独立行政法人国立病院機構
水戸医療センター

研 究 業 績 集

令和3年度

巻頭言

病院長　米野琢哉

水戸医療センターの基本方針として、「臨床研究を積極的に推進します」を掲げています。令和 3 年度は、COVID-19 対応に追われながらも、日常診療を黙々とこなし、臨床研究にも真摯に取り組んでいただきました。職員の皆様のご努力に敬意をはらいたいと思います。

臨床研究の推進は、診療の質向上のためにも必須です。様々な職種の方々が研究に取り組むことによって、診療の活性化にもつながると期待しております。病院としても、臨床研究部を中心に、資金提供、研究に必要な文書作成のアドバイスなど研究実施のサポートを継続していきます。今後も是非臨床研究にチャレンジしてみてください。

2021年度　　受託研究実績金額　　8,373万円

（治験・製造販売後臨床試験・製造販売後調査）

契約種類別グラフ

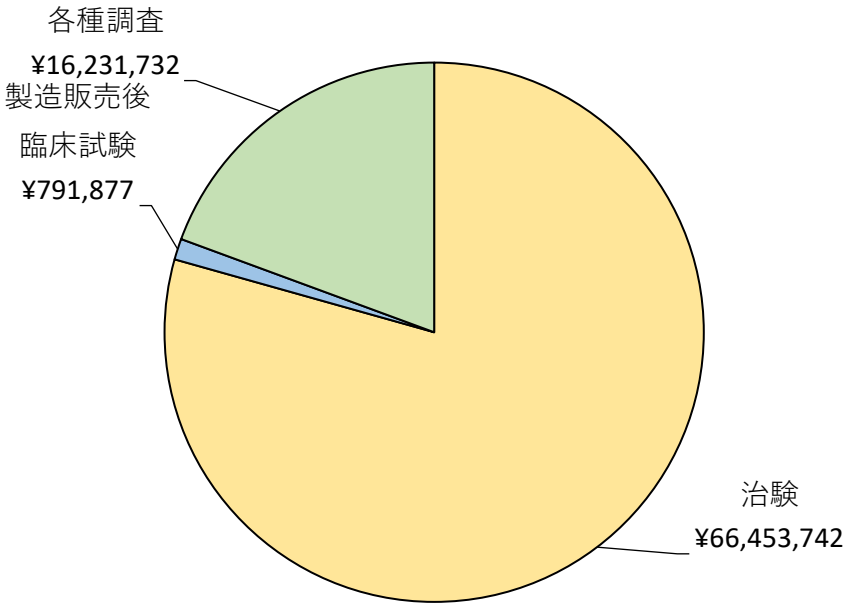

診療科別グラフ

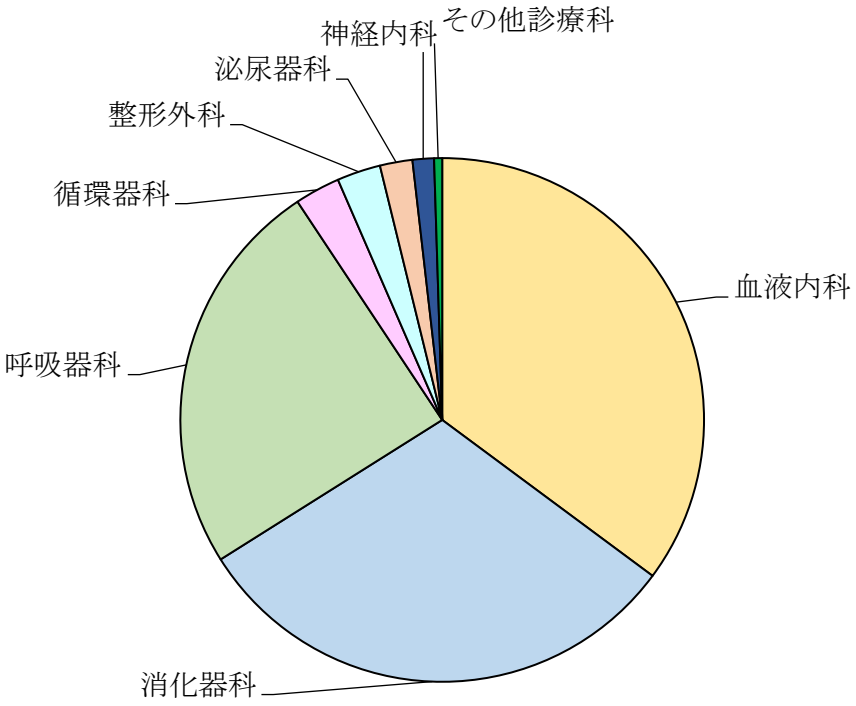

受託研究実績報告

①　受託研究実績金額　（治験・製造販売後臨床試験・製造販売後調査）

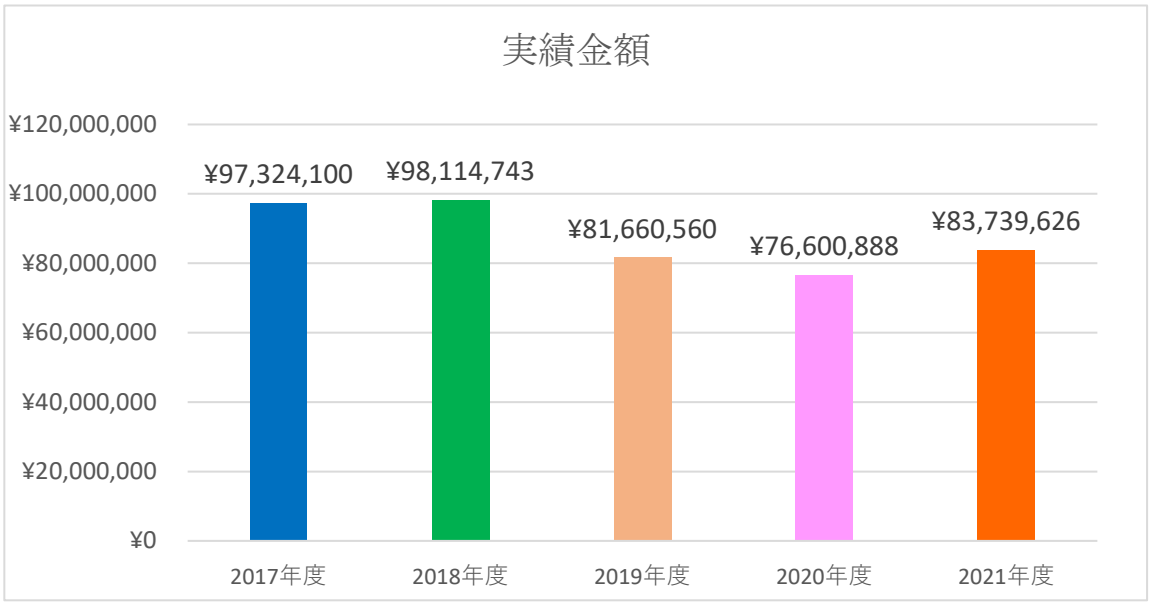

②　治験・製造販売後臨床試験　新規登録症例数

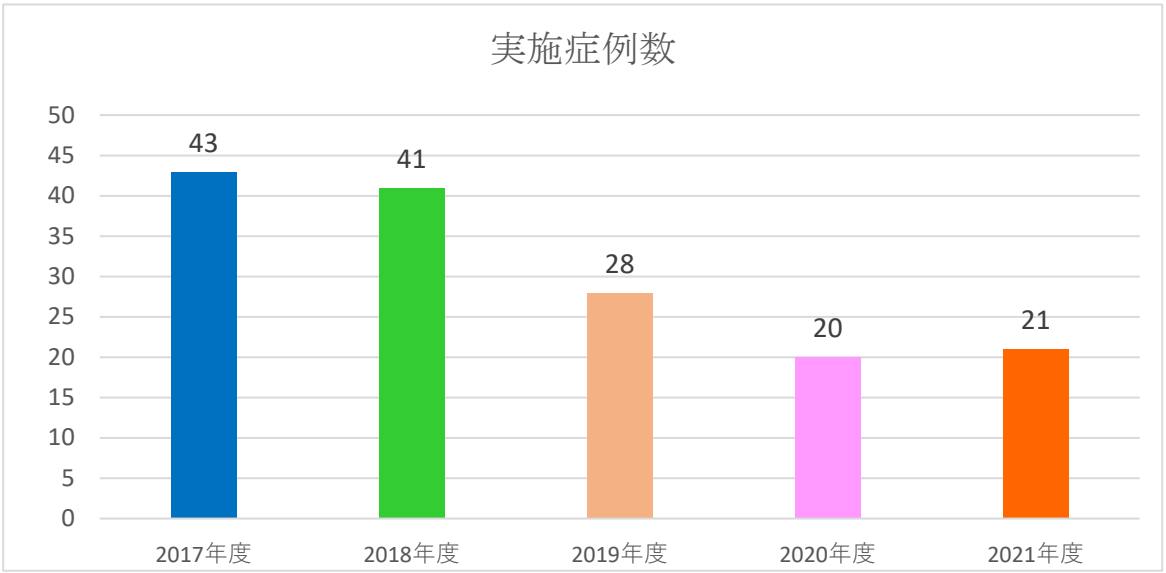

NHOネットワーク共同研究　新規症例登録数

研究責任者	研究課題名(採択番号)	研究代表者(施設名)	文書同意 有・無	当該施設 新規登録 症例数
堤 育代	未治療濾胞性リンパ腫における Obinutuzumabの治療成績、QOL、費用対効果、予後に関する多施設前向きコホート研究 （採択番号：H31-NHO(血液)-01）	堤育代 (水戸医療センター)	有	6
吉沢和朗	筋強直性ジストロフィー患者における脳梗塞発症頻度とCHADS2スコアによる予測の有用性についての前向き研究 （採択番号：H31-NHO(神経)-01）	吉田亘佑 (旭川医療センター)	有	1
吉田近思	B細胞性急性リンパ性白血病におけるターゲットキャプチャーRNA-seqを用いたサブタイプ診断の実行可能性に関する研究 （採択番号　H31-NHO(血液)－02）	安田貴彦 (名古屋医療センター)	有	2
箭内英俊	根治照射不能な進行非小細胞肺癌患者における免疫チェックポイント阻害剤の効果予測因子としての栄養/免疫学的指標の臨床的意義に関する前向き観察研究 （採択番号　H31-NHO(癌呼)-02）	岡本龍郎 （九州がんセンター ）	有	9
吉田近思	レジストリーデータを利用したAYA世代DLBCLの臨床的・生物学的特性を明らかにする観察研究 （採択番号：R3-NHO(血液)-01）	鈴木康裕 (名古屋医療センター)	無	2

競争的研究費

項目	研究課題名	研究者名	研究事業名☒	主任 分担	研究費 受領日	研究費 （単位：円）
厚生労働科学研究費	新型インフルエンザ等の感染症発生時のリスクマネジメントに資する感染症のリスク評価及び公衆衛生時対策の強化のための研究	安田　貢	国立病院機構 三重病院	分担	R3.6.24	500,000
厚生労働科学研究費	心停止後臓器提供数の減少への効果的な対策に資する研究	湯沢賢治	水戸医療センター	主任	R3.6.30	3,000,000
科学研究費助成事業 （学術研究助成基金助成金）	医師の病院前診察における網羅的文献データベース構築とエビデンス診療ギャップの解明	堤　悠介	水戸医療センター	主任	R3.7.9	585,000
科学研究費助成事業 （学術研究助成基金助成金）	次世代型肘検診から野球肘の病態解明 ～エコー検診と車載型小型MRIの融合～	小川　健	水戸医療センター	主任	R3.7.9	1,014,000
厚生労働科学研究費	HAMならびに類縁疾患の患者レジストリを介した診療連携モデルの構築によるガイドラインの活用促進と医療水準の均てん化に関する研究(20HA2001)	湯沢賢治	聖マリアンナ医科大学	分担	R3.8.30	300,000
日本医療研究開発機構研究費	遺伝子関連情報を基軸にした効率的免疫抑制管理による革新的長期管理ロジック開発（21ek0510033h0002）	湯沢賢治	東京女子医科大学	分担	R3.8.31	390,000
科学研究費助成事業 （科学研究費補助金）	臓器移植法制・法政策の包括的再検証―改正法施行10年目の現況を踏まえた提言(20H01430)	湯沢賢治	北海道大学大学院法学研究科	分担	R3.9.24	390,000
日本医療研究開発機構研究費	HAM-HTLV-1 陽性難治性疾患の患者レジストリ活用によるエビデンスの創出(21ek0109529s0301)	湯沢賢治	聖マリアンナ医科大学	分担	R3.9.29	390,000
日本医療研究開発機構研究費	新規HTLV-1感染モデルを用いたHAMの発症予防法・治療法の開発(21ek0109441s0202)	湯沢賢治	聖マリアンナ医科大学	分担	R3.9.29	910,000
民間セクターからの寄附金	腎代替療法の情報提供における腎移植に関する情報提供サイトに関する研究	湯沢賢治	中外製薬株式会社	主任	R3.10.20	200,000
民間セクターからの寄附金	腹水濾過濃縮再静注法の臨床応用への適応拡大の研究	小﨑浩一	中外製薬株式会社	主任	R3.10.20	200,000

英文論文

No	タイトル	著者 (※筆頭著者)	ポイント
1	Primary Intramuscular Classic Hodgkin Lymphoma: A Rare Case Report.	吉田近思	3.282
2	Venetoclax plus low-dose cytarabine in Japanese patients with untreated acute myeloid leukaemia ineligible for intensive chemotherapy	吉田近思	5.925
3	Impact of the Clinical Trials Act on Noncommercial Clinical Research in Japan: An Interrupted Time-series Analysis	※堤　育代	15.618
4	Venetoclax plus azacitidine in Japanese patients with untreated acute myeloid leukemia ineligible for intensive chemotherapy	吉田近思	5.925
5	Low-dose dasatinib in older patients with chronic myeloid leukaemia in chronic phase (DAVLEC): a single-arm, multicentre, phase 2 trial	吉田近思	33.153
6	A single-cell atlas of non-haematopoietic cells in human lymph nodes and lymphoma reveals a landscape of stromal remodelling	吉田近思	31.213
7	Alternating bortezomib-dexamethasone and lenalidomide-dexamethasone in patients with newly diagnosed multiple myeloma aged over 75 years	米野琢哉	3.794
8	The Conspicuousness of High Endothelial Venules in Angioimmunoblastic T-cell Lymphoma Is Due to Increased Cross-sectional Area, Not Increased Distribution Density	米野琢哉	7.137
9	A phase 2, open-label, multicenter study of ixazomib plus lenalidomide and dexamethasone in adult Japanese patients with relapsed and/or refractory multiple myeloma	米野琢哉	6.85
10	Rare Case of congenital coronary artery fistula coexistent and coalesced with aortopulmonary fistula	※大澤　匠	2
11	Soluble vascular endothelial growth factor receptor 2 and prognosis in patients with chronic heart failure	小泉智三	6.612

英文論文

No	タイトル	著者 (※筆頭著者)	ポイント
12	Cancer-related FGFR2 overexpression and gene amplification in Japanese patients with gastric cancer	石田博保	5.925
13	Cerebral Microbleeds, Cerebrospinal Fluid, and Neuroimaging Markers in Clinical Subtypes of Alzheimer's Disease	田代裕一	7.086
14	Recurrent Lobar Hemorrhages and Multiple Cortical Superficial Siderosis in a Patient of Alzheimer's Disease With Homozygous APOE ε2 Allele Presenting Hypobetalipoproteinemia and Pathological Findings of 18F-THK5351 Positron Emission Tomography: A Case Report	田代裕一	3.043
15	Right Proximal Common Carotid Artery Injury.	堤　悠介	5.697
16	Does statistical difference in the pre/post quasi-experimental study mean the utility of multimodal educational intervention in targeted normoxia in critically ill trauma patients?	堤　悠介	2.8485
17	The Japanese Clinical Practice Guidelines for Management of Sepsis and Septic Shock 2020 (J-SSCG 2020).	堤　悠介	4.76
18	Around ten percent of most recent Cochrane reviews included outcomes in their literature search strategy and were associated with potentially exaggerated results: A research-on-research study.	堤　悠介	10.407
19	The inclusion of outcomes in search strategies for Cochrane Reviews: authors' reply.	堤　悠介	4.7035
20	Minimal important changes in standard deviation units are highly variable and no universally applicable value can be determined.	堤　悠介	10.407
21	Substance use disorder treatment success: assessing patient-reported use improvement and provider-evaluated treatment completion	堤　悠介	6.007

英文論文

No	タイトル	著者 (※筆頭著者)	ポイント
22	Association between time to treatment failure and peripheral eosinophils in patients with non-small cell lung cancer treated with immune checkpoint inhibitors	中村亮太	8.218
23	National survey on deceased donor organ transplantation during the COVID-19 pandemic in Japan.	湯沢賢治	5.54
24	A multicentric study on the newly developed reconstruction locking plate for midshaft clavicular fracture.	※小川　健	8
25	High-definition magnetic resonance images on medial elbow injuries in preadolescent Little Leaguers	小川　健	4.805
26	Squamous cell carcinoma arising from an ischial pressure ulcer initially suspected to be necrotizing soft tissue infection: A case report	※笠井丈博	5.374
27	Emphysematous cystitis due to Streptococcus salivarius infection in a patient with a neurogenic bladder	※岡田脩平	2
28	Extramedullary plasmacytoma of the ureter	※岡田脩平	2
29	Odors Associated With Autobiographical Memory Induce Visual Imagination of Emotional Scenes as Well as Orbitofrontal-Fusiform Activation	井田正博	8.152
30	Effects of Magnetic Resonance Imaging With Axial Traction of the Thumb Carpometacarpal Joint on Articular Cartilage Visibility: A Feasibility Study	小川　健	3
31	Difference in Rupture Risk Between Familial and Sporadic Intracranial Aneurysms An Individual Patient Data Meta-analysis	山崎友郷	14.8
32	Preoperative Evaluation and Surgical Simulation for Osteochondritis Dissecans of the Elbow Using Three-Dimensional MRI-CT Image Fusion Images	小川　健	6.992
33	Sex Difference and Rupture Rate of Intracranial Aneurysms: An Individual Patient Data Meta-Analysis	山崎友郷	13.17

和文論文

No	論文名	著者 (※筆頭著者)	ポイント
1	臨床研究法実施後の臨床研究の現状と展望	堤　育代	1.000
2	慢性期慢性骨髄性白血病の治療	※吉田近思	1.500
3	後天性血小板機能異常による著明な出血傾向を呈したtriple negative原発性骨髄線維症	堤　育代	1.000
4	敗血症にobesity paradoxはあるのか？	堤　悠介	1.000
5	11　PROBAST：予測モデル研究〈渡部 純　堤 悠介〉	堤　悠介	1.000
6	CASE 2　2型糖尿病で急性冠動脈症候群を発症した患者に対するリキセナチドの効果〈堤 悠介　辻本 康〉	堤　悠介	1.000
7	2回の生体腎移植後に発症した急性虫垂炎に対し腹腔鏡下虫垂切除術を施行した1例	※小﨑浩一	1.500
8	COVID-19と腎移植医療	湯沢賢治	1.000
9	デオキシスパーガリン	※湯沢賢治	1.500
10	日本移植学会2020年症例登録 統計報告	※湯沢賢治	1.500
11	腎移植臨床登録集計報告（2021） 2020年実施症例の集計報告と追跡調査結果	湯沢賢治	1.000
12	日本の臓器提供と臓器移植の現状	※湯沢賢治	1.500
13	2回の生体腎移植後に発症した急性虫垂炎に対し腹腔鏡下虫垂切除を施行した1例	湯沢賢治	1.000
14	HTLV-1陽性臓器移植のエビデンス・プラクティスギャップに関する全国アンケート調査	湯沢賢治	1.000
15	COVID-19感染流行期における理想的な臓器摘出を創出するためのアンケート調査の結果−厚生労働科学特別研究事業による調査研究−	湯沢賢治	1.000
16	整形トピックス　上腕骨外側上顆炎の重症度診断や病態把握に有効な高分解能MRI	※小川　健	1.500
17	肘関節terrible triad injuryの治療戦略　前方要素の修復は必須か?	※小川　健	1.500
18	セメントステムを用いた上方アプローチによる人工骨頭置換術の短期成績	※森田純一郎	1.500

和文論文

No	論文名	著者 (※筆頭著者)	ポイント
19	上腕骨近位端骨折に対する保存療法の実際	小川　健	1.000
20	RSA術後の装具固定は2週間で可能か?	小川　健	1.000
21	MRIにて腱板筋筋腹の信号変化を認めた拘縮肩の特徴	小川　健	1.000
22	橈骨遠位端骨折術後に総指伸筋腱(示指)皮下断裂をきたした1例	小川　健	1.000
23	大学野球選手における上腕骨内側上顆下端の異常所見と学齢期線習量との関係	小川　健	1.000
24	腸間膜膿瘍を形成した小腸間膜放線菌症の1例	※栗原秀輔	1.500
25	戦略的視点で見るCT救急撮影～常に考える意識と行動が患者を救う～	※田中善啓	1.500
26	改訂第3版救急撮影ガイドライン	※田中善啓	1.500
27	熱傷による急性呼吸窮迫症候群に対し、頭部挙上位により酸素化が改善した1症例	※石井俊介	1.500

国際学会

学会名	演題名	演者名	発表年月日
63nd ASH Annual Meeting and Exposition	Importance of the Duration of TKI Treatment in Treatment-free Remission of Chronic Phase Chronic Myeloid Leukemia: Results of D-FREE Trial	吉田近思	R3.12.6
American Heart Association Scientific Sessions 2021	Association Between Frailty and Vascular Endothelial Growth Factor Families in Patients with Heart Failure: The PREHOSP-CHF Study	小泉智三	R3.11.16
Japanese Society of Cardiology Annual Scientific Sessions 2021	A Case of Recurrent Heart Failure on Well-controlled Eosinophilic Granulomatous with Polyangitis	南健太郎	R4.3.11
American Heart Association Scientific Sessions 2021	Association Between Age and the von-Willebrand Factor ADAMTS 13 Axis in Patients with ST elevation Myocardial infarction	大澤　匠 伊藤雄太 小泉智三	R3.11.13～11.15
European Society of Cardiology Asia with APSC &AFC	Comparison of VWF-ADAMTS 13 axis involvement in atrial fibrillation and sinus rhythm in patients with ST-elevation myocardial infarction	大澤　匠	R3.12.2
76th Annual Meeting of the American Society Surgery of Hand	Chronological change in postoperative magnetic resonance imaging for Kienböck’s disease using an original grading system	小川 健	R3.9.29
Japanese Society of Cardiology Annual Scientific Sessions 2021	Association Between Age and the ADAMTS 13 von-Willebrand Factor Axis in Patients with Acute Arterial Thrombosis (STEMI and Aculte Ischemic Stroke)	大澤　匠	R4.3.13
第76回日本消化器外科学会	Experience of cell-free and concentrated ascites reinfusion therapy (CART) in our hospital.	小﨑　浩一	R3.7.9

国内学会

学会名	演題名	演者名	発表年月日
第40回茨城造血器疾患研究会	Dasatinib+PSLで寛解導入療法後にponatinib hyper CVADで地固めを行ったPh+ALL	坪井宥璃	R3.5.19
第83回日本血液学会学術集会	初発慢性期慢性骨髄性白血病に対するボスチニブ治療の経験	坪井宥璃	R3.9.23
第83回日本血液学会学術集会	Venetoclax plus LDAC in untreated AML ineligible for intensive chemotherapy in expanded access study	吉田近思	R3.9.25
第16回日本血液学会関東甲信越地方会	初発μBCR-ABL陽性慢性期慢性骨髄性白血病に対するボスチニブ治療	坪井宥璃	R4.3.19
第61回日本呼吸器学会学術講演会	一次治療Osimertinibを用いた161例の臨床的検討：茨城県内他施設調査研究	沼田岳士	R3.4.23
第218回茨城内科学会	子宮筋腫術後再発に対しホルモン療法中、両肺に転移をきたした1例	船橋　恒（退職）	R3.10.17
第6回桜の郷チェストカンファレンス	呼吸器領域における興味深い症例の提示	箭内英俊	R3.11.25
第6回桜の郷チェストカンファレンス	COVID-19とインフルエンザについて	遠藤健夫	R3.11.25
水戸医療センター出張講座	肺の生活習慣病　COPD	遠藤健夫	R4.1.26
水戸医療センターがん市民セミナー	もっと知ってほしい肺がんのこと	遠藤健夫	R4.2.20
第24回日本臨床救急医学会総会・学術集会パネルディスカッション	「茨城県におけるCOVID-19医療体制構築～県庁医療調整本部活動とCOVID-19医療システム（i-HOPE）～」	安田　貢	R3.6.11
第45回茨城県救急医学会	「茨城県におけるCOVID-19医療体制構築～県庁医療調整本部活動とCOVID-20医療システム（i-HOPE）～」	安田　貢	R3.9.11
第75回国立病院総合医学会	「茨城県における進捗状況医療体制構築-行政と医療の連携、県庁医療調整本部活動とCOVID-19医療システム（i-HOPE)-」	安田　貢	R3.10.23
第35回日本外傷学会総会・学術集会	クラスタリングを用いた外傷死の分類-どのような患者を救命できそうか?	堤　悠介	R3.5.28

国内学会

学会名	演題名	演者名	発表年月日
第75回国立病院総合医学会	2015年9月関東・東北豪雨での茨城県常総水害について	石上耕司	R3. 10. 23
第121回日本外科学会定期学術集会	当院の腹壁瘢痕ヘルニア手術症例の検討	小崎浩一	R3. 4. 10
第38回日本呼吸器外科学会学術集会	肺癌手術症例における術後骨格筋減少の意義	中村亮太	R3. 5. 21
第38回日本呼吸器外科学会学術集会	浸潤性非小細胞肺癌手術症例における術前SLX上昇の意義	栗原秀輔	R3. 5. 21
第66回日本透析医学会学術集会	当院の持続的血液濾過透析におけるAN69ST膜の現状	小崎浩一	R3. 6. 5
第186回日本胸部外科学会　関東甲信越地方会	1秒率36. 3%のCOPD合併の食道癌に、左半腹臥位胸腔鏡下食道切除を行なった1例	加藤丈人	R3. 6. 5
第186回日本胸部外科学会　関東甲信越地方会	右上葉肺癌患者の血管走行異常の一例	栗原秀輔	R3. 6. 5
第29回日本乳癌学会学術総会	術後27年で胸壁再発を来した乳癌の一例	島　正太郎	R3. 7. 1～7. 3
第29回日本乳癌学会学術総会	術前抗ホルモン療法を行った高齢者乳癌32例の検討	森　千子	R3. 7. 1～7. 3
第76回日本消化器外科学会総会	幽門側胃切除術後再建法が骨格筋量減少に及ぼす影響	米山　智	R3. 7. 8
第75回日本食道癌学会学術集会	組織オキシメータを用いた再建胃管の血流評価	加藤丈人	R3. 9. 23～9. 24
第9回茨城医学会麻酔科分科会	（講演）茨城県の臓器移植の現状、その未来	小崎浩一	R3. 10. 2
第42回日本アフェレシス学会学術大会	非代償性肝硬変に伴う難治性腹水に対する腹水濾過濃縮再静注法	小崎浩一	R3. 10. 17
第68回日本臨床検査医学会学術集会	献腎移植後に発症した後天性IgA欠損症の1例	小崎浩一	R3. 11. 11
第55回茨城人工透析談話会	抗ドナー抗体陽性レシピエントに術前脱感作療法を施行した先行的生体腎移植の一例	小崎浩一	R3. 11. 14
第249回茨城外科学会	腸間膜膿瘍を形成した小腸間膜放線菌症の1例	栗原秀輔	R3. 11. 13
第83回日本臨床外科学会総会	白線ヘルニア、臍ヘルニア、左半月線ヘルニアを併発した1手術症例	河原将人	R3. 11. 18～11. 20
第18回CART研究会学術集会	（ワークショップ・基調講演）なぜ当院で低温保存腹水を用いた腹水濾過濃縮再静注法(CART)を始めたのか	小崎浩一	R3. 11. 27

国内学会

学会名	演題名	演者名	発表年月日
第34回日本内視鏡外科学会総会	反復する成人胃軸捻転症に対して腹腔鏡下胃固定術を行った一例	米山　智	R3.12.2
第34回日本内視鏡外科学会総会	胆嚢軸捻転症に対し腹腔鏡下胆嚢摘出術を施行した1例	小﨑浩一	R3.12.4
第34回日本外科感染症学会総会学術集会	免疫抑制下にある腎移植患者の手術部位(SSI)に対する周期的持続灌流併用局所陰圧閉鎖療法（NPWTi-d）の有用性	小﨑浩一	R3.12.17
第55回日本臨床腎移植学会	Dual kidney transplantation の一例	小﨑浩一	R4.2.25
第58回日本腹部救急医学会総会	初診時の診断が困難であったコレステロール塞栓症による小腸狭窄・穿孔の1例	成田保和	R4.3.25
第58回日本腹部救急医学会総会	術前診断が困難であった紙製食品飾りの誤飲によるS状結腸穿孔を呈した1例	森　貴昭	R4.3.25
茨城県脳心連携講演会	虚血性脳血管障害に対する治療の現状	加藤徳之	R3.5.31
我が街脳卒中を考える会	茨城県央地区における脳卒中連携	加藤徳之	R3.7.13
第80回日本脳神経外科総会	脳動脈瘤コイル塞栓術に要するコイル数の検討	加藤徳之	R3.10.27
第80回日本脳神経外科総会	重症くも膜下出血における予後予測と水頭症の治療	宮本智志	R3.10.27
第37回日本脳神経血管内治療学会	脳動脈瘤コイル塞栓術に要するコイル数の検討	加藤徳之	R3.11.25
第37回日本脳神経血管内治療学会	血栓回収療法中にマイクロカテーテルにより生じたdirect-carotid-cvernous fistulaの１例	宮本智志	R3.11.25
第57回日本移植学会総会	日本移植学会のCOVID-19に対する取り組み	湯沢賢治	R3.9.19
第40回日本心臓移植研究会学術集会	COVIDから心臓移植患者を守り心臓移植医療を維持するために－日本移植学会の取り組みから得られた知見－	湯沢賢治	R3.10.3
第48回日本肩関節学会学術集会	胸郭出口症候群の補助診断としてMRIは有効である	小川　健	R3.10.29

国内学会

学会名	演題名	演者名	発表年月日
第70回東日本整形災害外科学会雑誌	骨欠損に対する自家骨皮下埋没保存移植の経験　Preserving Autograft in Subcutaneous Space(PASS法)	中川翔太 森田純一郎 小川　健	R3.9.18
第64回日本手外科学会学術集会	母指CM関節症に対する鏡視下滑膜切除術の治療結果と成績不良例の検討	小川　健	R3.4.22
第36回東日本手外科研究会	キーンベック病に対する骨髄血移植・創外固定・低出力超音波併用治療	小川　健	R4.3.5
第32会日本臨床スポーツ医学会学術集会	大学野球投手における無症候性腱板損傷の経時的変化	小川　健	R3.11.13
第32会日本臨床スポーツ医学会学術集会	大学野球部員における手関節掌屈・背屈筋力の特性	小川　健	R3.11.13
第32会日本臨床スポーツ医学会学術集会	車載型ポータブルMRIによる上腕骨離断性骨軟骨炎検診の有用性	小川　健	R3.11.13
第94回日本整形外科学会学術集会	Composite beamの臨床成績は悪いのか -Chanrey Slite PlusとC-stemの長期成績の比較検討-	中川翔太	R3.5.20
第47回日本骨折治療学会学術集会	外傷性胸腰椎骨折と椎体癒合の関係	中川翔太 森田純一郎	R3.7.3
第47回日本骨折治療学会学術集会	セメントステムを用いた上方アプローチによる人工骨頭置換術の経験	森田純一郎 中川翔太	R3.7.3
第47回日本骨折治療学会学術集会	上腕骨顆上骨折変形治癒に対するmodified step-cut osteotomyの小経験	森田純一郎	R3.7.3
第17回茨城形成外科研究会	特発性血小板減少性紫斑病患者における眼窩コンパートメント症候群の一例	笠井丈博	R3.6.11
第48回日本マイクロサージャリー学会学術集会	神経・血管吻合後剥脱皮膚を植皮として用いた右手掌デグロービング損傷の一例	笠井丈博	R3.12.3
第120回茨城地方会	転移性腎癌に対するカボサンチニブ投与後に胃穿孔を生じた1例	岡田脩平	R3.6.19
第121回茨城地方会	精索腫瘍との鑑別が困難であったMeshomaの1例	岡田脩平	R3.10.17
第122回茨城地方会	ECIRS施行後にHydroperitoneumによってAbdominal Compartment Syndromeを発症した1例	岡田脩平	R4.2.5

国内学会

学会名	演題名	演者名	発表年月日
第35回日本泌尿器内視鏡学会総会	当科におけるロボット支援腎部分切除術の初期成績	飯沼昌宏	R3.11.18～11.13
第75回国立病院総合医学会	新型コロナウイルス感染症におけるオンライン・電話診療を受診した患者の処方調査	田所あき穂	R3.10.23～11.20
第75回国立病院総合医学会	院内製剤業務における 管理体制の向上に向けた取り組み	川又康平	R3.10.23～11.20
茨城県がん診療連携協議会研修部会薬剤師研修分科会	がん化学療法に対するペグフィルグラスチム併用における発熱性好中球減少症発現率に関する観察研究 ～非ホジキンリンパ腫～	小島卓也	R3.11.20
日本臨床腫瘍薬学会学術大会2022	免疫チェックポイント阻害剤で腎障害を来した症例における全生存期間の検討：後ろ向き観察研究	久保田将史	R4.3.12～3.13
第35回日本外傷学会総会・学術集会	外傷診療における2管球CT装置の有用性	田中善啓	R3.5.28
第45回茨城県救急医学会	COVID-19における放射線部門の感染対策：ハイブリッドチームの有用性	田中善啓	R3.9.11
第75回国立病院総合医学会	Pusher現象合併した重度麻痺高齢患者が腹臥位により端坐位保持可能に至った一症例	柳澤宏昭	R3.10.23
第75回国立病院総合医学会	急性期病院における脳血管障害患者の運転再開と高次脳機能評価の関連；アンケートを用いた実態調査	中津川秦生	R3.10.23
第86回日本循環器学会学術集会	高齢心不全患者における入院中の摂取エネルギー量と短期(90日以内)有害事象との関連	矢野博義	R4.3.12
第21回CRCと臨床試験のあり方を考える会議2021in横浜【Web開催】	治験検査資材管理方法の統一化への取り組み	本橋和樹	R3.10.2～11.14

令和３年度院内臨床研究課題

研究代表者	課題名	配分額
相澤哲史	神経内科患者における心拍変動係数（ＣＶＲ-Ｒ）による自立神経機能評価の有用性についての観察研究	390,000
小﨑浩一	腹水濾過濃縮再静注法（CART）における採取腹水長期常温保存の臨床使用への可能性の検討	1,700,000
中村亮太	肺癌手術症例における、周術期骨格筋減少の程度についての研究	300,000
米山　智	幽門側胃切除例における、術後骨格筋減少の程度についての研究	400,000
山崎友郷	脳内出血に対するＮａｖｉｇａｔｉｏｎ下血種吸引術＋ウロキナーゼ注入による安全性と効果の検討　後ろ向き研究	500,000
小川　健	牽引下MRIによる母指ＣＭ関節の軟骨評価に関する研究	290,000
森田純一郎	メガネ型デバイスを用いた複合現実を用いた骨盤骨折手術シミュレーションの有用性を検討する研究	650,000
中川翔太	新鮮骨粗鬆症性椎体骨折患者の1週間安静入院による保存加療に関する臨床研究	330,000
細谷恵美	抗がん剤治療における血管外漏出のリスク因子を探索する後ろ向き症例集積研究	450,000
木村梨奈	当院におけるDICの発生や治療の現状、ナルデメジンの使用状況と効果	360,000
石井俊介	血液内科に入院中のリハビリテーション患者におけるがん治療関連心機能障害の現状調査－後ろ向き観察研究－	150,000
矢野博義	高齢心不全患者における入院中の摂取エネルギー量と栄養状態が予後（総死亡・再入院）に及ぼす影響の検討　後ろ向き症例集積研究	150,000
田中善啓	仮想透視画像作成専用ソフトを用いたＩＶＲの被ばく及び造影剤原料の検討	350,000
湯沢賢治	腹腔鏡手術シミュレーターを用いたVR腹腔鏡手術トレーニングの試み	2,860,000

水戸医療センター

令和3年度　代表的論文

Internal Medicine
The Japanese Society of Internal Medicine

doi: 10.2169/internalmedicine.7524-21
Intern Med Advance Publication
http://internmed.jp

【 CASE REPORT 】

Primary Intramuscular Classic Hodgkin Lymphoma: A Rare Case Report

Yuya Kamura[1], Ikuyo Tsutsumi[1], Yukiko Miura[1], Masanori Seki[1], Takuya Komeno[1], Haruo Ohtani[2], Yukinori Inadome[3] and Chikashi Yoshida[1]

Abstract:

Hodgkin lymphoma (HL) is a hematologic malignancy that typically presents with lymphadenopathy. We herein report a patient with HL who presented with an intramuscular mass that required differentiation from an inflammatory lesion. A 65-year-old Japanese woman was referred to our hospital with a chief complaint of chronic and expanding tumor in her left thigh. By surgical resection, she was diagnosed with primary intramuscular, Epstein-Barr virus-positive, mixed-cellularity classic HL. She received combined modality therapy, resulting in a complete response. Primary intramuscular classic HL is extremely rare. It should be listed as a differential diagnosis of intramuscular tumors.

Key words: classic Hodgkin lymphoma (CHL), muscle, primary intramuscular lymphoma

(Intern Med Advance Publication)
(DOI: 10.2169/internalmedicine.7524-21)

Introduction

Hodgkin lymphoma (HL) is a hematologic malignancy that typically presents with lymphadenopathy, predominantly affecting the cervical, axillary, and mediastinal lymph nodes (1, 2). A biopsy is essential for the diagnosis of HL in order to confirm the pathological features, such as Reed-Sternberg cells derived from germinal center B-cells surrounded by inflammatory cells (3). HL is divided into two major types based on the immunophenotype and morphology of the tissue: nodular lymphocyte-predominant HL and classic HL (CHL). Furthermore, there are four subtypes of CHL: nodular sclerosis CHL, lymphocyte-rich CHL, mixed-cellularity CHL, and lymphocyte-depleted CHL (4).

Soft-tissue masses can generally be classified as mesenchymal tumors, skin appendage lesions, metastatic tumors, other tumors and tumorlike lesions, or inflammatory lesions (5). Primary intramuscular lymphoma is uncommon and rarely reported in HL.

We herein report a case of primary intramuscular CHL of the left thigh that responded to chemotherapy followed by radiotherapy.

Case Report

A 65-year-old Japanese woman was referred to our hospital with a chief complaint of swelling of her left thigh. She had noticed the mass 11 months earlier, and it gradually enlarged without pain. Subsequently, it was accompanied by enlargement of a left inguinal lymph node. Although a tissue biopsy was performed before her referral to our center, the histopathological diagnosis was inflammatory granuloma with necrosis debris and no evidence of malignancy. She had no B-symptoms, such as night sweats, a fever, or weight loss. Her medical history included type 2 diabetes mellitus and pulmonary fibrosis.

On a physical examination, she had a large (11×13 cm), firm, irregular and nontender mass in the left thigh with a solitary lymph node (1×1 cm) in the left inguinal region. No other lymphadenopathy or hepatosplenomegaly was identified. Laboratory investigations showed a normal white blood cell count (5,600 cells/μL: neutrophils, 50.0%; lymphocytes, 35.0%; and monocytes 9.0%) and a normal serum C-reactive protein level. Elevated serum lactate dehydrogenase (LDH) levels were observed (236 IU/L). The liver and kidney func-

[1]Department of Hematology, National Hospital Organization Mito Medical Center, Japan, [2]Department of Pathology, Mito Saiseikai General Hospital, Japan and [3]Department of Pathology, National Hospital Organization Mito Medical Center, Japan
Received: March 10, 2021; Accepted: April 12, 2021; Advance Publication by J-STAGE: June 5, 2021
Correspondence to Dr. Chikashi Yoshida, c.yoshida@mitomedical.org

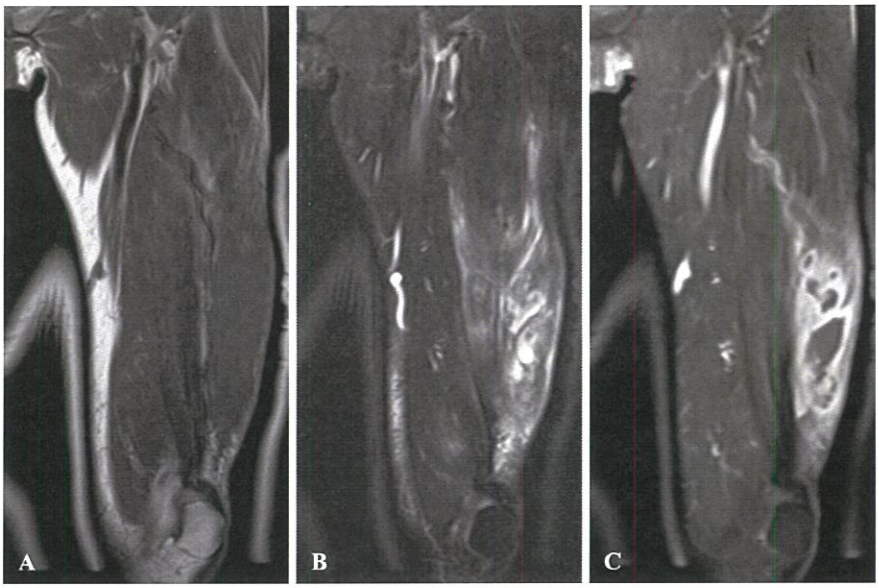

Figure 1. Coronal MR images of the left thigh. T1-weighted imaging revealed an intermediate signal intensity of the lesion compared with other normal muscle (A), while fat suppression T2-weighed imaging revealed increased signal intensity (B). Gadolinium-contrast enhancement demonstrated a series of cystic changes in the left vastus lateralis muscle (C).

tions were within the normal range. A serology test against hepatitis B, C, and anti-HIV were negative.

Contrast-enhanced computed tomography (CT) showed a low-density, irregularly shaped mass with rim enhancement in the left vastus lateralis muscle. Magnetic resonance imaging (MRI) was also performed to evaluate the nature of the lesion (Fig. 1). T1-weighted imaging revealed an intermediate signal intensity of the lesion compared with other normal muscle, while fat suppression T2-weighed imaging revealed an increased signal intensity of the lesion. Gadolinium-enhanced MRI demonstrated a series of cystic changes in the left vastus lateralis muscle, suggesting intramuscular abscess as a differential diagnosis at that time. We therefore performed soft tissue mass excision at the left thigh.

The histological examination of the surgical specimen showed that the central part of the tumor was mostly necrotic (Fig. 2A) with large, atypical cells, small lymphocytes, and macrophages infiltrating the periphery of the tumor (Fig. 2B). Some of the large, atypical cells were binuclear and pleomorphic and identified as Reed-Sternberg cells (Fig. 2C). An immunohistochemical examination revealed the large, atypical cells to be positive for CD30 (Fig. 2D), weakly positive for PAX5 (Fig. 2E), and completely negative for CD20 (Fig. 2F) and CD79a (Fig. 2G). They were also positive on Epstein-Barr virus-encoded small RNA *in situ* hybridization (EBER-ISH) (Fig. 2H). The disease was finally diagnosed as mixed-cellularity CHL. Fluorine-18 fluorodeoxyglucose positron emission tomography (^{18}F-FDG-PET)/CT from the head to upper thigh conducted after the surgery showed an abnormal accumulation of FDG only in the left inguinal lymph node (Fig. 3A-C). A bone marrow biopsy showed no evidence of tumor involvement. Based on these findings, we diagnosed her with Ann Arbor stage IIEA CHL of the primary left thigh muscle.

Although ABVD (doxorubicin, bleomycin, vinblastine, dacarbazine) chemotherapy was indicated for the initial treatment of this patient, the history of pulmonary fibrosis prompted us to refrain from using bleomycin because of possible pulmonary toxicity. Thus, she underwent 4 cycles of AVD chemotherapy that included doxorubicin 25 mg/m^2, vinblastine 6 mg/m^2, and dacarbazine 375 mg/m^2 on days 1 and 15 of a 28-day cycle. She did not experience any serious adverse events and tolerated the regimen well. Subsequently, involved-field radiation therapy (IFRT) was performed on the left thigh and left inguinal lymph node (total dose of 40 Gy in 20 fractions). After those series of treatments, the patient achieved a complete response and has been undergoing treatment-free follow-up for five years.

Discussion

HL characteristically presents with supradiaphragmatic lymphadenopathy. Extranodal involvement (including primary and secondary) of HL is less frequent, being noted in 15%-30% of HL cases (6). Among extranodal sites, the liver and lungs are the most common, followed by the bones (7). Muscle involvement was found in 0.32% of autopsy cases of CHL (8).

HL infrequently originates in extranodal organs. Indeed, there have only been two cases of primary intramuscular HL reported in the literature (9, 10), both of them involving gluteal tumors. Utkan et al. (9). described the first case of CHL in a 68-year-old man presenting with a history of pain-

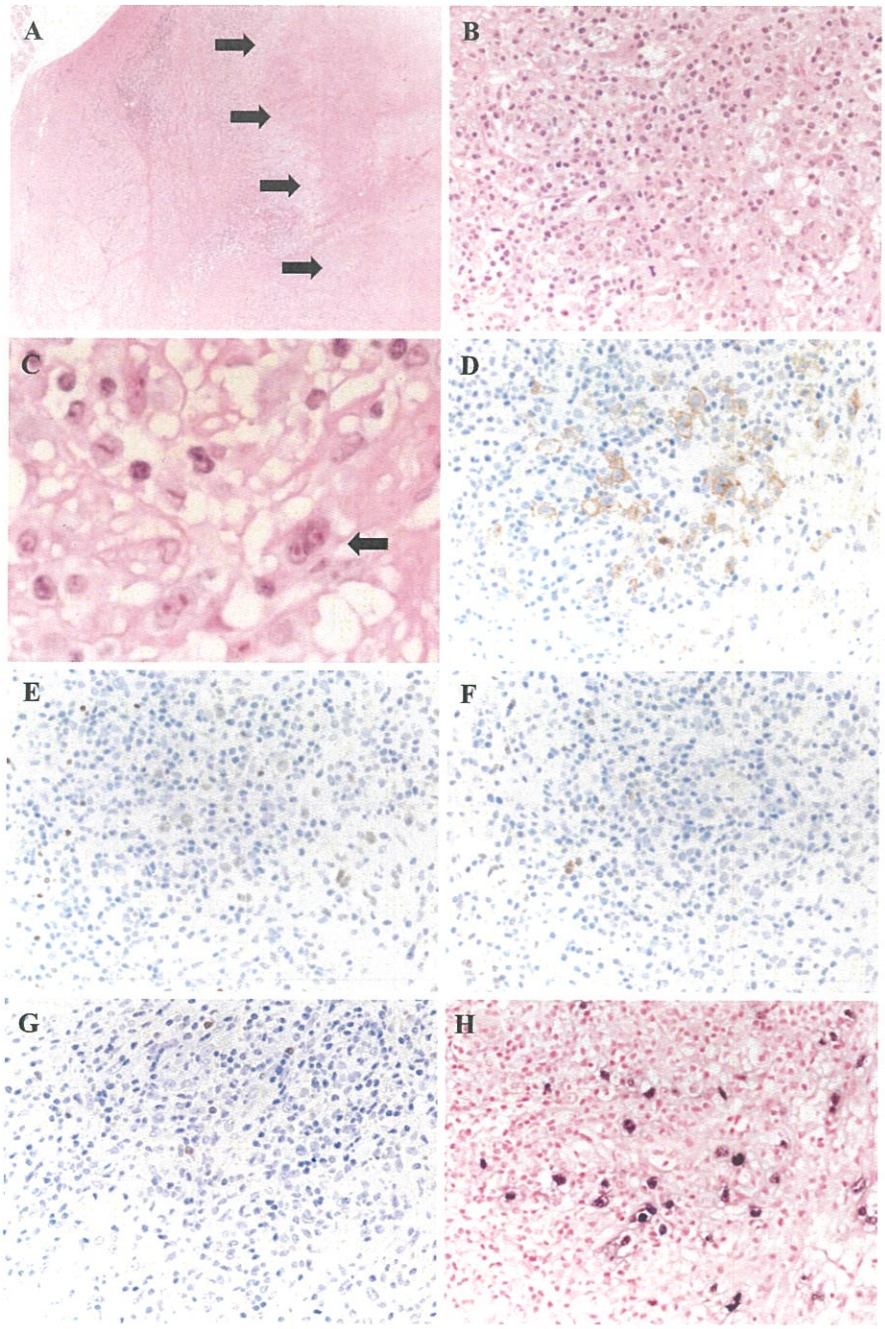

Figure 2. **A histopathological examination of the left thigh mass. Hematoxylin and Eosin staining (A: ×40, B: ×400, C: ×600) showed the central part of the tumor to be mostly necrotic (arrows in A), with large, atypical cells, small lymphocytes, and macrophages infiltrating the periphery of the tumor. Some of the large, atypical cells were binuclear and pleomorphic and were identified as Reed-Sternberg cells (arrow in C). An immunohistochemical examination revealed the atypical cells to be positive for CD30 (D: ×400) and weakly positive for PAX5 (E: ×400) but negative for CD20 (F: ×400) and CD79a (G: ×400). They were also positive for EBER-ISH (H: ×400).**

ful right gluteal swelling for 2 months with hypercalcemia, anemia, leukocytosis, and mild thrombocytosis. MRI revealed an approximately 15-cm mass infiltrating the gluteal and iliopsoas muscles. CT revealed no abnormalities except for a 2×2.5-cm right inguinal lymph node. A histological examination of the gluteal mass demonstrated nodular sclerosis CHL. There was no description of the Epstein-Barr virus (EBV) presence. The patient received six cycles of ABVD chemotherapy and achieved a complete response.

Jonjić et al. reported another case of primary intramuscular CHL in a 78-year-old man presenting with left gluteal lump (10). A laboratory examination showed an elevated erythrocyte sedimentation rate, anemia, and leukocytosis. [18] F-FDG-PET/CT revealed an over 10-cm-large FDG-avid

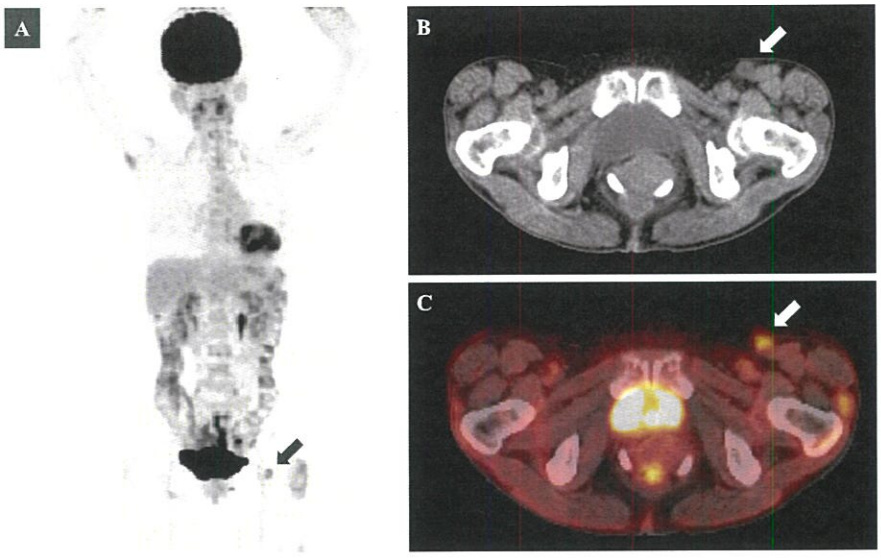

Figure 3. **^{18}F-FDG-PET maximum intensity projection image (A) of the head to the upper thigh taken after resection of the left thigh mass showed a single focal uptake (arrow in A), corresponding to the 10-mm-wide left inguinal lymph node indicated by the arrows on axial CT (B) and fused axial PET/CT (C).**

Table. **A Summary of the Reported Cases of Primary Intramasucular Classic Hodgkin Lymphoma.**

Reference Number	Age	Sex	B-symptoms	Location	Stage	Subtype	EBV	Treatment	OS
9	68	Male	NR	Right gluteal muscle	II E	Nodular sclerosis	NR	ABVD	Alive at 15 mo (CR)
10	78	Male	+	Left gluteal muscle	II EB	Nodular sclerosis	-	IFRT 44 Gy	NR (achieved CR)
Present case	65	Female	-	Left vastus lateralis muscle	II EA	Mixed cellularity	+	AVD+IFRT 40 Gy	Alive at 60 mo (CR)

OS: Overall survival, NR: Not recorded,+: positive, -: negative, ABVD: Doxorubicin, bleomycin, vinblastine, dacarbazine, mo: month, IFRT: involved-field radiation therapy, CR: Complete response, AVD: Doxorubicin, vinblastine, dacarbazine

mass in the left gluteal region and no other lesions. An excisional biopsy of the mass demonstrated nodular sclerosis CHL. EBER-ISH was negative. IFRT was performed, resulting in a complete response.

In the present patient, the third reported case of primary intramuscular CHL, there was some suspicion that the left inguinal lymph node was the primary lesion. However, this is chronologically unlikely, as the patient initially presented with the thigh swelling, followed by left inguinal lymphadenopathy. In addition, the inguinal lymph node was only 1 cm in diameter, whereas the thigh mass was over 10 cm large. Considering the pre/post temporal relationship and the size of the lesion, we determined that left thigh muscle lesion to be the primary one. These three cases of primary intramuscular HL are summarized in Table.

The association between EBV infection and the development of HL has been widely investigated and has been found to vary by region, economic status, and age, suggesting that environmental factors may be involved in the development of HL. Endoplasmic reticulum stress associated with the viral infection has been shown to be involved in the pathogenesis of HL (11). In addition, it has been reported that positivity of EBER-ISH is associated with a high frequency of extranodal involvement in patients with CHL (12). Reed-Sternberg cells and Hodgkin cells with a rich inflammatory background ensure their survival through the selective recruitment of cells in their microenvironment, constitutional activation of anti-apoptotic pathways, and elaborate evasion of the host immune system (13). As in the two previous cases (9, 10), the present case developed at an advanced age. Reed-Sternberg cells were positive for EBER-ISH, as shown in Fig. 2F. Taken together, these findings suggest that immunodeficiency along with aging and infection with EBV may contribute to the development of extranodal CHL. However, due to the extremely limited number of cases available, it is difficult to clarify the factors associated with the genesis of CHL primarily in muscle.

In conclusion, muscle involvement of HL is uncommon, and primary intramuscular CHL in particular is extremely rare. Nevertheless, it should be considered as a differential diagnosis in patients presenting with intramuscular tumors. Further studies are required to elucidate the clinical features

and pathogenesis of this rare form of disease.

The authors state that they have no Conflict of Interest (COI).

Acknowledgement

We are grateful to Prof. Junia V. Melo (University of Adelaide, Australia) for the language editorial assistance.

References

1. Shimabukuro-Vornhagen A, Haverkamp H, Engert A, et al. Lymphocyte-rich classical Hodgkin's lymphoma: clinical presentation and treatment outcome in 100 patients treated within German Hodgkin's Study Group trials. J Clin Oncol **23**: 5739-5745, 2005.
2. Laurent C, Do C, Gourraud PA, de Paiva GR, Valmary S, Brousset P. Prevalence of Common Non-Hodgkin Lymphomas and Subtypes of Hodgkin Lymphoma by Nodal Site of Involvement: A Systematic Retrospective Review of 938 Cases. Medicine (Baltimore) **94**: e987, 2015.
3. Marafioti T, Hummel M, Foss HD, et al. Hodgkin and reed-sternberg cells represent an expansion of a single clone originating from a germinal center B-cell with functional immunoglobulin gene rearrangements but defective immunoglobulin transcription. Blood **95**: 1443-1450, 2000.
4. Swerdlow SH, Campo E, Pileri SA, et al. The 2016 revision of the World Health Organization classification of lymphoid neoplasms. Blood **127**: 2375-2390, 2016.
5. Beaman FD, Kransdorf MJ, Andrews TR, Murphey MD, Arcara LK, Keeling JH. Superficial soft-tissue masses: analysis, diagnosis, and differential considerations. Radiographics **27**: 509-523, 2007.
6. Guermazi A, Brice P, de Kerviler E E, et al. Extranodal Hodgkin disease: spectrum of disease. Radiographics **21**: 161-179, 2001.
7. Li ZM, Zhu YJ, Xia Y, Huang JJ, Jiang WQ. Clinical characteristics of the patients with Hodgkin's lymphoma involving extranodal sites. Chin J Cancer **31**: 342-347, 2012.
8. Komatsuda M, Nagao T, Arimori S. An autopsy case of malignant lymphoma associated with remarkable infiltration in skeletal muscles. Rinsho Ketsueki (The Japanese Journal of Clinical Hematology) **22**: 891-895, 1981 (in Japanese).
9. Utkan G, Buyukcelik A, Yalcin B, et al. Extranodal Hodgkin disease presenting with gluteal mass and hypercalcemia. South Med J **99**: 1149-1150, 2006.
10. Jonjić N, Valković T, Vujaklija DV, Ilijaš KM. Diagnostic challenge of soft tissue extranodal Hodgkin lymphoma in core-needle biopsy: case report. Scott Med J 36933020941262, 2020.
11. Piris MA, Medeiros LJ, Chang KC. Hodgkin lymphoma: a review of pathological features and recent advances in pathogenesis. Pathology **52**: 154-165, 2020.
12. Kiliçarslan A, Öztürk V, Yikilmaz AŞ, et al. Evaluation of the Prognostic Importance of c-Myc and Bcl-2 Expressions and the Presence of Epstein-Barr Virus in Classical Hodgkin Lymphoma. Turk Patoloji Derg **34**: 199-206, 2018.
13. Bienz M, Ramdani S, Knecht H. Molecular Pathogenesis of Hodgkin Lymphoma: Past, Present, Future. Int J Mol Sci **21**: 6623, 2020.

JJCO Japanese Journal of Clinical Oncology

Japanese Journal of Clinical Oncology, 2021, 51(9)1372–1382
https://doi.org/10.1093/jjco/hyab112
Advance Access Publication Date: 29 July 2021
Original Article

OXFORD

Original Article

Venetoclax plus low-dose cytarabine in Japanese patients with untreated acute myeloid leukaemia ineligible for intensive chemotherapy

Takahiro Yamauchi[1,*], Chikashi Yoshida[2], Kensuke Usuki[3], Satoru Takada[4], Itaru Matsumura[5], Nobuaki Dobashi[6], Yasushi Miyazaki[7], Toshihiro Miyamoto[8], Hiroatsu Iida[9], Norio Asou[10], Junya Kuroda[11], Satoshi Ichikawa[12], Norio Komatsu[13], Wellington Mendes[14], Hideyuki Honda[15], Sumiko Okubo[16], Misaki Kurokawa[15], Qi Jiang[14], Andrew Wei[17], and Kenichi Ishizawa[18]

[1]Department of Hematology and Oncology, University of Fukui Hospital, Fukui, Japan, [2]Department of Hematology, National Hospital Organization, Mito Medical Center, Ibaraki, Japan, [3]Department of Hematology, NTT Medical Center Tokyo, Tokyo, Japan, [4]Leukemia Research Center, Saiseikai Maebashi Hospital, Maebashi, Japan, [5]Department of Hematology and Rheumatology, Kindai University Hospital, Osaka, Japan, [6]Division of Clinical Oncology/Hematology, The Jikei University Daisan Hospital, Tokyo, Japan, [7]Department of Hematology, Atomic Bomb Disease Institute, Nagasaki University, Nagasaki, Japan, [8]Medicine and Biosystemic Science, Graduate School of Medical Sciences, Kyushu University, Fukuoka, Japan, [9]Department of Hematology, National Hospital Organization Nagoya Medical Center, Nagoya, Japan, [10]Department of Hematology, Saitama Medical University International Medical Center, Hidaka, Japan, [11]Division of Hematology and Oncology, Department of Medicine, Kyoto Prefectural University of Medicine, Kyoto, Japan, [12]Department of Hematology, Tohoku University Hospital, Sendai, Japan, [13]Department of Hematology, Juntendo University School of Medicine, Tokyo, Japan, [14]AbbVie Inc., North Chicago, IL, USA, [15]AbbVie GK, Tokyo, Japan, [16]AbbVie GK, Osaka, Japan, [17]Department of Clinical Haematology, The Alfred Hospital and Monash University, Melbourne, VIC, Australia and [18]Department of Third Internal Medicine, Yamagata University Hospital, Yamagata, Japan

*For reprints and all correspondence: Takahiro Yamauchi, Department of Hematology and Oncology, University of Fukui Hospital, 23-3 Matsuokashimoaizuki, Eiheiji Fukui 910-1193, Japan. E-mail: tyamauch@u-fukui.ac.jp

Received 13 May 2021; Editorial Decision 24 June 2021; Accepted 26 June 2021

Abstract

Background: In a multinational phase 3 trial (VIALE-C), venetoclax plus low-dose cytarabine prolonged overall survival vs placebo plus low-dose cytarabine in patients with newly diagnosed acute myeloid leukaemia ineligible for intensive chemotherapy, although it was not statistically significant. Herein, we assess the benefit of venetoclax plus low-dose cytarabine in the Japanese subgroup of VIALE-C patients ($n = 27$).

Methods: VIALE-C, a randomized (2:1), double-blind study (NCT03069352), enrolled untreated patients (≥18 years) with acute myeloid leukaemia. Patients received venetoclax (600 mg days 1–28, 4-day ramp-up in cycle 1) or placebo in 28-day cycles with low-dose cytarabine (20 mg/m^2 days 1–10). The primary endpoint was median overall survival.

Results: In the Japanese subgroup, at a 6-month follow-up from the primary analysis, median overall survival for venetoclax ($n = 18$) and placebo ($n = 9$), plus low-dose cytarabine, was 4.7

and 8.1 months, respectively (hazard ratio, 0.928, 95% confidence intervals : 0.399, 2.156). The rate of complete remission plus complete remission with incomplete blood count recovery was higher with venetoclax plus low-dose cytarabine (44.4%) vs placebo plus low-dose cytarabine (11.1%). All patients experienced at least 1 adverse event. The most common grade ≥3 adverse events with venetoclax or placebo, plus low-dose cytarabine, were febrile neutropenia (50.0% vs 44.4%, respectively) and thrombocytopenia (27.8% vs 44.4%, respectively). Serious adverse events were reported in 50.0 and 33.3% of patients in the venetoclax and placebo, plus low-dose cytarabine arms, respectively; pneumonia was the most common (22.2% each).

Conclusions: Limited survival benefit in the Japanese subgroup can be attributed to small patient numbers and to baseline imbalances observed between treatment arms, with more patients in the venetoclax plus low-dose cytarabine arm presenting poor prognostic factors. Venetoclax plus low-dose cytarabine was well tolerated in Japanese patients with acute myeloid leukaemia ineligible for intensive chemotherapy.

Key words: acute myeloid leukaemia, venetoclax, low-dose cytarabine, VIALE-C, Japan

Introduction

Acute myeloid leukaemia (AML), although relatively rare, is the most common adult leukaemia in Japan accounting for ∼70% of myeloid leukaemias (1,2). The incidence of AML is age dependent with a median age at diagnosis in Japan of 65 years (3). Survival rates for patients with AML are the lowest amongst all leukaemias. Retrospective population-based studies that included the overall AML population (young adult to elderly) observed relatively low 5-year overall survival (OS) rates of 10–20% (4–7).

Standard first-line therapy for adults with newly diagnosed AML is intensive chemotherapy (1,8). However, many patients are ineligible for intensive therapy because of advanced age or comorbidities (3,9,10). When compared with younger adult patients with AML, elderly patients with AML also have increased frequencies of adverse prognostic factors such as unfavourable risk karyotype and secondary AML (11), leading to a poorer prognosis (12–14). Less intensive treatment options include azacitidine, decitabine or low-dose cytarabine (LDAC) (8) with only LDAC monotherapy approved in Japan (prior to March 2021) for the treatment of patients with AML who are ineligible for intensive chemotherapy (10). However, reported rates of complete remission (CR) or CR with incomplete blood count recovery (CRi) are ≤30% (3,15–17), underscoring the need for additional new treatment options.

Venetoclax, a selective inhibitor of B-cell leukaemia/lymphoma-2 (BCL2), has been evaluated either alone or in combination with other active agents in several hematologic malignancies (18–24). Venetoclax and cytarabine have complementary mechanisms of action that provide a biologic rationale for evaluation in AML. Cancer cell survival is mediated by BCL2 family members, including BCL2, BCL-X_L, and MCL1. In AML, BCL2 promotes chemoresistance, the survival of leukemic progenitor and blast cells, and has been associated with poor outcomes (25,26). Resistance to the BCL2 inhibitor venetoclax may be mediated by other pro-survival factors, like MCL1, that sequester endogenous BCL2 homology (BH)3-only proteins released by venetoclax upon binding to BCL2. In preclinical models, cytarabine synergized with venetoclax by enhancing BH3-only activity and/or suppressing MCL1 to promote apoptosis (27,28).

Venetoclax-based therapy in elderly patients with previously untreated AML was assessed in 2 large phase 1b/2 studies (24,29). Combination therapy with venetoclax plus azacitidine or decitabine resulted in a CR plus CRi rate of 67% and a median OS of 17.5 months (29). When combined with LDAC, venetoclax produced a CR plus CRi rate of 54% and median OS of 10.1 months (24). These results prompted the initiation of 2 phase 3 placebo-controlled trials to compare azacitidine (VIALE-A) or LDAC (VIALE-C) with or without venetoclax (30,31). Both studies enrolled patients globally and included patients from Japan. In the VIALE-A study, the addition of venetoclax to azacitidine significantly increased the CR plus CRi rate (66% vs 28%; $P < 0.001$) and median OS (14.7 vs 9.6 months; hazard ratio [HR]: 0.66; $P < 0.001$) compared with the control group (30). In the VIALE-C study at a 6-month follow-up analysis, the addition of venetoclax to LDAC significantly increased the CR plus CRi rate (48% vs 13%; $P < 0.001$) compared with the control group; median OS was 8.4 months vs 4.1 months (HR, 0.70; $P = 0.040$) (31).

Venetoclax has been approved for use in the USA and several other countries in combination with azacitidine, decitabine, or LDAC in patients with newly diagnosed AML ≥75 years of age who are ineligible for intensive induction chemotherapy; in March 2021, venetoclax in combination with azacitidine or LDAC was approved in Japan. Here we present efficacy and safety outcomes in the subgroup of Japanese patients with AML ineligible for intensive chemotherapy who participated in the VIALE-C study.

Methods

Study design

VIALE-C (NCT03069352) is a phase 3 randomized, double-blind placebo-controlled, multicenter study that assessed the efficacy and safety of venetoclax plus LDAC compared with placebo plus LDAC in treatment-naive patients with AML who were ineligible for intensive chemotherapy (31). The primary endpoint of the study was OS and secondary endpoints included response rates (CR, CR plus CRi, proportion of patients with CR plus CRi by initiation of cycle 2), transfusion independence rates, and event-free survival (EFS). The study was conducted in accordance with the International Council for Harmonization requirements, Good Clinical Practice guidelines, and the Declaration of Helsinki. The protocol was reviewed and approved by an independent ethics committee/institutional review board at each site before initiation. All patients provided written informed consent before participating.

Patients

Full eligibility criteria have been published previously (31). Briefly, eligible patients were adults (≥18 years) with newly diagnosed AML, as defined by the World Health Organization (32). Patients were ineligible for standard induction therapy either due to age (≥75 years) or lack of fitness, defined by the presence of at least 1 of the following: Eastern Cooperative Oncology Group (ECOG) performance status 2 or 3, history of congestive heart failure requiring treatment or ejection fraction ≤50% or chronic stable angina, diffusion capacity of the lung for carbon monoxide ≤65% or forced expiratory volume in 1 second ≤65%, creatinine clearance ≥0.5 to <0.75 ml/s/m^2, moderate hepatic impairment with total bilirubin >1.5 to ≤3.0 times the upper limit of normal, or other comorbidities deemed incompatible with standard therapy. Patients with secondary AML could have received prior therapy for myelodysplastic syndromes (MDS). Main exclusion criteria comprised a projected life expectancy <12 weeks, prior therapy for AML (except for hydroxyurea either prior to or during the first cycle of treatment) and previous treatment with cytarabine for any indication.

Randomization and treatment

Patients were randomized 2:1 via interactive response technology to either venetoclax plus LDAC or placebo plus LDAC. Randomization was stratified by AML status (*de novo* vs secondary), patient age (<75 vs ≥75 years) and region (USA, Europe, China, Japan and rest of world).

Venetoclax was administered orally once daily (QD), and to avoid the risk of tumour lysis syndrome (TLS), dosing began at 100 mg on day 1 of cycle 1 and increased stepwise over 4 days (ramp-up period) to reach the target dose of 600 mg (100 mg day 1, 200 mg day 2, 400 mg day 3, 600 mg days 4–28 of cycle 1). Venetoclax was given at the target dose of 600 mg QD in all subsequent 28-day cycles. During the ramp-up period and until 24 hours after the target dose of venetoclax was reached, all patients were hospitalized to monitor for TLS and received TLS prophylaxis (uric acid-reducing agents and hydration). Patients in the placebo arm received a placebo (identical-looking tablet) in the same manner as venetoclax. All patients received subcutaneous LDAC at a dose of 20 mg/m^2 QD on days 1–10 of each 28-day cycle. Treatment was continued until disease progression (PD), unacceptable toxicity or other pre-established treatment discontinuation criteria were met (31).

Assessments

Disease assessments were performed on bone marrow samples collected at screening, end of cycles 1 and 4, and every three cycles thereafter (in the absence of PD) until 2 consecutive samples confirmed stable achievement of CR or CRi. Disease assessments were also performed when relapse was suspected and/or at the final study visit. Clinical responses were defined according to the modified International Working Group criteria for AML (33), and PD was defined as per European LeukemiaNet recommendations (34). Details on the criteria for evaluating disease assessment have been reported previously in the primary publication of this study (31). OS was defined as the time from study randomization to death due to any cause. EFS was defined as the time from study randomization to PD, confirmed relapse from CR or CRi, treatment failure (failure to achieve CR, CRi, partial remission or morphologic leukaemia-free state as assessed by the investigator) or death from any cause. Post-baseline transfusion independence was defined as a period of at least 56 consecutive days without transfusions of either red blood cells (RBCs) or platelets occurring between the first dose of study drug and 30 days after the last dose of study drug.

Safety evaluations were performed throughout the study. Patients were monitored for adverse events (AEs), serious AEs, vital signs, laboratory measures, and clinically significant cardiac, pulmonary or radiologic findings. AEs were defined as those that occurred between the first dose of study drug until 30 days after the last dose of study drug. AEs were graded according to the National Cancer Institute Common Terminology Criteria for Adverse Events Version 4.03.

Statistical methods

Efficacy analyses were performed on the full analysis set, consisting of all patients who were randomized, whereas safety analyses were performed on all patients who received at least 1 dose of study drug. The pre-planned sample size for the VIALE-C study was 210 patients (randomized 2:1) to detect a statistically significant reduction in mortality of 45.5%, with 90% power at an alpha level of 0.05. OS, and EFS were analysed using Kaplan–Meier methodology and compared between treatment arms using the log-rank test. The HR was estimated using the Cox proportional-hazards model. Cox proportional-hazard regression models with stepwise variable selection were performed on OS in the Japan region as sensitivity analyses to identify relevant prognostic factors for OS and to better understand the treatment effect on OS when adjusting for these factors. Response rates and transfusion-independence outcomes were compared between treatment arms using the Cochran–Mantel–Haenszel test and 95% confidence intervals (CIs) were determined using the Clopper–Pearson Exact method.

For this analysis, baseline characteristics and study outcomes are described for the Japanese subgroup. The data cutoff for the primary analysis of the study was 15 February 2019; the cutoff for the 6-month follow-up analysis presented herein was 15 August 2019.

Results

Patient demographics and baseline characteristics

Between May 2017 and the data cutoff for the 6-month follow-up analysis of 15 August 2019, 211 patients were enrolled across 21 countries. Of the 211 patients,14 sites in Japan enrolled 27 (12.8%) patients who received venetoclax plus LDAC (n = 18) or placebo plus LDAC (n = 9). The median age was 81 (range: 60–89) years for patients treated with venetoclax plus LDAC and 78 (range: 71–85) years for those treated with placebo plus LDAC. Demographics and baseline characteristics of the Japanese subgroup are shown in Table 1. Treatment arms were balanced in terms of patient age (85% of patients ≥75 years; venetoclax plus LDAC vs placebo plus LDAC: 83.3% vs 88.9%), the proportion of patients with *de novo* AML, and the prevalence of transfusion dependence. Some imbalances were observed between the venetoclax plus LDAC and placebo plus LDAC arms, including the proportion of patients with AML with myelodysplasia-related changes (venetoclax plus LDAC vs placebo plus LDAC: 55.6% vs 44.4%), bone marrow blast count ≥50% (27.8% vs 11.1%), poor cytogenetic risk (55.6% vs 33.3%), tumour protein 53 (*TP53*) mutations (43.8% vs 22.2%), fms-like tyrosine kinase 3 (*FLT3*) mutations (18.8% vs 0%), nucleophosmin (*NPM1*) mutations (6.3% vs 22.2%) and prior use of hypomethylating agents (HMAs) (16.7% vs 33.3%). More than half of the patients in the venetoclax plus LDAC treatment arm (n = 10 [55.6%]) and n = 4 [44.4%] patients in the placebo plus LDAC arm had ≥2 reasons for ineligibility to receive intensive therapies.

Table 1. Patient demographics and baseline characteristics

Characteristic	Placebo + LDAC (*n* = 9)	Venetoclax + LDAC (*n* = 18)
Age		
Median, years (range)	78 (71–85)	81 (60–89)
≥75 years, *n* (%)	8 (88.9)	15 (83.3)
Male, *n* (%)	4 (44.4)	12 (66.7)
ECOG performance status, *n* (%)		
0	3 (33.3)	5 (27.8)
1	3 (33.3)	10 (55.6)
2	2 (22.2)	3 (16.7)
3	1 (11.1)	0
AML type, *n* (%)		
De novo	6 (66.7)	13 (72.2)
Secondary	3 (33.3)	5 (27.8)
Secondary AML type, *n*/*N* (%)		
Treatment-related AML	0/3	1/5 (20.0)
Prior hematologic disorder	3/3 (100.0)	4/5 (80.0)
Myelodysplasia-related changes, *n* (%)	4 (44.4)	10 (55.6)
Prior treatment with HMAs, *n* (%)	3 (33.3)	3 (16.7)
Bone marrow blast count, *n* (%)		
<30%	4 (44.4)	7 (38.9)
≥30%–<50%	4 (44.4)	6 (33.3)
≥50%	1 (11.1)	5 (27.8)
Cytogenetic risk, *n* (%)		
Favourable	0	0
Intermediate	6 (66.7)	8 (44.4)
Poor	3 (33.3)	10 (55.6)
Somatic mutations, *n*/*N* (%)		
TP53	2/9 (22.2)	7/16 (43.8)
FLT3	0/9	3/16 (18.8)
IDH1/2	2/9 (22.2)	3/16 (18.8)
NPM1	2/9 (22.2)	1/16 (6.3)
Baseline hepatic impairment	3 (33.3)	8 (44.4)
Baseline renal impairment	8 (88.9)	18 (100.0)
Transfusion dependent[a] at baseline, *n* (%)		
RBC or platelet	7 (77.8)	14 (77.8)
RBC	6 (66.7)	13 (72.2)
Platelet	3 (33.3)	8 (44.4)
Number of reasons for ineligibility to receive intensive therapy, *n* (%)		
1	5 (55.6)	8 (44.4)
2	4 (44.4)	9 (50.0)
3	0	1 (5.6)
≥4	0	0

[a]Transfusion dependence defined as transfusion within 56 days before first dose of study drug.

AML, acute myeloid leukaemia; ECOG, Eastern Cooperative Oncology Group; *FLT3*, fms-like tyrosine kinase 3; HMA, hypomethylating agent; *IDH*, isocitrate dehydrogenase; LDAC, low-dose cytarabine; *NPM1*, nucleophosmin; RBC, red blood cell; *TP53*, tumour protein 53.

The median treatment duration in the venetoclax plus LDAC and placebo plus LDAC arms was 2.1 (range: 0.2–23.5) months and 1.9 (range: 0.3–14.6) months, respectively. The proportion of patients who received any post-study treatment and intensive chemotherapy as post-study treatment was markedly higher in the placebo plus LDAC arm (77.8 and 55.6%, respectively) than in the venetoclax plus LDAC arm (27.8 and 16.7%, respectively; Table 2). The most common post-study treatments in the placebo plus LDAC arm were cytarabine (66.7%), aclarubicin hydrochloride (33.3%), and hydroxycarbamide (33.3%); azacitidine, cytarabine, daunorubicin and gemtuzumab ozogamicin (11.1% each) were the most common for patients in the venetoclax plus LDAC arm. Individual chemotherapy drugs were noted, but treatment regimens were not.

Overall, as of the data cutoff date, 26 patients in the Japanese subgroup (venetoclax plus LDAC, *n* = 17; placebo plus LDAC, *n* = 9) had discontinued treatment. The primary reasons for study drug discontinuation were (venetoclax plus LDAC vs placebo plus LDAC): treatment failure (22.2% vs 44.4%), PD (11.1% vs 33.3%), physician decision (16.7% vs 11.1%), AE not related to PD (16.7% vs 0%), withdrawal of consent (11.1% each), morphologic relapse (11.1% vs 0%) and AE related to PD (5.6% vs 0%).

Efficacy

OS outcomes in the Japanese subgroup at the primary analysis and at the 6-month follow-up analysis are shown in Fig. 1A and B, respectively. At both analyses, median OS was 4.7 months in the

Table 2. Summary of post-study treatment

Treatment, *n* (%)	Placebo + LDAC (*n* = 9)	Venetoclax + LDAC (*n* = 18)
Any post-study treatment	7 (77.8)	5 (27.8)
Intensive chemotherapy	5 (55.6)	3 (16.7)
Aclarubicin/aclarubicin hydrochloride	4 (44.4)	1 (5.6)
Cytarabine	4 (44.4)	2 (11.1)
Daunorubicin/daunorubicin hydrochloride	2 (22.2)	3 (16.7)

Treatment regimen was not collected, only individual chemotherapy drug.
LDAC, low-dose cytarabine.

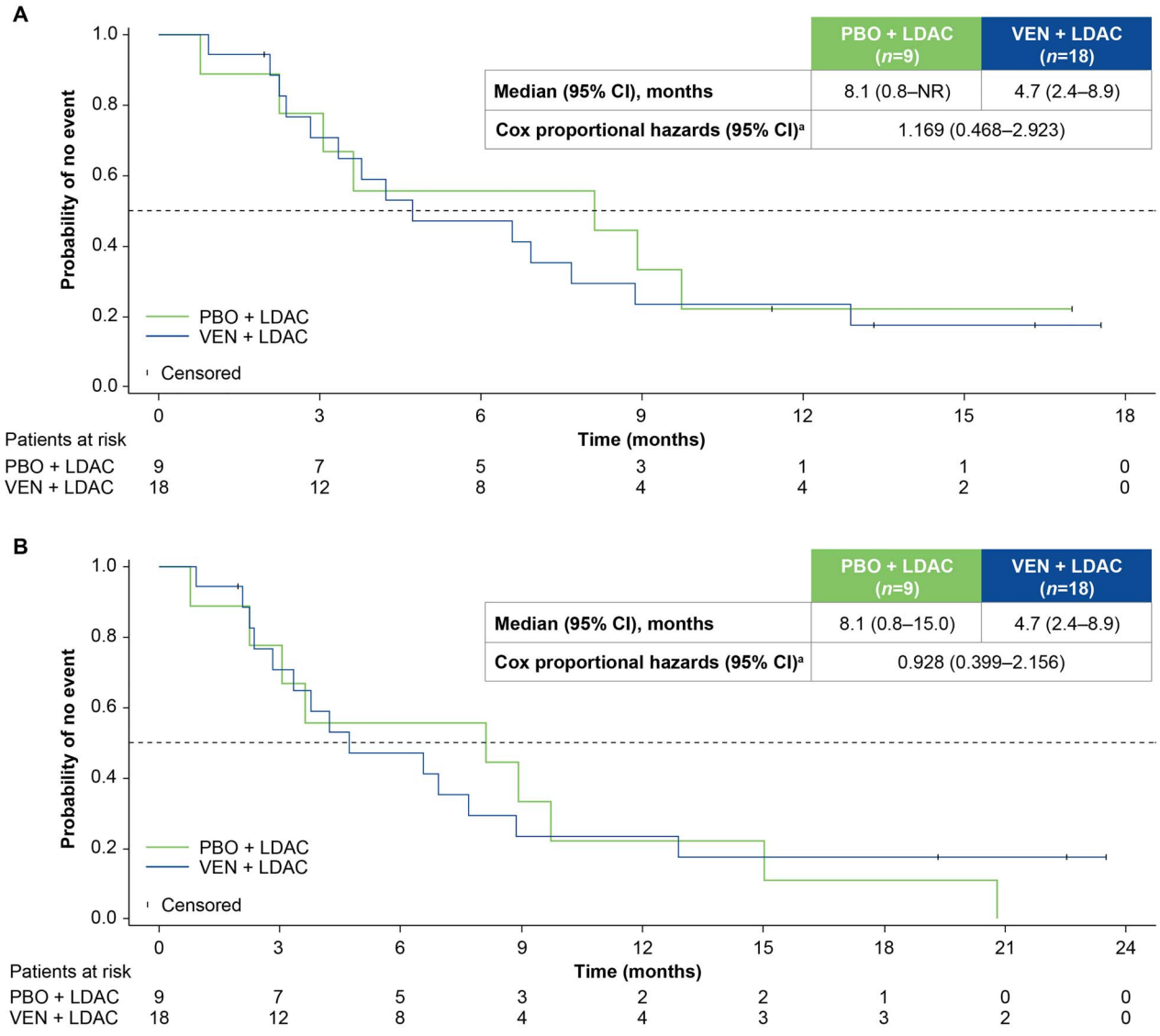

Figure 1. Overall survival (OS) by treatment arm at the primary analysis (A) and 6-month follow-up (B). [a]Unstratified Cox proportional hazards model. CI, confidence interval; HR, hazard ratio; LDAC, low-dose cytarabine; PBO, placebo; VEN, venetoclax.

venetoclax plus LDAC arm, and 8.1 months in the placebo plus LDAC arm. The HR at the 6-month follow-up was 0.928 (95% CI: 0.399–2.156). Considering the observed imbalance in baseline patient characteristics, a stepwise multivariate Cox regression analysis was performed to identify pre-treatment factors associated with OS. Factors included in the analysis were treatment arm, age, sex, AML status, bone marrow blast count, ECOG performance status, cytogenetic risk, prior use of HMAs and mutation status of *FLT3*, isocitrate dehydrogenase (*IDH*) and *NPM1*. To estimate the adjusted treatment effect, inclusion of treatment arm was forced into the model. Based on the stepwise variable selection, cytogenetic risk was identified as being significantly correlated with OS. At the 6-month follow-up, the HR for cytogenetic risk (intermediate vs poor) was 0.264 (95% CI: 0.102–0.685; $P = 0.006$). The covariate-adjusted HR

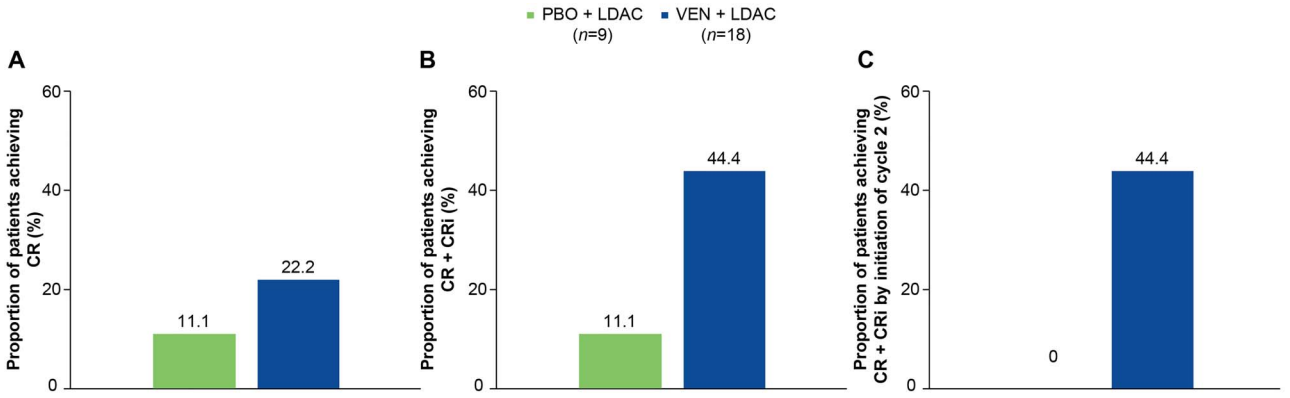

Figure 2. Rates of complete response (CR) (A), CR + CR with incomplete blood count recovery (CRi) (B), and CR + CRi by initiation of cycle 2 (C). LDAC, low-dose cytarabine; PBO, placebo; VEN, venetoclax.

for treatment arm (venetoclax plus LDAC vs placebo plus LDAC) was 0.800 (95% CI: 0.337–1.898), which was similar to that observed in the primary analysis.

Response rates for the Japanese subgroup are summarized in Fig. 2. The rates of CR and CR plus CRi were consistently higher in patients treated with venetoclax plus LDAC (22.2 and 44.4%, respectively) than in patients treated with placebo plus LDAC (11.1% each). The proportion of patients achieving CR plus CRi by initiation of cycle 2 was also higher in the venetoclax plus LDAC arm (44.4%) vs the placebo plus LDAC arm (0%).

Median EFS was numerically higher in the venetoclax plus LDAC arm vs the placebo plus LDAC arm both at the primary analysis (3.7 vs 2.2 months; HR: 0.565; 95% CI: 0.197–1.624; Fig. 3A) and at the 6-month follow-up (3.7 vs 2.2 months; HR: 0.620; 95% CI: 0.246–1.566; Fig. 3B).

The proportion of patients with post-baseline transfusion independence was similar across treatment groups in the Japanese subgroup (Fig. 4A). The median time to transfusion independence (RBC plus platelet) was shorter in the venetoclax plus LDAC arm than in the placebo plus LDAC arm (50 vs 96 days, respectively; Fig. 4B). One of 14 (7.1%) patients who were transfusion-dependent at baseline achieved transfusion independence during treatment with venetoclax plus LDAC, and 1 of 7 (14.3%) transfusion-dependent patients assigned to placebo plus LDAC achieved transfusion independence.

Safety

All patients in the Japanese subgroup experienced at least 1 AE (Table 3). The most frequently reported AEs (≥40% of patients) of any grade for the venetoclax plus LDAC or placebo plus LDAC arms, respectively, were nausea (66.7% vs 22.2%), febrile neutropenia (50.0% vs 44.4%), vomiting (50.0% vs 11.1%), decreased appetite (33.3% vs 44.4%), hypokalemia (33.3% vs 44.4%), thrombocytopenia (27.8% vs 44.4%) and pyrexia (22.2% vs 44.4%). The most frequently reported grade ≥ 3 AEs in the venetoclax plus LDAC or placebo plus LDAC arms, respectively, were hematologic: febrile neutropenia (50.0% vs 44.4%) and thrombocytopenia (27.8% vs 44.4%). Grade ≥ 3 pneumonia was reported in 3/18 (16.7%) patients in the venetoclax plus LDAC arm and in 3/9 (33.3%) in the placebo plus LDAC arm.

Serious AEs were reported in 9/18 (50.0%) and 3/9 (33.3%) patients in the venetoclax plus LDAC and placebo plus LDAC arms, respectively; pneumonia was the most common (22.2% each; Table 4). TLS was not observed in any patients in the Japanese subgroup. Fourteen (77.8%) patients died in the venetoclax plus LDAC arm and 9 (100.0%) in the placebo plus LDAC arm, mainly because of PD (61.1 and 77.8%, respectively). The rate of death within 60 days of initiating study treatment was similar in both treatment group (11.1% each).

AEs led to study treatment discontinuation in 6/18 (33.3%) and 0/9 patients treated with venetoclax plus LDAC and placebo plus LDAC, respectively, including pneumonia (11.1% vs 0%), and neutropenia, congestive heart failure, acute pancreatitis, fatigue, decreased appetite, intracranial haemorrhage and organizing pneumonia (5.6% vs 0% for each). Dose interruption and/or reduction occurred in 11/18 (61.1%) patients in the venetoclax plus LDAC arm and 4/9 (44.4%) patients in the placebo plus LDAC arm. The most common AEs (≥10% of patients) leading to dose interruption and/or reduction were (venetoclax plus LDAC vs placebo plus LDAC): febrile neutropenia (16.7% vs 11.1%), thrombocytopenia (11.1% each), decreased neutrophil count (11.1% vs 0%), upper GI haemorrhage (11.1% vs 0%), atrial fibrillation (5.6% vs 11.1%), pneumonia (5.6% vs 11.1%), cellulitis (0% vs 11.1%) and fasciitis (0% vs 11.1%).

Discussion

In this small subgroup of Japanese patients participating in VIALE-C ($n = 27$), the unadjusted OS appeared comparable though unbalanced covariates may have obscured the observation of treatment effect. At a 6-month follow-up analysis, the addition of venetoclax to LDAC showed a median OS of 4.7 months vs 8.1 months with placebo plus LDAC. In contrast, median OS of the total VIALE-C study population at a 6-month follow-up was 8.4 and 4.1 months for venetoclax plus LDAC and placebo plus LDAC, respectively (31).

Several important factors may have influenced outcomes in the Japanese subgroup. First, the number of patients in the subgroup was small (venetoclax plus LDAC, $n = 18$; placebo plus LDAC, $n = 9$). Second, patients in the venetoclax plus LDAC arm were more likely to have high-risk features at baseline than patients in the placebo plus LDAC arm, including a poor-risk cytogenetic profile (55.6% vs 33.3%, respectively), which was shown to correlate with OS. After adjusting for cytogenetic risk in Japanese patients, the HR for the venetoclax plus LDAC treatment arm was 0.800 (95%

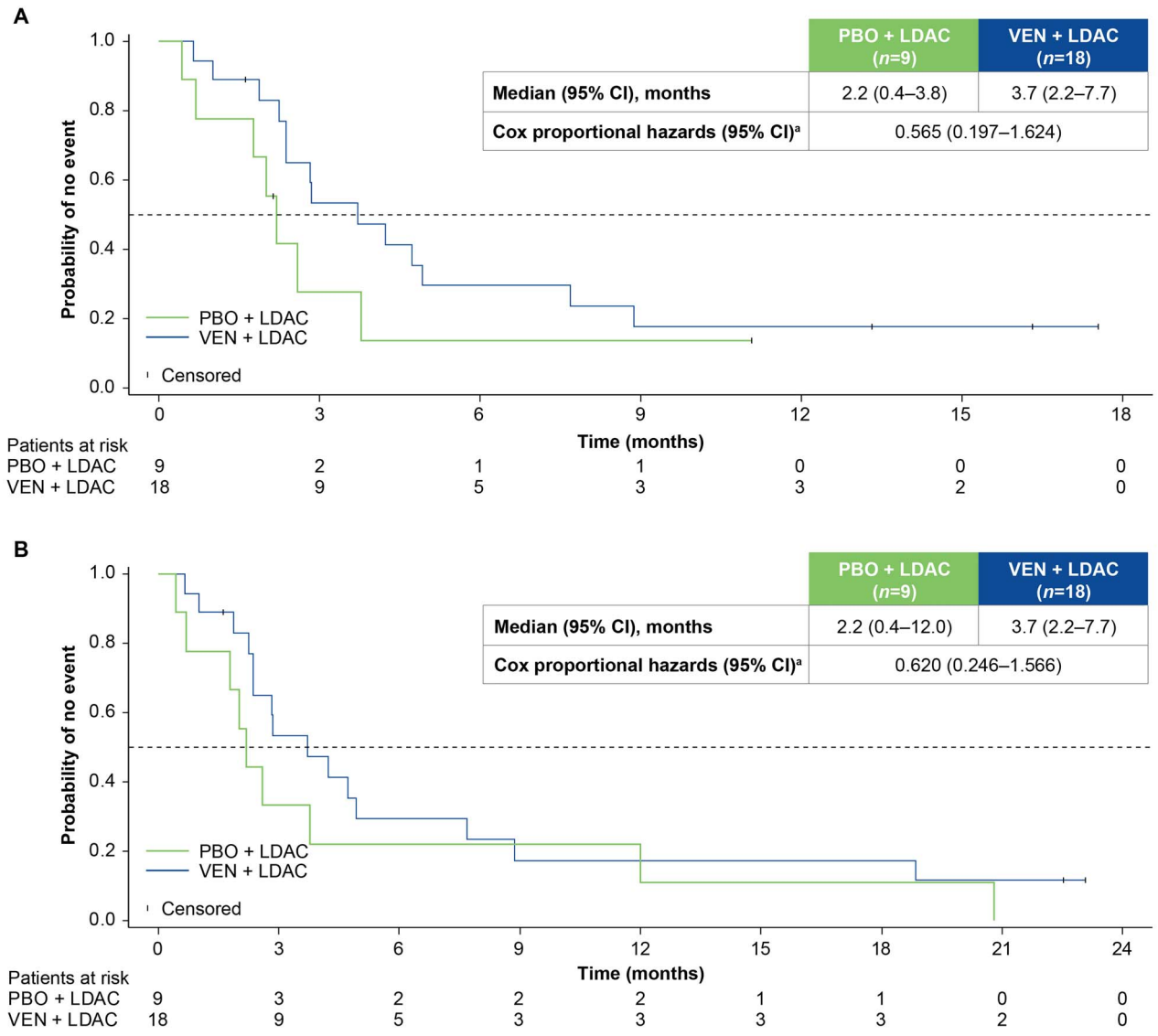

Figure 3. Event-free survival (EFS) by treatment arm at the primary analysis (A) and 6-month follow-up (B). [a]Stratified by AML state (*de novo* vs secondary) and age (18–74 vs ≥75 years). AML, acute myeloid leukaemia; CI, confidence interval; LDAC, low-dose cytarabine; PBO, placebo; VEN, venetoclax.

CI: 0.337–1.898). Last, patients in the Japanese subgroup assigned to the venetoclax plus LDAC arm were less likely to receive post-study treatment than those in the placebo plus LDAC arm (27.8% vs 77.8%, respectively), including intensive chemotherapy (16.7% vs 55.6%, respectively), which may have reduced the ability to detect the effects of study treatment on OS in this subgroup. It is noteworthy that the decision to administer post-study treatment and the choice of regimen to be used was at the investigator's discretion. The selection of further therapy was dependent upon important intermediate events during the study, such as treatment failure or PD. In the Japanese subgroup of the VIALE-C study, treatment failure and PD were reported as the primary reason for study discontinuation at least twice as often in the placebo plus LDAC arm (33.3 and 44.4%, respectively) compared with venetoclax plus LDAC arm (11.1 and 22.1%, respectively). The increased use of intensive chemotherapy as salvage treatment in Japanese patients compared with the total study population (29.6% vs 12.7%, respectively), and the greater use amongst Japanese patients randomized to the placebo plus LDAC arm compared with the venetoclax plus LDAC arm (*n* = 5/9 [55.6%] vs 3/18 [16.7%], respectively), may have reduced the ability to detect the effect of study treatment on survival within the Japanese subgroup.

A broad consensus on criteria for selection of the ideal 'unfit' patient with AML for inclusion in clinical trials was lacking and remains the subject of scientific debate. The structure for identifying patients who would not be suitable for intensive treatment in the VIALE-C, as well as the VIALE-A study, was based on age ≥ 75 years or age ≥ 18 to 74 years plus at least 1 criterion associated with lack of fitness for intensive induction chemotherapy (e.g. ECOG performance status of 2 or 3, particular defined comorbid conditions) (30,31). It is noteworthy that eligibility criteria for VIALE-C include prior MDS treated with HMAs, whereas VIALE-A excluded pre-treated MDS. Thus, VIALE-C included more patients with refractory MDS than VIALE-A, which may partially explain the difference in

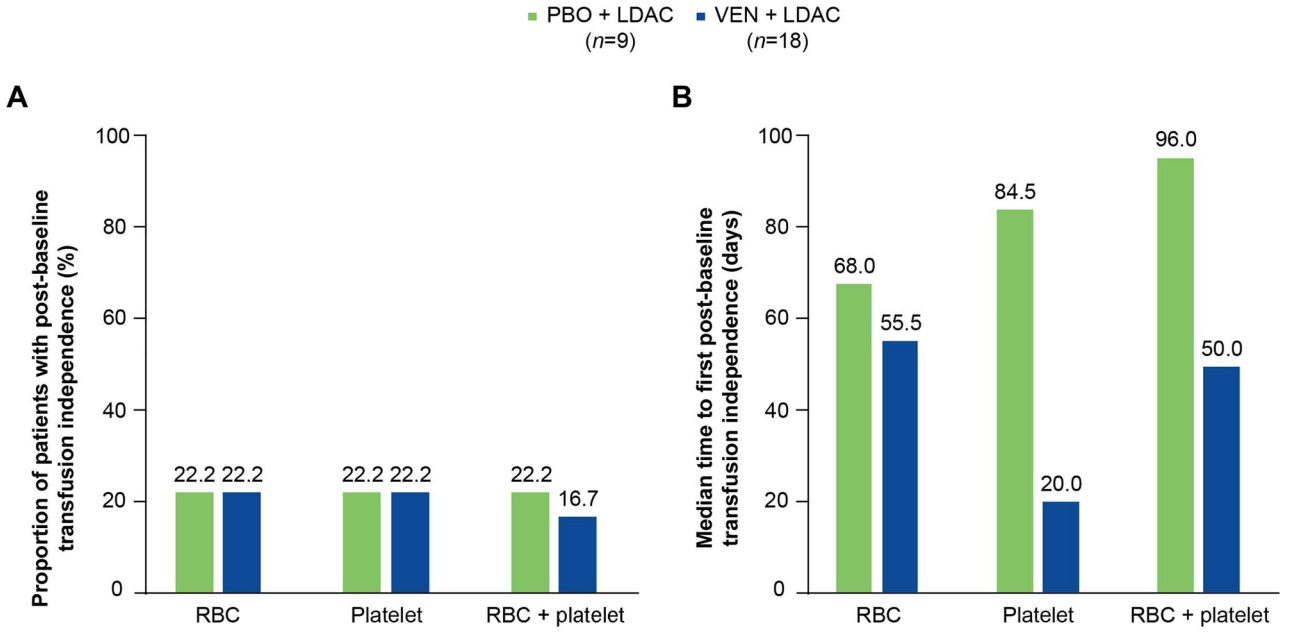

Figure 4. Proportion of patients with post-baseline transfusion independence (A) and median time to post-baseline transfusion independence (B), by treatment arm. Post-baseline transfusion independence was defined as a period of at least 56 consecutive days without transfusions. LDAC, low-dose cytarabine; PBO, placebo; RBC, red blood cell; VEN, venetoclax.

median OS between both studies. In a commentary by Löwenberg et al., it was noted that by using these inclusion criteria, a considerable proportion of the study population for these trials may not have only been 'unfit', but potentially 'frail' (e.g. patients had ECOG performance status of 3). Thus, a proportion of enrolled patients might have been too frail to benefit from almost any antileukemic treatment that introduces toxicities (35).

Despite the imbalances between treatment arms in baseline characteristics (e.g. poor cytogenetic risk, bone marrow blast count ≥50%, prior treatment with HMAs, *TP53*, *NPM1*, or *FLT3* mutation, and AML with myelodysplasia-related changes) and older median age, the addition of venetoclax to LDAC was associated with an increased CR plus CRi rate in Japanese patients (44.4% vs 11.1%), and all responses to treatment with venetoclax plus LDAC were achieved within the first cycle of therapy (vs 0% with placebo plus LDAC). The transfusion-independence rate was similar in the venetoclax plus LDAC and placebo plus LDAC arms likely due to the small patient numbers. In addition, transfusion prescription was not defined within the protocol and was at the investigator's discretion which could depend on institutional/regional guidelines. However, transfusion independence (RBC plus platelet) was achieved more rapidly with venetoclax plus LDAC compared with placebo plus LDAC (median 50 vs 96 days, respectively).

Of note, the differences in rates of post-study treatment received between treatment arms did not obscure the treatment effect of venetoclax plus LDAC when evaluating EFS as a secondary endpoint. At the 6-month follow-up, the Japanese subgroup reported a median EFS of 2.2 months in the placebo plus LDAC arm compared with 3.7 months in the venetoclax plus LDAC arm (HR: 0.620; 95% CI: 0.246–1.566), which was an opposite trend relative to the OS observation. It is noteworthy that the analysis of treatment arms shows a separation of EFS curves that implies benefit of venetoclax plus LDAC over placebo plus LDAC prior to receipt of subsequent salvage therapy. These data suggest that patients treated with venetoclax plus LDAC derived clinical benefit from therapy.

The safety profile of venetoclax plus LDAC was consistent with previous studies of venetoclax in AML, including the total study population of VIALE-C (24,29–31). AEs consisted mainly of hematologic events, such as febrile neutropenia and thrombocytopenia, and GI AEs (e.g. grade 1 or 2 nausea and vomiting). No cases of TLS were reported in the Japanese subgroup.

Despite the limitations of the current analysis (e.g. small patient numbers, imbalances between treatment arms in baseline characteristics, impact of post-study treatment), the data indicate a tolerable safety profile along with a trend toward beneficial improvements for patients treated with venetoclax plus LDAC in comparison to placebo plus LDAC. Treatment with venetoclax plus LDAC was well tolerated and led to higher CR plus CRi rates in comparison to treatment with placebo plus LDAC. These results support the consideration of venetoclax plus LDAC as a first-line treatment option for Japanese patients with AML ineligible for intensive chemotherapy.

Data sharing and data accessibility statement

AbbVie is committed to responsible data sharing regarding the clinical trials we sponsor. This includes access to anonymized, individual, and trial-level data (analysis data sets), as well as other information (e.g. protocols and Clinical Study Reports), as long as the trials are not part of an ongoing or planned regulatory submission. This includes requests for clinical trial data for unlicensed products and indications.

These clinical trial data can be requested by any qualified researchers who engage in rigorous, independent scientific research, and will be provided following review and approval of a research proposal and statistical analysis plan and execution of a data sharing

Table 3. Adverse events (AEs) reported in ≥15% of patients in the venetoclax plus low-dose cytarabine (LDAC) arm only

AE, *n* (%)	Placebo + LDAC (*n* = 9)		Venetoclax + LDAC (*n* = 18)	
	Any grade	Grade ≥ 3	Any grade	Grade ≥ 3
Any	9 (100.0)	8 (88.9)	18 (100.0)	17 (94.4)
Hematologic				
Febrile neutropenia	4 (44.4)	4 (44.4)	9 (50.0)	9 (50.0)
Leukopenia	0	0	3 (16.7)	3 (16.7)
Neutropenia	0	0	3 (16.7)	3 (16.7)
Thrombocytopenia	4 (44.4)	4 (44.4)	5 (27.8)	5 (27.8)
Nonhematologic				
Back pain	1 (11.1)	0	3 (16.7)	0
Constipation	3 (33.3)	0	5 (27.8)	0
Decreased appetite	4 (44.4)	0	6 (33.3)	1 (5.6)
Decreased weight	0	0	3 (16.7)	0
Delirium	1 (11.1)	0	3 (16.7)	0
Diarrhoea	2 (22.2)	0	5 (27.8)	0
Dry skin	0	0	3 (16.7)	0
Epistaxis	0	0	3 (16.7)	0
Fatigue	0	0	3 (16.7)	1 (5.6)
Hypokalemia	4 (44.4)	3 (33.3)	6 (33.3)	3 (16.7)
Increased blood bilirubin	0	0	3 (16.7)	0
Insomnia	2 (22.2)	0	5 (27.8)	0
Malaise	2 (22.2)	0	3 (16.7)	0
Nausea	2 (22.2)	0	12 (66.7)	0
Oropharyngeal pain	1 (11.1)	0	3 (16.7)	1 (5.6)
Peripheral edema	3 (33.3)	0	4 (22.2)	0
Pneumonia	3 (33.3)	3 (33.3)	5 (27.8)	3 (16.7)
Proctalgia	0	0	4 (22.2)	0
Pyrexia	4 (44.4)	1 (11.1)	4 (22.2)	1 (5.6)
Transfusion reaction	0	0	4 (22.2)	0
Upper GI haemorrhage	0	0	3 (16.7)	1 (5.6)
Vomiting	1 (11.1)	0	9 (50.0)	0

GI, gastrointestinal.

Table 4. Serious adverse events (AEs) reported in all patients

Serious AE, *n* (%)	Placebo + LDAC (*n* = 9)	Venetoclax + LDAC (*n* = 18)
Any	3 (33.3)	9 (50.0)
Pneumonia	2 (22.2)	4 (22.2)
Multiple organ dysfunction syndrome	1 (11.1)	0
Enterococcal infection	1 (11.1)	0
Upper GI haemorrhage	0	2 (11.1)
Congestive cardiac failure	0	1 (5.6)
GI haemorrhage	0	1 (5.6)
Intracranial haemorrhage	0	1 (5.6)
Acute pancreatitis	0	1 (5.6)
Acute cholecystitis	0	1 (5.6)
Neutrophil count decreased	0	1 (5.6)
WBC count decreased	0	1 (5.6)

GI, gastrointestinal; LDAC, low-dose cytarabine; WBC, white blood cell.

agreement. Data requests can be submitted at any time, and the data will be accessible for 12 months, with possible extensions considered. For more information on the process, or to submit a request, visit the following link: https://www.abbvie.com/our-science/clinical-trials/clinical-trials-data-and-information-sharing/data-and-information-sharing-with-qualified-researchers.html.

Author contributions

Takahiro Yamauchi: investigation and writing (reviewing and editing). Chikashi Yoshida: investigation and writing (reviewing and editing). Kensuke Usuki: investigation and writing (reviewing and editing). Satoru Takada: investigation and writing (reviewing and editing). Itaru Matsumura: investigation and writing (reviewing and

editing). Nobuaki Dobashi: investigation and writing (reviewing and editing). Yasushi Miyazaki: investigation and writing (reviewing and editing). Toshihiro Miyamoto: investigation and writing (reviewing and editing). Hiroatsu Iida: investigation and writing (reviewing and editing). Norio Asou: investigation and writing (reviewing and editing). Junya Kuroda: investigation and writing (reviewing and editing). Satoshi Ichikawa: investigation and writing (reviewing and editing). Norio Komatsu: investigation and writing (reviewing and editing). Wellington Mendes: supervision, writing (original draft preparation) and writing (reviewing and editing). Hideyuki Honda: formal analysis, data curation and writing (reviewing and editing). Sumiko Okubo: formal analysis, data curation and writing (reviewing and editing). Misaki Kurokawa: formal analysis, data curation and writing (reviewing and editing). Qi Jiang: formal analysis, data curation and writing (reviewing and editing). Andrew Wei: investigation and writing (reviewing and editing). Kenichi Ishizawa: investigation and writing (reviewing and editing).

Acknowledgements

AbbVie and the authors thank all the trial investigators and the patients who participated in this clinical trial as well as Sathej Gopalakrishnan and Jiuhong Zha for their contributions to this publication. Medical writing support was provided by Mary L. Smith, PhD, CMPP from Aptitude Health, Atlanta, GA, USA and funded by AbbVie.

Funding

Venetoclax is being developed in a collaboration between AbbVie and Genentech. AbbVie sponsored the study, contributed to its design, collection, analysis and interpretation of the data, and participated in the writing, review and approval of the manuscript. All authors had access to relevant data and participated in the drafting, review and approval of this manuscript. No honoraria or payments were made for authorship.

Conflict of interest statement

Takahiro Yamauchi has received research support and honoraria from and has served as an advisor for AbbVie, Astellas Pharma, Boehringer Ingelheim, Chugai Pharmaceutical Co., Ltd, Gilead Sciences, Inc., Mundipharma, Jansen (research support only), Ono Pharmaceutical, Otsuka Pharmaceutical Co., Ltd, Pfizer, Solasia Pharma, SymBio, Takeda and Teijin Pharma. Chikashi Yoshida has received honoraria from AbbVie GK, Astellas Pharma, Bristol-Myers Squibb, Daiichi Sankyo Co. Ltd, Janssen Pharmaceutical KK, Meiji Seika Pharma Co., Ltd, Nippon Shinyaku Co., Ltd, Novartis Pharma KK and Otsuka Pharmaceutical Co., Ltd Kensuke Usuki has received research funding from AbbVie, Alexion, Astellas Pharma, Chugai Pharmaceutical Co., Ltd, Daiichi Sankyo Co., Gilead Sciences, Inc., Sumitomo Dainippon Pharma and SymBio, and has received honoraria from Novartis. Satoru Takada has nothing to disclose. Itaru Matsumura has received research funding from Chugai Pharmaceutical Co., Ltd, Eisai, Kyowa Kirin Co. Ltd, Shionogi & Co. Ltd and Sumitomo Dainippon Pharma, and has served on a speakers bureau for Astellas Pharma, Bristol-Myers Squibb, Inc., Daiichi Sankyo Co. Ltd, Janssen Pharmaceutical KK, Novartis Pharma KK, Otsuka Pharmaceutical Co., Ltd and Pfizer Japan Inc. Nobuaki Dobashi from Otsuka Pharmaceutical Co., Ltd. Yasushi Miyazaki has received honoraria from Astellas Pharma, Celgene, Chugai Pharmaceutical Co., Ltd, Kyowa Kirin, Nippon Shinyaku, Novartis, Otsuka Pharmaceutical Co., Ltd and Sumitomo Dainippon Pharma, and has received research funding from Chugai Pharmaceutical Co., Ltd and Sumitomo Dainippon Pharma. Toshihiro Miyamoto has received honoraria from AbbVie, Astellas Pharmaceutical Co., Ltd, Astellas Amgen Pharmaceutical Co., Ltd, Bristol-Myers Squibb, Celgene, Merch Sharp & Dohme, Otsuka Pharmaceutical Co., Ltd and Takeda Pharmaceutical Co. Hiroatsu Iida has received research funding from Chugai Pharmaceutical Co., Ltd, and has received honoraria from Astellas Pharma, Celgene, Janssen and Novartis. Norio Asou has received research funding from AbbVie; Astellas Pharma, Chugai Pharmaceutical Co., Ltd, Eisai and Sumitomo Dainippon Pharma; has served on a speakers bureau for Asahi Kasei, Fuji Pharma, Nippon Shinyaku and Sumitomo Dainippon Pharma; and has received honoraria from Novartis and Nippon Shinyaku. Junya Kuroda has received honoraria from AbbVie, Astellas Pharma, Bristol-Myers Squibb, Celgene, Chugai Pharmaceutical Co., Ltd, Daiichi Sankyo Co., Eisai, Fujimoto Pharmaceutical, Janssen Pharmaceutical KK, Kyowa Kirin, Nippon Shinyaku, Ono Pharmaceutical, Otsuka Pharmaceutical Co., Ltd, Pfizer, Sanofi, Sumitomo Dainippon Pharma and Takeda Pharmaceutical; has received research funding: from AbbVie, Asahi Kasei, Astellas Pharma, Bristol-Myers Squibb, Celgene, Chugai Pharmaceutical Co., Ltd, Daiichi Sankyo Co., Eisai, Fujimoto Pharmaceutical, Kyowa Kirin, MSD, Nippon Shinyaku, Ono Pharmaceutical, Otsuka Pharmaceutical Co., Ltd, Pfizer, Sanofi, Shionogi, Sumitomo Dainippon Pharma, Sysmex, Taiho Pharmaceutical and Takeda Pharmaceutical; and has served as a consultant for AbbVie, Bristol-Myers Squibb, Celgene, Janssen Pharmaceutical KK and Sanofi. Satoshi Ichikawa from Chugai Pharmaceutical Co., Ltd. Norio Komatsu has received research funding from Bristol-Myers Squibb KK, Chugai Pharmaceutical Co., Ltd, Fujifilm Wako Pure Chemical Corporation, Fuso Pharmaceutical Industries, Ltd, Kyowa Hakko Kirin Co., Ltd, Otsuka Pharmaceutical Co., Ltd, Novartis Pharma KK, Pfizer Japan Inc., PharmaEssentia Japan KK, Shire Japan KK, Sumitomo Dainippon Pharma and Takeda Pharmaceutical Co., Ltd; has received advisory fees from AbbVie GK, Celgene KK, Japan Tobacco Inc. (Funding provided was intended only to support the investigator and does not support the manuscript or any work involved in producing the manuscript. The manuscript content is not in any way related to the tobacco industry), Novartis Pharma KK, Otsuka Pharmaceutical Co., Ltd, PharmaEssentia Japan KK and Shire Japan KK; has served on a speakers bureau for Novartis Pharma KK, Shire Japan KK and Takeda Pharmaceutical Co., Ltd; and served as a member of safety assessment committee in the M13–834 clinical trial. Wellington Mendes, Hideyuki Honda, Sumiko Okubo, Misaki Kurokawa and Qi Jiang are employees of AbbVie and may own stock. Andrew Wei has received research funding from AbbVie, Amgen, AstraZeneca, Celgene/BMS, Novartis, Servier and F.Hoffmann-La Roche; has received honoraria from AbbVie, Amgen, Astellas, AstraZeneca, Celgene/Bristol-Myers Squibb, Genentech, Janssen, MacroGenics, Novartis, Pfizer and Servier; has served on advisory boards for AbbVie, Amgen, Astellas, AstraZeneca, Celgene/Bristol-Myers Squibb, Genentech, Janssen, MacroGenics, Novartis, Pfizer and Servier; has served on a speakers bureau for Novartis, AbbVie and Celgene/Bristol-Myers Squibb; has served as a consultant for Servier; is a former employee of the Walter and Eliza Hall Institute of Medical Research, which receives royalties in relation to venetoclax, and is entitled to a fraction of these payments. Kenichi Ishizawa has received research funding from AbbVie, Bayer, Novartis and SymBio, and has served on a speakers bureau for Celgene, Chugai Pharmaceutical Co., Ltd, Eisai, Novartis, Ono Pharmaceutical and Takeda.

Statement of prior presentation

Results of this study have been partially presented at the 43rd Annual Meeting of the Japan Society for Hematopoietic Cell Transplantation Congress, Virtual, 5–7 March 2021.

Statement on originality of the work

The manuscript represents original work and has not been submitted for publication elsewhere nor previously published.

Abbreviations

AE, adverse event; AML, acute myeloid leukaemia; BCL2, B-cell leukaemia/lymphoma-2; BH, BCL2 homology; CI, confidence interval; CR, complete remission; CRi, complete remission with incomplete blood count recovery; ECOG, Eastern Cooperative Oncology Group; EFS, event-free survival; *FLT3*, fms-like tyrosine kinase 3; GI, gastrointestinal; HMA, hypomethylating agent; HR, hazard ratio; *IDH*, isocitrate dehydrogenase; LDAC, low-dose cytarabine; MDS, myelodysplastic syndromes; *NPM1*, nucleophosmin; OS, overall survival; PBO, placebo; QD, once daily; RBC, red blood cell; TLS, tumour lysis syndrome; *TP53*, tumour protein 53; VEN, venetoclax; WBC, white blood cell.

References

1. Miyawaki S. Clinical studies of acute myeloid leukemia in the Japan Adult Leukemia Study Group. *Int J Hematol* 2012;96:171–7.
2. Niino M, Matsuda T. Type distribution of myeloid leukemia from Cancer Incidence in Five Continents Vol. X. *Jpn J Clin Oncol* 2016;46:394.
3. Tasaki T, Yamauchi T, Matsuda Y, et al. The response to induction therapy is crucial for the treatment outcomes of elderly patients with acute myeloid leukemia: single-institution experience. *Anticancer Res* 2014;34:5631–6.
4. Bhayat F, Das-Gupta E, Smith C, McKeever T, Hubbard R. The incidence of and mortality from leukaemias in the UK: a general population-based study. *BMC Cancer* 2009;9:252.
5. Phekoo KJ, Richards MA, Møller H, Schey SA. South Thames Haematology Specialist Committee. The incidence and outcome of myeloid malignancies in 2,112 adult patients in southeast England. *Haematologica* 2006;91:1400–4.
6. Pulte D, Gondos A, Brenner H. Improvements in survival of adults diagnosed with acute myeloblastic leukemia in the early 21st century. *Haematologica* 2008;93:594–600.
7. Ohnishi H, Imataki O, Kawachi Y, Ide M, Kawakami K, Waki M, et al. Age is an independent adverse prognostic factor for overall survival in acute myeloid leukemia in Japan. *World J Hematol* 2014;3:105–14.
8. Heuser M, Ofran Y, Boissel N, et al. Acute myeloid leukaemia in adult patients: ESMO Clinical Practice Guidelines for diagnosis, treatment and follow-up. *Ann Oncol* 2020;31:697–712.
9. Kantarjian H, Ravandi F, O'Brien S, et al. Intensive chemotherapy does not benefit most older patients (age 70 years or older) with acute myeloid leukemia. *Blood* 2010;116:4422–9.
10. Kiyoi H, Yamaguchi H, Maeda Y, Yamauchi T. JSH practical guidelines for hematological malignancies, 2018: I. leukemia-1. Acute myeloid leukemia (AML). *Int J Hematol* 2020;111:595–613.
11. Grimwade D, Hills RK, Moorman AV, et al. Refinement of cytogenetic classification in acute myeloid leukemia: determination of prognostic significance of rare recurring chromosomal abnormalities among 5876 younger adult patients treated in the United Kingdom Medical Research Council trials. *Blood* 2010;116:354–65.
12. Estey E. Acute myeloid leukemia and myelodysplastic syndromes in older patients. *J Clin Oncol* 2007;25:1908–15.
13. Dombret H, Raffoux E, Gardin C. Acute myeloid leukemia in the elderly. *Semin Oncol* 2008;35:430–8.
14. Pollyea DA, Kohrt HE, Medeiros BC. Acute myeloid leukaemia in the elderly: a review. *Br J Haematol* 2011;152:524–42.
15. He P-F, Zhou J-D, Yao D-M, et al. Efficacy and safety of decitabine in treatment of elderly patients with acute myeloid leukemia: a systematic review and meta-analysis. *Oncotarget* 2017;8:41498–507.
16. Dombret H, Seymour JF, Butrym A, et al. International phase 3 study of azacitidine vs conventional care regimens in older patients with newly diagnosed AML with >30% blasts. *Blood* 2015;126:291–9.
17. Kantarjian HM, Thomas XG, Dmoszynska A, et al. Multicenter, randomized, open-label, phase III trial of decitabine versus patient choice, with physician advice, of either supportive care or low-dose cytarabine for the treatment of older patients with newly diagnosed acute myeloid leukemia. *J Clin Oncol* 2012;30:2670–7.
18. Fischer K, Al-Sawaf O, Fink A-M, et al. Venetoclax and obinutuzumab in chronic lymphocytic leukemia. *Blood* 2017;129:2702–5.
19. Kumar S, Kaufman JL, Gasparetto C, et al. Efficacy of venetoclax as targeted therapy for relapsed/refractory t(11;14) multiple myeloma. *Blood* 2017;130:2401–9.
20. Moreau P, Chanan-Khan A, Roberts AW, et al. Promising efficacy and acceptable safety of venetoclax plus bortezomib and dexamethasone in relapsed/refractory MM. *Blood* 2017;130:2392–400.
21. Roberts AW, Davids MS, Pagel JM, et al. Targeting BCL2 with venetoclax in relapsed chronic lymphocytic leukemia. *N Engl J Med* 2016;374:311–22.
22. Seymour JF, Kipps TJ, Eichhorst B, et al. Venetoclax–rituximab in relapsed or refractory chronic lymphocytic leukemia. *N Engl J Med* 2018;378:1107–20.
23. Stilgenbauer S, Eichhorst B, Schetelig J, et al. Venetoclax in relapsed or refractory chronic lymphocytic leukaemia with 17p deletion: a multicentre, open-label, phase 2 study. *Lancet Oncol* 2016;17:768–78.
24. Wei AH, Strickland SA Jr, Hou J-Z, et al. Venetoclax combined with low-dose cytarabine for previously untreated patients with acute myeloid leukemia: results from a phase Ib/II study. *J Clin Oncol* 2019;37:1277–84.
25. Del Poeta G, Venditti A, Del Principe MI, et al. Amount of spontaneous apoptosis detected by Bax/Bcl-2 ratio predicts outcome in acute myeloid leukemia (AML). *Blood* 2003;101:2125–31.
26. Lagadinou ED, Sach A, Callahan K, et al. BCL-2 inhibition targets oxidative phosphorylation and selectively eradicates quiescent human leukemia stem cells. *Cell Stem Cell* 2013;12:329–41.
27. Teh T-C, Nguyen N-Y, Moujalled DM, et al. Enhancing venetoclax activity in acute myeloid leukemia by co-targeting MCL1. *Leukemia* 2018;32:303–12.
28. Niu X, Zhao J, Ma J, et al. Binding of released bim to Mcl-1 is a mechanism of intrinsic resistance to ABT-199 which can be overcome by combination with daunorubicin or cytarabine in AML cells. *Clin Cancer Res* 2016;22:4440–51.
29. DiNardo CD, Pratz K, Pullarkat V, et al. Venetoclax combined with decitabine or azacitidine in treatment-naive, elderly patients with acute myeloid leukemia. *Blood* 2019;133:7–17.
30. DiNardo C, Jonas B, Pullarkat V, et al. Azacitidine and venetoclax in previously untreated acute myeloid leukemia. *N Engl J Med* 2020;383:617–29.
31. Wei AH, Montesinos P, Ivanov V, et al. Venetoclax plus LDAC for newly diagnosed AML ineligible for intensive chemotherapy: a phase 3 randomized placebo-controlled trial. *Blood* 2020;135:2137–45.
32. Arber DA, Orazi A, Hasserjian R, et al. The 2016 revision to the World Health Organization classification of myeloid neoplasms and acute leukemia. *Blood* 2016;127:2391–405.
33. Cheson BD, Bennett JM, Kopecky KJ, et al. Revised recommendations of the International Working Group for Diagnosis, standardization of response criteria, treatment outcomes, and reporting standards for therapeutic trials in acute myeloid leukemia. *J Clin Oncol* 2003;21:4642–9.
34. Döhner H, Estey E, Grimwade D, et al. Diagnosis and management of AML in adults: 2017 ELN recommendations from an international expert panel. *Blood* 2017;129:424–47.
35. Löwenberg B, Huls G. The long road: improving outcome in elderly "unfit" AML? *Blood* 2020;11;135:2114–5.

Journal of Epidemiology

Original Article J Epidemiol 2022;32(1):27-33

Impact of the Clinical Trials Act on Noncommercial Clinical Research in Japan: An Interrupted Time-series Analysis

Ikuyo Tsutsumi[1,2], Yusuke Tsutsumi[3,4], Chikashi Yoshida[2], Takuya Komeno[2], and Yuichi Imanaka[1]

[1]Department of Healthcare Economics and Quality Management, Kyoto University Graduate School of Medicine, Kyoto, Japan
[2]Department of Hematology, National Hospital Organization Mito Medical Center, Ibaraki, Japan
[3]Department of Emergency Medicine, National Hospital Organization Mito Medical Center, Ibaraki, Japan
[4]Department of Healthcare Epidemiology, Kyoto University Graduate School of Medicine, Kyoto, Japan

Received February 9, 2021; accepted July 5, 2021; released online October 23, 2021

ABSTRACT

Background: The number of new noncommercial clinical studies conducted in Japan declined within the first year of the implementation of the Clinical Trials Act (CTA) on April 1, 2018. This study aimed to examine the impact of the CTA's enforcement on the number of new noncommercial clinical studies registered in the Japanese Clinical Trial Registry.

Methods: An interrupted time-series design was used in the analysis, which was conducted from April 2015 to March 2019. We collected data for studies registered in the Clinical Trial Registry, managed by the University Hospital Medical Information Network.

Results: In total, 35,811 studies were registered; of these, 16,455 fulfilled the eligibility criteria. The difference in the trend of monthly number of new studies after CTA enforcement decreased significantly by 15.0 (95% confidence interval [CI], −18.7 to −11.3), and the level decreased by 40.8 (95% CI, −68.2 to −13.3) studies from the pre-enforcement to the post-enforcement period. Multigroup analyses indicated that the act exerted a significant effect on the trend of new clinical studies, particularly those with smaller sample sizes, interventional study designs, and nonprofit funding sponsors.

Conclusions: The number of Japanese noncommercial clinical studies declined significantly following implementation of the CTA. It is necessary to establish a system to promote clinical studies in Japan while ensuring transparency and safety.

Key words: Clinical Trials Act; interrupted time-series analysis; clinical research

INTRODUCTION

Recently, various regulations and laws have been developed for clinical research worldwide because research misconduct and inappropriate relationships between pharmaceutical companies and researchers have become serious problems. Such "research scandals" have recently become important ethical issues in Japan as well. It was exposed that data falsification and conflicts of interest occurred in research conducted in various fields, resulting in papers being withdrawn in several clinical studies and serious confusion in clinical practice.[1] Research misconduct can impair data accuracy and cause disadvantages to research participants and those who would benefit from the results.

Commercial clinical trials, conducted to obtain national marketing approval for drugs and medical devices, are legally regulated by the International Conference on Harmonization Good Clinical Practice Guideline in Japan. Meanwhile, non-commercial clinical studies, including non-commercial interventional studies and non-interventional studies, are regulated by the Ethical Guidelines for Medical and Health Research Involving Human Subjects, which are not legally enforceable.

To improve the conduct of clinical studies by ensuring trust in clinical studies and thereby promote public health and hygiene, the Clinical Trials Act (CTA) was established by the Ministry of Health, Labour and Welfare (MHLW) in Japan and enforced since April 1, 2018.[2] It aimed to define procedures for the conduct of clinical studies, appropriate provision of the management of reviews by certified review boards (CRBs), and systems for disclosure of information regarding funding or other benefits for clinical studies.[3] The CTA mainly regulates the "specified clinical trials" which are defined as the noncommercial interventional studies receiving funds or benefits from manufacturers and that using unapproved/off-label use drugs/medical devices. The Act also covers noncommercial interventional studies other than "specified clinical trials", which is not mandatory, but recommended (duty of effort). The commercial trials that are conducted to obtain national marketing approval for drugs and medical devices are exempted from the CTA. The CTA requires 1) contracts and disclosure of information regarding research funding; 2) review of the implementation plan and adverse events by a CRB authorized by the MHLW; 3) compliance with implementation standards for monitoring, conflict of interest

Address for correspondence. Yuichi Imanaka, Department of Healthcare Economics and Quality Management, Kyoto University Graduate School of Medicine, Kyoto, Japan (e-mail: imanaka-y@umin.net).

DOI https://doi.org/10.2188/jea.JE20210051
HOMEPAGE http://jeaweb.jp/english/journal/index.html

management, and record preservation; and 4) disclosure of the implementation plan to the MHLW.

While legal regulations for clinical studies have been implemented in various countries to ensure transparency, overregulation can sometimes limit clinical studies, particularly those of a noncommercial nature.[5,6] In the European Union (EU), the number of studies submitted for research grants or ethical review has declined by 30% to 50%, while the proportion of noncommercial studies has decreased from 40% to 14% since Directive 2001/20/EC was adopted in April 2001 and launched in May 2004.[7,8] Similarly, in Japan, there is the concern that the new law could reduce the number of studies conducted at study institutes lacking financial support, but this has not been examined previously. This study aimed to clarify the association between the enforcement of the CTA and the number of studies newly registered in the Japanese Clinical Trial Registry, using an interrupted time-series analysis design.

METHODS

Data source

We collected data from the Clinical Trials Registry managed by the University hospital Medical Information Network Clinical Trials Registry (UMIN-CTR),[9] which is part of the Japan Primary Registries Network (JPRN). The JPRN consists of the following three clinical study registration agencies: UMIN-CTR; Japan Pharmaceutical Information Center Clinical Trial Information[10]; and the Clinical Trials Registry operated by the Center for Clinical Trials of the Japan Medical Association.[11] The JPRN is a clinical trial registry that meets the criteria of the International Committee of Medical Journal Editors and was authorized by the World Health Organization (WHO) Primary Registry on August 16, 2008.[12] UMIN-CTR welcomes the registration of all academic clinical studies, including both commercial and noncommercial clinical trials, and both interventional and noninterventional studies. However, in practice, pharmaceutical company-led commercial clinical trials are registered in the Japan Pharmaceutical Information Center Clinical Trial Information, and physician-led commercial and medical device clinical trials are registered at the Center for Clinical Trials, Japan Medical Association. Additionally, the newly established clinical study database, the Japan Registry of Clinical Trials (jRCT), was added to the JPRN and approved by the WHO Primary Registry on December 5, 2018. The UMIN-CTR provides open .csv files, including daily snapshots of studies registered in the database. We downloaded the file from the UMIN-CTR website on April 1, 2019.[9]

Outcomes

The primary outcome was the change in the trend, defined as the difference in changes (slope) in the monthly number of new clinical studies before and after the enforcement of the CTA. The secondary outcome was the change in the monthly number of new clinical studies, defined as the difference in the monthly number of new clinical studies from the end of the pre-CTA period to the period immediately following the enforcement of the CTA. Additionally, the study focused on differences in the effects of the CTA on the following factors: sample size ($\leq$100 or $>$100), study objectives (malignancy or nonmalignancy), study design (interventional or noninterventional), and type of funding sponsor (for-profit or nonprofit).

Data selection

The inclusion criterion was an anticipated study start date between April 1, 2015, and March 31, 2019. The exclusion criteria were the exclusion of Japan from the study region and commercial trials requiring Investigational New Drug applications to the MHLW, because these trials were applicable to the International Conference on Harmonization Good Clinical Practice Guideline rather than the CTA. We included noninterventional studies, such as observational studies and meta-analyses, in this study since one of the study objectives was to determine whether the number of regulated interventional studies had been more affected by the Clinical Trials Act compared to unregulated designs.

Statistical analysis

Descriptive analyses were performed based on the baseline characteristics of studies before and after the enforcement of the CTA. Continuous variables are presented as medians (interquartile ranges [IQRs]), and categorical variables are presented as frequencies and percentages. A Wilcoxon rank-sum test was performed to compare continuous variables, and Pearson's chi-squared test was used in between-group comparisons of categorical or binary variables. An interrupted time-series analysis (ITSA) design[13,14] was used to assess the association between the enforcement of the CTA and changes in the trends and the monthly number of new studies. The intervention of interest was the enforcement of the CTA. The first month of the intervention period was set as April 2018, and the analysis period lasted for 48 months, from April 2015 to March 2019. To create the time-series dataset, the aggregate number of studies for each month from April 2015 to March 2019 was tabulated according to the anticipated study start date. We performed ITSA using two ordinary least-squares regression-based approaches.[15]

The following regression equation was used in the single-group analysis[15–18]:

$$Y_t = \beta_0 + \beta_1 T_t + \beta_2 X_t + \beta_3 X_t T_t + \epsilon_t$$

The following regression equation was used in the multigroup analysis[14–17]:

$$Y_t = \beta_0 + \beta_1 T_t + \beta_2 X_t + \beta_3 X_t T_t + \beta_4 Z + \beta_5 Z T_t + \beta_6 Z X_t + \beta_7 Z X_t T_t + \epsilon_t$$

Y_t represents the monthly number of studies measured at time point t, and T_t represents the time since April 2015. X_t is a dummy variable representing the enforcement of the CTA (eg, pre-CTA period was 0, otherwise 1). In the single-group analysis, β_0 represents the number of studies in the first month of the study (ie, April 2015). β_1 represents the slope of the monthly number of studies (trend) before the implementation of the CTA. β_2 represents the change in the monthly number of studies from the end of the pre-CTA period (level change) to the period immediately following the enforcement of the CTA. β_3 indicates the slope change following the enforcement of the CTA. In the multigroup analysis, β_0 to β_3 represents the value for the control group, and β_4 to β_7 represents the value for the comparison group. β_4 represents the difference in the number of studies during the first month of the study between the control group and comparison group (difference in level) prior to enforcement of the CTA. β_5 represents the difference in the slopes of the monthly number of studies between the control group and comparison group (difference in trend) prior to enforcement of the CTA. β_6

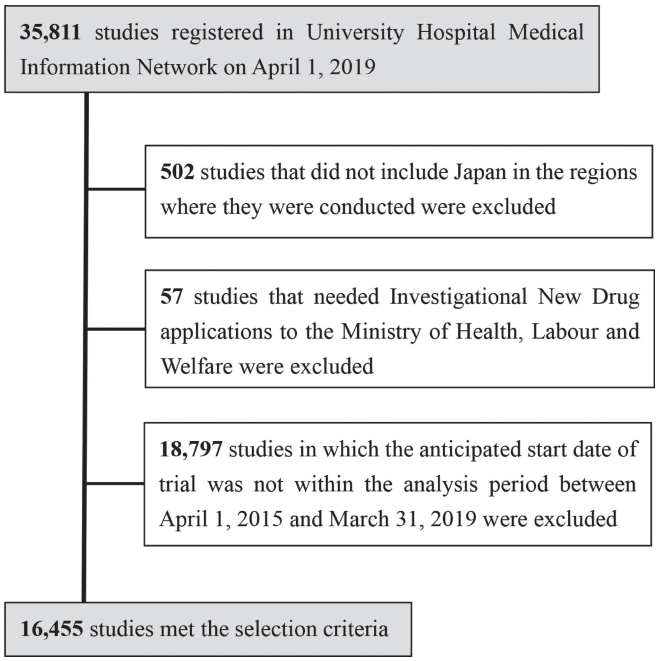

Figure 1. Flow diagram of data selection. MHLW, Ministry of Health, Labour and Welfare; UMIN-CTR, University hospital Medical Information Network.

represents the difference in levels immediately following enforcement of the CTA between the control group and comparison group. β_7 represents the difference in slopes (trends) in the pre- and post-CTA periods between the control group and comparison group. Calendar month was included as a dummy variable, to account for seasonality. Newey-West standard errors were used to deal with autocorrelation and possible heteroskedasticity.[15] All statistical tests were two-sided, and the significance level was set at 5%. All analyses were performed using Stata SE version 14.2 (Stata Corp, College Station, TX, USA). The requirement for ethics committee approval was waived because all the data are publicly available online and comprise only aggregate values, without any personally identifiable information.

RESULTS

Figure 1 shows the flow chart for data selection. We downloaded all data for 35,811 studies in the UMIN-CTR on April 1, 2019. The 502 studies that were not conducted in Japan and the 57 that involved Investigational New Drug applications to the MHLW were excluded according to the exclusion criteria. Additionally, 18,797 studies in which the anticipated study start date was not between April 1, 2015, and March 31, 2019, were excluded from the analysis. Therefore, 16,455 studies ultimately met the selection criteria.

Table 1 shows the baseline characteristics of studies initiated between April 2015 and March 2019. The proportion of interventional studies conducted after the enforcement of the CTA was lower relative to that of those conducted before the enforcement of the CTA (from 70.8% to 66.6%, $P < 0.001$). Regarding disease classification, the proportion of studies involving internal medicine and surgery conducted after the enforcement of the CTA was lower relative to that of those conducted before (from 43.0% to 40.0% and from 12.6% to 9.3%, respectively; $P = 0.002$). Moreover, the proportion of studies involving malignancy decreased after the law was enforced (from 24.4% to 21.7%, $P < 0.001$). Conversely, the proportion of studies involving healthy people increased after the enforcement (from 22.6% to 29.0%, $P < 0.001$). Regarding types of funding organizations, the most common was self-funded, followed by for-profit organizations and Japanese governmental offices, both before and after the enforcement of the CTA.

Figure 2 and Table 2 shows the results of the single-group ITSA for the monthly number of new studies. During the pre-enforcement period, the trend in the number of new studies increased by 1.64 (95% CI, 0.71–2.57, $P = 0.001$) each month. In contrast, during the post-CTA period, this trend was expected to decline significantly, by 13.3 (95% CI, −17.1 to −9.63, $P < 0.001$) studies every month. The difference in trends before and after the enforcement of the CTA was −15.0 (95% CI, −18.7 to −11.3, $P < 0.001$) studies. Furthermore, there was a significant decline in levels (−40.8; 95% CI, −68.2 to −13.3, $P = 0.005$) after the enforcement.

Figure 3 and Table 3 represent the results of the multigroup ITSA examining the effects of the CTA on various factors such as sample size, study design, and type of funding sponsor. As shown in Figure 3A, the pre-CTA trend for studies with sample sizes >100 increased by 0.53 (95% CI, 0.22–0.84, $P = 0.001$) monthly, which did not show a significant difference from those of studies with sample sizes ≤100 (0.65; 95% CI, −0.29 to 1.58, $P = 0.17$). In contrast, the post-CTA trend for studies with sample sizes >100 decreased by 2.99 (95% CI, −5.33 to −0.65, $P = 0.013$) monthly, while studies with sample sizes ≤100 showed a significant difference from those of studies with sample sizes >100 (−7.33; 95% CI, −10.6 to −4.11, $P < 0.001$). There was no significant difference in level changes between studies with sample sizes ≤100 and >100 during the period immediately following the enforcement of the CTA (−15.8; 95% CI, −45.4 to 13.8, $P = 0.29$).

Moreover, Figure 3B shows the effects of the CTA according to study design. The pre-CTA trend in noninterventional studies did not increase significantly (0.14; 95% CI, −0.24 to 0.52, $P = 0.47$), while interventional studies increased significantly by 1.36 (95% CI, 0.54–2.19, $P = 0.001$) per month. The post-CTA trend for noninterventional studies decreased by 2.78 (95% CI, −5.21 to −0.35, $P = 0.026$) per month, while interventional studies showed a significant difference from that for noninterventional studies (−7.78; 95% CI, −10.5 to −5.05, $P < 0.001$). There was a significant difference in level changes between interventional and noninterventional studies during the period immediately following the enforcement of the CTA (−40.6; 95% CI, −65.0 to −16.2, $P = 0.001$).

Furthermore, Figure 3C represents the results of the ITSA according to the type of funding sponsor. The pre-CTA trend for studies funded by for-profit sponsors increased at a rate of 1.10 (95% CI, 0.68–1.52, $P < 0.001$) studies per month, which did not differ significantly from studies funded by nonprofit sponsors (−0.55; 95% CI, −1.44 to 0.34, $P = 0.22$). In contrast, the post-CTA trend for studies funded by for-profit sponsors decreased at a rate of 1.61 (95% CI, −3.99 to 0.77, $P = 0.18$) studies per month, while studies funded by nonprofit sponsors showed a significant difference from that for studies funded by for-profit sponsors (−10.1; 95% CI, −12.0 to −8.27, $P < 0.001$). There was no significant difference in level changes between studies funded

Table 1. Baseline characteristics of studies that began between April 2015 and March 2019

	Total $N = 16,455$	Before the Act $n = 13,095$	After the Act $n = 3,360$	P value
Study design, N (%)				
Interventional	11,506 (69.9%)	9,268 (70.8%)	2,238 (66.6%)	<0.001***
Observational	4,656 (28.3%)	3,574 (27.3%)	1,082 (32.2%)	
Other (eg, meta-analysis)	248 (1.5%)	208 (1.6%)	40 (1.2%)	
Not selected	45 (0.3%)	45 (0.3%)	0 (0.0%)	
Sample size, median (IQR)[a]	50 (25–110)	50 (25–110)	50 (24–116.5)	0.97
Category by sample size, N (%)[a]				
≤100	12,261 (74.6%)	9,769 (74.7%)	2,492 (74.2%)	0.52
>100	4,175 (25.4%)	3,307 (25.3%)	868 (25.8%)	
Basic objectives (primary outcome), N (%)				
Safety	1,238 (7.5%)	977 (7.5%)	261 (7.8%)	<0.001***
Efficacy	7,165 (43.5%)	5,622 (42.9%)	1,543 (45.9%)	
Safety and efficacy	4,413 (26.8%)	3,650 (27.9%)	763 (22.7%)	
Bioequivalence	171 (1.0%)	136 (1.0%)	35 (1.0%)	
Bioavailability	190 (1.2%)	158 (1.2%)	32 (1.0%)	
Pharmacokinetics	143 (0.9%)	117 (0.9%)	26 (0.8%)	
Pharmacodynamics	48 (0.3%)	46 (0.4%)	2 (0.1%)	
Pharmacokinetics and pharmacodynamics	79 (0.5%)	63 (0.5%)	16 (0.5%)	
Other	3,008 (18.3%)	2,326 (17.8%)	682 (20.3%)	
Disease classification by specialty, N (%)				
Internal medicine	6,971 (42.4%)	5,628 (43.0%)	1,343 (40.0%)	0.002**
Surgery	1,961 (11.9%)	1,649 (12.6%)	312 (9.3%)	<0.001***
Medicine, other	6,814 (41.4%)	5,498 (42.0%)	1,316 (39.2%)	0.003**
Dental medicine	491 (3.0%)	384 (2.9%)	107 (3.2%)	0.44
Nursing	416 (2.5%)	317 (2.4%)	99 (2.9%)	0.083
Healthy people	3,926 (23.9%)	2,953 (22.6%)	973 (29.0%)	<0.001***
Not applicable	887 (5.4%)	661 (5.0%)	226 (6.7%)	<0.001***
Disease classification by malignancy, N (%)				
Malignancy	3,927 (23.9%)	3,198 (24.4%)	729 (21.7%)	<0.001***
Other	12,528 (76.1%)	9,897 (75.6%)	2,631 (78.3%)	
Category of funding organization, N (%)				
For-profit organization	3,186 (19.4%)	2,491 (19.0%)	695 (20.7%)	<0.001***
Self-funding	5,388 (32.7%)	4,407 (33.7%)	981 (29.2%)	
Japanese governmental office	1,995 (12.1%)	1,518 (11.6%)	477 (14.2%)	
Nonprofit foundation	453 (2.8%)	357 (2.7%)	96 (2.9%)	
Local government	282 (1.7%)	234 (1.8%)	48 (1.4%)	
Government offices of other countries	161 (1.0%)	121 (0.9%)	40 (1.2%)	
Outside Japan	51 (0.3%)	38 (0.3%)	13 (0.4%)	
Other	4,939 (30.0%)	3,929 (30.0%)	1,010 (30.1%)	

IQR, interquartile range.
[a]Data for 19 of 13,095 studies were missing in the sample before the act's enforcement.
*$P < 0.05$; **$P < 0.01$; ***$P < 0.001$.

Table 2. Results of the single-group ITSA for monthly number of new studies

	β	95% CI			P
Trend before the enforcement of the CTA : β_1	1.64	0.71	–	2.57	0.001**
Trend after the enforcement of the CTA : $\beta_1+\beta_3$	−13.3	−17.1	–	−9.63	<0.001***
Difference in trend before and after the enforcement of the CTA : β_3	−15.0	−18.7	–	−11.3	<0.001***
Difference in level before and after the enforcement of the CTA : β_2	−40.8	−68.2	–	−13.3	0.005**

CI, confidence interval; CTA, Clinical Trials Act.
*$P < 0.05$; **$P < 0.01$; ***$P < 0.001$.

by for- and nonprofit sponsors during the period immediately following the enforcement of the CTA (4.71; 95% CI, −14.6 to 24.0, $P = 0.63$).

DISCUSSION

The results of the single-group ITSA showed that the total number of new studies declined significantly in both trends and levels following the enforcement of the CTA in April 2018. The current data indicated that the enforcement of the CTA exerted a strong negative effect on the number of new clinical studies. The analysis of various factors, using the multigroup ITSA method, showed that the trend decreased significantly for all types of studies after the new legal regulation, especially those with smaller sample sizes, interventional study designs, and nonprofit funding sponsors. The result suggests that enforcement of the

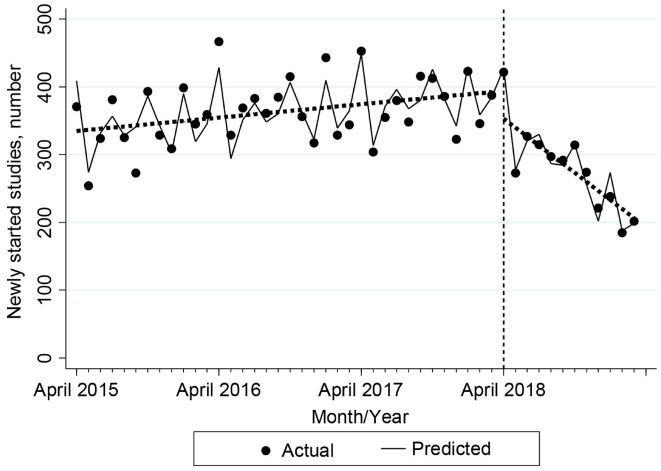

Figure 2. Results of the single-group ITSA for monthly number of new studies. The points on the figure represent the actual monthly number of studies. The solid lines indicate the predicted monthly number of studies adjusted by calendar month. Dotted lines represent trends (slopes) in monthly numbers of studies. Level change after the enforcement of the Clinical Trials Act (CTA) is defined as the difference from the end of the dotted line during the pre-act period to the starting point of the dotted line during the post-act period. CI, confidence interval; ITSA, interrupted time-series analysis.

CTA particularly affected studies with limited human resources and financial support. Prior to implementation, there were no legal restrictions in Japan on noncommercial clinical studies. After introduction of the new law, CRBs authorized by the MHLW reviewed study plans, adverse event reports, and the exact status of conflicts of interest of all physicians involved in the studies.[2–4] These improvements seek to increase the transparency of the procedures involved in clinical studies and flow of expenses, which contribute to the prevention of research misconduct. However, substantial research funding is needed to disburse expensive commission fees for review by a CRB and management costs, including personnel expenses for following requirements mandated by the CTA, as compared to the period prior to its introduction. Therefore, it can be difficult for researchers who do not have sufficient human resources and funds to conduct new clinical research.

Before the CTA was enacted in 2018, new ethical guidelines were established in 2015; the Act on the Protection of Personal Information was revised in 2015 and enacted in 2017. Therefore, it was necessary to confirm whether the decline in new research in the past few years was due to the CTA and not these factors. In this study, we used ITSA to show that there was a significant decrease in new clinical studies before and after the CTA was implemented. We also conducted analyses using ITSA, before and after the implementation of the new ethical guidelines and the revised Act on the Protection of Personal Information, and confirmed that there was no significant decrease in the number of new clinical studies after the implementation of each (data not shown).

Since 2001, each country in the EU has developed its own directives for clinical studies to maintain the quality of studies based on Directive 2001/20/EC. Thus, in most countries, the

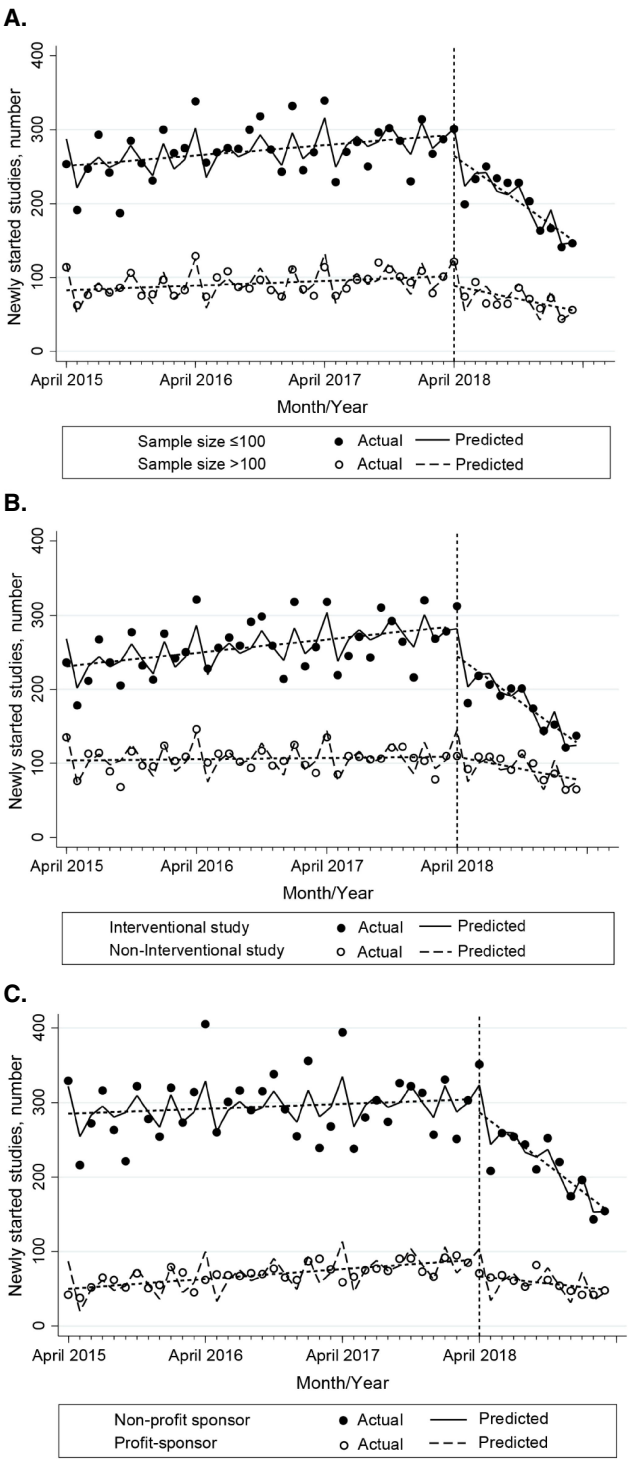

Figure 3. Results of the multigroup ITSA for monthly number of new studies. (**A**) ITSA according to sample size. (**B**) ITSA according to study design. (**C**) ITSA according to type of funding sponsor. The points on the graph represent the actual monthly number of studies. Solid lines indicate the predicted monthly number of studies adjusted by calendar month. Dotted lines represent trends (slopes) in monthly number of studies. Level change after the enforcement of the Clinical Trials Act (CTA) is defined as the difference from the end of the dotted line during pre-act period to the starting point of the dotted line during post-act period. CI, confidence interval; ITSA, interrupted time-series analysis.

Table 3. Results of the multigroup ITSA for monthly number of new studies

	Sample size ≤100 vs Sample size >100				Interventional studies vs Non-interventional studies				Non-profit sponsor vs Profit sponsor			
	β	95% CI		P	β	95% CI		P	β	95% CI		P
Pre-CTA trend for studies with sample sizes >100 :β_1	0.53	0.22	0.84	0.001**	0.14	−0.24	0.52	0.47	1.10	0.68	1.52	<0.001***
Post-CTA trend for studies with sample sizes >100 :$\beta_1+\beta_3$	−2.99	−5.33	−0.65	0.013*	−2.78	−5.21	−0.35	0.026*	−1.61	−3.99	0.77	0.18
Difference in trend for studies with sample sizes >100 before and after the enforcement of the CTA :β_3	−3.52	−5.80	−1.24	0.003**	−2.92	−5.40	−0.44	0.021*	−2.71	−4.89	−0.53	0.016*
Difference in level for studies with sample sizes >100 before and after the enforcement of the CTA :β_2	−12.9	−33.8	8.01	0.22	−0.08	−16.9	16.7	0.99	−22.7	−42.4	−3.12	0.024*
Difference in Pre-CTA trend between studies with sample sizes ≤100 and those >100 :β_5	0.65	−0.29	1.58	0.17	1.36	0.54	2.19	0.001**	−0.55	−1.44	0.34	0.22
Difference in Post-CTA trend between studies with sample sizes ≤100 and those >100 :$\beta_5+\beta_7$	−7.33	−10.6	−4.11	<0.001***	−7.78	−10.5	−5.05	<0.001***	−10.1	−12.0	−8.27	<0.001***
Difference in trend before and after the enforcement of the CTA between studies with sample sizes ≤100 and those >100 :β_7	−7.97	−11.3	−4.62	<0.001***	−9.14	−12.0	−6.31	<0.001***	−9.56	−11.6	−7.52	<0.001***
Difference in level before and after the enforcement of the CTA between studies with sample sizes ≤100 and those >100 :β_6	−15.8	−45.4	13.8	0.29	−40.6	−65.0	−16.2	0.001**	4.71	−14.6	24.0	0.63

CI, confidence interval; CTA, Clinical Trials Act.
*$P < 0.05$; **$P < 0.01$; ***$P < 0.001$.

number of noncommercial studies has decreased, particularly those funded by nonprofit sponsors,[19–21] because regulatory bodies impose highly demanding stipulations and expensive fees for the submission of studies to ethics committees. There are similar concerns in Japan that the CTA may also overly regulate clinical studies regardless of the study subject and magnitude of the risk to participants. Only a limited number of organizations with an accessible labor force and adequate financial resources could conduct clinical studies with larger sample sizes, which may limit the scopes of study domains. Indeed, a Japanese questionnaire survey showed that the investigators' desire for support systems when conducting clinical studies was significantly higher after the implementation of the CTA than before.[21] Furthermore, it may cause a decline in the number of new researchers who conduct innovative clinical research. It is essential to develop a system in which physicians can obtain appropriate support to conduct research. We may be able to follow the model developed in Italy, where the number of clinical studies increased after the introduction of legal regulation.[21] This is apparently because Italy implemented policy changes that include waiving of ethical review fees, prompt approval by ethics review boards, financial support for research expenses or management, and alleviation of regulations on investigator-driven study for noncommercial research.[22–24]

This study was subject to a few limitations. First, it did not include jRCT data analyzed in this study. Although the jRCT was enforced in April 2018, the actual registration begun in April 2019. In addition, there were only six new studies registered in the jRCT, but not in UMIN-CTR, within the current analysis period between April 1, 2015, and March 31, 2019, as reported in the WHO International Clinical Trials Registry Platform. This suggests that exclusion of the jRCT data has little impact on the current results. Second, we could analyze the data for only 1 year after the enforcement of the CTA. It may be essential to carry out medium- and long-term analysis for examining the impact of the CTA on clinical research in Japan. Nevertheless, the current analysis contributes to identifying the key issues faced by Japanese clinical research under the new legal regulation, which can be used to address them quickly. Finally, it is difficult to assess whether the introduction of the CTA can in fact reduce clinical research with inadequate transparency and reliability, which is the original purpose of the legislation, despite the decrease in newly initiated research found in this study. Further study from an alternative perspective may be needed to clarify this issue.

In conclusion, the number of noncommercial clinical studies decreased 1 year after the implementation of the CTA in Japan. Establishing a new system to promote clinical research in Japan while ensuring research transparency and safety is vital.

ACKNOWLEDGMENTS

We would like to thank Editage (www.editage.jp) for English language editing.

Conflicts of interest: None declared.

Funding source: This research did not receive any specific grant from funding agencies in the public, commercial, or not-for-profit sectors.

Author contributions: Ikuyo Tsutsumi — conceptualization, data curation, formal analysis, investigation, methodology, writing, original draft. Yusuke Tsutsumi — methodology, writing, review & editing. Chikashi Yoshida — conceptualization, review & editing. Takuya Komeno — conceptualization, review & editing. Yuichi Imanaka — conceptualization, methodology, review & editing, supervision.

REFERENCES

1. Sawano T, Ozaki A, Saito H, Shimada Y, Tanimoto T. Payments from pharmaceutical companies to authors involved in the Valsartan scandal in Japan. *JAMA Netw Open*. 2019;2(5):e193817.
2. Ministry of Health, Labour and Welfare. About the Clinical Trials Act. https://www.mhlw.go.jp/stf/seisakunitsuite/bunya/0000163417.html; 2019 Accessed 12.12.2019. [Japanese].
3. Ministry of Health, Labour and Welfare. Clinical Trials Act (Act No. 16 of April 14, 2017). 2017. https://www.mhlw.go.jp/file/06-Seisakujouhou-10800000-Iseikyoku/0000213334.pdf; 2019 Accessed 12.12.2019. [Japanese].
4. Tashiro S. How the clinical research act will change clinical research in Japan. *Gan To Kagaku Ryoho*. 2018;45(7):1011–1016.
5. Morice AH. The death of academic clinical trials. *Lancet*. 2003;361(9368):1568.
6. The Lancet. Who's afraid of the European Clinical Trials Directive? *Lancet*. 2003;361(9376):2167.

7. Bosch X. Europe's restrictive rules strangling clinical research. *Nat Med*. 2005;11(12):1260.
8. McMahon AD, Conway DI, Macdonald TM, McInnes GT. The unintended consequences of clinical trials regulations. *PLoS Med*. 2009;3(11):e1000131.
9. University hospital Medical Information Network (UMIN). UMIN Clinical Trials Registry (UMIN-CTR). https://www.umin.ac.jp/ctr/index.htm; 2013 Accessed 17.06.2020.
10. Japan Pharmaceutical Information Center. Japic Clinical Trials Information. https://www.clinicaltrials.jp/cti-user/common/Top.jsp; 2019 Accessed 12.08.2019. [Japanese].
11. The Japan Medical Association Center for Clinical Trials. JMACCT Clinical Trials Registry. https://dbcentre3.jmacct.med.or.jp/JMACTR/Default_Eng.aspx; 2019 Accessed 12.08.2019.
12. World Health Organization. International Clinical Trials Registry Platform (ICTRP). https://www.who.int/ictrp/network/primary/en/; 2019 Accessed 11.09.2019.
13. Wagner AK, Soumerai SB, Zhang F, Ross-Degnan D. Segmented regression analysis of interrupted time series studies in medication use research. *J Clin Pharm Ther*. 2002;27(4):299–309.
14. Bernal JL, Cummins S, Gasparrini A. Interrupted time series regression for the evaluation of public health interventions: a tutorial. *Int J Epidemiol*. 2017;46(1):348–355.
15. Linden A. Conducting interrupted time-series analysis for single- and multiple-group comparisons. *Stata J*. 2015;15(2):480–500.
16. Linden A, Adams JL. Applying a propensity score-based weighting model to interrupted time series data: improving causal inference in programme evaluation. *J Eval Clin Pract*. 2011;17(6):1231–1238.
17. Simonton DK. Cross-sectional time-series experiments: some suggested statistical analyses. *Psychol Bull*. 1977;84(3):489–502.
18. Simonton DK. Erratum to Simonton. *Psychol Bull*. 1977;84(6):1097.
19. Frewer LJ, Coles D, Champion K, et al. Has the European clinical trials directive been a success? *BMJ*. 2010;340:c1862.
20. Hartmann M, Hartmann-Vareilles F. The clinical trials directive: how is it affecting Europe's noncommercial research? *PLoS Clin Trials*. 2006;1(2):e13.
21. Chuma M, Takechi K, Yagi K, et al. Academic investigators' interest in promoting specified clinical trials: questionnaire survey before and after implementation of the Clinical Trial Act. *J Med Invest*. 2021;68(1.2):71–75.
22. Hartmann M. Impact assessment of the European clinical trials directive: a longitudinal, prospective, observational study analyzing patterns and trends in clinical drug trial applications submitted since 2001 to regulatory agencies in six EU countries. *Trials*. 2012;13:53.
23. Filibeck U, Addis A, Tomino C, Martini N. European clinical trials directive: the Italian position. *Lancet*. 2004;363(9421):1651–1652.
24. Gazzetta Ufficiale. GU Serie Generale n.43 del 22-02-2005. https://www.gazzettaufficiale.it/eli/gu/2005/02/22/43/sg/pdf 2019; 2019 Accessed 12.11.2019. [Italian].

JJCO Japanese Journal of Clinical Oncology

Japanese Journal of Clinical Oncology, 2022, 52(1)29–38
https://doi.org/10.1093/jjco/hyab170
Advance Access Publication Date: 5 November 2021
Original Article

OXFORD

Original Article

Venetoclax plus azacitidine in Japanese patients with untreated acute myeloid leukemia ineligible for intensive chemotherapy

Kazuhito Yamamoto[1,*], Atsushi Shinagawa[2], Courtney D. DiNardo[3], Keith W. Pratz[4], Kenichi Ishizawa[5], Toshihiro Miyamoto[6], Norio Komatsu[7], Yasuhiro Nakashima[8], Chikashi Yoshida[9], Noriko Fukuhara[10], Kensuke Usuki[11], Takahiro Yamauchi[12], Noboru Asada[13], Norio Asou[14], Ilseung Choi[15], Yasushi Miyazaki[16], Hideyuki Honda[17], Sumiko Okubo[18], Misaki Kurokawa[17], Ying Zhou[19], Jiuhong Zha[19], Jalaja Potluri[19], and Itaru Matsumura[20]

[1]Department of Hematology and Cell Therapy, Aichi Cancer Center, Nagoya, Aichi, Japan, [2]Department of Internal Medicine, Hitachi General Hospital, Hitachi, Ibaraki, Japan, [3]Department of Leukemia, Division of Cancer Medicine, University of Texas MD Anderson Cancer Center, Houston, TX, USA, [4]Leukemia Program, Division of Medicine, University of Pennsylvania, Philadelphia, PA, USA, [5]Department of Third Internal Medicine, Yamagata University Hospital, Yamagata, Japan, [6]Department of Medicine and Biosystemic Science, Kyushu University Graduate School of Medical Sciences, Fukuoka, Japan, [7]Department of Hematology, Juntendo University School of Medicine, Tokyo, Japan, [8]Department of Hematology, Graduate School of Medicine, Osaka City University, Osaka, Japan, [9]Department of Hematology, National Hospital Organization, Mito Medical Center, Ibaraki, Japan, [10]Department of Hematology, Tohoku University Graduate School of Medicine, Sendai, Japan, [11]Department of Hematology, NTT Medical Center Tokyo, Tokyo, Japan, [12]Department of Hematology and Oncology, University of Fukui Hospital, Fukui, Japan, [13]Department of Hematology and Oncology, Okayama University Hospital, Okayama, Japan, [14]Department of Hematology, Saitama Medical University International Medical Center, Hidaka, Saitama, Japan, [15]Department of Hematology, National Hospital Organization, Kyushu Cancer Center, Fukuoka, Japan, [16]Department of Hematology, Atomic Bomb Disease Institute, Nagasaki University, Nagasaki, Japan, [17]AbbVie GK, Tokyo, Japan, [18]AbbVie GK, Osaka, Japan, [19]AbbVie, Inc., North Chicago, IL, USA and [20]Department of Hematology and Rheumatology, Kindai University Hospital, Osaka, Japan

*For reprints and all correspondence: Kazuhito Yamamoto, Aichi Cancer Center, Department of Hematology and Cell Therapy, 1-1 Kanokoden, Chikusa Ward, Nagoya, Aichi 464-8681, Japan. E-mail: kyamamoto@aichi-cc.jp

Received 11 August 2021; Editorial Decision 30 September 2021; Accepted 15 October 2121

Abstract

Background: The phase 3 VIALE-A trial (NCT02993523) reported that venetoclax-azacitidine significantly prolonged overall survival compared with placebo-azacitidine in patients with newly diagnosed acute myeloid leukemia ineligible for intensive chemotherapy. Herein, efficacy and safety of venetoclax-azacitidine are analyzed in the Japanese subgroup of VIALE-A patients.
Methods: Eligible Japanese patients were randomized 2:1 to venetoclax-azacitidine ($N = 24$) or placebo-azacitidine ($N = 13$). Primary endpoints for Japan were overall survival and complete response (CR) + CR with incomplete hematologic recovery (CRi). Venetoclax (target dose 400 mg) was given orally once daily. Azacitidine (75 mg/m^2) was administered subcutaneously or intravenously on Days 1–7 of each 28-day cycle.

Results: Median follow-up was 16.3 months (range, 1.0–20.3). Median overall survival was not reached with venetoclax-azacitidine (hazard ratio 0.409 and 95% confidence interval: 0.151, 1.109); overall survival estimate was higher with venetoclax-azacitidine than placebo-azacitidine at 12 (67 and 46%) and 18 months (57 and 31%), respectively. CR and CRi rates were 67% with venetoclax-azacitidine and 15% with placebo-azacitidine. Most common any-grade adverse events were febrile neutropenia (79 and 39%), thrombocytopenia (54 and 77%), constipation (54 and 54%) and decreased appetite (54 and 38%) in the venetoclax-azacitidine and placebo-azacitidine arms, respectively. Only 1 patient in the venetoclax-azacitidine arm, and no patients in the placebo-azacitidine arm, had grade 4 febrile neutropenia that led to treatment discontinuation.
Conclusions: This Japanese subgroup analysis of VIALE-A demonstrates comparable safety and efficacy outcomes compared with the global study and supports venetoclax-azacitidine as first-line standard-of-care for Japanese treatment-naive patients with acute myeloid leukemia who are ineligible for intensive chemotherapy.

Key words: acute myeloid leukemia, venetoclax, azacitidine, VIALE-A, Japan

Introduction

Acute myeloid leukemia (AML) is the most common type of adult leukemia, with the highest incidence worldwide found in the USA, Western Europe and Australia (1). In Japan, AML is the most common leukemia, accounting for ∼70% of myeloid leukemias (2,3). AML primarily affects older adults, with a third of patients in Japan being diagnosed at ≥75 years of age (4). The 5-year survival rate was 39.2% among Japanese patients with leukemias diagnosed between 2006 and 2008 (5). Current treatment for younger adults in Japan consists of intensive induction chemotherapy with idarubicin or daunorubicin plus cytarabine (2,6). In addition, patients achieving remission are advised to continue with consolidation therapy consisting of high-dose cytarabine or non–cross-resistant agents, and allogeneic stem cell transplant for eligible patients. However, many patients with newly diagnosed AML are not eligible for intensive chemotherapy because of advanced age or the presence of comorbidities (6–8). Treatment options for these patients are limited and include low-intensity therapy with the hypomethylating agents (HMAs) azacitidine or decitabine, and low-dose cytarabine [LDAC; (9,10)].

In Japan, for patients ≥65 years of age who are ineligible for standard therapy (idarubicin or daunorubicin plus cytarabine) on the basis of their performance status, comorbidities or cytogenetic abnormalities, treatment with LDAC is recommended (6). However, outcomes with less intensive regimens such as decitabine, azacitidine or LDAC remain poor, with expected rates of complete response (CR) or CR with incomplete blood count recovery (CRi) lower than 30%, and median overall survival (OS) of <1 year (11–13). More effective and well-tolerated treatment options are needed for patients with AML ineligible for intensive chemotherapy.

Venetoclax is a selective inhibitor of B-cell leukemia/lymphoma-2 (BCL2) that has been studied in several hematologic malignancies as monotherapy or in combination with other agents (14–21). Two large phase 1b/2 studies have assessed venetoclax-based therapy in combination with low-intensity regimens in older patients with previously untreated AML (21,22). When combined with azacitidine or decitabine, venetoclax therapy resulted in a CR + CRi rate of 67% and a median OS of 17.5 months (22). A subsequent confirmatory phase 3 placebo-controlled trial (VIALE-A; NCT02993523) compared the efficacy and safety of venetoclax plus azacitidine (venetoclax-azacitidine) with placebo plus azacitidine (placebo-azacitidine) in treatment-naive patients with AML ineligible for standard induction therapy (23). The venetoclax-azacitidine combination regimen significantly increased OS [14.7 and 9.6 months, respectively; hazard ratio (HR), 0.66; 95% confidence interval (CI): 0.52, 0.85 and $P < 0.001$] and the CR + CRi rate (66 and 28%; $P < 0.001$) compared with the placebo-azacitidine regimen (23).

The biologic rationale for combining venetoclax with azacitidine in AML is based on their complementary mechanisms of action. The BCL2 family members, including BCL2, BCL-X_L and MCL1, mediate cancer cell survival by sequestering proapoptotic proteins. BCL2 is upregulated in AML, promotes chemoresistance, enhances the survival of leukemic progenitor and blast cells and has been associated with poor outcomes (24,25). In preclinical studies, venetoclax had additive or synergistic effects when combined with azacitidine in primary cells from patients with AML (26,27), where azacitidine was shown to downregulate MCL1 protein levels (27).

Venetoclax has been approved in the USA (28), and in >25 other countries for use in combination with azacitidine, decitabine or LDAC in patients with newly diagnosed AML who are ≥75 years of age, or those with comorbidities that preclude the use of intensive induction chemotherapy. Japan has the most aged population worldwide (29), and elderly patients with AML have limited treatment options. In March 2021, venetoclax in combination with azacitidine or LDAC was approved in Japan. The Japanese subgroup analyses aimed to provide evidence that safety and efficacy outcomes in the Japanese subgroup were comparable to the global population. Here, we present the results of the subgroup analysis of Japanese patients with AML ineligible for intensive chemotherapy who participated in the VIALE-A trial comparing venetoclax-azacitidine with placebo-azacitidine.

Materials and methods

Study design

VIALE-A (NCT02993523) is a phase 3, randomized, double-blind, placebo-controlled and multicenter study that assessed the efficacy and safety of venetoclax-azacitidine compared with placebo-azacitidine in patients with previously untreated AML who were ineligible for intensive chemotherapy (23). The dual primary endpoints for Japan were OS and CR + CRi rates. Key secondary endpoints included CR + CR with partial hematologic recovery (CRh) rates, response rates at the start of Cycle 2 and

transfusion-independence rates. The study was conducted in accordance with the International Council for Harmonization requirements, Good Clinical Practice guidelines and the Declaration of Helsinki. The study protocol was reviewed and approved by an independent ethics committee/institutional review board at each study site. All patients provided written informed consent.

Patients

Full eligibility criteria have been reported previously (23). In brief, the study enrolled treatment-naive adult (≥18 years of age) patients with a confirmed diagnosis of AML [per the World Health Organization classification (30)], who were ineligible for standard induction chemotherapy because of age (≥75 years) or comorbidities. The existence of at least one of the following conditions precluded the use of intensive induction chemotherapy: Eastern Cooperative Oncology Group (ECOG) performance status 2 or 3, history of congestive heart failure requiring treatment, an ejection fraction ≤50%, chronic stable angina, diffusion capacity of the lung for carbon monoxide ≤65%, forced expiratory volume in 1 second (s) of ≤65%, creatinine clearance 0.5 ml/s to <0.75 ml/s, moderate hepatic impairment with total bilirubin >1.5 to ≤3.0 times the upper limit of normal or other comorbidities considered incompatible with standard therapy. Patients needed to have a projected life expectancy of ≥12 weeks to be included in the trial, and those who had received previous treatment for myelodysplastic syndromes or AML were excluded.

Randomization and treatment

Eligible patients were randomized 2:1 via interactive response technology to either venetoclax-azacitidine or placebo-azacitidine. Randomization was stratified by patient age (<75 and ≥75 years), region (USA, European Union, China, Japan and rest of world) and cytogenetic risk (intermediate and poor).

Venetoclax was given orally once daily. Patients were hospitalized for monitoring and tumor lysis syndrome (TLS) prophylaxis for the first 4 days of treatment in Cycle 1, until 24 h after the target dose of venetoclax was reached. This included uric acid-reducing agents, intravenous hydration and laboratory assessments. To mitigate the risk of TLS, venetoclax dosing started at 100 mg on Day 1 of Cycle 1, increasing to 200 mg on Day 2 and reaching the target dose of 400 mg on Day 3. The 400mg daily dosing was maintained until Day 28 of Cycle 1 and on Days 1–28 in all subsequent cycles. Patients in the control arm received oral placebo according to the same schedule. Azacitidine was administered to patients in both study arms at a dose of 75 mg/m^2 subcutaneously or intravenously for the first 7 days of each 28-day cycle. Treatment was continued until disease progression, withdrawal of consent or other protocol-defined criteria for discontinuation were met.

Assessments

OS was defined as the time from study randomization to death due to any cause. Bone marrow assessments were performed at screening, at the end of Cycle 1 and every 3 cycles thereafter until 2 successive samples indicated CR or composite CR (CR or CR + CRi). Details on the disease evaluation criteria have been reported previously in the primary publication of this study (23). In brief, responses were assessed according to the modified International Working Group criteria for AML (31) and disease progression was defined per European LeukemiaNet criteria (32). Transfusion independence was defined as at least 56 consecutive days with no transfusion of either red blood cells (RBCs) or platelets between the first and last day of treatment.

Safety evaluations were performed throughout the study in all patients who received at least 1 dose of either venetoclax or placebo (in combination with azacitidine). Adverse events (AEs) were graded according to the National Cancer Institute Common Terminology Criteria for Adverse Events Version 4.03. AEs were defined as those occurring between the first dose of study drug until 30 days after discontinuation of treatment.

Statistical analyses

Baseline characteristics and treatment outcomes are descriptive for this subgroup analysis.

The data cutoff for the Japanese subgroup analysis presented here was 4 January 2020, the same cutoff used for the primary analysis of VIALE-A. The efficacy analyses were performed on the full analysis set, which included the intent-to-treat population who underwent randomization. Safety analyses were performed in all patients who received at least 1 dose of study drug (venetoclax or placebo, in combination with azacitidine).

Power and sample size determinations for the global phase 3 study have been reported previously (23). OS distribution was estimated using the Kaplan–Meier methodology, and comparisons between treatment arms used the log-rank test stratified by age and cytogenetic risk. The HR between the treatment groups was estimated with the Cox proportional hazards model with the same stratification factors. Response rates and transfusion independence outcomes were compared between treatment arms using the Cochran–Mantel–Haenszel test, with age and cytogenetic risk as stratification factors. The 95% CIs were determined with the Clopper–Pearson exact method.

Results

Patients

Between 6 February 2017 and 31 May 2019, of the 48 patients screened in Japan from 15 sites, 37 (77%) were randomized to the study arms, including 24 patients assigned to venetoclax-azacitidine and 13 to placebo-azacitidine. A total of 19 patients (10 venetoclax-azacitidine and 9 placebo-azacitidine) discontinued study, all because of death. Death was related to disease progression in 84.2% (16/19) of cases.

Patient demographics and baseline characteristics of the Japanese subgroup are summarized in Table 1. The proportion of patients ≥75 years of age was higher in the venetoclax-azacitidine arm than in the placebo-azacitidine arm (79 and 69%, respectively). The venetoclax-azacitidine arm also had a higher proportion of patients with ECOG performance status 0 or 1 (75 and 62%) and intermediate-risk cytogenetics (75 and 69%). On the other hand, more patients in the placebo-azacitidine arm had ≥50% blasts in bone marrow (54 and 42%, respectively) and baseline grade 3 or 4 neutropenia (92 and 79%). The main reason for ineligibility to receive intensive chemotherapy was advanced age (≥75 years) in both treatment arms (79% with venetoclax-azacitidine and 69% with placebo-azacitidine). In general, no significant differences in baseline characteristics were observed between the venetoclax-azacitidine and placebo-azacitidine arms.

Efficacy

At a median follow-up of 16.3 months (range, 1.0–20.3) median OS was not reached (NR) in the venetoclax-azacitidine arm (95% CI: 10.6, NR) and was 8.6 months (95% CI: 2.7, NR) in the placebo-azacitidine arm, with a stratified Cox proportional HR of 0.41 (95%

Table 1. Patient demographics and baseline characteristics

Characteristic	Venetoclax-azacitidine (*n* = 24)	Placebo-azacitidine (*n* = 13)
Age		
Median, years (range)	77.5 (68–85)	77.0 (67–86)
≥ 75 years, *n* (%)	19 (79.2)	9 (69.2)
Male, *n* (%)	14 (58.3)	9 (69.2)
AML type, *n* (%)		
De novo	20 (83.3)	10 (76.9)
Secondary	4 (16.7)	3 (23.1)
Secondary AML type, *n*/*N* (%)		
Prior MDS or CMML	3/4 (75.0)	3/3 (100)
Treatment-related AML	1/4 (25.0)	0/3
ECOG performance status, *n* (%)		
0 or 1	18 (75.0)	8 (61.5)
2 or 3	6 (25.0)	5 (38.5)
Blast count, *n* (%)		
< 30%	7 (29.2)	4 (30.8)
≥ 30% to <50%	7 (29.2)	2 (15.4)
≥ 50%	10 (41.7)	7 (53.8)
AML with myelodysplasia-related changes, *n* (%)	9 (37.5)	5 (38.5)
Cytogenetic risk, *n* (%)		
Intermediate	18 (75.0)	9 (69.2)
Poor	6 (25.0)	4 (30.8)
Somatic mutations, *n*/*N* (%)		
IDH1 or *IDH2*	6/21 (28.6)	4/13 (30.8)
FLT3	2/23 (8.7)	2/12 (16.7)
NPM1	0/14	6/9 (66.7)
TP53	2/14 (14.3)	0/9
Baseline Grade 3 or 4 cytopenias, *n* (%)		
Neutropenia	19 (79.2)	12 (92.3)
Grade 3	3 (12.5)	3 (23.1)
Grade 4	16 (66.7)	9 (69.2)
Anemia	8 (33.3)	5 (38.5)
Thrombocytopenia	7 (29.2)	4 (30.8)
Baseline transfusion dependence,[a] *n* (%)		
RBCs	2 (8.3)	2 (15.4)
Platelets	0	1 (7.7)
≥2 reasons for ineligibility to receive intensive therapy,[b] *n* (%)	8 (33.3)	7 (53.8)

[a]Baseline transfusion dependence defined as RBC or platelet transfusion within 8 weeks prior to the first dose of study drug or randomization.
[b]Patients could report more than 1 reason.
Abbreviations: AML, acute myeloid leukemia; CMML, chronic myelomonocytic leukemia; ECOG, Eastern Cooperative Oncology Group; *FLT3*, fms-like tyrosine kinase 3; *IDH*, isocitrate dehydrogenase; MDS, myelodysplastic syndrome; *NPM1*, nucleophosmin; RBC, red blood cell; TP53, tumor protein 53.

CI: 0.15, 1.11; Fig. 1). The estimated OS was 67% (95% CI: 44.3, 81.7) with venetoclax-azacitidine and 46% (95% CI: 19.2, 69.6) with placebo-azacitidine at 12 months, and 57% (95% CI: 33.9, 74.1) and 31% (95% CI: 6.5, 60.2), respectively, at 18 months.

Response rates and event-free survival (EFS) are shown in Fig. 2. Rates of CR and CR + CRi were higher in the venetoclax-azacitidine arm than in the placebo-azacitidine arm, with 67% of patients assigned to venetoclax-azacitidine and 15% of patients assigned to placebo-azacitidine achieving CR + CRi (Fig. 2a). The median time to first response (CR or CRi) was 1.2 months (range, 0.8–2.9) for venetoclax-azacitidine and 3.1 months (range, 3.0–3.2) for placebo-azacitidine. Half of the patients in the venetoclax-azacitidine arm achieved CR + CRi by the start of Cycle 2 compared with no patients in the placebo-azacitidine arm. The addition of venetoclax to azacitidine also resulted in a significant improvement in EFS [16.3 months (95% CI: 7.9, NR)] compared with 3.4 months (95% CI: 1.5, 14.5) with placebo-azacitidine (HR, 0.229; 95% CI: 0.088, 0.596 and $P = 0.001$; Fig. 2b).

Sixteen patients (67%; 95% CI: 45, 84) receiving venetoclax-azacitidine and 2 patients (15%; 95% CI: 2, 45) receiving placebo-azacitidine achieved post-baseline RBC and platelet transfusion independence while on treatment (Fig. 3). The median duration of RBC and platelet transfusion independence was 122 days (range, 57–557) for venetoclax-azacitidine, and 328 days (range, 312–344) for placebo-azacitidine. RBC transfusion independence was achieved in 75% of patients in the venetoclax-azacitidine arm (95% CI: 53.3, 90.2) and 23% in the placebo-azacitidine arm (95% CI: 5.0, 53.8). Platelet transfusion independence was achieved in 79% of patients in the venetoclax-azacitidine arm (95% CI: 57.8, 92.9) and 31% in the placebo-azacitidine arm (95% CI: 9.1, 61.4). The median number of post-baseline RBC transfusions was 11 (range, 2–47) and 8 (range, 2–45) in the venetoclax-azacitidine and placebo-azacitidine arms, respectively, with a median number of post-baseline platelet transfusions of 11 (range, 1–69) and 15 (range, 1–66) for each arm, respectively. One of 2 patients who were RBC transfusion dependent at baseline

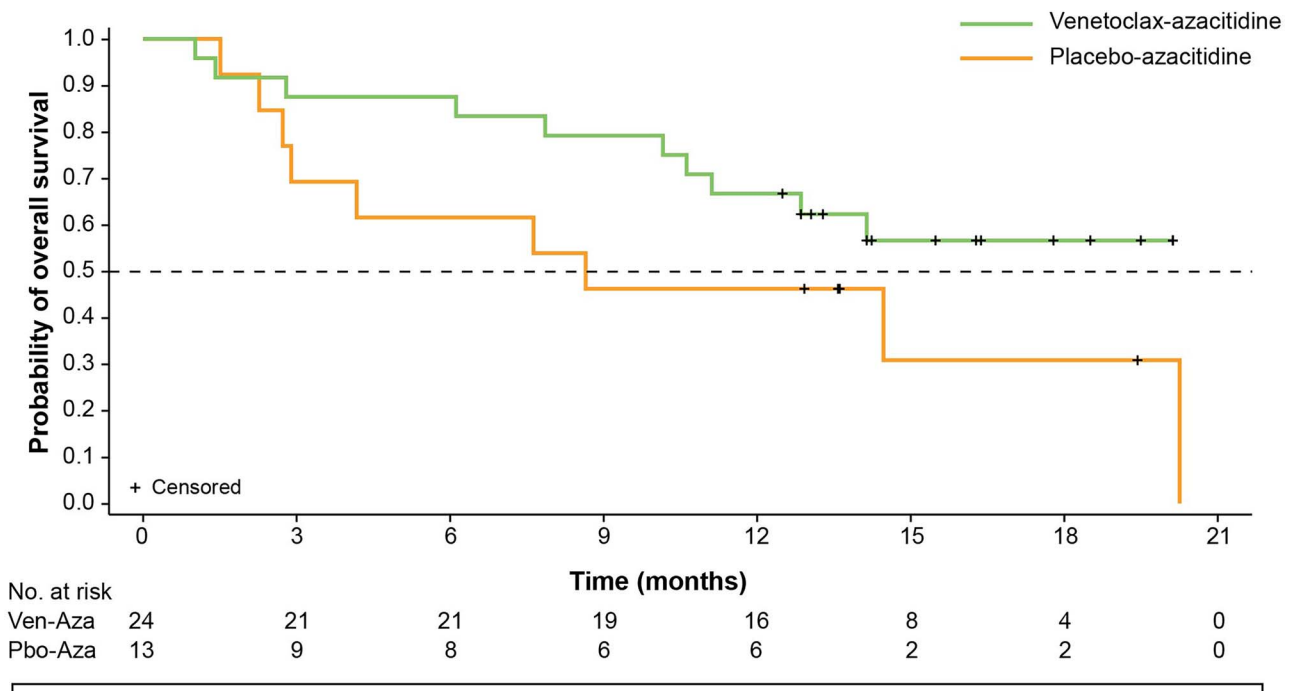

	Events	Survival estimate (%) (95% CI) Month 12	Month 18	Median (months) (95% CI)	Log-rank *P*-value	Cox proportional HR (95% CI)[a]
Ven-Aza (N = 24)	10	66.7 (44.3, 81.7)	56.6 (33.9, 74.1)	NR (10.6, NR)	0.070	0.41 (0.15, 1.11)
Pbo-Aza (N = 13)	9	46.2 (19.2, 69.6)	30.8 (6.5, 60.2)	8.6 (2.7, NR)		

Figure 1. OS by treatment arm. [a]Stratified by age (18 to <75, ≥75 years) and cytogenetic risk (intermediate, poor). Aza, azacitidine; CI, confidence interval; HR, hazard ratio; NR, not reached; OS, overall survival; Pbo, placebo; Ven, venetoclax.

became transfusion independent during treatment with venetoclax-azacitidine, whereas neither of the 2 transfusion-dependent patients assigned to placebo-azacitidine achieved transfusion independence. Only 1 patient was dependent on platelet transfusions at baseline and remained transfusion dependent during treatment with placebo-azacitidine.

Safety

Median duration of exposure to venetoclax/placebo was longer in the venetoclax-azacitidine arm than in the placebo-azacitidine arm [12.3 months (range, 0.9–20.0) and 1.8 months (range, 0.5–13.9)], respectively. Patients received a median of 8 treatment cycles (range, 1–19) with venetoclax-azacitidine and 2 treatment cycles (range, 1–15) with placebo-azacitidine. The most frequent reason for discontinuation of study drug within the placebo-azacitidine arm was disease progression.

All patients reported at least 1 AE of any grade. Table 2 summarizes AEs reported in ≥20% of patients in either treatment arm. The most common Grade ≥3 AEs (venetoclax-azacitidine and placebo-azacitidine, respectively) were mainly hematologic, including febrile neutropenia (79 and 39%), thrombocytopenia (50 and 77%), neutropenia (38 and 23%), leukopenia (33 and 31%) and anemia (21 and 15%; Table 2). Grade ≥3 pneumonia was observed in 21% of patients in the venetoclax-azacitidine arm and 15% of patients in the placebo-azacitidine arm. The most common nonhematologic AEs (any grade; venetoclax-azacitidine and placebo-azacitidine, respectively) included decreased appetite (54 and 31%), constipation (54 and 54%), diarrhea (46 and 46%), vomiting (42 and 23%) and nausea (38 and 31%; Table 2).

Serious AEs were reported in 67% of patients treated with venetoclax-azacitidine and 31% of patients treated with placebo-azacitidine; those occurring in ≥5% of patients in the venetoclax-azacitidine arm are summarized in Table 3. Serious AEs (venetoclax-azacitidine and placebo-azacitidine, respectively) included febrile neutropenia (42 and 0%), neutropenia (17 and 0%), pneumonia (13 and 8%) and leukopenia (8 and 0%). All patients were hospitalized to receive TLS prophylaxis and for monitoring, per protocol; no cases of TLS were reported in either treatment arm. To prevent the occurrence of clinically relevant infections, 79% of patients in the venetoclax-azacitidine arm and 77% of patients in the placebo-azacitidine arm received anti-infection prophylaxis.

AEs led to treatment discontinuation in 4 patients: 2 (8%) patients in the venetoclax-azacitidine arm (1 patient with Grade 4 febrile neutropenia and 1 with celiac artery occlusion leading to death), and 2 (15%) patients in the placebo-azacitidine arm [1 patient with Grade 3 fatigue and Grade 4 neutropenia and 1 patient with Grade 4 acute kidney injury (AKI)]. AEs led to venetoclax/placebo dose interruptions in 16 (67%) patients receiving venetoclax-azacitidine most commonly due to febrile neutropenia (n = 9), neutropenia (n = 6) and infection (n = 6), and in 4 (31%) patients treated with placebo-azacitidine due to febrile neutropenia and thrombocytopenia (n = 1), neutropenic enterocolitis and heart failure (n = 1), AKI (n = 1) and pneumonia (n = 1).

Death within 30 days of starting study treatment occurred in 1 (4%) patient treated with venetoclax-azacitidine (due to celiac artery occlusion) and in no patients treated with placebo-azacitidine. There were no deaths due to febrile neutropenia in either arm of the study.

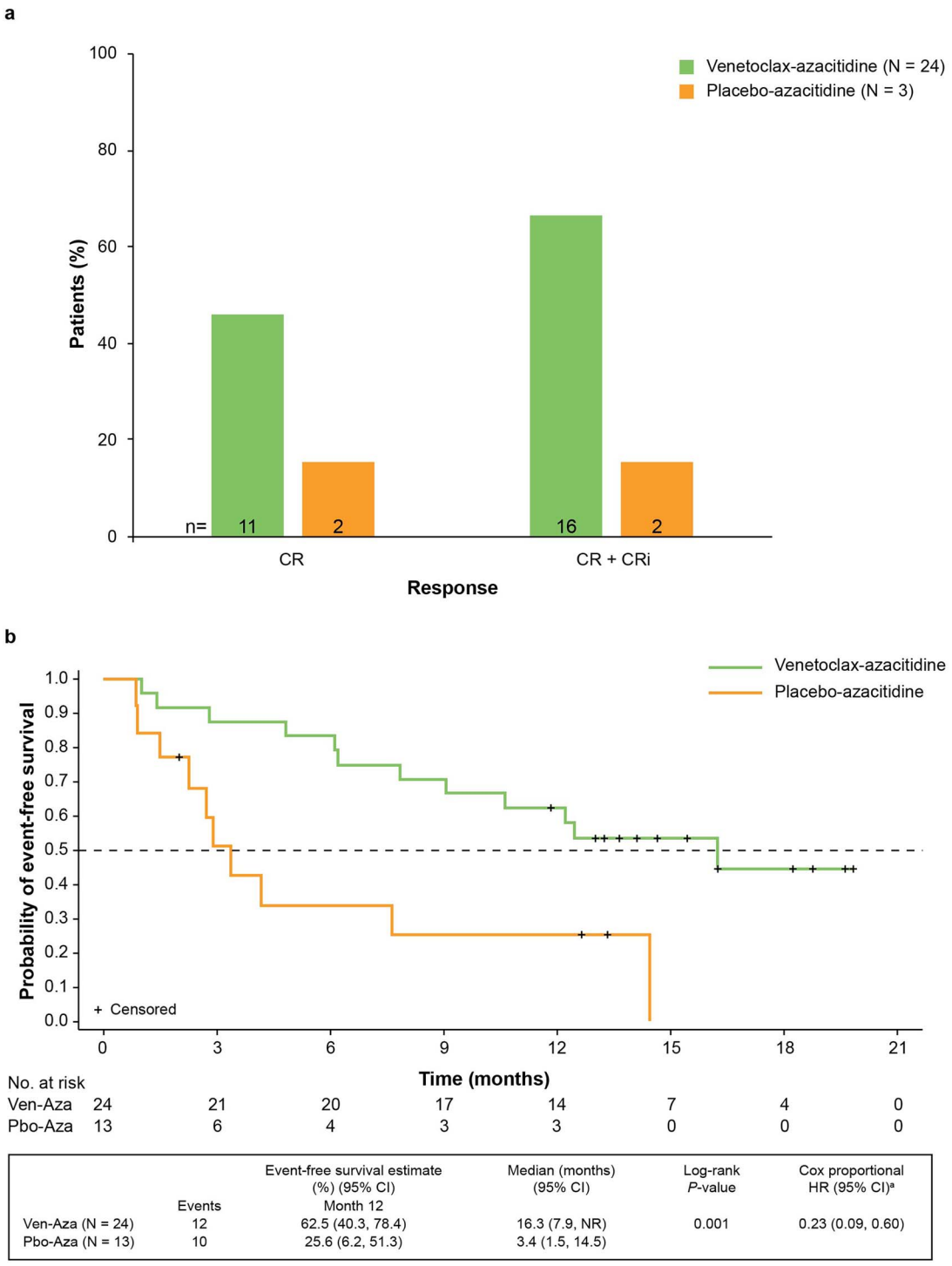

	Events	Event-free survival estimate (%) (95% CI) Month 12	Median (months) (95% CI)	Log-rank *P*-value	Cox proportional HR (95% CI)[a]
Ven-Aza (N = 24)	12	62.5 (40.3, 78.4)	16.3 (7.9, NR)	0.001	0.23 (0.09, 0.60)
Pbo-Aza (N = 13)	10	25.6 (6.2, 51.3)	3.4 (1.5, 14.5)		

Figure 2. Rates of CR and CR+CRi (a), and investigator-assessed event-free survival (b). [a]Stratified by age (18 to <75, ≥75 years) and cytogenetic risk (intermediate, poor). Aza, azacitidine; CI confidence interval; CR, complete response; CRi, CR with incomplete blood count recovery; HR, hazard ratio; Pbo, placebo; Ven, venetoclax.

Discussion

This analysis in the Japanese subgroup of the VIALE-A trial in patients with untreated AML ineligible for intensive chemotherapy demonstrated similar efficacy and safety outcomes as were seen in the overall population, despite the shorter median follow-up period for the Japanese subgroup analysis [16.3 vs 20.5 months (23)]. Importantly, no AEs specific to Japanese patients were observed.

Specifically, the median OS in the Japanese subgroup (NR with venetoclax-azacitidine and 8.6 months with placebo-azacitidine) was consistent with that in the overall population, where the median OS was 14.7 and 9.6 months, respectively. The composite CR + CRi rates for the Japanese subgroup (67 and 15%, respectively), were also consistent with the response outcomes in the overall population (66 and 28%, respectively; $P < 0.001$), which included patients from the USA, Europe, China, Japan and the rest of the world.

Table 2. Adverse events reported in ≥20% of patients in either arm

	Venetoclax-azacitidine (*n* = 24)		Placebo-azacitidine (*n* = 13)	
AE, *n* (%)	**Any grade**	**Grade ≥3**	**Any grade**	**Grade ≥3**
Any	24 (100)	24 (100)	13 (100)	12 (92.3)
Hematologic events	23 (95.8)	23 (95.8)	11 (84.6)	11 (84.6)
Thrombocytopenia	13 (54.2)	12 (50.0)	10 (76.9)	10 (76.9)
Neutropenia	9 (37.5)	9 (37.5)	3 (23.1)	3 (23.1)
Febrile neutropenia	19 (79.2)	19 (79.2)	5 (38.5)	5 (38.5)
Grade 3		18 (75.0)		5 (38.5)
Grade 4		1 (4.2)		0
Anemia	5 (20.8)	5 (20.8)	3 (23.1)	2 (15.4)
Leukopenia	8 (33.3)	8 (33.3)	4 (30.8)	4 (30.8)
Disseminated intravascular coagulation	1 (4.2)	1 (4.2)	3 (23.1)	0
Nonhematologic events				
Pneumonia	6 (25.0)	5 (20.8)	2 (15.4)	2 (15.4)
Nausea	9 (37.5)	1 (4.2)	4 (30.8)	0
Constipation	13 (54.2)	0	7 (53.8)	0
Diarrhea	11 (45.8)	1 (4.2)	6 (46.2)	1 (7.7)
Vomiting	10 (41.7)	0	3 (23.1)	0
Stomatitis	10 (41.7)	0	2 (15.4)	0
Decreased weight	6 (25.0)	1 (4.2)	1 (7.7)	0
Increased alanine aminotransferase	5 (20.8)	2 (8.3)	1 (7.7)	1 (7.7)
Hypokalemia	6 (25.0)	4 (16.7)	4 (30.8)	3 (23.1)
Pyrexia	7 (29.2)	0	4 (30.8)	0
Fatigue	1 (4.2)	0	1 (7.7)	1 (7.7)
Decreased appetite	13 (54.2)	1 (4.2)	4 (30.8)	1 (7.7)
Insomnia	6 (25.0)	0	1 (7.7)	0
Malaise	8 (33.3)	0	1 (7.7)	0

Abbreviation: AE, adverse event.

Table 3. Serious adverse events (any grade) occurring in ≥5% of patients

Serious AE, *n* (%)	Venetoclax-azacitidine (*n* = 24)	Placebo-azacitidine (*n* = 13)
Any	16 (66.7)	4 (30.8)
Febrile neutropenia	10 (41.7)	0
Neutropenia	4 (16.7)	0
Leukopenia	2 (8.3)	0
Pneumonia	3 (12.5)	1 (7.7)

*Abbreviation:*AE, adverse event.

Also, the higher rate of response for patients in the venetoclax-azacitidine arm in the Japanese subgroup analysis, compared with those in the placebo-azacitidine arm, correlated with a greater incidence of post-baseline transfusion independence (RBC + platelet: 67 and 15%, respectively). Responses were also reached earlier with venetoclax-azacitidine compared with placebo-azacitidine (median time to first response 1.2 and 3.1 months, respectively), with half of the patients in the venetoclax-azacitidine arm achieving a response by the start of Cycle 2.

The difference in median EFS between treatment groups was more marked in the Japanese subgroup (16.3 months with venetoclax-azacitidine and 3.4 months with placebo-azacitidine) than in the overall population (9.8 and 7.0 months, respectively). Therefore, these results support that the addition of venetoclax to HMA therapy improves the currently dismal outcomes achieved in elderly Japanese patients with AML treated with HMAs alone (11–13).

The median duration of exposure to venetoclax treatment was longer in the Japanese subgroup (12.3 months) compared with the overall population (7.6 months). Japanese patients randomized to placebo-azacitidine however, received a median of 2 treatment cycles (median duration of exposure 1.8 months), compared with a median of 4.5 treatment cycles for the overall population. Due to the double-blind design of this trial, early treatment discontinuation was at investigator discretion on the basis of lack of response, and a Japanese-specific signature cannot be confirmed.

However, the safety profile of venetoclax-azacitidine in the Japanese subgroup was consistent with safety data from the overall study population and with previous reports on the use of venetoclax in AML (22), with the most common AEs associated with venetoclax-azacitidine being hematologic or gastrointestinal. The incidence of grade 3 or 4 febrile neutropenia was higher in Japanese patients across treatment groups (79% with venetoclax-azacitidine and 39% with placebo-azacitidine) compared with the

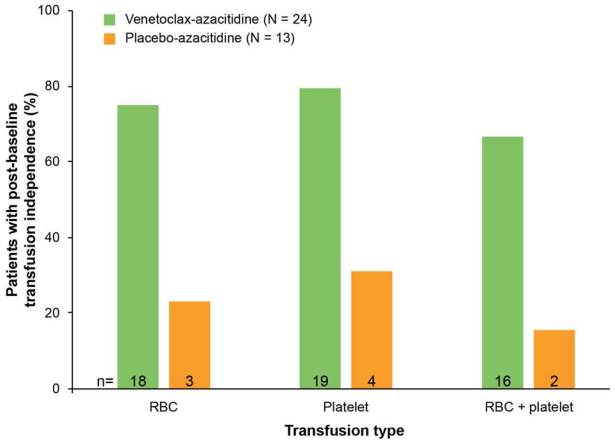

Figure 3. Proportion of patients with post-baseline transfusion independence. Transfusion independence was defined as a period of 56 days or more without transfusion. RBC, red blood cell.

overall population (42% with venetoclax-azacitidine and 19% with placebo-azacitidine). Notably, rates of infection and treatment discontinuation or death due to febrile neutropenia were similar in the Japanese and overall populations (23). These results suggest that febrile neutropenia was manageable with appropriate monitoring and intervention, including with venetoclax dose interruptions and the use of granulocyte-colony stimulating factor (G-CSF) per investigator discretion (28).

Some key differences in baseline characteristics were noted between the overall population and the Japanese subgroup, including a preponderance of patients ≥75 years of age (Japanese subgroup and overall population, 76 and 61%, respectively), with ECOG performance status of 0 or 1 (70 and 55%), with intermediate-risk cytogenetics (73 and 63%), and with baseline Grade 3 or 4 neutropenia (84 and 69%).

Venetoclax pharmacokinetics in patients with AML have been described using a population pharmacokinetics model (33). Although Asian patients had 67% higher relative bioavailability of venetoclax compared with non-Asian patients, the range of venetoclax exposures (area under the plasma concentration-time curve at steady state) was similar in the two groups. Covariate analysis to evaluate the relationship between venetoclax exposure and safety in patients with previously untreated AML identified that Asian patients were more likely to have treatment-emergent Grade ≥3 neutropenia regardless of treatment with placebo or venetoclax in combination with an HMA. However, the predicted net effect of venetoclax on treatment-emergent Grade ≥3 neutropenia was similar both for Asian and non-Asian patients (33).

Importantly, the safety and efficacy results with venetoclax-azacitidine described here were also generally similar to those reported in a phase 1/2 trial in Japan that enrolled 6 elderly (≥75 years) patients with untreated relapsed/refractory AML [NCT02265731; (34)]. With a median exposure time to venetoclax of 12.3 months in this study and 10.3 months in the phase 1/2 study, the majority of patients in both studies experienced at least 1 Grade ≥3 treatment-emergent AE (phase 3, 100%; phase 1/2, 83%), of which the most common were hematologic (phase 3: febrile neutropenia [79%], thrombocytopenia [50%], neutropenia [38%]; phase 1/2: lymphopenia [67%], febrile neutropenia [67%], thrombocytopenia [50%] and leukopenia [50%]). Equal proportions of patients in both studies experienced serious AEs (67%). Of note, the CR rates in Japanese patients in the VIALE-A study are higher than the reported rates with LDAC, the current standard of care in Japan for elderly patients with poor-risk cytogenetics (6,8).

The small number of patients analyzed (n = 37) in this investigation of a geographic population is a limitation of this study. Nevertheless, the data indicate that venetoclax-azacitidine was effective with an expected (similar to that of the overall population) and manageable safety profile in the Japanese subgroup of VIALE-A.

The combination of venetoclax and azacitidine could be considered a first-line standard of care for Japanese patients with previously untreated AML who are not candidates for intensive induction therapy.

Acknowledgments

AbbVie and the authors thank all the trial investigators and the patients who participated in this clinical trial. Medical writing support was provided by Rebecca Crepeau, PhD from Aptitude Health, Atlanta, GA, USA, and funded by AbbVie.

Funding

Venetoclax is being developed in a collaboration between AbbVie and Genentech. AbbVie and Genentech funded this study (NCT02993523) and participated in the study design, research, analysis, data collection, interpretation of data, reviewing and approval of the publication. All authors had access to relevant data and participated in the drafting, review and approval of this publication. No honoraria or payments were made for authorship.

Conflict of interest statements

Kazuhito Yamamoto has received honoraria from Chugai, Eisai, Mundipharma and Takeda, and has received research funding from AbbVie, Celgene, Chugai, Eisai, Incyte/IQVIA, SymBio and Zenyaku. **Atsushi Shinagawa** and **Ilseung Choi** declare that they have no conflicts of interest. **Courtney D. DiNardo** has received institutional research support from AbbVie, Agios, Bayer, Calithera, Celgene, Bristol-Myers Squibb, Cleave and Daiichi Sankyo, and has served as a consultant and on advisory boards for AbbVie, Agios, Celgene, Bristol-Myers Squibb, Daiichi Sankyo, Immune-Onc, Novartis, Takeda and Notable Labs. **Keith W. Pratz** has served in a consulting/advisory role for AbbVie, Astellas Pharma, Boston BioMedical, Bristol-Myers Squibb, Celgene and Jazz Pharmaceuticals, and has received research funding from AbbVie, Agios, Daiichi Sankyo and Millennium. **Kenichi Ishizawa** has received research funding from Novartis, AbbVie, Bayer and SymBio, and has served on a speakers' bureau for Celgene, Chugai, Eisai, Novartis, Ono Pharmaceutical and Takeda. **Toshihiro Miyamoto** has received honoraria from AbbVie, Amgen KK, Astellas Pharma, Bristol-Myers Squibb, Celgene, Merck Sharp & Dohme, Otsuka Pharmaceutical and Takeda. **Norio Komatsu** has received research funding from Bristol-Myers Squibb KK, Chugai, Fujifilm Wako Pure Chemical Industries, Fuso Pharmaceutical, Kyowa Kirin, Novartis Pharma KK, Otsuka Pharmaceutical, Pfizer Japan, PharmaEssentia Japan KK, Shire Japan KK, Sumitomo Dainippon Pharma and Takeda, and has received advisory fees from AbbVie GK, Celgene KK, Japan Tobacco Inc., Novartis KK, Otsuka Pharmaceutical, PharmaEssentia Japan KK and Shire Japan KK, and has served on speakers' bureaus

for Novartis KK, Shire Japan KK and Takeda, and as a member of safety assessment committee in the M13–834 clinical trial. **Yasuhiro Nakashima** has received research funding from AbbVie GK, Amgen KK, Astellas Pharma, Celgene and Novartis, and has received honoraria from Amgen KK. **Chikashi Yoshida** has received honoraria from AbbVie GK, Astellas Pharma, Bristol-Myers Squibb, Daiichi Sankyo, Janssen Pharmaceutical KK, Meiji Seika Pharma, Nippon Shinyaku, Novartis KK and Otsuka Pharmaceutical. **Noriko Fukuhara** has received research funding from AbbVie, Bayer, Eisai, Gilead Sciences, Ono Pharmaceutical and Solasia Pharma, and has received honoraria from Chugai and Kyowa Kirin. **Kensuke Usuki** has received research funding from AbbVie, Apellis Pharmaceuticals, Astellas-Amgen-Biopharma, Astellas Pharma, Bristol-Myers Squibb, Celgene, Chugai, Daiichi Sankyo, Gilead, Janssen Pharmaceuticals, Kyowa Kirin, Mundipharma, Nippon Boehringer Ingelheim, Nippon Shinyaku, Novartis Pharma KK, Ono Pharmaceutical, Otsuka Pharmaceutical, Pfizer, Sumitomo Dainippon Pharma, SymBio and Takeda, and has served on a speakers' bureau for Astellas Pharma, Bristol-Myers Squibb, Celgene, Daiichi Sankyo, Eisai, Kyowa Kirin, Merck Sharp & Dohme, Nippon Shinyaku, Novartis Pharma KK, Ono Pharmaceutical, Otsuka Pharmaceutical, PharmaEssentia, SymBio, Takeda and Yakult. **Takahiro Yamauchi** has received research funding from AbbVie, Astellas Pharma, Boehringer Ingelheim, Chugai, Janssen Pharmaceutical, Nippon Shinyaku, Ono Pharmaceutical, Otsuka Pharmaceutical, Pfizer, Solasia Pharma, Sumitomo Dainippon Pharma and Teijin Pharma. **Noboru Asada** has received honoraria from AbbVie, Astellas Pharma, Celgene, Chugai, Eisai, Kyowa Kirin, Novartis, Otsuka and Sanofi. **Norio Asou** has received research funding from AbbVie, Astellas Pharma, Chugai, Eisai and Sumitomo Dainippon Pharma, and has served on a speakers' bureau for Asahi Kasei, Fuji Pharma, Nippon Shinyaku and Sumitomo Dainippon Pharma, and has received honoraria from Nippon Shinyaku and Novartis. **Yasushi Miyazaki** has received honoraria from Astellas Pharma, Celgene, Chugai, Kyowa Kirin, Nippon Shinyaku, Novartis, Otsuka Pharmaceutical and Sumitomo Dainippon Pharma, and has received research funding from Chugai and Sumitomo Dainippon Pharma. **Hideyuki Honda**, **Sumiko Okubo**, **Misaki Kurokawa**, **Ying Zhou**, **Jiuhong Zha** and **Jalaja Potluri** are employees of AbbVie and may own stock. **Itaru Matsumura** has received research funding from Chugai, Eisai, Kyowa Kirin, Shionogi and Sumitomo Dainippon Pharma, and has served on a speakers' bureau for Astellas Pharma, Bristol-Myers Squibb, Daiichi Sankyo Janssen Pharmaceutical, Novartis, Otsuka Pharmaceutical and Pfizer.

Data sharing and data accessibility

AbbVie is committed to responsible data sharing regarding the clinical trials we sponsor. This includes access to anonymized, individual and trial-level data (analysis data sets), as well as other information (e.g. protocols and Clinical Study Reports), as long as the trials are not part of an ongoing or planned regulatory submission. This includes requests for clinical trial data for unlicensed products and indications.

These clinical trial data can be requested by any qualified researchers who engage in rigorous, independent scientific research and will be provided following review and approval of a research proposal and Statistical Analysis Plan (SAP) and execution of a Data Sharing Agreement (DSA). Data requests can be submitted at any time and the data will be accessible for 12 months, with possible extensions considered. For more information on the process, or to submit a request, visit the following link: https://www.abbvie.com/our-science/clinical-trials/clinical-trials-data-and-information-sharing/data-and-information-sharing-with-qualified-researchers.html.

References

1. Deschler B, Lübbert M. Acute myeloid leukemia: epidemiology and etiology. *Cancer* 2006;107:2099–107.
2. Miyawaki S. Clinical studies of acute myeloid leukemia in the Japan Adult Leukemia Study Group. *Int J Hematol* 2012;96:171–7.
3. Niino M, Matsuda T. Type distribution of myeloid leukemia from cancer incidence in five continents Vol. X. *Jpn J Clin Oncol* 2016;46:394.
4. Cancer Information Service. *Cancer Statistics in Japan; Table Download. 2. Incidence (National Estimates)*. https://ganjoho.jp/en/professional/statistics/table_download.html (4 August 2021, date last accessed).
5. Cancer Information Service. *Cancer Statistics in Japan; Table Download. 5. Survival*. https://ganjoho.jp/en/professional/statistics/table_download.html (4 August 2021, date last accessed).
6. Kiyoi H, Yamaguchi H, Maeda Y, Yamauchi T. JSH practical guidelines for hematological malignancies, 2018: I. Leukemia–1. Acute myeloid leukemia (AML). *Int J Hematol* 2020;111:595–613.
7. Kantarjian H, Ravandi F, O'Brien S, et al. Intensive chemotherapy does not benefit most older patients (age 70 years or older) with acute myeloid leukemia. *Blood* 2010;116:4422–9.
8. Tasaki T, Yamauchi T, Matsuda Y, et al. The response to induction therapy is crucial for the treatment outcomes of elderly patients with acute myeloid leukemia: single-institution experience. *Anticancer Res* 2014;34:5631–6.
9. Heuser M, Ofran Y, Boissel N, et al. Acute myeloid leukaemia in adult patients: ESMO clinical practice guidelines for diagnosis, treatment and follow-up. *Ann Oncol* 2020;31:697–712.
10. National Comprehensive Cancer Network. *NCCN Clinical Practice Guidelines in Oncology (NCCN Guidelines®). Acute Myeloid Leukemia*. Version 3.2021. 2020. https://www.nccn.org/professionals/physician_gls/pdf/aml.pdf (4 August 2021, date last accessed).
11. He PF, Zhou JD, Yao DM, et al. Efficacy and safety of decitabine in treatment of elderly patients with acute myeloid leukemia: a systematic review and meta-analysis. *Oncotarget* 2017;8:41498–507.
12. Dombret H, Seymour JF, Butrym A, et al. International phase 3 study of azacitidine vs conventional care regimens in older patients with newly diagnosed AML with >30% blasts. *Blood* 2015;126:291–9.
13. Kantarjian HM, Thomas XG, Dmoszynska A, et al. Multicenter, randomized, open-label, phase III trial of decitabine versus patient choice, with physician advice, of either supportive care or low-dose cytarabine for the treatment of older patients with newly diagnosed acute myeloid leukemia. *J Clin Oncol* 2012;30:2670–7.
14. Konopleva M, Pollyea DA, Potluri J, et al. Efficacy and biological correlates of response in a phase II study of venetoclax monotherapy in patients with acute myelogenous leukemia. *Cancer Discov* 2016;6:1106–17.
15. Fischer K, Al-Sawaf O, Bahlo J, et al. Venetoclax and obinutuzumab in patients with CLL and coexisting conditions. *N Engl J Med* 2019;380:2225–36.
16. Kumar S, Kaufman JL, Gasparetto C, et al. Efficacy of venetoclax as targeted therapy for relapsed/refractory t(11;14) multiple myeloma. *Blood* 2017;130:2401–9.
17. Moreau P, Chanan-Khan A, Roberts AW, et al. Promising efficacy and acceptable safety of venetoclax plus bortezomib and dexamethasone in relapsed/refractory MM. *Blood* 2017;130:2392–400.
18. Roberts AW, Davids MS, Pagel JM, et al. Targeting BCL2 with venetoclax in relapsed chronic lymphocytic leukemia. *N Engl J Med* 2016;374:311–22.
19. Seymour JF, Kipps TJ, Eichhorst B, et al. Venetoclax-rituximab in relapsed or refractory chronic lymphocytic leukemia. *N Engl J Med* 2018;378:1107–20.
20. Stilgenbauer S, Eichhorst B, Schetelig J, et al. Venetoclax in relapsed or refractory chronic lymphocytic leukaemia with 17p deletion: a

multicentre, open-label, phase 2 study. *Lancet Oncol* 2016;17:768–78.
21. Wei AH, Strickland SA Jr, Hou JZ, et al. Venetoclax combined with low-dose cytarabine for previously untreated patients with acute myeloid leukemia: results from a phase Ib/II study. *J Clin Oncol* 2019;37:1277–84.
22. DiNardo CD, Pratz K, Pullarkat V, et al. Venetoclax combined with decitabine or azacitidine in treatment-naive, elderly patients with acute myeloid leukemia. *Blood* 2019;133:7–17.
23. DiNardo CD, Jonas BA, Pullarkat V, et al. Azacitidine and venetoclax in previously untreated acute myeloid leukemia. *N Engl J Med* 2020;383:617–29.
24. Del Poeta G, Venditti A, Del Principe MI, et al. Amount of spontaneous apoptosis detected by Bax/Bcl-2 ratio predicts outcome in acute myeloid leukemia (AML). *Blood* 2003;101:2125–31.
25. Lagadinou ED, Sach A, Callahan K, et al. BCL-2 inhibition targets oxidative phosphorylation and selectively eradicates quiescent human leukemia stem cells. *Cell Stem Cell* 2013;12:329–41.
26. Bogenberger JM, Delman D, Hansen N, et al. Ex vivo activity of BCL-2 family inhibitors ABT-199 and ABT-737 combined with 5-azacytidine in myeloid malignancies. *Leuk Lymphoma* 2015;56:226–9.
27. Tsao T, Shi Y, Kornblau S, et al. Concomitant inhibition of DNA methyltransferase and BCL-2 protein function synergistically induce mitochondrial apoptosis in acute myelogenous leukemia cells. *Ann Hematol* 2012;91:1861–70.
28. VENCLEXTA® (venetoclax tablets). [prescribing information]. North Chicago, IL: AbbVie Inc.; 2020.
29. United Nations. Department of Economic and Social Affairs. *World Population Ageing*. 2017. https://www.un.org/en/development/desa/population/publications/pdf/ageing/WPA2017_Highlights.pdf (4 August 2021, date last accessed).
30. Arber DA, Orazi A, Hasserjian R, et al. The 2016 revision to the World Health Organization classification of myeloid neoplasms and acute leukemia. *Blood* 2016;127:2391–405.
31. Cheson BD, Bennett JM, Kopecky KJ, et al. Revised recommendations of the international working group for diagnosis, standardization of response criteria, treatment outcomes, and reporting standards for therapeutic trials in acute myeloid Leukemia. *J Clin Oncol* 2003;21:4642–9.
32. Döhner H, Estey E, Grimwade D, et al. Diagnosis and management of AML in adults: 2017 ELN recommendations from an international expert panel. *Blood* 2017;129:424–47.
33. Eckert D, Brackman D, Menon R, et al. Venetoclax exposure-efficacy and exposure-safety relationships in subjects with treatment-naïve acute myeloid leukemia who are ineligible for intensive chemotherapy. *Blood* 2020;136:52. https://doi.org/10.1182/blood-2020-136425.
34. Taniguchi S, Yamauchi T, Choi I, et al. Venetoclax in combination with azacitidine in Japanese patients with acute myeloid leukaemia: phase 1 trial findings. *Jpn J Clin Oncol* 2021;51:857–64.

Low-dose dasatinib in older patients with chronic myeloid leukaemia in chronic phase (DAVLEC): a single-arm, multicentre, phase 2 trial

Kazunori Murai, Hiroshi Ureshino, Takashi Kumagai, Hideo Tanaka, Kaichi Nishiwaki, Satoshi Wakita, Koiti Inokuchi, Toshihiro Fukushima, Chikashi Yoshida, Nobuhiko Uoshima, Toru Kiguchi, Masayuki Mita, Jun Aoki, Satoshi Kimura, Kaori Karimata, Kensuke Usuki, Joji Shimono, Yoshiaki Chinen, Junya Kuroda, Yasufumi Matsuda, Kensuke Nakao, Takaaki Ono, Katsumichi Fujimaki, Hirohiko Shibayama, Chisaki Mizumoto, Tomoharu Takeoka, Katsuhiro Io, Takeshi Kondo, Masatomo Miura, Yousuke Minami, Takayuki Ikezoe, Jun Imagawa, Ayako Takamori, Atsushi Kawaguchi, Junichi Sakamoto, Shinya Kimura

Lancet Haematol 2021; 8: e902–11

See **Comment** page e867

Department of Hematology, Iwate Prefectural Central Hospital, Morioka, Japan (K Murai MD); **Division of Hematology, Respiratory Medicine and Oncology, Department of Internal Medicine** (H Ureshino MD, Prof Sh Kimura MD), **and Education and Research Center for Community Medicine** (Prof A Kawaguchi PhD), **Faculty of Medicine, Saga University, Saga, Japan; Department of Hematology, Ome Municipal General Hospital, Ome, Japan** (T Kumagai MD); **Department of Hematology, Hiroshima City Asa Hospital, Hiroshima, Japan** (H Tanaka MD); **Division of Clinical Oncology and Hematology, Department of Internal Medicine, The Jikei University Kashiwa Hospital, Kashiwa, Chiba, Japan** (K Nishiwaki MD); **Department of Hematology, Nippon Medical School, Tokyo, Japan** (S Wakita MD, Prof K Inokuchi MD); **Department of Hematology and Immunology, Kanazawa Medical University, Kanazawa, Japan** (T Fukushima MD); **Department of Hematology, National Hospital Organization Mito Medical Center, Ibarakimachi, Japan** (C Yoshida MD); **Department of Hematology, Japanese Red Cross Kyoto Daini Hospital, Kyoto Japan** (N Uoshima MD); **Department of Hematology, Chugoku Central Hospital, Fukuyama, Japan** (T Kiguchi MD); **Department of Hematology, Shirakawa Kosei General Hospital, Shirakawa, Japan** (M Mita MD); **Department of Hematology, Yokohama City University**

Summary

Background ***BCR-ABL1*** **tyrosine kinase inhibitors (TKIs) are commonly initiated in older patients with chronic myeloid leukaemia in the chronic phase at standard doses. However, because of their safety profile in this population, appropriate therapy has not been established. We aimed to investigate whether a lower than standard dose of dasatinib was an appropriate therapy for older patients with chronic myeloid leukaemia in the chronic phase.**

Methods **DAsatinib, Very Low-dose, for Elderly CML-CP patients (DAVLEC) was a multicentre, single-arm, phase 2 trial done in 25 Japanese hospitals. We enrolled patients older than 70 years with newly diagnosed chronic myeloid leukaemia in the chronic phase, ECOG performance status 0–2, and no previous treatment for CML other than hydroxyurea within 4 weeks. Second-generation TKI dasatinib was given orally at a starting dose of 20% of the standard dose (20 mg/day). If the treatment was assessed as optimal response at 3 months, 6 months, and 9 months and adverse events were grade 2 or better (according to the NCI Common Toxicity Criteria v 4.0), the same dose was continued. If response was suboptimal and adverse events were grade 2 or better, the dose was increased by 20 mg/day. Once a dose reduction had been made because of a grade 3 or worse adverse event, there were no further dose increases. Treatment was discontinued if assessed as failure (disease progression to the accelerated phase or acute phase). The primary endpoint was the achievement of major molecular response at 12 months, assessed using a per-protocol analysis. This trial is registered at with the UMIN clinical trial registry, UMIN000024548, and has completed its planned observation period.**

Findings **Between Nov 1, 2016, and Oct 30, 2019, 52 patients received first-line dasatinib therapy at 20 mg/day. The median age at diagnosis was 77·5 years (73·5–83·0). 35 (67%) patients were male and 17 (33%) were female. 31 (60%) of 52 patients reached major molecular response at 12 months (one-sided 95% CI 48–71), with a median follow-up of 366 days (IQR 353–372). Grade 3–4 adverse events were reported in 12 (23%) patients. Neutropenia was the most frequent grade 3–4 adverse event, occurring in three (6%) patients. No treatment-related deaths were observed.**

Interpretation **Low-dose dasatinib at 20mg/day is worthy of consideration as a starting dose for older patients with newly diagnosed chronic myeloid leukaemia in the chronic phase. However, this dose needs to be further studied in a larger cohort and with a more ethnically diverse population.**

Funding **Bristol-Myers Squibb.**

Introduction

BCR-ABL1 tyrosine kinase inhibitors (TKIs) improves the life expectancy of patients with chronic myeloid leukaemia close to that of the general population.[1] Furthermore, some patients can discontinue TKIs without relapse.[2] The DASISION trial showed that patients newly diagnosed with CML in the chronic phase treated with the second-generation TKI dasatinib (100 mg/day) had significantly higher and faster rates of major molecular response than had patients treated with imatinib.[3] We reported that almost half of patients with chronic myeloid leukaemia in the chronic phase who had a sustained deep molecular response for at least 1 year could discontinue dasatinib without relapse [4,5]

More than 20% of patients with CML are older than 70 years.[6] Most older patients have comorbid health conditions and polypharmacy problems. Furthermore, comorbidity at diagnosis is strongly negatively correlated with overall survival in patients with CML patients.[7] TKIs are commonly initiated in older patients at standard dose. However, because of the safety concerns of TKIs in this population, the optimal therapy for older patients has not been established. The first-generation

Research in context

Evidence before this study

We searched PubMed and ClinicalTrials.gov, using the following search terms: "chronic myeloid leukaemia", "ABL tyrosine kinase inhibitor (TKI)", "dasatinib", "elderly", "older", "reduced" or "dose", for articles published between Jan 1, 2001, and Dec 1, 2020, in any language. We identified ten articles suggesting the appropriate dosage of dasatinib in older patients with chronic myeloid leukaemia in the chronic phase. These studies suggested that dasatinib dosing should be reduced in older patients, but findings were mainly based on retrospective studies and dose reduction was at most 50 mg/day, half the standard dose in prospective studies. No prospective studies examined the effect of 20 mg/day, 20% of the standard dose, in older patients with chronic myeloid leukaemia in the chronic phase.

Added value of this study

The first-generation TKI imatinib, associated with fewer cardiovascular complications and cheaper than second-generation TKIs, is often used for older patients with chronic myeloid leukaemia in the chronic phase. Because patients treated with second-generation TKIs including dasatinib had significantly improved overall survival and higher treatment-free remission rate than did patients treated with imatinib, dasatinib used at an appropriate dose was expected to provide a greater benefit than that of imatinib in older patients with chronic myeloid leukaemia in the chronic phase when used at an appropriate dose. In this study, dasatinib was given orally at 20% of the standard dose (20 mg/day). This starting dose was then optimised on the basis of activity and occurrence of adverse events. At 12 months, 31 (60%) patients had major molecular response, 14 (27%) a molecular response (MR) 4.0, and seven (13%) a MR4.5. Grade 3–4 adverse events were observed in 12 (23%) of 52 patients and pleural effusion was observed only in four patients. These findings showed that the treatment strategy of increasing or decreasing the dasatinib dose from a starting dose of 20 mg/day while monitoring therapeutic effects and adverse events was active and well tolerated in older patients with chronic myeloid leukaemia in the chronic phase.

Implications of all the available evidence

Our findings together with previous studies on reducing the dose of dasatinib suggest that the standard dose (100 mg/day) is not absolute and dasatinib should be used with an appropriate reduced dose in older patients with chronic myeloid leukaemia in the chronic phase.

TKI imatinib, associated with fewer cardiovascular complications than second-generation TKIs, is often used for older patients.[8] Even imatinib, however, raised safety issues, such as renal dysfunction and anaemia.[9] Patients treated with second-generation TKIs had significantly improved overall survival than did patients treated with imatinib.[10] Generally, a slightly lower dose of anticancer agent is selected than the dose that causes dose limiting toxicity. However, many molecularly targeted agents do not reach dose limiting toxicity and, in such cases, whether the dose selected in a clinical trial is truly optimal might be unclear. A reduced dose of 50 mg/day dasatinib was active in patients with chronic myeloid leukaemia in the chronic phase in a single-centre, phase 2 trial, suggesting that lower doses might be also effective.[11] A single-centre, retrospective study suggested that 20% of the standard dose of dasatinib (≤20 mg/day) was active and well tolerated for older patients with chronic myeloid leukaemia in the chronic phase.[12] However, evidence from single-centre results is insufficient. Additionally, in these studies the method of treatment was chosen on a case-by-case basis by each attending physician, therefore, insufficient evidence exists to generalise this finding to the treatment of older patients with CML.

Thus, we prospectively investigated the activity and safety of low-dose dasatinib in older patients with newly diagnosed chronic myeloid leukaemia in the chronic phase.

Methods

Study design and patients

We did a multicentre, single-arm, phase 2 study at 25 hospitals in Japan (appendix p 73). Patients were eligible if they were aged 70 years or older and had newly diagnosed chronic myeloid leukaemia in the chronic phase and did not received previous CML therapy other than hydroxyurea for a maximum of 1 month. Other eligibility criteria were an Eastern Cooperative Oncology Group (ECOG) performance status of 0–2, and adequate organ function. We adopted the European LeukemiaNet (ELN) 2013 criteria to define accelerated phase and blast phase CML.[13] To make the protocol as useful as possible for real-world clinical practice, the type of transcript was not examined because the frequency of non-b2a2 or b3a2 is low (approximately 1–2%) in Japanese patients[14] and the examination of transcript type is not covered by national insurance in Japan. Exclusion criteria were: (1) a history of treatment with TKI or interferon; (2) a history of the following significant or uncontrollable cardiovascular disorders or their complications including obvious pleural effusion, myocardial infarction within 6 months, angina pectoris within 3 months, congestive cardiac failure within 3 months, congenital QT prolongation syndrome, or QTc interval prolongation by 500 ms or more on 12-lead electrocardiogram; (3) second cancer; (4) hypersensitivity to dasatinib; and (5) being deemed ineligible for the study by the attending physician.

Medical Center, Yokohama, Japan (J Aoki MD); **Department of Hematology, Fukushima Medical University, Fukushima, Japan** (Sa Kimura MD, Prof T Ikezoe MD); **Department of Hematology, Heart Life Hospital, Nakagusuku, Japan** (K Karimata MD); **Department of Hematology, NTT Medical Center Tokyo, Japan** (K Usuki MD); **Department of Hematology, Asahikawa City Hospital, Asahikawa, Japan** (J Shimono MD); **Division of Hematology and Oncology, Department of Medicine, Kyoto Prefectural University of Medicine, Kyoto, Japan** (Y Chinen MD, Prof J Kuroda MD); **Department of Hematology and Oncology, University of Fukui, Fukui, Japan** (Y Matsuda MD); **Department of Hematology/Oncology, Shiga General Hospital, Moriyama, Japan** (K Nakao MD); **Divison of Hematology, Hamamatsu University School of Medicine, Hamamatsu, Japan** (T Ono MD); **Department of Hematology, Fujisawa City Hospital, Fujisawa, Japan** (K Fujimaki MD); **Osaka University Graduate School of Medicine, Department of Hematology and Oncology, Suita, Japan** (H Shibayama MD); **Division of Haematology and Immunology, Otsu Red Cross Hospital, Otsu, Japan** (C Mizumoto MD, T Takeoka MD); **Department of Hematology, Kansai Electric Power Hospital, Osaka, Japan** (K Io MD); **Blood Disorders Center, Aiiku Hospital, Sapporo, Japan** (T Kondo MD); **Department of Pharmacy, Akita University Hospital, Akita, Japan** (Prof M Miura PhD); **Department of Hematology, National Cancer Center Hospital East, Kashiwa, Japan** (Y Minami MD); **Department of Haematology and Oncology, Research Institute for Radiation Biology and Medicine, Hiroshima University, Hiroshima, Japan** (J Imagawa MD); **Clinical Research Center, Saga University Hospital, Saga, Japan** (A Takamori PhD); **Tokai Central Hospital, Kakamigahara, Japan** (Prof J Sakamoto MD)

Correspondence to:
Prof Shinya Kimura, Division of Hematology, Respiratory Medicine and Oncology, Department of Internal Medicine, Faculty of Medicine, Saga University, Saga, 849-8501, Japan
shkimu@cc.saga-u.ac.jp

See Online for appendix

This study was done according to the Declaration of Helsinki and was approved by Saga University and each participating hospital. All participants provided written informed consent. The study protocol is given in the appendix (pp 11–71).

Procedures

Patients received once-daily dasatinib started at a dose of 20 mg (Bristol-Myers Squibb, Princeton, NJ, USA). If the treatment effect was assessed as an optimal response (according to ELN criteria) at 3 months, 6 months, and 9 months, and adverse events were grade 2 or better (according to the NCI Common Toxicity Criteria for Adverse Events v 4.0), then treatment was continued without changing the dose. If the treatment effect was assessed as warning and adverse events were grade 2 or better, then the daily dose of dasatinib was increased by 20 mg per day. Once a dose reduction had been made because of a grade 3 or worse adverse event, the patient continued treatment at the same dose without further dose increases, even if the treatment effect was assessed as warning. If the treatment effect was assessed as failure, including disease progression to the accelerated phase or acute phase, then the protocol treatment was discontinued, and a more appropriate treatment was provided at the discretion of the attending physician. Administration of dasatinib was suspended if haematological toxicity of grade 3 or higher or non-haematological toxicity of grade 3 or higher were observed during all treatment periods. Treatment was resumed after recovery from toxicity by reducing the daily dose of dasatinib by 20 mg. If 20 mg/day dasatinib caused toxicity, then the frequency of administration was reduced to alternate-day administration of 20 mg, and if this regimen resulted in adverse events of grade 3 or worse, the protocol treatment was discontinued.

Quantification of *BCR-ABL1* mRNA in peripheral blood was measured using the *BCR-ABL1* mRNA international scale (IS) at a central laboratory (Bio Medical Laboratories, Tokyo, Japan) using a commercially available measurement kit, ODK1201 (Otsuka Pharmaceutical, Tokyo, Japan).[15] *ABL1* was used as housekeeping gene. A complete cytogenetic response MR2·0 was defined as a *BCR-ABL1* IS 1%, major molecular response (or MR3·0) as *BCR-ABL1* IS 0·1% or less, MR4·0 as *BCR-ABL1* IS 0·01% or less, and MR4·5

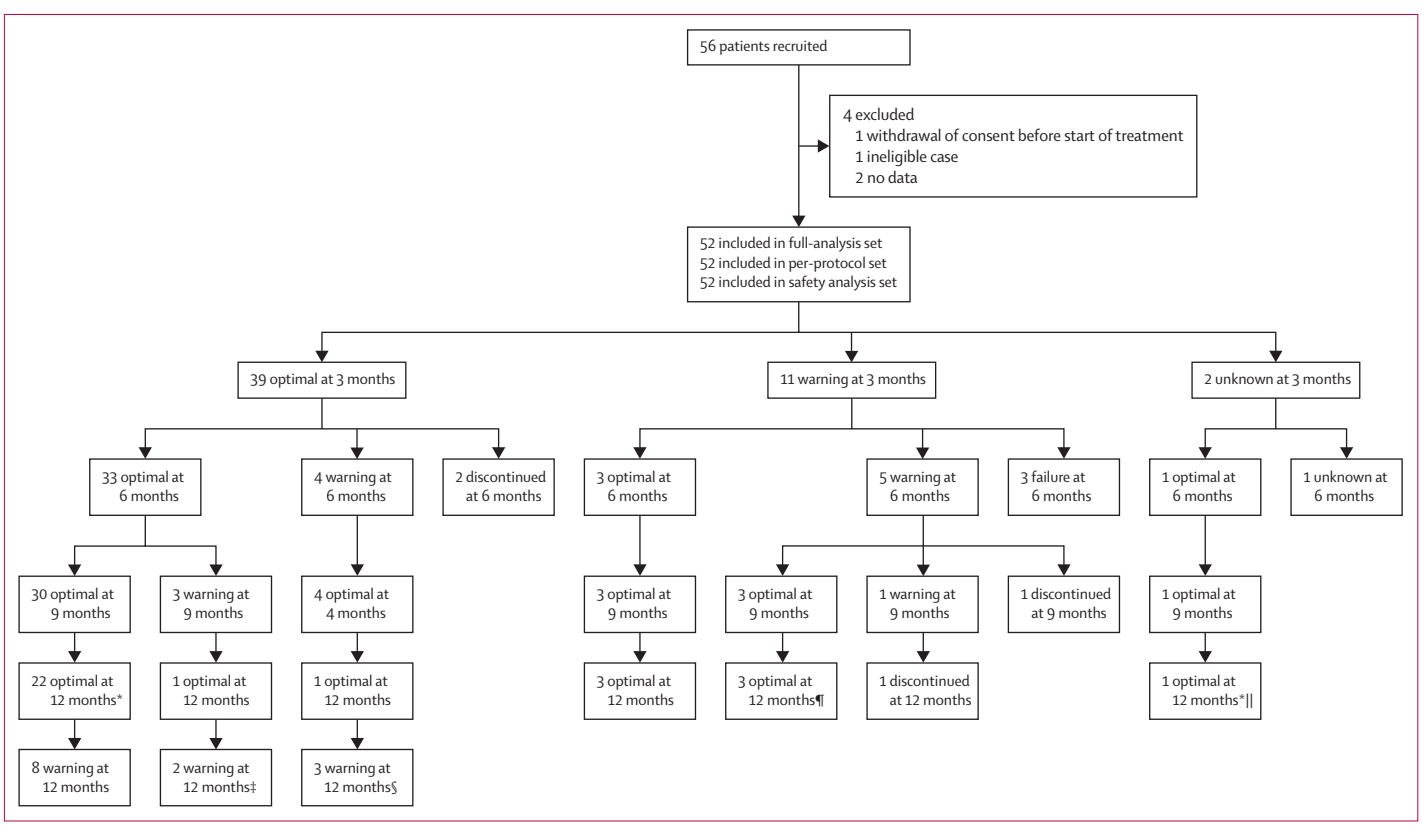

Figure 1: **Trial profile**

52 patients received 20 mg/day dasatinib as first-line therapy. *Continued treatment with dasatinib 20 mg/day alone. †One patient had optimal response at 3 months, but this patient did not achieve early molecular response. ‡One patient was unable to increase the dose of dasatinib at 9 months because of an adverse event. This patient received dasatinib 20 mg/day during the clinical trial. §One patient was unable to increase the dose of dasatinib at 6 months because of an adverse event. This patient received dasatinib 20 mg/day during the clinical trial. ¶One patient was unable to increase the dose of dasatinib at 6 months because of a medical condition. This patient received dasatinib 40 mg/day between 6 months and 12 months. ||One patient had missing data at 3 months. This patient reached major molecular response at 12 months with treatment with dasatinib 20mg.

as *BCR-ABL1* IS 0·0032% or less. Treatment activity was assessed at 3 months, 6 months, 9 months, and 12 months after treatment initiation (appendix p 1), as per ELN 2013 recommendations,[6,13] and was centrally reviewed. Because ELN 2013 does not stipulate criteria at 9 months, the criteria for assessing treatment effects at 6 months were followed at this timepoint. For adverse event monitoring, chest X-ray, electrocardiogram, and peripheral blood tests were done at 1 month, 3 months, 6 months, 9 months, and 12 months, and adverse events were assessed continuously from the time of signed informed consent until final follow-up date. Blood cell counts and immunophenotypic examinations were done as previously described.[4]

We assessed the halving time of *BCR-ABL1* IS at 3 months. It might be more accurate to use *BCR* as a control gene to calculate halving time[16] However, only ODK1201, which uses *ABL1* as a control gene, has been approved for use under national insurance in Japan. This kit was reported to accurately measure up to IS 144·6867%.[15] Therefore, we adopted the method reported by Fava and colleagues to calculate halving time using *ABL* as a control gene.[17]

Plasma samples were collected 2 h and 24 h after dasatinib administration at 1 month and 12 months for pharmacokinetic analysis to identify the minimum and maximum plasma concentrations of dasatinib. Dasatinib concentrations were measured by liquid chromatograph-tandem mass spectrometry analysis at Akita University, Akita, Japan.[18]

Failure to conduct drug administration, laboratory tests, and assessment of toxicity and activity in compliance with the protocol was regarded as protocol deviation. Protocol deviations falling under several of the following categories were regarded as a violation: (1) those affecting the assessment of the endpoints of the study, (2) those attributable to the investigator or study site, (3) those that were intentional or systematic, (4) those that were hazardous or considered tremendous deviation, (5) those that were clinically inappropriate. Deviations were defined as protocol deviations that were not considered violations or acceptable deviations. Acceptable deviations were defined as protocol deviations within the acceptable range defined for each study before or after the study between the study group or research representative or research secretariat and the data centre. Deviations in the acceptable range defined in advance were not listed in the monitoring report.

	Participants (n=52)
Age at enrolment, years	77·5 (73·5–83·0)
Sex	
Male	35 (67%)
Female	17 (33%)
ECOG performance status	
0	43 (83%)
1	8 (15%)
2	1 (2%)
Patients who received hydroxycarbamide	7 (4%)
Duration of hydroxycarbamide administration, days	0 (0–11·5)
BCR-ABL1 international scale	102·12% (88·73–126·00)
Sokal	
Low	2/49 (4%)
Intermediate	39/49 (80%)
High	8/49 (16%)
Hasford	
Low	12/49 (25%)
Intermediate	35/49 (71%)
High	2/49 (4%)
EUTOS	
Low	45/51 (88%)
High	6/51 (12%)
Comorbidity	
Yes	33 (63%)
Past medical history*	
Yes	38 (73%)
Medication for other conditions†	
Yes	47 (90%)

Data are n (%), n/N%, or median (IQR). All participants were Japanese. ECOG=Eastern Cooperative Oncology Group. EUTOS=European Treatment Outcome Study. *Patients who were not currently receiving treatment but had previous disease (appendix p 2). †Patients who were taking some medication for comorbidities (appendix p 2).

Table 1: **Baseline patient characteristics**

Outcomes

The primary endpoint of this study was achievement of major molecular response (MR3·0) at 12 months, as in the DASISION study.[3] Secondary endpoints were: (1) achievement of deep molecular response (MR4·0 or MR4·5) 12 months after treatment initiation; (2) incidence of all-grade adverse events or adverse events of grade 3 or 4; (3) treatment discontinuation due to adverse events during the 12-month treatment period; (4) treatment discontinuation due to disease progression or treatment failure during the 12 month treatment period; (5) association of CML prognostic scoring systems including Sokal score, Hasford score, and European Treatment and Outcome Study (EUTOS) score; (6) association of halving time of *BCR-ABL1* levelswith activity 3 months after treatment initiation; (7) association of the plasma concentration of dasatinib with treatment activity and adverse events; and (8) association of peripheral blood T cell and natural killer cell profiles with treatment activity and adverse events. No post-hoc or exploratory endpoints were considered in this study.

Statistical analysis

The initial sample size in this study was designed as follows. The major molecular response rate at 1 year in

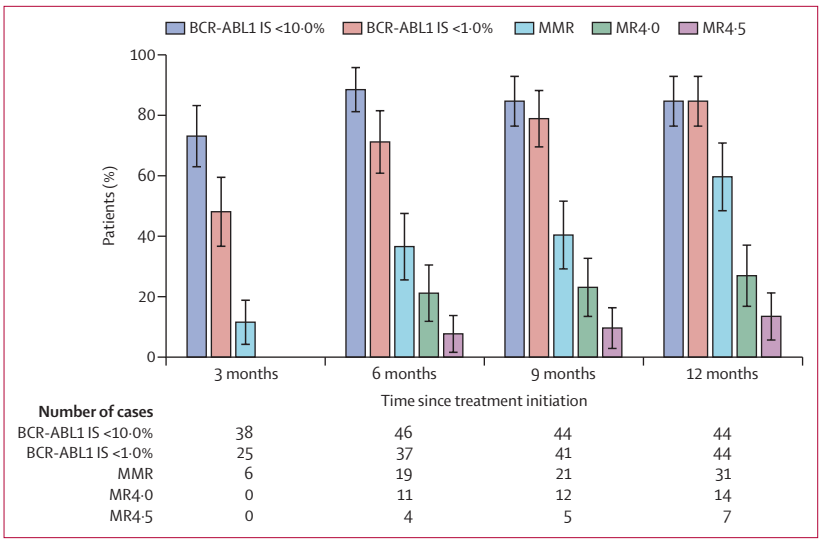

Number of cases	3 months	6 months	9 months	12 months
BCR-ABL1 IS <10·0%	38	46	44	44
BCR-ABL1 IS <1·0%	25	37	41	44
MMR	6	19	21	31
MR4·0	0	11	12	14
MR4·5	0	4	5	7

Figure 2: **Cumulative treatment response in eligible patients**
Error bars indicate one-sided 95% CIs. At 12 months, the estimated rate of complete cytogenetic response was 85% (95% CI 76–93), of MMR was 60% (48–71), of MR4·0 was 27% (17–37), and of MR4·5 was 14% (6–21). *BCR-ABL1* IS=*BCR-ABL1* international scale. MMR=major molecular response. MR4·0=*BCR-ABL1* IS 0·01% or lower. MR4·5=*BCR-ABL1* IS 0·0032% or lower.

the DASISION trial for first-line dasatinib at 100 mg per day was 46%.[3] On the basis of these data, we set the threshold major molecular response for older patients at 48%. We expected a slight improvement in the major molecular response rate and set the expected major molecular response at 53% as an alternative proportion. In the DASISION trial, the major molecular response rate with imatinib was 28% at 12 months, therefore, the non-inferiority margin was 10%, based on half of the major molecular response rate difference (38% [48% minus 10%] as null proportion). Under this condition, the number of patients required for normal approximation of binomial distribution with a significance level of 5% and power of 90% was calculated as 95. Additionally, taking dropouts due to protocol violations into consideration, the target number of patients to be enrolled was set at 100; however, no protocol deviations occurred.

However, the final sample size was recalculated due to ethical considerations, given that 1 year after starting this study, 13 (72%) of 18 patients had reached major molecular response. We used the Lee and Liu method[19] to calculate the predicted probabilities on the basis of these results. The predicted probability of non-inferiority of the major molecular response of the new treatment over the major molecular response of the standard treatment (38%) was assumed to be at least 95% when the expected number of patients was 50. This predicted probability value was greater than 0·99. This simulation led the effectiveness and safety committee to suggest that the number of patients recruited should be reduced to 50 for ethical reasons and this protocol amendment (Aug 15, 2019) was approved by the Saga University institutional review board.

The primary and secondary outcomes and safety were assessed in all patients who completed dasatinib treatment for 12 months. Patients for whom data necessary for analysis could not be obtained or who withdrew consent before treatment were excluded. For the primary endpoint, non-inferiority of major molecular response rate at 12 months and its one-sided 95% CI, estimated with the normal approximation, was considered to be established if the lower limit was shown to lie above the non-inferiority threshold of 38%. If the lower limit of the major molecular response was above not only the non-inferiority but also the superiority threshold of 48%, superiority was also considered to be established. For the baseline variables and secondary endpoints, Fisher's exact tests or Mann–Whitney tests were done. The significance level for the primary non-inferiority hypothesis test indicated one-sided 0·05 and for all other secondary endpoints indicated two-sided 0·05. Statistical analyses were done using SAS (version 9.4) and R (version 3.2.3). The study was registered in with the UMIN clinical trial registry, UMIN000024548.

Role of the funding source

The funder of the study had no role in study design, data collection, data analysis, data interpretation, or writing of the report.

Results

Between Nov 1, 2016, and Oct 30, 2019, 56 patients with newly diagnosed chronic myeloid leukaemia in the chronic phase were assessed for eligibility(figure 1). The first patient was enrolled on April 12, 2017. Median follow-up was 366 days (IQR 353–372).

Four (7%) patients withdrew their participation. 52 patients received 20 mg per day of dasatinib as first-line therapy (figure 1). The median age at diagnosis was 77·5 years (IQR, 73.5–83.0; table 1). 35 (67%) patients were male and 17 (33%) were female (table 1). Although 43 (83 %) of 52 patients had an ECOG performance status of 0, 38 (73%) patients had other illnesses before CML diagnosis, 33 (64%) patients had comorbidities at or after diagnosis of CML, and 47 (90%) patients needed to take medication regularly (appendix p 2). 44 (85%) patients received dasatinib therapy for 12 months (appendix p 3).

At 12 months, 31 (60%) of 52 patients had major molecular response (one-sided 95% CI 48–71; figure 2). The calculated major molecular response was higher than the lower confidence limit of 38%, which was set according to results from the DASISION trial and took into account a non-inferiority margin of 10% (p=0·0007). Another endpoint to test for superiority, the percentage of patients achieving major molecular response (48%), was higher than the major molecular response rate in the DASISON trial (p=0·047). Of the 31 patients who reached

	MMR at 12 months (n=31)	Non-MMR at 12 months (N=21)	p value	MMR at 12 months, dose unadjusted (n=23)	Non-MMR at 12 months, dose unadjusted (n=29)	p value
***BCR-ABL1* mRNA international scale**						
At diagnosis	n=28; 97·40 (76·23–122·18)	n=21; 112·56 (94·69–143·84)	0·0470	n=21; 93·63 (74·34–111·60)	n=28; 111·60 (94·55–137·82)	0·0160
1 month	n=28; 35·00 (20·22–64·89)	n=19; 48·64 (36·35–69·81)	0·1320	n=20; 25·51 (11·16–43·30)	n=27; 63·63 (39·60–73·71)	0·00028
3 months	n=30; 0·41 (0·19–3·46)	n=20; 4·26 (2·03–13·03)	0·0020	n=22; 0·33 (0·10–0·43)	n=28; 5·89 (2·11–17·12)	<0·0001
Halving time						
0–3 months	n=27; 11·4 (9·7–19·1)	n=20; 18·3 (16·1–27·9)	0·0050	n=20; 10·5 (9·5–11·6)	n=27; 19·4 (16·6–35·3)	<0·0001

Data are n or median (IQR), unless otherwise indicated. Initial dasatinib dose was 20 mg and dosing was adjusted according to the therapeutic effect and side-effects. MMR=major molecular response.

Table 2: **Association of response outcomes with BCR-ABL1 mRNA international scale and halving time**

major molecular response at 12 months, 23 patients did not require the initial dose of 20 mg dasatinib to be changed.

The median *BCR-ABL1* IS was 1·47% at 3 months (IQR 0·37–8·39; n=50; appendix p 4). 39 (75%) patients had an optimal response according to ELN 2013 recommendations (figure 1), 38 (73%) patients had *BCR-ABL1* IS less than 10% at 3 months (early molecular response at 3 months), and 25 (48%) patients had *BCR-ABL1* IS 1·0% or less (MR2·0) at 3 months (figure 2).

Regarding secondary endpoints, at 12 months, 14 patients had MR4.0 (27% [one-sided 95% CI 16·8–37·0) and seven patients had MR4.5 (13·5% [5·7–21·3; figure 2). Eight (15%) patients discontinued because of treatment failure (n=3), withdrawal of consent (n=2), drug-related adverse events (n=1), or other reasons (n=2; appendix pp 3, 5). No patients who discontinued from the study or interrupted their treatment because of adverse events transformed to accelerated phase or blast phase.

We found no correlation between the Sokal, Hasford, and EUTOS risk scores and the major molecular response rate at 12 months (appendix p 6). Therefore, we compared *BCR-ABL1* IS at diagnosis, 1 month, and 3 months in patients who had major molecular response at 12 months and in patients who did not have major molecular response (table 2). *BCR-ABL1* IS values at 3 months and at diagnosis were significantly lower in patients who had major molecular response at 12 months than in patients who did not have major molecular response. We compared *BCR-ABL1* IS (at diagnosis, 1 month, and 3 months) and halving time in patients who reached major molecular response on protocol treatment (dose-adjusted treatment) versus in those who did not reach MMR (by dose-adjusted treatment). We then compared *BCR-ABL1* IS (at diagnosis, 1 month, and 3 months) and halving time in patients who reached major molecular response on dasatinib 20 mg alone versus those who did not. We did not compare patients who had major molecular response at 12 months (dose-adjusted treatment group) with the group using 20 mg/day of dasatinib only. Interestingly, *BCR-ABL1* IS was statistically low throughout the study in patients who had major molecular response at 12 months with 20 mg/day dasatinib (table 2).

We used receiver operating characteristic (ROC) curve analysis to identify the optimal threshold values for predicting major molecular response at 12 months using *BCR-ABL1* IS. The cutoff value at 3 months for all treatment methods used in this study and for 20 mg dasatinib was 0·662% (appendix p 7). Next, we analysed the relationship between the halving time of *BCR-ABL1* IS during the initial 3 months of the study and major molecular response at 12 months. The median halving time was 15·7 days and was widely distributed (IQR 10·6–23·7; n=47; appendix p 4). Moreover, ROC curve analysis suggested that the optimal halving time for obtaining major molecular response at 12 months was 12·5 days (the cut-off value at 3 months for all patients) and 12·0 days (the cut-off value at 3 months for 20 mg dasatinib; appendix p 7). We attempted to predict major molecular response at 12 months using various cut-off values at 3 months (early molecular response, complete cytogenetic response, *BCR-ABL1* IS 0·662%, and halving time ≤12·5 days). All cut-off values seemed to be predictive of major molecular response at 12 months, except for early molecular response (appendix p 8); however, these findings need further validation.

Treatment-related adverse events of all grades were reported in 50 (96%) of 52 patients (table 3). However, eosinophilia, basophilia, increased lactate dehydrogenase, and increased C-reactive protein were thought to be due to the condition of CML itself, rather than adverse events of dasatinib. Pleural effusion was observed in four patients but pulmonary hypertension was not observed. Five patients had median dose interruptions of 7 days (IQR 5–36 days) due to haematological (n=3) and non-haematological adverse events (n=2). Three patients required dose reductions to 20 mg every other day, one patient discontinued for drug-related toxicity (QT prolongation), and none died of treatment-related causes (appendix p 3, 5).

The time to reach maximum plasma concentrations is approximately 2 h after dosing and dasatinib has a short half-life (less than 4 h).[20] Sampling times were baseline and 2 h after dasatinib administration. We compared the groups that reached major molecular response at 12 months and those that did not. Although we found no statistical difference in maximum plasma concent-

	Grade 1–2	Grade 3	Grade 4
Adverse events	38 (73%)	11 (21%)	1 (2%)
Haematological			
Leukocytopenia	13 (25%)	0	0
Neutropenia	6 (12%)	3 (6%)	0
Eosinophilia	8 (15%)	0	0
Basophilia	19 (37%)	0	0
Lymphocytosis	1 (2%)	0	0
Anaemia	33 (63%)	1 (2%)	1 (2%)
Thrombocytopenia	18 (35%)	1 (2%)	0
Non-haematological			
Superficial oedema	2 (4%)	0	0
Pleural effusion	4 (8%)	0	0
Diarrhoea	1 (2%)	0	0
Myalgia	2 (4%)	0	0
Musculoskeletal pain	3 (6%)	0	0
Rash	3 (6%)	0	0
Fatigue	8 (15%)	1 (2%)	0
Arrhythmia	3 (6%)	1 (2%)	0
Long QT syndrome	0	1 (2%)	0
Dyspnoea	4 (8%)	2 (4%)	0
Acute heart failure	0	1 (2%)	0
Pneumonia	0	2 (4%)	0
Urinary-tract infection	1 (2%)	1 (2%)	0
Cataract	0	1 (2%)	0
Hypoalbuminemia	24 (46%)	0	0
Increased total bilirubin	4 (8%)	0	0
Increased ALT	15 (29%)	0	0
Increased AST	17 (33%)	1 (2%)	0
Increased LDH	21 (40%)	0	0
Increased BUN	22 (42%)	0	0
Increased creatinine	13 (25%)	0	0
Increased NT-pro BNP	25 (48%)	0	0
Elevated C-reactive protein	22 (42%)	0	0
Hyponatremia	8 (15%)	0	0
Potassium abnormality	15 (29%)	0	0
Chloride abnormalities	16 (31%)	0	0
Hypocalcaemia	9 (17%)	0	0

Grade 1-2 events occurring in 10% or more patients and all grade 3-4 events are shown. There were no fatal (grade 5) events. ALT=alanine transaminase. AST=aspartate aminotransferase. LDH=lactate dehydrogenase. BUN=blood urea nitrogen. NT-pro BNP=N-terminal pro-brain natriuretic peptide.

Table 3: **Summary of adverse events during treatment (n=52)**

rations 2 h after dasatinib administration at 1 month between these two groups, we found a statistical difference at 2 h after dasatinib administration at 12 months (p=0·011) in patients who had major molecular response (23·5 ng/mL) and those who did not (8·0 ng/mL). However, in patients who received only 20 mg dasatinib, we found no significant difference in maximum plasma concentrations 2 h after dasatinib administration at 12 months between those who had major molecular response and those who did not (appendix p 9). In terms of trough levels, we found no significant difference in baseline measures at 1 month and 12 months between patients with grade 3–4 adverse events and those with non-grade 3–4 adverse events (appendix p 9).

Notably, only one patient developed lymphocytosis (table 3). We found no statistical difference in the lymphocyte profile between the major molecular response and non-major molecular response groups (appendix p 10).

Discussion

In patients with chronic myeloid leukaemia in the chronic phase treated with an initial dose of 20 mg/day dasatinib, 60% of patients had major molecular response at 12 months, and almost half of patients had major molecular response by 12 months without a dose escalation. The major molecular response rate of this study was similar to that obtained in the dasatinib group of the DASISION trial (100 mg/day).[3]

Generally, using quantitative RT-PCR of *BCR-ABL1* mRNA, the plot of *BCR-ABL1* mRNA expression results in a biphasic decrease in TKI-sensitive patients. This biphasic decrease consists of an initial steep decrease and a second moderate decrease. The initial steep slope is attributed to a reduction of proliferating differentiated leukaemic cells, and the secondary slope results from a slower reduction of quiescent leukaemic stem cells.[21] Halving time of *BCR-ABL1* mRNA from the point of diagnosis to that of 3 months has a trend similar to this initial decline of circulating BCR-ABL1-positive leukaemic cells. Short halving time indicates reduced circulating CML cells (both proliferating differentiated leukaemic cells and stem cells). In this study, we found a significant difference in median halving time at 3 months after initiation of dasatinib between patients who had major molecular response at 12 months and those who did not. This finding is consistent with previous reports.[22]

Early molecular response has been recognised as an essential predictor of having a favourable overall survival and progression-free survival.[23] In this study, early molecular response was the first checkpoint for increasing the dasatinib dose; 73% of patients had early molecular response, and of these 63% had major molecular response at 12 months. To increase the sensitivity to predict major molecular response at 12 months, the optimal cutoff for *BCR-ABL1* IS at 3 months was 0·662% for all treatment methods and 20 mg/day dasatinib only. Although the therapeutic doses of dasatinib used in this study differ from the dose of TKIs used in previous studies, a clinical trial showed that achieving MR2.0 at 3 months was essential for achieving a favourable outcome.[24] These results indicate that rapid downregulation of *BCR-ABL1* is necessary to achieve a favourable outcome,[22] regardless of the dose of TKI.

Although trial comparison might be done with caution because of different observation periods and age groups

between trials, we compared the results of DAVLEC with two other studies, DASISSION[3] and an Italian real-life cohort of patients with chronic myeloid leukaemia in the chronic phase older than 65 years who received front-line dasatinib.[25] The compared safety outcomes were pleural effusion and haematological toxicity, which are often associated with dasatinib treatment. Grade 1–2 pleural effusions accounted for 14% of adverse events in the DASISION trial,[3] 14% in the Italian cohort,[25] and 8% in DAVLEC; grade 3–4 effusions accounted for 1% of adverse events in the DASISION trial, 5% in the Italian cohort, and none in DAVLEC; and grade 3–4 neutropenia accounted for 21% of adverse events in the DASISION trial and 6% in DAVLEC. These results suggest that the treatment algorithm used in DAVLEC was relatively safe.

Because older patients are more likely to have multiple comorbidities and receive several medications, which was reflected in the patients enrolled in this study, administering full-dose TKIs might be harmful.[7] To prevent pleural effusion during dasatinib therapy, the trough plasma concentration of dasatinib should be kept below 2·5 ng/mL.[20] In the present study, the trough concentration of dasatinib was sufficiently low when measured at 1 month and 12 months of treatment. As a result, the incidence of adverse events tended to be lower than in the DASISION trial.

In this study, the median concentration of dasatinib 2 h after administration was 50 ng/mL or less, which is generally an active dose of dasatinib in patients who had major molecular response as well as those who did not. The median concentration 2 h after administration at 12 months in patients who had major molecular response was significantly higher than in patients who did not. The IQR in the major molecular response group was also wider than in the non-major molecular response group. These results might mean that dose increases were given to patients who did not have an optimal response during treatment.

A high concentration of dasatinib (50–100 nM, approximately 25–50 ng/mL) transiently inhibits *BCR-ABL1*, leading to irreversible apoptosis of CML cells. Additionally, intermediate concentrations of dasatinib (3–25 nM, approximately 1–13 ng/mL) with extended treatment times produce progressively more cytotoxicity.[26] The standard dasatinib dose, 100 mg/day, was determined from a clinical study of patients with chronic myeloid leukaemia in the chronic phase who were resistant or intolerant to imatinib.[27] No dose-finding studies exist for dasatinib in newly diagnosed patients with chronic myeloid leukaemia in the chronic phase. In older patients, aging or polypharmacy might slow the metabolism of dasatinib, leading to prolonged *BCR-ABL1* inhibition. Hence, dasatinib could be allowed to act over an extended time (≥1 day) to achieve an optimal therapeutic response. In addition to age and polypharmacy, blood dasatinib concentrations are higher in East Asians including Japanese individuals than in non-East Asians at the same dose of dasatinib,[28] possibly leading to activity with a smaller dose of dasatinib in Japanese patients with CML. Previous investigations indicated that both pharmacokinetic and pharmacodynamic analyses were essential to achieve the best therapeutic effect of dasatinib treatment.[29,30] Therefore, the initial dose of dasatinib for newly diagnosed patients with chronic myeloid leukaemia in the chronic phase might need to be re-examined.

From the analyses of three large clinical trials, lymphocytosis develops in a minimum of 32% of patients after dasatinib treatment initiation.[31] However, lymphocytosis was only reported in one (2%) patient in this study . The reason for this finding was not clear but could be related to an inadequate immune response in older patients or because the plasma concentration of dasatinib was low. Therefore, a relationship might not exist between the immunological effect of dasatinib and whether a patient reaches major molecular response. Alternatively, a relationship might exist, but this relationship could be dependent on immune system factors other than the interaction between TKI and CML cells. On the other hand, the low lymphocytosis might be associated with the generally low incidence of adverse events.[32]

Our study had several limitations. First, there was no control group for comparison. Second, for reasons unknown, there was a sex imbalance. If the proportion of men and women had been similar, the results might have been different. Third, whether very low-dose dasatinib can lead to treatment-free remission, which is another therapy goal[2,4,5] for patients with chronic myeloid leukaemia in the chronic phase, is unclearfrom our data. Fourth, all our patients were Japanese, which limits the generalisability of the findings due to lack of ethnic diversity and also due to the fact that in the health-care system of Japan patients are often diagnosed with CML at an earlier stage than in other countries. Fifth, mutation analysis was not conducted in the trial, even in poor responders. The protocol did not specify the detection of mutations because the trial was done in line with general clinical practice as much as possible and in Japan, testing for mutations is self-funded. Sixth, assessment of patient-reported outcomes, which are important to assess patients' quality of life, were not planned as part of the study.

In conclusion, the DAVLEC study showed that a starting dose of dasatinib of 20 mg/day was active and well-tolerated in older patients with chronic myeloid leukaemia in the chronic phase. Furthermore, rapid *BCR-ABL1* downregulation was an essential indicator of a favourable molecular response, regardless of the dose of TKI used. Further long-term follow-up will be necessary to confirm the results of this study.

Contributors

KM, HU, and ShK made substantial contributions to the study conception, design, analysis, and data interpretation. KM, HU, TKu, HT, KN, SW, KI, TF, CY, NU, MM, JA, SaK, KK, KU, TKi, JS, YC, JK, YMa, KN, TO, KF, HS, CM, TT, TKo, YMi, KI, TI, JI, and ShK enrolled patients and collected data. MM performed pharmacokinetic analysis.

AT and AK performed the statistical analyses. KM, HU, and ShK wrote the paper and critically reviewed the drafts and all authors approved the final version. KM, HU, AT, AK, and ShK had access to the raw data. ShK had final responsibility for the decision to submit the study for publication as a corresponding author. JSh enrolled the patients and collected data. JSa critically reviewed the draft.

Declaration of interests

KM has received honoraria from Bristol-Myers Squibb, Novartis, Pfizer, Celgene, Eisai, Sanofi, Janssen, and Otsuka Pharmaceuticals. TKu received honoraria from Bristol-Myers Squibb, Novartis, Pfizer, and Otsuka Pharmaceuticals. HT received honoraria from Bristol-Myers Squibb, Novartis, Pfizer, and Otsuka Pharmaceuticals. KN received grants from Kyowa-Kirin, and honoraria from Alexion. CY received honoraria from Bristol-Myers Squibb, Novartis KK, Pfizer Japan, Otsuka Pharmaceutical, AbbVie GK, Janssen Pharmaceutical KK, Nippon Shinyaku, and Chugai Pharmaceutical. NU received honoraria from Eisai and Janssen Pharmaceutical. KU received grants from Astellas Pharma, AbbVie, Apellis, SymBio, Daiichi-Sankyo, Novartis, Janssen, Otsuka, Astellas Amgen Biopharma, Takeda, Nippon-Shinyaku, Bristol-Myers Squibb, Amgen, Alexion, Incyte, Ono, Kyowa-Kirin, Celgene, Sumitomo-Dainippon, Chugai, Pfizer, Mundi, Yakult, MSD, Gilead, and Nippon-Boehringer-Ingelheim and honoraria from Novartis, Bristol-Myers-Squibb, Sanofi, Pfizer, Abbvie, Takeda, Ono, Kyowa-Kirin, Astellas, Alexion, Eisai, MSD, Otsuka, Celgene, Daiichi-Sankyo, Nippon-Shinyaku, PharmaEssentia, Yakult, SymBio, Alexion, and Chugai. JK received grants from Bristol-Myers Squibb, Sysmex, Celgene, Ono Pharmaceutical, Otsuka Pharmaceutical, Sanofi, Kyowa Kirin, Sanofi, Chugai Pharmaceutical, Eisai, Dainippon Sumitomo Pharma, Nippon Shinyaku, Takeda, Shionogi, Asahi Kasei, Daiichi Sankyo, MSD, Taiho Pharmaceutical, and Abbvie; has received honoraria from Bristol–Myers Squibb, Janssen Pharmaceutical KK, Celgene Corporation, Ono Pharmaceutical, Takeda, Sanofi, Kyowa Kirin, Chugai Pharmaceutical, Eisai, Astellas Pharma, Nippon Shinyaku, Dainippon Sumitomo Pharma, Symbio, Daiichi Sankyo, Fujimoto Pharmaceutical, Abbvie, and Otsuka Pharmaceutical; and consulting fees from Janssen Pharmaceutical KK, Bristol-Myers Squibb, Sanofi, and Abbvie. TO received grants from Celgene, Kyowa Hakko Kirin, Chugai Pharmaceutical, TAIHO Phamaceutical; and honoraria from Celgene, Kyowa Hakko Kirin, Chugai Pharmaceutical, Novartis, Bristol-Myers Squibb, Pfizer, Otsuka Pharmaceutical, ONO Pharmaceutical, Takeda Pharmaceutical, Astellas Pharma, Eisai Pharmaceuticals, Janssen Pharm, Daiichi Sankyo, and Mundipharma. KF received honoraria from Bristol-Myers Squibb, Novartis, Pfizer, and Otsuka Pharmaceuticals. HS received honoraria from Takeda, Ono, Novartis, Janssen, Chugai, Eizai, Nippon Shinyaku, Sanofi, AstraZeneca, Bristol-Myers Squibb, Otsuka, Mundi Pharma and Kyowa Kirin; and research funding from Janssen, Ono, Celgene, Novartis, Sanofi, AstraZeneca, AbbVie, and Chugai. TKo received honoraria from Bristol-Myers Squibb, Novartis, Pfizer, Otsuka Pharmaceuticals, and Abbvie; and has served in an advisory role for Astellas Pharma and Otsuka Pharmaceutical. YMi received honoraria from Bristol-Myers Squibb, Novartis, Pfizer, and Astellas; and research funding from Ono and CMIC Holdings. ShK has received honoraria from Bristol-Myers Squibb, Novartis, Pfizer, and Otsuka Pharmaceuticals; and research funding from Bristol-Myers Squibb, Pfizer, Otsuka Pharmaceuticals, and Ohara Pharmaceuticals. All other authors declare no competing interests.

Data sharing

Individual participant data that underlie the results reported in this Article, after de-identification, will be made available beginning 9 months and ending 36 months following Article publication. The protocol will be available in English or Japanese. Proposals should be directed to shkimu@cc.saga-u.ac.jp. To gain access, data requestors will need to sign a data access agreement.

Acknowledgments

This study was funded by Bristol-Myers Squibb. The DAVLEC trial was supported by the Epidemiological and Clinical Research Information Network, which collected the data. We thank all of the doctors who enrolled the patients.

References

1 Bower H, Björkholm M, Dickman PW, Höglund M, Lambert PC, Andersson TM. Life expectancy of patients with Chronic myeloid leukemia approaches the life expectancy of the general population. *J Clin Oncol* 2016; **34:** 2851–57.

2 Mahon FX, Réa D, Guilhot J, et al. Discontinuation of imatinib in patients with chronic myeloid leukaemia who have maintained complete molecular remission for at least 2 years: the prospective, multicentre Stop Imatinib (STIM) trial. *Lancet Oncol* 2010; **11:** 1029–35.

3 Kantarjian H, Shah NP, Hochhaus A, et al. Dasatinib versus imatinib in newly diagnosed chronic-phase chronic myeloid leukemia. *N Engl J Med* 2010; **362:** 2260–70.

4 Imagawa J, Tanaka H, Okada M, et al. Discontinuation of dasatinib in patients with chronic myeloid leukaemia who have maintained deep molecular response for longer than 1 year (DADI trial): a multicentre phase 2 trial. *Lancet Haematol* 2015; **2:** e528–35.

5 Kimura S, Imagawa J, Murai K, et al. Treatment-free remission after first-line dasatinib discontinuation in patients with chronic myeloid leukaemia (first-line DADI trial): a single-arm, multicentre, phase 2 trial. *Lancet Haematol* 2020; **7:** e218–25.

6 Hochhaus A, Baccarani M, Silver RT, et al. European LeukemiaNet 2020 recommendations for treating chronic myeloid leukemia. *Leukemia* 2020; **34:** 966–84.

7 Saussele S, Krauss MP, Hehlmann R, et al. Impact of comorbidities on overall survival in patients with chronic myeloid leukemia: results of the randomized CML study IV. *Blood* 2015; **126:** 42–49.

8 Luskin MR, DeAngelo DJ. How to treat chronic myeloid leukemia (CML) in older adults. *J Geriatr Oncol* 2018; **9:** 291–95.

9 Crugnola M, Castagnetti F, Breccia M, et al. Outcome of very elderly chronic myeloid leukaemia patients treated with imatinib frontline. *Ann Hematol* 2019; **98:** 2329–38.

10 Kizaki M, Takahashi N, Iriyama N, et al. Efficacy and safety of tyrosine kinase inhibitors for newly diagnosed chronic-phase chronic myeloid leukemia over a 5-year period: results from the Japanese registry obtained by the New TARGET system. *Int J Hematol* 2019; **109:** 426–39.

11 Naqvi K, Jabbour E, Skinner J, et al. Long-term follow-up of lower dose dasatinib (50 mg daily) as frontline therapy in newly diagnosed chronic-phase chronic myeloid leukemia. *Cancer* 2020; **126:** 67–75.

12 Itamura H, Kubota Y, Shindo T, Ando T, Kojima K, Kimura S. Elderly Patients with chronic myeloid leukemia benefit from a dasatinib dose as low as 20 mg. *Clin Lymphoma Myeloma Leuk* 2017; **17:** 370–74.

13 Baccarani M, Deininger MW, Rosti G, et al. European LeukemiaNet recommendations for the management of chronic myeloid leukemia: 2013. *Blood* 2013; **122:** 872–84.

14 Ito T, Tanaka H, Tanaka K, et al. Insertion of a genomic fragment of chromosome 19 between BCR intron 19 and ABL intron 1a in a chronic myeloid leukaemia patient with micro-BCR-ABL (e19a2) transcript. *Br J Haematol* 2004; **126:** 752–53.

15 Nakamae H, Yoshida C, Miyata Y, et al. A new diagnostic kit, ODK-1201, for the quantitation of low major BCR-ABL mRNA level in chronic myeloid leukemia: correlation of quantitation with major BCR-ABL mRNA kits. *Int J Hematol* 2015; **102:** 304–11.

16 Branford S, Yeung DT, Parker WT, et al. Prognosis for patients with CML and >10% BCR-ABL1 after 3 months of imatinib depends on the rate of BCR-ABL1 decline. *Blood* 2014; **124:** 511–18.

17 Fava C, Rege-Cambrin G, Dogliotti I, et al. Early BCR-ABL1 reduction is predictive of better event-free survival in patients with newly diagnosed chronic myeloid leukemia treated with any tyrosine kinase inhibitor. *Clin Lymphoma Myeloma Leuk* 2016; **16** (suppl): S96–100.

18 Miura M, Takahashi N. Routine therapeutic drug monitoring of tyrosine kinase inhibitors by HPLC-UV or LC-MS/MS methods. *Drug Metab Pharmacokinet* 2016; **31:** 12–20.

19 Lee JJ, Liu DD. A predictive probability design for phase II cancer clinical trials. *Clin Trials* 2008; **5:** 93–106.

20 Miura M. Therapeutic drug monitoring of imatinib, nilotinib, and dasatinib for patients with chronic myeloid leukemia. *Biol Pharm Bull* 2015; **38:** 645–54.

21 Fassoni AC, Baldow C, Roeder I, Glauche I. Reduced tyrosine kinase inhibitor dose is predicted to be as effective as standard dose in chronic myeloid leukemia: a simulation study based on phase III trial data. *Haematologica* 2018; **103:** 1825–34.

22 Murai K, Yamaguchi K, Ito S, et al. Rapid reduction in BCR-ABL1 transcript predicts deep molecular response in dasatinib-treated chronic-phase chronic myeloid leukaemia patients. *Eur J Haematol* 2018; **100:** 27–35.

23 Marin D, Ibrahim AR, Lucas C, et al. Assessment of BCR-ABL1 transcript levels at 3 months is the only requirement for predicting outcome for patients with chronic myeloid leukemia treated with tyrosine kinase inhibitors. *J Clin Oncol* 2012; **30:** 232–38.

24 Jabbour E, Kantarjian HM, O'Brien S, et al. Front-line therapy with second-generation tyrosine kinase inhibitors in patients with early chronic phase chronic myeloid leukemia: what is the optimal response? *J Clin Oncol* 2011; **29:** 4260–65.

25 Latagliata R, Stagno F, Annunziata M, et al. Frontline Dasatinib Treatment in a "Real-Life" Cohort of Patients Older than 65 Years with Chronic Myeloid Leukemia. *Neoplasia* 2016; **18:** 536–40.

26 Shah NP, Kasap C, Weier C, et al. Transient potent BCR-ABL inhibition is sufficient to commit chronic myeloid leukemia cells irreversibly to apoptosis. *Cancer Cell* 2008; **14:** 485–93.

27 Shah NP, Kantarjian HM, Kim DW, et al. Intermittent target inhibition with dasatinib 100 mg once daily preserves efficacy and improves tolerability in imatinib-resistant and -intolerant chronic-phase chronic myeloid leukemia. *J Clin Oncol* 2008; **26:** 3204–12.

28 Chuah CT, Nakamae H, Shen ZX, Bradley-Garelik MB, Kim DW. Efficacy and safety of dasatinib versus imatinib in the East Asian subpopulation of the DASISION trial of newly diagnosed chronic myeloid leukemia in chronic phase. *Leuk Lymphoma* 2014; **55:** 2093–100.

29 Vainstein V, Eide CA, O'Hare T, Shukron O, Druker BJ. Integrating in vitro sensitivity and dose-response slope is predictive of clinical response to ABL kinase inhibitors in chronic myeloid leukemia. *Blood* 2013; **122:** 3331–34.

30 Ishida Y, Murai K, Yamaguchi K, et al. Pharmacokinetics and pharmacodynamics of dasatinib in the chronic phase of newly diagnosed chronic myeloid leukemia. *Eur J Clin Pharmacol* 2016; **72:** 185–93.

31 Schiffer CA, Cortes JE, Hochhaus A, et al. Lymphocytosis after treatment with dasatinib in chronic myeloid leukemia: Effects on response and toxicity. *Cancer* 2016; **122:** 1398–407.

32 Nagata Y, Ohashi K, Fukuda S, Kamata N, Akiyama H, Sakamaki H. Clinical features of dasatinib-induced large granular lymphocytosis and pleural effusion. *Int J Hematol* 2010; **91:** 799–807.

nature cell biology

RESOURCE

https://doi.org/10.1038/s41556-022-00866-3

Check for updates

OPEN

A single-cell atlas of non-haematopoietic cells in human lymph nodes and lymphoma reveals a landscape of stromal remodelling

Yoshiaki Abe[1], Mamiko Sakata-Yanagimoto[2,3,4] ✉, Manabu Fujisawa[2], Hiroaki Miyoshi[5], Yasuhito Suehara[3], Keiichiro Hattori[3], Manabu Kusakabe[2,3], Tatsuhiro Sakamoto[2,3], Hidekazu Nishikii[2,3], Tran B. Nguyen[2], Yohei Owada[6], Tsuyoshi Enomoto[6], Aya Sawa[7], Hiroko Bando[8], Chikashi Yoshida[9], Rikako Tabata[10], Toshiki Terao[10], Masahiro Nakayama[11], Koichi Ohshima[5], Kensuke Usuki[12], Tatsuya Oda[6], Kosei Matsue[10] and Shigeru Chiba[2,3] ✉

The activities of non-haematopoietic cells (NHCs), including mesenchymal stromal cells and endothelial cells, in lymphomas are reported to underlie lymphomagenesis. However, our understanding of lymphoma NHCs has been hampered by unexplained NHC heterogeneity, even in normal human lymph nodes (LNs). Here we constructed a single-cell transcriptome atlas of more than 100,000 NHCs collected from 27 human samples, including LNs and various nodal lymphomas, and it revealed 30 distinct subclusters, including some that were previously unrecognized. Notably, this atlas was useful for comparative analyses with lymphoma NHCs, which revealed an unanticipated landscape of subcluster-specific changes in gene expression and interaction with malignant cells in follicular lymphoma NHCs. This facilitates our understanding of stromal remodelling in lymphoma and highlights potential clinical biomarkers. Our study largely updates NHC taxonomy in human LNs and analysis of disease status, and provides a rich resource and deeper insights into LN and lymphoma biology to advance lymphoma management and therapy.

Lymphomas are haematological malignancies that often develop from LNs[1]. Despite advances in treatments, most lymphoma subtypes remain incurable. Therefore, new therapeutic approaches are needed, including those that target the tumour microenvironment[2,3]. In lymphomas, as in solid cancers[4,5], the activities of NHCs, such as mesenchymal stromal cells (SCs) and endothelial cells, are thought to facilitate lymphomagenesis and therefore have potential as therapeutic targets[2,3]. Indeed, some lymphoma subtypes are reported to exhibit unique interactions with NHCs[6–9]; however, lymphoma NHC research is far behind that of solid cancers[10]. In particular, follicular lymphoma (FL) cells are considered to actively interact with NHCs to promote emergence and expansion[9,11,12]. SC-derived CXCL12 recruits FL cells in cooperation with CXCL13 (produced by follicular dendritic cells (FDCs)), which contribute to the follicular localization of tumour cells and their proliferation[9,13]. Other FDC-derived molecules, including BAFF (encoded by *TNFSF13B*), interleukin-15 and HGF, may have anti-apoptotic effects on FL cells[14–16]. Unfortunately, a complete understanding of the temporal and spatial associations that underlie these activities is hampered by the heterogeneity of NHCs. In fact, definitive NHC classification has not yet been achieved in humans, even in normal LNs[17,18]. Moreover, the identification of alterations in LN NHC (LNNHC) heterogeneity in the context of lymphomas is barely underway.

Major subsets of NHCs in LNs, as determined by morphology and topological localization, include blood endothelial cells (BECs), which include high endothelial venules (HEVs), lymphatic endothelial cells (LECs) and non-endothelial SCs (NESCs)[18–20]. Examples of NESCs include T-zone reticular cells (TRCs), medullary reticular cells, perivascular cells and follicular SCs (FSCs), such as FDCs and marginal reticular cells (MRCs)[18–20]. Although recent investigations of NHC heterogeneity have used single-cell RNA sequencing (scRNA-seq) technology[21–26], human LN BECs and NESCs have yet to be comprehensively analysed at single-cell resolution.

To address this issue, scRNA-seq was used in this study to construct an atlas of human NHCs in LNs and lymphoma. We aimed to identify previously unrecognized NHC heterogeneity in human LNs and to distinguish NHCs from lymphomas to define the global influences of lymphoma cells on the NHC niche. This approach can provide deep insights into lymphoma stromal biology and resources applicable to future studies of lymphomas and identify potential stroma-derived biomarkers that may serve as clinical indicators and/or therapeutic targets.

[1]Department of Hematology, Graduate School of Comprehensive Human Sciences, University of Tsukuba, Tsukuba, Japan. [2]Department of Hematology, Faculty of Medicine, University of Tsukuba, Tsukuba, Japan. [3]Department of Hematology, University of Tsukuba Hospital, Tsukuba, Japan. [4]Division of Advanced Hemato-Oncology, Transborder Medical Research Center, University of Tsukuba, Tsukuba, Japan. [5]Department of Pathology, School of Medicine, Kurume University, Kurume, Japan. [6]Department of Gastrointestinal and Hepato-Biliary-Pancreatic Surgery, Faculty of Medicine, University of Tsukuba, Tsukuba, Japan. [7]Department of Breast-Thyroid-Endocrine Surgery, University of Tsukuba Hospital, Tsukuba, Japan. [8]Department of Breast and Endocrine Surgery, Faculty of Medicine, University of Tsukuba, Tsukuba, Japan. [9]Department of Hematology, National Hospital Organization, Mito Medical Center, Higashiibaraki, Japan. [10]Division of Hematology/Oncology, Department of Internal Medicine, Kameda Medical Center, Kamogawa, Japan. [11]Department of Otolaryngology, Head and Neck Surgery, University of Tsukuba, Tsukuba, Japan. [12]Department of Hematology, NTT Medical Center Tokyo, Tokyo, Japan. ✉e-mail: sakata.mamiko@fb3.so-net.ne.jp; schiba-tky@umin.net

Results

Transcriptional features of major NHC components. To profile NHCs in human LNs and lymphomas, we performed scRNA-seq and data integration of NHCs extracted from LN samples without tumour cell infiltration (metastasis-free LNs (MFLNs)) from nine patients with a neoplasm and nodal FL samples from ten patients (Fig. 1a, Extended Data Fig. 1a–c and Supplementary Table 1). Gene mutations identified in FL samples are presented in Supplementary Tables 1 and 2. Graph-based clustering of integrated cells led to the identification of three major NHC components (BECs, LECs and NESCs) and three contaminating haematopoietic cell components (lymphocytes, plasma cells and dendritic cells) on the uniform manifold approximation and projection (UMAP) (Fig. 1b). Cell-type annotation was performed by analysing the expression levels of canonical gene markers (Fig. 1c) and differentially expressed genes (DEGs) (Fig. 1d and Supplementary Table 3). Clustered NHCs were uniformly distributed across patients, cohorts, sample collection sites and patient age (Fig. 1b and Extended Data Fig. 1d,e). Notably, expression of the marker *PDPN*, which has been used to isolate LECs in previous scRNA-seq studies[22–24], was either partially decreased or absent in LECs (Extended Data Fig. 1f). Accordingly, the proportion of LECs among NHCs detected by flow cytometry was slightly smaller than that determined using scRNA-seq, although we observed concordance in the proportion of each NHC component between both methods (Fig. 1e and Extended Data Fig. 1g).

To identify subclusters within each of these three major NHC components, we extracted each NHC component in silico and subjected it to re-clustering. Notably, NHCs of MFLNs and FL were similarly distributed (Fig. 1f), which is in contrast to observations in solid cancers[27,28]. Here we first sought to construct a single-cell atlas of NHCs in MFLNs.

Ten subclusters of human LN BECs. We identified arterial, capillary and venous BECs (Fig. 2a). Venous BECs were most prevalent in MFLNs, followed by capillary and arterial BECs (Fig. 2b). For this annotation, we used known markers, including *GJA4* for arterial BECs, *CA4* for capillary BECs and *ACKR1* for venous BECs[29–31] (Fig. 2c,d and Supplementary Table 4).

Unsupervised clustering of BECs further revealed ten transcriptionally distinct subclusters: large arteries (ABECs); arteries surrounding the LN capsule (caBECs); arterioles (aBECs); tip cells (tBECs); capillary BECs (cBECs); transitional BECs between capillary BECs and activated HEVs (C-aHEVs); activated HEVs (aHEVs); homeostatic HEVs (hHEVs); CXCL10$^+$ HEVs (CXCL10-HEVs); and large veins (VBECs) (Fig. 2e,f). Each subcluster exhibited more than 100 DEGs that helped clearly distinguish the groups (Fig. 2g–i and Extended Data Fig. 2a).

ABECs, aBECs, tBECs, cBECs and VBECs had plausible counterparts with similar gene expression profiles in mouse tissues, including LNs[25,32], or in other human tissues[28] (Supplementary Note). Although mice exhibit one HEV cluster in LNs[25], human LN HEVs were composed of three subclusters (aHEVs, hHEVs and CXCL10-HEVs). aHEVs were characterized by a prominent expression of *G0S2* (Fig. 2h, Extended Data Fig. 2b and Supplementary Table 5), which is upregulated following induction of cell-cycle progression[33], and *SELE* (Fig. 2h,i and Extended Data Fig. 2a,b), which is upregulated by inflammation[34]. By contrast, hHEVs expressed *SELE* at low levels (Fig. 2i and Extended Data Fig. 2a,b). Notably, C-aHEVs and aHEVs both expressed stress-related genes, including those associated with heat shock proteins, NF-κB activation, JNK activation and shear stress[35] (Extended Data Fig. 2b and Supplementary Table 6), which suggests that these subclusters respond to active cell deformation or damage.

We next performed trajectory analysis on integrated MFLN BEC data using the Monocle 3 pipeline[36]. We were able to identify all BEC subclusters in a cell object generated using Monocle 3 (Extended Data Fig. 2c). Trajectory of the arterial component flowed from ABECs to aBECs and cBECs, finally reaching tBECs (Fig. 2j). Similarly, trajectory of the venous component initially traced HEV subclusters (aHEVs and hHEVs), then proceeded to capillary subclusters (C-aHEVs and cBECs) and finally to tBECs (Fig. 2j). These findings support the idea that tBEC migration in LNs generates new capillary BECs[37].

Gene ontology (GO) analysis revealed that factors involved in blood vessel development are enriched in ABECs, caBECs, aBECs and tBECs (Fig. 2k and Supplementary Table 7), which is in agreement with their arterial or tip cell characteristic. Leukocyte migration and cellular extravasation signatures were most enriched in aHEVs (Fig. 2k). Molecules associated with apoptosis were enriched in C-aHEVs and aHEVs (Fig. 2k). Moreover, as reported in mice[25], CXCL10-HEVs expressed molecules associated with interferon and cytokine signalling (Fig. 2k).

Immunofluorescence (IF) analysis of BECs stained with GJA5, SSUH2 or INSR identified them as large arterial BECs in LNs (ABECs), arterial BECs outside LNs (caBECs) and arterioles (aBECs), respectively (Extended Data Fig. 2d–f). We also detected tBECs as cells stained positive for LY6H or PGF in the tips of PLVAP$^+$ cBECs (Fig. 2l and Extended Data Fig. 2g). HEVs strongly expressing SELE (aHEVs) were frequently observed in interfollicular regions (IFRs) (Fig. 2l), which indicates that IFRs may serve as niches that play pivotal roles in promoting the influx of immune cells into LNs. Moreover, staining for PLVAP, HES1 and the HEV marker MECA-79 revealed that PLVAP$^+$HES1$^+$ capillaries (C-aHEVs) and MECA-79$^+$HES1$^+$ HEVs (aHEVs) (Extended Data Fig. 2b) were localized near each other (Extended Data Fig. 2h). Notably, CXCL10-HEVs were frequently observed in IFRs and were localized exclusively in the vicinity of aHEVs (Fig. 2l and Extended Data Fig. 2i). These findings, together with the GO analysis, suggest that rare CXCL10-HEVs may activate cellular trafficking of adjacent HEVs through cytokine signalling, which results in the heterogeneity of human HEVs.

In summary, our single-cell atlas of LN BECs identified three, three and four transcriptionally distinct subclusters in arterial, capillary and venous BECs, respectively, which demonstrates the unique heterogeneity of these cells in humans (Extended Data Fig. 2j–l).

Eight subclusters of human LN LECs. A human LEC atlas[22,23] recently proposed the following six LEC subclusters: subcapsular sinus (SCS) ceiling LECs (cLECs; LEC I); SCS floor LECs (fLECs;

Fig. 1 | Single-cell survey of NHC components in LNs and FL. a, Study overview of the experimental and analytical workflows. FACS, fluorescence-activated cell sorting; MACS, magnetic-activated cell sorting; SSC, side scatter. **b**, UMAP plots of stroma-enriched cells from nine human MFLN samples and ten FL samples, coloured by cell type (top). Major NHC components from MFLN samples and FL samples are shown separately (bottom left and bottom right, respectively). **c**, Expression levels of marker genes used to identify cell types. Red arrowheads show cells expressing the indicated marker genes. **d**, Heatmap showing the expression of top-ranking marker genes for each major NHC component. Key genes are indicated on the left. **e**, Correlation of the proportions of BECs, LECs and NESCs among stroma-enriched cells, as evaluated using flow cytometry (FCM) analysis and scRNA-seq, coloured according to patient cohort. Circles indicate biologically independent samples ($n=9$ MFLN, $n=10$ FL). ρ denotes Spearman's rank correlation coefficient. $^{***}P=4.0\times10^{-6}$ (BEC), $^{***}P=8.0\times10^{-6}$ (LEC), $^{***}P=2.5\times10^{-6}$ (NESC) (two-sided Spearman's rank correlation test). **f**, UMAP plots of LN BECs, LECs and NESCs after re-clustering analysis shown according to patient cohort. Statistical source data are provided.

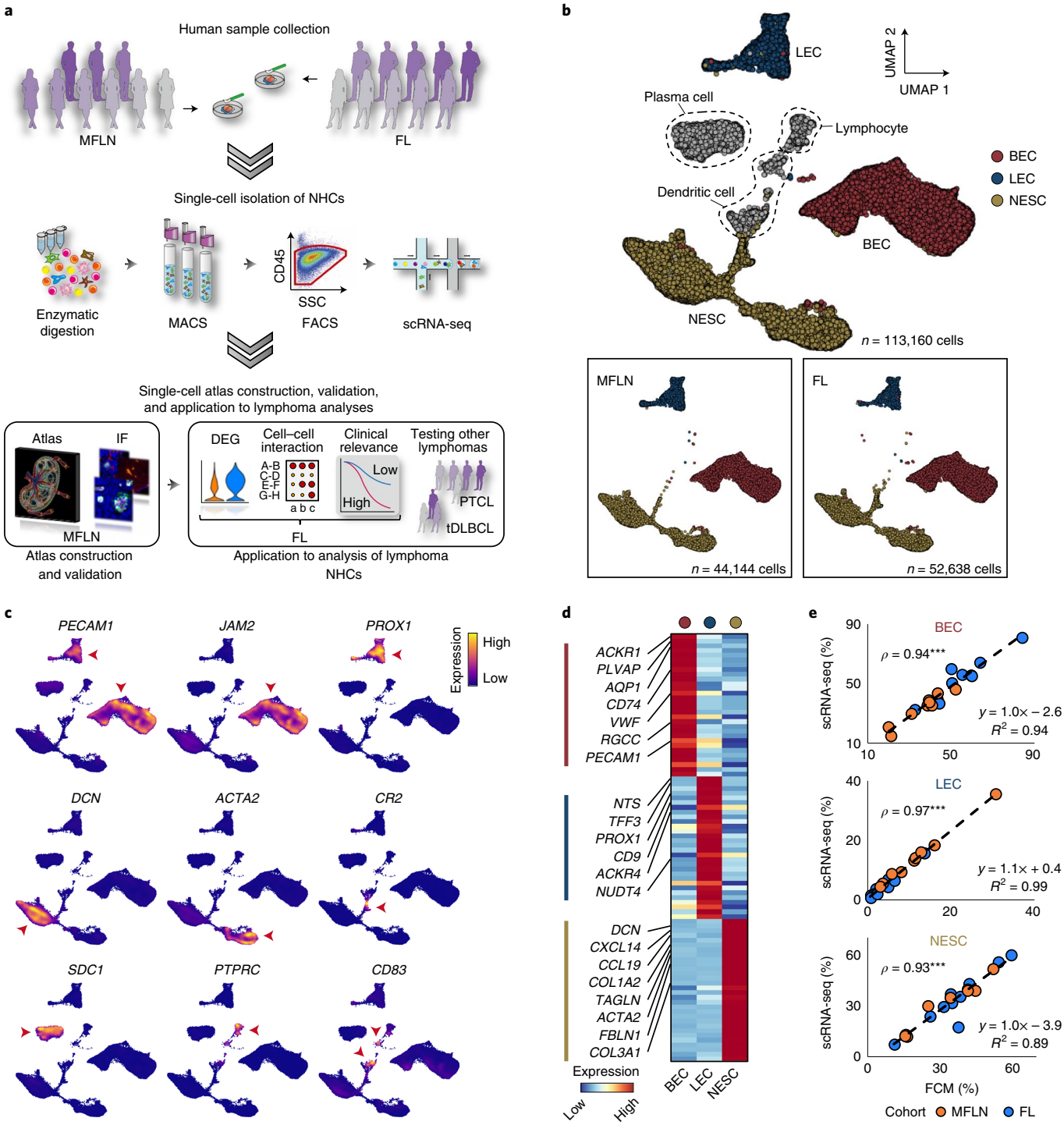
a
Human sample collection
MFLN
FL
Single-cell isolation of NHCs
Enzymatic digestion
MACS
CD45
SSC
FACS
scRNA-seq
Single-cell atlas construction, validation, and application to lymphoma analyses
Atlas
IF
MFLN
Atlas construction and validation
DEG
Cell–cell interaction
A-B
C-D
E-F
G-H
a b c
Clinical relevance
Low
High
Testing other lymphomas
PTCL
tDLBCL
FL
Application to analysis of lymphoma NHCs
b
LEC
UMAP 2
UMAP 1
Plasma cell
Lymphocyte
Dendritic cell
BEC
LEC
NESC
BEC
NESC
n = 113,160 cells
MFLN
n = 44,144 cells
FL
n = 52,638 cells
c
PECAM1
JAM2
PROX1
Expression
High
Low
DCN
ACTA2
CR2
SDC1
PTPRC
CD83
d
ACKR1
PLVAP
AQP1
CD74
VWF
RGCC
PECAM1
NTS
TFF3
PROX1
CD9
ACKR4
NUDT4
DCN
CXCL14
CCL19
COL1A2
TAGLN
ACTA2
FBLN1
COL3A1
Expression
Low
High
BEC
LEC
NESC
e
BEC
ρ = 0.94***
y = 1.0× – 2.6
R² = 0.94
LEC
ρ = 0.97***
y = 1.1× + 0.4
R² = 0.99
NESC
ρ = 0.93***
y = 1.0× – 3.9
R² = 0.89
scRNA-seq (%)
FCM (%)
Cohort
MFLN
FL
f
BEC
LEC
NESC
MFLN
FL

LEC II); particular SCS cLECs that cover medullary regions (LEC III); capillary LECs in surrounding tissues (LEC IV); valve LECs (LEC V); and LECs of medullary and cortical sinuses (LEC VI).

Accordingly, we performed unsupervised clustering of MFLN LECs, DEGs and trajectory analyses, and IF staining to compare results across studies (Fig. 3a–c, Extended Data Fig. 3a–l and Supplementary Tables 8 and 9). A detailed report of our findings is included in the Supplementary Note. In brief, we initially identified seven LEC subclusters: cLECs; bridge LECs (bLECs); fLECs and perifollicular sinus LECs (pfsLECs); collecting vessel LECs (collectLECs); medullary sinus LECs (msLECs); LECs on the upstream side of valves (Up-valves); and LECs on the downstream side of valves (Down-valves) (Fig. 3a–c and Extended Data Fig. 3a–c). Additional subclustering analysis divided the single fLEC and pfsLEC subcluster into fLECs and pfsLECs[23] (Extended Data Fig. 3d–f). Furthermore, IF staining revealed PAI1$^+$, MFAP4$^+$, PTX3$^+$ and MARCO$^+$ LECs (the latter three noted as LEC III, LEC IV and LEC VI, respectively[22]) as bLECs, collectLECs, msLECs and pfsLECs, respectively (Extended Data Fig. 3i–l). Our analysis therefore identified a total of eight LEC subclusters and unify data from recent reports[22–24] (Fig. 3d,e).

Twelve subclusters of human LN NESCs. NESCs were divided into the following 12 subclusters: SCs at capsule adventitia (advSCs); SFRP4$^+$ SCs (SFRP4-SCs); SFRP2$^+$ SCs (SFRP2-SCs); SCs enriched for tumour necrosis factor (TNF) signalling (TNF-SCs); C7$^+$ SCs (C7-SCs); AGT$^+$ SCs (AGT-SCs); TRCs; pericytes (PCs); smooth muscle cells (SMCs) with high or low ATF3 expression (ATF3^{hi} or ATF3^{lo} SMCs); MRCs; and FDCs (Fig. 4a,b and Extended Data Fig. 4a). TRCs, PCs, MRCs and FDCs were annotated on the basis of conventional taxonomy[18]. The results that contributed to the annotation of these known subclusters are included in the Supplementary Note.

DEG analysis revealed that NESC subclusters exhibited more than 100 DEGs each (Fig. 4c). advSCs showed the highest *CD34* expression among NESCs (Fig. 4d) and are considered the human counterpart of mouse CD34$^+$ SCs observed at adventitia of the LN capsule[21]. Both SFRP4-SCs and SFRP2-SCs shared *SFRP2* expression and were discriminated by higher *SFRP4* expression in the former (Fig. 4d,e). SFRP4-SCs also showed relatively high *INMT* expression (Supplementary Table 10), which suggests that they are the counterpart of mouse Inmt$^+$ SCs observed exclusively at medullary cords[21]. TNF-SCs were specifically characterized by *PTX3* expression, and C7-SCs by abundant *C7* expression (Fig. 4d,e). AGT-SCs expressed *AGT* and high levels of the apolipoprotein genes *APOE* and *APOC1* (Fig. 4d,e). ATF3^{hi} and ATF3^{lo} SMCs both expressed muscle-specific *MYH11* and *PLN* (Fig. 4d,e), but differed in the expression of genes associated with cellular responses to stress or mechanical stimuli (Fig. 4f and Supplementary Table 11). Notably, *TNFSF13B*, which encodes B-cell-activating factor belonging to the TNF family (BAFF) and is thought to define FDCs[20], was expressed by both MRCs and FDCs but at higher levels by MRCs (Fig. 4d,e).

Trajectory analysis revealed that MRCs were connected to TNF-SCs and C7-SCs (Fig. 4g and Extended Data Fig. 4b), which indicates that the latter two subclusters might differentiate into MRCs. Additional analysis showed a continuous trajectory from SMC subclusters to PCs, TRCs, MRCs and finally to FDCs in human LNs (Fig. 4h and Extended Data Fig. 4c), which is consistent with findings in mice of fibroblastic reticular cells in the splenic white pulp[38].

GO analysis revealed that advSCs expressed high levels of genes involved in the formation of elastic fibres and the extracellular matrix (ECM)[39] (Fig. 4i and Supplementary Table 12). In agreement with the preferential localization of mouse Inmt$^+$ SCs at the medulla[21], their human counterparts, SFRP4-SCs, expressed high levels of genes involved in ECM formation (Fig. 4i and Supplementary Table 12). TNF-SCs expressed genes associated with TNF signalling (*IL6* and *CCL2*) (Fig. 4i and Supplementary Tables 10 and 12), which suggests that they function in the chemotaxis of CCR2-expressing T cells, monocytes and dendritic cells to antigen sites[40]. C7-SCs expressed genes related to chemotaxis regulation (Fig. 4i), including *CXCL12* (Fig. 4d), which supports transendothelial T-cell migration across HEVs[41]. Top DEGs for AGT-SCs included *APOE*, *AGT* and *LPL*, which participate in remodelling of protein–lipid complexes and plasma lipoprotein particles (Fig. 4i and Supplementary Tables 10 and 12), which suggests that AGT-SCs may participate in lipid metabolism or transport.

IF staining was performed to identify the localization of each subcluster in LNs (Extended Data Fig. 4d–o). Fibroblasts positive for decorin (encoded by *DCN*), a strong marker of advSCs, SFRP4-SCs, SFRP2-SCs, TNF-SCs and C7-SCs (Extended Data Fig. 4d), were widely distributed in the adventitia, IFRs and medulla (Extended Data Fig. 4e). FBN1$^+$ SCs (advSCs) (Fig. 4d) were observed at the capsule adventitia, as observed in mice[21] (Extended Data Fig. 4f). SFRP2$^+$ SCs (SFRP2-SCs and SFRP4-SCs) were preferentially distributed in the medulla (Extended Data Fig. 4g). PTX3$^+$ SCs (TNF-SCs) were observed in IFRs (Extended Data Fig. 4h). C7-SCs were most frequent in the outer cortex, excluding follicles (Extended Data Fig. 4i), which is consistent with their proposed role in facilitating immune cell migration. AGT$^+$ cells were found on outer regions of the IFRs, frequently situated between SCSs and HEVs (Extended Data Fig. 4j). SMCs were observed as α-smooth muscle actin$^+$ (encoded by *ACTA2*), MYH11$^+$ or PLN$^+$ cells (Fig. 4d) around not only arterial BECs but also some HEVs (Extended Data Fig. 4k,l). ATF3 was positive in some SMCs around HEVs in the IFRs (aHEVs), as well as around arteries (Extended Data Fig. 4l). In line with the DEG analysis between SMC subclusters, ATF3$^+$ SMCs were also marked by HSP70 (encoded by *HSPA1A*) expression (Extended Data Fig. 4m), which probably reflects cell damage induced by blood flow[42] and/or immune cell trafficking.

To summarize, we identified 12 NESC subclusters, thereby showing unanticipated heterogeneity, linked to the distribution of other NHC subsets and LN niches (Extended Data Fig. 4p–r).

We accomplished a single-cell atlas of NHC components in human LNs (Extended Data Fig. 4p). Additional

Fig. 2 | A single-cell atlas of human LN BECs. a, UMAP plot of MFLN BECs coloured according to classification of arterial, capillary and venous BECs. **b**, The proportions of arterial, capillary and venous BECs in MFLN samples. **c**, Expression levels of arterial, capillary and venous BEC marker genes. **d**, Heatmap showing the expression of top-ranking marker genes of arterial, capillary and venous BECs. Key genes are indicated on the left. **e**, UMAP plot of ten MFLN BEC subclusters identified by unsupervised clustering. **f**, Prevalence of each BEC subcluster in MFLN samples. **g**, Number of DEGs per BEC subcluster. **h**, Heatmap showing the expression of top-ranking marker genes for each BEC subcluster. Key genes are indicated on the left. **i**, Violin plots representing the expression of top marker genes for each BEC subcluster. **j**, Single-cell BECs ordered according to pseudotime developmental stages. Dark winding lines in the cell object indicate putative developmental trajectories. Cell regions are assigned to BEC subclusters based on subcluster-defining gene expression levels. **k**, GO enrichment analysis of DEGs for each BEC subcluster. **l**, IF staining of PLVAP (white) and LY6H (red) (top left) to identify tBECs; MECA-79 (green), SELE (white) and CXCL10 (red) (top right) to identify aHEVs and CXCL10-HEVs; and MECA-79 (green), SELE (white) and CD31 (red) (bottom) to discriminate aHEVs (arrowheads) from hHEVs. Dashed lines indicate follicles. Scale bars, 50 μm (grey) or 200 μm (white). Representative images from one of three independent experiments are shown.

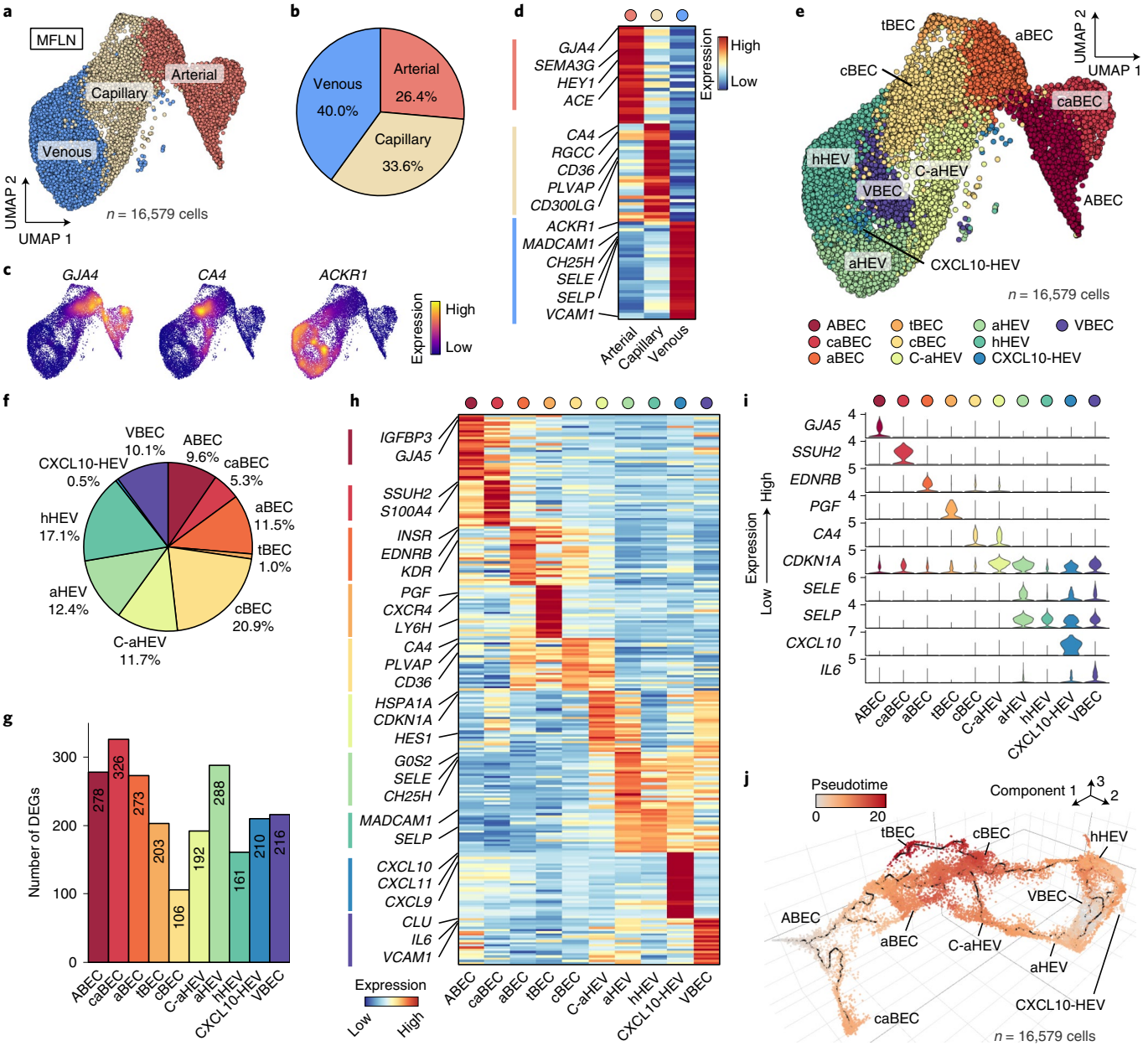
a
MFLN
Arterial
Capillary
Venous
UMAP 2
UMAP 1
n = 16,579 cells
b
Venous 40.0%
Arterial 26.4%
Capillary 33.6%
c
GJA4
CA4
ACKR1
Expression
High
Low
d
GJA4
SEMA3G
HEY1
ACE
CA4
RGCC
CD36
PLVAP
CD300LG
ACKR1
MADCAM1
CH25H
SELE
SELP
VCAM1
Expression
High
Low
Arterial
Capillary
Venous
e
tBEC
aBEC
cBEC
caBEC
hHEV
C-aHEV
VBEC
ABEC
aHEV
CXCL10-HEV
UMAP 2
UMAP 1
n = 16,579 cells
ABEC
caBEC
aBEC
tBEC
cBEC
C-aHEV
aHEV
hHEV
CXCL10-HEV
VBEC
f
VBEC 10.1%
ABEC 9.6%
caBEC 5.3%
aBEC 11.5%
tBEC 1.0%
cBEC 20.9%
C-aHEV 11.7%
aHEV 12.4%
hHEV 17.1%
CXCL10-HEV 0.5%
g
Number of DEGs
0
100
200
300
278
326
273
203
106
192
288
161
210
216
ABEC
caBEC
aBEC
tBEC
cBEC
C-aHEV
aHEV
hHEV
CXCL10-HEV
VBEC
h
IGFBP3
GJA5
SSUH2
S100A4
INSR
EDNRB
KDR
PGF
CXCR4
LY6H
CA4
PLVAP
CD36
HSPA1A
CDKN1A
HES1
G0S2
SELE
CH25H
MADCAM1
SELP
CXCL10
CXCL11
CXCL9
CLU
IL6
VCAM1
Expression
Low
High
ABEC
caBEC
aBEC
tBEC
cBEC
C-aHEV
aHEV
hHEV
CXCL10-HEV
VBEC
i
GJA5
SSUH2
EDNRB
PGF
CA4
CDKN1A
SELE
SELP
CXCL10
IL6
Expression
Low
High
ABEC
caBEC
aBEC
tBEC
cBEC
C-aHEV
aHEV
hHEV
CXCL10-HEV
VBEC
j
Pseudotime
0
20
Component 1
2
3
tBEC
cBEC
hHEV
VBEC
ABEC
aBEC
C-aHEV
aHEV
CXCL10-HEV
caBEC
n = 16,579 cells
k
Blood vessel development
Regulation of cell adhesion
Muscle structure development
ECM organization
Leukocyte migration
Response to growth factor
Focal adhesion
Muscle cell differentiation
Notch signalling pathway
ECM proteoglycans
Laminin interactions
Cellular extravasation
Smooth muscle cell differentiation
Cytokine-mediated signalling pathway
Attenuation phase
Apoptosis
Regulation of innate immune response
Interferon signalling
Regulation of inflammatory response
Regulation of IκK/NFκB signalling
−log10(P)
0
15
l
DAPI PLVAP LY6H
tBEC
DAPI MECA-79
SELE CXCL10
aHEV and CXCL10-HEV
DAPI MECA-79
SELE CD31
SELE
aHEV and hHEV
IFR
Follicle
T-zone

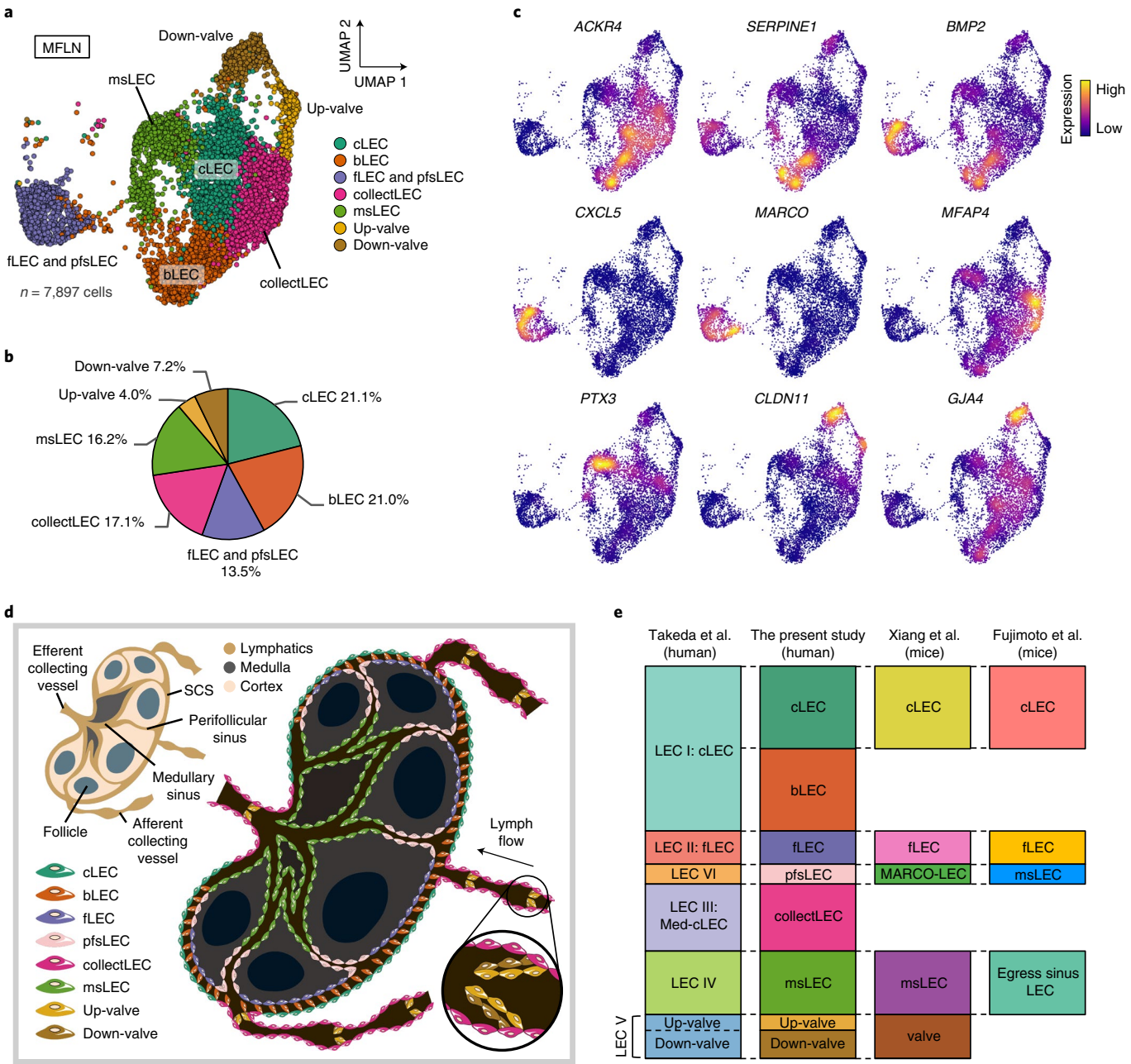

Fig. 3 | A single-cell atlas of human LN LECs. a, UMAP plot of MFLN LEC subclusters identified by unsupervised clustering. **b**, The prevalence of each LEC subcluster in MFLN samples. **c**, Expression levels of marker genes for each LEC subcluster. **d**, Schematic showing the topological localization of eight LEC subclusters in the LN. **e**, Comparison of subclusters identified here with those previously characterized (Takeda et al.[22], Xiang et al.[23] and Fujimoto et al.[24]). Bar heights of the previous studies are adjusted to cell numbers (belonging to each subcluster) identified in this study.

basic profiles of the atlas are described in the Supplementary Note, Extended Data Figs. 5a–c and 6a,b and Supplementary Tables 13 and 14.

Remodelling of NHC proportions in FL. Using this atlas, we next sought to explore alterations in FL NHCs at subcluster levels by comparing them with MFLN counterparts (Fig. 5a and Extended Data Fig. 7a). Overall, the proportion of BECs were markedly increased in FL relative to MFLNs, whereas the proportion of LECs decreased (Fig. 5a). Moreover, the proportion of arterial subclusters were increased in FL BECs (Fig. 5a). In FL NESCs, the proportion of FDCs was greatly increased (Fig. 5a). Notably, MRCs were also greatly increased in FL, whereas advSCs, SFRP4-SCs, SFRP2-SCs and TNF-SCs were decreased (Fig. 5a).

Subcluster-specific transcriptional changes in FL stroma. We next performed multistep DEG analyses in NHC subclusters of MFLNs and FL by monitoring differences in gene expression between mesenteric LNs (mLNs) and peripheral LNs (pLNs) (Extended Data Fig. 6a,b, Supplementary Tables 13 and 14 and Supplementary Note). We observed the greatest differences in MRCs, followed by TRCs, SMC subclusters, PCs and FDCs (Fig. 5b and Supplementary Tables 15–17). Figure 5c shows the expression levels of the top three DEGs upregulated in FL NHC subclusters in comparison

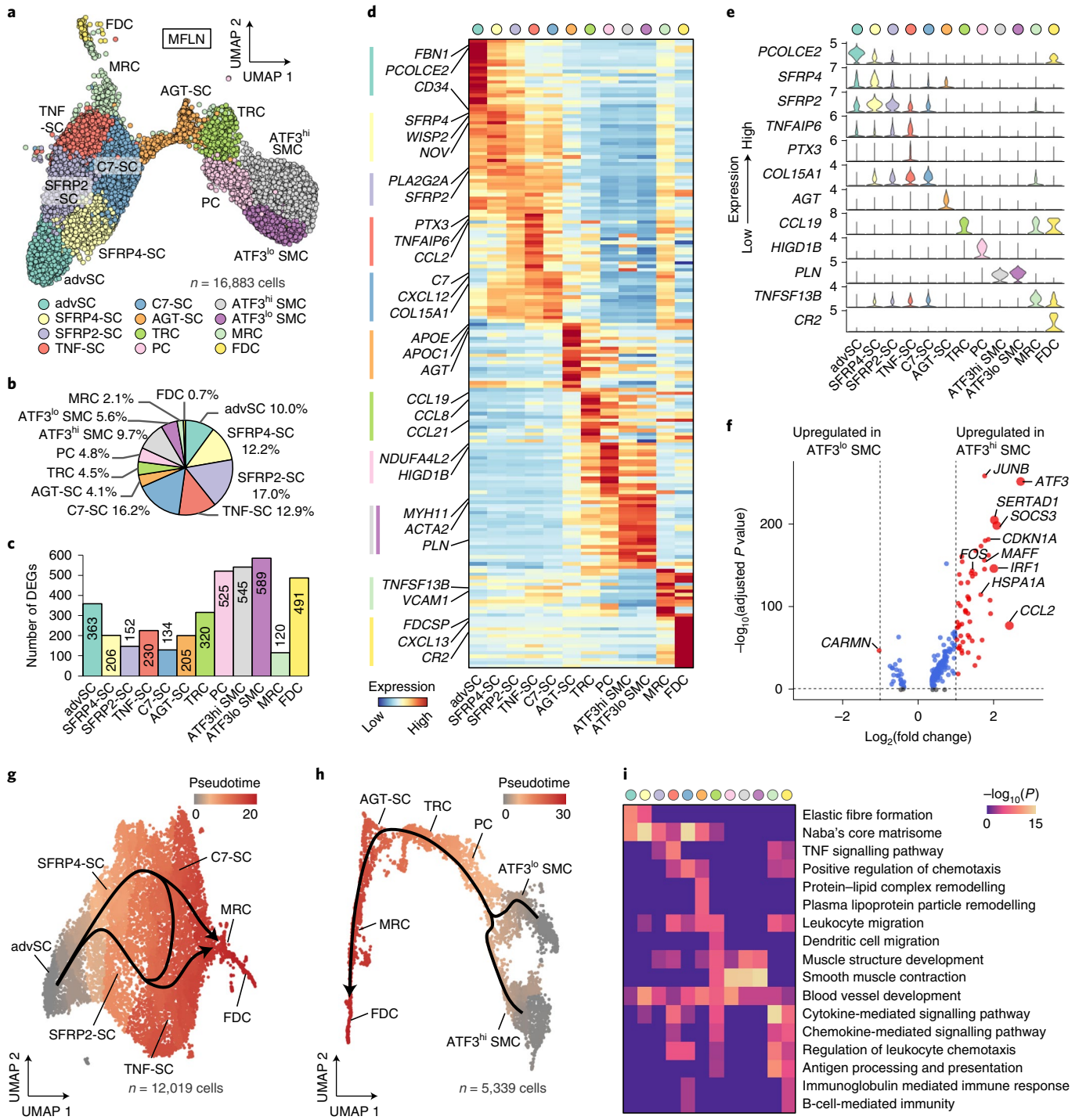

Fig. 4 | A single-cell atlas of human LN NESCs. a, UMAP plot of MFLN NESC subclusters identified by unsupervised clustering. **b**, The prevalence of each NESC subcluster in MFLN samples. **c**, Number of DEGs per NESC subcluster. **d**, Heatmap showing the expression of top-ranking marker genes for each NESC subcluster. Key genes are indicated on the left. **e**, Violin plots representing top marker genes for each NESC subcluster. **f**, Volcano plot of upregulated or downregulated genes between ATF3^{hi} and ATF3^{lo} SMCs. Significance was determined as an adjusted $P < 0.05$ (two-sided Wilcoxon rank-sum test with Bonferroni correction) (blue dots) and $\log_2$ fold-change of ≥1 (red dots). Larger dots indicate log2 fold-change of ≥2. Key genes are labelled. **g**,**h**, Pseudotime developmental stages of single cells in advSCs, SFRP4-SCs, SFRP2-SCs, TNF-SCs, C7-SCs, MRCs and FDCs (**g**) or in SMC subclusters, PCs, TRCs, AGT-SCs, MRCs and FDCs (**h**). Dark winding lines in the cell objects indicate putative developmental trajectories. Cell regions are assigned to each subcluster based on subcluster-defining gene expressions. **i**, GO enrichment analysis of DEGs for each NESC subcluster.

to their MFLN counterparts. In MRCs, *CXCL13* was most markedly upregulated, and GO terms related to lymphocyte migration were enriched (Fig. 5c, Extended Data Fig. 7b,c and Supplementary Tables 17 and 18), which suggests that MRCs, in addition to FDCs, function in the accumulation of malignant B cells[13]. The expression of *TNFSF13B* was significantly enhanced in FL NESC subclusters, including SFRP4-SCs and AGT-SCs (Extended Data Fig. 7b). *IL15* and *HGF* expression levels also tended to be increased in

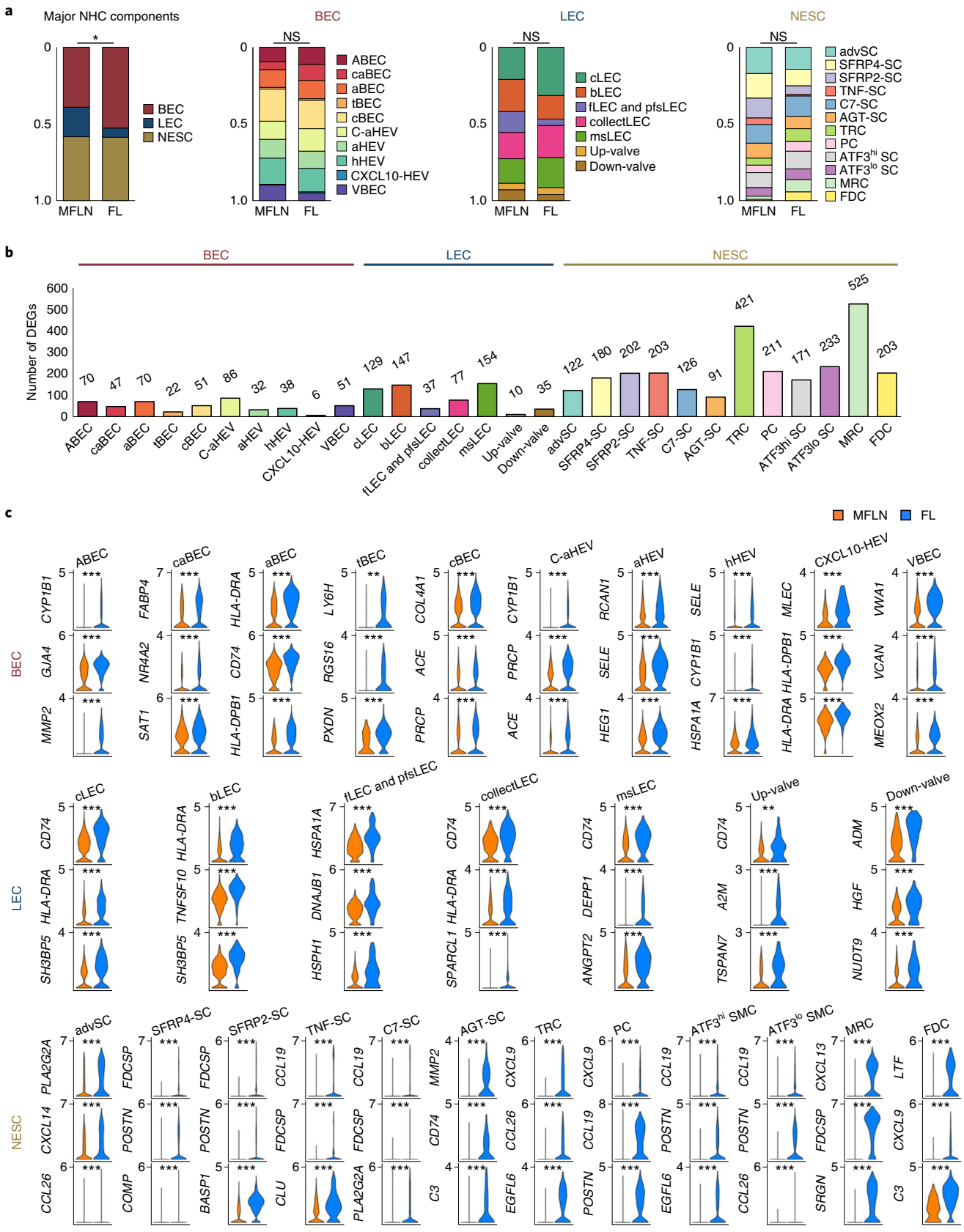

Fig. 5 | Compositional and transcriptional changes in FL stroma. a, Differences between MFLN and FL NHC compositions based on major NHC components, and BEC, LEC and NESC subclusters. *$P = 0.010$ (two-sided Chi-squared test). NS, not significant. **b**, Number of DEGs upregulated in FL NHC subclusters compared to MFLN counterparts. **c**, Violin plots of the top three DEGs upregulated in FL NHC subclusters compared to MFLN counterparts. **$P < 0.01$, ***$P < 0.001$ (two-sided Wilcoxon rank-sum test with Bonferroni correction). Exact *P* values are provided in Supplementary Tables 15–17. Statistical source data are provided.

some FL NESC subclusters, although this finding was not significant (Extended Data Fig. 7b). Notably, in some NESC subclusters, we observed marked upregulation of genes relevant to solid cancers but previously not associated with lymphomagenesis. Among them, *POSTN*, which encodes periostin (a protein secreted by cancer-associated fibroblasts (CAFs) and promotes the formation of cancer stem cell, perivascular and premetastatic niches[43]), was substantially upregulated in TRCs and PCs and in SMC subclusters of FL (Fig. 5c, Extended Data Fig. 7b and Supplementary Table 17). The expression of *EGFL6*, which encodes EGFL6 (a member of the EGF-like superfamily that reportedly promotes tumour cell growth by stimulating angiogenesis[44,45]), was highly upregulated in TRCs, SMC subclusters and MRCs (Fig. 5c, Extended Data Fig. 7b and Supplementary Table 17). CAFs positive for fibroblast activation protein (FAP) are associated with an immunosuppressive environment, which hampers immunotherapy[46–48]. Intriguingly, *FAP* was most upregulated in FSCs (MRCs and FDCs) (Extended Data Fig. 7b and Supplementary Table 17), which indicates that FSCs may create an immunological environment that favours malignant cells in FL.

In FL BECs, *GJA4* was upregulated in arterial subclusters, ABECs and aBECs (Fig. 5c and Supplementary Table 15), a pattern that is reflective of arterial vessel development[29]. Other genes involved in blood vessel development or ECM organization were upregulated in almost all subclusters (Extended Data Fig. 7c and Supplementary Tables 15 and 18). FL HEV subclusters showed high *SELE* expression (Fig. 5c and Supplementary Table 15), which is suggestive of inflammation and HEV activation[49,50]. Indeed, FL HEV subclusters expressed genes that regulate cellular adhesion and migration (Extended Data Fig. 7c and Supplementary Tables 15 and 18). Notably, expression of the tip cell markers *LY6H*, *PXDN*, *PGF* and *LOX* was markedly upregulated in FL tBECs (Fig. 5c and Supplementary Table 15), which suggests that they are involved in the acceleration of angiogenesis. The significant decrease in the proportion of LECs in FL suggests that there is widespread lymphatic damage. IF staining confirmed that the LEC density was lower in FL compared with that in MFLNs (Extended Data Fig. 7d,e). Many FL LEC subclusters also showed upregulation of heat shock genes as well as *CD74*, which reportedly functions in wound healing[51] (Fig. 5c, Extended Data Fig. 7c and Supplementary Tables 16 and 18). CD74 overexpression was confirmed in FL LECs by IF staining (Extended Data Fig. 7f,g).

Landscape of intercellular interactions in FL stroma. To assess the NHC–malignant B-cell crosstalk underlying FL growth, we performed scRNA-seq of cryopreserved CD45$^+$ cells from nine FL samples (FL 2–FL 10) and extracted gene expression profiles of malignant B-cell clusters in silico from each (Extended Data Figs. 1c and 8a–d). We then performed intercellular ligand–receptor interaction analyses between FL NHC subclusters and malignant B cells using CellPhoneDB[52]. Thereafter, we extracted significant interactions that were considered upregulated in FL NHC subclusters relative to the corresponding MFLN subclusters.

We identified a total of 58 interactions, including some previously uncharacterized in FL (Fig. 6a). In BECs, we noted that overexpression of JAG1, which is reportedly observed in B-cell lymphoma BECs and associated with aggressive lymphoma phenotypes[53], was limited to only larger arterial BEC subclusters (ABECs and caBECs) (Fig. 6a). Interactions mediated through adhesion molecules, including the SELE–CD44 interaction[54,55], were activated mainly in HEV subclusters (C-aHEVs, aHEVs and hHEVs) (Fig. 6a), which suggests that these HEV subclusters may contribute to the haematogenous expansion of FL cells[54,56]. Interactions that promote cancer cell death and mediated by TNFSF10 were markedly upregulated in several LEC subclusters[57] (Fig. 6a), which suggests that LECs may antagonize lymphoma development. In NESCs, interactions associated with TNF signalling, cell adhesion, PDGF signalling and chemokine signalling were differentially activated among subclusters (Fig. 6a). Notably, overexpression of CXCL12, which reportedly supports FL cell migration, adhesion and activation[58], was observed in advSCs (Fig. 6a). Moreover, interactions via BAFF were upregulated, even in medullary SCs (SFRP4-SCs), which suggests that stromal remodelling in FL supports the extrafollicular expansion of malignant B cells[59]. In advSCs and medullary SC subclusters, interactions mediated by stroma-derived CD70 were enhanced (Fig. 6a). Interactions mediated through PDGFRB, which promotes cell migration and angiogenesis[60], were enhanced in TRCs and PCs (Fig. 6a), which suggests that during FL expansion, mechanisms other than CCR7–CCL19/CCL21 signalling may drive the homing of malignant B cells to the T-cell zone[61]. Instead, the CCR7–CCL19 interaction was extended to non-TRC SCs (TNF-SCs and PCs) (Fig. 6a). Consistent with the DEG analyses of MFLNs and FL, the CXCL13–CXCR5 axis[9,13] was activated in MRCs and FDCs (Fig. 6a).

Enhanced CD70–CD27 interaction across FL stroma. Based on the above interactome analysis results, we next sought to explore an interaction that can potentially be targeted in lymphoma. We carefully surveyed candidate interactions from the perspective of novelty in the field. We noted that the CD70–CD27 interaction in solid and haematological cancers has attracted increasing attention[62–65], whereas interactions mediated by stroma-derived CD70 have rarely been investigated. Accordingly, we focused on the CD70–CD27 interaction for functional validation to verify the usefulness of our atlas-based analyses and to propose a potential mechanism in the stroma relevant to FL progression. Initially, we confirmed that

Fig. 6 | Dissection of stroma–malignant B-cell interactions in FL. a, Enhanced interactions across FL NHC subclusters and malignant B cells ($B_{malignant}$). Circle size indicates the negative $\log_{10}$ of adjusted *P* values (Methods). Circles are coloured when a stroma-derived factor is upregulated in relevant FL subclusters. **b**, IF staining for MECA-79 (cyan), DCN (red) and CD70 (green) in MFLN and FL samples. Scale bars, 200 µm. Representative images from one of three independent experiments are shown. **c**, Proportions of CD70$^+$ area in medullary and adventitia regions of MFLN ($n=3$) and FL ($n=3$) samples. Circles represent biologically independent samples. Bars indicate the median. $^{**}P=0.0095$ (two-sided unpaired *t*-test). **d**, Binding of FL CD19$^+$CD10$^+$ cells to CD70-Fc protein with an anti-CD27 blocking antibody or isotype human IgG. The histograms represent three independent experiments (FL13) with the count in arbitrary units. **e**, Blocking of FL CD19$^+$CD10$^+$ cell binding to CD70-Fc protein after treating cells with an anti-CD27 blocking antibody ($n=3$) or isotype mouse IgG1 ($n=3$) in CD27$^+$ FL samples (FL11–FL14). Proportions of cells bound to CD70-Fc protein were adjusted by subtracting nonspecific binding observed with human IgG. CD70-Fc protein binding to cells treated with isotype mouse IgG1 was set to 100% in each experiment. Circles represent independent experiments. Bars indicate the median. $^{**}P=0.0022$, $^{***}P=7.3\times10^{-4}$ (FL11), $^{***}P=2.2\times10^{-4}$ (FL12), $^{***}P=7.6\times10^{-4}$ (FL13) (two-sided paired *t*-test). **f**, Representative malignant B-enriched cell (FL14) adhesion to medullary regions of FL in the presence of an isotype mouse IgG1 or anti-CD27 antibody. Orange dots indicate adherent cells. Yellow dashed lines indicate medullary regions. Scale bars, 200 µm. **g**, Blocking of malignant B-enriched cell (FL11, FL13 and FL14) adhesion to FL medullary regions (per mm^2) after treating cells with an anti-CD27 blocking antibody ($n=3$) or isotype mouse IgG1 ($n=3$). Adhesion of cells treated with isotype mouse IgG1 was set to 100% in each experiment. Circles represent independent experiments. Bars indicate the median. $^{*}P=0.041$ (FL11), $^{*}P=0.027$ (FL14), $^{**}P=0.0050$ (two-sided paired *t*-test). Statistical source data are provided.

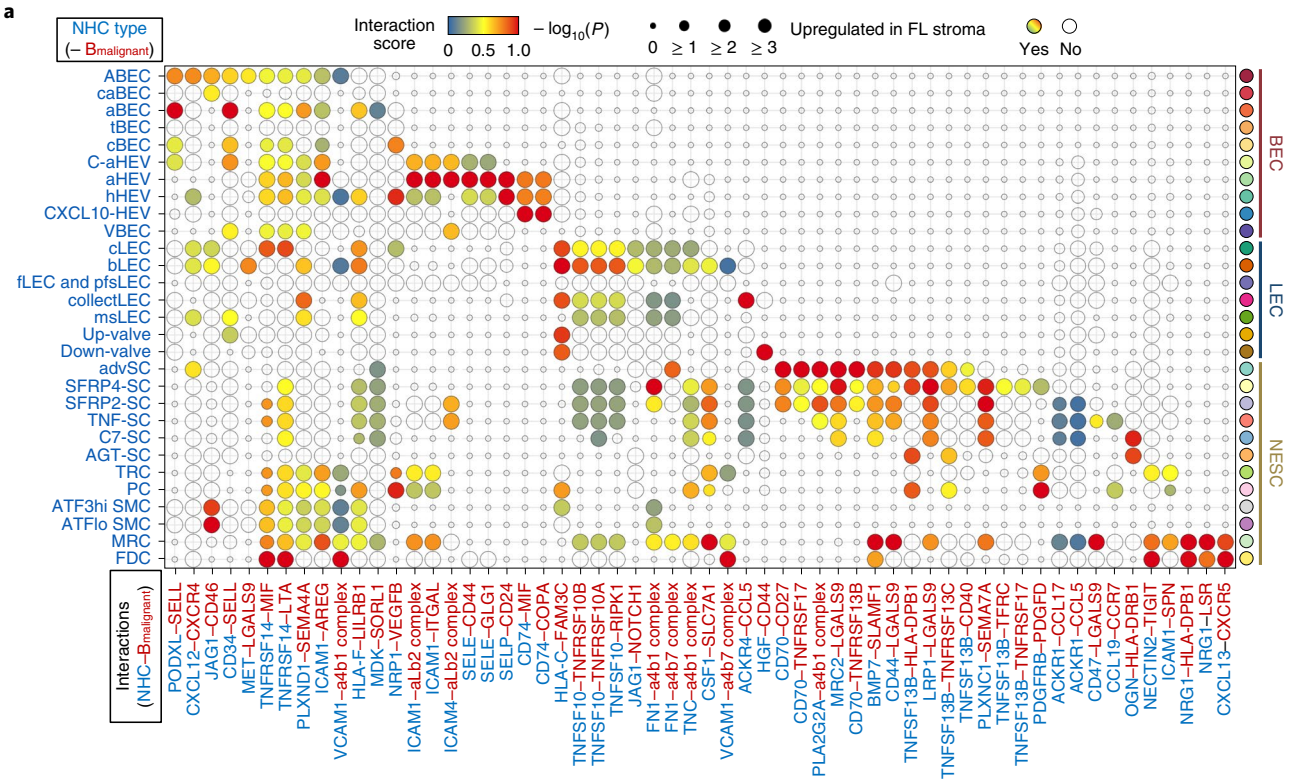
a
NHC type (– Bmalignant)
Interaction score
– log10(P)
0 0.5 1.0
0 ≥ 1 ≥ 2 ≥ 3
Upregulated in FL stroma
Yes No
ABEC
caBEC
aBEC
tBEC
cBEC
C-aHEV
aHEV
hHEV
CXCL10-HEV
VBEC
cLEC
bLEC
fLEC and pfsLEC
collectLEC
msLEC
Up-valve
Down-valve
advSC
SFRP4-SC
SFRP2-SC
TNF-SC
C7-SC
AGT-SC
TRC
PC
ATF3hi SMC
ATFlo SMC
MRC
FDC
BEC
LEC
NESC
Interactions (NHC–Bmalignant)
PODXL–SELL
CXCL12–CXCR4
JAG1–CD46
CD34–SELL
MET–LGALS9
TNFRSF14–MIF
TNFRSF14–LTA
PLXND1–SEMA4A
ICAM1–AREG
VCAM1–a4b1 complex
HLA-F–LILRB1
MDK–SORL1
NRP1–VEGFB
ICAM1–aLb2 complex
ICAM1–ITGAL
ICAM4–aLb2 complex
SELE–CD44
SELE–GLG1
SELP–CD24
CD74–MIF
CD74–COPA
HLA-C–FAM3C
TNFSF10–TNFRSF10B
TNFSF10–TNFRSF10A
TNFSF10–RIPK1
JAG1–NOTCH1
FN1–a4b1 complex
FN1–a4b7 complex
TNC–a4b1 complex
CSF1–SLC7A1
VCAM1–a4b7 complex
ACKR4–CCL5
HGF–CD44
CD70–CD27
CD70–TNFRSF17
PLA2G2A–a4b1 complex
MRC2–LGALS9
CD70–TNFRSF13B
BMP7–SLAMF1
CD44–LGALS9
TNFSF13B–HLA-DPB1
LRP1–LGALS9
TNFSF13B–TNFRSF13C
TNFSF13B–CD40
PLXNC1–SEMA7A
TNFSF13B–TFRC
TNFSF13B–TNFRSF17
PDGFRB–PDGFD
ACKR1–CCL17
ACKR1–CCL5
CD47–LGALS9
CCL19–CCR7
OGN–HLA-DRB1
NECTIN2–TIGIT
ICAM1–SPN
NRG1–HLA-DPB1
NRG1–LSR
CXCL13–CXCR5

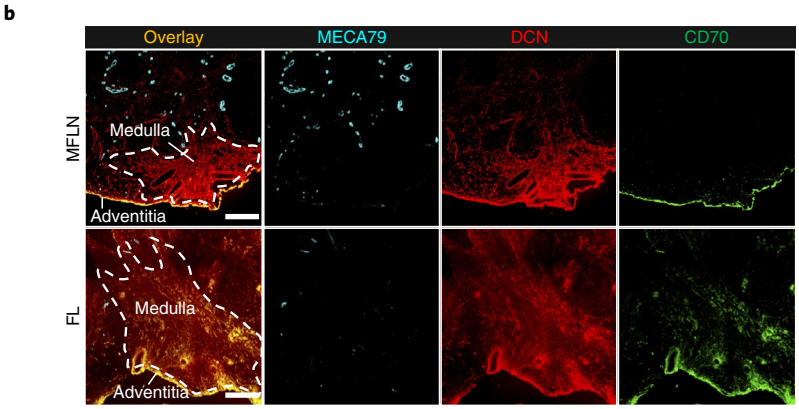
b
Overlay
MECA79
DCN
CD70
MFLN
FL
Medulla
Adventitia
Medulla
Adventitia

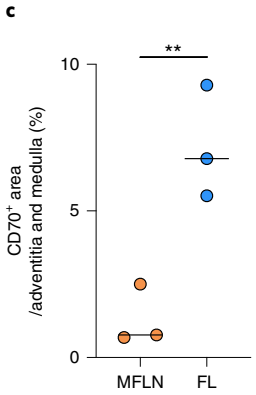
c
CD70+ area /adventitia and medulla (%)
10
5
0
**
MFLN
FL

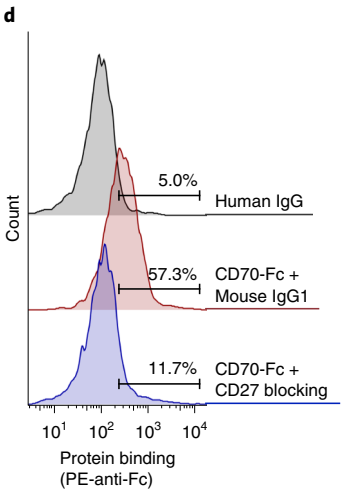
d
Count
5.0%
Human IgG
57.3%
CD70-Fc + Mouse IgG1
11.7%
CD70-Fc + CD27 blocking
10^1 10^2 10^3 10^4
Protein binding (PE-anti-Fc)

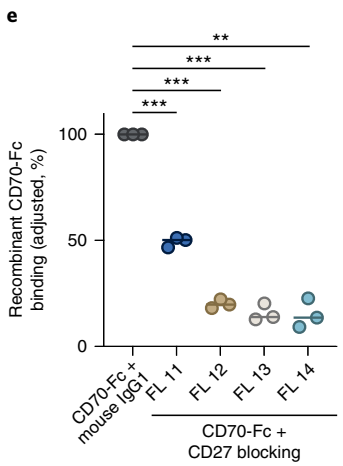
e
Recombinant CD70-Fc binding (adjusted, %)
100
50
0
**
***
***
***
CD70-Fc + mouse IgG1
FL 11
FL 12
FL 13
FL 14
CD70-Fc + CD27 blocking

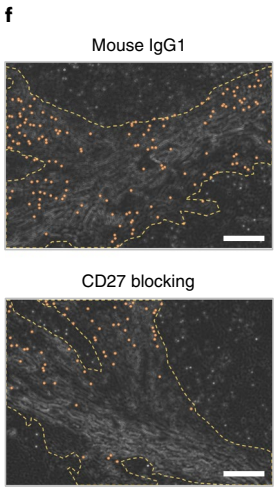
f
Mouse IgG1
CD27 blocking

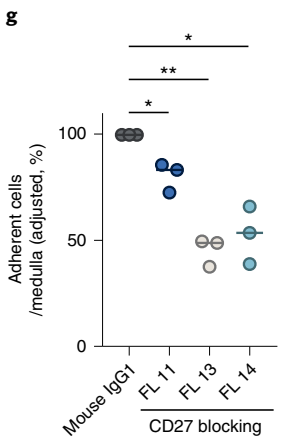
g
Adherent cells /medulla (adjusted, %)
100
50
0
*
**
*
Mouse IgG1
FL 11
FL 13
FL 14
CD27 blocking

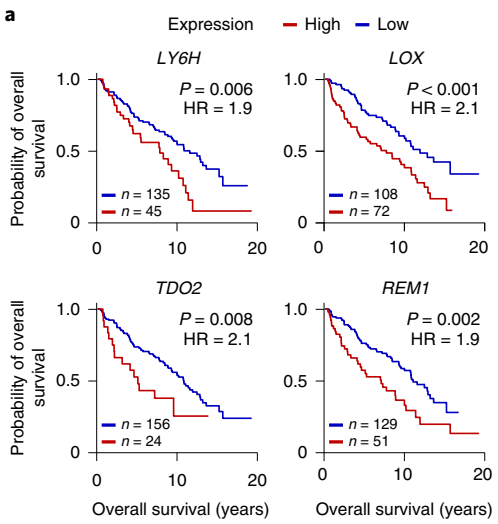

b

	Variables	Univariate Cox regression HR (95% CI)	Univariate Cox regression *P* value	Multivariate Cox regression HR (95% CI)	Multivariate Cox regression *P* value
Representative NHC subcluster	IPI, high and intermediate	3.12 (1.96–4.96)	<0.001	2.35 (1.46–3.80)	<0.001
	ASCT, not performed	0.61 (0.26–1.41)	0.24	–	–
tBEC	*LY6H* expression, high	1.86 (1.18–2.93)	0.006	1.98 (1.17–3.34)	0.010
tBEC	*LOX* expression, high	2.07 (1.37–3.13)	<0.001	2.07 (1.31–3.26)	0.001
	PTGIS expression, high	1.63 (1.07–2.46)	0.020	1.11 (0.65–1.91)	0.68
TRC	*TDO2* expression, high	2.09 (1.19–3.76)	0.009	1.95 (1.05–3.62)	0.033
TRC	*REM1* expression, high	1.92 (1.25–2.95)	0.002	1.63 (1.01–2.64)	0.044
	PIEZO2 expression, high	2.03 (1.12–3.68)	0.019	1.57 (0.79–3.10)	0.19
	CHI3L1 expression, high	2.23 (1.35–3.70)	0.001	1.57 (0.91–2.71)	0.10

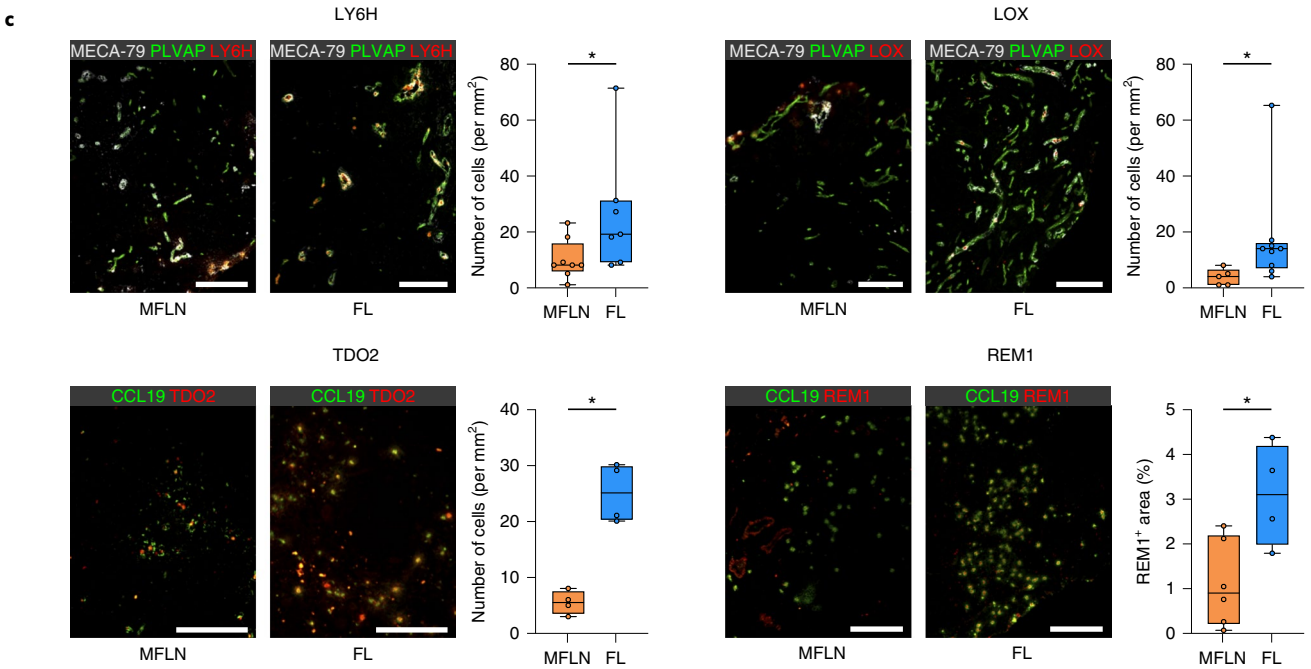

Fig. 7 | Identification of stroma-derived prognostic markers in FL. a, Kaplan–Meier curves showing the overall survival of patients newly diagnosed with FL ($n = 180$) based on the expression level of *LY6H*, *LOX*, *TDO2* and *REM1*. Statistical analysis was performed using the two-sided log-rank test. HR, hazard ratio. **b**, Univariate and multivariate Cox regression analyses predicting overall survival ($n = 180$). Statistical analysis was performed using two-sided Cox proportional-hazards analysis. Significant gene expression in multivariate analysis is indicated by text shaded in red. Representative NHC subcluster denotes subclusters in which indicated gene expression is most greatly upregulated in FL. CI, confidence interval. **c**, Left: images of IF staining for LY6H, LOX, TDO2 and REM1 in representative MFLN and FL samples. Scale bars, 200 μm. Right: the box plots show the interquartile range (box limits), median (centre line), minimum to maximum values (whiskers), and biologically independent samples (circles) for quantification of cell number (for LY6H, LOX and TDO2) or area (for REM1) positive for each protein in MFLN and FL samples (MFLN, $n = 8$, 5, 4 and 6; FL, $n = 7$, 9, 4 and 4 for LY6H, LOX, TDO2 and REM1, respectively). *$P = 0.029$ (LY6H), *$P = 0.010$ (LOX), *$P = 0.029$ (TDO2), *$P = 0.038$ (REM1) (two-sided Mann–Whitney *U*-test). Statistical source data are provided.

CD70 is overexpressed in FL medullary and adventitial SCs by IF staining (Fig. 6b,c). We next examined the gene and protein expression levels of the CD70 ligand CD27 in the B cells of FL samples. Single-cell transcriptomic analysis of FL B cells showed that *CD27* was significantly upregulated in malignant B cells compared with non-malignant B cells (Extended Data Fig. 8e). Consistent with these results, flow cytometry analysis of FL haematopoietic cells showed that the $CD19^+CD10^+$ cell population (malignant B-cell enriched fraction) in 5 out of 8 (62.5%) biologically independent samples was positive for CD27, and its expression was also significantly higher in the $CD19^+CD10^+$ population than in the $CD19^+CD10^-$ population (non-malignant B-cell fraction) (Extended Data Fig. 8f,g). Among the five $CD27^+$ FL samples, four (80.0%) showed unequivocal binding to recombinant human CD70-Fc protein (Fig. 6d). The binding of malignant B-enriched cells to CD70-Fc protein was significantly inhibited by the treatment of the cells with an anti-CD27 function-blocking antibody in all four cases (Fig. 6d,e). Next, we performed ex vivo cell adhesion assays using FL frozen sections and malignant B-enriched cells. The number of malignant B-enriched cells adhered to the medullary regions was

significantly decreased following treatment with the anti-CD27 antibody (Fig. 6f,g).

Prognostic implications of stroma-derived markers in FL. Next, we tested the applicability of our single-cell analysis of NHCs in the search for clinically relevant factors. To correlate niche-specific or subcluster-specific alterations in NHCs with survival of patients with FL, we utilized a bulk microarray dataset of 180 FL biopsy samples from newly diagnosed patients with available survival information[66].

We narrowed down multivariate analysis candidates to seven genes (*LY6H*, *LOX*, *PTGIS*, *TDO2*, *REM1*, *PIEZO2* and *CHI3L1*) expressed at minimal levels in FL haematopoietic cells but at high levels in FL BEC or NESC subclusters compared with MFLN counterparts. We hypothesized that they were probably associated with unfavourable prognosis (Fig. 7a and Extended Data Fig. 9a–e). In the multivariate analysis, increased expression of the tip cell markers *LY6H* and *LOX*, as well as *TDO2* and *REM1*, were associated with an unfavourable prognosis, even after adjustment for the international prognostic index[67] (Fig. 7b).

For each of the four genes, we performed IF staining in MFLN and FL samples. Cells expressing LY6H, LOX, TDO2 or REM1 were increased in FL compared with those in MFLNs (Fig. 7c).

Findings from the additional prognostic analyses are described in the Supplementary Note, Extended Data Fig. 9f,g and Supplementary Table 19.

Observation of NHC subclusters across lymphomas. Finally, we examined whether our single-cell atlas was applicable to different lymphoma subtypes. We also investigated a more aggressive FL stromal remodelling phenotype. To this end, we performed scRNA-seq of stroma-enriched cells from five nodal peripheral T-cell lymphoma (PTCL) samples and three diffuse large B-cell lymphoma transformed from FL (tDLBCL) samples (Fig. 1a, Extended Data Fig. 1c and Supplementary Table 20). Detailed findings are described in the Supplementary Note and Extended Data Fig. 10a–h. In brief, NHC subclusters were detectable in PTCL and tDLBCL data and we observed distinct alterations in tDLBCL stroma that probably represented a terminal form of stromal remodelling in FL.

Discussion

Here we presented a human LNNHC map at single-cell resolution that was useful for exploring changes in lymphoma NHCs.

First, we shed light on differences in mouse and human LNNHC heterogeneity. Overall, our findings suggest that human LNs harbour unique NHC subpopulations that have not been detected in murine LNs, which emphasizes the need for further human studies. As in previous studies that used fresh human LN samples[22,26], we used MFLNs from patients with tumours to construct the atlas. Notably, a detailed analysis of LNNHCs from an individual with a benign tumour indicated that the clustering was comparable between samples from the individual with a benign tumour and patients with a malignant tumour (Supplementary Note). This observation suggests minimal or negligible influence of malignancy-derived factors on our atlas.

Second, multistep DEG analyses revealed subcluster-specific changes in FL, including those with a previously unknown function in lymphoma. We found that upregulation of some of the known intercellular interactions across FL NHCs and malignant B cells extended to unanticipated NHC subclusters and, conversely, other interactions were enhanced in limited NHC subclusters. These observations largely increase the resolution of our understating of stromal remodelling in lymphoma. Additionally, these findings may be of clinical importance, as these may be considered as potential stroma-derived prognostic factors. Notably, two tip-cell markers were upregulated in FL and could serve as prognostic factors. LOX enzymatic activity is reported to drive tumour angiogenesis by activating PDGFRβ signalling in vascular SMCs, which is consistent with our DEG analysis that FL SMCs expressed *PDGFRB* at high levels[68]. Meanwhile, our observation of *LY6H* expression in tip cells has not previously been described in mouse or human endothelial cells. We also identified *TDO2* as a prognostic predictor of FL. *TDO2* may function to attract regulatory T cells, antagonize $CD8^+$ T-cell activity and accelerate myeloid cell tolerogenicity[69]. *REM1* overexpression in TRCs and PCs was also associated with unfavourable FL outcomes. Thus, further analysis of this gene, which has been scarcely explored, and its relevance to the lymphoma stroma is warranted. As the enrichment of the FL TRC signature per se was not prognostic (Supplementary Note), qualitative rather than quantitative alterations in certain NHC subpopulations may affect the chemoresistance and prognosis of FL more precisely. In addition to these prognostic factors, many upregulated genes with or without a known pro-tumorigenic function were included in our dataset, which makes our atlas a powerful discovery tool for additional therapeutic targets.

Third, we found that the CD70–CD27 interaction via stroma-derived CD70 was enhanced in FL. Although the role of CD70 has increasingly been investigated in the context of interplays across various immune cells and cancer cells[64,65], lymphoma SCs have not been explored as a source of CD70. A recent report suggested that CD70 expressed by CAFs supports tumour progression in solid cancers by facilitating cancer cell migration[70]. Consistent with these findings, we confirmed binding between CD70 and malignant B cells that could be blocked by an antagonist against the CD70 ligand CD27. CD70 was upregulated in extrafollicular FL SCs, which suggests that CD70 may facilitate the infiltration of lymphoma cells into extrafollicular regions during tumour progression. Our analysis therefore proposes stroma-derived CD70 as a potential biomarker and therapeutic target for FL.

Last, we found that NHC heterogeneities in LNs were detectable even in aggressive lymphomas, thereby confirming the usefulness of our NHC atlas to characterize the stroma of various lymphoma subtypes. In particular, alterations in tDLBCL stroma harmonized with those in FL, thereby supporting the findings from the analysis of FL stroma. Furthermore, our findings indicate that extrafollicular SCs, including TRCs and medullary SCs, not only promote extrafollicular infiltration of FL cells but simultaneously differentiate into FSCs and are finally replaced by FSCs in more advanced phenotypes. This reflects a unique stromal transition that corresponds to the FSC-dependent growth of FL[71].

Limitations of this study include the quantity of samples, which may not be sufficient to identify all NHC subpopulations or to precisely determine the correlation between the NHC heterogeneities in the transcriptome data and patient characteristics, such as genomic alterations. Second, we cannot completely exclude the possibility that our atlas is influenced by unknown factors from a distant malignancy. Third, our study was not designed to analyse other lymphoma subtypes or non-lymphoma diseases. Finally, further functional validation is required to confirm our findings relevant to each NHC subcluster.

In summary, our LNNHC atlas is of value to lymphoma researchers as it largely updates the NHC taxonomy in human LNs in the context of lymphoma. This study provides a platform for future research that aims to deepen our understanding of LN or lymphoma biology and to improve lymphoma management.

Online content

Any methods, additional references, Nature Research reporting summaries, source data, extended data, supplementary information, acknowledgements, peer review information; details of author contributions and competing interests; and statements of data and code availability are available at https://doi.org/10.1038/s41556-022-00866-3.

Received: 26 February 2021; Accepted: 10 February 2022;
Published online: 24 March 2022

References

1. Swerdlow, S. et al. *WHO Classification of Tumours of Haematopoietic and Lymphoid Tissues* 4th edn (WHO Press, 2017).
2. Scott, D. W. & Gascoyne, R. D. The tumour microenvironment in B cell lymphomas. *Nat. Rev. Cancer* **14**, 517–534 (2014).
3. Höpken, U. E. & Rehm, A. Targeting the tumor microenvironment of leukemia and lymphoma. *Trends Cancer* **5**, 351–364 (2019).
4. De Palma, M., Biziato, D. & Petrova, T. V. Microenvironmental regulation of tumour angiogenesis. *Nat. Rev. Cancer* **17**, 457–474 (2017).
5. Sahai, E. et al. A framework for advancing our understanding of cancer-associated fibroblasts. *Nat. Rev. Cancer* **20**, 174–186 (2020).
6. Ruan, J., Hajjar, K., Rafii, S. & Leonard, J. P. Angiogenesis and antiangiogenic therapy in non-Hodgkin's lymphoma. *Ann. Oncol.* **20**, 413–424 (2009).
7. Lenz, G. et al. Stromal gene signatures in large-B-cell lymphomas. *N. Engl. J. Med.* **359**, 2313–2323 (2008).
8. Medina, D. J. et al. Mesenchymal stromal cells protect mantle cell lymphoma cells from spontaneous and drug-induced apoptosis through secretion of B-cell activating factor and activation of the canonical and non-canonical nuclear factor κB pathways. *Haematologica* **97**, 1255–1263 (2012).
9. Mourcin, F., Pangault, C., Amin-Ali, R., Amé-Thomas, P. & Tarte, K. Stromal cell contribution to human follicular lymphoma pathogenesis. *Front. Immunol.* **3**, 280 (2012).
10. Valkenburg, K. C., de Groot, A. E. & Pienta, K. J. Targeting the tumour stroma to improve cancer therapy. *Nat. Rev. Clin. Oncol.* **15**, 366–381 (2018).
11. Carbone, A. et al. Follicular lymphoma. *Nat. Rev. Dis. Primers* **5**, 83 (2019).
12. Guilloton, F. et al. Mesenchymal stromal cells orchestrate follicular lymphoma cell niche through the CCL2-dependent recruitment and polarization of monocytes. *Blood* **119**, 2556–2567 (2012).
13. Husson, H. et al. CXCL13 (BCA-1) is produced by follicular lymphoma cells: role in the accumulation of malignant B cells. *Br. J. Haematol.* **119**, 492–495 (2002).
14. Tjin, E. P. et al. Functional analysis of HGF/MET signaling and aberrant HGF-activator expression in diffuse large B-cell lymphoma. *Blood* **107**, 760–768 (2006).
15. Lwin, T. et al. Lymphoma cell adhesion-induced expression of B cell-activating factor of the TNF family in bone marrow stromal cells protects non-Hodgkin's B lymphoma cells from apoptosis. *Leukemia* **23**, 170–177 (2009).
16. Epron, G. et al. Monocytes and T cells cooperate to favor normal and follicular lymphoma B-cell growth: role of IL-15 and CD40L signaling. *Leukemia* **26**, 139–148 (2012).
17. Link, A. et al. Fibroblastic reticular cells in lymph nodes regulate the homeostasis of naive T cells. *Nat. Immunol.* **8**, 1255–1265 (2007).
18. Krishnamurty, A. T. & Turley, S. J. Lymph node stromal cells: cartographers of the immune system. *Nat. Immunol.* **21**, 369–380 (2020).
19. Chang, J. E. & Turley, S. J. Stromal infrastructure of the lymph node and coordination of immunity. *Trends Immunol.* **36**, 30–39 (2015).
20. Fletcher, A. L., Acton, S. E. & Knoblich, K. Lymph node fibroblastic reticular cells in health and disease. *Nat. Rev. Immunol.* **15**, 350–361 (2015).
21. Rodda, L. B. et al. Single-Cell RNA sequencing of lymph node stromal cells reveals niche-associated heterogeneity. *Immunity* **48**, 1014–1028.e16 (2018).
22. Takeda, A. et al. Single-cell survey of human lymphatics unveils marked endothelial cell heterogeneity and mechanisms of homing for neutrophils. *Immunity* **51**, 561–572.e5 (2019).
23. Xiang, M. et al. A single-cell transcriptional roadmap of the mouse and human lymph node lymphatic vasculature. *Front. Cardiovasc. Med.* **7**, 52 (2020).
24. Fujimoto, N. et al. Single-cell mapping reveals new markers and functions of lymphatic endothelial cells in lymph nodes. *PLoS Biol.* **18**, e3000704 (2020).
25. Brulois, K. et al. A molecular map of murine lymph node blood vascular endothelium at single cell resolution. *Nat. Commun.* **11**, 3798 (2020).
26. Kapoor, V. N. et al. Gremlin 1^{+} fibroblastic niche maintains dendritic cell homeostasis in lymphoid tissues. *Nat. Immunol.* **22**, 571–585 (2021).
27. Lambrechts, D. et al. Phenotype molding of stromal cells in the lung tumor microenvironment. *Nat. Med.* **24**, 1277–1289 (2018).
28. Goveia, J. et al. An integrated gene expression landscape profiling approach to identify lung tumor endothelial cell heterogeneity and angiogenic candidates. *Cancer Cell* **37**, 21–36.e13 (2020).
29. Fang, J. S. et al. Shear-induced Notch–Cx37–p27 axis arrests endothelial cell cycle to enable arterial specification. *Nat. Commun.* **8**, 2149 (2017).
30. Fleming, R. E. et al. Carbonic anhydrase IV expression in rat and human gastrointestinal tract regional, cellular, and subcellular localization. *J. Clin. Invest.* **96**, 2907–2913 (1995).
31. Thiriot, A. et al. Differential DARC/ACKR1 expression distinguishes venular from non-venular endothelial cells in murine tissues. *BMC Biol.* **15**, 45 (2017).
32. Kalucka, J. et al. Single-cell transcriptome atlas of murine endothelial cells. *Cell* **180**, 764–779.e20 (2020).
33. Heckmann, B. L., Zhang, X., Xie, X. & Liu, J. The G0/G1 switch gene 2 (G0S2): regulating metabolism and beyond. *Biochim. Biophys. Acta* **1831**, 276–281 (2013).
34. Veerman, K., Tardiveau, C., Martins, F., Coudert, J. & Girard, J. P. Single-cell analysis reveals heterogeneity of high endothelial venules and different regulation of genes controlling lymphocyte entry to lymph nodes. *Cell Rep.* **26**, 3116–3131.e5 (2019).
35. Bondareva, O. et al. Identification of atheroprone shear stress responsive regulatory elements in endothelial cells. *Cardiovasc. Res.* **115**, 1487–1499 (2019).
36. Trapnell, C. et al. The dynamics and regulators of cell fate decisions are revealed by pseudotemporal ordering of single cells. *Nat. Biotechnol.* **32**, 381–386 (2014).
37. Phng, L. K. & Gerhardt, H. Angiogenesis: a team effort coordinated by Notch. *Dev. Cell* **16**, 196–208 (2009).
38. Cheng, H. W. et al. Origin and differentiation trajectories of fibroblastic reticular cells in the splenic white pulp. *Nat. Commun.* **10**, 1739 (2019).
39. Naba, A. et al. The matrisome: in silico definition and in vivo characterization by proteomics of normal and tumor extracellular matrices. *Mol. Cell. Proteom.* **11**, M111.014647 (2012).
40. Severino, P. et al. Human lymph node-derived fibroblastic and double-negative reticular cells alter their chemokines and cytokines expression profile following inflammatory stimuli. *Front. Immunol.* **8**, 141 (2017).
41. Phillips, R. & Ager, A. Activation of pertussis toxin-sensitive CXCL12 (SDF-1) receptors mediates transendothelial migration of T lymphocytes across lymph node high endothelial cells. *Eur. J. Immunol.* **32**, 837–847 (2002).
42. Xu, Q., Schett, G., Li, C., Hu, Y. & Wick, G. Mechanical stress-induced heat shock protein 70 expression in vascular smooth muscle cells is regulated by Rac and Ras small G proteins but not mitogen-activated protein kinases. *Circ. Res.* **86**, 1122–1128 (2000).
43. González-González, L. & Alonso, J. Periostin: a matricellular protein with multiple functions in cancer development and progression. *Front. Oncol.* **8**, 225 (2018).
44. Noh, K. et al. Differential effects of EGFL6 on tumor versus wound angiogenesis. *Cell Rep.* **21**, 2785–2795 (2017).
45. An, J. et al. EGFL6 promotes breast cancer by simultaneously enhancing cancer cell metastasis and stimulating tumor angiogenesis. *Oncogene* **38**, 2123–2134 (2019).
46. Cremasco, V. et al. FAP delineates heterogeneous and functionally divergent stromal cells in immune-excluded breast tumors. *Cancer Immunol. Res.* **6**, 1472–1485 (2018).
47. Costa, A. et al. Fibroblast heterogeneity and immunosuppressive environment in human breast cancer. *Cancer Cell* **33**, 463–479.e10 (2018).
48. Kieffer, Y. et al. Single-cell analysis reveals fibroblast clusters linked to immunotherapy resistance in cancer. *Cancer Discov.* **10**, 1330–1351 (2020).
49. Ley, K. The role of selectins in inflammation and disease. *Trends Mol. Med.* **9**, 263–268 (2003).
50. Silva, M., Videira, P. A. & Sackstein, R. E-selectin ligands in the human mononuclear phagocyte system: implications for infection, inflammation, and immunotherapy. *Front. Immunol.* **8**, 1878 (2017).
51. Farr, L., Ghosh, S. & Moonah, S. Role of MIF cytokine/CD74 receptor pathway in protecting against injury and promoting repair. *Front. Immunol.* **11**, 1273 (2020).
52. Vento-Tormo, R. et al. Single-cell reconstruction of the early maternal–fetal interface in humans. *Nature* **563**, 347–353 (2018).
53. Cao, Z. et al. Angiocrine factors deployed by tumor vascular niche induce B cell lymphoma invasiveness and chemoresistance. *Cancer Cell* **25**, 350–365 (2014).
54. Wallach-Dayan, S. B. et al. CD44-dependent lymphoma cell dissemination: a cell surface CD44 variant, rather than standard CD44, supports in vitro lymphoma cell rolling on hyaluronic acid substrate and its in vivo accumulation in the peripheral lymph nodes. *J. Cell Sci.* **114**, 3463–3477 (2001).
55. Higashi, M. et al. CD44 expression during tumor progression of follicular lymphoma. *Oncol. Rep.* **22**, 1135–1140 (2009).
56. Drillenburg, P. & Pals, S. T. Cell adhesion receptors in lymphoma dissemination. *Blood* **95**, 1900–1910 (2000).
57. Ashkenazi, A. Targeting death and decoy receptors of the tumour-necrosis factor superfamily. *Nat. Rev. Cancer* **2**, 420–430 (2002).
58. Pandey, S. et al. IL-4/CXCL12 loop is a key regulator of lymphoid stroma function in follicular lymphoma. *Blood* **129**, 2507–2518 (2017).
59. Novak, A. J. et al. Genetic variation in B-cell-activating factor is associated with an increased risk of developing B-cell non-Hodgkin lymphoma. *Cancer Res.* **69**, 4217–4224 (2009).

60. Gerli, M. F. M. et al. Combined Notch and PDGF signaling enhances migration and expression of stem cell markers while inducing perivascular cell features in muscle satellite cells. *Stem Cell Rep.* **12**, 461–473 (2019).
61. Rehm, A. et al. Cooperative function of CCR7 and lymphotoxin in the formation of a lymphoma-permissive niche within murine secondary lymphoid organs. *Blood* **118**, 1020–1033 (2011).
62. Jacobs, J. et al. CD70: an emerging target in cancer immunotherapy. *Pharmacol. Ther.* **155**, 1–10 (2015).
63. Starzer, A. M. & Berghoff, A. S. New emerging targets in cancer immunotherapy: CD27 (TNFRSF7). *ESMO Open* **4**, e000629 (2020).
64. Yang, Z. Z. et al. TGF-β upregulates CD70 expression and induces exhaustion of effector memory T cells in B-cell non-Hodgkin's lymphoma. *Leukemia* **28**, 1872–1884 (2014).
65. Al Sayed, M. F. et al. CD70 reverse signaling enhances NK cell function and immunosurveillance in CD27-expressing B-cell malignancies. *Blood* **130**, 297–309 (2017).
66. Leich, E. et al. Follicular lymphomas with and without translocation t(14;18) differ in gene expression profiles and genetic alterations. *Blood* **114**, 826–834 (2009).
67. International Non-Hodgkin's Lymphoma Prognostic Factors Project. A predictive model for aggressive non-Hodgkin's lymphoma. *N. Engl. J. Med.* **329**, 987–994 (1993).
68. Baker, A. M. et al. Lysyl oxidase plays a critical role in endothelial cell stimulation to drive tumor angiogenesis. *Cancer Res.* **73**, 583–594 (2013).
69. Opitz, C. A. et al. The therapeutic potential of targeting tryptophan catabolism in cancer. *Br. J. Cancer* **122**, 30–44 (2020).
70. Jacobs, J. et al. Unveiling a CD70-positive subset of cancer-associated fibroblasts marked by pro-migratory activity and thriving regulatory T cell accumulation. *Oncoimmunology* **7**, e1440167 (2018).
71. Béguelin, W. et al. Mutant EZH2 induces a pre-malignant lymphoma niche by reprogramming the immune response. *Cancer Cell* **37**, 655–673.e11 (2020).

Methods

Human samples. This study was approved by the Ethics Committee of the University of Tsukuba Hospital and the review boards of associated institutions that provided human samples (Kameda Medical Center, NTT Medical Center Tokyo and Mito Medical Center) and conducted according to all relevant ethical regulations regarding human participants. Written informed consent was obtained from all participants. The participants were not compensated for taking part in the study. For scRNA-seq, MFLN samples were prospectively collected from patients with a neoplasm ($n=9$) who had undergone surgical LN dissection between January and June 2020. Non-sentinel LNs without enlargement (<1 cm) were used. The collected LNs were verified as malignancy-free via flow cytometry analysis of pan-cytokeratin negativity (Extended Data Fig. 1b). Nodal FL ($n=10$), PTCL ($n=5$) and tDLBCL ($n=3$) samples were also prospectively collected between August 2019 and May 2020. Furthermore, for functional experiments, additional nodal FL samples ($n=8$) were collected between May 2020 and August 2021. Lymphoma diagnosis of tissue specimens was made pathologically, phenotypically and/or referring to results of cytogenetic examinations, including fluorescence in situ hybridization analysis by expert haematopathologists.

Single-cell isolation of LNNHCs. After collection, LN or lymphoma samples were immediately minced and digested for 1 h with RPMI 1640 medium (Sigma-Aldrich, R8758) with 5% fetal bovine serum (FBS) containing 0.2 mg ml^{-1} collagenase P (Sigma-Aldrich, 11213857001), 0.8 mg ml^{-1} dispase (Gibco, 17105041) and 0.1 mg ml^{-1} DNase I (Worthington, LS002139), with continuous agitation. Cells were then filtered through a 70-µm mesh, and red blood cells were lysed in 1% ammonium-chloride-potassium buffer. Thereafter, haematopoietic cells and contaminated red blood cells were depleted using human CD45 (130-045-801) and CD235a (130-050-501) microbeads according to the manufacturer's instructions (Miltenyi Biotec). For MFLN samples, the remaining single-cell suspension was incubated with phycoerythrin (PE)-anti-CD45 (BioLegend; 1:500) in combination with Alexa Fluor 488-pan-cytokeratin (ThermoFisher Scientific; 1:500), allophycocyanin (APC)-anti-podoplanin (BioLegend; 1:500) and PE-cyanin 7 (PE-Cy7)-anti-CD31 (BioLegend; 1:500). For lymphoma samples, PE-anti-CD45 was mixed with fluorescein isothiocyanate (FITC)-anti-CD31 (BioLegend; 1:500), APC-anti-podoplanin (BioLegend; 1:500) and PE-Cy7-anti-CD34 (BioLegend; 1:500). The samples were incubated for 20 min, then 7-AAD viability staining solution (ThermoFisher Scientific, 00-6993-50; 1:1,000) was added and incubated for 10 min in the dark on ice. CD45$^-$ live cells were sorted using a FACSAria II or III (BD Bioscience) after removing doublets by gating with a FSC-H versus FCS-W plot and a SSC-H versus SSC-W plot. Flow cytometry data were analysed using FlowJo software (Tree Star, v.10.7.1). CD45$^+$ cells were cryopreserved in FBS plus 10% dimethylsulfoxide in liquid nitrogen.

Library preparation, sequencing and data pre-processing. Sorted CD45$^-$ cells were converted to barcoded scRNA-seq libraries using Chromium Single Cell 3′ reagent kits (V3) (10X Genomics) according to the manufacturer's instructions (CG000183 Rev A), aiming for 5,000–8,000 cells per library. Library quality control and quantification were performed using a KAPA Library Quantification kit for Illumina platforms (Kapa Biosystems, KK4873) and a 2100 Bioanalyzer High Sensitivity DNA kit (Agilent, 5067-4626). Libraries were sequenced on an Illumina HiSeq X Ten system with an average depth of 31,439 reads per cell, then mapped to the human genome (build GRCh38) and demultiplexed using CellRanger pipelines (10X Genomics, v.3.1.0).

Data processing and cell clustering of individual cases. Pre-processed data from each sample were further processed and analysed individually using the R package Seurat (v.3.2.2) on RStudio (v.3.5.0 or v.4.0.2). After removing ribosomal genes, genes expressed in fewer than 3 cells and cells expressing fewer than 200 genes, we filtered out cells with fewer than 200 unique feature counts (low-quality cells). Cells with unique feature counts greater than three times the median value (possible doublets) and/or cells with more than twice the median number of mitochondrial genes (possible apoptotic or lysed cells) were also removed. We then normalized data using the NormalizeData function and extracted highly variable features using the FindVariableFeatures function. Normalized data underwent a linear transformation (scaling) and principal component analysis (PCA) based on variable features using the RunPCA function. Graph-based clustering was then performed according to gene expression profiles using the FindNeighbors and FindClusters functions with default parameters, and results were visualized using a nonlinear dimensional reduction UMAP technique running RunUMAP and DimPlot functions. Cell clusters were annotated based on the expression of canonical markers, including *PECAM1* and *JAM2* for BECs, *PECAM1* and *PROX1* for LECs, *ACTA2* for SMCs, *CCL19* and *CCL21* for TRCs, *CR2* for FDCs, *DCN* for other NESCs, *PTPRC* for contaminating lymphocytes, *SDC1* for plasma cells, and *CCR7* and *CD83* (in cells weakly *PTPRC*$^+$) for dendritic cells[22,72,73]. *MKI67* and *TOP2A* expression levels were used to identify clusters of an aggressively proliferative nature. For the FL sample 3, which came from a patient with intra-submandibular gland FL, any distinct clusters negative for all canonical markers and positive for keratin genes (indicating glandular tissue contamination) were removed. All other cases were confirmed to consist solely of these major clusters. We confirmed a negligible presence of ambient RNA contamination in single-cell NHC data, and found an imperceptible influence of potential RNA contamination on clustering results in all LN and lymphoma samples by using the DecontX (in the celda package, v.1.6.1) and SoupX (v.1.5.2) packages (data not shown)[74,75].

Data integration with batch effect collection. We performed canonical correlation analysis[76] to identify shared sources of variation across multiple datasets using the FindIntegrationAnchors function and integrated them using anchors from the IntegrateData function with canonical correlation dimensions of 20. Integrated data were scaled and underwent PCA as performed in individual datasets.

Supervised annotation and unsupervised clustering of LNNHCs. We performed graph-based clustering of PCA-reduced integrated data and supervised annotation, as described in 'Data processing and cell clustering of individual cases' above. Clusters characterized by extremely low unique feature counts (low-quality cells) were removed.

Next, we extracted the three major NHC components (BECs, LECs and NESCs) in silico and performed scaling, PCA-based dimensional reduction and unsupervised graph-based subclustering of each component. We removed subclusters that were considered possible doublets as characterized by high expressions of marker genes for different NHC components and incongruously high unique feature counts. In BEC subclustering, we also performed supervised annotation for the identification of arterial, capillary and venous BECs using canonical markers for each BEC component[29–32].

DEG analysis. DEG analysis was performed using the FindMarkers or FindAllMarkers functions with a minimum of 20% of the gene-expressing cells and a minimum log fold-change of 0.25 in gene expression between each cluster and other clusters. We primarily used the Wilcoxon rank-sum test for DEG detection. To confirm detected DEGs, we also used the model-based analysis of single-cell transcriptomics (MAST) method[77]. DEGs were defined as genes confirmed to show an adjusted *P* value (based on the Bonferroni correction) of <0.05 by using both methods. Results of the Wilcoxon rank-sum test were used to construct DEG lists and volcano plots. Volcano plots were created using the R package EnhancedVolcano (v.1.8.0). DEG analysis to compare corresponding clusters between mLN and pLN samples and between MFLN and FL samples was performed in a similar manner using the cut-off parameters described above.

For DEG analyses between MFLN and FL NHC subclusters, we adopted a multistep approach. Several previous studies had indicated differences in gene and protein expression between mLNs and pLNs[78–81]. Therefore, we initially profiled DEGs between mLNs and pLNs among MFLNs at subcluster levels (Supplementary Table 13 and Supplementary Note). Referring to this profile, we identified DEGs upregulated in FL by removing those detected between mLNs and pLNs. We also performed DEG analysis between MFLN and FL NHC subclusters using only pLN samples (MFLN 7–MFLN 9 and FL 2–FL 10) to support the reliability of the detected DEGs.

GO enrichment analysis of DEGs in particular clusters was performed using Metascape (http://metascape.org)[82].

Trajectory analysis. We performed trajectory analysis using the Monocle 3 package (v.0.2.3)[36] in RStudio on integrated BEC, NESC and LEC data constructed using Seurat. Data pre-processing was performed using the preprocess_cds function, with the number of dimensions set at 100. Dimensionality reduction and clustering were performed using the reduce_dimension and cluster_cells functions, respectively. We then fit a principal graph within each cluster using the learn_graph function and visualized the order of cells in pseudotime by plot_cells or plot_cells_3d functions, as appropriate with the pseudotime colouring option.

Single-cell analysis of FL haematopoietic cells. We performed single-cell analysis of cryopreserved CD45$^+$ cells from nine FL samples (FL 2–FL 10). After thawing, cell suspensions were filtered through a 70-µm mesh and incubated with 7-AAD viability staining solution for 10 min in the dark. The 7-AAD$^-$ live cells were sorted using a FACSAria II or III after removing doublets, then were converted to barcoded scRNA-seq libraries, as performed for CD45$^-$ cells. Library preparation, sequencing and data processing were performed as for CD45$^-$ cells. Data quality control, processing and graph-based clustering were performed in each individual case using the Seurat package, with dimension and resolution parameters of 50 and 0.5, respectively. Thereafter, we identified malignant B-cell populations by detecting restrictions of light chain kappa/lambda genes, as suggested by previous studies[83,84]. In brief, we projected the B-cell marker *CD79A* and the light chain genes *IGKC* (for light chain kappa) and *IGLC2* (for light chain lambda) to cell clusters on the UMAP plot of each sample (Extended Data Fig. 8a). We then calculated the ratio of cells expressing *IGLC2* and *IGKC* with expression levels of >1 and >2, respectively, in each B-cell cluster. We defined B-cell clusters with a ratio of >2.0 or <0.25 as malignant (Extended Data Fig. 8b).

Malignant B-cell signature analysis in FL B cells. To support the reliability of malignant B-cell detection, we performed signature analysis on data from FL B cells. We developed a gene set that represents a malignant B-cell signature based on the recent single-cell analysis of FL B cells reported by Andor et al.[83]. We carefully selected genes that were described as significantly upregulated in malignant compared to non-malignant B cells in a uniform manner among different FL samples[83]. Selected genes are listed in Supplementary Table 21. A malignant B-cell signature score was calculated in B cells of all nine FL samples using the GSVA package (v.1.38.2)[85] and depicted using the FeaturePlot and VlnPlot functions of Seurat.

Intercellular ligand–receptor interaction analysis. We investigated interactions between NHC subclusters and malignant B cells of nine FL samples (FL2–FL10) using the CellPhoneDB package (v.2.1.1)[52] on Python (v.3.6). Gene expression information relevant to each NHC subcluster in integrated FL NHCs was used for NHC data, whereas gene expression information relevant to malignant B-cell clusters in each FL sample was separately used for malignant B-cell data, as gene expression profiles of malignant B cells vary greatly among samples. We then performed pairwise comparisons between NHC subclusters and malignant B-cell clusters. In brief, we derived potential ligand–receptor interactions based on the expression of a receptor gene by one lineage subpopulation and a ligand gene by another. We filtered genes expressed in >20% of cells in any given subpopulation. We then permuted the cluster labels of all input cells 1,000 times and calculated the mean interaction score (the average receptor expression level in a subpopulation multiplied by the average ligand expression level in the interacting subpopulation), which generated a null distribution of the mean interaction score for each ligand–receptor pair in each pairwise comparison across subpopulations. Thereafter, we located observed mean interaction scores that were the same or higher than the actual mean score in the null distribution and calculated the proportion of the observed scores, conferring a *P* value for the likelihood of specificity of a given ligand–receptor complex to a given cluster pair. To consider interactions between FL NHCs and FL malignant B cells, we selected only interactions with a *P* value of <0.05 in more than half of FL cases (>4 cases). Furthermore, to assess subcluster-specific lymphomagenesis mechanisms in FL stroma, we extracted interactions that included a molecule in which gene expression was significantly upregulated in at least one FL NHC subcluster compared with that in the corresponding MFLN subcluster. We integrated interaction scores and *P* values of interactions between pairs consisting of the same NHC subcluster and malignant B-cell clusters from different FL samples, as previously described[84]. In brief, we calculated mean interaction scores for pairs that included the same NHC subcluster and malignant B-cell clusters from different FL samples, then normalized the mean interaction scores per interaction. We also combined *P* values of interactions for pairs that consisted of the same NHC subcluster and malignant B-cell clusters from different FL samples using Fisher's method. The *P* values were corrected using the Benjamini–Hochberg method. In Fig. 6a, circles are coloured when gene expression for the indicated stroma-derived factor is upregulated in relevant FL subclusters compared to that in the MFLN counterparts (log fold-change >0 and adjusted *P* value <0.05).

IF staining. Human LN and lymphoma samples were immediately embedded in OCT compound (Sakura Finetek Japan, 45833) and frozen in hexane cooled with dry ice. Samples were sliced to 3-µm thickness with a cryostat at −20 °C. Sections were dried for 1 h at 20 °C, fixed for 10 min in 4% paraformaldehyde, incubated for 10 min with 0.1% Triton X-100 (Sigma-Aldrich, T9284) for permeabilization, and then treated with 10% goat serum (Sigma-Aldrich, G9023) in PBS or serum-free protein blocking buffer (Dako, X0909) (when using non-goat-derived secondary antibodies) for 30 min. Sections were stained overnight at 4 °C with primary antibodies listed in Supplementary Table 22. After several washes with tris-buffered saline with tween 20 (Sigma-Aldrich, P9416), sections were stained for 1 h with combinations of the following secondary antibodies at 20 °C: AF488-goat-anti-rat IgG (ThermoFisher Scientific), AF594-goat-anti-rabbit IgG (ThermoFisher Scientific), AF594-donkey-anti-goat IgG (ThermoFisher Scientific) and AF647-goat-anti-mouse IgG (ThermoFisher Scientific). A TrueVIEW Autofluorescence Quenching kit (Vector, SP-8500) was used to decrease possible tissue autofluorescence per the manufacturer's instructions. Sections were then mounted in mounting medium with 4,6-diamidino-2-phenylindole (DAPI; Vector, H-1200). Stained samples were imaged using a Leica DMi8 S Platform with the Thunder imaging system (3D Live Cell & 3D Cell Culture & 3D assay). Analysed LNs were verified as malignancy-free by pan-cytokeratin staining. Quantitative analysis of acquired images was performed using ImageJ software (National Institute of Health, v.2.1.0). As LNs and FL carry localized structures, we randomly acquired at least five different regions of interest within each sample and used the median values for statistical analysis.

Flow cytometry analysis of FL haematopoietic cells. To analyse the expression of CD27 in malignant FL B cells and to perform the binding/adhesion assays described below, we used additionally collected cryopreserved FL samples (FL11–FL18). Clinical characteristics of patients in the additional FL cohort are described in Supplementary Table 23. After thawing, cells were filtered through a 70-µm mesh and incubated with PE-anti-CD27 (BioLegend; 1:500), FITC-anti-CD3 (BioLegend; 1:500), APC-anti-CD19 (Miltenyi Biotec; 1:500) and PE-Cy7-anti-CD10 (BioLegend; 1:500) antibodies for 20 min on ice. Cells were then incubated with 7-AAD viability staining solution for 10 min in the dark and analysed using a FACSAria II or III and FlowJo software.

Recombinant protein binding assay. Recombinant Fc chimera CD70 (SinoBiological, 10780-H01H) or human IgG (R&D systems, 1-001-A) was incubated with a single-cell suspension of FL haematopoietic cells for 10 min at 4 °C in RPMI with 10% FCS. To block CD70–CD27 binding, cells were incubated in the presence of anti-CD27 blocking antibody (R&D systems, MAB382) or isotype mouse IgG1 (R&D systems, MAB002) for 30 min at 4 °C before binding. After binding, the cells were washed, fixed using 4% paraformaldehyde for 10 min at 20 °C, incubated with PE-anti-human IgG Fc (R&D systems; 1:500), FITC-anti-CD3 (1:500), APC-anti-CD19 (1:500) and PE-Cy7-anti-CD10 (1:500) for 20 min at 4 °C, and analysed using flow cytometry (FACSAria II or III) and FlowJo software.

Ex vivo cell adhesion assay. Frozen FL sections were sliced at 6-µm thickness immediately before the assay. For malignant B-cell isolation, we used FL samples in which >90% B cells were confirmed to be malignant by flow cytometry. B cells were isolated from the FL haematopoietic cell suspension using an EasySep Release Human CD19 Positive Selection kit (StemCell Technologies, ST-17754). Cells were then treated with anti-CD27 blocking antibody or isotype mouse IgG1 for 30 min at 4 °C. Thereafter, 2×10^6 cells were applied on the sections and incubated with 60 r.p.m. rotation for 5 min, followed by incubation without rotation for 15 min. The incubation with and without rotation was repeated two more times. After incubation, the sections were gently washed with PBS, sealed with a cover glass and imaged using a Keyence BZ-X710 microscope (Keyence). Adherent cells were manually counted using ImageJ.

Prognostic analysis of stroma-derived markers in FL. To analyse the prognostic potential of gene expression patterns of NHCs in patients with FL, we used a bulk microarray dataset of 180 FL biopsy samples from independent, newly diagnosed cases[66]. To narrow candidates to stroma-specific genes, we initially selected DEGs upregulated in FL BEC and NESC subclusters relative to MFLN counterparts. These were narrowed down to those showing a log fold-change of >0.5 and <0.1% of cells with an expression level higher than 0 in FL haematopoietic cells (Extended Data Fig. 9a). We did not use genes upregulated in FL LEC subclusters, as the proportion of FL LECs was considerably decreased relative to MFLN LECs and the specificity of these genes to FL stroma was considered unlikely in analyses of bulk tissues. Next, we tested the expression of all candidate genes using the Kaplan–Meier method and two-sided log-rank test. Cut-off expression values of each gene for the Kaplan–Meier survival curves was determined using maximally selected rank statistics[86]. As many putative stroma-specific genes were upregulated in FL, it was possible that *P* value collection (for example, the Bonferroni method) greatly reduced the number of candidate genes, considering that the sample size in the dataset was not particularly large. Therefore, we extracted genes with reliable prognostic impacts using another approach (Extended Data Fig. 9a,c). We initially divided patients into three groups according to survival outcomes: a favourable group, which comprised patients alive 10 years after diagnosis; an unfavourable group, which comprised patients who died within 5 years of diagnosis; and an intermediate/indefinite group, which comprised the remaining patients (Extended Data Fig. 9c). We then compared the proportion of patients with higher expression of each candidate gene between favourable and unfavourable groups. Genes were considered prognostic when the proportion was significantly higher in the unfavourable group compared with that in the favourable group (Extended Data Fig. 9d). These prognostic genes were further subjected to multivariate analysis (Extended Data Fig. 9a).

To evaluate the prognostic efficiency of the FL TRC signature, we extracted the DEGs that were upregulated in FL TRCs in comparison to MFLN TRCs (Supplementary Table 17). We considered the DEGs with an expression level higher than 0 in <0.1% FL haematopoietic cells, <10% FL BECs and <10% FL LECs and were detectable in the microarray dataset[66]. A total of 11 extracted genes constituting the FL TRC signature are listed in Supplementary Table 19.

Whole-exome sequencing. Whole-exome sequencing was performed on genomic DNA extracted from nine FL samples (FL2–FL10). Libraries were prepared using SureSelect Human All Exon v.7 kits (Agilent Technologies, 5191-4004) according to the manufacturer's instructions and sequenced using an Illumina HiSeq X Ten system with a 150-bp paired-end protocol. We used the Genomon2 pipeline (v.2.6.2) for alignment of sequence and mutation calling. Somatic mutations with a Fisher's exact *P* value of <0.01 and an empirical Bayesian call *P* value of <0.0001 were adopted. Thereafter, mutations of synonymous single nucleotide variants, variants only in unidirectional reads, variants in intergenic, intronic, untranslated regions and noncoding RNA regions, and variants in repetitive genomic regions were excluded. Furthermore, known genetic alterations affecting at least 10% of FL[11] were screened for additional mutations. Finally, mutations derived from mapping errors were excluded using Integrative Genomics Viewer. Detected somatic mutations are listed in Supplementary Table 2.

Statistics and reproducibility. Statistical analysis was performed using R on RStudio or GraphPad Prism 9 (GraphPad, v.9.2.0). A two-sided *P* value of <0.05 was considered statistically significant.

Reporting Summary. Further information on research design is available in the Nature Research Reporting Summary linked to this article.

Data availability

The scRNA-seq data that support the findings of this study have been deposited at the European Genome-Phenome Archive (https://ega-archive.org) database and can be retrieved using the accession number EGAD00001008311. For survival analysis, a DNA microarray dataset from Leich et al.[66] was downloaded from the Gene Expression Omnibus (GEO) (accession number: GSE16131). For mapping of scRNA-seq data, GRCh38 (https://www.ncbi.nlm.nih.gov/assembly/GCF_000001405.39) was used. All other data are available from the corresponding authors on reasonable request. Source data are provided with this paper.

Code availability

The codes for key computational analyses are available on GitHub at https://github.com/yoshiakiabe1018/Stroma01. All of the packages used are available online.

References

72. Zhao, Q. et al. Single-cell transcriptome analyses reveal endothelial cell heterogeneity in tumors and changes following antiangiogenic treatment. *Cancer Res.* **78**, 2370–2382 (2018).
73. Baryawno, N. et al. A cellular taxonomy of the bone marrow stroma in homeostasis and leukemia. *Cell* **177**, 1915–1932.e16 (2019).
74. Yang, S. et al. Decontamination of ambient RNA in single-cell RNA-seq with DecontX. *Genome Biol.* **21**, 57 (2020).
75. Young, M. D. & Behjati, S. SoupX removes ambient RNA contamination from droplet-based single-cell RNA sequencing data. *GigaScience* https://doi.org/10.1093/gigascience/giaa151 (2020).
76. Butler, A., Hoffman, P., Smibert, P., Papalexi, E. & Satija, R. Integrating single-cell transcriptomic data across different conditions, technologies, and species. *Nat. Biotechnol.* **36**, 411–420 (2018).
77. Finak, G. et al. MAST: a flexible statistical framework for assessing transcriptional changes and characterizing heterogeneity in single-cell RNA sequencing data. *Genome Biol.* **16**, 278 (2015).
78. Streeter, P. R., Berg, E. L., Rouse, B. T., Bargatze, R. F. & Butcher, E. C. A tissue-specific endothelial cell molecule involved in lymphocyte homing. *Nature* **331**, 41–46 (1988).
79. Berlin, C. et al. α4β7 integrin mediates lymphocyte binding to the mucosal vascular addressin MAdCAM-1. *Cell* **74**, 185–195 (1993).
80. von Andrian, U. H. & Mempel, T. R. Homing and cellular traffic in lymph nodes. *Nat. Rev. Immunol.* **3**, 867–878 (2003).
81. Lee, M. et al. Transcriptional programs of lymphoid tissue capillary and high endothelium reveal control mechanisms for lymphocyte homing. *Nat. Immunol.* **15**, 982–995 (2014).
82. Zhou, Y. et al. Metascape provides a biologist-oriented resource for the analysis of systems-level datasets. *Nat. Commun.* **10**, 1523 (2019).
83. Andor, N. et al. Single-cell RNA-seq of follicular lymphoma reveals malignant B-cell types and coexpression of T-cell immune checkpoints. *Blood* **133**, 1119–1129 (2019).
84. Roider, T. et al. Dissecting intratumour heterogeneity of nodal B-cell lymphomas at the transcriptional, genetic and drug-response levels. *Nat. Cell Biol.* **22**, 896–906 (2020).
85. Hänzelmann, S., Castelo, R. & Guinney, J. GSVA: gene set variation analysis for microarray and RNA-seq data. *BMC Bioinformatics* **14**, 7 (2013).
86. Hothorn, T. & Zeileis, A. Generalized maximally selected statistics. *Biometrics* **64**, 1263–1269 (2008).

Acknowledgements

We thank our staff at associated institutions and departments for cooperation in collections of the human samples; E. Matsuzawa and Y. Sakashita for technical assistance; and A. Suzuki and Y. Suzuki (the University of Tokyo) for their support in the computational analysis of scRNA-seq data. Finally, we acknowledge E. Lamar for outstanding editorial assistance. This work was supported by Grants-in-Aid for Scientific Research (KAKENHI: JP20J20851 to Y.A., JP21H02945 to M.S.-Y., and JP19H03683 to S.C.) from the Ministry of Education, Culture, Sports, and Science of Japan; AMED under grant numbers JP21ck0106544 and JP21ck0106644 (to M.S.-Y.) and JP21cm0106505 (to S.C.); and Okinaka Memorial Institute for Medical Research, Foundation for Promotion of Cancer Research, and Takeda Science Foundation (to M.S.-Y.). The funders had no role in the study design, data collection and analysis, decision to publish or preparation of the manuscript.

Author contributions

Y.A. collected the human samples, performed all experiments and computational analyses, and generated all figures and tables. M.S.-Y. and M.F. developed experimental and analytical scRNA-seq systems and supported scRNA-seq experiments and analyses. H.M., T.B.N. and K.O. assisted in the immunostaining experiments. Y.S., K.H., M.K., T.S., H.N., Y.O., T.E., A.S., H.B., C.Y., R.T., T.T., M.N., K.U., T.O. and K.M. aided in human sample collection. M.S.-Y. conceived the study. Y.A., M.S.-Y. and S.C. designed the project and wrote the manuscript.

Competing interests

The authors declare no competing interests.

Additional information

Extended data is available for this paper at https://doi.org/10.1038/s41556-022-00866-3.

Supplementary information The online version contains supplementary material available at https://doi.org/10.1038/s41556-022-00866-3.

Correspondence and requests for materials should be addressed to Mamiko Sakata-Yanagimoto or Shigeru Chiba.

Peer review information *Nature Cell Biology* thanks the anonymous reviewers for their contribution to the peer review of this work. Peer reviewer reports are available.

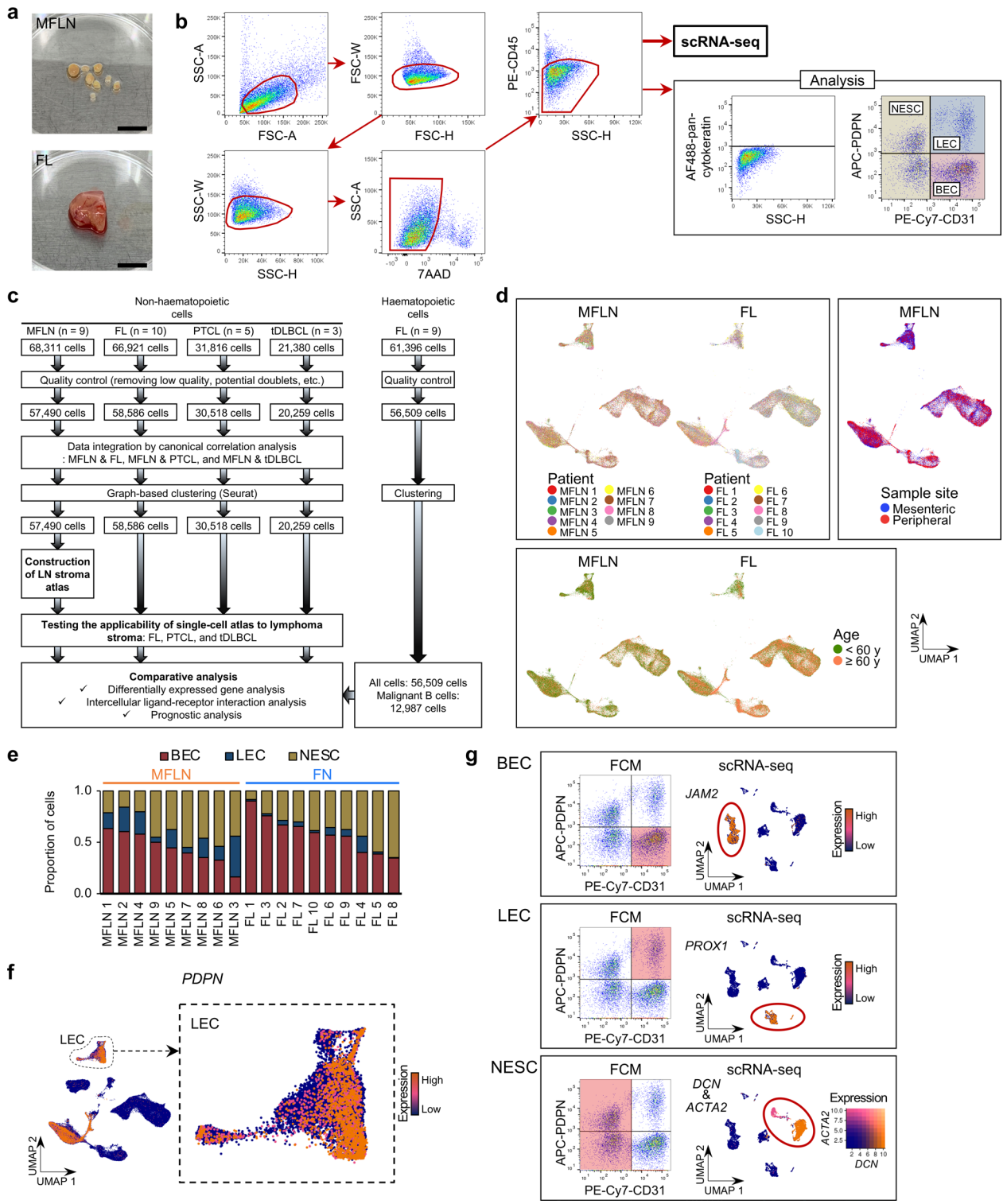

Extended Data Fig. 1 | Single-cell analysis of LN and lymphoma NHCs. a, Macroscopy of representative human metastasis-free lymph node (MFLN) (top) and follicular lymphoma (FL) (bottom) samples. Scale bars, 1 cm. **b**, Gating strategy for the isolation and analysis of non-haematopoietic cells (NHCs) in human LN and lymphoma in flow cytometry (see 'Single-cell isolation of LNNHCs' in the Methods section). BEC, blood endothelial cell; LEC, lymphatic endothelial cell; NESC, non-endothelial stromal cell; scRNA-seq, single-cell RNA sequencing. **c**, Overview of scRNA-seq analysis conducted in the present study. PTCL, peripheral T-cell lymphoma; tDLBCL, diffuse large B-cell lymphoma transformed from FL. **d**, UMAP plots of NHCs, colour coded by patients (top left), sites of sample collection (top right), and patient age (bottom), according to patient cohorts. **e**, Proportion of each major NHC component between MFLN (left) and FL (right) cohorts. **f**, *PDPN* expression in stroma-enriched cells from MFLN samples. High magnification image indicates heterogeneous *PDPN* expression levels among LECs. **g**, Strategy used to detect BECs (top), LECs (middle), and NESCs (bottom) using flow cytometry (FCM, red-coloured) or scRNA-seq (red circles) analysis in a representative case (MFLN 8).

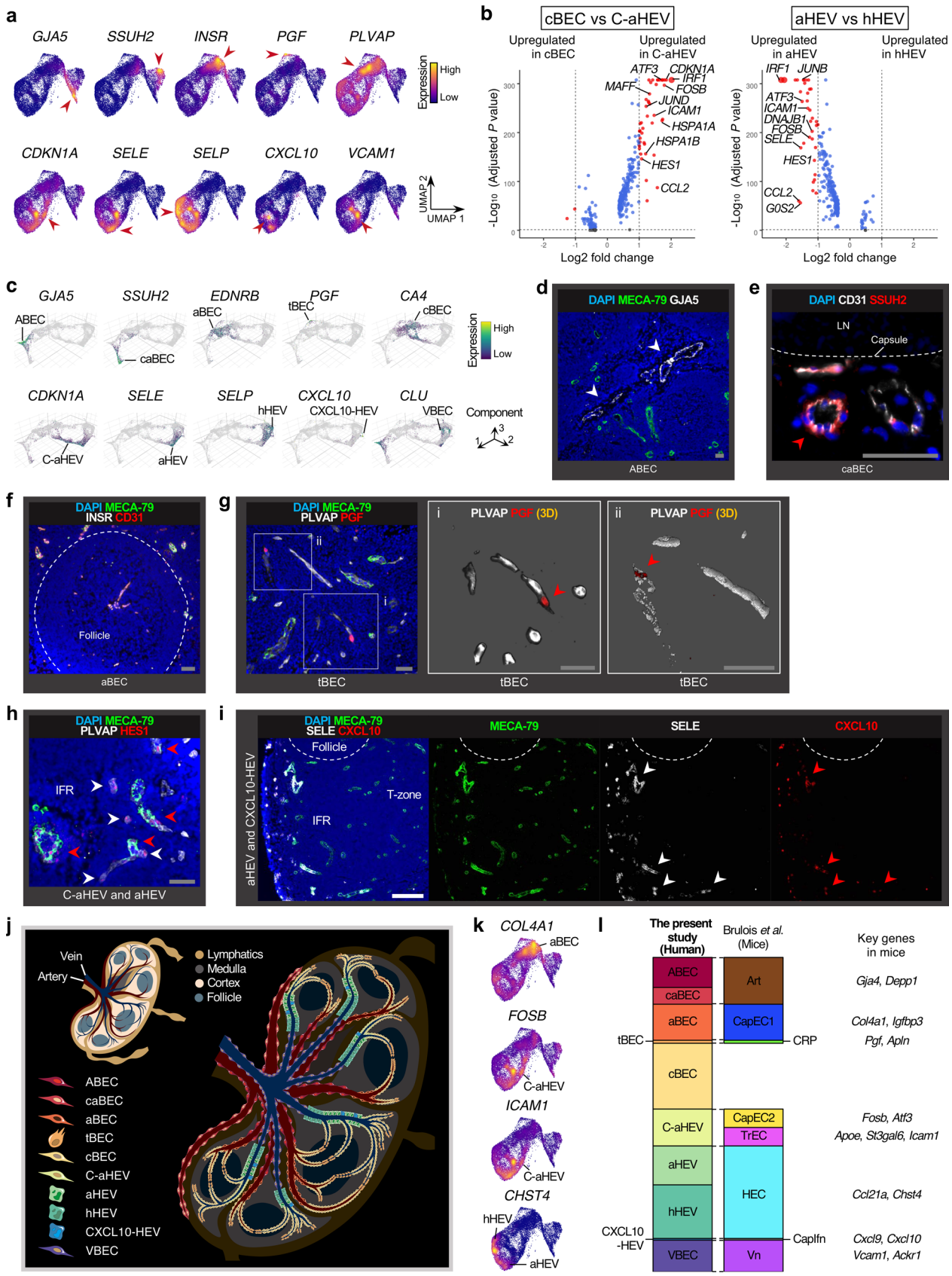

Extended Data Fig. 2 | See next page for caption.

Extended Data Fig. 2 | Dissection of human LN BECs at single-cell resolution. a, Expression of marker genes for each BEC subcluster. Red arrowheads show cells expressing indicated marker genes. **b**, Volcano plots of up- or down-regulated genes between cBECs and C-aHEVs (left) or between aHEVs and hHEVs (right). Significance was determined as an adjusted *P* value of <0.05 (two-sided Wilcoxon Rank-Sum test with Bonferroni correction) (blue-coloured dots) and log2 fold-change of ≥1 (red-coloured dots). Larger dots indicate log2 fold-change of ≥2. Key genes are labelled. **c**, Expression of marker genes for each BEC subcluster in a single-cell BEC object, generated by *Monocle 3*. **d–i**, IF staining of MECA-79 (green) and GJA5 (white) shows large arterial BECs (ABECs) (**d**, white arrowheads); CD31 (white) and SSUH2 (red) identify arteries surrounding LN capsule (caBECs) (**e**, red arrowhead); MECA-79 (green), INSR (white), and CD31 (red) identify arterioles (aBECs) (**f**); MECA-79 (green), PLVAP (white), and PGF (red). High magnification images (i and ii) are presented in 3D identifying tip cells (tBECs) (**g**, red arrowhead); MECA-79 (green), PLVAP (white), and HES1 (red) show activated HEVs (aHEVs) (red arrowheads) and transitional BECs between capillary BECs and aHEVs (C-aHEVs) (white arrowheads) (**h**); MECA-79 (green), SELE (white), and CXCL10 (red) to identify aHEVs and CXCL10-HEVs. Arrowheads show cells positive for indicated proteins (**i**). IFR, interfollicular region. Scale bars, 50 μm (grey), 200 μm (white). Representative images from one of three independent experiments are shown. **i**, LN schematic depicting topological localization of 10 BEC subclusters. **j**, Expression of marker genes for key mouse LN BEC subclusters (proposed by Brulois et al[25]) in our human data. **k**, Comparison of BEC subclusters identified here with those characterized in mice[25]. Bar heights of the mouse study are adjusted to the cell numbers (belonging to each subcluster) identified in this study. Key markers for mouse BEC subclusters[25] are listed on right.

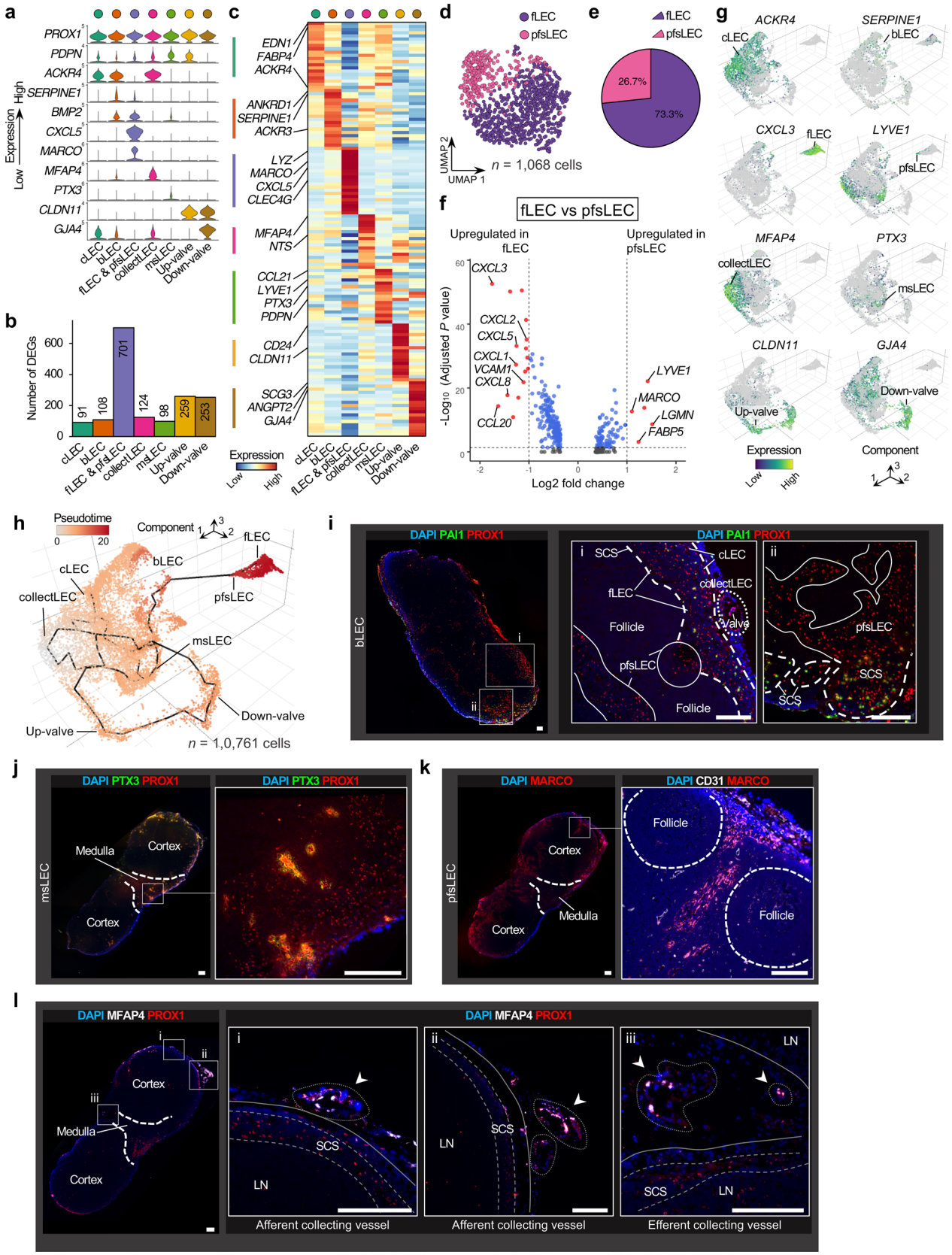

Extended Data Fig. 3 | See next page for caption.

Extended Data Fig. 3 | Dissection of human LN LECs at single-cell resolution. a, Violin plots showing expression of top marker genes for each LEC subcluster. **b**, Number of DEGs per LEC subcluster. **c**, Heatmap showing expression of top-ranking marker genes for each LEC subcluster. Key genes are indicated on the left. **d**, UMAP plot of fLECs and pfsLECs discriminated by unsupervised sub-clustering of a single 'fLEC and pfsLEC' subcluster. **e**, Composition of fLECs and pfsLECs in the 'fLEC and pfsLEC' subcluster. **f**, Volcano plot of up- or down-regulated genes in fLECs and pfsLECs. Significance was determined as an adjusted *P* value of <0.05 (two-sided Wilcoxon Rank-Sum test with Bonferroni correction) (blue-coloured dots) and log2 fold-change of ≥1 (red-coloured dots). Key genes are labelled. **g**, Expression of marker genes for each LEC subcluster in a single-cell LEC object, generated by *Monocle 3*. **h**, Single-cell LECs, ordered according to pseudo-time developmental stages. Dark winding lines indicate putative developmental trajectories. Cell regions are assigned to LEC subclusters based on marker gene expression. **i–l**, IF staining of PAI1 (green) and PROX1 (red) to identify bridge LECs (bLECs). Bold dashed lines in magnified images (i and ii) indicate subcapsular sinuses (SCSs). Solid lines indicate perifollicular sinuses. Scale bars, 500 μm (left panel), 200 μm (magnification panels) (**i**); PTX3 (green) and PROX1 (red) to identify medullary sinus LECs (msLECs). Dashed lines indicate boundaries between the LN cortex and medullary regions. High magnification image at right corresponds to boxed area at left. Scale bars, 200 μm (**j**); MARCO (red) for identification of perifollicular sinus LECs (pfsLECs). High magnification image at right shows staining of CD31 (white) and MARCO (red). Dashed lines indicate boundaries between the LN cortex and medullary regions (left) or follicles (right). Scale bars, 200 μm (**k**); MFAP4 (white) and PROX1 (red) to identify collecting vessel LECs (arrowheads). High magnification images show afferent (i and ii) or efferent (iii) collecting vessels. Bold dashed lines in left panel indicate boundaries between the LN cortex and medullary regions. Scale bars, 200 μm (**l**). Representative images from one of three independent experiments are shown.

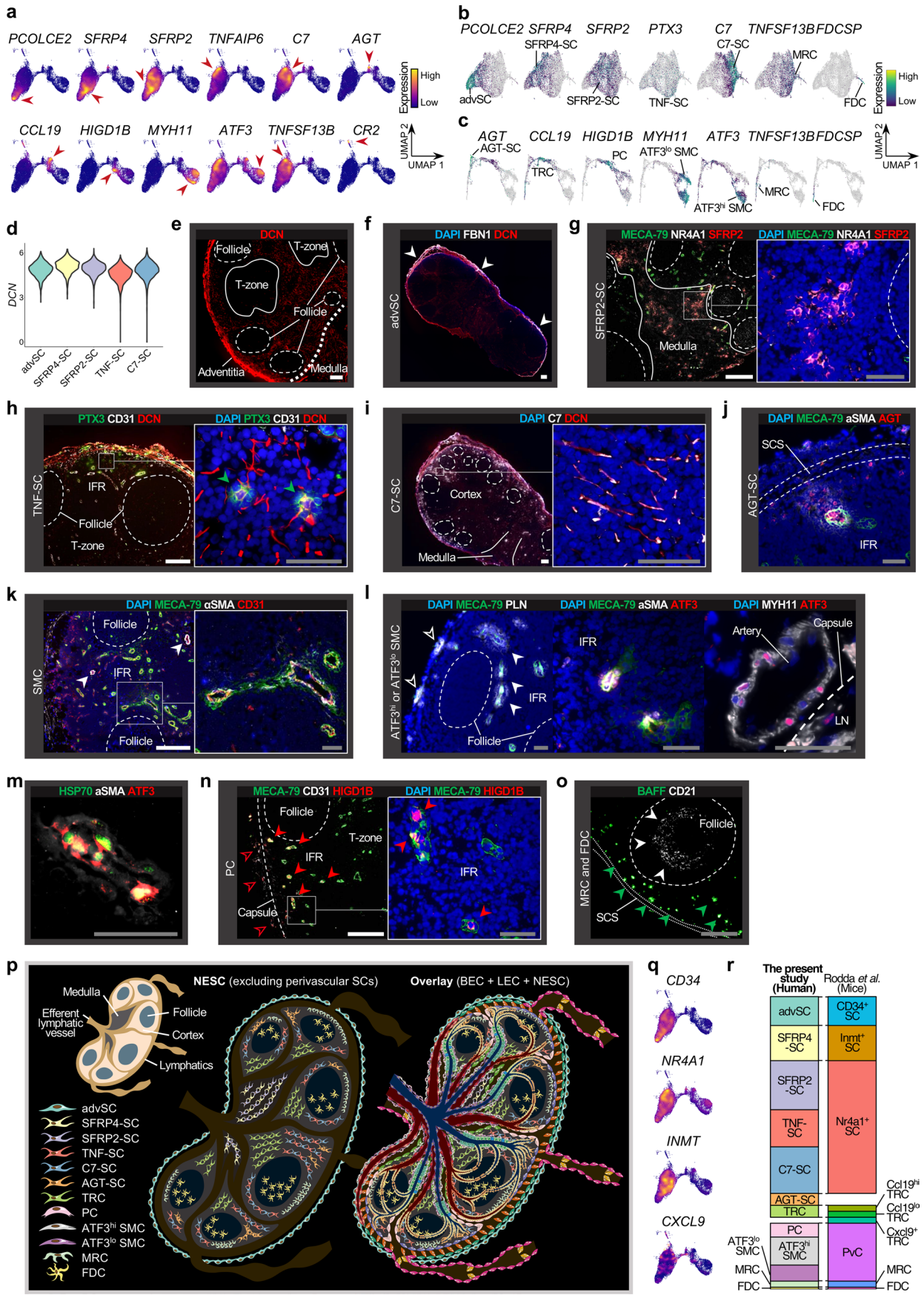

Extended Data Fig. 4 | See next page for caption.

Extended Data Fig. 4 | Dissection of human LN NESCs at single-cell resolution. a, Expression of marker genes for each NESC subcluster. Red arrowheads show cells expressing indicated marker genes. **b,c**, Marker gene expressions in a NESC object shown in Fig. 4g (**b**) or Fig. 4h (**c**). **d**, *DCN* expression in MFLN advSCs, SFRP4-SCs, SFRP2-SCs, TNF-SCs, and C7-SCs. **e–o**, IF staining of DCN showing DCN-positive fibroblasts (**e**); FBN1 (white) and DCN (red) to identify SCs in the capsule adventitia (advSC) (arrowheads) (**f**); MECA-79 (green), NR4A1 (a marker of LN fibroblastic reticular cells; white)[21], and SFRP2 (red) to identify SFRP2-SCs (**g**); PTX3 (green), CD31 (white), and DCN (red) to identify TNF-SCs (green arrowheads) (**h**); C7 (white) and DCN (red) to identify C7-SCs (**i**); MECA-79 (green), α-smooth muscle actin (αSMA, white), and AGT (red) to identify AGT-SCs (**j**); MECA-79 (green), αSMA (white), and CD31 (red) to identify SMCs. White arrowheads indicate SMCs around arteries (**k**); MECA-79 (green) and PLN (white) identifying SMCs around HEVs (filled arrowheads) and arteries (empty arrowheads) (left); MECA-79 (green), αSMA (white), and ATF3 (red) identifying $ATF3^{hi}$ SMCs around HEVs (middle); and MYH11 (white) and ATF3 (red) showing $ATF3^{hi}$ and $ATF3^{lo}$ SMCs around arteries (**l**); HSP70 (green), αSMA (white), and ATF3 (red) on SMCs (**m**); MECA-79 (green), CD31 (white), and HIGD1B (red) identifying PCs around arteries (empty arrowheads) and HEVs (filled arrowheads) (**n**); BAFF (green) and CD21 (white) identifying MRCs (green arrowheads) and FDCs (white arrowheads), respectively (**o**). IFR, interfollicular region; LN, lymph node; SCS, subcapsular sinus. Scale bars, 50 μm (grey),200 μm (white). Representative images from one of three independent experiments are shown. **p**, LN schematic depicting NESC subclusters excluding perivascular SCs (left) and an overlay image of all BEC, LEC, and NESC subclusters (right). **q**, Expression of marker genes for key mouse LN NESC subclusters[21] in our human data. **r**, Comparison of NESC subclusters identified here with those characterized in mice[21].

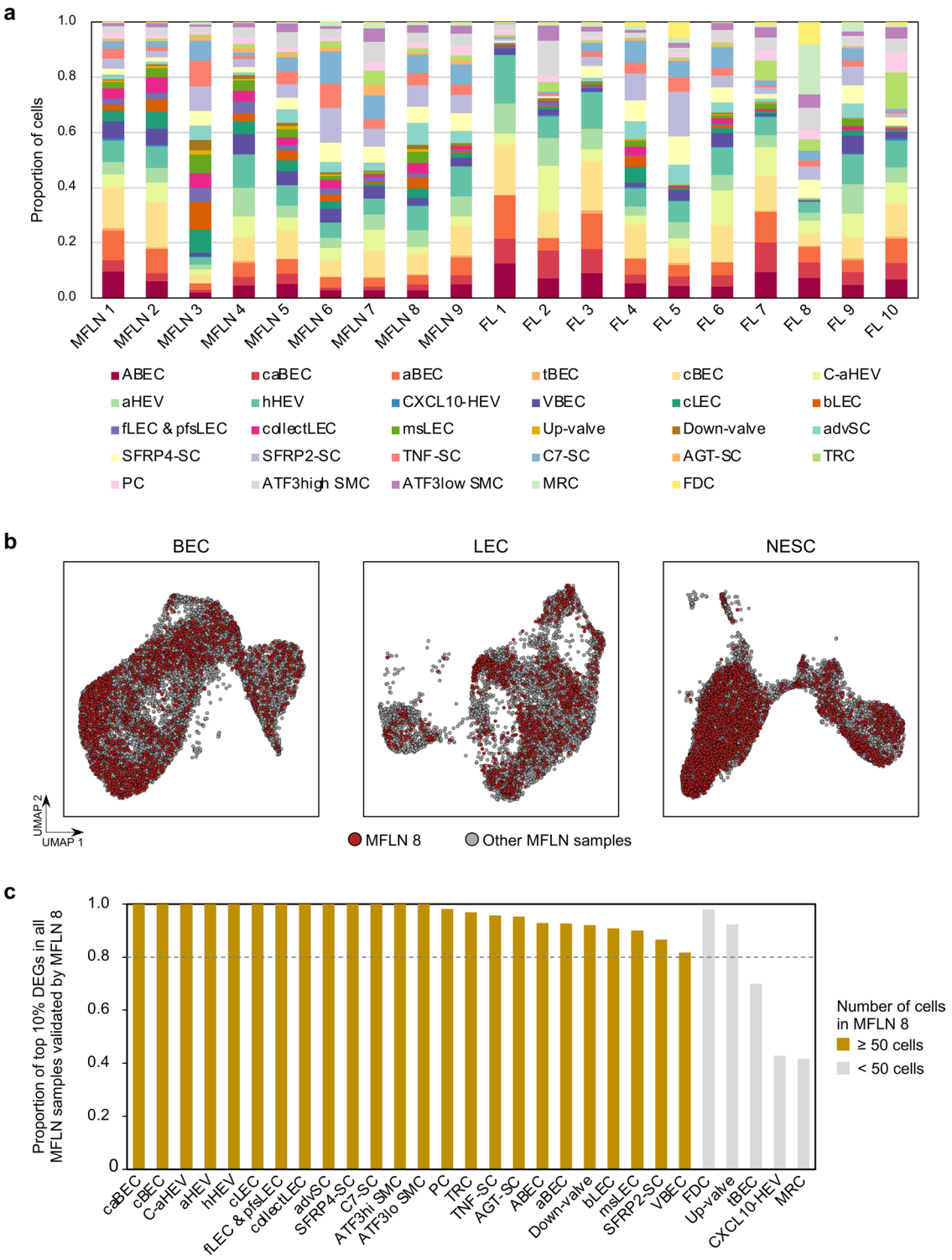

Extended Data Fig. 5 | Overview of LNNHC atlas. a, Proportion of each NHC subcluster based on patients in the MFLN and FL cohorts. **b**, UMAP plot of major NHC components from MFLN samples, highlighting NHCs from a patient with a benign tumour (MFLN 8) (red dots). **c**, Proportions of top DEGs detected using all MFLN data and validated by DEGs in MFLN 8 according to NHC subclusters. Top DEGs were defined as the top 10% of DEGs of each NHC subcluster, calculated using all MFLN data (listed in Supplementary Table 3,8,10). Bars of subclusters with >50 cells in MFLN 8 were highlighted by ochre colouring. Dashed line indicates 80% validation.

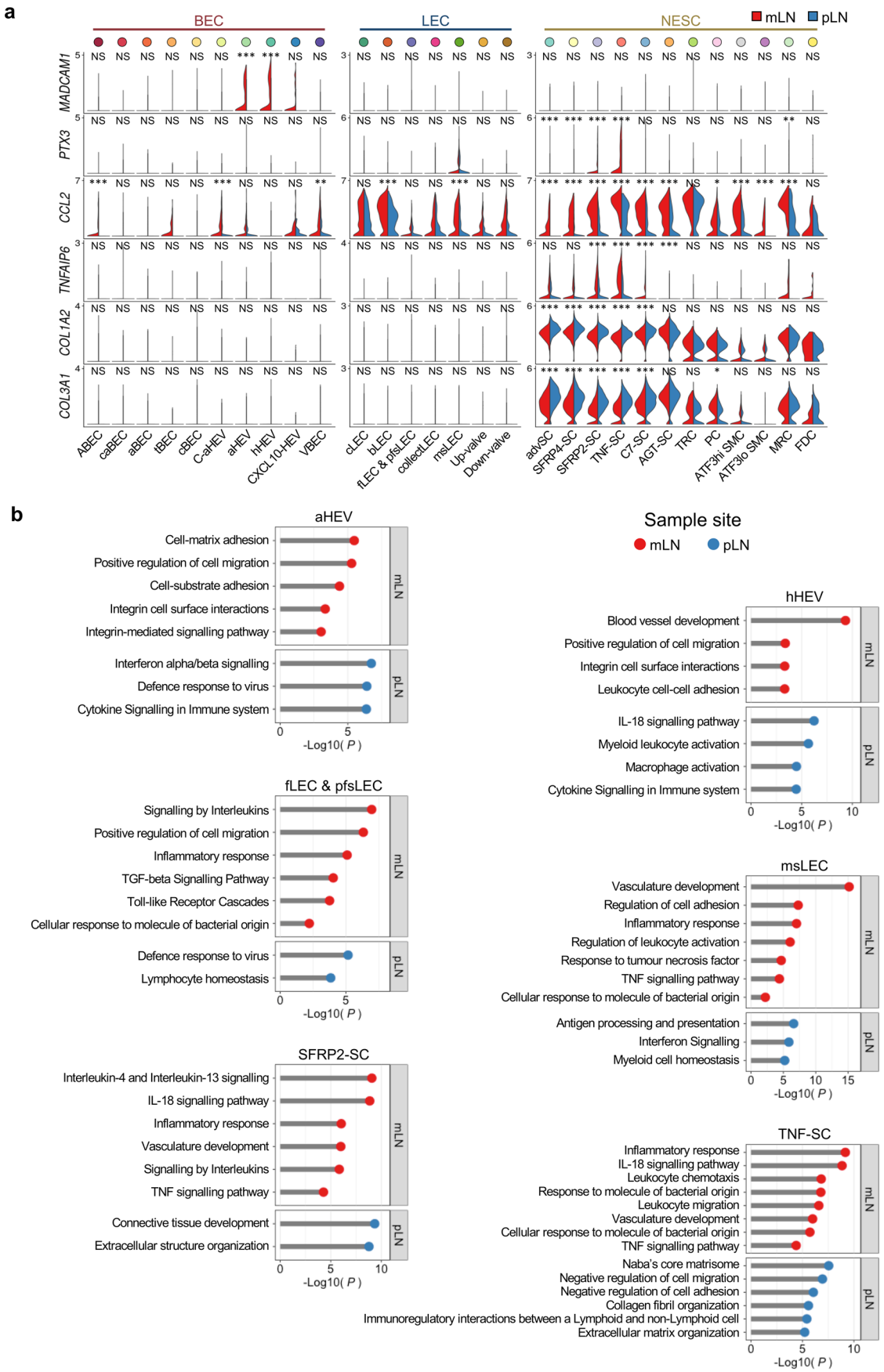

Extended Data Fig. 6 | See next page for caption.

Extended Data Fig. 6 | Comparative analyses between mesenteric and peripheral LNs. a, Violin plots comparing expressions of key genes between mLN (red) and pLN (blue) samples according to NHC subclusters. $^{*}P < 0.05$, $^{**}P < 0.01$, $^{***}P < 0.001$ (two-sided Wilcoxon Rank-Sum test with Bonferroni correction). NS, not significant. The exact *P* values are provided in Supplementary Table 13. **b**, Key gene ontologies of DEGs upregulated in mLN (red) or pLN (blue) compared with the other LN type according to representative NHC subclusters.

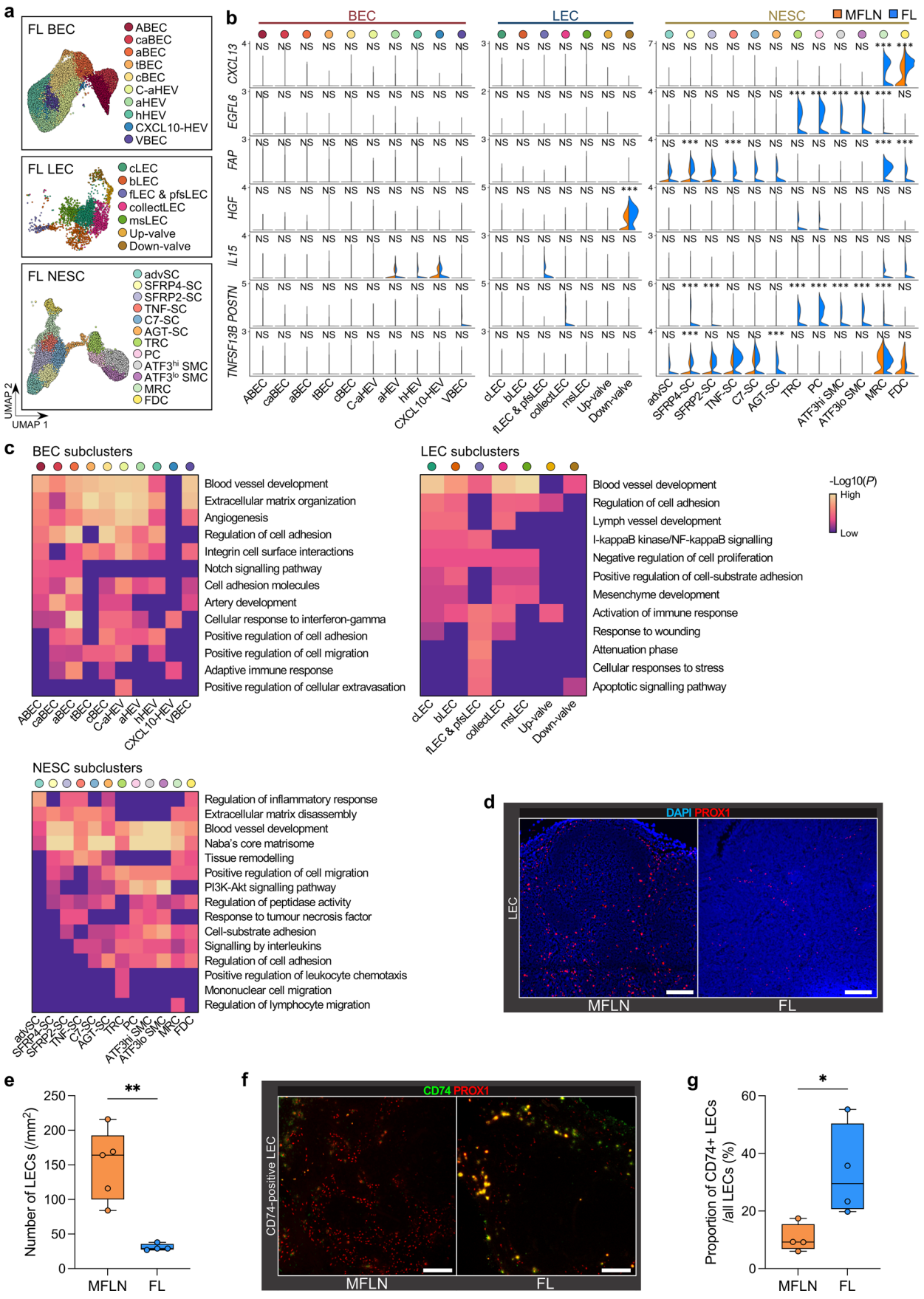

Extended Data Fig. 7 | See next page for caption.

Extended Data Fig. 7 | Alterations of gene expression profiles in FL stroma. a, UMAP plots of FL BEC (top), LEC (middle), and NESC (bottom) subclusters. **b**, Violin plots comparing expressions of key genes between MFLN (orange) and FL (blue) samples, according to NHC subclusters. ***$P < 0.001$ (two-sided Wilcoxon Rank-Sum test with Bonferroni correction). NS, not significant. The exact P values are provided in Supplementary Table 15–17. **c**, Gene ontology changes in FL NHC subclusters. GO enrichment analysis of DEGs upregulated in FL BEC (top left), LEC (top right), or NESC (bottom left) subclusters relative to MFLN counterpart subclusters. **d**, IF staining of PROX1 (red) showing LEC distribution in representative MFLN (left) and FL (right) samples. Scale bars, 200 μm. **e**, Number of PROX1-positive LECs per mm^2, detected by IF staining in biologically independent MFLN ($n = 5$) and FL ($n = 4$) samples. The box plots show the interquartile range (box limits), median (centre line), minimum to max values (whiskers), and samples (circles). **$P = 0.0025$ (two-sided unpaired t-test). **f**, IF staining of CD74 (green) and PROX1 (red) showing CD74-positive LECs in representative MFLN (left) and FL (right) samples. Scale bars, 200 μm. **g**, Proportions of CD74-positive LECs among PROX1-positive LECs (%) detected by IF staining in biologically independent MFLN ($n = 4$) and FL ($n = 4$) samples. The box plots show the interquartile range (box limits), median (centre line), minimum to max values (whiskers), and samples (circles). *$P = 0.033$ (two-sided unpaired t-test). The statistical source data are provided.

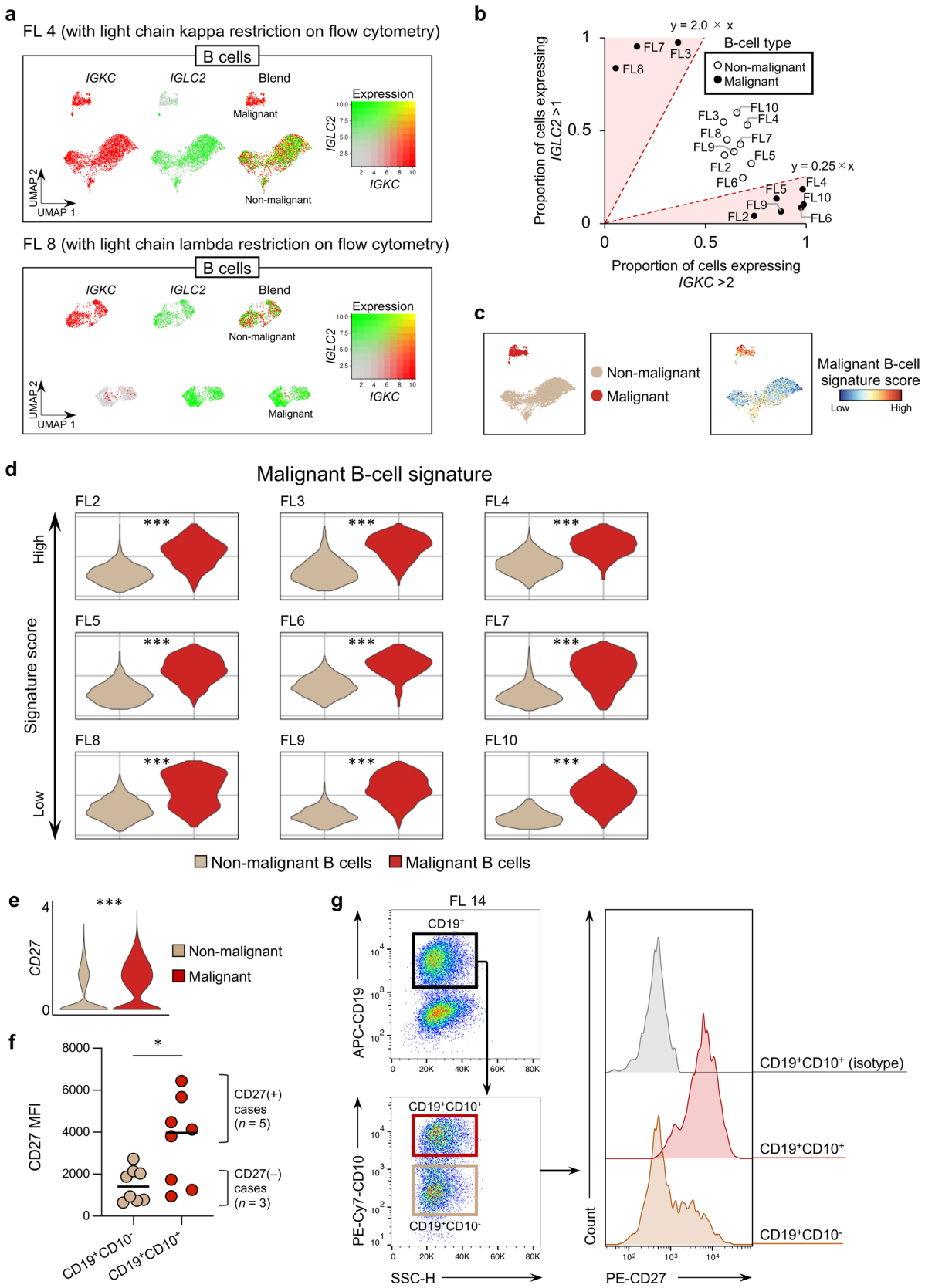

Extended Data Fig. 8 | See next page for caption.

Extended Data Fig. 8 | Interactome analysis across FL stroma and malignant B cells. a, Strategies used to identify malignant B-cell components in FL samples *in silico*. Shown are representative cases with light chain kappa (FL 4; top) or lambda (FL 8; bottom) restrictions confirmed by flow cytometry analysis (data not shown). After identifying B-cell components by detecting *CD79A* expression, we assessed expression of *IGKC* (for light chain kappa) and *IGLC2* (for light chain lambda). Clusters with cells expressing *IGKC* and those expressing *IGLC2* were considered non-malignant B cells, while clusters with cells expressing only one of these genes were considered malignant B cells. **b**, Scatter plot showing clear discrimination of malignant (filled circles) from non-malignant (empty circles) B-cell clusters in each FL sample, based on the ratio of cells expressing *IGLC2* (expression level >1; y-axis) to those expressing *IGKC* (expression level >2; x-axis,). Red-shaded areas indicate regions in which the ratio was >2.0 or <0.25. **c**, Representative UMAP plots showing B cells from FL 4 according to B-cell types (beige; non-malignant, red; malignant) (left panel) or malignant B-cell signature score (right panel). **d**, Violin plots showing malignant B-cell signature score in extracted non-malignant and malignant B cells, according to different FL samples (FL 2–10). $^{***}P = 1.1 \times 10^{-204}$ (FL 2), $^{***}P = 0$ (FL 3), $^{***}P = 3.3 \times 10^{-176}$ (FL 4), $^{***}P = 0$ (FL 5), $^{***}P = 4.2 \times 10^{-122}$ (FL 6), $^{***}P = 0$ (FL 7), $^{***}P = 4.2 \times 10^{-161}$ (FL 8), $^{***}P = 3.7 \times 10^{-256}$ (FL 9), $^{***}P = 2.5 \times 10^{-81}$ (FL 10) (two-sided Wilcoxon Rank-Sum test with Bonferroni correction). **e**, Violin plots showing the expression of *CD27* in non-malignant and malignant B cells. $^{***}P = 0$ (two-sided Wilcoxon Rank-Sum test with Bonferroni correction). **f**, Comparison of CD27 mean fluorescence intensity (MFI) between FL $CD19^+CD10^-$ (non-malignant B-cell fraction) and $CD19^+CD10^+$ (malignant B-cell fraction) cells. Circles represent biologically independent samples ($n = 8$; FL 11–18). $^{*}P = 0.039$ (two-sided Wilcoxon matched-pairs signed rank test). **g**, Flow cytometry analysis of CD27 expression on $CD19^+CD10^-$ and $CD19^+CD10^+$ cells of a representative FL sample (FL 14). The statistical source data are provided.

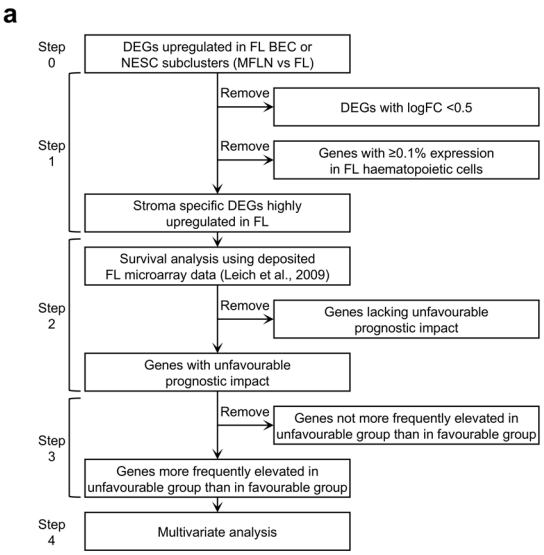

b Step 2

Genes with unfavourable prognostic impact (revealed in the Step 2)

Gene	Representative NHC subcluster	LogFC (FL vs MFLN)	Percentage in FL haematopoietic cells (%)	HR	*P* value
GJA4	ABEC	0.604	0.087	2.1	0.006
FABP4	caBEC	0.689	0.023	2.3	0.001
LY6H	tBEC	1.052	0.051	2.1	0.006
LOX	tBEC	0.534	0.007	2.1	< 0.001
PXDN	tBEC	0.629	0.076	1.6	0.048
SELE	hHEV	0.752	0.005	1.8	0.030
CHRDL1	AGT-SC	0.570	0.035	1.7	0.027
PTGIS	advSC	0.521	0.042	1.6	0.019
EGFL6	TRC	1.568	0.064	1.8	0.049
TDO2	TRC	0.866	0.005	2.1	0.008
REM1	TRC	0.575	0.011	1.9	0.002
PIEZO2	TRC	0.511	0.058	2.0	0.017
ABCC9	PC	0.698	0.012	2.5	0.044
CHI3L1	MRC	0.735	0.044	2.2	0.001

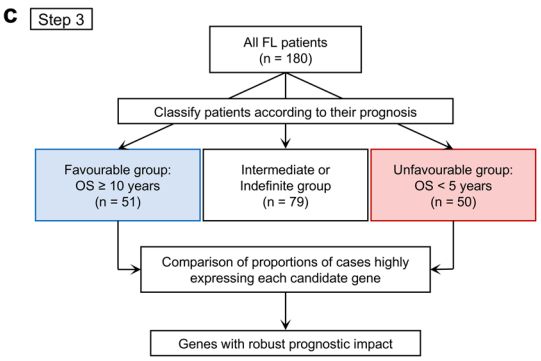

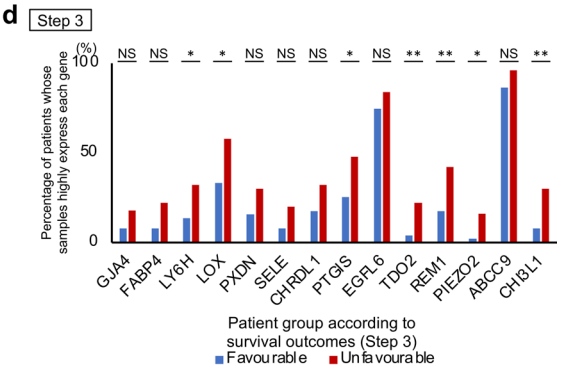

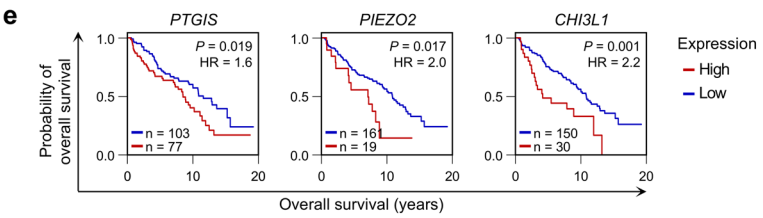

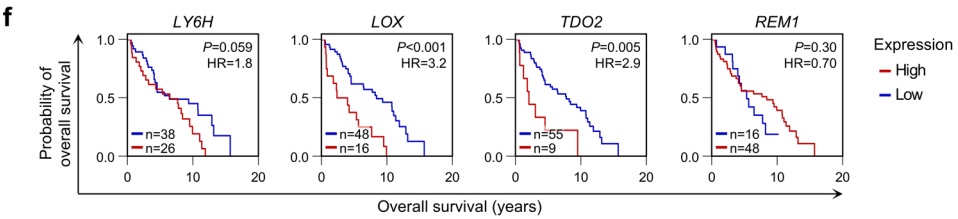

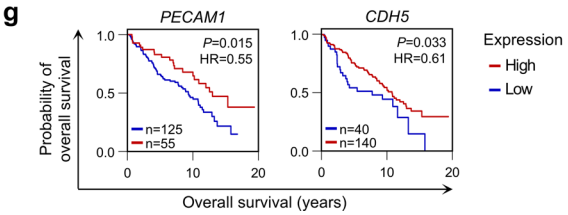

Extended Data Fig. 9 | See next page for caption.

Extended Data Fig. 9 | Exploring stroma-derived prognostic markers in FL. a, Scheme of stepwise survival analysis using public data from FL patients[66] to identify stroma-derived prognostic markers. **b**, Genes with unfavourable prognostic impact, as revealed by survival analysis using Kaplan–Meier methods with the two-sided log-rank test (Step 2). Representative NHC subcluster denotes subclusters in which indicated gene expression is most greatly upregulated. FC, fold-change; HR, hazard ratio. **c**, Strategies used to confirm prognostic impact of candidate genes identified in Step 2 (Step 3). OS, overall survival. **d**, Results of analysis performed in Step 3. Shown is the proportion of patients whose samples highly expressed indicated genes in favourable or unfavourable prognostic groups. $^{*}P = 0.034$ (*LY6H*), $^{*}P = 0.017$ (*LOX*), $^{*}P = 0.024$ (*PTGIS*), $^{*}P = 0.014$ (*PIEZO2*), $^{*}P = 0.027$ (*CHI3L1*), $^{**}P = 0.0077$ (*TDO2*), $^{**}P = 0.0092$ (*REM1*) (two-sided Fisher's exact test). NS, not significant. **e**, Kaplan–Meier curves showing overall survival of newly diagnosed FL patients (n = 180) based on expression of *PTGIS*, *PIEZO2*, and *CHI3L1*. Statistical analysis was performed using the two-sided log-rank test. **f**, Estimation of overall survival based on expression of *LY6H*, *LOX*, *TDO2*, and *REM1* in the FL patients of the intermediate prognosis group (n = 64, two-sided log-rank test). **g**, Estimation of overall survival based on expression of *PECAM1* and *CDH5* (n = 180, two-sided log-rank test). The statistical source data are provided.

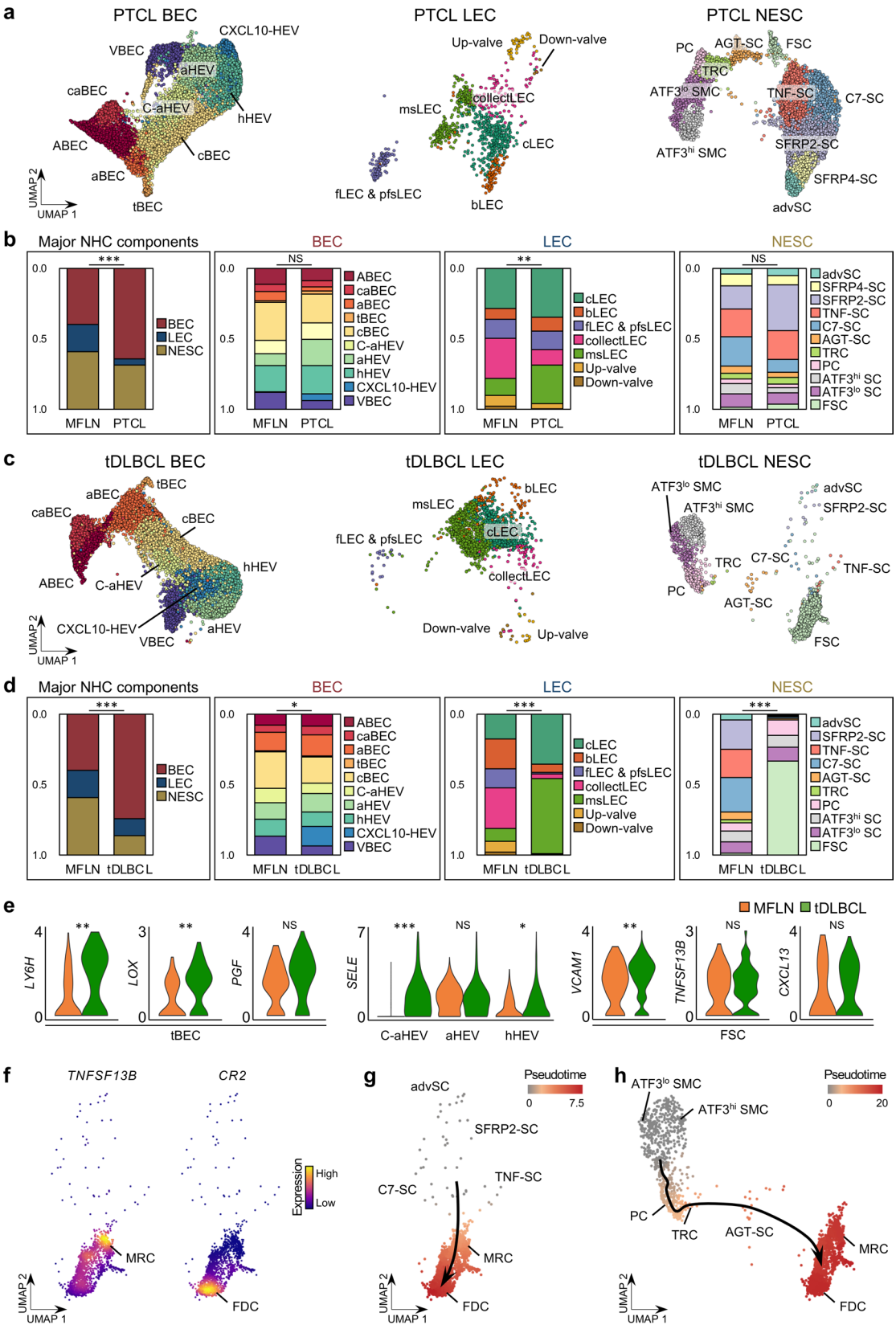

Extended Data Fig. 10 | See next page for caption.

Extended Data Fig. 10 | Applicability of the LNNHC atlas to PTCL and tDLBCL stroma. a, UMAP plots of PTCL BEC (left), LEC (middle), and NESC (right) subclusters. **b**, Compositional differences between PTCL and MFLN NHCs based on major NHC components, BEC subclusters, LEC subclusters, and NESC subclusters (from left to right). $^{**}P = 0.0076$, $^{***}P = 2.7 \times 10^{-4}$ (two-sided chi-squared test). NS, not significant. **c**, UMAP plots of tDLBCL BEC (left), LEC (middle), and NESC (right) subclusters. **d**, Compositional differences between tDLBCL and MFLN NHCs based on major NHC components, BEC subclusters, LEC subclusters, and NESC subclusters (from left to right). $^{*}P = 0.030$, $^{***}P = 3.4 \times 10^{-6}$ (Major NHC components), $^{***}P = 6.3 \times 10^{-16}$ (LEC), $^{***}P = 1.1 \times 10^{-23}$ (NESC) (two-sided chi-squared test). **e**, Violin plots comparing expressions of key genes between MFLN (orange) and tDLBCL (green) samples according to selected NHC subclusters. $^{*}P = 0.015$, $^{**}P = 0.0039$ (*LY6H*), $^{**}P = 0.0090$ (*LOX*), $^{**}P = 0.0075$ (*VCAM1*), $^{***}P = 8.0 \times 10^{-111}$ (two-sided Wilcoxon Rank-Sum test with Bonferroni correction). NS, not significant. **f**, Expression of *TNFSF13B* (left) and *CR2* (right) in tDLBCL follicular stromal cells identifying MRCs and FDCs, respectively. **g,h**, Pseudo-time developmental stages in tDLBCL advSCs, SFRP2-SCs, TNF-SCs, C7-SCs, MRCs, and FDCs (**g**) or in tDLBCL SMC subclusters, PCs, TRCs, AGT-SCs, MRCs, and FDCs (**h**). Dark winding lines in the cell objects indicate putative developmental trajectories. The statistical source data are provided.

nature research

Corresponding author(s): Mamiko Sakata-Yanagimoto

Last updated by author(s): Jan 20, 2022

Reporting Summary

Nature Research wishes to improve the reproducibility of the work that we publish. This form provides structure for consistency and transparency in reporting. For further information on Nature Research policies, see our Editorial Policies and the Editorial Policy Checklist.

Statistics

For all statistical analyses, confirm that the following items are present in the figure legend, table legend, main text, or Methods section.

n/a	Confirmed
☐	☒ The exact sample size (*n*) for each experimental group/condition, given as a discrete number and unit of measurement
☐	☒ A statement on whether measurements were taken from distinct samples or whether the same sample was measured repeatedly
☐	☒ The statistical test(s) used AND whether they are one- or two-sided *Only common tests should be described solely by name; describe more complex techniques in the Methods section.*
☐	☒ A description of all covariates tested
☐	☒ A description of any assumptions or corrections, such as tests of normality and adjustment for multiple comparisons
☐	☒ A full description of the statistical parameters including central tendency (e.g. means) or other basic estimates (e.g. regression coefficient) AND variation (e.g. standard deviation) or associated estimates of uncertainty (e.g. confidence intervals)
☐	☒ For null hypothesis testing, the test statistic (e.g. *F*, *t*, *r*) with confidence intervals, effect sizes, degrees of freedom and *P* value noted *Give P values as exact values whenever suitable.*
☒	☐ For Bayesian analysis, information on the choice of priors and Markov chain Monte Carlo settings
☐	☒ For hierarchical and complex designs, identification of the appropriate level for tests and full reporting of outcomes
☐	☒ Estimates of effect sizes (e.g. Cohen's *d*, Pearson's *r*), indicating how they were calculated

Our web collection on statistics for biologists contains articles on many of the points above.

Software and code

Policy information about availability of computer code

Data collection	FACSAria II and III (BD Biosciences) were used for acquisition of flow cytometry data. Chromium Single Cell 3' Reagent kits (V3) (10X Genomics) were used for single-cell RNA library preparation. Libraries were sequenced on an Illumina HiSeq X Ten system, mapped to the human genome (build GRCh38), and demultiplexed using CellRanger pipelines (10x Genomics, version 3.1.0).
Data analysis	Flowcytometric data were analyzed using FlowJo software (Tree Star Inc. v10.7.1). Single-cell data was analyzed using R package Seurat (R. Satija Lab. v3.2.2) on RStudio (v3.5.0 or v4.0.2). Monocle 3 package (Trapnell Lab. v0.2.3) was used for trajectory analysis on single-cell data. CellPhoneDB package (Teichlab. v2.1.1) was used on Python (v3.6) for intercellular ligand–receptor interaction analysis. GO enrichment analysis was performed using metascape (http://metascape.org). GSVA package (https://github.com/rcastelo/GSVA. v1.38.2) was used for gene signature analyses. DecontX (in celda package. Campbell Lab. v1.6.1) and SoupX (v1.5.2) were used for the detection of ambient RNA contamination. For analysis of whole-exome sequencing, the Genomon2 pipeline (v2.6.2) was used for sequence alignment and mutation calling. Statistical analyses were performed using R on Rstudio or GraphPad Prism 9 (GrphPad, v9.2.0) Please find detailed descriptions for each analysis in the Methods section. The codes for key computational analyses are available on GitHub at http://github.com/yoshiakiabe1018/Stroma01.

For manuscripts utilizing custom algorithms or software that are central to the research but not yet described in published literature, software must be made available to editors and reviewers. We strongly encourage code deposition in a community repository (e.g. GitHub). See the Nature Research guidelines for submitting code & software for further information.

Data

Policy information about availability of data

All manuscripts must include a data availability statement. This statement should provide the following information, where applicable:

- Accession codes, unique identifiers, or web links for publicly available datasets
- A list of figures that have associated raw data
- A description of any restrictions on data availability

scRNA-seq data that support the findings of this study have been deposited at the European Genome-Phenome Archive (https://ega-archive.org) database and can be retrieved using the accession number EGAD00001008311. For survival analysis, a DNA microarray dataset from Leich et al66 was downloaded from the Gene Expression Omnibus (GEO) (accession number: GSE16131). For mapping of scRNA-seq data, GRCh38 (https://www.ncbi.nlm.nih.gov/assembly/GCF_000001405.39) was used. All other data are available from the corresponding authors on reasonable request. Source data are provided with this paper.

Field-specific reporting

Please select the one below that is the best fit for your research. If you are not sure, read the appropriate sections before making your selection.

☒ Life sciences ☐ Behavioural & social sciences ☐ Ecological, evolutionary & environmental sciences

For a reference copy of the document with all sections, see nature.com/documents/nr-reporting-summary-flat.pdf

Life sciences study design

All studies must disclose on these points even when the disclosure is negative.

Sample size	No statistical method was used to determine sample size a priori. The number of human lymph node and lymphoma samples was highly restricted due to the limited availability of these samples in clinical settings.
Data exclusions	Pre-processed single-cell data from each sample were further processed and analysed individually using R package Seurat on RStudio. After removing ribosomal genes, genes expressed in fewer than 3 cells, and cells expressing fewer than 200 genes, we filtered out cells with less than 200 unique feature counts (low quality cells). Cells with unique feature counts greater than three times the median value (possible doublets) and/or cells with more than twice the median number of mitochondrial genes (possible apoptotic or lysed cells) were also removed. After the data integration and clustering analysis, we removed data of NHC subclusters considered possible doublets as characterized by high expressions of marker genes for different NHC components and incongruously high unique feature counts.
Replication	All experiments were independently replicated at least once to verify reproducibility.
Randomization	Not relevant - no treatment group.
Blinding	Not relevant - no treatment group.

Reporting for specific materials, systems and methods

We require information from authors about some types of materials, experimental systems and methods used in many studies. Here, indicate whether each material, system or method listed is relevant to your study. If you are not sure if a list item applies to your research, read the appropriate section before selecting a response.

Materials & experimental systems

n/a	Involved in the study
☐	☒ Antibodies
☒	☐ Eukaryotic cell lines
☒	☐ Palaeontology and archaeology
☒	☐ Animals and other organisms
☐	☒ Human research participants
☒	☐ Clinical data
☒	☐ Dual use research of concern

Methods

n/a	Involved in the study
☒	☐ ChIP-seq
☐	☒ Flow cytometry
☒	☐ MRI-based neuroimaging

Antibodies

Antibodies used	Flow cytometric analysis: PE-anti-CD45 (BioLegend. Cat# 304058), AF488-anti-pan-cytokeratin (ThermoFisher Scientific. Cat# 53-9003-82), FITC-anti-CD31 (Biolegend, 303103), APC-anti-podoplanin (Biolegend. Cat# 337021), PE-Cy7-anti-CD31 (Biolegend. Cat# 303117), PE-Cy7-anti-CD34 (Biolegend, 343515). PE-anti-CD27 (Biolegend, 302842), FITC-anti-CD3 (Biolegend, 300406), APC-anti-CD19 (Miltenyi Biotec, 130-113-165), PE-Cy7-anti-CD10 (Biolegend. Cat# 312214). The dilution for each antibody is described in the Methods section of the manuscript.

Recombinant protein binding assay: PE-anti-human IgG Fc (R&D systems, FAB110P). The dilution is described in the Methods section of the manuscript.

Functional blocking: anti-CD27 blocking antibody (R&D systems, MAB382), isotype mouse IgG1 (R&D systems, MAB002).

Antibodies used for immunofluorescence staining were listed in Supplementary Table 9.

Validation

All the antibodies used in this study have been tested by the manufacturer and have been cited by other authors and references are available on the manufacturer's websites. We provide catalog numbers for all the antibodies in the Methods section of the manuscript or in Supplementary Table 9 as readers can retrieve the information of the antibodies. We have further evaluated the specificity of the antibodies in our samples by analyzing the distribution of the antibody signals and the absence of the antibody signals in the regions where the target protein was not supposed to be expressed.

Human research participants

Policy information about studies involving human research participants

Population characteristics

Supplementary Table 1 summarises the characteristics of patients in metastasis-free lymph node and follicular lymphoma cohorts. Metastasis-free lymph node cohort consists of neoplasm-bearing patients (n = 9) who had undergone surgical LN dissection. The median age of the patients in this cohort is 66 years old. Follicular lymphoma cohort consists of 10 patients with the median age of 59. Among the follicular lymphoma patients, six patients were newly diagnosed cases. Most of the follicular lymphoma patients (n = 9) were with pathological grade of 1-2.
Supplementary Table 7 summarises the characteristics of patients in peripheral T-cell lymphoma cohort and diffuse large B-cell lymphoma transformed from follicular lymphoma cohort. Peripheral T-cell lymphoma cohort consists of five newly diagnosed patients with various subtypes of lymphoma with the median age of 78. Diffuse large B-cell lymphoma transformed from follicular lymphoma cohort consists of three patients.
Additional follicular lymphoma samples for functional experiments were collected from eight patients. Characteristics of follicular lymphoma patients in the additional cohort is summarised in Supplementary Table 10.

Recruitment

Samples were prospectively collected from patients who agreed to participate in the study. There were no other criteria for patient selection. There is no self-selection bias or other biases in recruitment.

Ethics oversight

This study was approved by the Ethics Committee of the University of Tsukuba Hospital and the review boards of associated institutions that provided human samples (Kameda Medical Center, NTT Medical Center Tokyo, and Mito Medical Center) and conducted according to all relevant ethical regulations regarding human patients. Written informed consent was obtained from all participating patients. The participants were not compensated for their participation.

Note that full information on the approval of the study protocol must also be provided in the manuscript.

Flow Cytometry

Plots

Confirm that:

☒ The axis labels state the marker and fluorochrome used (e.g. CD4-FITC).

☒ The axis scales are clearly visible. Include numbers along axes only for bottom left plot of group (a 'group' is an analysis of identical markers).

☒ All plots are contour plots with outliers or pseudocolor plots.

☒ A numerical value for number of cells or percentage (with statistics) is provided.

Methodology

Sample preparation

Single-cell isolation of LN non-haematopoietic cells: After collection, LN or lymphoma samples were immediately minced and digested for 1 h with RPMI 1640 medium (Sigma-Aldrich, R8758) with 5% fetal bovine serum containing 0.2 mg/ml collagenase P (Sigma-Aldrich, 11213857001), 0.8 mg/ml dispase (Gibco, 17105041), and 0.1 mg/ml DNase 1 (Worthington, LS002139), with continuous agitation. Cells were then filtered through a 70 µm mesh and red blood cells were lysed in 1% ammonium-chloride-potassium buffer. Thereafter, haematopoietic cells and contaminated red blood cells were depleted using human CD45 (130-045-801) and CD235a (130-050-501) microbeads according to the manufacturer's instructions (Miltenyi Biotec). For MFLN samples, the remaining single-cell suspension was incubated with phycoerythrin (PE)-anti-CD45 (Biolegend) in combination with Alexa Fluor 488-pan-cytokeratin (ThermoFisher Scientific), allophycocyanin (APC)-anti-podoplanin (Biolegend), and PE-cyanin 7 (PE-Cy7)-anti-CD31 (Biolegend). For lymphoma samples, PE-anti-CD45 was mixed with fluorescein isothiocyanate-anti-CD31 (Biolegend), APC-anti-podoplanin, and PE-Cy7-anti-CD34 (Biolegend). The samples were incubated for 20 min, then 7-AAD Viability Staining Solution (ThermoFisher Scientific, 00-6993-50) was added and incubated for 10 min in the dark on ice. CD45-negative live cells were sorted using FACSAria II or III (BD Bioscience) after removing doublets by gating with a FSC-H versus FCS-W plot and a SSC-H versus SSC-W plot.

Single-cell isolation of FL haematopoietic cells: After thawing, cell suspensions were filtered through a 70 µm mesh and incubated with 7-AAD Viability Staining Solution for 10 min in the dark.

Flow cytometric analysis of FL haematopoietic cells: After thawing, cells were filtered through a 70 µm mesh, and incubated with PE-anti-CD27 (Biolegend), FITC-anti-CD3 (Biolegend), APC-anti-CD19 (Miltenyi Biotec), and PE-Cy7-anti-CD10 (Biolegend)

antibodies for 20 min on ice. Cells were then incubated with 7-AAD Viability Staining Solution for 10 min in the dark and analysed using FACSAria II or III.

Recombinant protein binding assay: Recombinant Fc chimera CD70 (SinoBiological, 10780-H01H) or human IgG (R&D systems, 1-001-A) was incubated with a single-cell suspension of FL haematopoietic cells for 10 min at 4 ºC in RPMI with 10% FCS. To block CD70–CD27 binding, malignant B cells were incubated in the presence of anti-CD27 blocking antibody (R&D systems, MAB382) or isotype mouse IgG1 (R&D systems, MAB002) for 30 min at 4 ºC before binding. After binding, the cells were washed, fixed by 4% PFA for 10 min at 20 ºC and incubated with PE-anti-human IgG Fc (R&D systems), FITC-anti-CD3, APC-anti-CD19, and PE-Cy7-anti-CD10 for 20 min at 4 ºC.

Instrument

FACSAria II and III (BD Biosciences)

Software

Data collection: FACSAria II and III (BD Biosciences)
Data analysis: FlowJo (Tree Star Inc. v10.7.1)

Cell population abundance

The purity of sorted fractions was not determined for each sorting because FACS was used justed to enrich cell fractions of interest, followed by scRNA-seq which finally identifies the cell-type of sorted cells.

Gating strategy

All captured cells were first gated for singlet cells with a FSC-H versus FCS-W plot and a SSC-H versus SSC-W plot. Thereafter, dead cells were removed as 7-AAD-positive cells.
Non-haematopoietic cells: From singlets, CD45-negative (SSC-H vs PE-CD45).
Blood endothelial cells: From non-haematopoietic cells, CD31-positive and PDPN-negative (PE-Cy7-CD31 vs APC-PDPN).
Lymphatic endothelial cells: From non-haematopoietic cells, CD31-positive and PDPN-positive (PE-Cy7-CD31 vs APC-PDPN).
Non-endothelial stromal cells: From non-haematopoietic cells, CD31-negative (PE-Cy7-CD31 vs APC-PDPN).
FL malignant B cells: From singlets, CD19-positive (SSC-H vs APC-CD19), followed by CD10-positive (SSC-H vs PE-Cy7-CD10).
FL non-malignant B cells: From singlets, CD19-positive (SSC-H vs APC-CD19), followed by CD10-negative (SSC-H vs PE-Cy7-CD10).
CD70-Fc-bound FL malignant B cells: From FL malignant B cells, human IgG Fc-positive (SSC-H vs PE-anti-human IgG Fc).

☒ Tick this box to confirm that a figure exemplifying the gating strategy is provided in the Supplementary Information.

ORIGINAL PAPER

Nagoya J. Med. Sci. **84**. 80–90, 2022
doi:10.18999/nagjms.84.1.80

Alternating bortezomib-dexamethasone and lenalidomide-dexamethasone in patients with newly diagnosed multiple myeloma aged over 75 years

Akihiro Yokoyama[1,2], Akiko Kada[3], Toshiya Kagoo[1], Michihiro Hidaka[4], Hiroatsu Iida[5], Yasuhiko Miyata[5], Akiko M. Saito[3], Morio Sawamura[6], Takuya Komeno[7], Kazutaka Sunami[8], Naoki Takezako[9] and Hirokazu Nagai[5]

[1]*Division of Hematology, Department of Internal Medicine, National Hospital Organization Tokyo Medical Center, Tokyo, Japan*
[2]*Division of Transfusion Medicine, National Hospital Organization Tokyo Medical Center, Tokyo, Japan*
[3]*Department of Clinical Trials and Research, Clinical Research Center, National Hospital Organization Nagoya Medical Center, Nagoya, Japan*
[4]*Department of Hematology, National Hospital Organization Kumamoto Medical Center, Kumamoto, Japan*
[5]*Department of Hematology, National Hospital Organization Nagoya Medical Center, Nagoya, Japan*
[6]*Department of Hematology, National Hospital Organization Shibukawa Medical Center, Shibukawa, Japan*
[7]*Department of Hematology, National Hospital Organization Mito Medical Center, Ibaraki, Japan*
[8]*Department of Hematology, National Hospital Organization Okayama Medical Center, Okayama, Japan*
[9]*Department of Hematology, National Hospital Organization Disaster Medical Center of Japan, Tachikawa, Japan*

ABSTRACT

More than 40% of Japanese patients with multiple myeloma (MM) are over 75 years of age at diagnosis. Regardless of the treatment benefits, complications and relapses obstruct long-term survival. We conducted a phase II, open-label, single-arm, multicenter clinical trial to assess the efficacy and safety of alternating bortezomib-dexamethasone (Bd) and lenalidomide-dexamethasone (Ld) (Bd/Ld) treatment in MM patients aged over 75 years (MARBLE trial). Patients received Bd therapy from days 1 to 35 and Ld therapy from days 36 to 63. For Bd therapy, patients were administered bortezomib 1.3 mg/m^2 and oral dexamethasone 20 mg on days 1, 8, 15, and 22. For Ld therapy, they were administered lenalidomide 15 mg from days 36 to 56 and dexamethasone 10 mg on days 36, 43, 50, and 57. They underwent six treatment cycles in total, each consisting of a 63-day regimen. In total, 10 patients were enrolled, with a median age of 81 years. Efficacy was not evaluated because the patients were fewer than planned. The overall response rate was 80.0% and complete response rate 40.0%. Seventy percent of patients completed the study treatment. Progression-free survival and overall survival at 2 years were 40.0% and 80.0%, respectively. Adverse events of grade 3 or higher, including anemia, decreased lymphocyte count, neutropenia, and hypokalemia, were observed in eight patients. Alternating chemotherapy with Bd/Ld might be feasible, but its efficacy should be verified further.

Keywords: myeloma, alternating therapy, bortezomib, lenalidomide, dexamethasone

Received: November 25, 2020; accepted: May 21, 2021

Corresponding Author: Akihiro Yokoyama, MD, PhD
Division of Hematology, Department of Internal Medicine and Division of Transfusion Medicine, National Hospital Organization Tokyo Medical Center, 2-5-1 Higashigaoka, Meguro-ku, Tokyo 152-8902, Japan
Tel: +81- 3-3411-0111 , E-mail: yokoyama.akihiro.sa@mail.hosp.go.jp

Abbreviations:
AEs: adverse events
ASCT: autologous stem cell transplantation
BMP: bortezomib/melphalan/prednisone
Bd: bortezomib-dexamethasone
Bd/Ld: bortezomib-dexamethasone and lenalidomide-dexamethasone
CI: confidence interval
CRR: complete response rate
FIRST trial: Frontline Investigation of Revlimid and Dexamethasone Versus Standard Thalidomide trial
Ld: lenalidomide plus low-dose dexamethasone
MM: multiple myeloma
NDMM: newly diagnosed multiple myeloma
ORR: overall response rate
OS: overall survival
PFS: progression-free survival
TTR: time to response
UMIN: University Hospital Medical Information Network
VGPR: very good partial response
VISTA trial: Velcade as Initial Standard Therapy in Multiple Myeloma: Assessment with Melphalan and Prednisone trial

INTRODUCTION

Multiple myeloma (MM) is caused by an accumulation of cancerous plasma cells, the terminally differentiated form of B-lymphocytes, in the bone marrow, and it is characterized by the production of an abnormal protein called monoclonal immunoglobulin (M-protein) by the tumor cells. This refractory disease shows several clinical symptoms, including hypercalcemia, renal insufficiency, anemia, and bone osteolytic changes, otherwise known as CRAB criteria, even in the novel agent era.[1]

Nevertheless, radical improvements in treatment outcomes have been accomplished by treatment with high-dose melphalan plus autologous stem cell transplantation (ASCT) as well as with novel chemotherapeutic agents, including bortezomib, lenalidomide, and thalidomide. However, these treatments have failed to improve long-term survival in elderly patients, who are generally ineligible for ASCT. Therefore, the greatest therapeutic benefits of these treatments are limited to patients under 70 years of age, mainly due to adverse events (AEs).[2]

Based on data from randomized phase III trials, the following two treatment options are recommended for elderly patients: bortezomib/melphalan/prednisone (BMP), based on the Velcade as Initial Standard Therapy in Multiple Myeloma: Assessment with Melphalan and Prednisone (VISTA) trial[3] and lenalidomide plus low-dose dexamethasone (Ld), based on the Frontline Investigation of Revlimid and Dexamethasone Versus Standard Thalidomide (FIRST) trial.[4] In Japan, both BMP and Ld are approved as front-line options.

Further, combination therapy with bortezomib-dexamethasone (Bd) has been investigated, mainly by the UPFRONT trial, a community-based phase IIIB study in the US, performed to compare three front-line regimens based on bortezomib (Bd, BMP, and Bd plus thalidomide) in ASCT-ineligible patients with MM; the study results suggested that a Bd treatment regimen balances efficacy and safety in elderly MM patients.[5]

To further improve the treatment outcome in this population, a triplet combination of bort-

ezomib plus Ld administered in a modified dose and schedule was examined; it was found to be a well-tolerated and effective treatment option for newly diagnosed MM (NDMM) patients aged over 65 years.[6]

Presently, despite the known benefits of these novel agents, most patients pass away after repeated relapses. There is little evidence supporting alternating chemotherapy as a treatment strategy for MM. The international phase II trial by Mateos MV et al comparing BMP and Ld administered in a sequential (121 patients) and alternating (120 patients) manner did not show differences in efficacy and safety between the two groups.[7] In this study, Ld was administered after the start of bortezomib treatment because Ld was not approved for newly diagnosed or untreated MM in Japan when this study was designed. In our study, we investigated an alternating chemotherapy regimen of Bd and Ld (alkylator-free regimen) with respect to balancing safety, tolerability, and efficacy in elderly patients with ASCT-ineligible NDMM. We assumed that the side effects will be suppressed by alternating two drugs with different mechanisms of action as an initial treatment strategy for MM, leading to high efficacy and improved survival. Furthermore, we detected chromosomal abnormalities in patients using fluorescence in situ hybridization (FISH) and assessed whether the alternating treatment strategy suppresses clonal evolution.

METHODS

Trial design

In this phase II, open-label, single-arm, multicenter trial, we assessed the efficacy and safety of alternating Bd and Ld as an induction therapy for NDMM patients aged 75 years or more who were ineligible for ASCT. Patients who satisfied the eligibility criteria were enrolled in the study. The details of this study are described elsewhere.[8]

This study was performed at 22 facilities in Japan and was registered in the Clinical Trial Registry of the University Hospital Medical Information Network (UMIN), Japan (Registration Number: UMIN000013773).

Interventions

Patients were enrolled in the trial within 4 weeks of diagnosis and began treatment according to the study protocol. Patients received Bd therapy from days 1 to 35 (for 35 days) and Ld therapy from days 36 to 63 (for 28 days). Patients underwent a total of six treatment cycles, each consisting of a 63-day regimen, as mentioned above. The starting doses of bortezomib and lenalidomide were adjusted based on patient age, general condition, and renal function.

For Bd therapy, patients were administered bortezomib 1.3 mg/m^2 and oral dexamethasone 20 mg on days 1, 8, 15, and 22. The site of bortezomib administration was rotated between sessions to avoid consecutive injections at the same site (eg, left thigh, right thigh, abdomen). Following Bd therapy, patients were administered lenalidomide 15 mg from days 36 to 56 and dexamethasone 10 mg on days 36, 43, 50, and 57 as Ld therapy. A physician decided whether each patient should receive treatment in an inpatient or outpatient setting.

It was recommended to administer antibacterial agents, antifungal agents, or sulfamethoxazole-trimethoprim to prevent infectious diseases and to use anticoagulants or antiplatelet agents to prevent deep vein thrombosis in patients who were concerned about the increase in the risk of venous thromboembolism.

We performed the chromosome test (G-binding) and FISH test at baseline 2–4 weeks before the treatment started. The myeloma FISH panel included the following: Vysis LSI IGH/CCND1 XT Dual Color Dual Fusion Probes probe to detect t(11;14)(q13;q32), Vysis LSI IGH/FGFR3

Dual Color Dual Fusion Probes to detect t(4;14)(p16;q32), Vysis LSI IGH/MAF Dual Color Dual Fusion Probes probe to detect t(14;16)(q32;q23), Vysis LSI IGH/MYC/CEP 8 Tri-Color Dual Fusion FISH Probes to detect t(8;14)(q24;q32), Vysis LSI D13s319/13q34 FISH Probes to detect deletion of 13q14, Vysis LSI TP53 SpectrumOrange/ CEP 17 SpectrumGreen Probes to detect deletion of p53 (17p13.1), CKS1B/CEN1p Dual Color FISH Probe to detect chromosome 1q21 gain, AHCYL1/CEN1p Dual Color FISH Probe to detect deletion of 1p13, and CDKN2C/CEN1p Dual Color FISH Probe to detect deletion of 1p32.

Further, we conducted a comprehensive geriatric assessment, including the Cumulative Illness Rating Scale for Geriatrics, at baseline.[9]

Sample size

One trial reported that Ld therapy achieved an overall response rate (ORR) of 70.4% in untreated MM patients aged 75 years or older.[10] In contrast, the EVOLUTION study revealed ORRs of 85% and 88% for bortezomib-lenalidomide-dexamethasone and bortezomib-dexamethasone-cyclophosphamide-lenalidomide therapies in a population of untreated MM patients, respectively.[11] We expected our approach of alternating chemotherapy with Bd and Ld to achieve an ORR of 88%. Thereby, the required sample size was calculated as $n = 32$, assuming an expected response rate of 88%, a threshold response rate of 70.4%, $\alpha = 0.05$ (one-sided), and $\beta = 0.2$ (80% power), based on a binomial distribution. However, we set the sample size at 35 according to a dropout rate of 10%.

Statistical methods

The primary endpoint was the ORR during the period of alternating chemotherapy with Bd and Ld. Secondary endpoints were AEs, the proportion of treatment continuation, complete response rate (CRR), very good partial response (VGPR), progression-free survival (PFS), overall survival (OS), and time to response (TTR).

ORR, CRR and VGPR were estimated with 90% confidence intervals (CIs). Survival curves of PFS, OS and TTR were calculated using the Kaplan–Meier method; CI was calculated using Greenwood's formula. Further, the occurrence of worst-grade AEs, grade-3 or higher AEs, and serious AEs were calculated.

RESULTS

Patient demographics

Ten patients were enrolled between October 2014 and March 2016 from three centers of the National Hospital Organization in Japan. The study ended before reaching the target sample size because of slow accrual. All patients (five men and five women) were included in the intention-to-treat analysis. Patient characteristics are shown in Table 1.

Table 1 Patient characteristics

	n (%)*
Number of patients	
Gender	10
Male	5 (50.0%)
Female	5 (50.0%)

Age (years)	81 (76–85)
Durie & Salmon System stage	
II	2 (20.0%)
III	8 (80.0%)
International Staging System stage	
I	1 (10.0%)
II	5 (50.0%)
III	4 (40.0%)
ECOG Performance Status score	
1	3 (30.0%)
2	3 (30.0%)
3	4 (40.0%)
Serum M protein type	
IgG	4 (40.0%)
IgA	5 (50.0%)
BJP	1 (10.0%)
Bone lesion	
Osteoporosis	3 (30.0%)
Osteolytic lesions	2 (20.0%)
Extensive bone destruction and major fractures	5 (50.0%)
Translocation karyotype/Chromosome abnormality	
t(11;14)(q13;q32), other	1 (10.0%)
Other	1 (10.0%)
Chromosome 13 abnormalities -13/13q-	1 (10.0%)
FISH abnormalities (n = 9)	
t(4;14)(p16;q32)	3 (33.3%)
t(8;14)(q24;q32)	1 (11.1%)
t(11;14)(q13;q32)	2 (22.2%)
del(17p)	1 (11.1%)
del(1p32.3)	1 (11.1%)
1q21 gain	5 (55.6%)
del(13)	5 (55.6%)
Other (n = 3)	1 (33.3%)
Serum β2-microglobulin (mg/L)	5.3 (3.1–9.5)
Albumin (g/dL)	3.2 (2.5–4.0)
Hb (g/dL)	4.4 (3.9–4.9)
Creatinine clearance (mL/min)	45.8 (31.8–66.7)
Ca (mg/dL)	9.5 (7.2–11.3)
LDH (U/L)	167 (121–253)
Ratio of bone marrow plasma cells	41.6 (9.0–80.4)
Comorbidity[#]	
Vascular	6 (60.0%)
Respiratory	2 (20.0%)
Eyes, ears, nose, throat, and larynx	1 (10.0%)

Liver, pancreas, and biliary	1 (10.0%)
Renal	5 (50.0%)
Neurologic	1 (10.0%)
Endocrine and breast	2 (20.0%)
Psychiatric illness	1 (10.0%)

*Data are presented as median (range) or number (%).
BJP: Bence Jones proteinuria
Ca: calcium
ECOG: Eastern Cooperative Oncology Group
FISH: fluorescence in situ hybridization
Hb: hemoglobin
IgA: immunoglobulin A
IgG: immunoglobulin G
LDH: lactate dehydrogenase
#Scores ≥ 2, assessed with the Cumulative Illness Rating Scale-Geriatric during comprehensive geriatric assessment.

The median age was 81 years (range, 76–85 years). Eight patients (80.0%) had stage III MM according to the Durie and Salmon system. All patients had Eastern Cooperative Oncology Group Performance Status score ≥ 1; three (30.0%) had score 1, three (30.0%) had score 2, and four (40.0%) had score 3. In terms of the serum M protein type, five (50.0%), four (40.0%), and one (10.0%) patients had IgA, IgG, and Bence Jones protein, respectively. In one patient, the translocation karyotype was t(11;14)(q13;q32). FISH abnormalities were observed as follows: five patients with 1q21 gain, five with del(13), three with t(4;14)(p16;q32), two with t(11;14)(q13;q32), one with t(8;14)(q24;q32), one with del(17p), and one with del(1p32.3). Six patients were categorized into the high-risk subgroup with chromosomal abnormalities: t(4;14), t(14;16), del(17p), or 1q21 gain, as determined by the International Myeloma Working Group and Mayo Clinic.[12,13] All patients had bone lesions, and the median serum β2-microglobulin level of 5.3 mg/L (range 3.1–9.5 mg/L) was high. Among out of the 10 patients, 7 (70.0%) completed the trial planned six treatment of 6 cycles.

The remaining three patients discontinued up to six cycles of Bd therapy, during four cycles of Bd therapy, and after three cycles of Bd therapy. The reasons for early treatment discontinuation were extended treatment interval (n = 2) and patient request (n = 1).

Outcomes

The maximum effect of patient response is shown in Table 2.

Table 2 Maximum effect of patient response

	sCR	CR	VGPR	PR	SD	Total (n)	ORR
Bd/Ld	3	1	2	2	2	10	80.0%

Bd: bortezomib-dexamethasone
Ld: lenalidomide-dexamethasone
sCR: stringent complete response
CR: complete response
VGPR: very good partial response
PR: partial response
SD: stable disease

The ORR was 80.0% (90% CI: 49.3–96.3%), CRR was 40%, and VGPR rate was 20% for Bd/Ld alternating treatment, with seven patients (70.0%) having completed the planned six cycles of study treatment. In two patients, the effect worsened when the treatment was switched from Ld to Bd.

At the cut-off date (January 15, 2018), the median follow-up time was 27 months. The 2-year OS and PFS were 80.0% and 40.0% (95% CI: 40.9–94.6%, 12.3–67.0%), respectively (Fig. 1).

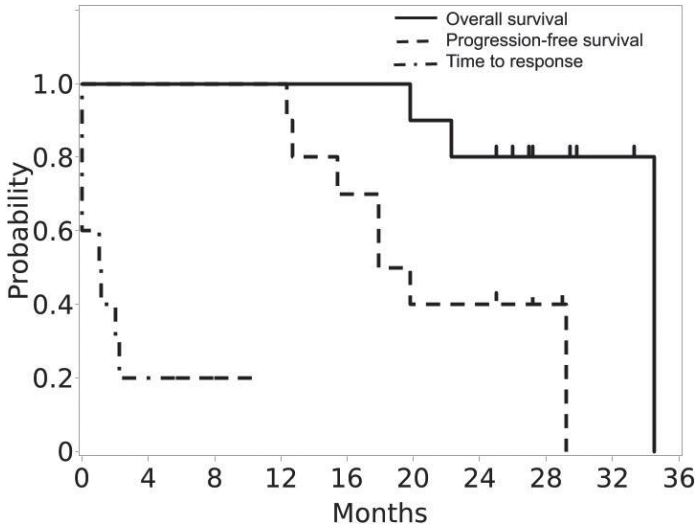

Fig. 1 Kaplan-Meier curve for overall survival, progression-free survival, and time to response

Four out of six patients with relapse or disease progression received the first salvage therapy with immunomodulatory drugs (IMiDs). Moreover, two patients additionally received second salvage therapy with IMiDs or bortezomib. Regarding the response time, the probability at 10 months was 20.0% (95% CI: 3.1–47.5%). Three patients from the high-risk subgroup died during the follow-up period due to myeloma.

Of the total 10 patients, 8 had AEs of grade 3 or higher, the most common of which were hematologic toxicities, such as anemia, lymphocyte count decrease, neutropenia, platelet count decrease, and white blood cell decrease, as shown in Table 3. Grade 4 AEs of neutropenia, lymphocyte count decrease, platelet count decrease, and white blood cell decrease were observed in one patient during cycle 4 of Bd therapy.

Table 3 Adverse events of grade 3 or more

Cycle	1		2		3		4		5		6	
	Bd	Ld	Bd	Ld	Bd	Ld	Bd	Ld	Bd	Ld	Bd	Ld
n	10	10	10	10	10	9	9	8	8	8	7	7

Anemia	3	1	2	1	1	0	1	0	0	0	0	0
Diarrhea	0	0	1	0	0	0	0	0	0	0	0	0
Nausea	0	1	0	0	0	0	0	0	0	0	0	0
Infections, infestations, and others	0	0	0	0	0	0	1	0	0	0	0	0
Lymphocyte count decrease	1	2	0	2	0	0	1	0	0	0	0	1
Neutropenia	2	0	1	1	1	1	1	0	0	0	0	0
Platelet count decrease	1	1	0	0	0	0	1	0	0	0	0	0
White blood cell count decrease	1	1	1	1	1	1	1	0	0	0	0	0
Anorexia	0	0	0	0	0	0	1	0	0	0	0	0
Hypokalemia	0	0	1	2	1	1	0	0	0	0	0	0
Hyponatremia	1	0	0	0	0	0	0	0	0	0	0	0
Back pain	1	0	0	0	0	0	0	0	0	0	0	0
Bone pain	1	0	0	0	0	0	0	0	0	0	0	0

Two patients experienced unexpected serious AEs; one had grade 2 arthralgia and the other grade 3 musculoskeletal and connective tissue disorders. The former was diagnosed as osteoarthritis of the hip; subsequently, bortezomib on day 22 was omitted, and the patient recovered after undergoing joint arthroplasty. The latter was diagnosed as a fracture of the right femoral neck and was resolved with an arthroplasty. We discontinued the study treatment for the latter patient.

In terms of its association with the number of treatment cycles, the number of AEs of grade

3 or higher decreased after cycle 4 of Ld treatment, and only one case of lymphocyte count decrease occurred at cycle 6 of Ld treatment.

DISCUSSION AND CONCLUSION

In the present study, we evaluated the feasibility and efficacy of alternating Bd and Ld treatments in elderly patients with NDMM.

We hypothesized that the study treatment would be effective because patients would receive first-line therapy with drugs of different mechanisms of action during each cycle; this would suppress the myeloma cells while reducing severe toxicity. Our results did not support the hypothesis in terms of efficacy, as the ORR, the primary endpoint, was 80.0% in this study, and its lower limit of 90% CI was below the threshold value of 70.4%. However, the 2-year PFS and OS of 40.0% and 80.0%, respectively, were comparable to those reported in elderly patients in the FIRST trial[14] or the UPFRONT study,[15] despite this MARBLE trial having 55.6% of patients with high-risk cytogenetics. Further, with respect to toxicity, the incidence of hematologic and non-hematologic AEs or serious AEs was similar to that reported previously.[7,14] Because Ld was approved in our country after the start of this study, it was not possible to enroll the planned number of patients in this study, and the study was discontinued early.

All patients received at least three cycles of Bd/Ld treatment, and 70.0% of them completed six cycles (54 weeks), suggesting that this study treatment was well-tolerated even in elderly patients with MM.[7] Further, considering that our study was aimed at patients aged over 75 years and that 70.0% of these patients completed the study treatment, our results for AEs are better than those reported in previous studies with elderly patients.[7,14]

Moreover, the treatment of patients aged 75 years or more needs to be optimized. Although the number of subjects was too small to draw any conclusions from this study, the alternating chemotherapy strategy based on a combination of proteasome inhibitors and IMiDs still has the potential to become one of the treatment options for elderly MM patients. This strategy can be applied in combination with anti-CD38 monoclonal antibodies.

The Bd/Ld alternating therapy is widely indicated in patients with standard-risk (other than high-risk subgroup), who face difficulty in using a combination of proteasome inhibitors and IMiDs owing to AEs and who can visit the hospital to receive Bd therapy once a week.

To summarize, the study suggests that alternating Bd/Ld treatment might be tolerable in elderly patients with NDMM; however, its efficacy was not determined because the number of patients was smaller than planned.

AUTHOR CONTRIBUTIONS

AY and AK equally contributed to this work.

ACKNOWLEDGEMENTS

This study was supported by an operating expense grant for research from the National Hospital Organization.

DECLARATIONS

Statement of ethics

Written informed consent was obtained from every participant in the study.

This trial was approved by the Central Ethics Review Committee for Clinical Research of the National Hospital Organization on July 20, 2014 (H26-0320002).

Conflicts of interest statement

AK reports personal fees from Bayer Yakuhin, Ltd., as a member of the independent data monitoring committee of clinical trials outside the submitted work. KS received research funding from Ono Pharmaceutical, MSD, Celgene, AbbVie, Takeda Pharmaceutical, Sanofi, Bristol-Myers Squibb, Daiichi Sankyo, Janssen, Novartis, Alexion Pharma, and GlaxoSmithKline and received honoraria from Ono Pharmaceutical, Celgene, Takeda Pharmaceutical, and Bristol-Myers Squibb. The other authors have no conflicts of interest to declare.

Funding sources

This study was supported by an operating expense grant for research from the National Hospital Organization.

REFERENCES

1 Munshi NC, Longo DL, Anderson KC. Plasma cell disorders. In: *Harrison's Principles of Internal Medicine*. 20th ed. New York:McGraw-Hill Medical;2018:793.
2 Brenner H, Gondos A, Pulte D. Recent major improvement in long-term survival of younger patients with multiple myeloma. *Blood*. 2008;111:2521–2526. doi:10.1182/blood-2007-08-104984.
3 San Miguel JF, Schlag R, Khuageva NK, et al. Bortezomib plus melphalan and prednisone for initial treatment of multiple myeloma. *N Engl J Med*. 2008;359:906–917. doi:10.1056/NEJMoa0801479.
4 Facon T, Dimopoulos MA, Dispenzieri A, et al. Final analysis of survival outcomes in the phase 3 FIRST trial of up-front treatment for multiple myeloma. *Blood*. 2018;131:301–310. doi:10.1182/blood-2017-07-795047.
5 Niesvizky R, Flinn IW, Rifkin R, et al. Community-based phase IIIB trial of three UPFRONT bortezomib-based myeloma regimens. *J Clin Oncol*. 2015;33:3921–3929. doi:10.1200/JCO.2014.58.7618.
6 O'Donnell EK, Laubach JP, Yee AJ, et al. A phase 2 study of modified lenalidomide, bortezomib and dexamethasone in transplant-ineligible multiple myeloma. *Br J Haematol*. 2018;182:222–230. doi:10.1111/bjh.15261.
7 Mateos MV, Martínez-López J, Hernández MT, et al. Sequential vs alternating administration of VMP and Rd in elderly patients with newly diagnosed MM. *Blood*. 2016;127:420–425. doi:10.1182/blood-2015-08-666537.
8 Yokoyama A, Kada A, Saito AM, et al. Phase II Study of Treatment for Newly Diagnosed Multiple Myeloma Patients Over 75 Years Old with Alternating Bortezomib/dexamethasone and Lenalidomide/dexamethasone: the MARBLE Trial. *Acta Med Okayama*. 2019;73(6):547–552. doi:10.18926/AMO/57722.
9 Tucci A, Ferrari S, Bottelli C, et al. A comprehensive geriatric assessment is more effective than clinical judgment to identify elderly diffuse large cell lymphoma patients who benefit from aggressive therapy. *Cancer*. 2009;115(19):4547–4553. doi:10.1002/cncr.24490.
10 Vesole DH, Jacobus S, Rajkumar SV, et al. Lenalidomide plus low-dose dexamethasone (Ld): Superior one- and two-year survival regardless of age compared to lenalidomide plus high-dose dexamethasone (LD). *Blood*. 2010;116:abstract 308. doi:10.1182/blood.V116.21.308.308.
11 Kumar S, Flinn I, Richardson PG, et al. Randomized, multicenter, phase 2 study (EVOLUTION) of combinations of bortezomib, dexamethasone, cyclophosphamide, and lenalidomide in previously untreated multiple myeloma. *Blood*. 2012;119:4375–4382. doi:10.1182/blood-2011-11-395749.
12 Palumbo A, Avet-Loiseau H, Oliva S, et al. Revised International Staging System for Multiple Myeloma: A Report From the International Myeloma Working Group. *J Clin Oncol*. 2015;33:2863–2869. doi:10.1200/JCO.2015.61.2267.
13 Dingli D, Ailawadhi S, Bergsagel PL, et al. Therapy for relapsed multiple myeloma: Guidelines from the

Mayo stratification for myeloma and risk-adapted therapy. *Mayo Clin Proc*. 2017;92:578–598. doi:10.1016/j.mayocp.2017.01.003.

14 Hulin C, Facon T, Shustik C, et al. Effect of age on efficacy and safety outcomes in patients (Pts) with newly diagnosed multiple myeloma (NDMM) receiving lenalidomide and low-dose dexamethasone (Rd): The first trial. *Blood*. 2014;124:81. doi:10.1182/blood.V124.21.81.81.

15 Niesvizky R, Flinn IW, Rifkin R, et al. Efficacy and safety of three bortezomib-based combinations in elderly, newly diagnosed multiple myeloma patients: Results from all randomized patients in the community-based, phase 3b UPFRONT study. *Blood*. 2011;118:478. doi:10.1182/blood.V118.21.478.478.

Journal of Histochemistry & Cytochemistry 2021, Vol. 69(10) 645–657

DOI: 10.1369/00221554211048551
journals.sagepub.com/home/jhc
SAGE

The Conspicuousness of High Endothelial Venules in Angioimmunoblastic T-cell Lymphoma Is Due to Increased Cross-sectional Area, Not Increased Distribution Density

Akiya Kogami, Mana Fukushima, Hitomi Hoshino, Takuya Komeno, Tadakazu Okoshi, Masataka Murahashi, Tomoya O. Akama, Junya Mitoma, Haruo Ohtani, and Motohiro Kobayashi

Department of Tumor Pathology, Faculty of Medical Sciences, University of Fukui, Eiheiji, Japan (AK, MF, HH, MM, MK); Omachi Municipal General Hospital, Omachi, Japan (MF, MK); Department of Hematology, National Hospital Organization Mito Medical Center, Ibaraki, Japan (TK); Department of Pathology, Japanese Red Cross Fukui Hospital, Fukui, Japan (TO); Department of Pharmacology, Kansai Medical University, Hirakata, Japan (TOA); Department of Medical Life Sciences, School of Medical Life Sciences, Kyushu University of Health and Welfare, Nobeoka, Japan (JM); and Department of Pathology, Mito Saiseikai General Hospital, Mito, Japan (HO)

Summary

Angioimmunoblastic T-cell lymphoma (AITL) is a T-cell lymphoma of follicular helper T-cell origin. Histologically, neoplastic T-cells proliferate to form clusters adjacent to or between arborizing high endothelial venules (HEVs). HEVs in normal lymph nodes express sulfated glycans called peripheral lymph node addressin (PNAd); however, it remains unclear whether PNAd is also expressed on HEVs in AITL. Furthermore, although it is widely accepted that HEVs are conspicuous in AITL due to their proliferation, quantitative histological support for this concept is lacking. To investigate these issues, we employed monoclonal antibodies recognizing PNAd, namely, MECA-79, HECA-452, and 297-11A, and performed quantitative immunohistochemical analysis of HEVs in 36 AITL-affected and 67 normal lymph nodes. Staining with all three antibodies confirmed that AITL HEVs express PNAd. Moreover, AITL HEVs were bound calcium-dependently by L-selectin-IgM fusion proteins, indicating that they function in the recruitment of L-selectin-expressing lymphocytes. Unexpectedly, HEV distribution density was not increased but rather decreased in AITL compared with normal lymph nodes, but HEV cross-sectional area in AITL was significantly greater than that seen in normal lymph nodes. Overall, these results indicate that the prominence of AITL HEVs is likely due to increased cross-sectional area rather than increased distribution density. (J Histochem Cytochem 69:645–657, 2021)

Keywords

CD34, *N*-acetyllactosamine, sialyl Lewis x (sLe^x)

Introduction

Angioimmunoblastic T-cell lymphoma (AITL) is one of the most common subtypes of peripheral T-cell lymphoma (PTCL), accounting for roughly 20% of PTCL.[1] Currently, neoplastic T-cells are thought to originate from follicular helper T-cells, which, under normal conditions, play pivotal roles in the formation and maintenance of germinal centers and B-cell differentiation.[2] In AITL, neoplastic T-cells proliferate against a background consisting of reactive host immune cells, including B-cells (often with a blast form), plasma cells,

Received for publication June 1, 2021; accepted September 7, 2021.

Corresponding Author:
Motohiro Kobayashi, Department of Tumor Pathology, Faculty of Medical Sciences, University of Fukui, 23-3 Matsuoka-Shimoaizuki, Eiheiji, Fukui 910-1193, Japan.
E-mail: motokoba@u-fukui.ac.jp

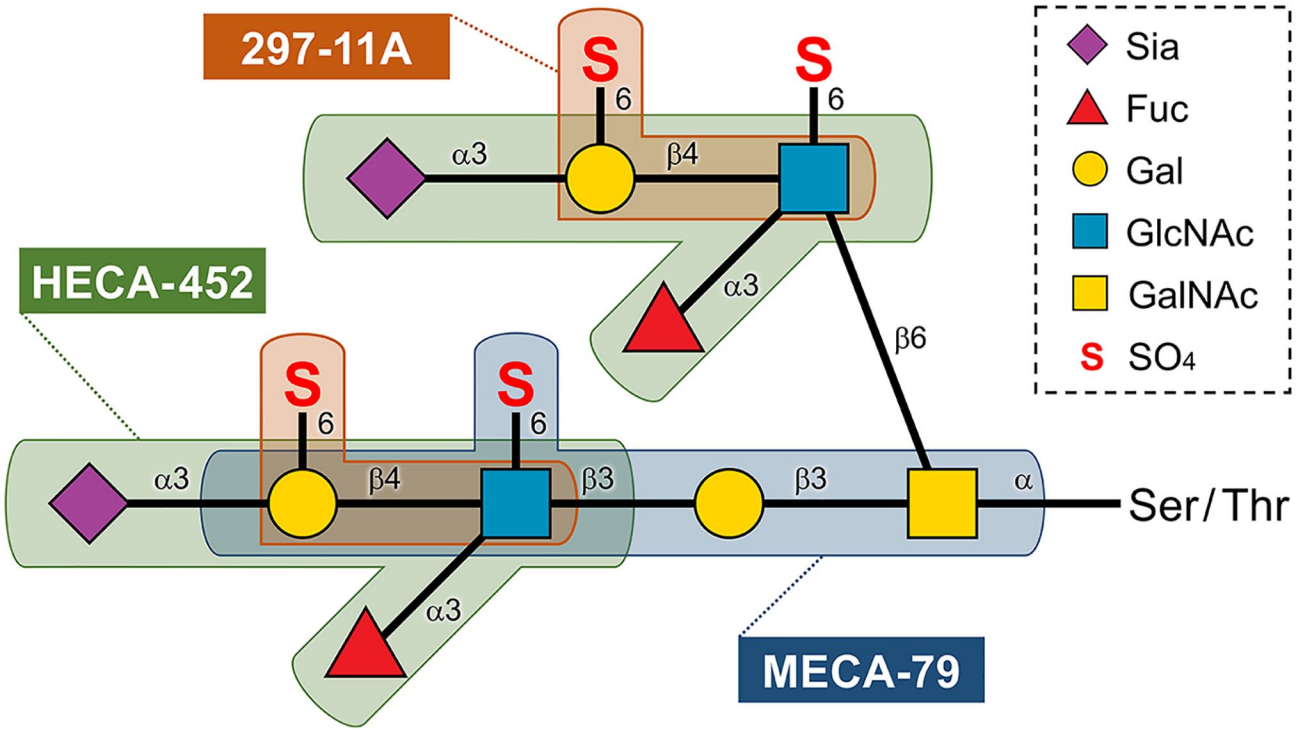

Figure 1. Glycan structure of 6,6′-disulfo sLe^x attached to both extended core 1 and core 2-branched *O*-glycans, one of the most fully glycosylated and sulfated forms of putative L-selectin ligands. Epitopes are shown for MECA-79, HECA-452, and 297-11A monoclonal antibodies.[1–3,5–8]

eosinophils, and macrophages, as well as an irregularly expanded meshwork of follicular dendritic cells (FDCs) and arborizing high endothelial venules (HEVs).[3,4]

HEVs are specialized venules composed of tall and plump endothelial cells located mainly in T-cell zones, such as paracortical and interfollicular areas; however, some HEVs are also present in B-cell zones, particularly in the periphery of lymphoid follicles.[5] Under physiological conditions, HEVs function to recruit lymphocytes from the circulation to the lymphoid parenchyma. HEVs express a series of glycoproteins, including CD34 decorated with sulfated sialyl Lewis x (sLe^x) glycans, collectively called peripheral lymph node addressin (PNAd).[6–8] Expression of PNAd in HEV-like vessels is reportedly induced in various chronic inflammatory diseases,[9] and we also reported such PNAd expression in chronic *Helicobacter pylori* gastritis,[10] ulcerative colitis,[11] autoimmune pancreatitis,[12] chronic prostatitis associated with benign prostatic hyperplasia,[13] eosinophilic chronic rhinosinusitis (ECRS),[14] and, most recently, oral lichen planus.[15] The relatively weak, transient adhesive interaction between PNAd on HEVs (as well as HEV-like vessels) and L-selectin on circulating lymphocytes results in lymphocyte rolling along the luminal face of HEVs, followed by chemokine-dependent lymphocyte activation, integrin-mediated lymphocyte firm attachment to endothelium, and platelet endothelial cell adhesion molecule 1 (PECAM-1)-mediated lymphocyte transmigration across blood vessels.[8,16]

PNAd is often detected using the monoclonal antibody MECA-79,[17] whose epitope has been shown to be 6-sulfo [i.e. *N*-acetylglucosamine (GlcNAc)-6-*O*-sulfated] *N*-acetyllactosamine (LacNAc) attached to extended core 1 *O*-glycans, Galβ1→4(SO_4→6)GlcNAcβ1→3Galβ1→3GalNAcα1→Ser/Thr (in which Gal is galactose and GalNAc is *N*-acetylgalactosamine) (Fig. 1).[18] This epitope overlaps with 6-sulfo sLe^x, Siaα2→3Galβ1→4[Fucα1→3(SO_4→6)]GlcNAcβ1→R (in which Sia is sialic acid and Fuc is fucose), the L-selectin recognition determinant. This determinant can be also detected by the monoclonal antibody HECA-452, whose epitope has been shown to be sLe^x tetrasaccharide, Siaα2→3Galβ1→4(Fucα1→3)GlcNAcβ1→R, regardless of GlcNAc- and/or Gal-6-*O*-sulfation (Fig. 1).[19–21] GlcNAc-6-*O*-sulfation of sLe^x moieties is required for optimal L-selectin binding and is catalyzed cooperatively by GlcNAc-6-*O*-sulfotransferase 1 (GlcNAc6ST-1) and GlcNAc-6-*O*-sulfotransferase 2 (GlcNAc6ST-2).[22,23] On the contrary, HEVs in peripheral lymph nodes also express sialyl 6′-sulfo (i.e., Gal-6-*O*-sulfated) LacNAc-capped *O*-glycans, Siaα2→3(SO_4→6)

Galβ1→4GlcNAcβ1→R, which can be detected with the antibody 297-11A (Fig. 1), which we recently developed.[24] Gal-6-*O*-sulfation of sLe^x moieties also comprises an L-selectin-binding determinant in vitro[25] and is catalyzed by keratan sulfate Gal-6-*O*-sulfotransferase (KSGal6ST).[26] However, it remains to be determined whether these sulfated sLe^x-related glycans are also expressed in HEVs formed in AITL. Furthermore, although it is widely accepted that HEV proliferation is a histological hallmark of AITL, to our knowledge, there are no reports of quantitative histological analysis of HEVs to confirm this idea.

This study consists of two parts: functional analysis of the carbohydrate moiety of PNAd expressed in HEVs, and quantitative and morphometric analysis of HEVs. First, we conducted immunohistochemical staining with a battery of anti-PNAd monoclonal antibodies and confirmed that sulfated sLe^x, which is expressed in normal lymph node HEVs, is also expressed in HEVs formed in AITL. Then, we used selectin-IgM fusion proteins to determine whether sulfated sLe^x expressed in these HEVs potentially functions as an L-selectin ligand. In the second part of our analysis, we asked whether HEV distribution density (specifically, the number per unit area) in AITL differed from that seen in normal lymph nodes and how HEV cross-sectional area in AITL compared with that seen in normal lymph nodes. Our analysis indicated overall that HEVs formed in AITL show increased cross-sectional area, rather than increased distribution density.

Materials and Methods

Human Tissue Samples

Formalin-fixed, paraffin-embedded (FFPE) tissue blocks of biopsied lymph nodes with a diagnosis of AITL were obtained from the pathology archives of University of Fukui Hospital (Eiheiji, Japan), National Hospital Organization Mito Medical Center (Ibaraki, Japan), Omachi Municipal General Hospital (Omachi, Japan), and the Japanese Red Cross Fukui Hospital (Fukui, Japan). Using hematoxylin and eosin (H&E) staining with adjunctive immunohistochemical staining for CD3 (rabbit polyclonal, cat. no. A0452; Dako, Glostrup, Denmark), CD4 (mouse monoclonal IgG_1, clone 1F6, cat. no. NCL-CD4-1F6; Leica Biosystems, Newcastle Upon Tyne, UK), CD10 (mouse monoclonal IgG_1, clone 56C6, cat. no. 413261; Nichirei Biosciences, Tokyo, Japan), CD20 (mouse monoclonal IgG_{2a}, clone L26, cat. no. M0755; Dako), CD21 (mouse monoclonal IgG_1, clone 1F8, cat. no. M0784; Dako), BCL6 (mouse monoclonal IgG_1, clone P1F6, cat. no. 413761; Nichirei Biosciences), CXCL13 (goat polyclonal, cat. no. AF801; R&D Systems, Minneapolis, MN), and CXCR5 (rabbit polyclonal, cat. no. GTX100351; GeneTex, Irvine, CA), histological diagnosis of AITL was re-evaluated by certified pathologists (AK, MF, HO and MK) according to the latest edition of the World Health Organization (WHO) classification (revised 4th edition).[4] From that analysis, we selected specimens with histological findings in best agreement with AITL (n=36 from 19 patients; mean age, 73.7 ± 12.2 years; male:female = 12:7). FFPE tissue blocks of surgically resected axillary lymph nodes negative for metastasis (n=67 from 19 patients; mean age, 59.2 ± 12.8 years; male:female = 1:18) were collected as controls. Analysis of human lymph node tissues was approved by the Ethics Committee of the Faculty of Medical Sciences, University of Fukui (reference number 20160100, approved on December 7, 2016; reference number 20200193, approved on April 14, 2021).

Monoclonal Antibodies

The following monoclonal antibodies were used as primary antibodies: QBEND10 (mouse IgG_1, cat. no. IM0786; Immunotech, Marseille, France) recognizing human CD34, a marker of vascular endothelial cells[27]; MECA-79 (rat IgM, cat. no. 553863; BD Biosciences, Franklin Lakes, NJ)[17]; HECA-452 (rat IgM, cat. no. 550407; BD Biosciences)[19]; and 297-11A (mouse IgM).[24] Epitopes for MECA-79, HECA-452, and 297-11A are shown in Fig. 1.

Expression of MECA-79 and 297-11A Epitopes in Lec2 Cells

To express the minimum epitope of MECA-79, Lec2 cells (obtained from American Type Culture Collection, Manassas, VA), a mutant CHO line that lacks sialic acid modification due to inactivation of the Golgi CMP-sialic acid transporter,[28] were co-transfected with pcDNA1-GlcNAc6ST-2[29,30] and pcDNA3-β1,3-*N*-acetylglucosaminyltransferase 3 (β3GlcNAcT-3)[18] (the latter harboring a neomycin resistance gene) at a 9:1 ratio using Lipofectamine Plus (Thermo Fisher Scientific; Waltham, MA) according to the manufacturer's instructions. We then selected stable transformants in 400 μg/ml of Geneticin (Sigma-Aldrich; St. Louis, MO). Cells positive for MECA-79 were cloned by limited dilution, resulting in Lec2/β3GlcNAcT-3/GlcNAc6ST-2 cells. Cells were then transiently transfected with either pcDNA3-KSGal6ST[26] or empty pcDNA3 (mock). After 36 hr, cells were dissociated into monodispersed cells using phosphate-buffered saline (PBS) containing 0.5 mM ethylenediaminetetraacetic acid (EDTA) and then doubly immunostained

with MECA-79 and 297-11A. Expression of both glycoepitopes was assayed simultaneously by flow cytometry using an FACSCanto II (BD Biosciences) with FlowJo software (Tree Star; Ashland, OR).

Immunohistochemistry

Immunohistochemical staining for MECA-79 and HECA-452 was conducted using an indirect method as described,[14] and staining for CD34 and 297-11A was carried out using the Histofine system (Nichirei Biosciences), as per the manufacturer's instructions. For 297-11A staining, to remove sialic acid, which inhibits 297-11A binding, sections were preincubated at 37C for 90 min in a humidified chamber with 0.2 U/ml neuraminidase from *Arthrobacter ureafaciens* (Nacalai Tesque; Kyoto, Japan) dissolved in 50 mM sodium acetate (pH 5.2).[31] Double immunofluorescence staining for MECA-79 and 297-11A was performed essentially as described.[32]

L- and E-Selectin-IgM Chimera In Situ Binding Assays

To obtain L- or E-selectin-IgM chimeric proteins, COS-1 cells were transiently transfected with pcDNA1.1-L-selectin•IgM or pcDNA1.1-E-selectin•IgM, respectively.[10] Transfected cells were cultured 3 days and conditioned media were recovered. L- and E-selectin-IgM binding to CHO cells expressing non-sulfated sLe^x attached to core 2-branched *O*-glycans (named CHO/CD34/F7/C2) and to those expressing its GlcNAc-6-*O*-sulfated form (designated CHO/CD34/F7/C2/LSST)[31] was assayed by flow cytometry, as described.[21,33] L- and E-selectin-IgM chimera in situ binding assays on FFPE tissue sections were carried out as described,[10] with modification. In brief, after quenching endogenous peroxidase activity and blocking nonspecific protein binding, sections were incubated with conditioned media containing L- or E-selectin-IgM chimeras for 30 min and washed with Dulbecco's modified Eagle medium (DMEM; Thermo Fisher Scientific). Sections were then incubated 30 min with horseradish peroxidase (HRP)-conjugated goat anti-human IgM antibody (Millipore; Billerica, MA) and washed with DMEM. The color reaction was developed using Betazoid DAB Chromogen Kit (Biocare Medical; Pacheco, CA). Sections were briefly counterstained with hematoxylin. Negative controls were washed using DMEM supplemented with 5 mM EDTA to chelate calcium ions. In the E-selectin-IgM chimera in situ binding assay, sections were preincubated with CSLEX1 monoclonal antibody (mouse IgM, cat. no. 551344; BD Biosciences), which binds exclusively to non-sulfated sLe^x,[20,21] as a means to detect 6-sulfo sLe^x only.

Quantification of HEVs

Immunostained slides were scanned with NanoZoomer RS (Hamamatsu Photonics; Hamamatsu, Japan) to obtain whole slide images. The area of each lymph node (mm^2) and the number of vessels positive for CD34, MECA-79, HECA-452, or 297-11A in the entire area of each lymph node were determined using NDP.view2 Plus software (Hamamatsu Photonics). We then divided the number of vessels positive for CD34, MECA-79, HECA-452, or 297-11A in each lymph node by the area of corresponding lymph node to calculate the distribution density of vessels of interest. In addition, the number of HEVs positive for MECA-79, HECA-452, or 297-11A was divided by the number of CD34-positive vessels to determine their proportion in total vessels. To determine the mean cross-sectional area of one HEV, as well as the total cross-sectional area of HEVs present in a unit area (1 mm^2), regions in H&E-stained sections with densely distributed HEVs were selected from five cases each of AITL-affected or normal lymph nodes, and for each HEV present in a region, we determined the inner area surrounded by the basement membrane.

Statistical Analysis

Data are expressed as mean ± SD. Differences between groups were statistically analyzed by two-tailed unpaired *t*-test using GraphPad Prism 7 software (GraphPad Software; La Jolla, CA). *P* values less than 0.05 were considered significant.

Results

HEVs Formed in AITL Express Sulfated sLe^x That Constitutes PNAd

AITL cases examined here showed histopathological features typical of AITL,[4] in which lymphoma cells proliferate throughout the lymph node, and normal lymph node architecture is effaced (Fig. 2A). Against a background of reactive host immunoblasts, plasma cells, and eosinophils, small to medium-sized lymphocytes with clear-to-pale cytoplasm (so-called clear cells) proliferate to form clusters adjacent to or between arborizing HEVs (Fig. 2B). Normal lymph node HEVs reportedly constitutively express a series of glycoproteins, including CD34 decorated with sulfated sLe^x, which constitutes PNAd.[6,7] To determine whether

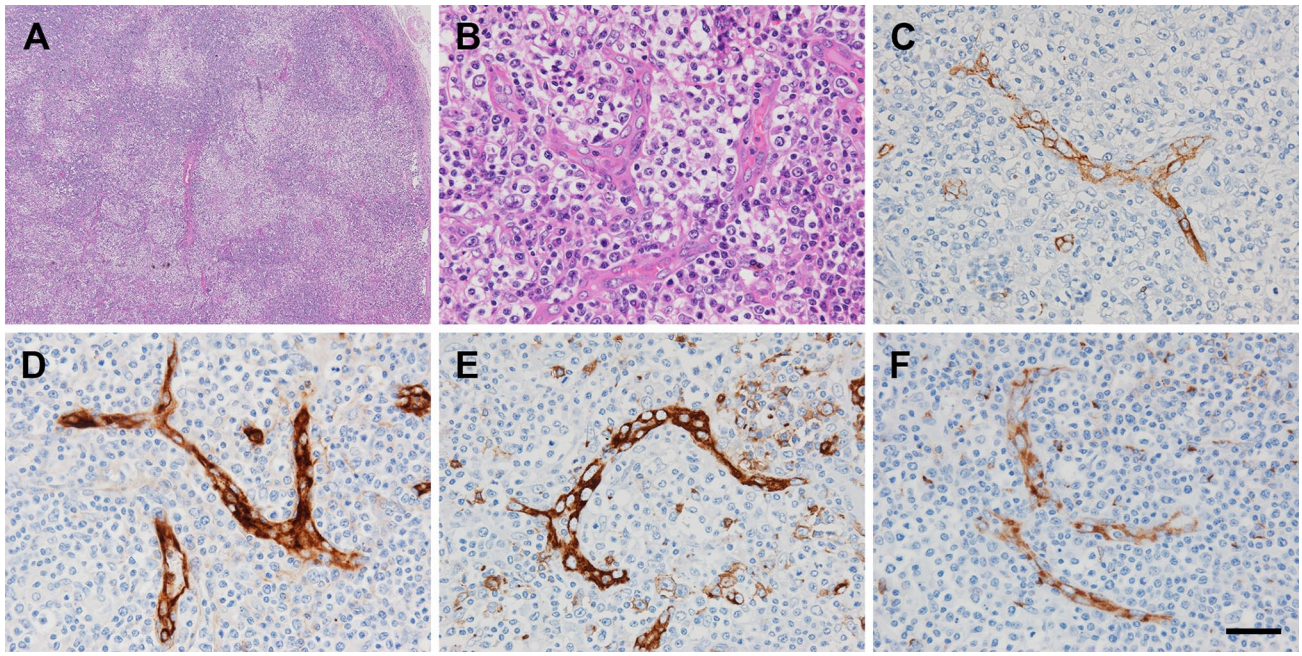

Figure 2. Immunohistochemical profiles of HEVs formed in AITL. (A, B) Histology of AITL. Normal lymph node architecture is effaced due to proliferation of lymphoma cells throughout the lymph node (A). Lymphoma cells with "clear cell" features proliferate to form clusters adjacent to or between arborizing HEVs (B). H&E staining. (C–F) HEVs formed in AITL stain positively for CD34 (C), MECA-79 (D), HECA-452 (E), and 297-11A (F). Signals were visualized with 3,3'-diaminobenzidine (DAB) (brown), and tissues were counterstained with hematoxylin. Bar = 400 μm for panel A and 40 μm for the rest. Abbreviations: HEVs, high endothelial venules; AITL, angioimmunoblastic T-cell lymphoma; H&E, hematoxylin and eosin.

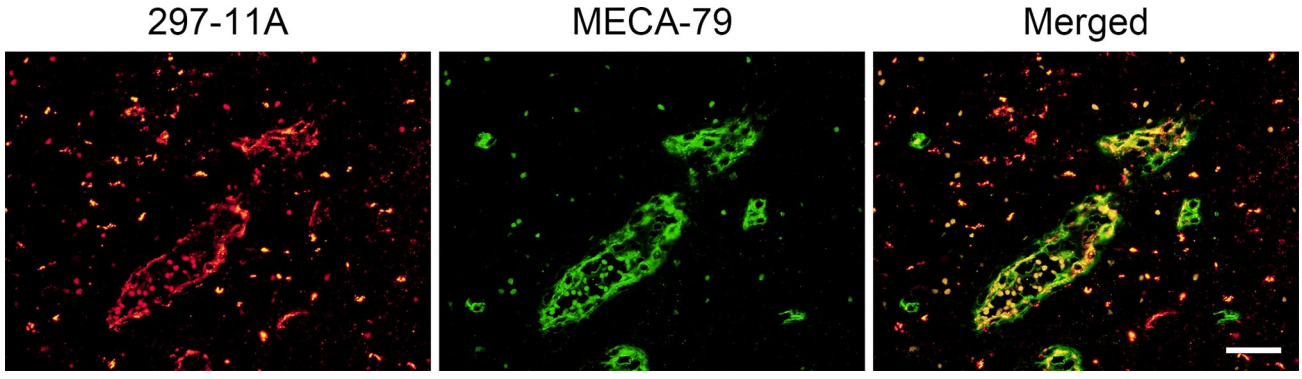

Figure 3. Dual immunofluorescence of HEVs formed in AITL for 297-11A (red) and MECA-79 (green). Yellow signals in Merged indicate colocalization of both carbohydrate antigens. Bar = 40 μm. Abbreviations: HEVs, high endothelial venules; AITL, angioimmunoblastic T-cell lymphoma.

HEVs formed in AITL are decorated with sulfated sLe^x, we conducted immunohistochemical staining for CD34, MECA-79, HECA-452, and 297-11A. In addition to CD34 (Fig. 2C), HEVs formed in AITL were positive for MECA-79 (Fig. 2D), and a proportion were also positive for HECA-452 (Fig. 2E) or 297-11A (Fig. 2F) (see "The Proportion of HEVs in Total Blood Vessels Does Not Increase in AITL" below for detailed quantitative data). Given the glycoepitopes recognized by these antibodies (see Fig. 1), this result indicates that as in normal lymph node, HEVs formed in AITL express sulfated sLe^x.

Gal-6-O-sulfation of LacNAc in the MECA-79 Epitope Does Not Inhibit Reactivity to MECA-79

We then conducted double immunofluorescence staining of AITL tissues with MECA-79 and 297-11A antibodies and found that, overall, 297-11A and MECA-79 signals on HEVs colocalized (Fig. 3), a pattern described

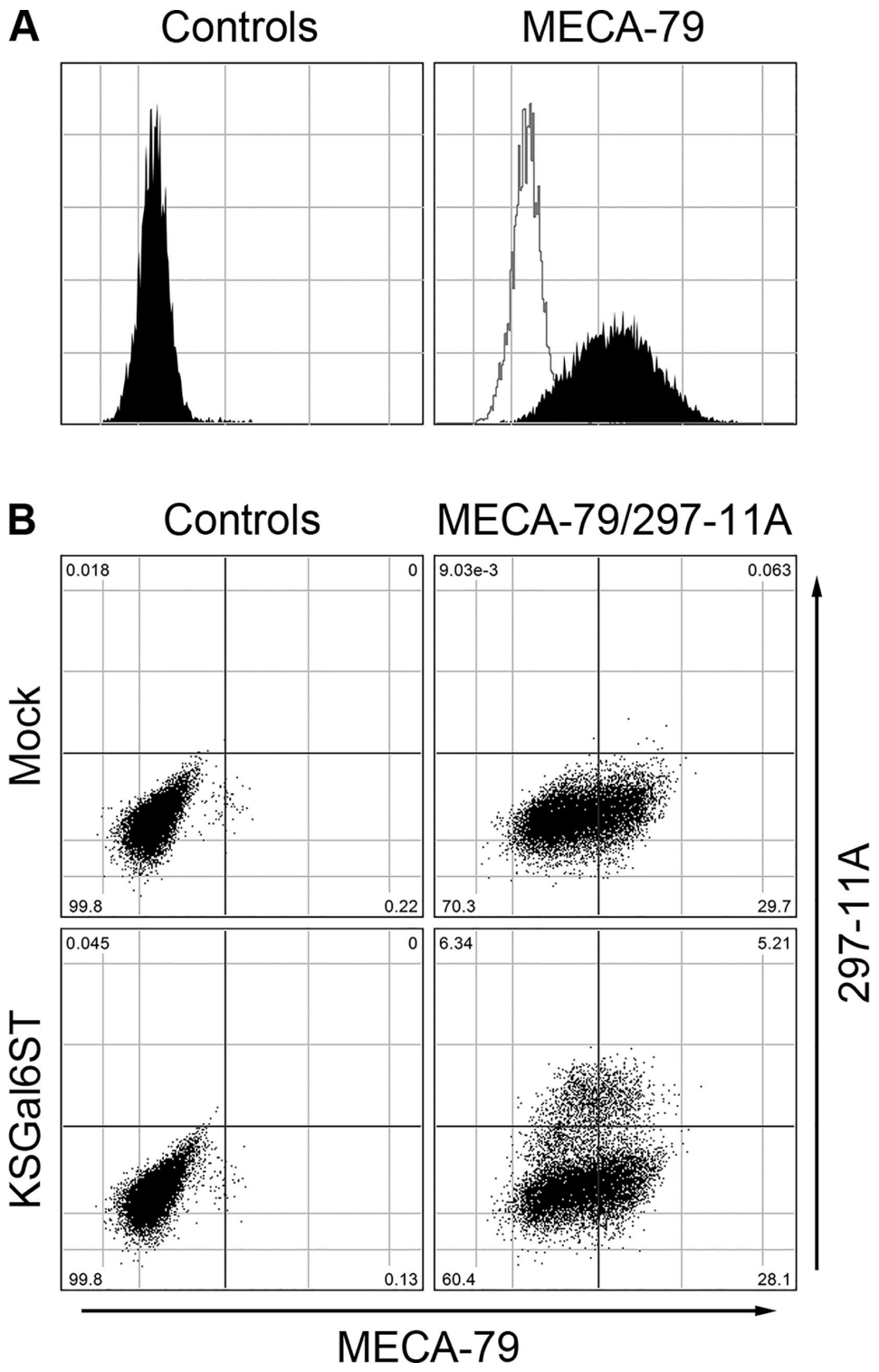

Figure 4. Gal-6-*O*-sulfation of LacNAc in the MECA-79 epitope does not inhibit reactivity to MECA-79. (A) Stable expression of the MECA-79 minimum epitope in Lec2/β3GlcNAcT3/GlcNAc6ST-2 cells (filled histogram in right panel). Filled histogram in the left panel and open histogram in the right panel represent negative controls in which the primary antibody was replaced with isotype-matched immunoglobulin. X- and Y-axes indicate fluorescence intensity and number of events, respectively. Note that cells expressing the MECA-79 epitope are distributed normally, indicating that they are of a single clone. (B) Lec2/β3GlcNAcT-3/GlcNAc6ST-2 cells were transiently transfected with empty vector (mock; upper panels) or KSGal6ST cDNA (lower panels), and then doubly immunostained with MECA-79 and 297-11A (right panels). Left panels represent negative controls replacing primary antibodies with isotype-matched immunoglobulins. X- and Y-axes indicate fluorescence intensity originating from MECA-79 and 297-11A, respectively. Abbreviations: LacNAc, *N*-acetyllactosamine; cDNA, complementary DNA.

in normal lymph node HEVs.[24] The minimum MECA-79 epitope is reportedly 6-sulfo LacNAc attached to extended core 1 *O*-glycans, and it is known that α2,3-sialylated and/or α1,3-fucosylated forms of this structure are also recognized by MECA-79 antibody (see Fig. 1).[18] To determine whether 6′-*O*-sulfation (Gal-6-*O*-sulfation) of LacNAc in the MECA-79 epitope alters its reactivity to MECA-79, we first established Lec2/β3GlcNAcT-3/GlcNAc6ST-2 cells, which express the minimum MECA-79 epitope (Fig. 4A). We then transfected these cells with either KSGal6ST cDNA to express the 297-11A epitope in addition to the MECA-79 epitope or the empty vector (mock) and then evaluated the expression levels of both epitopes simultaneously by flow cytometry. As shown in Fig. 4B (right upper panel), 29.8% (29.7% + 0.1%) of mock-transfected cells were MECA-79-positive, whereas in cells transfected with KSGal6ST cDNA, 33.3% (28.1% + 5.2%) of cells were MECA-79-positive (Fig. 4B, right lower panel). Importantly, expression levels of the MECA-79 epitope in the 297-11A-positive cell population were not attenuated relative to those seen in the 297-11A-negative cell population (Fig. 4B, right lower panel). This result indicates that Gal-6-*O*-sulfation of LacNAc—that is, formation of the 297-11A epitope—in the MECA-79 epitope does not inhibit reactivity to MECA-79.

Sulfated sLe^x Expressed in AITL HEVs Potentially Functions as an L-Selectin Ligand

Although both L- and E-selectin reportedly bind to 6-sulfo sLe^x,[33,34] binding affinity to 6-sulfo sLe^x of IgM fusion proteins of these two selectins has not been fully evaluated. Thus, we first assayed their binding affinity to 6-sulfo sLe^x by flow cytometry using CHO cells expressing 6-sulfo sLe^x, as well as control CHO cells expressing non-sulfated sLe^x. As shown in Fig. 5A (blue histograms), L-selectin-IgM chimeras did not bind to CHO cells expressing non-sulfated sLe^x (upper panel) but did bind to CHO cells expressing 6-sulfo sLe^x, although the signal intensity was weak (lower panel). On the contrary, E-selectin-IgM chimeras showed comparable binding to CHO cells expressing either non-sulfated sLe^x or 6-sulfo sLe^x (Fig. 5A, red histograms). It should be noted that E-selectin-IgM chimeras bound to 6-sulfo sLe^x more readily than did L-selectin-IgM chimeras (Fig. 5A, lower panel). This finding indicates that, at least in vitro, E-selectin-IgM chimeras possess higher capacity to bind to 6-sulfo sLe^x than do L-selectin-IgM chimeras and thus could serve as a sensitive functional probe for 6-sulfo sLe^x.

We then conducted L- and E-selectin-IgM chimera in situ binding assays to investigate whether sulfated sLe^x expressed in AITL HEVs functions as an L-selectin ligand. Both L-selectin-IgM (Fig. 5B) and E-selectin-IgM (Fig. 5C) bound calcium-dependently not only to HEVs in normal lymph nodes but also to those formed in AITL, although the signal intensity of the L-selectin-IgM chimera in AITL HEVs (Fig. 5B, arrows) was much less than that seen in normal lymph node HEVs. It is noteworthy that E-selectin-IgM chimera binding to these HEVs was preserved even after incubation of tissue sections with anti-non-sulfated sLe^x antibody CSLEX1 (Fig. 5C, with CSLEX1). These findings collectively indicate that HEVs formed in AITL possess some selectin-binding ability, albeit limited.

HEV Distribution Density in AITL Decreases Rather Than Increases

Given reports that vascularity in AITL often increases as does HEV arborization,[4] we investigated these changes by performing quantitative immunohistochemical analysis of HEVs using 36 AITL-affected lymph nodes and 67 normal axillary lymph nodes as controls. To calculate vessel distribution density, specifically, the number of vessels per unit area, we first determined the area of each lymph node. Not surprisingly, the area of AITL-affected lymph nodes (52.2 ± 59.7 mm^2) was greater than that of normal lymph nodes (19.3 ± 19.8 mm^2) with high statistical significance ($p<0.001$) (Fig. 6A). Consequently, the distribution density of total vessels in AITL (62.5 ± 20.6/mm^2) was less than that of normal lymph nodes (110.8 ± 35.4/mm^2) with high statistical significance ($p<0.001$) (Fig. 6B). As for HEVs, the distribution density of MECA-79-positive HEVs in AITL (31.0 ± 16.1/mm^2) was less than that of normal lymph nodes (47.8 ± 14.9/mm^2) with high statistical significance ($p<0.001$) (Fig. 6C). Similarly, the distribution density of both HECA-452-positive and 297-11A-positive HEVs in AITL (14.2 ± 8.9/mm^2 and 7.8 ± 12.4/mm^2, respectively) was less than that seen in normal lymph nodes (30.2 ± 13.1/mm^2 and 17.3 ± 19.9/mm^2, respectively) with statistical significance ($p<0.001$ and $p=0.011$, respectively) (Fig. 6D and E, respectively). These findings indicate that rather than increasing, vascularity in AITL decreases relative to normal lymph nodes, as does HEV distribution density.

The Proportion of HEVs in Total Blood Vessels Does Not Increase in AITL

We next assessed the proportion of HEVs in total vessels. As shown in Fig. 7A, the proportion of MECA-79-positive HEVs among CD34-positive total vessels in AITL (50.2% ± 22.2%) and in normal lymph nodes (46.2% ± 17.1%) was comparable ($p=0.320$). Similarly, the proportion of 297-11A-positive HEVs among total vessels in AITL (11.9% ± 17.3%) and in normal lymph

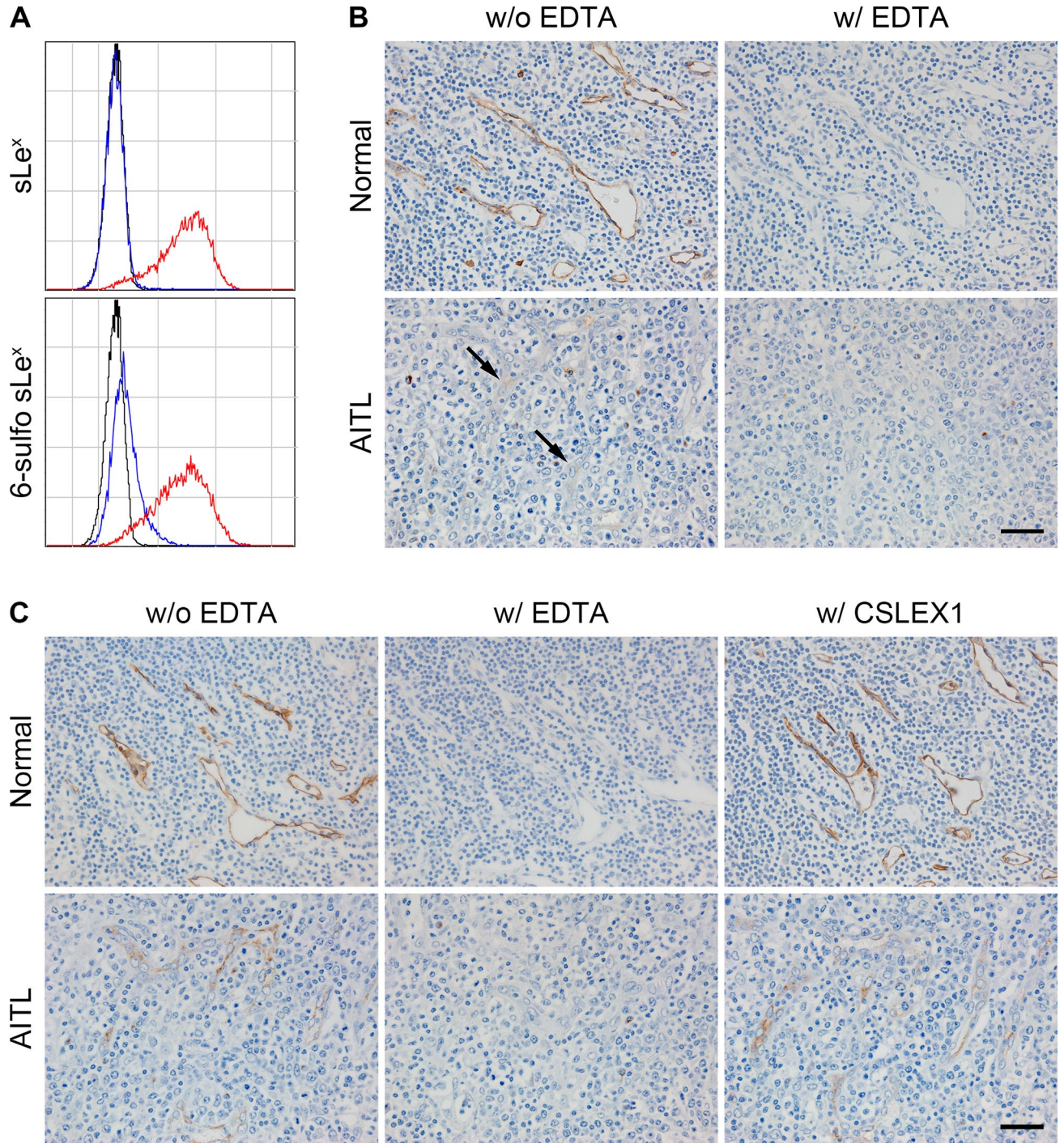

Figure 5. L- and E-selectin-IgM chimera binding assays. (A) Flow cytometric analysis of L-selectin-IgM (blue histograms) and E-selectin-IgM (red histograms) chimera binding to CHO cells expressing non-sulfated sLe^x (upper panel) or 6-sulfo sLe^x (lower panel). Black histograms represent negative controls performed using conditioned medium from untransfected COS-1 cells. X- and Y-axes indicate fluorescence intensity and number of events, respectively. (B, C) L-selectin-IgM (B) and E-selectin-IgM (C) in situ binding assays on FFPE tissue sections of normal (upper panels) and AITL-affected (lower panels) lymph nodes. Both L- and E-selectin-IgM chimeras bind to HEVs in the presence of calcium ions (without EDTA), but binding is completely abrogated in the absence of calcium ions (with EDTA). Note very weak L-selectin-IgM binding to HEVs formed in AITL (arrows). E-selectin-IgM chimera binding to HEVs is maintained even after incubating sections with CSLEX1 antibody, which binds exclusively to non-sulfated sLe^x (with CSLEX1). Signals were visualized with DAB (brown), and tissues were counterstained with hematoxylin. Bar = 40 μm. Abbreviations: FFPE, formalin-fixed, paraffin-embedded; AITL, angioimmunoblastic T-cell lymphoma; HEVs, high endothelial venules; EDTA, ethylenediaminetetraacetic acid.

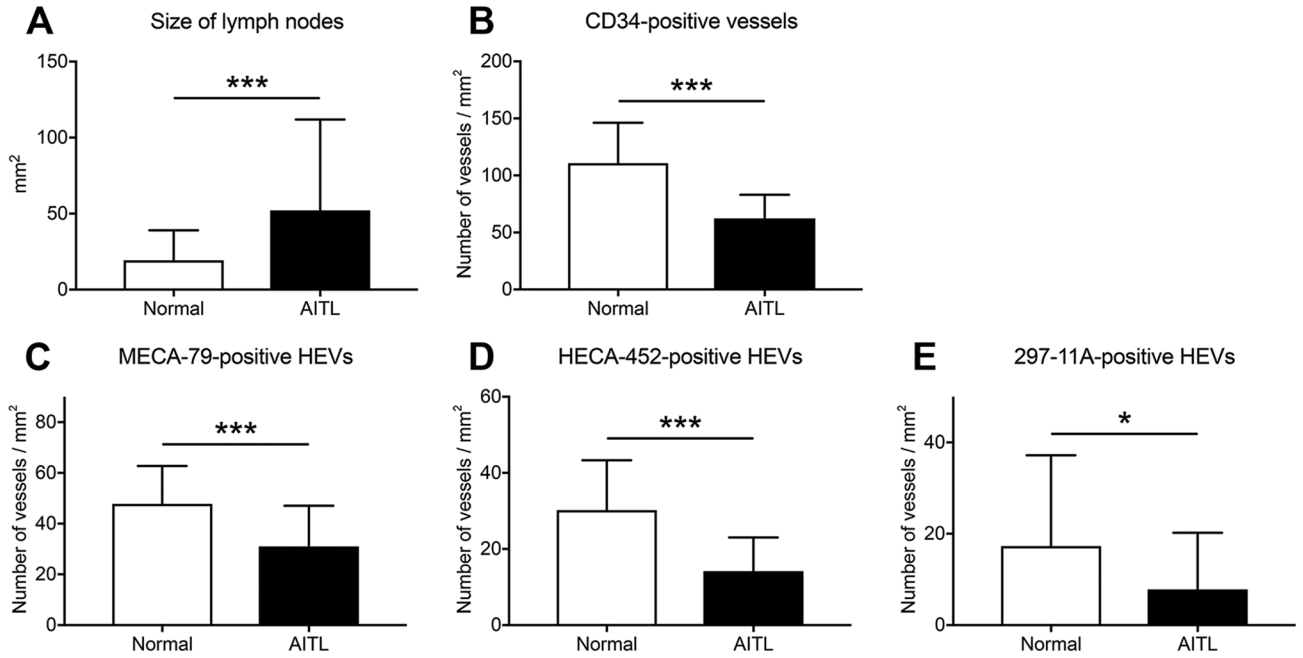

Figure 6. Distribution density of HEVs. (A) The size (area) of normal (n=67; open boxes) and AITL-affected (n=36; filled boxes) lymph nodes. (B–E) Distribution density of vessels immunoreactive for CD34 (B), MECA-79 (C), HECA-452 (D), or 297-11A (E) in normal and AITL-affected lymph nodes. Data are presented as means with SD. Abbreviations: HEVs, high endothelial venules; AITL, angioimmunoblastic T-cell lymphoma. *$p < 0.05$; ***$p < 0.001$.

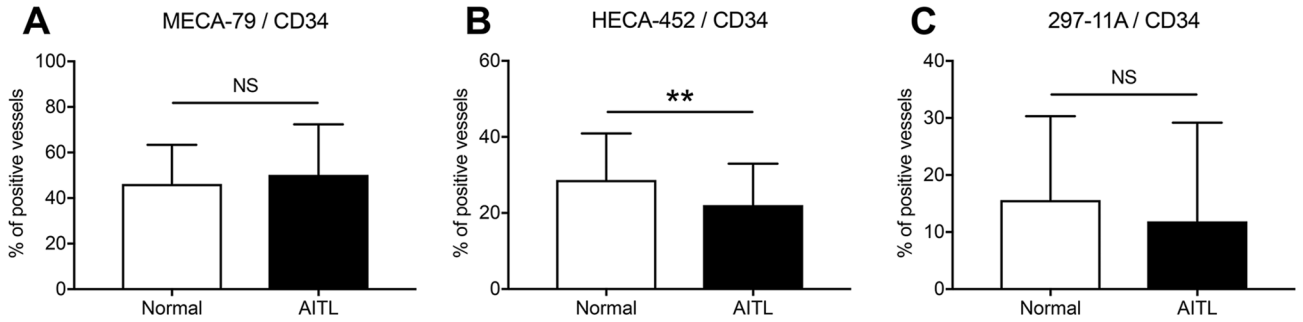

Figure 7. The proportion of HEVs immunoreactive for MECA-79 (A), HECA-452 (B), or 297-11A (C) among CD34-positive total vessels in normal (n=67; open boxes) and AITL-affected (n=36; filled boxes) lymph nodes. Data are presented as means with SD. Abbreviations: HEVs, high endothelial venules; AITL, angioimmunoblastic T-cell lymphoma; NS, not significant. **p<0.01.

nodes (15.6% ± 14.7%) did not differ significantly (p=0.249) (Fig. 7C). These findings indicate that among total vessels, the proportion of HEVs is comparable in AITL and normal lymph nodes. Interestingly, however, the proportion of HECA-452-positive HEVs among total vessels in AITL (22.1% ± 10.9%) was smaller than that seen in normal lymph nodes (28.7% ± 12.2%) with statistical significance (p=0.008) (Fig. 7B).

HEV Cross-sectional Area Increases in AITL

We next performed a careful review of H&E-stained tissue specimens and found that HEVs formed in AITL (Fig. 8B) were composed of higher endothelial cells with more plump cytoplasm and a larger cross-sectional area than those seen in normal lymph nodes (Fig. 8A). Also, it is noteworthy that in some AITL HEVs, neoplastic "clear cell" T-cells infiltrate the space between endothelial cells and basement membrane and appear to push the basement membrane outward, resulting in increased cross-sectional area of HEVs (Fig. 8C). Thus, we first measured the cross-sectional area of every single HEV in AITL-affected and normal lymph nodes. As shown in Fig. 8D, the mean cross-sectional area of an HEV in AITL (0.0014 ± 0.0012 mm^2) was greater than that seen in normal lymph nodes

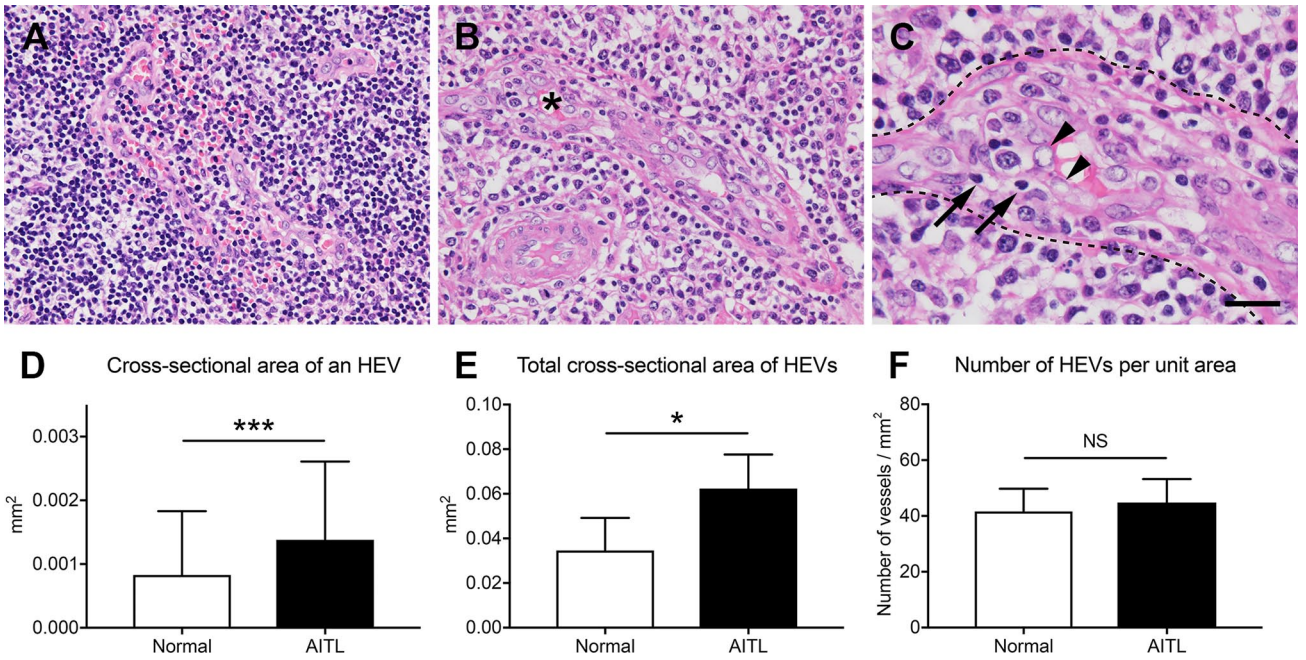

Figure 8. Increased cross-sectional area of HEVs in AITL-affected lymph nodes. (A–C) Photomicrographs of HEVs in normal (A) and AITL-affected (B and C) lymph nodes. Panel C is an enlarged view of the region indicated by asterisk in panel B. Note that in AITL, neoplastic T-cells (arrows) and reactive immunoblasts infiltrate the space between endothelial cells (arrowheads) and the basement membrane (dotted lines) likely pushing the basement membrane outward and resulting in increased cross-sectional area of HEVs. H&E staining. Bar = 40 μm for panels A and B and 20 μm for panel C. (D) The mean cross-sectional area of one HEV in normal (n=5; open box) and AITL-affected (n=5; filled box) lymph nodes. (E) The total cross-sectional area of HEVs present in a unit area (1 mm^2) of normal (n=5) and AITL-affected (n=5) lymph nodes. (F) The number of HEVs per unit area in the region assessed in (E) in normal (n=5) and AITL-affected (n=5) lymph nodes. Data are presented as means with SD. Abbreviations: HEVs, high endothelial venules; AITL, angioimmunoblastic T-cell lymphoma; NS, not significant. *p<0.05, ***p<0.001.

(0.0008 ± 0.0010 mm^2) with high statistical significance (p<0.001). We then calculated the total cross-sectional area of HEVs present in a unit area (1 mm^2) of lymph nodes. As shown in Fig. 8E, that area in AITL (0.062 ± 0.015 mm^2) was greater than that seen in normal lymph nodes (0.035 ± 0.015 mm^2) with statistical significance (p=0.019), whereas the number of HEVs present in the same region did not differ between normal and AITL-affected lymph nodes (41.6 ± 8.1/mm^2 and 44.8 ± 8.4/mm^2, respectively; p=0.558) (Fig. 8F).

Discussion

In this study, we demonstrate that HEVs formed in AITL express sulfated sLe^x that constitutes PNAd and potentially functions as an L-selectin ligand. Moreover, we demonstrate that the distribution density of HEVs does not increase but rather decrease in AITL compared with normal lymph nodes, whereas the proportion of HEVs in total blood vessels is essentially comparable between AITL and normal lymph nodes. On the contrary, we found that the cross-sectional area of HEVs in AITL was significantly greater than that seen in normal lymph nodes. These results overall indicate that the apparent increase in PNAd-expressing functional HEVs in AITL is likely due to increased cross-sectional area, not to increased distribution density.

HEV proliferation is a hallmark of AITL, as is described in the latest edition of the WHO classification.[4] Strikingly, however, here we found that the distribution density of not only total vessels but also HEVs in AITL was significantly less than that seen in normal lymph nodes. These findings suggest that AITL lymph nodes become enlarged due to proliferation of neoplastic T-cells and recruitment and/or proliferation of reactive host immune cells, possibly in response to humoral factors secreted by neoplastic T-cells,[3] whereas stromal components including HEVs do not increase, or even if they do, that increase is not to the same extent as the tumor parenchyma. Nevertheless, some pathologists report that HEVs apparently increase in number in AITL,[1] a perception that we attribute to increased HEV cross-sectional area. This phenomenon could be due to increased expression of lymphotoxin αβ (LT-αβ) secreted by neoplastic T-cells or reactive immunoblastic B-cells.[35] As LT-β receptor signaling is important for the formation and maintenance of HEV morphology, including endothelial cell cuboidal shape and vessel arborization,[36] increased

signaling in this pathway may contribute to the unusual morphology of HEVs seen in AITL. Alternatively, in AITL, neoplastic "clear cell" T-cells often proliferate to form clusters surrounding HEVs, and in some HEVs infiltrate the space between endothelial cells and basement membrane to expand the area surrounded by the basement membrane.

Overall, we feel our findings could be helpful in diagnosing AITL. Occasionally, tissue specimens that have a strong probability of being AITL lack prominent HEVs. In such cases, it is important to understand that it is not the number of HEVs that increases in AITL but rather their cross-sectional area. A consideration of this finding might prevent pathologists from erroneously ruling out a diagnosis of AITL in these circumstances.

Muramatsu[37] has reported that the number and proportion of HEVs, which were identified morphologically based on H&E and silver staining, were significantly greater in AITL than in normal lymph nodes. This result is inconsistent with our results reported here, potentially due to different methods used to identify HEVs. In the Muramatsu study, vessels with a diameter of less than 15 μm, even if they were composed of high endothelial cells, were classified as capillaries rather than HEVs. Thus, a substantial portion of small-sized PNAd-expressing vessels that we categorize as HEVs here might not have been classified as HEVs in the other study. As these vessels are frequently found in normal lymph nodes, it is plausible that the number of HEVs in normal lymph nodes was underestimated, resulting in an apparent relative increase in the number of HEVs in AITL.

We also demonstrate that HEVs formed in AITL express sulfated sLe^x recognized by MECA-79, and some are also positive for HECA-452 and 297-11A. This is an immunohistochemical profile similar to that seen in normal peripheral lymph node HEVs.[24] We previously demonstrated that sulfated sLe^x is also expressed in HEVs formed in lymphoid stroma of salivary Warthin's tumor,[38] testicular seminoma,[39] and a diffuse sclerosing variant of papillary thyroid carcinoma.[40] These HEVs presumably function in the histogenesis of distinct lymphoid stroma formed in these tumors. However, HEV function in AITL histogenesis remains uncharacterized. As AITL is composed not only of neoplastic T-cells but also of a variety of reactive host immune cells, it is tempting to speculate that HEVs formed in AITL may function to recruit these reactive host immune cells, particularly those expressing high levels of L-selectin such as naïve T- and B-cells.[5] Further studies are, however, required to test this hypothesis.

We also show for the first time that a Gal-6-*O*-sulfated form of the MECA-79 epitope is recognized by this antibody. Double immunofluorescence staining revealed that 297-11A signals on HEVs formed in AITL colocalized with MECA-79 signals, as is seen in HEVs in normal peripheral lymph nodes.[24] Furthermore, flow cytometric analysis revealed that Gal-6-*O*-sulfation of LacNAc, that is, formation of the 297-11A epitope, in the MECA-79 epitope does not attenuate reactivity to MECA-79. In addition, we previously demonstrated by glycan array analysis that GlcNAc-6-*O*-sulfation of Gal-6-*O*-sulfated LacNAc does not alter reactivity to 297-11A.[24] These findings overall indicate that KSGal6ST catalyzes Gal-6-*O*-sulfation of 6-sulfo LacNAc attached to extended core 1 *O*-glycans to form 6,6′-disulfo (both GlcNAc- and Gal-6-*O*-sulfated) LacNAc attached to extended core 1 *O*-glycans, which can be detected by both MECA-79 and 297-11A.

In in situ binding assay performed here, normal lymph node HEVs were readily bound by L-selectin-IgM chimeras. By contrast, HEVs formed in AITL were decorated very weakly with this chimera, indicating substantially diminished L-selectin-binding capacity of HEVs formed in AITL. On the contrary, E-selectin-IgM chimeras bound readily to HEVs in normal lymph nodes and relatively well to those formed in AITL. As E-selectin-IgM chimera binding was not abolished by pretreatment of tissue sections with CSLEX1 antibody, it is reasonable to conclude that E-selectin-IgM chimera binding to HEVs is mediated by 6-sulfo sLe^x. Thus, we propose that HEVs formed in AITL likely possess potential L-selectin-binding properties, albeit to a limited extent.

In this study, although the proportion of MECA-79-positive and 297-11A-positive HEVs in total vessels did not differ significantly between AITL-affected and normal lymph nodes, the proportion of HECA-452-positive HEVs in total vessels was significantly smaller in AITL compared with normal lymph nodes. Given the glycoepitopes recognized by MECA-79, 297-11A, and HECA-452 antibodies (see Fig. 1), this result suggests that GlcNAc-α1,3-fucosylation in sLe^x moieties is downregulated in AITL compared with normal lymph nodes. Hiraoka et al.[41] previously demonstrated that KSGal6ST competes with α1,3-fucosyltransferase 7 (FucT-7) for the same acceptor substrate, namely, LacNAc, and downregulates synthesis of 6-sulfo sLe^x by inhibiting α1,3-fucosylation. As GlcNAc-α1,3-fucosylation of 6-sulfo sLe^x moieties is a prerequisite for selectin binding,[42] L-selectin-binding capacity of HEVs may be decreased in AITL. This hypothesis is supported by the finding that both L- and E-selectin-IgM chimera binding to HEVs decreased in AITL, although the significance of this finding remains to be determined.

Acknowledgments

The authors thank Hisataka Kato, Takuya Suga, Shinichi Fujii, and Moriyasu Hattori for preparation of tissue sections; Maiko Yamanaka for immunohistochemical staining; Junko

Yamamoto for assisting with flow cytometry; Dr. Akifumi Muramoto for helpful discussion on statistical analysis; and Dr. Elise Lamar for critical reading of the manuscript.

Competing Interests

The author(s) declared no potential conflicts of interest with respect to the research, authorship, and/or publication of this article.

Author Contributions

All authors have contributed to this article as follows: AK designed and performed the research, analyzed the data, and wrote the manuscript; MF, HH, TK, and TO performed the research; MM wrote the manuscript; TOA and JM performed the research; HO analyzed the data and wrote the manuscript; and MK conceived of and designed the research, analyzed the data, and wrote the manuscript. All authors have read and approved the final manuscript.

Funding

The author(s) disclosed receipt of the following financial support for the research, authorship, and/or publication of this article: This work was supported in part by a Grant-in-Aid for Scientific Research (B) 21H02702 from the Japan Society for the Promotion of Science (to M.K.).

Literature Cited

1. Chiba S, Sakata-Yanagimoto M. Advances in understanding of angioimmunoblastic T-cell lymphoma. Leukemia. 2020;34(10):2592–606.
2. Ueno H, Banchereau J, Vinuesa CG. Pathophysiology of T follicular helper cells in humans and mice. Nat Immunol. 2015;16(2):142–52.
3. Ohtani H, Komeno T, Agatsuma Y, Kobayashi M, Noguchi M, Nakamura N. Follicular dendritic cell meshwork in angioimmunoblastic T-cell lymphoma is characterized by accumulation of $CXCL13^{+}$ cells. J Clin Exp Hematop. 2015;55(2):61–9.
4. Dogan A, Gaulard P, Jaffe ES, Müller-Hemelink HK, de Leval L. Angioimmunoblastic T-cell lymphoma and other nodal lymphomas of T follicular helper cell origin. In: Swerdlow SH, Campo E, Harris NL, Jaffe ES, Pileri SA, Stein H, Thiele J, editors. WHO classification of tumours of haematopoietic and lymphoid tissues. Revised 4th ed. Lyon: International Agency for Research on Cancer; 2017. p. 407–12.
5. Miyasaka M, Tanaka T. Lymphocyte trafficking across high endothelial venules: dogmas and enigmas. Nat Rev Immunol. 2004;4(5):360–70.
6. Berg EL, Robinson MK, Warnock RA, Butcher EC. The human peripheral lymph node vascular addressin is a ligand for LECAM-1, the peripheral lymph node homing receptor. J Cell Biol. 1991;114(2):343–9.
7. Michie SA, Streeter PR, Bolt PA, Butcher EC, Picker LJ. The human peripheral lymph node vascular addressin. An inducible endothelial antigen involved in lymphocyte homing. Am J Pathol. 1993;143(6):1688–98.
8. Butcher EC, Picker LJ. Lymphocyte homing and homeostasis. Science. 1996;272(5258):60–6.
9. Aloisi F, Pujol-Borrell R. Lymphoid neogenesis in chronic inflammatory diseases. Nat Rev Immunol. 2006; 6(3):205–17.
10. Kobayashi M, Mitoma J, Nakamura N, Katsuyama T, Nakayama J, Fukuda M. Induction of peripheral lymph node addressin in human gastric mucosa infected by *Helicobacter pylori*. Proc Natl Acad Sci U S A. 2004; 101(51):17807–12.
11. Suzawa K, Kobayashi M, Sakai Y, Hoshino H, Watanabe M, Harada O, Ohtani H, Fukuda M, Nakayama J. Preferential induction of peripheral lymph node addressin on high endothelial venule-like vessels in the active phase of ulcerative colitis. Am J Gastroenterol. 2007;102(7):1499–509.
12. Maruyama M, Kobayashi M, Sakai Y, Hiraoka N, Ohya A, Kageyama S, Tanaka E, Nakayama J, Morohoshi T. Periductal induction of high endothelial venule-like vessels in type 1 autoimmune pancreatitis. Pancreas. 2013;42(1):53–9.
13. Inamura S, Shinagawa T, Hoshino H, Sakai Y, Imamura Y, Yokoyama O, Kobayashi M. Appearance of high endothelial venule-like vessels in benign prostatic hyperplasia is associated with lower urinary tract symptoms. Prostate. 2017;77(7):794–802.
14. Tsutsumiuchi T, Hoshino H, Fujieda S, Kobayashi M. Induction of peripheral lymph node addressin in human nasal mucosa with eosinophilic chronic rhinosinusitis. Pathology. 2019;51(3):268–73.
15. Yoshida H, Imamura Y, Yoshimura H, Kobayashi M. Induction of high endothelial venule-like vessels in oral and cutaneous lichen planus: a comparative study. J Histochem Cytochem. 2020;68(5):343–50.
16. Muller WA, Weigl SA, Deng X, Phillips DM. PECAM-1 is required for transendothelial migration of leukocytes. J Exp Med. 1993;178(2):449–60.
17. Streeter PR, Rouse BT, Butcher EC. Immunohistologic and functional characterization of a vascular addressin involved in lymphocyte homing into peripheral lymph nodes. J Cell Biol. 1988;107(5):1853–62.
18. Yeh JC, Hiraoka N, Petryniak B, Nakayama J, Ellies LG, Rabuka D, Hindsgaul O, Marth JD, Lowe JB, Fukuda M. Novel sulfated lymphocyte homing receptors and their control by a core 1 extension β1,3-*N*-acetylglucosaminyltransferase. Cell. 2001;105(7): 957–69.
19. Duijvestijn AM, Horst E, Pals ST, Rouse BN, Steere AC, Picker LJ, Meijer CJ, Butcher EC. High endothelial differentiation in human lymphoid and inflammatory tissues defined by monoclonal antibody HECA-452. Am J Pathol. 1988;130(1):147–55.
20. Mitsuoka C, Sawada-Kasugai M, Ando-Furui K, Izawa M, Nakanishi H, Nakamura S, Ishida H, Kiso M, Kannagi R. Identification of a major carbohydrate capping group of the L-selectin ligand on high endothelial venules in human lymph nodes as 6-sulfo sialyl Lewis X. J Biol Chem. 1998;273(18):11225–33.
21. Mitoma J, Miyazaki T, Sutton-Smith M, Suzuki M, Saito H, Yeh JC, Kawano T, Hindsgaul O, Seeberger PH,

Panico M, Haslam SM, Morris HR, Cummings RD, Dell A, Fukuda M. The *N*-glycolyl form of mouse sialyl Lewis X is recognized by selectins but not by HECA-452 and FH6 antibodies that were raised against human cells. Glycoconj J. 2009;26(5):511–23.
22. Kawashima H, Petryniak B, Hiraoka N, Mitoma J, Huckaby V, Nakayama J, Uchimura K, Kadomatsu K, Muramatsu T, Lowe JB, Fukuda M. *N*-acetylglucosamine-6-*O*-sulfotransferases 1 and 2 cooperatively control lymphocyte homing through L-selectin ligand biosynthesis in high endothelial venules. Nat Immunol. 2005;6(11): 1096–104.
23. Uchimura K, Gauguet JM, Singer MS, Tsay D, Kannagi R, Muramatsu T, von Andrian UH, Rosen SD. A major class of L-selectin ligands is eliminated in mice deficient in two sulfotransferases expressed in high endothelial venules. Nat Immunol. 2005;6(11):1105–13.
24. Tsutsumiuchi M, Hoshino H, Kogami A, Tsutsumiuchi T, Yokoyama O, Akama TO, Kobayashi M. Preferential expression of sialyl 6'-sulfo *N*-acetyllactosamine-capped *O*-glycans on high endothelial venules in human peripheral lymph nodes. Lab Invest. 2019;99(10): 1428–41.
25. Patnode ML, Yu SY, Cheng CW, Ho MY, Tegesjö L, Sakuma K, Uchimura K, Khoo KH, Kannagi R, Rosen SD. KSGal6ST generates galactose-6-*O*-sulfate in high endothelial venules but does not contribute to L-selectin-dependent lymphocyte homing. Glycobiology. 2013; 23(3):381–94.
26. Akama TO, Nakayama J, Nishida K, Hiraoka N, Suzuki M, McAuliffe J, Hindsgaul O, Fukuda M, Fukuda MN. Human corneal GlcNAc 6-*O*-sulfotransferase and mouse intestinal GlcNAc 6-*O*-sulfotransferase both produce keratan sulfate. J Biol Chem. 2001;276(19):16271–8.
27. Fina L, Molgaard HV, Robertson D, Bradley NJ, Monaghan P, Delia D, Sutherland DR, Baker MA, Greaves MF. Expression of the CD34 gene in vascular endothelial cells. Blood. 1990;75(12):2417–26.
28. North SJ, Huang HH, Sundaram S, Jang-Lee J, Etienne AT, Trollope A, Chalabi S, Dell A, Stanley P, Haslam SM. Glycomics profiling of Chinese hamster ovary cell glycosylation mutants reveals *N*-glycans of a novel size and complexity. J Biol Chem. 2010;285(8):5759–75.
29. Hiraoka N, Petryniak B, Nakayama J, Tsuboi S, Suzuki M, Yeh JC, Izawa D, Tanaka T, Miyasaka M, Lowe JB, Fukuda M. A novel, high endothelial venule-specific sulfotransferase expresses 6-sulfo sialyl Lewis^x, an L-selectin ligand displayed by CD34. Immunity. 1999; 11(1):79–89.
30. Bistrup A, Bhakta S, Lee JK, Belov YY, Gunn MD, Zuo FR, Huang CC, Kannagi R, Rosen SD, Hemmerich S. Sulfotransferases of two specificities function in the reconstitution of high endothelial cell ligands for L-selectin. J Cell Biol. 1999;145(4):899–910.
31. Kobayashi M, Mitoma J, Hoshino H, Yu SY, Shimojo Y, Suzawa K, Khoo KH, Fukuda M, Nakayama J. Prominent expression of sialyl Lewis X-capped core 2-branched *O*-glycans on high endothelial venule-like vessels in gastric MALT lymphoma. J Pathol. 2011; 224(1):67–77.
32. Fujiwara M, Kobayashi M, Hoshino H, Uchimura K, Nakada T, Masumoto J, Sakai Y, Fukuda M, Nakayama J. Expression of long-form *N*-acetylglucosamine-6-*O*-sulfotransferase 1 in human high endothelial venules. J Histochem Cytochem. 2012;60(5):397–407.
33. Taga M, Hoshino H, Low S, Imamura Y, Ito H, Yokoyama O, Kobayashi M. A potential role for 6-sulfo sialyl Lewis X in metastasis of bladder urothelial carcinoma. Urol Oncol. 2015;33(11):496.e1–9.
34. Ohmori K, Kanda K, Mitsuoka C, Kanamori A, Kurata-Miura K, Sasaki K, Nishi T, Tamatani T, Kannagi R. P- and E-selectins recognize sialyl 6-sulfo Lewis X, the recently identified L-selectin ligand. Biochem Biophys Res Commun. 2000;278(1):90–6.
35. Foss HD, Anagnostopoulos I, Herbst H, Grebe M, Ziemann K, Hummel M, Stein H. Patterns of cytokine gene expression in peripheral T-cell lymphoma of angioimmunoblastic lymphadenopathy type. Blood. 1995; 85(10):2862–9.
36. Onder L, Danuser R, Scandella E, Firner S, Chai Q, Hehlgans T, Stein JV, Ludewig B. Endothelial cell-specific lymphotoxin-β receptor signaling is critical for lymph node and high endothelial venule formation. J Exp Med. 2013;210(3):465–73.
37. Muramatsu T. Vascular system of lymph nodes: vascular density of AILD and malignant lymphomas with special reference to HEV. Fukushima J Med Sci. 1987; 33(1):17–28.
38. Ohya A, Kobayashi M, Sakai Y, Kawashima H, Kageyama S, Nakayama J. Lymphocyte recruitment via high endothelial venules in lymphoid stroma of Warthin's tumour. Pathology. 2013;45(2):150–4.
39. Sakai Y, Hoshino H, Kitazawa R, Kobayashi M. High endothelial venule-like vessels and lymphocyte recruitment in testicular seminoma. Andrology. 2014;2(2): 282–9.
40. Low S, Sakai Y, Hoshino H, Hirokawa M, Kawashima H, Higuchi K, Imamura Y, Kobayashi M. High endothelial venule-like vessels and lymphocyte recruitment in diffuse sclerosing variant of papillary thyroid carcinoma. Pathology. 2016;48(7):666–74.
41. Hiraoka N, Petryniak B, Kawashima H, Mitoma J, Akama TO, Fukuda MN, Lowe JB, Fukuda M. Significant decrease in α1,3-linked fucose in association with increase in 6-sulfated *N*-acetylglucosamine in peripheral lymph node addressin of FucT-VII-deficient mice exhibiting diminished lymphocyte homing. Glycobiology. 2007;17(3):277–93.
42. Malý P, Thall A, Petryniak B, Rogers CE, Smith PL, Marks RM, Kelly RJ, Gersten KM, Cheng G, Saunders TL, Camper SA, Camphausen RT, Sullivan FX, Isogai Y, Hindsgaul O, von Andrian UH, Lowe JB. The α(1,3) fucosyltransferase Fuc-TVII controls leukocyte trafficking through an essential role in L-, E-, and P-selectin ligand biosynthesis. Cell. 1996;86(4):643–53.

International Journal of Clinical Oncology
https://doi.org/10.1007/s10147-021-02030-7

ORIGINAL ARTICLE

A phase 2, open-label, multicenter study of ixazomib plus lenalidomide and dexamethasone in adult Japanese patients with relapsed and/or refractory multiple myeloma

Shinsuke Iida[1] · Tohru Izumi[2,3] · Takuya Komeno[4] · Yasuhito Terui[5,6] · Takaaki Chou[7,8] · Takashi Ikeda[9] · Deborah Berg[10] · Shinichi Fukunaga[11] · Kenkichi Sugiura[12] · Makoto Sasaki[13]

Received: 2 June 2021 / Accepted: 12 September 2021

Abstract

Background TOURMALINE-MM1 was a global study that demonstrated a significant improvement in progression-free survival with ixazomib plus lenalidomide and dexamethasone compared with placebo plus lenalidomide and dexamethasone, in patients with relapsed and/or refractory multiple myeloma. The current study was conducted to evaluate further the efficacy and safety of ixazomib plus lenalidomide and dexamethasone in Japanese patients.

Methods This phase 2, open-label, single-arm, multicenter study enrolled patients aged ≥ 20 years with relapsed and/or refractory multiple myeloma at 16 sites in Japan. Patients refractory to lenalidomide or proteasome inhibitor-based therapy at any line were excluded. The primary endpoint was the rate of very good partial response or better in the response-evaluable analysis set. Secondary endpoints were progression-free survival, overall response rate, duration of response, time to progression, overall survival and safety.

Results In total, 34 patients were enrolled. The rate of very good partial response or better was 50.0% (95% confidence interval 31.9–68.1) and the overall response rate was 84.4% (95% confidence interval 67.2–94.7). Median progression-free survival was 22.0 months (95% confidence interval 17.3–not evaluable) and median overall survival was not estimable. The safety profile of ixazomib plus lenalidomide and dexamethasone in this study was similar to that in the TOURMALINE-MM1 study.

Conclusions The efficacy and safety of ixazomib plus lenalidomide and dexamethasone in Japanese patients with relapsed and/or refractory multiple myeloma are comparable with reported TOURMALINE-MM1 study results.

Clinicaltrials.gov identifier NCT02917941; date of registration September 28, 2016.

Keywords Ixazomib · RRMM · Efficacy · Safety · Japanese

✉ Shinsuke Iida
iida@med.nagoya-cu.ac.jp

[1] Department of Hematology and Oncology, Nagoya City University Graduate School of Medical Sciences, Kawasumi 1, Mizuho-cho, Mizuoho-ku, Nagoya-shi, Aichi, Japan

[2] Department of Hematology, Tochigi Cancer Center, Utsunomiya, Tochigi, Japan

[3] Department of Hematology, Sendai Medical Center, Sendai, Miyagi, Japan

[4] Department of Hematology, National Hospital Organization Mito Medical Center, Ibaraki, Japan

[5] Department of Hematology Oncology, Cancer Institute Hospital of Japanese Foundation for Cancer Research, Koto, Tokyo, Japan

[6] Department of Hematology, Saitama Medical University Hospital, Moroyama-machi, Saitama, Japan

[7] Department of Internal Medicine, Niigata Cancer Center Hospital, Niigata, Japan

[8] Niigata Kenshin Plaza, General Incorporated Foundation, Health Medicine Prevention Association, Niigata, Japan

[9] Division of Hematology and Stem Cell Transplantation, Shizuoka Cancer Center, Nagaizumi, Shizuoka, Japan

[10] Clinical Research and Development, Takeda Pharmaceutical Company Limited, Osaka, Japan

[11] Oncology Therapeutic Area Unit for Japan and Asia, Takeda Pharmaceutical Company Limited, Osaka, Japan

[12] Statistical & Quantitative Sciences, Data Sciences Institute, Research & Development, Takeda Pharmaceutical Company Limited, Osaka, Japan

[13] Division of Hematology, Department of Internal Medicine, Juntendo University School of Medicine, Tokyo, Japan

Published online: 02 October 2021

Introduction

Multiple myeloma (MM) is a malignant disease in which monoclonal plasma cells proliferate, mainly in the bone marrow. MM causes increases in monoclonal immunoglobulin (M-protein) production by myeloma cells, hematopoietic deterioration, bone destruction, hypercalcemia and renal failure. MM constitutes approximately 1% of all reported neoplasms and approximately 13% of hematologic cancers worldwide [1]. In Japan, the National Cancer Center estimated there would be 7,800 new cases of MM, with approximately 4500 deaths in 2019 [2].

The treatment landscape has shifted from autologous stem cell transplantation (ASCT) being the mainstay of therapy, to its combination with novel agent-based induction regimens and post-ASCT consolidation and maintenance treatments [3]. While historic treatment approaches focused on the use of cytotoxic drugs such as alkylating agents, anthracyclines and corticosteroids, the introduction of the first-in-class proteasome inhibitor (PI), bortezomib and immunomodulatory drugs (IMiDs) such as thalidomide and lenalidomide have improved treatment outcomes [4–7]. PIs and IMiDs currently remain the backbone of therapy throughout the MM treatment pathway [8, 9]. Monoclonal antibody drugs also play an important role [10].

Although some data have suggested an increasing cure fraction rate in front-line patients, MM is still generally regarded as incurable [11]. Most patients receive multiple lines of therapy, including combination regimens, over the course of their disease [12].

In an effort to further target the increased proteasome activity known to occur in MM and other cancers, ixazomib, a small molecule 20S PI, was developed. In contrast to bortezomib, ixazomib has demonstrated a faster dissociation rate from the proteasome; improved pharmacokinetics and pharmacodynamics, which may result in enhanced tumor penetration; and antitumor activity in a broader range of tumor xenografts [13]. The clinical benefit of ixazomib has been studied previously and ixazomib is being developed globally as a treatment option for relapse/refractory (RR)MM, newly diagnosed (ND)MM, maintenance monotherapy for MM and relapsed or refractory systemic light-chain amyloidosis [14–17]. In Japan, ixazomib is approved for the treatment of RRMM and more recently was approved as maintenance monotherapy.

The pivotal TOURMALINE-MM1 (MM1) study was a phase 3 global, randomized, double-blind, placebo-controlled study that evaluated the efficacy and safety of ixazomib combined with lenalidomide and dexamethasone (LenDex) versus placebo combined with LenDex, in patients with RRMM who had received at least one prior therapy [17]. The efficacy results of the primary analysis for the overall population demonstrated a statistically significant and clinically meaningful prolongation in the primary endpoint of progression-free survival (PFS) with the ixazomib plus LenDex regimen compared with the placebo plus LenDex regimen (median PFS of 20.6 months versus 14.7 months, respectively [hazard ratio 0.742; $p = 0.012$]), as assessed by an independent review committee [17].

In addition, the ixazomib plus LenDex regimen provided clinical benefit, as demonstrated by significant improvements in complete response (CR) rate, overall response rate (ORR) and rate of very good partial response (VGPR) or better (VGPR + CR), and longer disease control, as demonstrated by a significant improvement in time to progression (TTP) and a longer duration of response (DOR). Ixazomib in combination with LenDex has thus been shown to be an efficacious regimen [17].

However, the PFS data for the Japanese subpopulation in the MM1 study was limited [17]; hence, consistency with the overall population could not be concluded, and efficacy in Japanese patients remained to be confirmed.

The current study evaluated the efficacy and safety of ixazomib when administered with LenDex in Japanese patients with RRMM. In relapsed or refractory settings, significantly longer PFS or TTP have been demonstrated in patients with VGPR or better, compared with those with partial response (PR) [18]. Therefore, the endpoint of VGPR + CR rate is often clinically correlated with PFS. Hence, the primary objective of this study was to determine the rate of VGPR or better in the response-evaluable analysis set, which was agreed upon in a consultation meeting between the study sponsor and the Pharmaceuticals and Medical Devices Agency of Japan.

Materials and methods

Study design

This was a phase 2, open-label, single-arm, multicenter study, with patients enrolled at 16 study sites in Japan. Response was assessed according to the International Myeloma Working Group criteria every 4 weeks until progressive disease (PD) [19]. All patients were followed up for survival after progression, and patients were contacted every 12 weeks until death or termination of the study. Patients attended an end of treatment visit approximately 30 days after receiving their last dose of any study drug (ixazomib, lenalidomide or dexamethasone) and continued to be followed up for other assessments. Patients discontinuing study treatment prior to PD continued to be assessed for PD during the PFS follow-up portion of the study. Primary analysis was conducted approximately 12 months after the last

enrollment, and the final analysis was conducted after the final database lock, approximately 24 months after the last enrollment.

This study was conducted in compliance with Good Clinical Practice (GCP), Good Post-marketing Study Practice (GPSP) and all applicable local regulations and guidelines. All study-related documents were reviewed and approved by the local or central institutional review boards of all study sites. This study was also conducted in accordance with the Declaration of Helsinki, and the International Council for Harmonisation of Technical Requirements for Pharmaceuticals for Human Use (ICH) Harmonised Tripartite Guideline for GCP and GPSP, and all applicable regulations. Objectives and potential risks and benefits were explained to patients using the informed consent form approved by the institutional review board, with each patient having signed and dated the form before screening.

Patient selection

Important inclusion criteria were (1) Japanese patients ≥ 20 years with diagnosed MM and measurable disease with serum M-protein ≥ 1 g/dl, urine M-protein ≥ 200 mg/24 h or abnormal serum free light chain (FLC) ratio with involved FLC level ≥ 10 mg/dl and who were relapsed and/or refractory after receiving one to three prior therapies; (2) patients who had an Eastern Cooperative Oncology Group (ECOG) performance status of 0, 1 or 2. Patients who had received autologous transplants were also eligible for inclusion. Additional inclusion criteria are described in Online Resource 1.

An important exclusion criterion was patients who were refractory to lenalidomide or PI-based therapy at any line. Additional exclusion criteria are described in Online Resource 1.

Treatment

Patients received 4 mg of ixazomib on days 1, 8 and 15 plus lenalidomide (25 mg) on days 1 through 21, and dexamethasone (40 mg) on days 1, 8, 15 and 22 of a 28-day cycle. Patients with a low creatinine clearance of < 60 ml/min received a reduced lenalidomide dose of 10 mg once daily. Patients continued to receive treatment until progressive disease or unacceptable toxicity, whichever came first.

Endpoints

The primary endpoint was the rate of VGPR + CR in the response-evaluable analysis set. The secondary endpoints were PFS, ORR, DOR, TTP, safety and overall survival (OS). The definitions of secondary endpoints are described in Online Resource 2.

Statistical analysis

For the VGPR + CR rate and ORR, two-sided 95% confidence intervals (CIs) were calculated in the response-evaluable analysis set and the full analysis set (FAS). The response-evaluable population was defined as patients who received at least one dose of ixazomib, had measurable disease at baseline and had at least one post-baseline response assessment. For PFS, OS and TTP, Kaplan–Meier estimates (and the 25th, 50th [median] and 75th percentiles, if estimable) were calculated with their two-sided 95% CIs in the FAS. For DOR, the Kaplan–Meier estimates was calculated as well for responders. Based on the results of the MM1 study, a sample size of 27 was required to provide a point estimate of 48.1% for the expected VGPR + CR rate, which was higher than the threshold rate of 39.0% with 80% probability. Assuming a dropout rate of 10%, the target number of patients for this study was set to 30. All analyses were conducted with SAS version 9.2.

Results

Patient background

Patient demographics and baseline characteristics are described in Table 1. Of the 34 patients in the FAS, the median age was 67 years. Median time from initial diagnosis was 44.4 months, with 71% of MM diagnosed being of the IgG type.

At study entry, 82% of patients were International Staging System stage I, and 74% had an ECOG performance status of 0. Additionally, 29% of patients had a creatinine clearance of 30 to < 60 ml/min, 62% of patients only had one prior line of therapy, 91% of patients had relapsed disease and 9% of patients had refractory disease.

Overall, 68% of patients had undergone ASCT with a median time of 38.8 months since the time of last transplantation to the first dose at study entry. 91% of patients had previous exposure to PIs and 35% to IMiDs. 32% of patients had high-risk cytogenetic abnormalities, whereby cut-offs were 5% positive cells for del(17p), 3% for t(4;14) and 3% for t(14;16), of cells testing positive for these abnormalities.

Exposure

The study drug exposure is described in Table 2. The median number of treatment cycles for all study drugs was 20, with a median relative dose intensity of 86.0% for ixazomib, 81.6% for lenalidomide and 91.7% for dexamethasone.

Table 1 Patient demographics and baseline characteristics in the full analysis set

	Ixazomib + LenDex $N = 34$
Age (years)	
Median	67
Min, max	40, 78
Sex (*n*, %)	
Male	19 (56)
Female	15 (44)
Baseline body surface area (m^2)	
Median	1.62
Min, max	1.20, 2.03
Time since initial diagnosis to first dose at study entry (months)	
Median	44.4
Min, max	10, 176
Type of myeloma at initial diagnosis (*n*, %)	
IgG	24 (71)
IgA	4 (12)
Bence-Jones	5 (15)
Light chain only	1 (3)
ISS stage for myeloma at study entry (*n*, %)	
I	28 (82)
II	5 (15)
III	1 (3)
Creatinine clearance (ml/min) (*n*, %)	
30 to < 60	10 (29)
60 to < 90	15 (44)
90 to max	9 (26)
Baseline ECOG performance status (*n*, %)	
0	25 (74)
1	9 (26)
Prior therapy (*n*, %)	
Lines of prior therapy	
1	21 (62)
2	12 (35)
3	1 (3)
Patient population categories	
Relapsed patients[a]	31 (91)
Refractory patients[b]	3 (9)
Patients with ASCT	23 (68)
Prior IMiD therapy	
Exposed	12 (35)
Thalidomide[c]	5 (15)
Lenalidomide[c]	8 (24)
Naive	22 (65)
Prior PI therapy	
Exposed	31 (91)
Bortezomib[d]	30 (88)
Carfilzomib[d]	2 (6)
Naive	3 (9)
Cytogenetics	
Cytogenetics results	
High risk[e]	11 (32)
Standard	21 (62)
Not available	2 (6)
Chromosomal abnormalities	
Del 13 or 13q	15 (44)
Del 17 or 17p	4 (12)
t(4;14)	7 (21)
t(11;14)	2 (6)
t(14;16)	1 (3)

ASCT autologous stem cell transplantation, *ECOG* Eastern Cooperative Oncology Group, *IMiD* immunomodulatory drug, *PI* proteasome inhibitor, *ISS* International Staging System, *LenDex* lenalidomide and dexamethasone

[a]Relapsed was defined as patients who relapsed from at least one previous treatment but were not refractory to any previous treatment

[b]Refractory was defined as patients who were refractory to at least one previous treatment but did not relapse from any previous treatment

[c]One patient had been exposed to both thalidomide and lenalidomide

[d]One patient had been exposed to both bortezomib and carfilzomib

[e]High-risk cytogenetic abnormalities that were defined as containing t(4;14), t(14;16) or del(17p); cutoff values for defining the presence of t(4;14), t(14;16) and del(17p) were 3%, 3% and 5% positive cells, respectively

Efficacy

The response to treatment is described in Table 3. The primary endpoint of confirmed VGPR + CR rate was 50.0% (95% CI 31.9–68.1), which was above the threshold rate of 39.0% based on the results of the MM1 study. The ORR was 84.4% (95% CI 67.2–94.7) and the CR rate was 28.1% (95% CI 13.7–46.7), with the stringent CR rate being 25.0% (95% CI 11.5–43.4). In the high-risk and standard-risk cytogenetics subgroups, the ORRs were 72.7% and 90.5%, respectively. In the response-evaluable analysis set, stable disease was demonstrated in 15.6% of patients and no patients had PD as their best response.

The median DOR was not estimable for patients with VGPR or better. At the last assessment, no PD was documented in 78% of patients with CR ($n = 9$), 56% of patients with VGPR or better ($n = 16$) and 48% of patients with PR or better ($n = 27$). The median time to response was 2.9 months (95% CI 1.8–5.1) for VGPR or better and 1.0 months (95% CI 1.0–1.8) for PR or better.

PFS is described in Fig. 1. With a median follow-up of 28.1 months, median PFS was 22.0 months (95%

Table 2 Study drug exposure in the safety analysis set

	Ixazomib + LenDex $N = 34$			
	Ixazomib	Lenalidomide	Dexamethasone	Combination
Number of treatment cycles[a]				
Mean (standard deviation)	17.8 (9.3)	17.8 (9.3)	17.8 (9.3)	17.8 (9.3)
Median	20.0	20.0	20.0	20.0
Min, max	1, 32	1, 32	1, 32	1, 32
Relative dose intensity (%)				
Mean (standard deviation)	85.4 (12.8)	78.2 (18.7)	76.5 (25.0)	–
Median	86.0	81.6	91.7	–
Min, max	59, 100	40, 100	23, 100	–

LenDex lenalidomide and dexamethasone

[a]A treatment cycle was defined as a cycle in which the patient received any amount of ixazomib, lenalidomide or dexamethasone

Table 3 Summary of response to treatment in the response-evaluable analysis set

	Ixazomib + LenDex $N = 32$[a]		
	n	%	95% CI
CR	9	(28.1)	(13.7, 46.7)
sCR	8	(25.0)	(11.5, 43.4)
PR	18	(56.3)	(37.7, 73.6)
VGPR	7	(21.9)	(9.3, 40.0)
Overall response (≥ PR)	27	(84.4)	(67.2, 94.7)
VGPR or better (CR + VGPR)	16	(50.0)	(31.9, 68.1)
SD	5	(15.6)	(5.3, 32.8)
PD	0	(0.0)	(0.0, 10.9)

CI confidence interval, *CR* complete response, *LenDex* lenalidomide and dexamethasone, *PD* progressive disease, *PR* partial response, *sCR* stringent complete response, *SD* stable disease, *VGPR* very good partial response

[a] Response-evaluable population: among 34 subjects enrolled in the study, 32 subjects who received at least one dose of study drug, had measurable disease at baseline, and had at least one post-baseline response assessment. Two enrolled patients were not response-evaluable: one subject did not have any evaluable disease at baseline and one was not evaluable for response assessment

CI 17.3–not evaluable); and 18 patients (53%) had PD, including one death.

At the time of data cutoff, the OS data were not mature, and the median OS was not estimable.

Safety

The overall summary of treatment-emergent adverse events (TEAEs) is described in Table 4 and the most common TEAEs that were reported in ≥ 10% of patients are described in Table 5. All patients experienced at least one TEAE and drug-related TEAE during the study ($n = 34$ [100%]). Additionally, 85% of patients had at least 1 TEAE of Grade ≥ 3 and 79% of patients had a drug-related TEAE of Grade ≥ 3. The most common TEAEs of Grade ≥ 3 were neutropenia (21%), decreased platelet count (21%), decreased neutrophil count (18%), diarrhea (15%) and maculopapular rash (12%) (Table 6). Two deaths were observed, with one death due to adverse events (AEs) (subarachnoid hemorrhage and subdural hemorrhage) that were associated with a fall and without study drug causality, and another death due to primary disease or its complications after discontinuation of study treatment for PD.

Serious adverse events (SAEs) were experienced by 35% of patients ($n = 12$), with 29% experiencing drug-related SAEs. The most common SAEs were pneumonia (9%), diarrhea (6%) and fall (6%), while the most common drug-related SAEs were pneumonia (9%) and diarrhea (6%).

Overall, 32% of patients had at least one TEAE leading to the discontinuation of one or more of the three study drugs; the most common AE was neutropenia, which was reported in two patients. Additionally, 76% of patients had at least one TEAE resulting in dose reduction of any study drug, with the most common AE being maculopapular rash, which was reported in four patients. Two patients were diagnosed with a second malignancy while on study treatment: one patient was reported as having acute myeloid leukemia and the other had malignant lung neoplasm. Both of these AEs were serious, considered to be related to study treatment and resulted in discontinuation of study treatment. Patients were specifically followed up for second malignancies because of the increased risk with lenalidomide [20, 21].

TEAEs occurring in ≥ 20% of patients were constipation (50%), upper respiratory tract infection (47%), diarrhea (41%), rash (35%), nasopharyngitis (32%), nausea (29%), platelet count decreased (26%), influenza (24%), neutropenia (24%), chilblains (21%), dysgeusia (21%), fall (21%) and peripheral sensory neuropathy (21%).

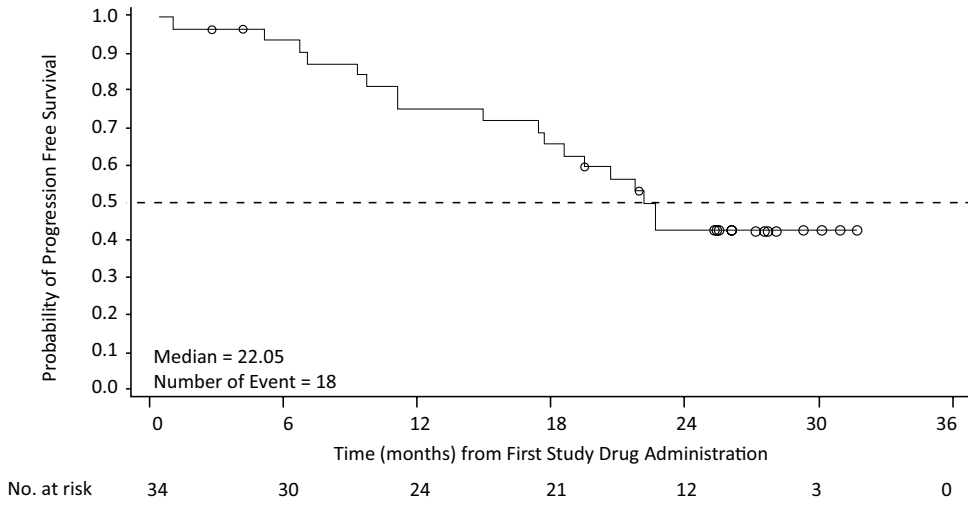

Fig. 1 Progression-free survival in the full analysis set

Table 4 Overall summary of TEAEs in the safety analysis set

	Ixazomib + LenDex *N* = 34 *n* (%)
Any AE	34 (100)
Grade 3 or higher AE	29 (85)
Drug-related AE	34 (100)
Drug-related Grade 3 or higher AE	27 (79)
SAE	12 (35)
Drug-related SAE	10 (29)
AEs resulting in any study drug dose reduction	26 (76)
AEs resulting in any study drug dose modification[a]	29 (85)
AEs resulting in any study drug discontinuation[b]	11 (32)
On-study deaths[c]	1 (3)

Dose reduction, dose modification and study drug discontinuation may have been in relation to any of the three drug regimens. On-study deaths were defined as deaths that occurred within 30 days of the last dose of study drug

AE adverse event, *LenDex* lenalidomide and dexamethasone, *SAE* serious adverse event, *TEAE* treatment-emergent adverse event

[a]Dose modification included dose reduction, dose increase, dose delay and dose discontinuation

[b]Study drug discontinuation may have been in relation to ≥ 1 of the three study drugs

[c]The subject died of subarachnoid hemorrhage and subdural hemorrhage during the study. The event was assessed to be associated with a fall; causality with the study drug was ruled out

Drug-related TEAEs occurring in ≥ 20% of patients were diarrhea (38%), constipation (38%), rash (29%), platelet count decreased (26%), nausea (24%), peripheral sensory neuropathy (21%), dysgeusia (21%) and neutropenia (21%). Drug-related TEAEs of Grade ≥ 3 occurring in ≥ 10% of patients were platelet count decreased (21%), neutrophil count decreased (18%), neutropenia (18%), diarrhea (15%) and maculopapular rash (12%).

A summary of TEAEs of clinical importance is presented in Table 7. The TEAEs of clinical importance were neutropenia, thrombocytopenia, heart failure, arrhythmia, myocardial infarction, nausea, vomiting, diarrhea, rash, maculopapular rash, urticaria, erythema multiforme, generalized rash, macular rash, peripheral sensory neuropathy and peripheral neuropathy.

AEs of clinical importance reported in this study were similar to those reported in the global MM1 study. No previously unknown safety concerns were identified in this study.

Discussion

In this study, all demographics and other baseline characteristics except race were similar to those of the MM1 study [17]. The efficacy of ixazomib when administered with LenDex in Japanese RRMM patients was similar to that in the intent-to-treat (ITT) population of the MM1 study. The confirmed VGPR + CR rate was 50.0% and the point estimate demonstrated in this study exceeded the threshold rate of 39.0%, which was based on the results of the MM1 study. The confirmed ORR and CR rates in this study (84.4% and 28.1%, respectively) were numerically better than those in the MM1 study (78% and 12%, respectively). The ORR for the high-risk subgroup was 72.7% and 90.5% for the standard-risk subgroup, although the number of patients with high-risk cytogenetics was small in this study. The favorable result for the primary efficacy endpoint was supported by the findings from the secondary efficacy endpoints, including PFS, DOR and TTP.

The safety profile of ixazomib when administered with LenDex in Japanese RRMM patients was similar to that in the ITT population of the MM1 study [17]. No new safety

Table 5 The most common (≥ 10%) TEAEs in the safety analysis set

	Ixazomib + LenDex *N* = 34 *n* (%)
Patients with at least 1 AE	34 (100)
Constipation	17 (50)
Upper respiratory tract infection	16 (47)
Diarrhea	14 (41)
Rash	12 (35)
Nasopharyngitis	11 (32)
Nausea	10 (29)
Platelet count decreased	9 (26)
Influenza	8 (24)
Neutropenia	8 (24)
Chilblains	7 (21)
Dysgeusia	7 (21)
Fall	7 (21)
Peripheral sensory neuropathy	7 (21)
Bronchitis	6 (18)
Neutrophil count decreased	6 (18)
Dental caries	5 (15)
Malaise	5 (15)
Edema peripheral	5 (15)
Pharyngitis	5 (15)
Maculopapular rash	5 (15)
Vomiting	5 (15)
Back pain	4 (12)
Dry skin	4 (12)
Hyperglycemia	4 (12)
Oropharyngeal pain	4 (12)
Pain in extremity	4 (12)
Pneumonia	4 (12)
Pyrexia	4 (12)
Stomatitis	4 (12)
Thrombocytopenia	4 (12)
Urticaria	4 (12)

AE adverse event, *LenDex* lenalidomide and dexamethasone, *TEAE* treatment-emergent adverse event

Table 6 Grade 3 or higher TEAEs in the safety analysis set

	Ixazomib + LenDex *N* = 34 *n* (%)
Neutropenia	7 (21)
Platelet count decreased	7 (21)
Neutrophil count decreased	6 (18)
Diarrhea	5 (15)
Maculopapular rash	4 (12)
Erythema multiforme	3 (9)
Pneumonia	3 (9)
White blood cell count decreased	3 (9)
Alanine aminotransferase increased	1 (3)
Anemia	1 (3)
Aspartate aminotransferase increased	1 (3)
Blood creatine phosphokinase increased	1 (3)
Cellulitis	1 (3)
Fall	1 (3)
Femoral neck fracture	1 (3)
Hyperglycemia	1 (3)
Hypertension	1 (3)
Hypophosphatemia	1 (3)
Hypotension	1 (3)
Leukemia	1 (3)
Lipase increased	1 (3)
Loss of consciousness	1 (3)
Lung neoplasm malignant	1 (3)
Lymphocyte count decreased	1 (3)
Malignant neoplasm of unknown primary seta[a]	1 (3)
Edema peripheral	1 (3)
Osteonecrosis of jaw	1 (3)
Pharyngitis	1 (3)
Pneumonitis	1 (3)
Rash generalized	1 (3)
Macular rash	1 (3)
Sebaceous nevus	1 (3)
Subarachnoid hemorrhage	1 (3)
Subdural hemorrhage	1 (3)
Thrombocytopenia	1 (3)
Tooth infection	1 (3)
Vomiting	1 (3)

Toxicity grade defined according to the National Cancer Institute Common Terminology Criteria for Adverse Events version 4.03

LenDex lenalidomide and dexamethasone, *TEAE* treatment-emergent adverse event

[a]Reported during the follow-up period

concerns were identified in this study, and the overall safety profile of ixazomib plus LenDex showed that this combination was well tolerated.

Diarrhea was the most commonly reported gastrointestinal AE of clinical importance. While antidiarrheal agents are not recommended for prophylactic use, they should be used appropriately as symptomatic treatment. In this study, antidiarrheal agents were administered if infectious causes were excluded.

Dermatological disorders were reported in 65% of patients, while they did not result in any patient discontinuing the study treatment, 24% of patients had their doses of ixazomib and/or lenalidomide reduced, and 32% had their doses of ixazomib and/or lenalidomide withheld. This corresponds with the incidence of rash observed in the Japanese subgroup enrolled in the MM1 study (70% reported rash)

Table 7 Summary of TEAEs of clinical importance[a] in the safety analysis set

N = 34, *n* (%)	Any Grade		≥ Grade 3		Treatment/response			
	Adverse event	Drug related	Adverse event	Drug related	Dose discontinuation	Dose reduction	Patient withdrawn from study[b]	Next cycle delayed
Blood toxicity								
Neutropenia	14 (41)	13 (38)	13 (38)	12 (35)	3 (9)	6 (18)	1 (3)	10 (29)
Thrombocytopenia	13 (38)	13 (38)	8 (24)	8 (24)	3 (9)	4 (12)	2 (6)	5 (15)
Cardiac disorders								
Cardiac failure	1 (3)	0	0	0	0	0	0	0
Gastrointestinal disorders								
Nausea	10 (29)	9 (26)	0	0	0	0	0	0
Vomiting	5 (15)	5 (15)	1 (3)	1 (3)	0	1 (3)	1 (3)	0
Diarrhea	14 (41)	13 (38)	5 (15)	5 (15)	0	2 (6)	4 (12)	0
Dermatologic disorders	22 (65)	20 (59)	9 (26)	8 (24)	0	8 (24)	11 (32)	2 (6)
Rash	12 (35)	10 (29)	0	0	0	0	2 (6)	0
Maculopapular rash	5 (15)	5 (15)	4 (12)	4 (12)	0	4 (12)	4 (12)	0
Urticaria	4 (12)	3 (9)	0	0	0	0	0	0
Erythema multiforme	3 (9)	3 (9)	3 (9)	3 (9)	0	2 (6)	3 (9)	0
Generalized rash	1 (3)	1 (3)	1 (3)	1 (3)	0	1 (3)	1 (3)	1 (3)
Macular rash	1 (3)	1 (3)	1 (3)	1 (3)	0	1 (3)	1 (3)	1 (3)
Peripheral neuropathy								
Peripheral sensory neuropathy	7 (21)	7 (21)	0	0	0	1 (3)	0	1 (3)
Peripheral neuropathy	1 (3)	1 (3)	0	0	0	0	0	0

TEAE treatment-emergent adverse event

[a]TEAEs of clinical importance was not based on a safety signal in the review of the clinical data; rather, they were considered of clinical importance owing to other factors that included, but were not limited to: (1) identification by searches of the clinical database considering the context of the intended patient population; (2) common adverse reactions for lenalidomide; (3) AEs reported at higher rates both across ixazomib clinical trials and within the MM1 study; and (4) adverse reactions reported with the commercially available PIs bortezomib and carfilzomib

[b]Some patients withdrew from the study due to multiple TEAEs

and higher than that reported in the overall population in the MM1 study (51% reported rash) [17], suggesting a slightly higher frequency of skin disorders developing in the Japanese population. However, this AE was manageable either by dose reduction or supportive care.

This study employed a dose modification guideline for rash that was modified from the MM1 study [17], and consistent with the Japanese package insert (i.e., ixazomib and lenalidomide were withheld in the event of Grade 2 rash not manageable by supportive care, until it recovered to Grade 1 or better). The successful management of rash may have contributed to the high relative dose intensity of lenalidomide while also maximizing exposure to ixazomib.

Supportive care and dose modification that are dependent on the patient's AEs seem an effective approach for continuous treatment, resulting in better outcomes. This is supported by the results in this study, with patients receiving a median of 20 treatment cycles and showing good responses.

This study has several clinical limitations. Its single-arm, open-label design may bias the interpretation of the study results. Secondly, the sample size and inclusion/exclusion criteria of the study limit the generalizability of its results. For example, 82% of patients were international staging system (ISS) stage I, 74% had an ECOG performance status of 0, 62% only had one prior line of therapy, 91% had relapsed disease and 68% had undergone ASCT. Hence, the generalizability of these results to patients with more advanced stage, poorer performance status or multiple lines of therapy, those with refractory disease or ASCT-ineligible patients may be limited.

In conclusion, ixazomib, when administered with LenDex, demonstrated efficacy in achieving a 50% rate of

confirmed VGPR or better in Japanese patients with RRMM, which was higher than the 39.0% threshold rate. The results demonstrated in this study are comparable with those in the MM1 study [17]. Likewise, the overall safety profile of ixazomib when administered with LenDex showed that this combination was well tolerated in this population.

Supplementary Information The online version contains supplementary material available at https://doi.org/10.1007/s10147-021-02030-7.

Acknowledgements The authors would like to thank all patients and their families, and all investigators who have contributed to this study; Yoshihide Kakimoto, MD, from the Medical Affairs of Takeda Pharmaceutical Co. Ltd. (Tokyo, Japan) for reviewing and providing valuable advice on this manuscript; and Yoichi Kase, PhD, from the Oncology Clinical Research Department of Takeda Pharmaceutical Co. Ltd. for providing valuable inputs on the study design. Medical writing assistance was provided by Darryl Lin and Ivan Olegario of MIMS Pte Ltd, which was funded by Takeda Pharmaceutical Co. Ltd., and complied with Good Publication Practice 3 ethical guidelines (Battisti et al. *Ann Intern Med.* 2015;163:461–4).

Authors' contributions SF, KS, DB and SI were involved in the study concept and design. All authors were involved in the acquisition, analysis or interpretation of data, and critical revision of the manuscript for important intellectual content. SF, KS and SI were involved in the drafting of the manuscript. KS was involved in statistical analysis. SF and DB were involved in obtaining funding. SF was involved in administrative, technical or material support. SI and SF were involved in the study supervision.

Funding This study was funded by Takeda Pharmaceutical Company Ltd. (Osaka, Japan).

Availability of data and material The authors do not plan to share individual participant's data supporting the results reported in this article because informed consent about external data sharing has not been obtained in any patient in the study due to investigator sites' policy. The redacted study protocol, redacted statistical analysis plan, in this article will be made available, within 3 months from initial request, to researchers who provide a methodologically sound proposal.

Declarations

Conflict of interest Shinsuke Iida reports research funding, honoraria and fees from Takeda Pharmaceutical Company Limited, during the conduct of the study; Honoraria and fees from Ono, Celgene, Janssen, Sanofi, Daiichi Sankyo and Takeda Pharmaceutical Company Limited; research funding from AbbVie, Bristol-Myers Squibb, Celgene, Daiichi Sankyo, GlaxoSmithKline, Ono and scholarship donations from Chugai, Kyowa Kirin, Ono, Sanofi and Takeda Pharmaceutical Company Limited, outside the submitted work. Takashi Ikeda reports honoraria and fees from Sanofi, outside the submitted work. Deborah Berg, Shinichi Fukunaga and Kenkichi Sugiura are employees of Takeda Pharmaceutical Company Limited, during the conduct of the study. Deborah Berg and Shinichi Fukunaga have stock ownership in Takeda Pharmaceutical Company Limited. Takaaki Chou has received honoraria from Takeda Pharmaceutical Company Limited, Ono, and BMS. Yasuhito Terui reports honoraria and fees from Celgene, Janssen, Merck Sharp & Dohme, Eisai, Ono, Takeda Pharmaceutical Company Limited, Chugai and AbbVie. Makoto Sasaki reports honoraria and lecture fees Takeda Pharmaceutical Company Limited. Tohru Izumi and Takuya Komeno have nothing to disclose.

Ethical approval All study-related documents were reviewed and approved by the local or central institutional review boards of all study sites.

Informed consent Objectives and potential risks and benefits were explained to patients using the informed consent form approved by the institutional review board, with each patient having signed and dated the form before screening.

References

1. Palumbo A, Anderson K (2011) Multiple myeloma. N Engl J Med 364(11):1046–1060
2. Japan National Cancer Center (2019). Projected cancer statistics, 2020. http://ganjoho.jp/reg_stat/statistics/stat/short_pred.html. Accessed 02 June 2021
3. Gay F, Engelhardt M, Terpos E et al (2018) From transplant to novel cellular therapies in multiple myeloma: European Myeloma Network guidelines and future perspectives. Haematologica 103(2):197–211
4. Dimopoulos M, Spencer A, Attal M et al (2007) Lenalidomide plus dexamethasone for relapsed or refractory multiple myeloma. N Engl J Med 357(21):2123–2132
5. Facon T, Mary JY, Hulin C et al (2007) Melphalan and prednisone plus thalidomide versus melphalan and prednisone alone or reduced-intensity autologous stem cell transplantation in elderly patients with multiple myeloma (IFM 99–06): a randomised trial. Lancet 370(9594):1209–1218
6. San Miguel JF, Schlag R, Khuageva NK et al (2008) Bortezomib plus melphalan and prednisone for initial treatment of multiple myeloma. N Engl J Med 359(9):906–917
7. Weber DM, Chen C, Niesvizky R et al (2007) Lenalidomide plus dexamethasone for relapsed multiple myeloma in North America. N Engl J Med 357(21):2133–2142
8. Iida S, Ishida T, Murakami H et al (2019) JSH practical guidelines for hematological malignancies, 2018: III. Myeloma-1. Multiple myeloma (MM). Int J Hematol 109(5):509–538
9. Kumar SK, Callander NS, Hillengass J et al (2019) NCCN guidelines insights: multiple myeloma, version 1.2020. J Natl Compr Cancer Netw 17(10):1154–1165
10. Yang Y, Li Y, Gu H et al (2020) Emerging agents and regimens for multiple myeloma. J Hematol Oncol 13(1):150–150
11. Barlogie B, Mitchell A, van Rhee F et al (2014) Curing myeloma at last: defining criteria and providing the evidence. Blood 124(20):3043–3051

12. Dimopoulos MA, Richardson PG, Moreau P et al (2014) Current treatment landscape for relapsed and/or refractory multiple myeloma. Nat Rev Clin Oncol 12(1):42–54
13. Kupperman E, Lee EC, Cao Y et al (2010) Evaluation of the proteasome inhibitor MLN9708 in preclinical models of human cancer. Can Res 70(5):1970–1980
14. Dimopoulos MA, Gay F, Schjesvold F et al (2019) Oral ixazomib maintenance following autologous stem cell transplantation (TOURMALINE-MM3): a double-blind, randomised, placebo-controlled phase 3 trial. Lancet 393(10168):253–264
15. Dimopoulos MA, Špička I, Quach H et al (2020) Ixazomib as postinduction maintenance for patients with newly diagnosed multiple myeloma not undergoing autologous stem cell transplantation: the phase III TOURMALINE-MM4 trial. J Clin Oncol 38(34):4030–4041
16. Dispenzieri A, Kastritis E, Wechalekar AD et al (2019) Primary results from the phase 3 tourmaline-al1 trial of ixazomib-dexamethasone versus physician's choice of therapy in patients (Pts) with relapsed/refractory primary systemic al amyloidosis (RRAL). Blood 134(Supplement_1):139–139
17. Moreau P, Masszi T, Grzasko N et al (2016) Oral ixazomib, lenalidomide, and dexamethasone for multiple myeloma. N Engl J Med 374(17):1621–1634
18. Chanan-Khan AA, Giralt S (2010) Importance of achieving a complete response in multiple myeloma, and the impact of novel agents. J Clin Oncol 28(15):2612–2624
19. Rajkumar SV, Harousseau J-L, Durie B et al (2011) Consensus recommendations for the uniform reporting of clinical trials: report of the International Myeloma Workshop Consensus Panel 1. Blood 117(18):4691–4695
20. U.S. Food and Drug Administration. REVLIMID Prescribing Information (2019) 4439576
21. Revlimid capsules® (lenalidomide) (2020) *Japan Package Insert.* 00065995

OPEN ACCESS

Rare case of congenital coronary artery fistula coexistent and coalesced with aortopulmonary fistula

Takumi Osawa , Yuta Ito, Tomomi Koizumi

Department of Cardiovascular Medicine, Mito Medical Center, Mito, Ibaraki, Japan

Correspondence to
Dr Takumi Osawa;
tosawa49710@gmail.com

Accepted 30 June 2021

SUMMARY

Coronary artery fistula (CAF) is an uncommon congenital heart disease. Furthermore, aortopulmonary fistula is a rare congenital heart disease of adult onset. We report the case of a 79-year-old man who presented with chest pain. ECG-gated cardiac CT and coronary artery angiography revealed an anomalous vessel arising from the right coronary cusp and a CAF from the left coronary descending artery. These fistulas coalesced and drained into the same portion of the pulmonary artery. Haemodynamic studies revealed that the estimated systemic-to-pulmonary flow ratio was 1.18. The mean pulmonary pressure was 14 mm Hg. We decided against surgical intervention due to his advanced age and lack of heart failure symptoms. The patient did not have any worsening heart failure and chest pain on follow-up. This was a rare case of CAF coexistent and coalesced with an aortopulmonary fistula.

BACKGROUND

Coronary artery fistula (CAF) is a very rare disease.[1] It is a communication between the coronary arteries and the cardiac chambers or other vessels. Aortopulmonary fistula is also a rare disease. We report a case where CAF and an aortopulmonary fistula coalesced and drained into the pulmonary artery (PA). We obtained a detailed anatomical information using multidetector CT angiography and coronary artery angiography.

CASE PRESENTATION

A 79-year-old man with a 3-month history of chest discomfort unrelated to exercise was admitted to our hospital. The patient reported a medical history of asthma and chronic obstructive pulmonary disease, which were well-controlled by medication. On initial examination, his blood pressure was 115/82 mm Hg, heart rate was 78 beats/min, respiratory rate was 12 breaths/min, pulse oximetric oxygen saturation was 98% in room air and his temperature was 36.2°C. The patient's height and weight were 170 cm and 66 kg, respectively. Clinical examination of the cardiovascular system revealed no murmurs, and the lungs were clear. His jugular venous pressure was not elevated, and he did not exhibit heart failure symptoms, such as shortness of breath and leg oedema.

INVESTIGATIONS

A 12-leads ECG revealed sinus rhythm and T-wave inversion in leads V1, V2 and V3. Transthoracic ECG illustrated one flow just above the pulmonary valve, preserved left ventricular ejection fraction, no enlargement of the left and right heart, trivial mitral regurgitation and trivial tricuspid regurgitation. ECG-gated cardiac CT revealed an anomalous vessel arising from the right coronary cusp (RCC) and a CAF from the left coronary descending artery (LAD; figure 1A,B). The abnormal blood vessels emerging from the RCC and the CAF emerging from the LAD coalesced, and drained into the PA (figure 1C). Coronary artery angiography revealed no significant stenosis of the coronary artery; however, it revealed fistulas originating in both the RCC and LAD (figure 2A,B; videos 1 and 2). These fistulas drained into the same portion of the main PA. Haemodynamic studies revealed that the estimated systemic-to-pulmonary flow ratio was 1.18 (table 1). Step-up of oxygen saturation was observed between the main PA and right ventricle outflow (table 2). The mean PA pressure was within normal range. Single-photon emission CT revealed no myocardial ischaemia.

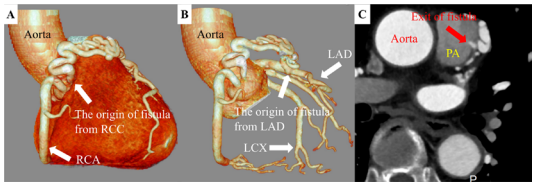

Figure 1 The ECG-gated cardiac CT revealing abnormal vessels arising from the LAD and RCC. (A) Right-lateral view illustrates the fistula from RCC. (B) Right-lateral view illustrates the fistula from the LAD. (C) Superior view illustrating the exit of fistulas. LAD, left coronary descending artery; LCX, left coronary circumflex artery; PA, pulmonary artery; RCA, right coronary artery; RCC, right coronary cusp.

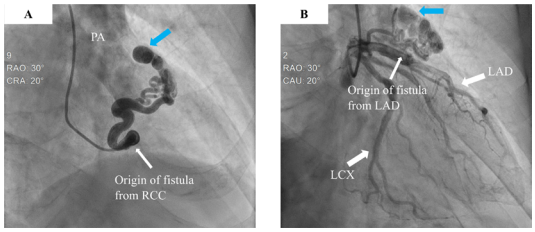

Figure 2 Angiography of coronary artery and fistulas. (A) Right-cranial view illustrating the fistula originating from the right coronary cusp. (B) Right-caudal view illustrating the fistula from the left coronary descending artery. The two fistulas draining into the same portion of the main PA. CAU. caudal; CRA, cranial; LAD, left coronary descending artery; LCX, left coronary circumflex artery; PA, pulmonary artery; RAO, right anterior oblique; RCC, right coronary cusp.

To cite: Osawa T, Ito Y, Koizumi T. *BMJ Case Rep* 2021;**14**:e244035. doi:10.1136/bcr-2021-244035

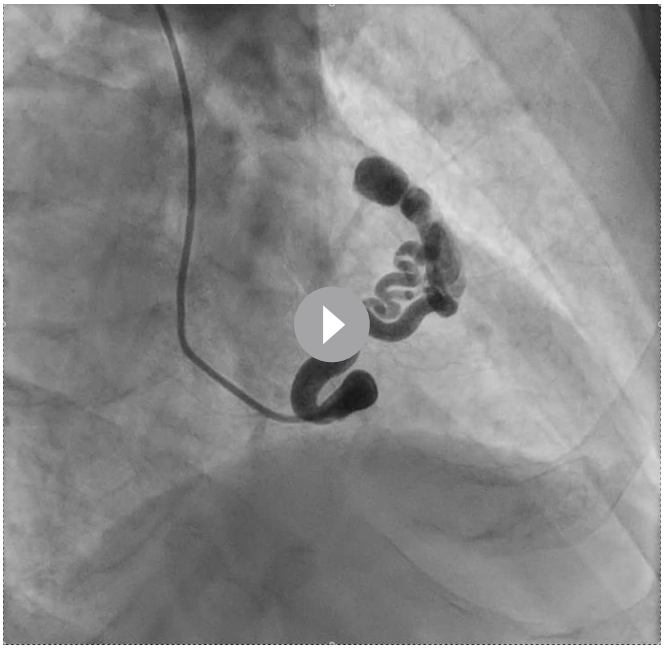

Video 1 Angiography of coronary artery and fistulas. Right cranial view illustrating the fistula originating from the right coronary cusp.

DIFFERENTIAL DIAGNOSIS

The differential diagnosis of this case included angina pectoris, myocarditis, pericarditis, musculoskeletal disease and oesophageal disease.

TREATMENT

The estimated systemic-to-pulmonary flow ratio was low, and single-photon emission CT revealed no ischaemic myocardium. We decided against surgical intervention due to his advanced age and lack of heart failure symptoms.

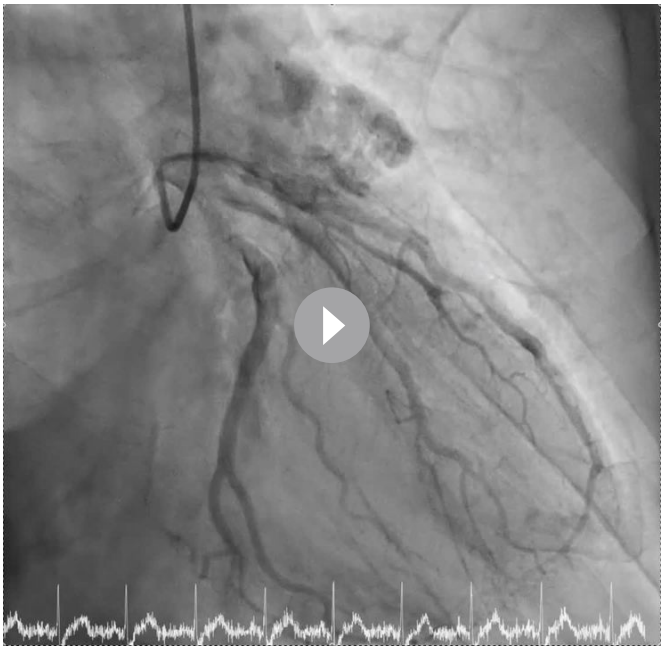

Video 2 Angiography of coronary artery and fistulas. Right caudal view illustrating the fistula from the left coronary descending artery.

Table 1 Haemodynamic studies of the case

Aorta s/d/m	162/106/130	mm Hg
Pulmonary capillary wedge a-wave/v-wave/mean	6/1/3	mm Hg
PA s/d/m	21/10/14	mm Hg
Right ventricle systolic/diastolic/EDP	26/6/10	mm Hg
Right atrium a a-wave/v-wave/mean	9/8/7	mm Hg
Heart rate	71	beats/min
Cardiac output (Fick)	7.15	L/min
Cardiac index (Fick)	3.97	L/min/m^2
Qp/Qs*	1.18	

The estimated systemic-to-pulmonary flow ratio is 1.18. The pulmonary artery pressure is within the normal range.
*Pulmonary blood flow/systemic blood flow ratio.
EDP, end-diastolic pressure; PA, pulmonary artery; s/d/m, systolic/diastolic/mean.

OUTCOME AND FOLLOW-UP

After discharge, the patient was carefully followed up.

DISCUSSION

We describe a rare case of a CAF. To our knowledge, this is the first documented case of congenital aortopulmonary fistula combined with CAF. These two fistulas were connected to each other.

CAF is a rare congenital anatomical abnormality of the coronary arteries. CAF prevalence is reportedly 0.9% of all congenital heart diseases.[1] CAF may arise from the LAD, left coronary circumflex artery or the right coronary artery. Congenital coronary-PA fistula is a CAF and its characteristics are poorly understood. The majority of CAFs arise from the left coronary artery.[2–4] The most common drainage site for CAF is PA (85%).[4] In this case, the fistula connected the left descending coronary artery to the PA.

Aortocardiac fistula is a rare condition. Aortopulmonary fistula is an aortocardiac fistula. There were no reports of the prevalence of the aortopulmonary fistula. The aortocardiac fistula is common in the aortic-right atrium (37%) and aortic-PA (25%).[5] The origin of the aortocardiac fistula in this case was RCC, namely the ascending aorta.

With the development of CT, it has become possible to determine the origins, drainage sites and the number of fistulas in detail.[6] As in this case, the results of CT can be used to determine examination methods and treatment strategies. Angiography of coronary artery and fistulas is an invasive study and has some

Table 2 Oxygen saturation

	O_2 saturation (%)
Right PA	76.2
Left PA	75.3
Main PA	75.9
Right ventricle outflow	69.6
Right ventricle apex	68.1
Right ventricle inflow	69.4
Superior vena cava	72
Right atrium	70.5
Inferior vena cava	76.2
Aorta	91.2

Illustration of the step-up of oxygen saturation between the main pulmonary artery and right ventricle outflow.
PA, pulmonary artery.

risks of complications. Also, the accurate diagnosis rate is low with invasive angiography.

The most commonly reported symptoms of CAF are chest pain (39%) and respiratory dyspnoea (25%), with murmur being the most common finding on physical examination (37%).[2] In this case, however, chest pain was the only symptom. The coronary 'steal phenomenon' is considered to be the primary cause of CAF without coronary artery stenosis. This mechanism is related to the flow from the high-pressure coronary artery to a low-resistance PA, owing to the pressure gradient. This symptom is associated with an increased myocardial oxygen demand during exercise or activity.

Researchers agree that the symptomatic patients should be treated. According to the American College of Cardiology/American Heart Association guidelines, 'percutaneous or surgical closure is a Class I recommendation for large fistulas regardless of symptoms, and for small or moderate fistulas with evidence of myocardial ischemia, arrhythmia, ventricular dysfunction, ventricular enlargement, or endarteritis'.[7] In this case, however, we decided to treat the patient conservatively for multiple reasons. First, his symptoms were atypical of angina pectoris and did not worsen on exertion. The frequency of his symptoms was approximately once a month. Second, he exhibited no symptoms of heart failure or pulmonary hypertension. Third, the mean PA pressure and estimated systemic-to-pulmonary flow ratio were low. Fourth, there were some risks associated with surgery due to his advanced age.

In conclusion, this was a rare case where CAF and an aortopulmonary fistula coalesced and drained into the PA.

Learning points

- To create awareness among physicians regarding the possibility of coexistence of exceedingly rare anatomical pathologies, coronary artery fistula and aortopulmonary fistula, which also coalesced before draining into the pulmonary artery. This case study will also help physicians understand its presentation.
- To understand that multidetector CT angiography is helpful in investigating for congenital coronary artery fistulas and can be used to plan the approach towards coronary artery angiography.
- To assess the risk of the diseases, examinations and anatomical evaluation about adult congenital heart diseases should be done.

Acknowledgements We are grateful to Dr Yasushi Kobayashi for helpful discussions and comments on the article.

Contributors TO and YI were part of the team that admitted the patient. TO and TK did the literature review and article write-up. All authors gave their final approval of the version to be published.

Funding The authors have not declared a specific grant for this research from any funding agency in the public, commercial or not-for-profit sectors.

Competing interests None declared.

Patient consent for publication Obtained.

Provenance and peer review Not commissioned; externally peer reviewed.

ORCID iD
Takumi Osawa http://orcid.org/0000-0002-1602-7529

REFERENCES

1 Lim JJ, Jung JI, Lee BY, *et al*. Prevalence and types of coronary artery fistulas detected with coronary CT angiography. *AJR Am J Roentgenol* 2014;203:W237–43.
2 Verdini D, Vargas D, Kuo A, *et al*. Coronary-Pulmonary artery fistulas: a systematic review. *J Thorac Imaging* 2016;31:380–90.
3 Kim MS, Jung JI, Chun HJ. Coronary to pulmonary artery fistula: morphologic features at multidetector CT. *Int J Cardiovasc Imaging* 2010;26:273–80.
4 Zhou K, Kong L, Wang Y, *et al*. Coronary artery fistula in adults: evaluation with dual-source CT coronary angiography. *Br J Radiol* 2015;88:20140754.
5 Foster TJ, Amin AH, Busu T, *et al*. Aorto-cardiac fistula etiology, presentation, and management: a systematic review. *Heart Lung* 2020;49:317–23.
6 Yun G, Nam TH, Chun EJ. Coronary artery fistulas: pathophysiology, imaging findings, and management. *Radiographics* 2018;38:688–703.
7 Warnes CA, Williams RG, Bashore TM, *et al*. ACC/AHA 2008 guidelines for the management of adults with congenital heart disease: Executive summary: a report of the American College of Cardiology/American heart association Task force on practice guidelines (writing Committee to develop guidelines for the management of adults with congenital heart disease). *Circulation* 2008;118:2395–451.

ESC HEART FAILURE
ESC Heart Failure 2021; **8**: 4187–4198
Published online 13 August 2021 in Wiley Online Library (wileyonlinelibrary.com) **DOI:** 10.1002/ehf2.13555

ORIGINAL RESEARCH ARTICLE

Soluble vascular endothelial growth factor receptor 2 and prognosis in patients with chronic heart failure

Moritake Iguchi[1]*, Hiromichi Wada[2], Tsuyoshi Shinozaki[3], Masahiro Suzuki[4], Yoichi Ajiro[5], Morihiro Matsuda[6], Akihiro Koike[7], Tomomi Koizumi[8], Masatoshi Shimizu[9], Yujiro Ono[10], Takashi Takenaka[11], Satoru Sakagami[12], Yukiko Morita[13], Kazuteru Fujimoto[14], Kazuya Yonezawa[15], Kazuro Yoshida[16,22], Akiyo Ninomiya[16], Toshihiro Nakamura[17], Junichi Funada[18], Yutaka Kajikawa[19], Yoshifumi Oishi[20], Toru Kato[21], Kazuhiko Kotani[23], Mitsuru Abe[1], Masaharu Akao[1], Koji Hasegawa[2] and for the PREHOSP-CHF Study Investigators

[1]*Department of Cardiology, National Hospital Organization Kyoto Medical Center, 1-1, Mukaihata-cho, Fukakusa, Fushimi-ku, Kyoto, 612-8555, Japan;* [2]*Division of Translational Research, National Hospital Organization Kyoto Medical Center, Kyoto, Japan;* [3]*Department of Cardiology, National Hospital Organization Sendai Medical Center, Sendai, Japan;* [4]*Department of Clinical Research, National Hospital Organization Saitama Hospital, Wako, Japan;* [5]*Division of Clinical Research, National Hospital Organization Yokohama Medical Center, Yokohama, Japan;* [6]*Division of Preventive Medicine Institute for Clinical Research, National Hospital Organization Kure Medical Center and Chugoku Cancer Center, Kure, Japan;* [7]*Department of Cardiology, National Hospital Organization Fukuokahigashi Medical Center, Koga, Japan;* [8]*Department of Cardiology, National Hospital Organization Mito Medical Center, Ibaraki, Japan;* [9]*Department of Cardiology, National Hospital Organization Kobe Medical Center, Kobe, Japan;* [10]*Department of Cardiology, National Hospital Organization Higashihiroshima Medical Center, Hiroshima, Japan;* [11]*Department of Cardiology, National Hospital Organization Hokkaido Medical Center, Sapporo, Japan;* [12]*Institute for Clinical Research, National Hospital Organization Kanazawa Medical Center, Kanazawa, Japan;* [13]*Department of Cardiology, National Hospital Organization Sagamihara Hospital, Sagamihara, Japan;* [14]*Department of Cardiology, National Hospital Organization Kumamoto Medical Center, Kumamoto, Japan;* [15]*Division of Clinical Research, National Hospital Organization Hakodate Hospital, Hakodate, Japan;* [16]*Department of Cardiology, National Hospital Organization Nagasakikawadana Medical Center, Higashisonogi, Japan;* [17]*Department of Cardiology, National Hospital Organization Kyushu Medical Center, Fukuoka, Japan;* [18]*Department of Cardiology, National Hospital Organization Ehime Medical Center, Toon, Japan;* [19]*Department of Cardiology, National Hospital Organization Fukuyama Medical Center, Fukuyama, Japan;* [20]*Department of Cardiology, National Hospital Organization Higashitokushima Medical Center, Itano, Japan;* [21]*Department of Clinical Research, National Hospital Organization Tochigi Medical Center, Utsunomiya, Japan;* [22]*Department of Cardiology, National Hospital Organization Nagasaki Hospital, Nagasaki, Japan; and* [23]*Division of Community and Family Medicine, Jichi Medical University, Shimotsuke, Japan*

Abstract

Aims Endothelial cell vascular endothelial growth factor receptor 2 (VEGFR-2) plays a pivotal role in angiogenesis, which induces physiological cardiomyocyte hypertrophy via paracrine signalling between endothelial cells and cardiomyocytes. We investigated whether a decrease in circulating soluble VEGFR-2 (sVEGFR-2) levels is associated with poor prognosis in patients with chronic heart failure (HF).

Methods and results We performed a multicentre prospective cohort study of 1024 consecutive patients with HF, who were admitted to hospitals due to acute decompensated HF and were stabilized after initial management. Serum levels of sVEGFR-2 were measured at discharge. Patients were followed up over 2 years. The outcomes were cardiovascular death, all-cause death, major adverse cardiovascular events (MACE) defined as a composite of cardiovascular death and HF hospitalization, and HF hospitalization. The mean age of the patients was 75.5 (standard deviation, 12.6) years, and 57% were male. Patients with lower sVEGFR-2 levels were older and more likely to be female, and had greater proportions of atrial fibrillation and anaemia, and lower proportions of diabetes, dyslipidaemia, and HF with reduced ejection fraction (<40%). During the follow-up, 113 cardiovascular deaths, 211 all-cause deaths, 350 MACE, and 309 HF hospitalizations occurred. After adjustment for potential clinical confounders and established biomarkers [N-terminal B-type natriuretic peptide (NT-proBNP), high-sensitivity cardiac troponin I, and high-sensitivity C-reactive protein], a low sVEGFR-2 level below the 25th percentile was significantly associated with cardiovascular death [hazard ratio (HR), 1.79; 95% confidence interval (CI), 1.16–2.74] and all-cause death (HR, 1.43; 95% CI, 1.04–1.94), but not with MACE (HR, 1.11; 95% CI, 0.86–1.43) or HF hospitalization (HR, 1.03; 95% CI, 0.78–1.35). The stratified analyses revealed that a low sVEGFR-2 level below the 25th percentile was significantly associated with cardiovascular death (HR, 1.76; 95% CI, 1.07–2.85) and all-cause death (HR, 1.49; 95% CI, 1.03–2.15) in the high-NT-proBNP group (above the median), but not in the low-NT-proBNP group. Notably, the patients with high-NT-proBNP and low-sVEGFR-2 (below the 25th percentile) had a 2.96-fold higher risk (95% CI, 1.56–5.85) for cardiovascular death and a 2.40-fold higher risk (95% CI, 1.52–3.83) for all-cause death compared with those with low-NT-proBNP and high-sVEGFR-2.

Conclusions A low sVEGFR-2 value was independently associated with cardiovascular death and all-cause death in patients with chronic HF. These associations were pronounced in those with high NT-proBNP levels.

Keywords Heart failure; Biomarker; Angiogenesis; Lymphangiogenesis; Mortality

Received: 22 March 2021; Revised: 9 July 2021; Accepted: 28 July 2021
**Correspondence to: Moritake Iguchi, Department of Cardiology, National Hospital Organization Kyoto Medical Center, 1-1, Mukaihata-cho, Fukakusa, Fushimi-ku, Kyoto 612-8555, Japan. Phone: +81 75-641-9161; Fax: +81 75-643-4325. Email: moritake@kuhp.kyoto-u.ac.jp*

Introduction

Despite current advances in therapy, heart failure (HF) remains a leading cause of hospitalization and mortality worldwide, and its prevalence is progressively increasing in aging societies.[1] HF is a clinical syndrome with several underlying aetiologies. Basic studies have demonstrated that dysfunction of angiogenesis is a major cause of the pathogenesis and progression of advanced HF, regardless of the aetiology[2]: cardiac tissue growth is angiogenesis-dependent, and disruption of coordinated cardiac hypertrophy and angiogenesis causes the transition from adaptive cardiac hypertrophy to decompensated HF.[3,4]

Vascular endothelial growth factor (VEGF) is a key cytokine in angiogenesis.[5] The VEGF family consists of five members [VEGF (or VEGF-A), placental growth factor, VEGF-B, VEGF-C, and VEGF-D] and three tyrosine kinase receptors (VEGFR-1, -2, and -3). Among the pathways involving these members, the VEGF/VEGFR-2 pathway plays a major role in angiogenesis. A recent study demonstrated that crosstalk between the endothelial cell VEGFR-2 and cardiac myocyte ErbB signalling pathways coordinates cardiac myocyte hypertrophy with angiogenesis, and thereby contributes to physiological cardiac growth.[6] A soluble form of VEGFR-2 (sVEGFR-2) is generated by proteolytic hydrolysis of membrane-bound VEGFR-2 or by alternative splicing,[7,8] and sVEGFR-2 can be measured in serum and plasma by immunoassay.[9] Circulating levels of sVEGFR-2 were reported to serve as a surrogate biomarker of VEGF-mediated tumour growth in patients with various cancers.[10–12] However, the clinical significance of sVEGFR-2 in patients with chronic HF (CHF) is unknown. We therefore performed a multicentre prospective cohort study to investigate the prognostic value of serum sVEGFR-2 levels in patients with CHF.

Methods

Study population

The PREHOSP-CHF study (Development of Novel Biomarkers to Predict REHOSPitalization in Chronic Heart Failure) is a nationwide, multicentre prospective cohort study to determine the predictive value of possible novel biomarkers related to angiogenesis or lymphangiogenesis for cardiovascular (CV) events in patients with CHF (UMIN Clinical Trials Registry: UMIN000021657). We enrolled 1065 patients with HF, who were admitted to hospitals due to acute decompensated HF and were stabilized after initial management, between December 2015 and October 2017 in the 21 National Hospital Organization institutions across Japan. The present study was conducted by nationally certified cardiologists. Acute decompensated HF was defined by the modified Framingham criteria. The exclusion criteria are described in the Supporting Information (Supplemental Methods section). After excluding 41 patients who were subsequently found to be ineligible (31 patients) or who withdrew consent (10 patients), a total of 1024 patients were included in the analyses. The study was approved by the central ethics committee of the National Hospital Organization headquarters and each institution's ethical committee. All of the patients provided written informed consent.

Exposures, sample collection, and biomarker measurement

The primary predictor was the serum level of sVEGFR-2 at the time of nearest discharge. The serum levels of sVEGFR-2, VEGF, and high-sensitivity C-reactive protein (hs-CRP) were measured with specific, commercially available ELISA kits according to the manufacturers' instructions: sVEGFR-2 and VEGF were measured using a Quantikine kit (R&D Systems, Minneapolis, MN), and hs-CRP was measured with a CycLex kit (Medical & Biological Laboratories [MBL], Nagano, Japan).[13] These assays were performed by an investigator masked to the sources of the samples. The serum levels of N-terminal pro-brain natriuretic peptide (NT-proBNP) were measured using a validated, sandwich electrochemiluminescence immunoassay (Elecsys; Roche Diagnostics, Indianapolis, IN). The sensitivities of the assays for VEGF, sVEGFR-2, and hs-CRP were 5.0, 4.6, and 28.6 pg/mL, respectively. The inter-assay/intra-assay coefficients of variation of ELISA for VEGF, sVEGFR-2, and hs-CRP were $<9\%/<7\%$, $\leq 7\%/<5\%$, and $<6\%/<4\%$, respectively. The sensitivity of the assay for NT-proBNP was 5 pg/mL, and the assay coefficients of variation at values of the measuring range (5–35 000 pg/mL) were $<10\%$. The high-sensitivity cardiac troponin I (hs-cTnI) values were measured using a cardiac

troponin assay (Architect Stat High-sensitive Troponin I; Abbott Laboratories, Abbott Park, IL). The limit of detection in this assay is 1.9 pg/mL (range, 0–50 000 pg/mL) and the 99th percentile cut-off is 26.2 pg/mL. Additional details are described in the Supporting Information (Supplemental Methods section).

Study endpoints

The endpoints in the analyses were CV death, all-cause death, major adverse cardiovascular events (MACE) defined as a composite of CV death and HF-related hospitalization, and HF-related hospitalization. Causes of death were adjudicated after consideration of all the available information and were classified according to the following pre-specified groups: CV death and non-CV death. CV death included death related to HF, acute coronary syndrome, stroke, and other vascular disease, and sudden death. Sudden death was defined as death related to fatal arrhythmia or unexplained death in a previously stable patient. Patients were followed up over 2 years. At the end of the follow-up period (Day 720), survival status and detailed information about MACE were available in 1009 patients (follow-up rate, 98.5%).

Statistical analysis

We divided the patients into quartiles according to their baseline sVEGFR-2 levels. The categorical variables are presented as numbers and percentages and were compared using a χ^2 test. The continuous variables are expressed as mean with standard deviation or median with interquartile range. On the basis of their distributions, the continuous variables were compared using ANOVA or the Kruskal–Wallis test. The *P* values for trends across the groups were calculated using the Cochran–Armitage test for categorical variables and the Jonckheere–Terpstra test for continuous variables. The cumulative incidences of clinical outcomes were estimated by the Kaplan–Meier method and Cox proportional hazard regression. For competing risk analyses, we used the Fine and Gray model to estimate the subdistribution hazard ratio (HR). The relationships between the baseline biomarker levels and the outcomes were investigated with the use of Cox proportional hazard regression. In our prior exploratory study of 254 CHF patients, the incidence of MACE over a 2 year follow-up period was 29.1% in a low sVEGFR-2 group (below the median) and 17.3% in a high sVEGFR-2 group. To realize 99% power for MACE, we estimated that a sample size of 785 patients was required. We increased this sample size by 20% to account for potential loss to follow-up, arriving at a final sample size of 1050 patients with an expected MACE incidence of 242 patients. We therefore included no more than 24 variables for the statistical analysis, because that was the highest number of variables supported by the anticipated incidence of MACE. We used four sets of models to confirm the consistency of the association between sVEGFR-2 levels and clinical events: Model 1, adjusted for age, sex, body mass index, and traditional CV risk factors (i.e. hypertension, diabetes, and dyslipidaemia), as well as established risk factors for HF [i.e. prior HF hospitalization, left ventricular dysfunction defined as an ejection fraction (EF) $<$ 40%, and NYHA class 3/4]; Model 2, adjusted for the covariates included in Model 1 and other CV risk factors [i.e. coronary artery disease, old myocardial infarction, atrial fibrillation (AF), chronic kidney disease (CKD, defined as an estimated glomerular filtration rate of less than 60 mL/min/1.73 m^2), anaemia (defined as haemoglobin levels of less than 13 g/dL in male participants and 12 g/dL in female participants), chronic obstructive pulmonary disease, and cerebrovascular disease]; Model 3, adjusted for the covariates included in Model 2 and prescription of renin–angiotensin system inhibitors (RAS-I), beta blockers, loop diuretics, and mineral corticoid receptor antagonists (MRA); and Model 4, adjusted for the covariates included in Model 3 and CV biomarkers [NT-proBNP, hs-cTnI, and hs-CRP ($>$1 mg/L)].

Subgroup analyses were performed based on the independent determinants for sVEGFR-2 level in the multiple regression analysis, EF category (HFpEF: HF with preserved EF ($\geq$50%); HFmrEF: HF with mid-range EF (40–49%); and HFrEF: HF with reduced EF [$<$40%]), and aetiology of HF (ischaemic or non-ischaemic).

All statistical tests were two-sided, and $P < 0.05$ was considered significant. Analyses were performed using JMP version 12 (SAS Institute, Cary, NC) and R, version 3.4.4 (R Foundation for Statistical Computing, Vienna, Austria).

Results

Baseline characteristics

The distribution of sVEGFR-2 values is shown in *Figure S1*. We divided the patients into four groups based on the quartile of the sVEGFR-2 levels (Quartile 1: sVEGFR-2 $<$ 5259 pg/mL; Quartile 2: 5259 pg/mL $\leq$ VEGFR-2 $<$ 6120 pg/mL; Quartile 3: 6120 pg/mL $\leq$ sVEGFR-2 $<$ 7210 pg/mL; and Quartile 4: sVEGFR-2 $\geq$ 7210 pg/mL). The baseline characteristics of the entire cohort and of the patients divided into quartiles of sVEGFR-2 levels are shown in *Tables 1* and *S1*. Patients with Quartile 1 sVEGFR-2 levels were older and had higher rates of female sex, lower body mass index, AF, and anaemia, while they had lower prevalence of diabetes and dyslipidaemia compared with those with Quartiles 2–4 sVEGFR-2 levels. Prevalence of HFpEF was higher in those with Quartile 1 sVEGFR-2 levels than in those with Quartiles 2–4 sVEGFR-2 levels.

Table 1 Baseline characteristics according to quartiles of sVEGFR-2

Variable *N*	Entire cohort 1024	Quartile 1 256	Quartile 2 256	Quartile 3 256	Quartile 4 256	*P* value	*P* for trend
Age (years)	75.5 (12.6)	80 (10.7)	77.3 (11.8)	74.7 (11.9)	70.2 (13.7)	<0.001	<0.001
Male gender	601 (58.7)	132 (51.6)	133 (52.0)	167 (65.2)	169 (66.0)	<0.001	<0.001
Body mass index (kg/m^2)	22.2 (4.9)	20.9 (4.1)	22 (4.8)	22.5 (4.4)	23.3 (5.7)	<0.001	<0.001
SBP (mmHg)	114.8 (17.8)	112.8 (17)	115.5 (17.3)	114.8 (18.6)	116.2 (18)	0.2	0.07
DBP (mmHg)	65.6 (12.6)	63.8 (12.9)	66.7 (13.0)	65 (12.5)	66.7 (11.9)	0.02	0.052
Pulse rate (bpm)	70.1 (13.6)	69.5 (13.9)	70.3 (13.6)	69.8 (13.8)	70.9 (13.2)	0.7	0.3
NYHA 3/4	139 (13.6)	34 (13.3)	38 (14.9)	36 (14.1)	31 (12.1)	0.8	0.6
HFpEF/mrEF/rEF	429/186/409 (41.9/18.2/39.9)	127/51/78 (49.6/19.9/30.5)	103/45/108 (40.2/17.6/42.2)	104/48/104 (40.6/18.8/40.6)	95/42/119 (37.1/16.4/46.5)	0.02	<0.001
Ischaemic aetiology	252 (24.6)	48 (18.8)	69 (27.0)	65 (25.4)	70 (27.3)	0.08	0.04
Hypertension	777 (75.9)	189 (73.8)	196 (76.6)	202 (78.9)	190 (74.2)	0.5	0.8
Diabetes	396 (38.7)	83 (32.4)	99 (38.7)	91 (35.5)	123 (48)	0.002	0.001
Dyslipidaemia	418 (40.8)	81 (31.6)	118 (46.1)	99 (38.7)	120 (46.9)	<0.001	0.005
Prior HF hospitalization	322 (31.4)	80 (31.3)	93 (36.3)	83 (32.4)	66 (25.8)	0.08	0.1
Coronary artery disease	319 (31.2)	74 (28.9)	87 (34.0)	77 (30.1)	81 (31.6)	0.6	0.7
Old myocardial infarction	181 (17.7)	33 (12.9)	48 (18.8)	48 (18.8)	52 (20.3)	0.1	0.04
AF	533 (52.1)	153 (59.8)	144 (56.3)	135 (52.7)	101 (39.5)	<0.001	<0.001
CKD	527 (51.5)	128 (50.0)	143 (55.9)	134 (52.3)	122 (47.7)	0.3	0.5
Anaemia[a]	577 (56.4)	174 (68.0)	143 (55.9)	138 (53.9)	122 (47.7)	<0.001	<0.001
COPD	77 (7.5)	22 (8.6)	23 (9.0)	21 (8.2)	11 (4.3)	0.1	0.06
Cerebrovascular disease	176 (17.2)	51 (19.9)	45 (17.6)	37 (14.5)	43 (16.8)	0.4	0.2
RAS-I	725 (70.8)	176 (68.8)	183 (71.5)	172 (67.2)	194 (75.8)	0.1	0.2
Beta blockers	752 (73.4)	167 (65.2)	189 (73.8)	195 (76.2)	201 (78.5)	0.005	<0.001
Loop diuretics	871 (85.1)	213 (83.2)	225 (87.9)	212 (82.8)	221 (86.3)	0.3	0.7
MRA	441 (43.1)	111 (43.4)	117 (45.7)	106 (41.4)	107 (41.8)	0.8	0.5
NT-proBNP (pg/mL)	1493 [664–3395]	1404 [674–3493]	1591 [680–3560]	1656 [706–3289]	1389 [598–3201]	0.7	0.5
hs-cTnI (pg/mL)	21.9 [12.1–47.4]	22.5 [13.4–47.8]	21.8 [12.0–45.6]	20.0 [10.5–44.6]	23.9 [13.8–52.6]	0.3	0.8
hs-CRP (mg/L)	2.48 [0.83–8.87]	2.74 [0.87–9.52]	2.35 [0.78–9.68]	2.05 [0.86–7.62]	3.11 [0.83–8.76]	0.4	0.8
VEGF (pg/mL)	377 [223–632]	324 [189–521]	401 [231–666]	366 [226–636]	438 [243–672]	<0.001	0.001

Continuous variables are expressed as the mean (standard deviation) or median [interquartile range] according to the distributions. Categorical variables are presented as numbers (percentages).

AF, atrial fibrillation; CKD, chronic kidney disease; COPD, chronic obstructive pulmonary disease; DBP, diastolic blood pressure; EF, ejection fraction; Hb, haemoglobin; HF, heart failure, HFmrEF, HF with mid-range EF; HFpEF, HF with preserved EF; HFrEF, HF with reduced EF; hs-CRP, high-sensitivity C-reactive protein; hs-cTnI, high sensitivity cardiac troponin I; MRA, mineral corticoid receptor antagonists; NT-proBNP, N-terminal pro-brain natriuretic peptide; RAS-I, renin angiotensin system inhibitor; SBP, systolic blood pressure; VEGF, vascular endothelial growth factor; VEGFR-2, soluble vascular endothelial growth factor receptor 2.

[a]Anaemia was defined as a haemoglobin level <13 g/dL in male participants and <12 g/dL in female participants.

In simple regression analyses, the sVEGFR-2 level was inversely correlated with EF, and positively correlated with the VEGF levels, but it was not significantly correlated with the levels of established CV biomarkers (NT-proBNP, hs-cTnI, and hs-CRP) (*Table S2*). Stepwise multiple regression analysis revealed that independent determinants of the sVEGFR-2 level were lower age, male gender, presence of diabetes, absence of AF and anaemia, and higher levels of NT-proBNP (*Table S2*).

Incidence of outcomes and Cox regression analyses

During the 720 day follow-up, a total of 113 (11.0%) CV deaths, 211 (20.6%) all-cause deaths, 350 (34.2%) MACE, and 309 (30.2%) HF-related hospitalizations occurred (*Table 2*). *Figure 1* shows the cumulative incidence of outcomes and unadjusted Cox proportional HRs according to quartiles of sVEGFR-2. The patients with Quartile 1 sVEGFR-2 levels showed the greatest risks of CV death [*P* = 0.01; HR, 1.54; 95% confidence interval (CI), 0.96–2.51 (vs. Quartile 2); HR, 1.75; 95% CI, 1.07–2.91 (vs. Quartile 3); HR, 2.32; 95% CI, 1.37–4.09 (vs. quartile 4)] and all-cause death [*P* = 0.004; HR, 1.51; 95% CI, 1.06–2.18 (vs. Quartile 2); HR, 1.57; 95% CI, 1.09–2.26 (vs. Quartile 3); HR, 1.94; 95% CI, 1.32–2.87 (vs. quartile 4)], but did not show a significantly higher risk of MACE (*P* = 0.7) or HF-related hospitalization (*P* = 0.97) than the other quartile groups. In contrast, quartiles of VEGF were not significantly associated with the risk of CV death, all-cause death, MACE, or HF-related hospitalization (*Figure S2*). Because there was an apparent threshold effect between Quartile 1 and Quartile 2 in the incidence of all-cause death and CV death, sVEGFR-2 was modelled as a dichotomous variable in subsequent analyses by applying a threshold of Quartile 1 vs. Quartiles 2–4. In competing risk analyses, the patients with Quartile 1 sVEGFR-2 also showed significantly higher incidence of CV death than those with Quartiles 2–4 (HR, 1.77; 95% CI 1.21–2.56), but not that of MACE (HR, 1.13; 95% CI, 0.89–1.43) or HF-related hospitalization (HR, 1.00; 95% CI, 0.77–1.29) (*Figure S3*).

Figure 2 shows the unadjusted and adjusted HRs of low sVEGFR-2 levels below the 25th percentile for the various outcomes. After adjusting for traditional risk factors, a low sVEGFR-2 level below the 25th percentile was significantly associated with the risk of CV death, but not with the risk of all-cause death, MACE, or HF-related hospitalization (*Figure 2*, Model 1). After additional adjustment for other potential clinical confounders, a low sVEGFR-2 level below the 25th percentile was significantly associated with the risk of CV death, but not with the risk of all-cause death, MACE, or HF-related hospitalization (*Figure 2*, Model 2). Even after additional adjustment for medications for HF, these associations were consistent (*Figure 2*, Model 3). Importantly, after additional adjustment for established CV biomarkers, a low sVEGFR-2 level below the 25th percentile was significantly associated with the risk of CV death (HR, 1.79; 95% CI, 1.16–2.74) and all-cause death (HR, 1.43; 95% CI, 1.04–1.94), but not with the risk of MACE (HR, 1.11; 95% CI, 0.86–1.43) or HF-related hospitalization (HR, 1.03; 95% CI, 0.78–1.35) (*Figure 2*, Model 4, *Table S3*).

Subgroup analyses

Figure 3 shows the results of subgroup analyses on the association of low sVEGFR-2 below the 25th percentile with CV death and all-cause death. A low sVEGFR-2 level below the 25th percentile was significantly associated with all-cause death in men, but not in women. The risk for CV death tended to be higher in those with a low sVEGFR-2 level below the 25th percentile compared with those with a high sVEGFR-2 level in men (HR, 1.67; 95% CI, 0.95–2.86), but not in women (HR, 1.25; 95% CI, 0.63–2.38).

Interestingly, a low sVEGFR-2 level below the 25th percentile was significantly associated with CV death (HR, 1.76; 95% CI, 1.07–2.85) and all-cause death (HR, 1.49; 95% CI, 1.03–2.15) in the high-NT-proBNP (>50th percentile) group, but not with either CV death (HR, 1.33; 95% CI, 0.50–3.52) or all-cause death (HR, 1.07; 95% CI, 0.56–1.99) in the low-NT-proBNP group after adjustment for potential clinical confounders (*Figure 3*).

Figure S4 shows the results of Kaplan–Meier analysis based on the subgroups of EF category. A low sVEGFR-2 level below the 25th percentile was associated with CV death (HR, 1.99; 95% CI, 1.20–3.22) and all-cause death (HR, 1.78; 95% CI, 1.24–2.53) in patients with HFpEF/HFmrEF, but not in those

Table 2 Incidence of events according to quartiles of sVEGFR-2

Event	Entire cohort	Quartile 1	Quartile 2	Quartile 3	Quartile 4
CV death	113 (11.0)	41 (16.0)	28 (10.9)	25 (9.8)	19 (7.4)
All-cause death	211 (20.6)	72 (28.1)	50 (19.5)	49 (19.1)	40 (15.6)
MACE (CV death + HF hospitalization)	350 (34.2)	94 (36.7)	85 (33.2)	85 (33.2)	86 (33.6)
HF hospitalization	309 (30.2)	77 (30.1)	74 (28.9)	77 (30.1)	81 (31.6)

Variables are presented as numbers (percentages).
CV, cardiovascular; HF, heart failure; MACE, major adverse cardiovascular events defined as a composite of CV death and HF-related hospitalization; sVEGFR-2, soluble vascular endothelial growth factor receptor 2.

Figure 1 Incidence of CV death (A), all-cause death (B), MACE (C), and HF-related hospitalization (D) according to the quartiles of baseline sVEGFR-2 levels during the follow-up period. CI, confidence interval; CV, cardiovascular; HF, heart failure; HR, hazard ratio, MACE, major adverse cardiovascular events defined as a composite of CV death and HF-related hospitalization; Q, quartile; sVEGFR-2, soluble vascular endothelial growth factor receptor 2.

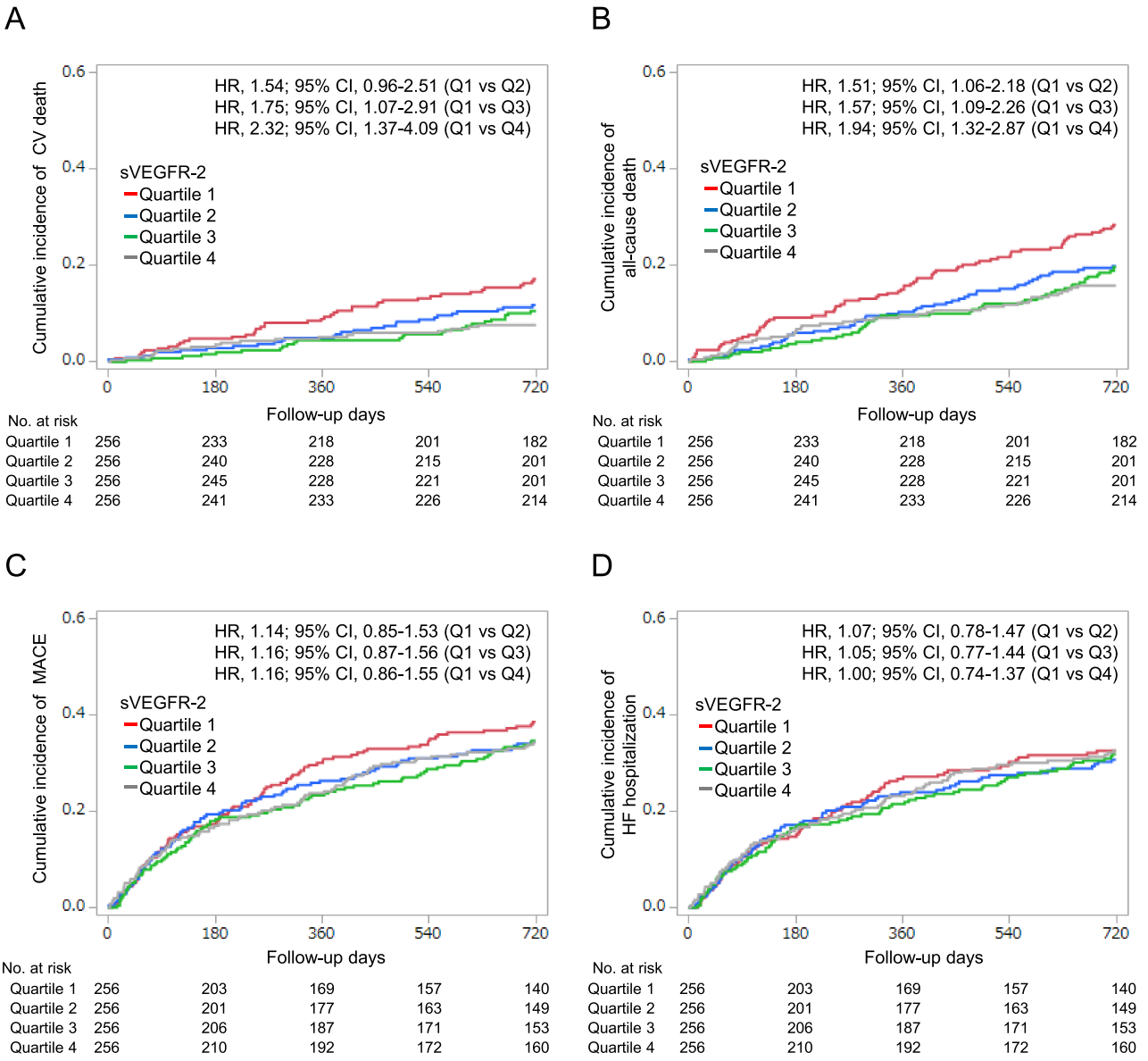

with HFrEF (HR for CV death, 1.29; 95% CI, 0.65–2.41; HR for all-cause death, 1.38; 95% CI, 0.84–2.21).

Figure S5 shows Kaplan–Meier analysis based on the aetiology of HF (ischaemic or non-ischaemic). A low sVEGFR-2 level below the 25th percentile was associated with CV death (HR, 1.99; 95% CI, 1.28–3.03) and all-cause death (HR, 1.66; 95% CI, 1.18–2.29) in patients with non-ischaemic aetiology, but not in those with ischaemic aetiology (HR for CV death, 0.43; 95% CI, 0.12–1.27; HR for all-cause death, 1.32; 95% CI, 0.66–2.54).

Risk stratification by NT-proBNP and sVEGFR-2

Figure 4 shows the cumulative incidence (A and B) and unadjusted and adjusted HRs (C) for CV death and all-cause death in patients divided into 4 groups based on the median of NT-proBNP and the 25th percentile of sVEGFR-2 levels. Notably, the high-NT-proBNP/low-sVEGFR-2 group exhibited the highest risks of CV death and all-cause death among the four groups, even after adjustment for potential clinical confounders and the established CV biomarkers (*Figure 4C*).

DOI: 10.1002/ehf2.13555

Figure 2 Multivariate Cox proportional hazard analysis for CV death, all-cause death, MACE, and HF-related hospitalization. Model 1: adjusted for age, sex, body mass index, and traditional cardiovascular risk factors (hypertension, diabetes, and dyslipidaemia), as well as established risk factors for HF [prior HF hospitalization, left ventricular dysfunction (ejection fraction < 40%), and NYHA class 3/4]. Model 2: adjusted for the covariates included in Model 1 and other CV risk factors (CAD, old myocardial infarction, AF, CKD, anaemia, chronic obstructive pulmonary disease, and cerebrovascular disease). Model 3: adjusted for the covariates included in Model 2 and prescription of RAS-I, beta blockers, loop diuretics, and MRA. Model 4: adjusted for the covariates included in Model 3 and CV biomarkers [NT-proBNP, hs-cTnI, and hs-CRP (>1 mg/L)]. AF, atrial fibrillation; BMI, body mass index; CAD, coronary artery disease; CKD, chronic kidney disease; hs-CRP, high sensitivity C-reactive protein; hs-cTnI, high sensitivity cardiac troponin I; MRA, mineral corticoid receptor antagonists; NT-proBNP, N-terminal pro-brain natriuretic peptide; RAS-I, renin angiotensin inhibitor. Other abbreviations are defined in *Figure 1*.

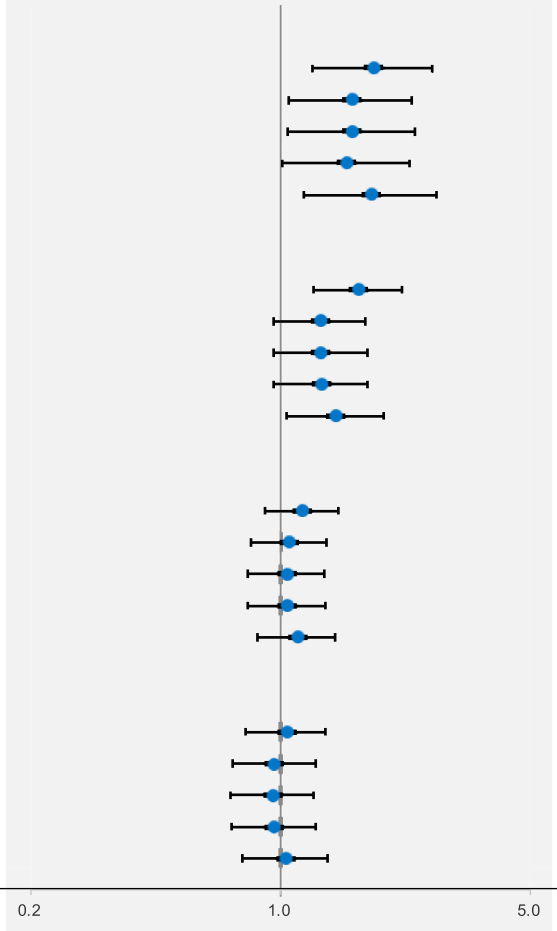

Outcomes	HR	95% CI Lower	95% CI Upper
CV death			
Unadjusted	1.82	1.23	2.65
Model-1	1.58	1.06	2.34
Model-2	1.59	1.05	2.37
Model-3	1.53	1.01	2.30
Model-4	1.79	1.16	2.74
All-cause death			
Unadjusted	1.65	1.24	2.19
Model-1	1.29	0.96	1.73
Model-2	1.30	0.95	1.75
Model-3	1.30	0.96	1.76
Model-4	1.43	1.04	1.94
MACE			
Unadjusted	1.15	0.91	1.45
Model-1	1.06	0.83	1.35
Model-2	1.04	0.81	1.33
Model-3	1.04	0.81	1.33
Model-4	1.11	0.86	1.43
HF hospitalization			
Unadjusted	1.04	0.80	1.34
Model-1	0.96	0.73	1.25
Model-2	0.95	0.73	1.24
Model-3	0.96	0.73	1.25
Model-4	1.03	0.78	1.35

These findings suggest the incremental prognostic value of sVEGFR-2 in combination with NT-proBNP in patients with CHF.

Discussion

This is the first dedicated and large-scale prospective cohort study to demonstrate that a low sVEGFR-2 level below the 25th percentile is significantly associated with the risk of CV and all-cause mortality in patients with CHF. These associations remain significant after adjustment for potential clinical confounders and the established CV biomarkers of NT-proBNP, hs-cTnI, and hs-CRP. Furthermore, the addition of a low sVEGFR-2 level below the 25th percentile to the model with potential clinical confounders significantly improved the prediction of CV and all-cause mortality in patients with high NT-proBNP levels. These findings suggest that the measurement of sVEGFR-2 provides prognostic information about CV and all-cause mortality beyond potential clinical confounders and the established CV biomarkers in clinical

Figure 3 Multivariate-adjusted stratified analyses of the associations of low sVEGFR-2 below the 25th percentile and the risks of CV death and all-cause death. Data were adjusted for the covariates included in Model 3 in *Figure 2*. *We divided the patients according to the median of NT-proBNP. EF, ejection fraction; LV, left ventricular. Other abbreviations are defined in *Figures 1* and *2*.

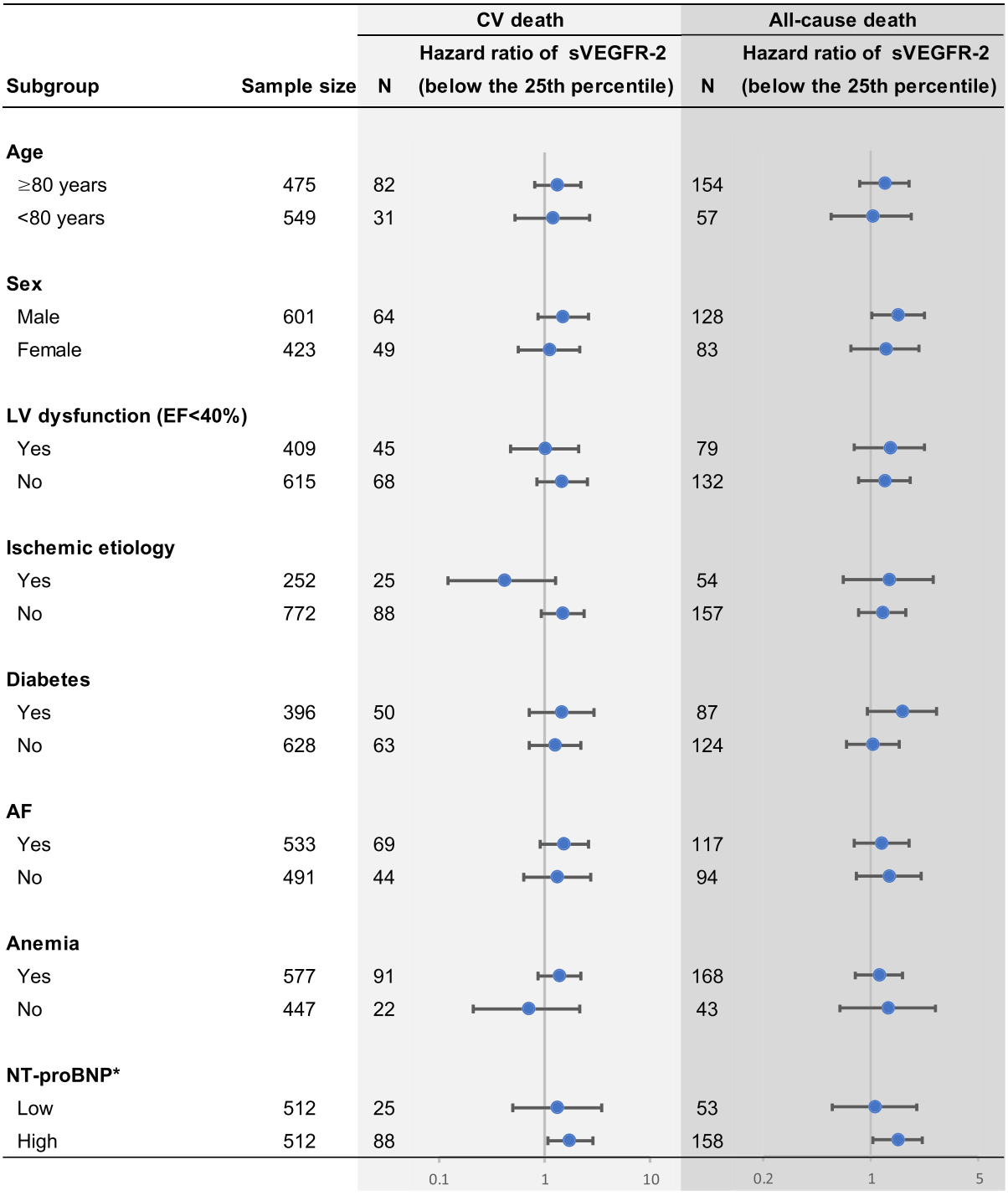

settings. The strengths of our investigation include the large sample size, multicentre prospective design, and high follow-up rate.

The underlying mechanism of the relationship between a low sVEGFR-2 value and poor prognosis in patients with CHF should be considered. VEGFR-2 is mainly expressed in

Figure 4 Incidence of CV death (A) and all-cause death (B) according to the combination of baseline sVEGFR-2 (lowest quartile) and NT-proBNP (above the median) levels during the follow-up period, and unadjusted and adjusted hazard ratios of the combination of sVEGFR-2 and NT-proBNP for CV death and all-cause death (C). The covariates included in each model are shown in *Figure 2*. Abbreviations are as defined in *Figures 1* and *2*.

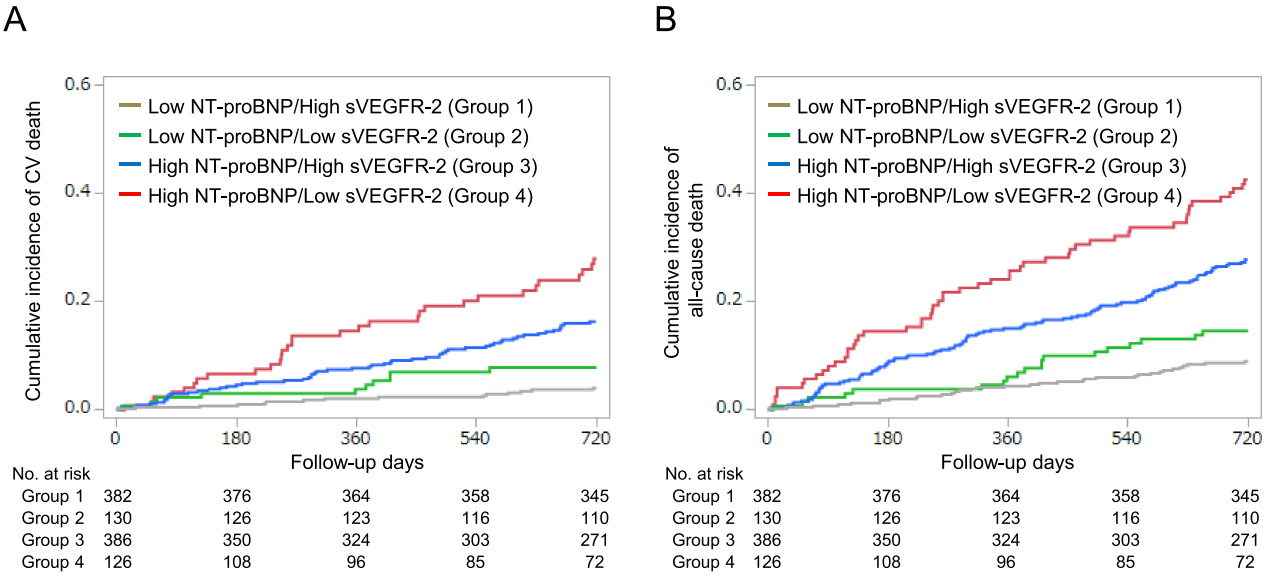

C

Subgroups	Hazard ratio for CV death	CV death HR	CV death 95% CI Lower	CV death 95% CI Upper	Hazard ratio for all-cause death	All-cause death HR	All-cause death 95% CI Lower	All-cause death 95% CI Upper
Unadjusted								
Low NT-proBNP/High sVEGFR-2		Reference				Reference		
Low NT-proBNP/Low sVEGFR-2		2.02	0.88	4.45		1.69	0.95	2.93
High NT-proBNP/High sVEGFR-2		4.25	2.47	7.78		3.45	2.37	5.16
High NT-proBNP/Low sVEGFR-2		7.87	4.32	14.98		5.94	3.88	9.22
Model 1								
Low NT-proBNP/High sVEGFR-2		Reference				Reference		
Low NT-proBNP/Low sVEGFR-2		1.53	0.66	3.41		1.19	0.66	2.07
High NT-proBNP/High sVEGFR-2		2.23	1.27	4.14		1.92	1.30	2.89
High NT-proBNP/Low sVEGFR-2		3.82	2.04	7.43		2.71	1.74	4.29
Model 2								
Low NT-proBNP/High sVEGFR-2		Reference				Reference		
Low NT-proBNP/Low sVEGFR-2		1.35	0.58	3.02		1.07	0.59	1.87
High NT-proBNP/High sVEGFR-2		1.65	0.93	3.12		1.58	1.06	2.42
High NT-proBNP/Low sVEGFR-2		2.93	1.55	5.78		2.33	1.48	3.71
Model 3								
Low NT-proBNP/High sVEGFR-2		Reference				Reference		
Low NT-proBNP/Low sVEGFR-2		1.23	0.52	2.77		1.07	0.59	1.88
High NT-proBNP/High sVEGFR-2		1.67	0.93	3.17		1.62	1.08	2.48
High NT-proBNP/Low sVEGFR-2		2.96	1.56	5.85		2.40	1.52	3.83
	0.1 1 10				0.1 1 10			

endothelial cells,[14] and a naturally occurring sVEGFR-2 was produced by proteolytic hydrolysis of membrane-bound VEGFR-2 or alternative splicing of VEGFR-2.[7,15] sVEGFR-2 protein and messenger RNA were found to be present in various tissues, including the skin, heart, spleen, kidney, ovary, and plasma in wild-type mice.[16] The VEGF/VEGFR-2 signalling pathway plays an important role in endothelial dysfunction,[17] which is one of the characteristic pathophysiological features of CHF.[18] Endothelium–cardiomyocyte interactions play essential roles in CV homeostasis; deranged endothelium-related signalling pathways have been implicated in the pathophysiology of HF.[19] A recent study demonstrated that cross talk between the endothelial VEGFR-2 and cardiomyocyte ErbB signalling pathways is required for adaptive cardiac

hypertrophy.[6] On the other hand, systemic vasoconstriction associated with endothelin dysfunction has been suggested to play a central role in HF pathogenesis: dysfunction of the endothelium leads to increased vascular stiffness and impaired arterial distensibility, augmenting myocardial damage.[20,21] Taken together, these findings indicate that a decrease in circulating sVEGFR-2 may reflect down-regulation of membrane-bound VEGFR-2 in cardiac and systemic endothelial cells, leading to a vulnerability to decompensated HF. Further investigation is necessary to clarify the mechanistic role of sVEGFR-2 in HF.

In the present study, the associations of low sVEGFR-2 with CV death and all-cause death were pronounced in patients with HFpEF. Not only cardiac microvascular rarefaction but also peripheral vascular dysfunction has been associated with impairment of cardiac reserve function in HFpEF.[22–25] These previous and our present findings may also support the idea that a low sVEGFR-2 reflects both cardiac and vascular endothelial dysfunction, leading to a deterioration of the prognosis in HFpEF.

The association between a low sVEGFR-2 value and all-cause death was significant in men, but not in women. The risk for CV death also tended to be higher in patients with low sVEGFR-2 compared with those with high sVEGFR-2 in men, but not in women. These results suggest the possibility of a sex difference in the pathophysiology of sVEGFR-2. Previous studies suggested a sex-based difference in the endogenous expression of VEGF.[26,27] Thus, systemic or CV expression of VEGF may affect the circulating sVEGFR-2 level and/or its association with prognosis in CHF. Future studies will be needed to define the mechanisms underlying the sex difference in the association between the sVEGFR-2 level and prognosis in CHF.

The associations of a low VEGFR-2 value with CV and all-cause deaths became prominent when adjusting for or stratifying based on NT-proBNP, a marker of increased left ventricular wall stress.[28] These findings may suggest that endothelial dysfunction itself does not lead to HF, but in combination with an increased left ventricular wall stress, it can lead to decompensated HF.

The VEGF/VEGFR2 signalling pathway plays a crucial role in tumour angiogenesis[29] as well as CV endothelial integrity. Since HF was subsequently noted in 2–4% of patients with cancers who were taking VEGF signalling pathway inhibitors,[30] it would be of interest to determine whether the sVEGFR-2 level can predict incident HF in combination with NT-proBNP among patients with cancer who are receiving VEGF signalling pathway inhibitors.

Study limitations

The present study has several limitations. First, the results were derived from a prospective observational study; therefore, they only reflect association and not causality. Second, the sources and the detailed physiological and pathological roles of sVEGFR-2 have not been elucidated.[7] Further investigations will be needed to answer these questions. Third, we did not repeatedly measure the sVEGFR-2 levels during the follow-up period. The predictive significance of a change in sVEGFR-2 levels in patients with HF is unclear. Fourth, we did not measure the levels of VEGF-C, a central regulator of lymphangiogenesis, and the other ligand for sVEGFR-2. Recently, we demonstrated that low VEGF-C is inversely and independently associated with the risk of all-cause mortality in patients with suspected or known coronary artery disease.[31] Future studies will define the prognostic value of VEGF-C in patients with CHF. Finally, because the PREHOSP-CHF study cohort consists exclusively of Asian individuals with HF, our results may not be generalizable to general Asian populations, or to other ethnic groups. Despite these limitations, the present study provides not only better risk stratification in patients with CHF but also deeper insight into the role of angiogenesis in the mechanisms of HF.

Conclusions

In a multicentre prospective cohort, a low sVEGFR-2 value was independently associated with CV death and all-cause death among patients with CHF, especially in those with high NT-proBNP levels.

Acknowledgements

We thank Mr Shuichi Ura, who substantially contributed to this work but passed away before this manuscript was drafted. We also thank the other members, co-operators, and participants of the PREHOSP-CHF study for their valuable contributions. The other members of the PREHOSP-CHF study group are listed in the Appendix of the Supporting Information.

The hs-cTnI values were measured at Abbott Japan LLC (Minato-ku, Tokyo, Japan).

Conflict of interest

None of the authors has any relationship relevant to the content of this paper to disclose.

Funding

The PREHOSP-CHF study is supported by a Grant-in-Aid for Clinical Research from the National Hospital Organization.

Supporting information

Additional supporting information may be found online in the Supporting Information section at the end of the article.

Figure S1. Distribution of the sVEGFR-2 levels. sVEGFR-2 = soluble vascular endothelial growth factor receptor 2.

Figure S2. Incidence of CV death (A), all-cause death (B), MACE (C), and HF-related hospitalization (D) according to the quartiles of baseline VEGF levels during the follow-up period. VEGF = vascular endothelial growth factor, CV = cardiovascular, MACE = major adverse cardiovascular events defined as a composite of CV death and HF-related hospitalization, HF = heart failure, HR = hazard ratio, CI = confidence interval.

Figure S3. Competing risk of death adjusted cumulative hazard curves for incident CV death (A), MACE (B), and HF-related hospitalization (C) in patients with and without low sVEGFR-2 levels below the 25th percentile during the follow-up period. sVEGFR-2 = soluble vascular endothelial growth factor receptor 2, CV = cardiovascular, MACE = major adverse cardiovascular events defined as a composite of CV death and HF-related hospitalization, HF = heart failure, HR = hazard ratio, CI = confidence interval.

Figure S4. Incidence of CV death (A) and all-cause death (B) between patients with and those without low sVEGFR-2 levels below the 25th percentile in the HFpEF/mrEF and HFrEF groups. Adjusted HR was calculated using the covariates included in model 3. sVEGFR-2 = soluble vascular endothelial growth factor receptor 2, CV = cardiovascular, HR = hazard ratio, CI = confidence interval, HF = heart failure, HFpEF = HF with preserved ejection fraction (EF), HFmrEF = HF with mid-range EF, HFrEF = HF with reduced EF.

Figure S5. Incidence of CV death (A) and all-cause death (B) between patients with and those without low sVEGFR-2 levels below the 25th percentile in the groups with HF with ischemic etiology and HF with non-ischemic etiology. Adjusted HR was calculated using the covariates included in model 3. sVEGFR-2 = soluble vascular endothelial growth factor receptor 2, CV = cardiovascular, HR = hazard ratio, CI = confidence interval, HF = heart failure.

Table S1. Baseline characteristics according to quartiles of sVEGFR-2.

Table S2. Simple and stepwise multiple regression analyses for the sVEGFR-2 level.

Table S3. Multiple Cox proportional hazard analysis for clinical outcomes.

References

1. Roger VL. Epidemiology of heart failure. *Circ Res.* 2013; **113**: 646–659.
2. Oka T, Akazawa H, Naito AT, Komuro I. Angiogenesis and cardiac hypertrophy. *Circ Res.* 2014; **114**: 565–571.
3. Shiojima I, Sato K, Izumiya Y, Schiekofer S, Ito M, Liao R, Colucci WS, Walsh K. Disruption of coordinated cardiac hypertrophy and angiogenesis contributes to the transition to heart failure. *J Clin Invest.* 2005; **115**: 2108–2118.
4. Izumiya Y, Shiojima I, Sato K, Sawyer DB, Colucci WS, Walsh K. Vascular endothelial growth factor blockade promotes the transition from compensatory cardiac hypertrophy to failure in response to pressure overload. *Hypertension.* 2006; **47**: 887–893.
5. Taimeh Z, Loughran J, Birks EJ, Bolli R. Vascular endothelial growth factor in heart failure. *Nat Rev Cardiol.* 2013; **10**: 519–530.
6. Kivelä R, Hemanthakumar KA, Vaparanta K, Robciuc M, Izumiya Y, Kidoya H, Takakura N, Peng X, Sawyer DB, Elenius K, Walsh K, Alitalo K. Endothelial cells regulate physiological cardiomyocyte growth via VEGFR2-mediated paracrine signaling. *Circulation.* 2019; **139**: 2570–2584.
7. Stevens M, Oltean S. Modulation of receptor tyrosine kinase activity through alternative splicing of ligands and receptors in the VEGF-A/VEGFR Axis. *Cells.* 2019; **8**: 288.
8. Abou-Fayçal C, Hatat AS, Gazzeri S, Eymin B. Splice variants of the RTK family: their role in tumour progression and response to targeted therapy. *Int J Mol Sci* 2017; **18**: 383.
9. Ebos JM, Bocci G, Man S, Thorpe PE, Hicklin DJ, Zhou D, Jia X, Kerbel RS. A naturally occurring soluble form of vascular endothelial growth factor receptor 2 detected in mouse and human plasma. *Mol Cancer Res.* 2004; **2**: 315–326.
10. Sallinen H, Heikura T, Koponen J, Kosma VM, Heinonen S, Ylä-Herttuala S, Anttila M. Serum angiopoietin-2 and soluble VEGFR-2 levels predict malignancy of ovarian neoplasm and poor prognosis in epithelial ovarian cancer. *BMC Cancer.* 2014; **14**: 696.
11. Jantus-Lewintre E, Sanmartín E, Sirera R, Blasco A, Sanchez JJ, Tarón M, Rosell R, Camps C. Combined VEGF-A and VEGFR-2 concentrations in plasma: diagnostic and prognostic implications in patients with advanced NSCLC. *Lung Cancer.* 2011; **74**: 326–331.
12. Ebos JM, Lee CR, Bogdanovic E, Alami J, Van Slyke P, Francia G, Xu P, Mutsaers AJ, Dumont DJ, Kerbel RS. Vascular endothelial growth factor-mediated decrease in plasma soluble vascular endothelial growth factor receptor-2 levels as a surrogate biomarker for tumor growth. *Cancer Res.* 2008; **68**: 521–529.
13. Wada H, Ura S, Kitaoka S, Satoh-Asahara N, Horie T, Ono K, Takaya T, Takanabe-Mori R, Akao M, Abe M, Morimoto T, Murayama T, Yokode M, Fujita M, Shimatsu A, Hasegawa K. Distinct characteristics of circulating vascular endothelial growth factor-a and C levels in human subjects. *PLoS One.* 2011; **6**: e29351.
14. Abhinand CS, Raju R, Soumya SJ, Arya PS, Sudhakaran PR. VEGF-A/VEGFR2 signaling network in endothelial cells relevant to angiogenesis. *J Cell Commun Signal* 2016; **10**: 347–354.
15. Albuquerque RJC, Hayashi T, Cho WG, Kleinman ME, Dridi S, Takeda A, Baffi JZ, Yamada K, Kaneko H, Green MG, Chappell J, Wilting J, Weich HA, Yamagami S, Amano S, Mizuki N, Alexander JS, Peterson ML, Brekken RA, Hirashima M, Capoor S, Usui T, Ambati BK, Ambati J. Alternatively spliced vascular endothelial growth factor receptor-2 is an essential endogenous inhibitor of lymphatic vessel growth. *Nat Med.* 2009; **15**: 1023–1030.
16. Pavlakovic H, Becker J, Albuquerque R, Wilting J, Ambati J. Soluble VEGFR-2:

an antilymphangiogenic variant of VEGF receptors. *Ann N Y Acad Sci.* 2010; **1207**: E7–E15.
17. Kliche S, Waltenberger J. VEGF receptor signaling and endothelial function. *IUBMB life.* 2001; **52**: 61–66.
18. Alem MM. Endothelial dysfunction in chronic heart failure: assessment, findings, significance, and potential therapeutic targets. *Int J Mol Sci* 2019; **20**: 3198.
19. Lim SL, Lam CS, Segers VF, Brutsaert DL, De Keulenaer GW. Cardiac endothelium-myocyte interaction: clinical opportunities for new heart failure therapies regardless of ejection fraction. *Eur Heart J.* 2015; **36**: 2050–2060.
20. Marti CN, Gheorghiade M, Kalogeropoulos AP, Georgiopoulou VV, Quyyumi AA, Butler J. Endothelial dysfunction, arterial stiffness, and heart failure. *J Am Coll Cardiol.* 2012; **60**: 1455–1469.
21. Redfield MM, Jacobsen SJ, Borlaug BA, Rodeheffer RJ, Kass DA. Age- and gender-related ventricular-vascular stiffening: a community-based study. *Circulation.* 2005; **112**: 2254–2262.
22. Mohammed SF, Hussain S, Mirzoyev SA, Edwards WD, Maleszewski JJ, Redfield MM. Coronary microvascular rarefaction and myocardial fibrosis in heart failure with preserved ejection fraction. *Circulation.* 2015; **131**: 550–559.
23. Kishimoto S, Kajikawa M, Maruhashi T, Iwamoto Y, Matsumoto T, Iwamoto A, Oda N, Matsui S, Hidaka T, Kihara Y, Chayama K, Goto C, Aibara Y, Nakashima A, Noma K, Higashi Y. Endothelial dysfunction and abnormal vascular structure are simultaneously present in patients with heart failure with preserved ejection fraction. *Int J Cardiol.* 2017; **231**: 181–187.
24. Lyle MA, Brozovich FV. HFpEF, a disease of the vasculature: a closer look at the other half. *Mayo Clin Proc.* 2018; **93**: 1305–1314.
25. Cuijpers I, Simmonds SJ, van Bilsen M, Czarnowska E, González Miqueo A, Heymans S, Kuhn AR, Mulder P, Ratajska A, Jones EAV, Brakenhielm E. Microvascular and lymphatic dysfunction in HFpEF and its associated comorbidities. *Basic Res Cardiol.* 2020; **115**: 39.
26. Crisostomo PR, Wang M, Herring CM, Markel TA, Meldrum KK, Lillemoe KD, Meldrum DR. Gender differences in injury induced mesenchymal stem cell apoptosis and VEGF, TNF, IL-6 expression: role of the 55 kDa TNF receptor (TNFR1). *J Mol Cell Cardiol.* 2007; **42**: 142–149.
27. Malamitsi-Puchner A, Tziotis J, Tsonou A, Protonotariou E, Sarandakou A, Creatsas G. Changes in serum levels of vascular endothelial growth factor in males and females throughout life. *J Soc Gynecol Investig.* 2000; **7**: 309–312.
28. Richards M, Troughton RW. NT-proBNP in heart failure: therapy decisions and monitoring. *Eur J Heart Fail.* 2004; **6**: 351–354.
29. Carmeliet P. VEGF as a key mediator of angiogenesis in cancer. *Oncology.* 2005; **69**: 4–10.
30. Dobbin SJH, Cameron AC, Petrie MC, Jones RJ, Touyz RM, Lang NN. Toxicity of cancer therapy: what the cardiologist needs to know about angiogenesis inhibitors. *Heart.* 2018; **104**: 1995–2002.
31. Wada H, Suzuki M, Matsuda M, Ajiro Y, Shinozaki T, Sakagami S, Yonezawa K, Shimizu M, Funada J, Takenaka T, Morita Y, Nakamura T, Fujimoto K, Matsubara H, Kato T, Unoki T, Takagi D, Ura S, Wada K, Iguchi M, Masunaga N, Ishii M, Yamakage H, Shimatsu A, Kotani K, Satoh-Asahara N, Abe M, Akao M, Hasegawa K. VEGF-C and mortality in patients with suspected or known coronary artery disease. *J Am Heart Assoc* 2018; **7**: e010355.

JJCO Japanese Journal of Clinical Oncology

Japanese Journal of Clinical Oncology, 2021, 51(10)1523–1533
https://doi.org/10.1093/jjco/hyab104
Advance Access Publication Date: 13 July 2021
Original Article

OXFORD

Original Article

Cancer-related FGFR2 overexpression and gene amplification in Japanese patients with gastric cancer

Keiko Minashi[1], Takeshi Yamada[2], Hisashi Hosaka[3], Kenji Amagai[4], Yoshiaki Shimizu[5], Hirokazu Kiyozaki[6], Mikio Sato[7], Atsuko Soeda[8], Shinji Endo[9], Hiroyasu Ishida[10], Toshiro Kamoshida[11], Yoshinori Sakai[12], and Kohei Shitara[13]

[1]Clinical Trial Promotion Department, Chiba Cancer Center, Chiba, Japan, [2]Department of Gastroenterology, University of Tsukuba Hospital, Tsukuba, Japan, [3]Department of Gastroenterology, Gunma Prefectural Cancer Center, Ota, Japan, [4]Department of Gastroenterology, Ibaraki Prefectural Central Hospital, Ibaraki Cancer Center, Kasama, Japan, [5]Department of Surgery, Narita Red Cross Hospital, Narita, Japan, [6]Department of Surgery, Saitama Medical Center, Jichi Medical University, Saitama, Japan, [7]Department of Gastroenterology, Ryugasaki Saiseikai Hospital, Ryuugasaki, Japan, [8]Department of Gastroenterology, Tsukuba Memorial Hospital, Tsukuba, [9]Department of Gastroenterology and Hepatology, Shinmatsudo Central General Hospital, Matsudo, Japan, [10]Department of Gastroenterology, National Health Organization, Mito Medical Center, Ibaraki, Japan, [11]Department of Gastroenterology, Hitachi, Ltd., Hitachi General Hospital, Hitachi, Japan, [12]Department of Gastroenterology, Tsuchiura Kyodo General Hospital, Tsuchiura, Japan and [13]Department of Gastrointestinal Oncology, National Cancer Center Hospital East, Kashiwa, Japan

*For reprints and all correspondence: Keiko Minashi, Clinical Trial Promotion Department, Chiba Cancer Center, 666-2 Nitona-cho Chuo-ku Chiba, 260-8717 Japan. E-mail: kminashi@chiba-cc.jp

Received 1 February 2021; Editorial Decision 10 June 2021; Accepted 18 June 2021

Abstract

Objective: Fibroblast growth factor receptor 2 (FGFR2) has been proposed as a novel druggable target in unresectable gastric cancer. FGFR2 alteration has been reported as associated with poor prognosis even in patients with gastric cancer who received systemic chemotherapy. This study aimed to evaluate the frequency of FGFR2 overexpression and gene amplification in clinical specimens from Japanese patients with recurrent or unresectable gastric cancer.

Methods: This observational study enrolled patients who were histologically or cytologically confirmed with unresectable HER2-negative or unknown gastric or gastroesophageal junctional adenocarcinoma treated with at least one previous chemotherapy. FGFR2 overexpression and gene amplification in the specimens were evaluated by immunohistochemical staining and fluorescence *in situ* hybridization methods, respectively.

Results: In a total of 173 eligible cases, FGFR2 immunohistochemistry score was evaluated as 0, 1, 2, 3 and 4 for 20, 80, 35, 28 and 10 cases, respectively. In 151 evaluable cases with FGFR2 immunohistochemistry scores of 1–4, *FGFR2* copy number expressed as fluorescence *in situ* hybridization signals were detected as <4, $\geq 4 < 10$ and ≥ 10 copies for 123, 16 and 12 cases, respectively. *FGFR2* copy number showed an increasing tendency along with higher FGFR2 immunohistochemistry scores in the corresponding specimen. The response rate and time to treatment failure for first line chemotherapy did not have any obvious relationship to FGFR2 immunohistochemistry score and *FGFR2* copy number.

Conclusions: Although FGFR2 overexpression and gene amplification were shown in Japanese patients with unresectable gastric cancer, these alterations did not impact the effects of cytotoxic agents as first line chemotherapy.

Key words: FGFR2 overexpression, FGFR2 gene amplification, gastric cancer, immunohistochemical staining, fluorescent *in situ* hybridization

Introduction

Gastric cancer (GC) is the fifth most prevalent cancer and the third leading cause of cancer-related death worldwide (1). Although surgery is the treatment of choice for GC, prognosis with advanced GC is still poor (2). It has been reported that 22–51% of GC patients who received radical surgery with curative intent develop recurrent disease (3,4). In patients with unresectable advanced or recurrent lesions, systemic chemotherapy can prolong median survival time to 13–14 months (5,6). Trastuzumab in patients with HER2-positive advanced GC, and an antiangiogenic agent (ramucirumab) and immune checkpoint inhibitors (nivolumab and pembrolizumab) introduced as later-line therapy in non-selective patients with metastatic GC have demonstrated modest survival benefits (7–12). Despite improved outcomes with these targeted molecular therapies, however, prognosis with advanced GC still remains wanting, and there is a critical need to develop more efficacious therapeutic agents.

The fibroblast growth factor (FGF)/FGF receptor (FGFR) signaling axis plays an important role in normal organ, vascular and skeletal development. On the other hand, activating *FGFR* gene abnormalities are reported in various tumor types, in which many of these *FGFR* abnormalities are considered a driving event (13–15). Genetic modifications or overexpression of FGFRs have been associated with tumorigenesis and disease progression in breast, lung, gastric, hematologic and other malignancies. The cancer types known to be connected to genetic abnormalities in FGFR include breast cancer [*FGFR1* and *FGFR2* gene amplifications at an incidence of 10 and ~1%, respectively; (16)], squamous cell lung cancer [*FGFR1* gene amplifications at an incidence of 20%; (17)], endometrial cancer [*FGFR2* activating mutation at an incidence of 12%; (16)], intrahepatic cholangiocarcinoma [*FGFR2* gene fusions at an incidence of 14%; (18)], bladder cancer [*FGFR3* activating mutation at an incidence of 50–60% for non-muscle invasive type; (16)], myeloma [*FGFR3* translocation at an incidence of 15%; (16)] and glioma [*FGFR3* gene fusions at an incidence of 8%; (19)]. It has also been reported that *FGFR2* gene amplification and FGFR2 overexpression is found in 1.8–15% (20) and 2.5–61.4% (21) of GC, respectively, and is associated with poor prognosis (22,23). In cases with diffuse type GC, up to a 10% incidence of *FGFR2* gene amplification in those with relatively poor prognosis has been reported (15). It has also been reported that *FGFR2* and *HER2* gene amplifications are mutually exclusive (24). Therefore, *FGFR2* amplification has attracted significant interest as a therapeutic target for *FGFR2*-amplified GC, and several development projects are ongoing (25). In this context, clarifying the frequency of *FGFR2* gene amplification and FGFR2 overexpression in GC may greatly contribute to the development of *FGFR2* inhibitors as a novel therapeutic option. To illuminate the significance of developing *FGFR2* inhibitors for GC, we aimed in this study to find the frequency of *FGFR2* gene amplification and FGFR2 overexpression in clinical specimens from HER2 negative/unknown Japanese patients with recurrent or unresectable GC.

Patients and methods

Study design

This study was a multicenter observational study.

Study population

This study included patients who were diagnosed with unresectable gastric or gastroesophageal junctional adenocarcinoma confirmed by histological or cytological methods. Patients who were diagnosed either to be seen as refractory for at least one systemic chemotherapy or as recurrent during or within 6 months after postoperative adjuvant chemotherapy/chemoradiation therapy were eligible. The other criteria for eligibility were as follows: (i) negative or unknown for HER2/neu status, (ii) age $\geq$ 20 years at written informed consent before enrollment in this study and (iii) clinical GC specimens at diagnosis or surgical resection were available. Patients whom the investigator judged to be ineligible for this study were excluded. It has been reported that *FGFR2* and *HER2* gene amplifications are almost always mutually exclusive (24), so we excluded HER2 positive patients to focus on *FGFR2* amplification in this study.

The World Medical Association Declaration of Helsinki on medical research protocols and ethics was followed throughout the study. Authorization for the use of the clinical specimens for research purposes was obtained from the institutional review board at each study location.

Study data collection on chemotherapy

In this study, we collected (regimen, duration, efficacy, etc.) data on only one regimen of chemotherapy received first after a diagnosis of unresectable or recurrent GC. Response rates and time to treatment failure (TTF) for chemotherapy prior to enrollment were calculated from case report data extracted from background medical records for each case with first line chemotherapy. Cases with first line chemotherapy were defined as those who had: non-curative resection, received first line chemotherapy and had first line chemotherapy data (on regimens, duration, efficacy, etc.); those who received first line chemotherapy and had first line chemotherapy data (on regimens, duration, efficacy, etc.); those who had curative resection but did not receive adjuvant chemotherapy, had recurrence, received first line chemotherapy and had first line chemotherapy data (on regimens, duration, efficacy, etc.) and; those who had curative resection and recurrence 6 months after adjuvant chemotherapy, received first line chemotherapy and had first line chemotherapy data (on regimens, duration, efficacy, etc.).

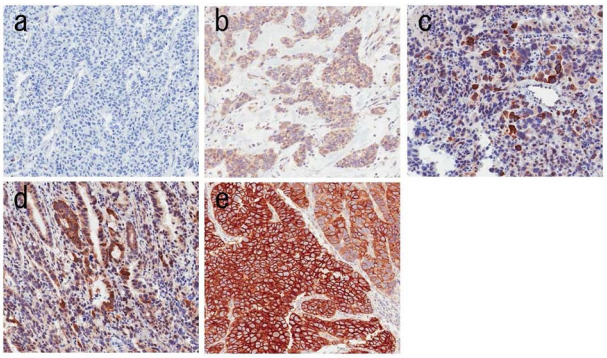

Figure 1. Representative immunohistochemical (IHC) images for the expression of fibroblast growth factor receptor 2 (FGFR2) protein in the gastric cancer clinical specimens in this study. Images a, b, c, d and e show IHC score expressions of 0, 1, 2, 3 and 4, respectively. See text for score definitions. Magnification: ×20 objective.

FGFR2 immunohistochemistry

To evaluate FGFR2 protein expression, immunohistochemistry (IHC) staining was performed using rabbit anti-FGFR2 polyclonal antibody (FGFR2 IHC kit, Nichirei Biosciences Inc., Tokyo, Japan) with 4 μm sections from formalin-fixed and paraffin-embedded tumor specimens. The staining intensity of each tumor cell and proportion of tumor cells with FGFR2 overexpression in each section was scored by two independent observers as follows: Score 0, <10% of tumor cells expressed weakly with FGFR2 but none expressed highly; Score 1, ≥10% of tumor cells expressed weakly with FGFR2 but none expressed highly; Score 2, <10% of tumor cells expressed highly with FGFR2; Score 3, ≥10%—<50% of tumor cells expressed highly with FGFR2 and Score 4, ≥50% of tumor cells expressed highly with FGFR2 (Fig. 1). The percentage of positive FGFR2 cells was calculated based on the positive area of the tumor cell region. The strong expression ant weak expression was evaluated based on the stainability of the core with strong expression and weak expression of CBA (cell block array) determined in the validation test.

FGFR2 fluorescence *in situ* hybridization

To evaluate *FGFR2* gene amplification, we used the fluorescence *in situ* hybridization (FISH) method with the 4 μm serial sections from the tumor specimens used for IHC examination. For this analysis, we used the tumor specimens with FGFR2 IHC scores of 1–4 because it is known that a tumor specimen with a IHC score of 0 rarely shows *FGFR2* gene amplification (26). More specifically, a human *FGFR2* gene probe prepared from genomic sequences of bacterial artificial chromosome clones RP11-7P17 and RP11-62L18 using *FGFR2* reverse and forward primer genes (Hokkaido System Science Co., Ltd., Sapporo, Japan) was fluorescently labeled in orange by nick translation. A human centromere 10 (CEP 10) gene probe (Vysis CEP 10 SpectrumGreen Probe, Abbott Molecular Inc., Des Plaines, USA) as reference, since the *FGFR2* gene is localized on human chromosome 10, was fluorescently labeled in green. After hybridization, single sets of 20 tumor cells in each section were evaluated for their average number of *FGFR2* signals and CEP 10 signals per tumor cell by two independent observers. A ratio of *FGFR2* signals to CEP 10 signals (FGFR2/CEP10) was calculated for each section. A representative FISH image of the *FGFR2* signals is shown in Fig. 2.

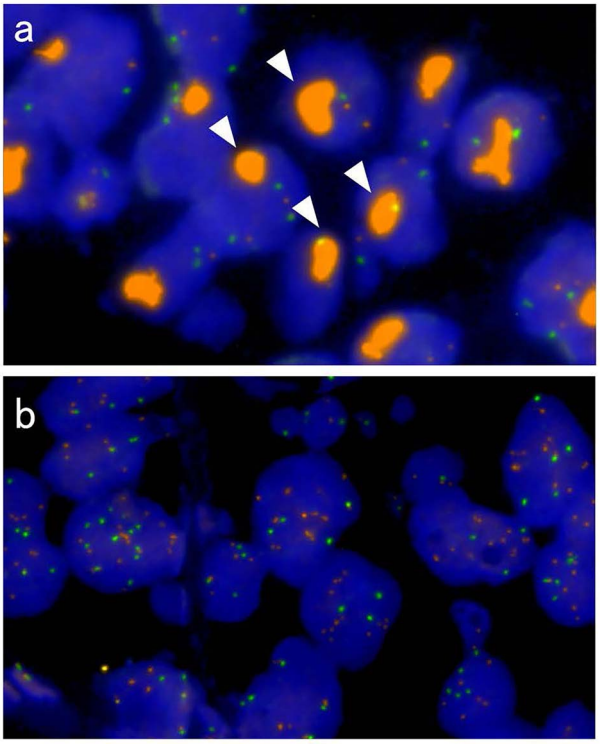

Figure 2. Representative FGFR2 fluorescence *in situ* hybridization (FISH) image in the clinical specimen of gastric cancer in this study. Each orange fluorescence image represented FGFR2 gene. (a) This figure showed 40 FGFR2 signals per tumor cell as well as clusters of FGFR2 signals (triangle arrows show representative examples). (b) This figure showed 13 FGFR2 signals per tumor cell.

Statistical analysis

Statistical significance in the distribution of baseline characteristics according to the FGFR2 IHC score or *FGFR2* copy number expressed by FISH signals per tumor cell was analyzed by χ^2-test or Fisher's exact test with $P < 0.05$ for the two-side significance level. In cases having data on TTF and best response with first line chemotherapy prior to enrollment, Kaplan–Meier plots for the TTF were drawn according to the FGFR2 IHC score or *FGFR2* copy number, and significance between the plots was analyzed using Logrank tests.

Results

Disposition and characteristics of cases

Among a total of 176 cases were enrolled maximally during the enrollment period from June 2018 to March 2020 (defined as the full analysis set, FAS); 3 cases did not meet inclusion criteria and were excluded, with the remaining 173 cases being defined as the per protocol set (PPS). Within the PPS, 140 cases having data with which to calculate TTF for a first line chemotherapy regimen just prior to enrollment were defined as the first line chemotherapy set (FLCS) (Table 1 and Fig. 3).

The primary analysis set was the PPS, consisting of 132 (76.3%) males and 41 (23.7%) females. Mean ± standard deviation for age was 67.4 ± 10.1 years (range 34–83 years). In the PPS, 92 cases (53.2%) had a primary tumor lesion at the enrollment. Primary tumors were located in the upper stomach (41 cases, 23.7%), middle

Table 1. Structured analysis population proportions: FGFR2 IHC score

Analysis set	FGFR2 by IHC					Total
	Score 0	Score 1	Score 2	Score 3	Score 4	
All enrolled patients	21	82	35	28	10	176
PPS	20 (95.2%)	80 (97.6%)	35 (100.0%)	28 (100.0%)	10 (100.0%)	173 (98.3%)
Patients excluded from PPS	1 (4.8%)	2 (2.4%)	0 (0.0%)	0 (0.0%)	0 (0.0%)	3 (1.7%)
FLCS	13 (61.9%)	65 (79.3%)	29 (82.9%)	24 (85.7%)	9 (90.0%)	140 (79.5%)

Abbreviations: PPS, per protocol set; FLCS, first line chemotherapy set.

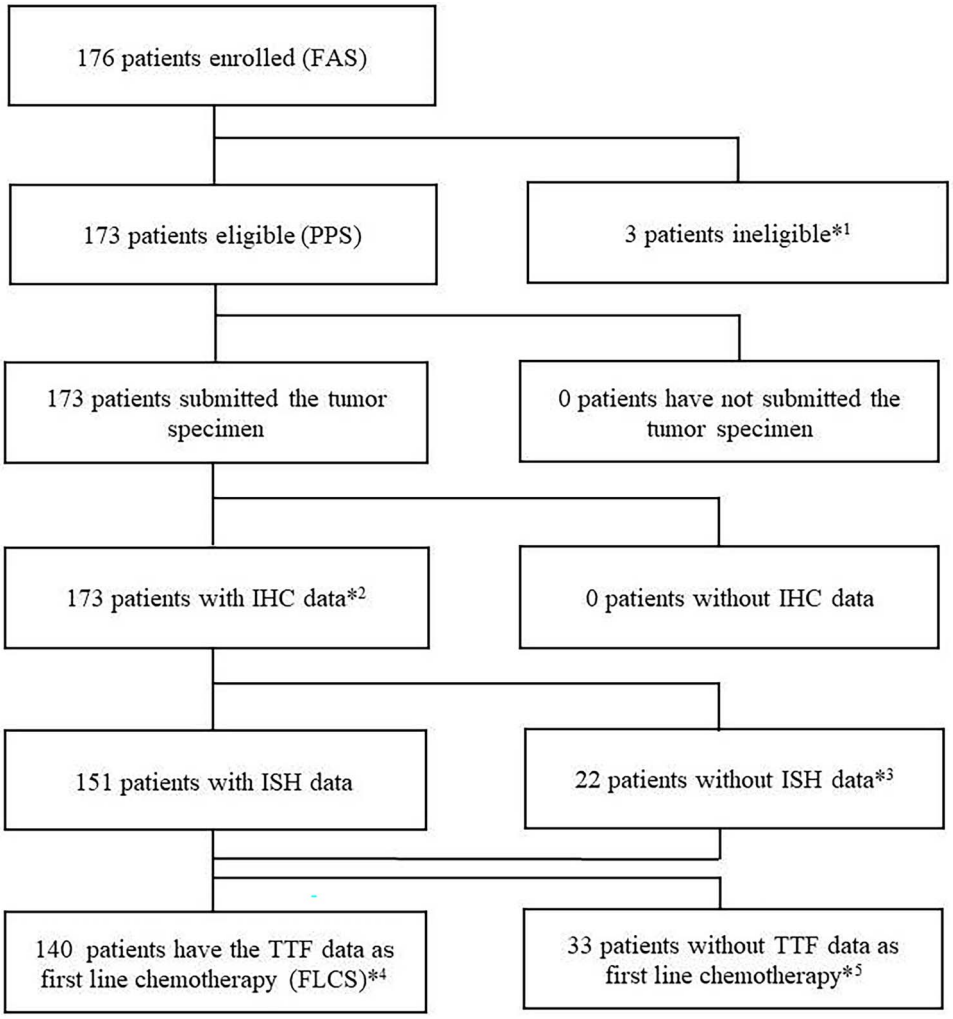

Figure 3. Patients flow diagram. FAS, full analysis set; PPS, per protocol set; FLCS, first line chemotherapy set; IHC, immunohistochemistry; ISH, *in situ* hybridization; TTF, time to treatment failure. *1 One patient was excluded from PPS due to deviation of inclusion criteria, 'after primary chemotherapy'. Two patients were excluded from PPS due to deviation of inclusion criteria, 'the patient obtained written informed consent form'. *2 Patients with IHC score 0, 1, 2, 3 or 4. *3 Twenty patients with IHC score 0 and 2 patients with IHC score 1, 2, 3 or 4 who have no ISH data due to specimen failure. *4 FLCS was composed with patients who had: non-curative resection, received first line chemotherapy and had first line chemotherapy data (on regimens, duration, efficacy, etc.); those who received first line chemotherapy and had first line chemotherapy data (on regimens, duration, efficacy, etc.); those who had curative resection but did not receive adjuvant chemotherapy, had recurrence, received first line chemotherapy and had first line chemotherapy data (on regimens, duration, efficacy, etc.) and; those who had curative resection and recurrence 6 months after adjuvant chemotherapy, received first line chemotherapy and had first line chemotherapy data (on regimens, duration, efficacy, etc.). *5 Thirty-three patients were excluded from FLCS for the following reasons. Two patients had no data for the duration of first line chemotherapy. Thirty-one patients had curative resection and recurrence during adjuvant chemotherapy or within 6 months after adjuvant chemotherapy, received second line chemotherapy.

stomach (49 cases, 28.3%), lower stomach (62 cases, 35.8%), esophagogastric junction (16 cases, 9.2%) or other (5 cases, 2.9%). Tumor specimens for 168 cases (97.1%) were from a primary lesion and the remaining 5 (2.9%) from a metastatic lesion. The most frequent histological types were: poorly differentiated adenocarcinoma (75 cases, 89.3%); signet ring cell carcinoma (7 cases, 8.3%) and mucinous

Table 2. Baseline characteristics of cases according to FGFR2 IHC score

Category		FGFR2 by IHC					Total	*P* value*	99% CI**
		Score 0	Score 1	Score 2	Score 3	Score 4			
N									
		20	80	35	28	10	173		
Age (years)									
	Mean	65.2	67.6	66.0	69.3	69.4	67.4		
	Std	11.7	9.6	12.9	6.2	9.1	10.1		
	Min	34	42	35	49	47	34		
	Median	66.5	69	70	69.5	71.5	69		
	Max	80	83	83	79	80	83		
Age category (years)									
	<65	7 (35.0%)	26 (32.5%)	12 (34.3%)	5 (17.9%)	2 (20.0%)	52 (30.1%)	0.5323	
	≧65	13 (65.0%)	54 (67.5%)	23 (65.7%)	23 (82.1%)	8 (80.0%)	121 (69.9%)		
Gender									
	Male	7 (35.0%)	64 (80.0%)	27 (77.1%)	25 (89.3%)	9 (90.0%)	132 (76.3%)	0.0004	
	Female	13 (65.0%)	16 (20.0%)	8 (22.9%)	3 (10.7%)	1 (10.0%)	41 (23.7%)		
Primary tumor (at registration)									
	Yes	8 (40.0%)	42 (52.5%)	18 (51.4%)	16 (57.1%)	8 (80.0%)	92 (53.2%)	0.3528	
	No	12 (60.0%)	38 (47.5%)	17 (48.6%)	12 (42.9%)	2 (20.0%)	81 (46.8%)		
Primary site									
	Upper stomach	5 (25.0%)	17 (21.3%)	12 (34.3%)	6 (21.4%)	1 (10.0%)	41 (23.7%)	0.2382	[0.2272, 0.2492]
	Middle stomach	8 (40.0%)	26 (32.5%)	7 (20.0%)	7 (25.0%)	1 (10.0%)	49 (28.3%)		
	Lower stomach	6 (30.0%)	26 (32.5%)	13 (37.1%)	13 (46.4%)	4 (40.0%)	62 (35.8%)		
	Esophagogastric junction	0 (0.0%)	9 (11.3%)	3 (8.6%)	2 (7.1%)	2 (20.0%)	16 (9.2%)		
	Others	1 (5.0%)	2 (2.5%)	0 (0.0%)	0 (0.0%)	2 (20.0%)	5 (2.9%)		
Main tissue type									
	Diffuse type	13 (65.0%)	39 (48.8%)	16 (45.7%)	11 (39.3%)	5 (50.0%)	84 (48.6%)	0.0567	
	Intestinal type	3 (15.0%)	38 (47.5%)	18 (51.4%)	15 (53.6%)	4 (40.0%)	78 (45.1%)		
	Unspecified adenocarcinoma	4 (20.0%)	2 (2.5%)	1 (2.9%)	2 (7.1%)	1 (10.0%)	10 (5.8%)		
	Others	0 (0.0%)	1 (1.3%)	0 (0.0%)	0 (0.0%)	0 (0.0%)	1 (0.6%)		
Diffuse type									
	Poorly differentiated adenocarcinoma	12 (92.3%)	35 (89.7%)	15 (93.8%)	9 (81.8%)	4 (80.0%)	75 (89.3%)	0.1893	
	Signet-ring cell carcinoma	1 (7.1%)	4 (10.3%)	0 (0.0%)	2 (18.2%)	0 (0.0%)	7 (8.3%)		
	Mucinous adenocarcinoma	0 (0.0%)	0 (0.0%)	1 (6.7%)	0 (0.0%)	1 (20.0%)	2 (2.4%)		
Intestinal type									
	Well differentiated	0 (0.0%)	12 (31.6%)	3 (16.7%)	4 (26.7%)	1 (25.0%)	20 (25.6%)	0.9331	
	Moderately differentiated	3 (100.0%)	24 (63.2%)	14 (77.8%)	10 (66.7%)	3 (75.0%)	54 (69.2%)		
	Papillary adenocarcinoma	0 (0.0%)	2 (5.3%)	1 (5.6%)	1 (6.7%)	0 (0.0%)	4 (5.1%)		

Analysis set: per protocol set.

*P value of Fisher's exact test.

**In case of estimation by Monte Carlo Method, 99% confidence interval (CI) is also described together with the P value.

carcinoma (2 cases, 2.4%); well differentiated adenocarcinoma (20 cases, 25.6%); moderately differentiated adenocarcinoma (54 cases, 69.2%) and papillary adenocarcinoma (4 cases, 5.1%; Table 2). None had been reported as positive for HER2/neu.

FGFR2 IHC score

Of the 173 PPS cases, FGFR2 IHC score was evaluated as 0, 1, 2, 3 and 4 for 20 (11.6%), 80 (46.2%), 35 (20.2%), 28 (16.2%) and 10 (5.8%) cases, respectively (Table 1). Looking at the distribution of baseline characteristics in the PPS according to FGFR2 IHC score, there were no significant differences in age, presence of primary tumor at registration or primary site of tumor and main tissue type, except for gender composition by which the proportion of females was higher than males at Score 0 and that of males was higher than females at Scores 1–4 (P = 0.0004; Table 2). The distribution of gender composition in the FLCS similarly showed a significant

Table 3. Structured analysis population proportions: *FGFR2* copy number

Analysis set	*FGFR2* copy number (copies/cell)			Total
	<4	≥4, <10	≥10	
All enrolled patients	124	17	12	153
PPS	123 (99.2%)	16 (94.1%)	12 (100.0%)	151 (98.7%)
Patients excluded from PPS	1 (0.8%)	1 (5.9%)	0 (0.0%)	2 (1.3%)
FLCS	101 (81.5%)	15 (88.2%)	10 (83.3%)	126 (82.4%)

Table 4. Relationship between FGFR2 IHC score and *FGFR2* signals

	FGFR2 by IHC					Total
	Score 0	Score 1	Score 2	Score 3	Score 4	
FGFR2 copy number (copies/cell)						
<4	–	73 (92.4%)	28 (82.4%)	21 (75.0%)	1 (10.0%)	123 (81.5%)
≥4, <10	–	6 (7.6%)	4 (11.8%)	5 (17.9%)	1 (10.0%)	16 (10.6%)
≥10	–	0 (0.0%)	2 (5.9%)	2 (7.1%)	8 (80.0%)	12 (7.9%)

Analysis set: per protocol set.

difference (P = 0.0036), whereas no significance was observed in other baseline FLCS characteristics according to FGFR2 IHC score (data not shown).

FGFR2 copy number

In the 151 cases of the PPS with FGFR2 IHC scores of 1–4, except for 2 cases who had no FISH result due to specimen failure, *FGFR2* copy numbers per tumor cell were detected as <4, ≥4 < 10 and ≥ 10 for 123 cases, 16 cases and 12 cases, respectively (Table 3). *FGFR2* copy number was moderately correlated with FGFR2/CEP10 ratio (r = 0.41 and P < 0.0001). In these 151 cases, the proportions that showed a ≥4 *FGFR2* copy number per tumor cell according to FGFR2 IHC scores of 1, 2, 3 and 4 were 6/79 (7.6%), 6/34 (17.7%), 7/28 (25.0%) and 9/10 (90.0%), respectively, and that showed a ≥10 *FGFR2* copy number per tumor cell were 0/79 (0.0%), 2/34 (5.9%), 2/28 (7.1%) and 8/10 (80.0%), demonstrating an increased tendency for the proportion of cases with amplified *FGFR2* copy number per tumor cell along with FGFR2 IHC score (Table 4). In addition, the mean ± standard deviation for *FGFR2* copy number per tumor cell according to FGFR2 IHC scores of 1, 2, 3 and 4 were 2.4 ± 0.6 (79 cases), 4.2 ± 6.1 (34 cases), 5.8 ± 11.9 (28 cases) and 25.5 ± 15.6 (10 cases), respectively, demonstrating that the average number of *FGFR2* copies increased along with FGFR2 IHC score and the average number of *FGFR2* copies at IHC score 2 exceeded 4. Looking at the distribution of baseline characteristics in the PPS according to *FGFR2* copy number, there were no significant differences in age, gender, presence of primary tumor at registration or main tissue type except with primary site of tumor (P = 0.0387) in which the proportion of upper or middle stomach primary sites with *FGFR2* copy number category of ≥10 seemed lower than those of <10 categories. Although not significant (P = 0.0956), the proportion of diffuse type primary tumors with a *FGFR2* copy number category of ≥10 seemed higher than those of <10 categories (Table 5).

Response to chemotherapy prior to enrollment according to FGFR2 IHC score

In the FLCS, the proportion of cases with pyrimidine fluoride plus a platinum anticancer agent as the first line chemotherapy regimen prior to enrollment was 116 cases (82.9%) and other agents accounted for 24 cases (17.1%). Response to chemotherapy regimen prior to enrollment according to FGFR2 IHC score is summarized in Table 6. Response rates for first line chemotherapy according to FGFR2 IHC scores of 0, 1, 2, 3 and 4 were 15.4, 33.8, 34.5, 37.5 and 55.6%, respectively (P = 0.4142). In addition, median values for TTF and Kaplan–Meier plots for TTF with first line chemotherapy (Table 6 and Fig. 4) revealed no statistical differences by FGFR2 IHC score (P = 0.3456, Logrank test).

Response to chemotherapy prior to enrollment according to *FGFR2* copy number

Response to the chemotherapy regimens according to *FGFR2* copy number is summarized in Table 7. The response rate for first line chemotherapy according to *FGFR2* copy number categories of <4, ≥4 < 10 and ≥10 were 33.7, 60.0 and 30.0%, respectively (P = 0.1464). In addition, the TTF with first line chemotherapy revealed no statistical difference by *FGFR2* copy number (P = 0.4607, Logrank test; Table 7 and Fig. 4).

Discussion

FGFR2 overexpression and *FGFR2* gene amplification have been identified as a novel oncogenic (15) and druggable target (27) in cancers including GC. In addition, FGFR2 overexpression and *FGFR2* gene amplification have been reported as associated with poor prognosis and lower response to chemotherapy in GC (22,23). Furthermore, bemarituzumab, a novel FGFR2b inhibitor, plus chemotherapy demonstrated significant progression-free and overall survival benefit compared with placebo plus chemotherapy in patients with

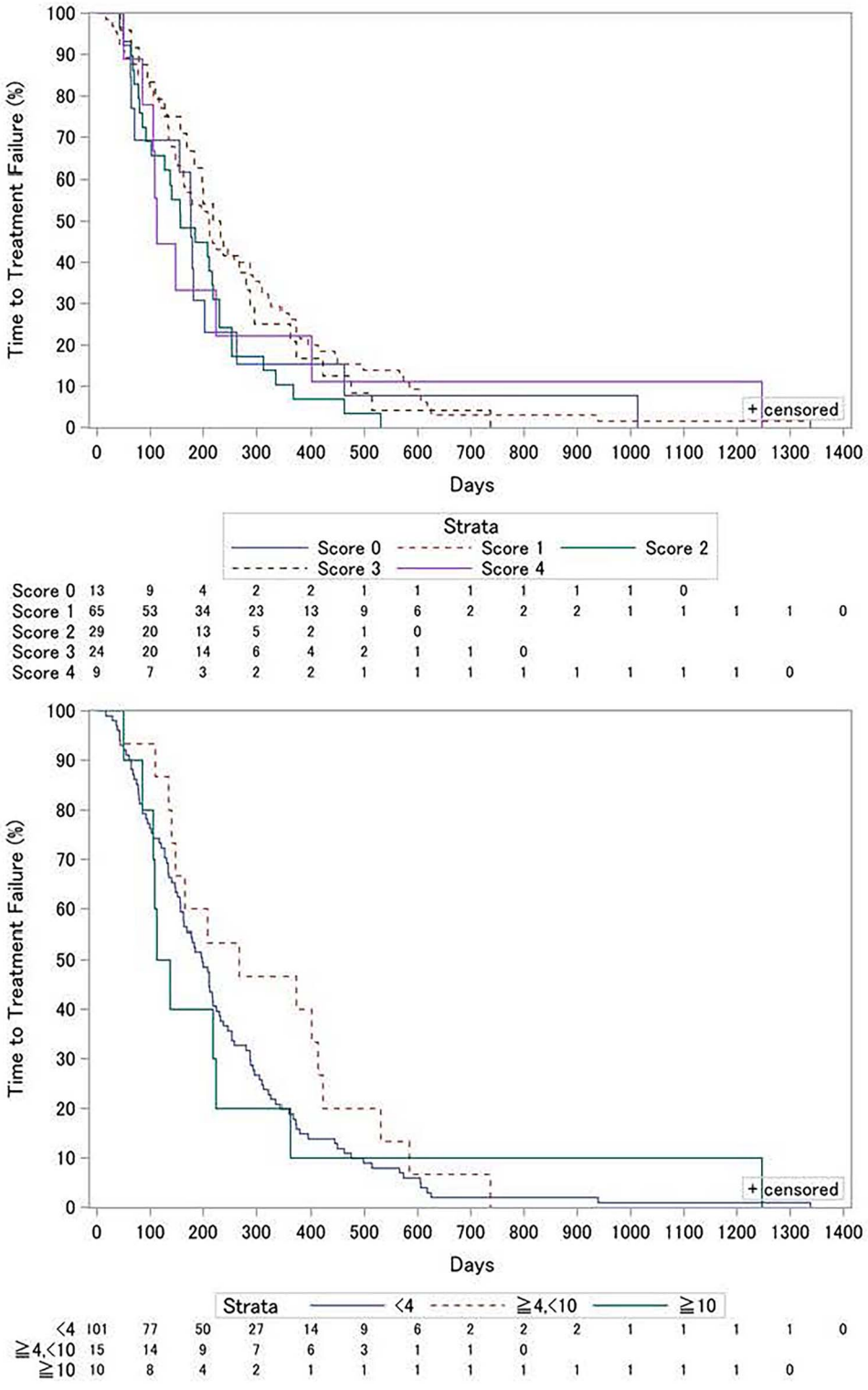

Figure 4. Kaplan–Meier plots of the TTF for first line chemotherapy. The upper and lower panel represented Kaplan–Meier plots according to FGFR2 IHC score 0–4 (P = 0.3456, Logrank test) and FGFR2 copy number category of <4, $\geq 4 < 10$ and ≥ 10 copies/cell (P = 0.4607, Logrank test), respectively.

Table 5. Baseline characteristics of cases according to *FGFR2* copy number

Category	*FGFR2* copy number (copies/cell)			*P* value*
	<4	≥4, <10	≥10	
N	123	16	12	
Age (years)				
Mean	67.2	70.3	67.4	
Std	10.2	8.2	9.4	
Min	35	46	47	
Median	69	72.5	70	
Max	83	77	80	
Age category (years)				
<65	39 (31.7%)	2 (12.5%)	4 (33.3%)	0.3194
≧65	84 (68.3%)	14 (87.5%)	8 (66.7%)	
Gender				
Male	99 (80.5%)	14 (87.5%)	10 (83.3%)	0.9201
Female	24 (19.5%)	2 (12.5%)	2 (16.7%)	
Primary tumor (at registration)				
Yes	67 (54.5%)	9 (56.3%)	8 (66.7%)	0.7404
No	56 (45.5%)	7 (43.8%)	4 (33.3%)	
Primary site				
Upper stomach	27 (22.0%)	6 (37.5%)	1 (8.3%)	0.0387
Middle stomach	34 (27.6%)	6 (37.5%)	1 (8.3%)	
Lower stomach	48 (39.0%)	3 (18.8%)	5 (41.7%)	
Esophagogastric junction	12 (9.8%)	1 (6.3%)	3 (25.0%)	
Others	2 (1.6%)	0 (0.0%)	2 (16.7%)	
Main tissue type				
Diffuse type	56 (45.5%)	7 (43.8%)	8 (66.7%)	0.0956
Intestinal type	63 (51.2%)	7 (43.8%)	3 (25.0%)	
Unspecified adenocarcinoma	4 (3.3%)	1 (6.3%)	1 (8.3%)	
Others	0 (0.0%)	1 (6.3%)	0 (0.0%)	
Diffuse type				
Poorly differentiated adenocarcinoma	49 (87.5%)	7 (100.0%)	7 (87.5%)	0.4839
Signet-ring cell carcinoma	6 (10.7%)	0 (0.0%)	0 (0.0%)	
Mucinous adenocarcinoma	1 (1.8%)	0 (0.0%)	1 (12.5%)	
Intestinal type				
Well differentiated	13 (20.6%)	4 (57.1%)	1 (33.3%)	0.0736
Moderately differentiated	47 (74.6%)	2 (28.6%)	2 (66.7%)	
Papillary adenocarcinoma	3 (4.8%)	1 (14.3%)	0 (0.0%)	
Specimen collection sites				
Primary tumor	119 (96.7%)	16 (100.0%)	12 (100.0%)	1
Liver	0 (0.0%)	0 (0.0%)	0 (0.0%)	
Lung	0 (0.0%)	0 (0.0%)	0 (0.0%)	
Abdominal lymph nodes	1 (0.8%)	0 (0.0%)	0 (0.0%)	
Peritoneal dissemination	2 (1.6%)	0 (0.0%)	0 (0.0%)	
Others	1 (0.8%)	0 (0.0%)	0 (0.0%)	

Analysis set: per protocol set.
**P* value of Fisher's exact test.

advanced GC (28). Thus, we aimed in this multicenter observational study to clarify the frequency of FGFR2 overexpression and *FGFR2* gene amplification using IHC and FISH methods as well as reliable baseline factors in Japanese patients with recurrent or unresectable GC.

In the present study, the proportion of the cases with FGFR2 overexpression as expressed by IHC scores of ≥1, ≥2, ≥3 or 4 was revealed to be 88.4, 42.2, 22.0 or 5.8%, respectively. It has been reported in a meta-analysis of studies on FGFR2 overexpression that GC patients have a wide range of FGFR2 overexpression frequencies from 2.5 to 61.4% (21). The frequency of FGFR2 overexpression found in the present study conducted in Japanese GC patients was demonstrated to be no less than in those studies.

It has been recognized that FGFR2 overexpression is often led by *FGFR* gene amplification (15). There have been multiple reports to-date that *FGFR2* gene amplification is associated with FGFR2 overexpression in gastric cancer (21,29), and FGFR2 protein overexpression has been noted to strongly correlate with *FGFR2* gene amplification, according to a report by Ahn et al. (26). On the other hand, Tuner et al. reported that FGFR2 overexpression was result

Table 6. Response to chemotherapy prior to enrollment according to FGFR2 IHC score

Category	FGFR2 by IHC					*P* value*
	Score 0	Score 1	Score 2	Score 3	Score 4	
N	13	65	29	24	9	
Best overall response: first line chemotherapy						
Complete response (CR)	0 (0.0%)	1 (1.5%)	0 (0.0%)	0 (0.0%)	0 (0.0%)	0.5074
Partial response (PR)	2 (15.4%)	21 (32.3%)	10 (34.5%)	9 (37.5%)	5 (55.6%)	
Stable disease (SD)	8 (61.5%)	17 (26.2%)	8 (27.6%)	6 (25.0%)	2 (22.2%)	
Non-CR/Non-PD	1 (7.7%)	13 (20.0%)	2 (6.9%)	5 (20.8%)	1 (11.1%)	
Progressive disease (PD)	1 (7.7%)	11 (16.9%)	9 (31.0%)	4 (16.7%)	1 (11.1%)	
Not evaluable (NE)	1 (7.7%)	2 (3.1%)	0 (0.0%)	0 (0.0%)	0 (0.0%)	
Response rate (CR + PR)	2 (15.4%)	22 (33.8%)	10 (34.5%)	9 (37.5%)	5 (55.6%)	0.4142
95% Confidence interval (%)	[4.3, 42.2]	[23.5, 46.0]	[19.9, 52.7]	[21.2, 57.3]	[26.7, 81.1]	
Disease control rate (CR + PR + SD + Non-CR/Non-PD)	11 (84.6%)	52 (80.0%)	20 (69.0%)	20 (83.3%)	8 (88.9%)	0.663
95% Confidence interval (%)	[57.8, 95.7]	[68.7, 87.9]	[50.8, 82.7]	[64.1, 93.3]	[56.5, 98.0]	
Time to treatment failure (TTF): first line chemotherapy						
N	13	65	29	24	9	
Median TTF	176	211	157	225	112	
95% Confidence interval (%)	[64.0, 202.0]	[162.0, 289.0]	[92.0, 218.0]	[157.0, 288.0]	[50.0, 401.0]	

Analysis set: FLCS (n = 140).

*P value of Fisher's exact test.

of abnormal transcriptional upregulation of the *FGFR2* gene (16). We also evaluated *FGFR2* gene amplification in this study. Because the *FGFR2* gene is known to localize on human chromosome 10, we evaluated the number of *FGFR2* copies per tumor cell on a basis of 4 copies/cell, or the equivalent of 2 times 2 copies/cell in normal cells, and set 3 categories for *FGFR2* copy number per tumor cell, i.e. <4, $\geq 4 < 10$ and ≥ 10 copies/cell. As a result, *FGFR2* copy numbers of <4, $\geq 4 < 10$ and ≥ 10 copies/cell were observed in 123, 16 and 12 cases out of 151 cases with an FGFR2 IHC score of ≥ 1, respectively. In addition, although no statistically significant difference was noted, the fact that an increasing tendency was observed in the proportion of cases who showed amplified *FGFR2* copy number per tumor cell along with their FGFR2 IHC score suggests a relationship between IHC score (FGFR2 overexpression) and *FGFR2* copy number expressed by FISH signals (*FGFR2* gene amplification). Taking these results into account, we consider it possible to estimate the *FGFR2* gene amplification with high reliability in clinically available GC specimen screening samples using the IHC method, which is more convenient than the FISH method.

Although many questions on the role of FGFR2 overexpression and *FGFR2* gene amplification in the pathogenesis and progression of GC have yet to be answered, it has been reported that a GC cell line established from GC patient with *FGFR2* gene amplification demonstrates significant inhibition of tumor cell growth and survival by the induction of *FGFR2* downregulation (30). Those results suggest that tumor progression in GC patients with FGFR2 overexpression and *FGFR2* gene amplification may in large part be associated with these FGFR abnormalities, and thus the establishment of optional chemotherapies that target these molecular factors would be highly desirable.

We also examined relationships between baseline characteristics and response to first line chemotherapy prior to enrollment, with FGFR2 IHC score and *FGFR2* copy number, to investigate predictive factors for FGFR2 overexpression and *FGFR2* gene amplification. For gender composition, the proportion of females with an FGFR2 IHC score of 0 was higher, whereas the proportion of males with FGFR2 IHC scores of 1–4 was higher, and an imbalance was thus observed. However, no difference was shown by way of *FGFR2* copy number. In addition, no gender effects on FGFR2 overexpression have been observed in other studies of FGFR2 overexpression in the primary tumors of GC patients by IHC (26,31). Our examination of other baseline characteristics revealed no relationships between FGFR2 IHC score and *FGFR2* copy number, and was consistent with other studies on FGFR2 overexpression (26,31) and *FGFR2* gene amplification (32,33) involving GC patients. Furthermore, we found no relationship to first line chemotherapy response in this study. At this point, it is widely recognized that a high-level *FGFR2* gene amplification and FGFR2 overexpression is associated with decreased overall survival and lower response to chemotherapy (30,34). Because our present study was small-sized, limited to HER2 negative cases, did not control for background chemotherapy regimen and did not evaluate overall survival, there are still issues to be investigated by way of confirming the association of FGFR2 with the response to chemotherapy.

Based on the above considerations, we believe it essential to clarify FGFR2 protein overexpression and/or *FGFR2* gene amplification in GC patients to confirm altered FGFR2 expression, and to develop the potential molecular-targeting therapeutic agents with FGFR2 inhibitors.

Conclusions

The present multicenter observational study took a detailed look at the frequency of FGFR2 overexpression and *FGFR2* gene amplification in Japanese patients with GC, and the effect of cytotoxic agents were similar regardless of whether patients had FGFR overexpression and gene amplification. These findings may contribute the development of promising therapeutic option for patients with recurrent or unresectable GC.

Table 7. Response to chemotherapy prior to enrollment according to *FGFR2* copy number

Category	*FGFR2* copy number (copies/cell)			*P* value*
	<4	≧4,<10	≧10	
N	101	15	10	
Best overall response: first line chemotherapy				
Complete response (CR)	1 (1.0%)	0 (0.0%)	0 (0.0%)	0.7098
Partial response (PR)	33 (32.7%)	9 (60.0%)	3 (30.0%)	
Stable disease (SD)	28 (27.7%)	2 (13.3%)	3 (30.0%)	
Non-CR/Non-PD	16 (15.8%)	3 (20.0%)	2 (20.0%)	
Progressive disease (PD)	21 (20.8%)	1 (6.7%)	2 (20.0%)	
Not evaluable (NE)	2 (2.0%)	0 (0.0%)	0 (0.0%)	
Response rate (CR + PR)	34 (33.7%)	9 (60.0%)	3 (30.0%)	0.1464
95% Confidence interval (%)	[25.2, 43.3]	[35.7, 80.2]	[10.8, 60.3]	
Disease control rate (CR + PR + SD + Non-CR/Non-PD)	78 (77.2%)	14 (93.3%)	8 (80.0%)	0.417
95% Confidence interval (%)	[68.1, 84.3]	[70.2, 98.8]	[49.0, 94.3]	
Time to treatment failure (TTF): first line chemotherapy				
N	101	15	10	
Median TTF	198	267	124.5	
95% Confidence interval (%)	[157.0, 218.0]	[135.0, 413.0]	[50.0, 224.0]	

Analysis set: FLCS with IHC score 1–4 (n = 126).

*P value of Fisher's exact test.

Funding

This work was supported by Taiho Pharmaceutical Co., Ltd., Tokyo, Japan.

Conflict of interest statement

Keiko Minashi received research grant from Astellas Pharma Inc., Daiichi Sankyo Co., Ltd., Mediscience Planning Inc., Merck Biopharma Co., Ltd., MSD K.K., Ono Pharmaceutical Co., Ltd., Taiho Pharmaceutical Co., Ltd. Takeshi Yamada received lecture fee from Daiichi Sankyo Co., Ltd., Eli Lilly Japan K.K., Merck Biopharma, Novartis, Ono Pharmaceutical Co., Ltd., Taiho Pharmaceutical Co., Ltd., Yakult Honsha. Kohei Shitara reports paid consulting or advisory roles for AbbVie, Astellas Pharma Inc., Bristol-Myers Squibb K.K., Eli Lilly Japan K.K., GSK, MSD K.K., Novartis, Ono Pharmaceutical Co., Ltd., Pfizer, Taiho Pharmaceutical Co., Ltd. and Takeda; honoraria from AbbVie, Novartis and Yakult; and research funding from Astellas Pharma Inc., Chugai Pharmaceutical Co., Ltd., Eli Lilly Japan K.K., Daiichi Sankyo Co. Ltd., MSD K.K., Ono Pharmaceutical Co., Ltd., Sumitomo Dainippon Pharma, Taiho Pharmaceutical Co., Ltd. and Medi Science, outside the submitted work.

References

1. Bray F, Ferlay J, Soerjomataram I, Siegel RL, Torre LA, Jemal A. Global cancer statistics 2018: GLOBOCAN estimates of incidence and mortality worldwide for 36 cancers in 185 countries. *CA Cancer J Clin* 2018;68:394–424.
2. Smyth EC, Verheij M, Allum W, Cunningham D, Cervantes A, Arnold D. Gastric cancer: ESMO clinical practice guidelines for diagnosis, treatment and follow-up. *Ann Oncol* 2016;27:v38–49.
3. Cardoso R, Coburn NG, Seevaratnam R, et al. A systematic review of patient surveillance after curative gastrectomy for gastric cancer: a brief review. *Gastric Cancer* 2012;15:S164–7.
4. Spolverato G, Ejaz A, Kim Y, et al. Rates and patterns of recurrence after curative intent resection for gastric cancer: a United States multi-institutional analysis. *J Am Coll Surg* 2014;219:664–75.
5. Koizumi W, Narahara H, Hara T, et al. S-1 plus cisplatin versus S-1 alone for first-line treatment of advanced gastric cancer (SPIRITS trial): a phase III trial. *Lancet Oncol* 2008;9:215–21.
6. Yamada Y, Higuchi K, Nishikawa K, et al. Phase III study comparing oxaliplatin plus S-1 with cisplatin plus S-1 in chemotherapy-naive patients with advanced gastric cancer. *Ann Oncol* 2015;26:141–8.
7. Bang YJ, Van Cutsem E, Feyereislova A, et al. Trastuzumab in combination with chemotherapy versus chemotherapy alone for treatment of HER2-positive advanced gastric or gastro-oesophageal junction cancer (ToGA): a phase 3, open-label, randomised controlled trial. *Lancet* 2010;376:687–97.
8. Al-Batran SE, Van Cutsem E, Oh SC, et al. Quality-of-life and performance status results from the phase III RAINBOW study of ramucirumab plus paclitaxel versus placebo plus paclitaxel in patients with previously treated gastric or gastroesophageal junction adenocarcinoma. *Ann Oncol* 2016;27:673–9.
9. Shitara K, Bang YJ, Satoru Iwasa S, et al. Trastuzumab deruxtecan in previously treated HER2-positive gastric cancer. *N Engl J Med* 2020;382:2419–30.
10. Kang YK, Boku N, Taroh Satoh T, et al. Nivolumab in patients with advanced gastric or gastro-oesophageal junction cancer refractory to, or intolerant of, at least two previous chemotherapy regimens (ONO-4538-12, ATTRACTION-2): a randomised, double-blind, placebo-controlled, phase 3 trial. *Lancet* 2017;390:2461–71.
11. Shitara K, Özgüroğlu M, Bang YJ, et al. Pembrolizumab versus paclitaxel for previously treated, advanced gastric or gastro-oesophageal junction cancer (KEYNOTE-061): a randomised, open-label, controlled, phase 3 trial. *Lancet* 2018;392:123–33.
12. Shitara K, Van Cutsem E, Bang YJ, et al. Efficacy and safety of pembrolizumab or pembrolizumab plus chemotherapy vs chemotherapy alone for patients with first-line, advanced gastric cancer: the KEYNOTE-062 phase 3 randomized clinical trial. *JAMA Oncol* 2020;6:1571–80.
13. Eswarakumar VP, Lax I, Schlessinger J. Cellular signaling by fibroblast growth factor receptors. *Cytokine Growth Factor Rev* 2005;16:139–49.

14. Fukumoto S. Actions and mode of actions of FGF19 subfamily members. *Endocr J* 2008;55:23–31.
15. Brooks AN, Kilgour E, Smith PD. Molecular pathways: fibroblast growth factor signaling: a new therapeutic opportunity in cancer. *Clin Cancer Res* 2012;18:1855–62.
16. Turner N, Grose R. Fibroblast growth factor signaling: from development to cancer. *Nat Rev Cancer* 2010;10:116–29.
17. Schildhaus HU, Nogova L, Wolf J, Buettner R. FGFR1 amplifications in squamous cell carcinomas of the lung: diagnostic and therapeutic implications. *Transl Lung Cancer Res* 2013;2:92–100.
18. Arai Y, Totoki Y, Hosoda F, Shirota T, Hama N, Nakamura H. Fibroblast growth factor receptor 2 tyrosine kinase fusions define a unique molecular subtype of cholangiocarcinoma. *Hepatology* 2014;59:1427–34.
19. Parker BC, Annala MJ, Cogdell DE, et al. The tumorigenic FGFR3-TACC3 gene fusion escapes miR-99a regulation in glioblastoma. *J Clin Invest* 2013;123:855–65.
20. Kim HS, Kim JH, Jang HJ. Pathologic and prognostic impacts of FGFR2 amplification in gastric cancer: a meta-analysis and systemic review. *J Cancer* 2019;10:2560–7.
21. Kim HS, Kim JH, Jang HJ, Han B, Zang DY. Pathological and prognostic impacts of FGFR2 overexpression in gastric cancer: a meta-analysis. *J Cancer* 2019;10:20–7.
22. Hosoda K, Yamashita K, Ushiku H, et al. Prognostic relevance of FGFR2 expression in stage II/III gastric cancer with curative resection and S-1 chemotherapy. *Oncol Lett* 2018;15:1853–60.
23. Seo S, Park SJ, Ryu MH, et al. Prognostic impact of fibroblast growth factor receptor 2 gene amplification in patients receiving fluoropyrimidine and platinum chemotherapy for metastatic and locally advanced unresectable gastric cancers. *Oncotarget* 2017;8:33844–54.
24. Das K, Gunasegaran B, Tan IB, Deng N, Lim KH, Tan P. Mutually exclusive FGFR2, HER2, and KRAS gene amplifications in gastric cancer revealed by multicolour FISH. *Cancer Lett* 2014;353:167–75.
25. Katoh M. FGFR inhibitors: effects on cancer cells, tumor microenvironment and whole-body homeostasis (Review). *Int J Mol Med* 2016;38:3–15.
26. Ahn S, Lee J, Hong M, et al. FGFR2 in gastric cancer: protein overexpression predicts gene amplification and high H-index predicts poor survival. *Mod Pathol* 2016;29:1095–103.
27. Dai S, Zhou Z, Chen Z, Xu G, Chen Y. Fibroblast growth factor receptors (FGFRs): structures and small molecule inhibitors. *Cell* 2019;8:614.
28. Wainberg ZA, Enzinger PC, Kang YK, et al. Randomized double-blind placebo-controlled phase 2 study of bemarituzumab combined with modified FOLFOX6 (mFOLFOX6) in first-line (1L) treatment of advanced gastric/gastroesophageal junction adenocarcinoma (FIGHT). *J Clin Oncol* 2021;39:3_suppl.160.
29. Tokunaga R, Imamura Y, Nakamura K, et al. Fibroblast growth factor receptor 2 expression, but not its genetic amplification, is associated with tumor growth and worse survival in esophagogastric junction adenocarcinoma. *Oncotarget* 2016;7:19748–61.
30. Xie L, Su X, Zhang L, et al. FGFR2 gene amplification in gastric cancer predicts sensitivity to the selective FGFR inhibitor AZD4547. *Clin Cancer Res* 2013;19:2572–83.
31. Hur JY, Chao J, Kim K, et al. High-level FGFR2 amplification is associated with poor prognosis and Lower response to chemotherapy in gastric cancers. *Pathol Res Pract* 2020;216:152878.
32. Su X, Zhan P, Gavine PR, et al. FGFR2 amplification has prognostic significance in gastric cancer: results from a large international multicentre study. *Br J Cancer* 2014;110:967–75.
33. Shoji H, Yamada Y, Okita N, et al. Amplification of FGFR2 gene in patients with advanced gastric cancer receiving chemotherapy: prevalence and prognostic significance. *Anticancer Res* 2015;35:5055–61.
34. Liu G, Xiong D, Xiao R, Huang Z. Prognostic role of fibroblast growth factor receptor 2 in human solid tumors: a systematic review and meta-analysis. *Tumour Biol* 2017;39:1010428317707424.

Cerebral Microbleeds, Cerebrospinal Fluid and Neuroimaging Markers in Clinical Subtypes of Alzheimer's Disease

MASAKI IKEDA[1*], Hiroo Kasahara[1], Sayaka Kodaira[1], Kazuaki Nagashima[1], Yukio Fujita[1], Kouki Makioka[1], Eriko Takai[1], Kimitioshi Hirayanagi[1], Natsumi Furuta[1], Etsuko Sanada[1], Ayumi Kobayashi[1], Shun Nagamine[1], Yasuo Harigaya[2], Noriaki Hattori[1], Tsuneo Yamazaki[1], Yuichi Tashiro[3], Kazuhiro Kishi[1], Hirotaka Shimada[1], Takayuki Suto[1], Yasujiro Sakai[1], Yukiko Tanaka[1], Yuko Aihara[1], Masakuni Amari[1], Haruyasu Yamaguchi[1], Koichi Okamoto[1], Masamitsu Takatama[1], Kenji Ishii[4], Tetsuya Higuchi[1], Yoshito Tsushima[1], Yoshio Ikeda[1]

[1]Gunma University, Japan, [2]Maebashi Red Cross Hospital, Japan, [3]Mito Medical Center, Japan, [4]Tokyo Metropolitan Institute of Gerontology, Japan

Submitted to Journal:
Frontiers in Neurology

Specialty Section:
Dementia and Neurodegenerative Diseases

Article type:
Original Research Article

Manuscript ID:
543866

Received on:
18 Mar 2020

Revised on:
24 Feb 2021

Journal website link:
www.frontiersin.org

Conflict of interest statement

The authors declare that the research was conducted in the absence of any commercial or financial relationships that could be construed as a potential conflict of interest

Author contribution statement

MI, HK, NK, FY, MK, HK, FN, NS, HY, HN, TY, SY, YT, TY, AY, AM, YH, OK, TM and YI collected the clinical data, interpreted the data, and MI wrote the manuscript. ET analyzed genomic DNA from the patient's blood samples and CSF biomarkers from the patient's CSF. ES and AK performed neuropsychological examinations. MI, SK, KI, TH and YT evaluated the neuroimaging information. KK, HS and TS organized the neuroimaging systems. MI and YI performed the clinical data analysis and evaluated the specificities and neurological significances.

Keywords

Alzheimer's disease, cerebral microbleeds, posterior cortical atrophy, CSF biomarkers, 99mTc ECD-SPECT, 11C PiB-PET, Logopenic variant of primary progressive aphasia

Abstract

Word count: 316

Lobar cerebral microbleeds (CMBs) in Alzheimer's disease (AD) are associated with cerebral amyloid angiopathy (CAA) due to vascular amyloid beta (Aβ) deposits. However, the relationship between lobar CMBs and clinical subtypes of AD remains unknown. Here, we enrolled patients with early- and late-onset amnestic dominant AD, logopenic variant of primary progressive aphasia (lvPPA) and posterior cortical atrophy (PCA) who were compatible with the AD criteria. We then examined the levels of cerebrospinal fluid (CSF) biomarkers (Aβ 1-42, Aβ 1-40, Aβ 1-38, phosphorylated tau 181 (P-Tau), total tau (T-Tau), neurofilament light chain (NFL), and chitinase 3-like 1 protein (YKL-40)), analyzed the number and localization of CMBs, and measured the cerebral blood flow (CBF) volume by 99mTc-ethyl cysteinate dimer single photon emission computerized tomography (99mTc ECD-SPECT), as well as the mean cortical standard uptake value ratio by 11C-labeled Pittsburgh Compound B-positron emission tomography (11C PiB-PET). Lobar CMBs in lvPPA were distributed in the temporal, frontal, and parietal lobes with the left side predominance, while the CBF volume in lvPPA significantly decreased in the left temporal area, where the number of lobar CMBs and the CBF volumes showed a significant inversely correlation. The CSF levels of NFL in lvPPA were significantly higher compared to the other AD subtypes and non-demented subjects. The numbers of lobar CMBs significantly increased the CSF levels of NFL in the total AD patients, additionally, among AD subtypes, the CSF levels of NFL in lvPPA predominantly were higher by increasing number of lobar CMBs. On the other hand, the CSF levels of Aβ 1-38, Aβ 1-40, Aβ 1-42, P-Tau, and T-Tau were lower by increasing number of lobar CMBs in the total AD patients. These findings may suggest that aberrant brain hypoperfusion in lvPPA was derived from the brain atrophy due to neurodegeneration, and possibly may involve the microcirculation aberration causing by lobar CMBs and cerebrovascular injuries, with the left side dominance, consequently leading to a clinical phenotype of logopenic variant.

Contribution to the field

Lobar CMBs in lvPPA were distributed in the temporal, frontal and parietal lobes with the left side predominance, while the CBF volume in lvPPA significantly decreased in the left temporal area, where the number of lobar CMBs and the CBF volumes showed a significant inversely correlation. Moreover, the CSF levels of NFL were significantly higher in lvPPA compared to the other AD subtypes, and non-demented subjects. Increased numbers of lobar CMBs significantly increased the CSF levels of NFL, while decreasing Abeta1-38. These findings may suggest the presence of aberrant metabolism in lvPPA derived from cerebrovascular injuries due to CAA and neurodegeneration. Moreover, with higher lobar CMBs prevalence of lobar CMBs and lower CBF volume, with left side predominance, lvPPA may involve the axonal neurodegeneration associated with AD pathology.

Ethics statements

Studies involving animal subjects

Generated Statement: No animal studies are presented in this manuscript.

Studies involving human subjects

Generated Statement: The studies involving human participants were reviewed and approved by the Gunma University Ethical Review Board for Medical Research Involving Human Subjects of Gunma University (Maebashi, Gunma, Japan), the Geriatrics Research Institute and Hospital (Maebashi, Gunma, Japan) and Maebashi Red Cross Hospital (Maebashi, Gunma, Japan). . The patients/participants provided their written informed consent to participate in this study.

Inclusion of identifiable human data

Generated Statement: No potentially identifiable human images or data is presented in this study.

Data availability statement

Generated Statement: The authors acknowledge that the data presented in this study must be deposited and made publicly available in an acceptable repository, prior to publication. Frontiers cannot accept a manuscript that does not adhere to our open data policies.

Original Research

Cerebral Microbleeds, Cerebrospinal Fluid and Neuroimaging Markers in Clinical Subtypes of Alzheimer's Disease

Masaki Ikeda[1,2,3]*, Sayaka Kodaira[4], Hiroo Kasahara[1], Eriko Takai[1], Kazuaki Nagashima[1], Yukio Fujita[1], Kouki Makioka[1], Kimitoshi Hirayanagi[1], Natsumi Furuta[1], Minori Furuta[1], Etsuko Sanada[1], Ayumi Kobayashi[1], Yasuo Harigaya[5], Shun Nagamine[1], Noriaki Hattori[6], Yuichi Tashiro[7], Kazuhiro Kishi[8], Hirotaka Shimada[8], Takayuki Suto[8], Hisashi Tanaka[9], Yasujiro Sakai[2], Tsuneo Yamazaki[10], Yukiko Tanaka[11], Yuko Aihara[12], Masakuni Amari[2], Haruyasu Yamaguchi[2,13], Koichi Okamoto[2], Masamitsu Takatama[2], Kenji Ishii[14], Tetsuya Higuchi[4], Yoshito Tsushima[4] and Yoshio Ikeda[1]

[1]Departments of Neurology, Gunma University Graduate School of Medicine, Maebashi, Japan.

[2]Department of Neurology, Geriatrics Research Institute and Hospital, Maebashi, Japan.

[3]Faculty of Health & Medical Care, Division of Common Education (Neurology), Saitama Medical University, Hidaka, Japan.

[4]Departments of Diagnostic Radiology and Nuclear Medicine, Gunma University Graduate School of Medicine, Maebashi, Japan.

[5]Department of Neurology, Maebashi Red Cross Hospital, Maebashi, Japan.

[6]Department of Neuropsychiatry, Jomo Hospital, Maebashi, Japan.

[7]Department of Neurology, Mito Medical Center, Mito, Japan.

[8]Department of Radiology, Gunma University Hospital, Maebashi, Japan.

[9]Department of Neuropsychiatry, Tanaka Hospital, Yoshioka, Japan.

[10]Department of Occupational therapy, Gunma University Graduate School of Health Sciences, Maebashi, Japan.

[11]Department of Geriatric Medicine, Uchida Hospital, Numata, Japan.

[12]Department of Neurology, Shinozuka Hospital, Fujioka, Japan.

[13]Tokyo Center for Dementia Research and Practices, Suginami-ku, Tokyo, Japan.

[14]Team for Neuroimaging, Tokyo Metropolitan Institute of Gerontology, Itabashi-ku, Tokyo, Japan.

Running title: Microbleeds and Biomarkers in AD subtypes

***Correspondence: Dr Masaki Ikeda**. E-mail: ikedam8@gmail.com

Present position: Faculty of Health & Medical Care, Division of Common Education (Neurology), Saitama Medical University. 1397-1 Yamane, Hidaka, Saitama, 350-1241, Japan.

Key words:

Alzheimer's disease, cerebral microbleeds, logopenic variant of primary progressive aphasia, posterior cortical atrophy, CSF biomarkers, ^{99m}Tc ECD-SPECT, ^{11}C PiB-PET

ABSTRACT

Lobar cerebral microbleeds (CMBs) in Alzheimer's disease (AD) are associated with cerebral amyloid angiopathy (CAA) due to vascular amyloid beta (Aβ) deposits. However, the relationship between lobar CMBs and clinical subtypes of AD remains unknown. Here, we enrolled patients with early- and late-onset amnestic dominant AD, logopenic variant of primary progressive aphasia (lvPPA) and posterior cortical atrophy (PCA) who were compatible with the AD criteria. We then examined the levels of cerebrospinal fluid (CSF) biomarkers (Aβ1-42, Aβ1-40, Aβ1-38, phosphorylated tau 181 (P-Tau), total tau (T-Tau), neurofilament light chain (NFL), and chitinase 3-like 1 protein (YKL-40)), analyzed the number and localization of CMBs, and measured the cerebral blood flow (CBF) volume by ^{99m}Tc-ethyl cysteinate dimer single photon emission computerized tomography (^{99m}Tc ECD-SPECT), as well as the mean cortical standard uptake value ratio by ^{11}C-labeled Pittsburgh Compound B-positron emission tomography (^{11}C PiB-PET). Lobar CMBs in lvPPA were distributed in the temporal, frontal, and parietal lobes with the left side predominance, while the CBF volume in lvPPA significantly decreased in the left temporal area, where the number of lobar CMBs and the CBF volumes showed a significant inversely correlation. The CSF levels of NFL in lvPPA were significantly higher compared to the other AD subtypes and non-demented subjects. The numbers of lobar CMBs significantly increased the CSF levels of NFL in the total AD patients, additionally,

among AD subtypes, the CSF levels of NFL in lvPPA predominantly were higher by increasing number of lobar CMBs. On the other hand, the CSF levels of Aβ1-38, Aβ1-40, Aβ1-42, P-Tau, and T-Tau were lower by increasing number of lobar CMBs in the total AD patients. These findings may suggest that aberrant brain hypoperfusion in lvPPA was derived from the brain atrophy due to neurodegeneration, and possibly may involve the microcirculation aberration causing by lobar CMBs and cerebrovascular injuries, with the left side dominance, consequently leading to a clinical phenotype of logopenic variant.

1 INTRODUCTION

Cerebral amyloid angiopathy (CAA) is caused by amyloid beta (Aβ) accumulation and is characterized by several pathological changes in the walls of small cortical and leptomeningeal capillaries, arterioles, and arteries (1–4). Lobar cerebral microbleeds (CMBs) are a neuroimaging marker of CAA, thought to reflect leakage of blood products and hemosiderin deposits from cerebral vessels damaged by Aβ deposition in Alzheimer's disease (AD) (5–7). The clinical presentations of atypical AD consist not only of amnestic symptoms, but also of language/speech disturbances and visuospatial cognitive deficits. Logopenic variant of primary progressive aphasia (lvPPA) (8–10) has been subsequently confirmed by the pathological findings of AD (11), and posterior cortical atrophy (PCA) (12, 13) has been reported to be

mainly based upon AD pathology (14). The three current global criteria characterizing AD include the two atypical presentations of lvPPA and PCA with memory loss and progressive cognitive decline (15–17). With regards to lvPPA and PCA, several reports have revealed the important evidences from neuroimaging (18–20) and cerebrospinal fluid (CSF) AD biomarkers (21–24). However, investigations of the four subtypes of AD (early onset AD (EOAD), late onset AD (LOAD), lvPPA, and PCA) have been scarcely reported in relation to CSF biomarkers and neuroimaging with lobar CMBs. While the current well-established CSF biomarkers for AD diagnosis include Aβ1-42, phosphorylated tau 181 (P-Tau) and total tau (T-Tau) (15–17), non-Aβ or non-tau CSF biomarker, neurofilament light chain (NFL) and chitinase 3-like 1 protein (YKL-40) have also became a point of focus as alternative biomarkers for AD (25–27). Quite recently, CSF levels of Aβ1-38 was reported to be lower in the CAA patients than the AD patients and the controls; while CSF NFL of CAA and AD patients was higher than control cases (28), although they were not atypical AD phenotypes. From these findings, we postulated that differences might exist in the CSF levels of NFL, YKL-40, and Aβ1-38, the number and distribution of cortical areas, the lateral predominance (left-right difference) of lobar CMBs localization, as well as the regional CBF (cerebral blood flow) volume and ^{11}C PiB retention may be apparent between the four subtypes of AD. Accordingly, we formulated the following hypotheses: (1) typical amnestic AD and atypical AD exhibit unique clinical characteristics,

CSF biomarkers, and frequency of apolipoprotein E gene (APOE) ε4 allele carriers; (2) the smaller soluble Aβ molecule, Aβ1-38, and the alternative biomarkers, NFL and YKL-40, could serve as CSF biomarkers of the AD subtypes; (3) the number of lobar CMBs at the cerebral areas, as well as the laterality predominance differs among the four AD subtypes; (4) regional CBF volume differs across the four AD subtypes and is correlated with the number of CMBs at the cerebral areas. To test these hypotheses and explore the heterogeneity of clinical AD, we sought to investigate the relationships between CMBs, CSF markers, CBF volumes, and ^{11}C PiB retention among the four AD subtypes.

2 MATERIALS AND METHODS

2.1 Participants

The spouse or family members of each AD patient provided written informed consent for the patient to participate in this study. The subjects who underwent lumbar punctures were recruited at Gunma University Graduate School of Medicine, the Geriatrics Research Institute and Maebashi Red Cross Hospital. Upon entering the study, subjects underwent a standardized clinical assessment, including medical history, physical and neurological examinations, neuropsychological examinations of Mini-Mental State Examination (MMSE) (29), Montreal Cognitive Assessment (MoCA) (30), Frontal assessment battery (FAB) (31), and brain MRI

scanning. A diagnosis of AD was reached in patients with a score equal to, or below 23 points on the MMSE (32), combined with information from caregivers on the patients' daily activities. The diagnosis of AD was also based upon the diagnostic criteria of the National Institute of Neurological and Communicative Diseases and Stroke-Alzheimer's Disease and Related Disorders Association (NINCDS-ADRDA) (33), in addition to adapted NIA/AA criteria and DSM-5 (15–17). Subjects were classified as non-demented (ND) if they scored more than 24 points on the MMSE, and/or if, based upon information on activities of daily living (ADL) provided by the family, they were considered to have a normal daily life that did not require any cognitive assistance. We classified AD patients into the following four clinical AD subtypes: (1) early-onset amnestic dominant deficit Alzheimer's disease (EOAD), in which the age at onset (AAO) of the memory disturbances is lower than 64 years old, (2) late-onset amnestic dominant deficit Alzheimer's disease (LOAD), in which AAO is 65 years or older, (3) logopenic variant type of primary progressive aphasia (lvPPA) (9), and (4) posterior cortical atrophy (PCA) (12, 13), in which the subjects initially suffer from visual agnosia and/or visuospatial cognitive deficits followed by memory loss, consistent with current diagnostic criteria for AD (15–17). All AD patients who participated in this study had CSF biomarkers and/or ^{11}C PiB-PET findings consistent with an underlying AD pathology. Exclusion criteria included patients with dementia who were clinically diagnosed with corticobasal syndrome

(CBS), progressive supranuclear palsy (PSP), dementia with Lewy bodies (DLB), frontotemporal dementia (FTD), vascular dementia (VaD), cerebral amyloid angiopathy-related inflammation (CAA-RI), or other neurodegenerative diseases characterized by dementia. No patient who participated in this study had autopsy performed.

2.2 Assessments of language/speech dysfunctions and visual agnosia/visuospatial cognitive deficits

Speech function was assessed using the Standard Language Test of Aphasia (SLTA) (10, 34), a battery of tests originally developed to assess multi-domain language function, including ‘‘Confrontation naming’’, ‘‘Word repetition’’, ‘‘Sentence repetition’’, ‘‘Auditory single-word comprehension’’, and ‘‘Auditory complex sentence comprehension commands’’. A proportion of patients were assessed using the WAB (Western Aphasia Battery: Kertesz A. J Speech Hear Disord. 1986). Visual cognitive functions were assessed using the Benton Visual Retention Test (BVRT) and/or VPTA (Visual Perception Test for Agnosia, edited by Japan Society for Higher Dysfunction: Brain Function Test committee, Tokyo, 1997). These assessments were carried out for the differential diagnosis of visual agnosia/visuospatial cognitive deficits. We examined AD patients who primarily presented with language/speech deficits and were diagnosed with logopenic variant type of primary progressive aphasia (lvPPA) according to the Consensus

Classification of the three clinical variants of PPA (9). We also examined AD patients who primarily presented with visual agnosia/visuospatial cognitive deficits dominant AD as posterior cortical atrophy (PCA) (12, 13).

2.3 Analyses of CSF levels of Aβ1-42, Aβ1-40, Aβ1-38, P-Tau, T-Tau, NFL, and YKL-40

Cerebrospinal fluid (CSF) was obtained by a lumbar puncture of the L3/L4 or L4/L5 intervertebral space, and the CSF samples were centrifuged for 10 min at 1,800 × g at 4 ℃ within 3 h of collection. Samples were divided into aliquots of 0.5 mL in polypropylene tubes and stored at -80 ℃ until analysis with ELISA kits for human CSF Aβ1-42 and Aβ1-40 (FUJIFILM Wako Pure Chemical Corporation, Osaka, Japan) (10, 35) and for CSF Aβ1-38 (IBL, Fujioka, Gunma, Japan) (10, 35). Inter-assay CVs (coefficients of variation) of the CSF Aβ1-42, Aβ1-40, and Aβ1-38 were less than 20 %, respectively (**supplementary Table 1**). All samples were measured by a single operator using the same reagents. Measurement of phosphorylated Tau (P-Tau) in CSF was performed using a sandwich ELISA INNOTEST® PHOSPHO-TAU (181P) (FUJIREBIO, Ghent, Belgium) as previously described elsewhere (10, 35). Human total tau (T-tau) was measured using a sandwich ELISA INNOTEST® T-Tau-Ag (FUJIREBIO, Ghent, Belgium) (36). Measurement of NFL (neurofilament light chain), a CSF marker of neurodegeneration and large fiber axonal degeneration, was performed using the

sandwich ELISA NF-light® (IBL International, Hamburg, Germany) (37, 38). CSF levels of YKL-40 (chitinase 3-like 1 protein), a CSF marker of glial neuroinflammation, was measured by the MicroVue™ YKL-40 EIA kits (Quidel, San Diego, CA, USA) (38–40). Inter-assay CVs of P-Tau, T-Tau, NFL, and YKL-40 were less than 20 %, respectively (**supplementary Table 1**). All samples were measured by a single operator using the same reagents.

2.4 Analyses of APOE allele

After obtaining informed consent for genetic testing of the apolipoprotein E gene (APOE) allele, we purified genomic DNA from lymphocytes in the peripheral blood of affected subjects. For the analysis of APOE allele polymorphism, purified genomic DNA samples were examined as previously described (10, 35).

2.5 Analyses of neuroimaging markers

2.5.1 MRI

All participants underwent a brain MRI (T2WI, T1WI, FLAIR, T2*WI (2-dimensional gradient recalled echo)) carried out on three different MRI scanners (Siemens 3.0T, Siemens 1.5T, and General Electric 1.5T) (**supplementary Table 2, 3**). CMBs were defined as homogenous, round areas with a signal void (of a diameter smaller than 10 mm) detected by T2*WI (7).

Lobar CMBs were defined as microbleeds restricted primarily to cortical areas of frontal, temporal, parietal, and occipital lobes bilaterally. We quantified the number of CMBs in deep white matter (DWM) and cerebellum, rated by MRI (axial T2*WI) according to the anatomical rating scale (MARS) (41). The number of CMBs on MRI T2*WI was determined independently, and a random order, by the first rater (M.I.) who was an experienced neurologist and the second rater (H.K.) who was an excellent neuroradiologist, both of whom were blinded to the clinical diagnosis of the patients. In cases of disagreement, the number of CMBs were ascertained by consensus. The number of CMBs were used to estimated inter-rater reliability by weighted kappa coefficient (0.827) carried out by statistical analyses in SPSS 24.0 (SPSS Inc. Chicago, IL, USA). All neuro-radiological analyses were conducted by PACS Imaging Workstation (Sectra AB, Stockholm, Sweden).

2.5.2 ^{99m}Tc ECD-SPECT studies

AD patients underwent ^{99m}Tc-ethyl cysteinate dimer single photon emission computerized tomography (^{99m}Tc ECD-SPECT) (FUJIFILM RI Toyama Chemical Co., Ltd., Chuo-ku, Tokyo, Japan) imaging as previously described (42). The degree of uptake of ^{99m}Tc ECD-SPECT and its AD diagnostic abilities are in excellent concordance with those of ^{18}F FDG-positron emission tomography (PET) (43). We assessed blood perfusion of CBF volumes in the brains

of patients with the four subtypes of AD by ^{99m}Tc ECD-SPECT bilaterally in five regions (frontal, temporal, parietal, occipital lobes, and cerebellum) according to previously published methodology (42, 43), however, we did not perform partial volume correction in this study. Each AD patient was placed in a supine position on the scanning bed with eyes closed during injection and during the sequent scanning period with a quiet examination dose of 600 MBq.

2.5.3 ^{11}C PiB-PET studies

^{11}C PiB (2-(4-aminophenyl)-6-hydroxybenzothiazole) was synthesized for ^{11}C PiB-PET (44), and ^{18}F-labeled fluorodeoxyglucose was also synthesized for PET (FDG-PET) in Gunma University hospital cyclotron according to previous reported methods (10, 44–48). We used a Discovery ST Elite scanner (General Electric Medical Systems, Milwaukee, WI, USA) for all PET studies. After an intravenous injection of ^{11}C-PiB (550 MBq), emission scans were acquired three-dimensionally without arterial sampling. Images were loaded on Xeleris workstation (General Electric Medical Systems, Milwaukee, WI), where ^{11}C PiB-PET images were co-registered with the respective ^{18}F FDG-PET images (10, 48). The ^{11}C PiB-PET images were rated as “positive” by visual inspection when the uptake level in the cerebral cortex was more prominent than those in the white matter (10, 47, 48). The standardized uptake value ratio (SUVR) represents a quantitative measure of tracer uptake, which is normalized to the mean

uptake in a reference region as well as published protocols (44–47) and our previous methods (48). The cerebellar cortex was selected as a reference region to evaluate the mean cortical SUVR (mcSUVR) of ^{11}C PiB-PET as ^{11}C PiB uptake in the cerebellar cortices does not differ between AD patients and healthy controls (44–47). Thus, since the cerebellar cortices are expected to have a lower fibrillary Aβ plaque burden than the cerebral cortices, the cerebellar cortex was used as a reference region to evaluate mcSUVR (46–47). Regions in the frontal cortical region (FRC), parietal cortical region (PAR), anterior cingulate region (ANC), posterior cingulate region (PCG), lateral temporal lobe cortical region (LTC), medial temporal lobe cortical region (MTC), and occipital cortical region (OCC) were selected to calculate the mcSUVR of the respective areas (44–48). Circular standard regions of interest (ROI) of 1 cm in diameter were placed on each cortical region of each ^{11}C PiB-PET images onto each cortical region of the ^{11}C PiB-PET image using the co-registered FDG-PET image (48). However, we did not perform partial volume correction. A standardized single ROI was placed over three regions of the FRC, three of the PAR, one of the ANC, one of the PCG, three of the LTC, one of the MTC, and one of the OCC in the ipsilateral side (48). The levels of regional ^{11}C PiB accumulation were summarized and the mcSUVR was calculated. Additionally, the mcSUVR at a total of 26 areas was used to calculate a global SUVR in each subject (48). Mean cortical

SUVR values were calculated in 31 participants (lvPPA: 4, PCA: 4, EOAD: 10, LOAD: 13) who underwent ^{11}C PiB-PET scans, in all 14 areas as described above.

2.6 Statistical analyses

Comparison analyses for demographic data (AAO, duration of illness, MMSE, MoCA, FAB, education years, hypertension, diabetes, hypercholesterolemia, and APOE ε4 allele carrier) were performed between the two clinical AD subgroups (the typical AD group and the atypical AD group) using either Mann-Whitney tests for continuous variables, or a chi-squared or Fisher's test for categorial variables. The chi-squared test applied for categorical variables, was also used to evaluate the association between the number of microbleeds between the two AD subtypes. Statistical comparisons of CSF Aβ1-38, Aβ1-40, Aβ1-42, P-Tau, T-Tau, NFL, and YKL-40 across the two AD subgroups and the ND group were performed using a one-way analysis of variance (ANOVA) ($p < 0.05$), Tuckey's test was used for post hoc comparison. If the non-normal distribution was identified for non-parametrical comparison using Mann-Whitney tests (defined as $p < 0.05$), Dunn's test was used for post hoc comparison.

A Kruskal-Wallis test, as well as one-way ANOVA and Dunn's test, used for post hoc comparison and correction for multiple comparisons, were applied to the following analyses: statistical comparisons of the CSF biomarkers across the four AD subgroups, comparison of

CBF volumes by ^{99m}ECD-SPECT among the frontal, temporal, parietal, and occipital lobe cortices and cerebellum, and comparisons of ^{11}C PiB retention among the frontal, temporal, parietal, and occipital lobe cortices. The correlation analysis among levels of the CBF volumes and the number of lobar CMBs was performed using Spearman's rank correlation tests at the four areas (frontal, temporal, parietal, and occipital) in the four AD subtypes. Correlation analysis for the levels of CSF markers and number of lobar CMBs was performed using Spearman's rank correlation tests in all AD patients.

Data were reported as mean ± SD (standard deviation). All statistical analyses were performed using SPSS software package (version 24: SPSS Inc., Chicago, IL, USA) applying a significance level of $p < 0.05$, and graphs were drafted using GraphPad Prism 7 (GraphPad Software, La Jolla, CA, USA)

2.7 Standard protocol approvals and patient consent

This study complied with the Declaration of Helsinki and was approved by the Gunma University Ethical Review Board for Medical Research Involving Human Subjects of Gunma University (Maebashi, Gunma, Japan), the Geriatrics Research Institute and Hospital (Maebashi, Gunma, Japan), and Maebashi Red Cross Hospital (Maebashi, Gunma, Japan). The spouse or family members of each AD patient provided written informed consent for the patient to

participate in the study.

3. RESULTS

3.2 Demographics and CSF biomarkers in typical AD and atypical AD

A total of 117 AD patients were enrolled, then divided into the 85 typical amnestic AD patients (39 EOAD and 46 LOAD) and the 32 atypical AD patients (20 lvPPA and 12 PCA). Clinical information of the AD patients and the 40 non-demented (ND) subjects, and CSF biomarkers of them (Aβ1-42, Aβ1-40, Aβ1-38, P-Tau, T-tau, NFL, and YKL-40) were also investigated (**Table 1**). CSF levels of Aβ1-42 were significantly lower in the typical AD (n = 85) and atypical AD (n = 32) groups compared to the ND group (n = 40) ($p < 0.0001$, respectively; **Table 1**). Meanwhile, CSF levels of P-Tau, T-Tau, NFL, and YKL-40 were significantly higher in both AD group compared to the ND group ($p < 0.0001$, respectively; **Table 1**). Additionally, the CSF levels of Aβ1-38 were significantly lower in the atypical AD compared to the typical AD group ($p = 0.002$), although the results of other CSF biomarkers and the prevalence of APOE ε4 allele did not differ significantly between the typical AD and atypical AD groups (**Table 1**).

3.1 Demographics of the four subtypes of AD patients

We then classified the AD patients into EOAD (n = 39), LOAD (n = 46), lvPPA (n = 20), and PCA (n = 12) according to the AD criteria (15, 16, 17). The AAO of PCA and EOAD were significantly lower than that of LOAD ($p < 0.0001$, $p < 0.0001$, respectively), and the AAO of PCA was significantly lower than that of lvPPA ($p = 0.046$), however, higher than that of EOAD ($p = 0.0002$). The total MoCA scores in lvPPA were significantly lower than those in LOAD ($p = 0.015$), while the total FAB scores in lvPPA were significantly lower than those in EOAD ($p = 0.045$; **Table 2**). In the neuropsychological examinations, the scores of auditory sentence comprehension of lvPPA were significantly lower than those of PCA ($p = 0.015$), EOAD ($p = 0.042$), and LOAD ($p = 0.0005$). The "intersecting pentagon" scores of PCA were significantly lower than those of EOAD ($p = 0.021$) and LOAD ($p = 0.0009$). The "Clock drawing test" scores of PCA were significantly lower than those of LOAD ($p = 0.028$). Additionally, the SLTA was performed as previously described for speech/language function (10), which revealed that the lvPPA patients presented with the hesitant speech and word-finding pauses due to impaired single word retrieval and difficulty with sentence repetition (data not shown), which agreed with the criteria described for lvPPA (8, 9).

3.3 Prevalence and localization of CMBs in the four clinical AD subtypes

The prevalence of lobar CMBs (1 ≦) in lvPPA (50.00%) was higher than those in the other three AD subtypes (EOAD: 23.08%, PCA: 25.00%, LOAD: 36.96%). Among the four AD subtypes, the prevalence of lobar CMBs in lvPPA was significantly higher than those in both PCA ($p = 0.036$), as well as higher, though not significantly, than EOAD ($p = 0.082$) and LOAD ($p = 0.322$) (**Table 3**). Comparison of the mean number of lobar CMBs per an AD patient with lobar CMBs was not significantly different across the four AD subtypes in the bilateral sides ($p = 0.312$), the right side ($p = 0.715$) and the left side ($p = 0.259$) (**Table 3**). The number of lobar CMBs in lvPPA tended to be higher in the right side than the left side, although comparison of the mean number of lobar CMBs between the right and left sides was not significant among the four AD subtypes ($p = 0.161$) (**Table 3**). Moreover, while the number of lobar CMBs in the frontal, temporal, and parietal lobes in lvPPA and LOAD tended to be higher than in PCA (**Figure 1A, B, C**), the number of lobar CMBs in the occipital area in LOAD tended to be higher than in the other subtypes of AD (**Figure 1D)**. Additionally, the total number of lobar CMBs in the frontal, temporal, parietal, and occipital lobes in lvPPA and LOAD was significantly higher than in PCA ($p = 0.0332$, $p = 0.0136$, respectively, **Figure 1F**). There was no significant difference in the number of CMBs in DWM among the four AD subtypes, although the number of CMBs on each side of the DWM was less than three in each AD patient (**Figure 1E**). Among

the four AD subtypes with lobar CMBs (lvPPA: n = 10, PCA: n = 3, EOAD: n = 9, LOAD: n = 17), lobar CMBs in lvPPA tended to be predominantly localized on the left side, rather than those on the right side of frontal, temporal, parietal, and occipital lobes (left side percentage of frontal (68.18%), temporal (65.91%), parietal (67.74%), occipital (70.00%) lobes and total areas (67.52%) shown in **Figure 1A, B, C, D, and F**). The total number of CMBs in frontal, temporal, parietal, and occipital lobe cortices in lvPPA tended to be higher in the left side compared to the right, although not significant (p = 0.1833) (**Figure 1F**), while there was no difference in the laterality dominance in the other subtypes of AD.

3.4 Diagnostic values of CSF biomarkers in the AD patients

We did not have data information of CSF from AD patients based upon with postmortem verification of AD diagnosis. We calculated diagnostic values of the CSF biomarkers of Aβ1-42 (cut off < 308.7), P-Tau (cut off > 47.43), T-Tau (cut off > 270.2), NFL (cut off > 858.8), and YKL-40 (cut off > 78.59) by the data from the typical AD (EOAD and LOAD) patients (n = 72) and non-dementia (ND) subjects (n = 33). These data were shown in **Table 4**.

3.5 Results of CSF biomarkers, APOE ε4 alleles, and global ^{11}C PiB-PET retention in the four AD subtypes

CSF biomarkers were analyzed in 18 patients with lvPPA, 12 with PCA, 34 with EOAD, and 38 with LOAD, in addition to the 33 ND subjects, by reference to the diagnostic values of CSF biomarkers (**3.4**) (**Table 5**). The CSF levels of Aβ1-42 (pg/ml) in the four AD subtypes were all significantly lower than those in ND (one-way ANOVA post hoc Dunn's test, $p < 0.0001$, respectively for all four AD subtypes), however, no significant differences were observed across the four AD subtypes (Kruskal-Willis test: $p = 0.983$). The Aβ1-40 (pg/ml) CSF levels did not differ significantly from those in ND (one-way ANOVA post hoc Dunn's test, $0.05 < p$), and no significant differences were found across the four AD subtypes (Kruskal-Willis test: $p = 0.379$). The Aβ1-38 (pg/ml) CSF levels of the AD subtypes were not significantly different from those in ND (Kruskal-Willis test: $p = 0.035$; post hoc difference, $0.05 < p$), nor were the CSF Aβ1-38 levels significantly different across the four AD subtypes ($0.05 < p$) (**Table 5**).

A total of 135 subjects were analyzed for the CSF levels of P-Tau, T-Tau, NFL, and YKL-40. The levels of CSF P-Tau were significantly higher in lvPPA, EOAD, LOAD, PCA compared with those in ND (ANOVA post hoc Dunn's test: $p < 0.0001$, $p < 0.0001$, $p < 0.0001$, $p = 0.0212$, respectively). Meanwhile, there were no significant differences observed in P-Tau across the four AD subtypes (Kruskal-Willis test: $p = 0.389$). The CSF levels of T-Tau (pg/ml) were higher in lvPPA, LOAD, EOAD and PCA than ND ($p < 0.0001$, respectively). However, no significant differences were observed in T-Tau across the four AD subtypes (Kruskal-Willis

test: p = 0.756). The CSF levels of NFL (pg/ml) were the highest in lvPPA, followed by LOAD, EOAD and PCA, and all four AD subgroups had higher levels than ND ($p < 0.0001$, $p < 0.0001$, $p < 0.0001$, $p = 0.036$, respectively). Across all four AD subtypes, the CSF levels of NFL in lvPPA were significantly higher than those in PCA ($p = 0.003$), EOAD ($p = 0.014$) and LOAD ($p = 0.045$). The CSF levels of YKL-40 (ng/ml) in lvPPA, LOAD, EOAD, and PCA were significantly higher than those in ND ($p < 0.0001$, $p < 0.0001$, $p < 0.001$, $p = 0.044$, respectively); meanwhile no significant difference was noted among the four AD subtypes (Kruskal-Willis test: $p = 0.148$) (**Table 5**). The prevalence of APOE ε4 allele carrier was the highest in EOAD (64.71%, n = 22/34), followed by lvPPA (55.56%, n = 10/18), LOAD (52.63%, n = 20/38), and PCA (41.67%, n = 5/12), with no significant differences among them (**Table 5**). There is no significant difference in global mcSUVR across all 14 areas among the four AD subtypes (**Table 5**).

3.6 Regional comparison of CBF volumes in the four clinical subtypes of AD

The number of AD patients examined by ^{99m}Tc ECD-SPECT were as follows: lvPPA: n = 17, PCA: n = 12, EOAD: n = 32, and LOAD: n = 36. In the frontal lobe, CBF volumes in lvPPA were significantly lower than those in LOAD ($p = 0.033$; **Figure 2A**). In the temporal lobe, the CBF volumes in lvPPA were significantly lower than those in EOAD ($p = 0.0011$) and LOAD

($p = 0.0002$; **Figure 2B**). In the parietal areas, the CBF volumes in PCA and lvPPA were lower than those in LOAD ($p < 0.0001$, respectively; **Figure 2C**). In the occipital lobe, the CBF volumes in PCA were significantly lower than those in EOAD ($p = 0.0098$) and LOAD ($p = 0.002$), while those in lvPPA were significantly lower than those in LOAD ($p = 0.0311$; **Figure 2D**). In the cerebellar region, there was no significant difference in the CBF volumes across all four AD subtypes (**Figure 2E**). Among the total CBF volumes, namely FTPO, including those of the frontal, temporal, parietal, and occipital lobes in the four AD subtypes, the mean CBF volumes in lvPPA were significantly lower than those in EOAD ($p = 0.047$) and LOAD ($p = 0.002$), while those in PCA were significantly lower than those in LOAD ($p = 0.0132$; **Figure 2F**). CBF volumes in lvPPA were significantly lower in the left side of the frontal, temporal, and parietal lobes than in the right side (*$p < 0.05$, **$p < 0.0001$, respectively, shown in **Figure 2A-D** and **2F**).

3.7 Correlation between CBF volume and number of lobar CMBs in the four AD subtypes

Spearman rank correlation tests revealed that the levels of CBF volume were significantly inversely correlated with the number of lobar CMBs in the left temporal region in lvPPA ($r = -0.382$, $p = 0.046$); bilateral (right; left) parietal region ($r = -0.397$, $p = 0.020$; $r = -0.345$, $p = 0.042$, respectively), bilateral (right; left) occipital region ($r= -0.353$, $p = 0.042$; $r= -0.408$, $p =$

0.043, respectively), and the bilateral (right; left) temporal region (r= -0.345, p = 0.042; r = -0.368, p = 0.027) in LOAD (**Table 6**).

3.8 Correlation between the number of lobar CMBs and the levels of CSF markers in the total AD and the levels of NFL in the AD subtypes

In the total AD subtypes, Spearman rank correlation tests revealed that the CSF levels of Aβ1-38, Aβ1-40, Aβ1-42, P-Tau and T-Tau were significantly negatively correlated with the amounts of lobar CMBs (r= -0.274, p = 0.004; r = -0.216, p = 0.019; r = -0.193, p = 0.049; r = -0.298, p = 0.0016; r = -0.331, p = 0.0005, respectively, by Spearman's rank correlation *t* tests), while the CSF levels of NFL were significantly positively correlated with the number of lobar CMBs (r = +0.397, p < 0.0001: Spearman *t* test), although YKL-40 showed no significant difference (**FIGURE 3 (A)-(G)**). CSF levels of NFL in the lvPPA patients showed significantly positive correlation with the number of lobar CMBs (r = +0.587, p = 0.005), while the EOAD and LOAD also show significant differences (r = +0.326, p = 0.034; r = +0.298, p = 0.046) (**FIGURE 3 (H)-(K)**).

4. DISCUSSION

The key findings of our study are as follows. First, the CSF levels of Aβ1-42 were significantly

lower in combined the typical AD group and the atypical AD than in the ND, while the CSF levels of P-Tau, T-Tau, NFL, and YKL-40 were significantly higher in the typical AD and atypical AD groups compared to the ND group. Second, the CSF levels of NFL in the four AD subtypes were significantly higher than those of ND, and the CSF levels of NFL were significantly higher in lvPPA than in PCA, EOAD, and LOAD among the four AD subtypes. While the CSF levels of YKL-40 of the four AD subtypes were higher than ND, however, YKL-40 did not show significant differences among the four AD subtypes. Third, among the four clinical AD subtypes, lvPPA had the highest prevalence of lobar CMBs (50%), which were distributed across the frontal, temporal, parietal, and occipital lobe cortices with a left side predominance. Meanwhile, LOAD had a tendency of a higher number of lobar CMBs in the occipital lobe cortices bilaterally than the other AD subtypes, although did not show significant difference. Among the four AD subtypes, the total number of lobar CMBs in lvPPA and LOAD were significantly higher than those in PCA. Fourth, the CBF volumes in lvPPA were reduced in the frontal, temporal, and occipital lobe areas, compared to those in the other AD subtypes, with a significant left side predominance, while the CBF volumes of PCA were significantly lower in the bilateral occipital and parietal lobes areas than in those of LOAD. Fifth, we identified a significant inverse correlation between the number of lobar CMBs and the CBF volume in the left temporal area in lvPPA, and in the bilateral temporal, parietal, and occipital

areas in LOAD; while those of PCA and EOAD showed similar inverse correlations, however, were not significant. The global ^{11}C PiB retention had no significant difference among the four AD subtypes. We found that higher number of lobar CMBs in the AD patients were significantly associated with lower amount of the smaller peptides Aβ1-38 and higher amount of NFL, although Aβ1-40, Aβ1-42, P-Tau and T-Tau have been reported (49, 50). Furthermore, CSF levels of NFL in the lvPPA patients was higher in a significantly positive correlation with the number of lobar CMBs ($p=0.005$), while the EOAD and LOAD also show significant differences ($p=0.034$, $p=0.0046$, respectively).

We describe our considerations about the results in this study as follows. (1) We demonstrated that the CSF levels of NFL and YKL-40 were significantly higher in the four AD subtypes than in ND. Moreover, among the four AD subtypes, the CSF levels of NFL in lvPPA were significantly higher than those in the other AD subtypes. Additionally, CSF levels of NFL in the lvPPA patients were higher in significantly positive correlation with the number of lobar CMBs. (2) Lobar CMBs in the four AD subtypes were most frequently detected in lvPPA, followed by LOAD, PCA, and EOAD. The APOE ε4 allele had the highest frequency in EOAD, which had the lowest prevalence of lobar CMBs, suggesting that the prevalence of lobar CMBs may be related not only to APOE ε4 allele carrier status, but also to other factors, such as advanced aging and higher AAO of dementia (lvPPA and LOAD). (3) The lvPPA group showed

a higher number of lobar CMBs in the frontal, temporal, and parietal lobe cortices, in contrast to those of EOAD and PCA, which may involve speech/language disturbances, resulting in logopenic speech, although the other AD subtypes did not show any laterality predominance of CMBs in distribution of cerebral cortices. Lobar microbleeds in typical amnestic LOAD and elderly people have been reported to be located predominantly in the occipital lobe cortices, presumably since aging and longevity might induce more severe CAA (5). (4) In lvPPA, AD pathology characterized by lobar CMBs with a clear left side predominance is likely to occur as a result of ischemic vascular pathology derived from lobar CMBs (51). However, although we observed high prevalence of lobar CMBs in left frontal areas, we observed a significant inverse correlation between CBF volume and the number of lobar CMBs in the left temporal region in lvPPA. In PCA, bilateral occipital and parietal lobes showed a decrease in CBF volumes, likely due to localized brain atrophy, possibly involving visuospatial cognitive syndromes. Consistent with three previously published reports (21–23), while the CSF levels of P-Tau, T-Tau, and NFL in all PCA patients were significantly higher than in the ND group, the lowest among all four AD groups was observed in PCA patients who also showed positive ^{11}C PiB retention, suggesting that PCA, based upon Aβ pathology, may not be as aggressive a disease of tau pathology and axonal neurodegeneration as the other AD subtypes. For this reason, PCA of the amnestic AD type was considered to have unique differential pathology

from that of typical AD even if compatible with AD criteria (52). The elevated CSF NFL levels were significantly related to longitudinal cognitive decline in AD and mild cognitive impairment (MCI) (25). Moreover, CSF NFL had a stronger correlation than those of T-Tau and P-Tau, leading to brain atrophy and progression of cognitive decline in AD (26). Pathologically, tau accumulation is reported to cause a great burden to cortical areas of the predominant hemisphere in lvPPA (53). With regards to lvPPA, the coexistence of AD pathology and argyrophilic thorny astrocytes clusters (ATAC) have been focused on intensely in tau immunoreactive pathology in fronto-temporo-parietal cortices as well as subcortical regions in lvPPA, suggesting that they may be markers of a process responsible for the prominent focal clinical manifestations of lvPPA based upon AD pathology (54, 55). Quite recently, Buciuc et al. reported that CAA pathology was the dominant risk factor of CMBs/SS (cortical superficial siderosis) in LPA (lvPPA) by neuroimaging-pathological analyses, they emphasized that CMB/SS were frequent in LPA patients (46%: 6/13) pathologically with moderate/severe CAA (56). They also described that they did not observe a higher frequency/number of CMBs/SS in the regions with the most severe CAA, nor observe a topolographic relationship between CMBs/SS location and regional PiB uptake or regional hypometabolism, although most CMBs/SS co-occurred with some degree of regional CAA. Their results were consistent with another neuroimaging-neuropathological study of CMBs/SS and CAA, where CMBs/SS

occurred at the sites with reduced CAA (57). We found a significant inverse correlation between CBF volume and the number of lobar CMBs in the left temporal region in lvPPA, although most frequent prevalence of lobar CMBs was left frontal areas, which might imply that lobar CMBs were not necessarily determinant for decreased CBF volume, but regional brain atrophy might reflect the decrease of CBF volume.

We found that CSF levels of NFL were significantly higher in lvPPA than those of other AD subtypes after controlling for multiple comparison, additionally, CSF NFL elevated by the increased number of lobar CMBs in lvPPA patients, presumably that lobar CMBs and/or CAA pathology in lvPPA might involve secondary and/or indirectly neuronal and axonal degeneration based upon AD pathology. Indeed, in analyses of functional neuronal connectivity in lvPPA patients, not only the language network (posterior superior temporal gyrus and inferior frontal lobe) but also the working memory network (frontal regions, inferior parietal lobule, superior, and middle temporal gyri) have been shown to be widely disturbed with a left side predominance by a resting-state fMRI study (58). Our findings of lvPPA imply that left predominant hypoperfusion may occur due to left dominant brain atrophy causing by neuronal and axonal degeneration, and possibly and/or partly due to microcirculation aberration causing by lobar CMBs and cerebrovascular injuries.

The limitation of this study was the absence of post-mortem autopsy analysis for any

of the patients, which prevented us from performing pathological diagnosis to support our clinical diagnosis. Nonetheless, to ensure that the atypical AD group (lvPPA and PCA) did not include patients with CBS, PSP, FTD, DLB, or other neurodegenerative diseases that present with dementia, we performed a careful clinical diagnosis in strict accordance with the current global criteria (8, 9, 13–17).

5. CONFLICT OF INTEREST

The authors declare that the research was conducted in the absence of any commercial or financial relationships that could be constructed as a potential conflict of interest.

6. AUTHOR CONTRIBUTION STATEMENT

MI, HK, KN, FY, MK, KH, NF, SN, YH, NH, YT, HT, SY, TY, YT, YA, MA, HY, KO, MT and YI collected the clinical data, interpreted the data, and MI wrote the manuscript. ET analyzed genomic DNA from the patient's blood samples and CSF biomarkers from the patient's CSF. ES and AK performed neuropsychological examinations. MI, SK, HK, TH, YT and KI evaluated the neuroimaging information. KK, HS and TS organized the neuroimaging systems. MI and YI performed the clinical data analysis and evaluated the specificities and neurological significances.

7. FUNDING

This study was supported by a Grant-in-Aid for Scientific Research (C) (M.I.:18K07491, T.Y.: 17K09790, T.H.: 19K08220, Y.T.: 18K07627, K.I.: 17K09813, Y.I.: 19K07813) from the Ministry of Education, Culture, Sports, Science and Technology of Japan, and a research program entitled ‘‘Dominantly Inherited Alzheimer’s Network-Japan (DIAN-J)’’ of the Ministry of Health, Labour and Welfare, also received an “Ai-no-bokin” (Donation of love) from a grant for dementia research from the JOMO-SHINBUN newspaper company (Maebashi, Gunma, Japan).

8. ACKNOWLEDGEMENTS

We especially thank Dr Hirofumi Kawakami, an Advanced Application Specialist who belongs to Headquarter of Academy, GE Healthcare Japan, for his excellent technical assistance. We thank Dr Mikio Shoji with academic discussions about this manuscript. We would like to thank Editage (www.editage.com) for English language editing.

9. DATA AVAILABILITY STATEMENT

All data generated or analyzed during this study are included in this published article.

LEGENDS

TABLE 1. Demographics and CSF biomarkers in typical/atypical AD patients

Differences between groups were analyzed using a chi-squared test for the categories of sex, hypertension, diabetes, and hypercholesterolemia, and a Kruskal-Wallis test, and variance was analyzed using post hoc Dunn tests (for age at onset, duration of illness, years of education, and total scores of MMSE, MoCA, and FAB, respectively). Data are presented as mean ± standard deviation. NA: not applicable. ND: non-demented subject. *$p < 0.0001$ comparing the ND and the typical and atypical AD groups combined.

TABLE 2. Demographics of the four subtypes of AD patients

Differences between groups were analyzed using a chi-squared test for the categories of sex, hypertension, diabetes, and hypercholesterolemia, and a Kruskal-Wallis test, and variance was analyzed using post hoc Dunn tests (for age at onset, duration of illness, years of education, total scores of MMSE, MoCA, FAB, respectively, and the sub-scores of Language, Calculation, Visuospatial functioning, and the Clock drawing test).

TABLE 3. Prevalence and mean number of lobar CMBs in the four subtypes of AD patients patients

Data are presented as mean ± standard deviation. Differences between groups were analyzed using a chi-squared test, and a Kruskal-Wallis test, and variance was analyzed using post hoc Dunn tests for mean lobar CMBs numbers (No.), respectively.

TABLE 4. Diagnostic values of CSF biomarkers in the typical AD patients vs. ND

AD: Alzheimer's disease, ND: non-dementia subjects, Aβ: Amyloid β, P-Tau: phosphorylated tau, T-tau: total tau, NFL: neurofilament light chain, YKL-40: chitinase 3-like 1 protein.

Table 5. CSF biomarkers, APOE ε4 alleles and global ^{11}C PiB-PET retention in the four subtypes of AD patients

A Kruskal-Wallis test, one-way ANOVA multiple comparison analysis and post hoc Dunn correction yielded the following results: CSF levels of Aβ1-42 were lower, and CSF levels of P-Tau, T-Tau, NFL, and YKL-40 were higher than those of ND: $^{a}p < 0.0001$, $^{b}p < 0.001$, $^{c}p < 0.01$, $^{d}p < 0.05$. Among the four subtypes of AD, CSF levels of NFL in lvPPA were significantly higher than those in PCA ($p = 0.003$), EOAD ($p = 0.014$), and LOAD ($p = 0.045$).

TABLE 6. Correlation between the levels of CBF volumes and the number of lobar CMBs in the four subtypes of AD patients

The levels of CBF volume were significantly correlated with the number of lobar CMBs at the left temporal lobe (r = -0.382, p = 0.046) in lvPPA, and at the right and the left temporal lobes (r = -0.345, p = 0.042; r = -0.368, p = 0.027, respectively), at the right and the left parietal lobes (r = -0.397, p = 0.020; r = -0.345, p = 0.042, respectively), and at the right and the left occipital areas (r = -0.353, p = 0.042; r = -0.408, p = 0.043, respectively) in LOAD.

FIGURE 1. Regional comparison of the number of CMBs in the four AD subtypes of AD

Number of lobar CMBs in frontal (**A**), temporal (**B**), parietal (**C**), occipital (**D**) lobes, and deep white matter (DWM) (**E**) of lvPPA, PCA, EOAD, and LOAD. Total number of lobar CMBs in frontal, temporal, parietal and occipital lobe cortices (**F**). *p < 0.05.

FIGURE 2. Regional comparison of CBF volumes in the four AD subtypes in ^{99m}Tc ECD-SPECT

CBF volumes in frontal (**A**), temporal (**B**), parietal (**C**), occipital (**D**) lobes and cerebellum (**E**) of lvPPA, PCA, EOAD and LOAD. Total CBF volumes, namely, Sum of (**A**)-(**D**), in frontal,

temporal, parietal and occipital lobes (**F**). *p < 0.05, **p < 0.01, ***p < 0.001, ****p < 0.0001.

FIGURE 3. Correlations between the number of lobar cerebral microbleeds, and cerebrospinal fluid levels of Aβ1-38, Aβ1-40 Aβ1-42, P-Tau, T-Tau, NFL and YKL-40 in the total AD subtypes, and CSF NFL in the lvPPA

Scatter plots presenting the correlations per patient between total number of lobar CMBs and CSF biomarkers, Aβ1-38 (**A**), Aβ1-40 (**B**), Aβ1-42 (**C**), P-Tau (**D**), T-Tau (**E**), NFL (**F**), and YKL-40 (**G**). The number of CMBs and the levels of CSF NFL in the lvPPA (**H**), the PCA (**I**) the EOAD (**J**), and the LOAD (**K**).

SUPPLEMENTAL TABLE 1.

Assay quality data of Inter-assay CVs (Coefficients of variation) %.

Inter-assay CVs of Aβ1-42, Aβ1-40 and Aβ1-38 were less than 15%, 15% and 20%, respectively. Inter-assay CVs of P-Tau, T-Tau, NFL, and YKL-40 were less than 15%, 20%, 20 % and 15 %, respectively.

SUPPLEMENTAL TABLE 2.

MRI parameters.

FA = Flip angle, ST = Slice thickness, TE = Time to echo, TI = Time for inversion, TR = Time to repeat.

SUPPLEMENTAL TABLE 3.

Distribution of patients across field strengths and sequences.

1.5 T and 3.0 T columns included all the patients scanned on these field strengths in the different AD subgroups. There was no significant difference among the four subgroups of AD across field strength and hemosiderin positive sequences.

REFERENCES

1. Vinters HV. Cerebral amyloid angiopathy. A critical review. *Stroke.* (1987) 18:311–24. doi: 10.116/01.str.18.2.311

2. Greenberg SM, Finklestein SP, Schaefer PW. Petechial hemorrhages accompanying lobar hemorrhage: detection by gradient-echo MRI. *Neurology.* (1996) 46:1751–54. doi: 10.1212/wnl.46.6.1751

3. Cordonnier C, van der Flier WM, Sluimer JD, Leys D, Barkhof F, Scheltens P. Prevalence and severity of microbleeds in a memory clinic setting. *Neurology.* (2006) 66:1356–60. doi: 10.1212/01.wnl.0000210535.20297

4. Viswanathan A, Greenberg SM. Cerebral amyloid angiopathy in the elderly. *Ann Neurol.* (2011) 70:871–80. doi: 10.1002/ana.22516

5. Pettersen JA, Sathiyamoorthy G, Gao FQ, Szilagyi G, Nadkarni NK, St George-Hyslop P, et al. Microbleed topography, leukoaraiosis, and cognition in probable Alzheimer disease from the Sunnybrook dementia study. *Arch Neurol.* (2008) 65:790–795. doi: 10.1001/archneur.65.6.790

6. Gregg NM, Kim AE, Gurol ME, Lopez OL, Aizenstein HJ, Price JC et al. Incidental Cerebral Microbleeds and Cerebral Blood Flow in Elderly Individuals. *JAMA Neurol*. (2015) 72:1021–8. doi: 10.1001/jamaneurol.2015.1359

7. Wardlaw JM, Smith EE, Biessels GJ, Cordonnier C, Fazekas F, Frayne R, et al. Neuroimaging standards for research into small vessel disease and its contribution to ageing

and neurodegeneration. *Lancet Neurol.* (2013) 12:822–38. doi: 10.1016/S1474–4422(13)70124–8

8. Mesulam MM. Primary progressive aphasia. *Ann Neurol.* (2001) 49:425–32

9. Gorno-Tempini ML, Hillis AE, Weintraub S, Kertesz A, Mendez M, Cappa SF, et al. Classification of primary progressive aphasia and its variants. *Neurology.* (2011) 76:1006–14. doi: 10.1212/WNL.0b013e31821103e6

10. Ikeda M, Tashiro Y, Takai E, Kurose S, Fugami N, Tsuda K, et al. CSF levels of Aβ1-38/Aβ1-40/Aβ1-42 and ^{11}C PiB-PET studies in three clinical variants of primary progressive aphasia and Alzheimer's disease. *Amyloid.* (2014) 21:238–45. doi: 10.3109/13506129.2014.949231

11. Rohrer JD, Rossor MN, Warren JD. Alzheimer's pathology in primary progressive aphasia. *Neurobiol Aging.* (2012) 33:744–52. doi: 10.1016/j.neurobiolaging.2010.05.020

12. Benson DF, Davis RJ, Snyder BD. Posterior cortical atrophy. *Arch Neurol.* (1988) 45:789–93. doi: 10.1001/archneur.1988.00520310107024

13. Crutch SJ, Lehmann M, Schott JM, Rabinovici GD, Rossor MN, Fox NC. Posterior cortical atrophy. *Lancet Neurol.* (2012) 11:170–78. doi: 10.1016/S1474–4422(11)70289–7

14. Tang-Wai DF, Graff-Radford NR, Boeve BF, Dickson DW, Parisi JE, Crook R, et al. Clinical, genetic, and neuropathologic characteristics of posterior cortical atrophy. *Neurology.* (2004) 63:1168–74. doi: 10.1212/01.wnl.0000140289.18472.15

15. McKhann GM, Knopman DS, Chertkow H, Hyman BT, Jack CR, Jr., Kawas CH, et al. The diagnosis of dementia due to Alzheimer's disease: Recommendations from the National Institute on Aging-Alzheimer's Association workgroups on diagnostic guidelines for Alzheimer's disease. *Alzheimers Dement.* (2011) 7:263–9. doi: 10.1016/j.jalz.2011.03.005

16. American Psychiatric Association (2013) Diagnostic and Statistical Manual of Mental Disorders, Fifth Edition: DSM-5. Arlington, VA: American Psychiatric Association

17. Dubois B, Feldman HH, Jacova C, Hampel H, Molinuevo JL, Blennow K, et al. Advancing research diagnostic criteria for Alzheimer's disease: the IWG-2 criteria. *Lancet Neurol* (2014) 13:614–29. Erratum in: *Lancet Neurol.* (2014) 13:757. doi: 10.1016/S1474–4422(14)70090–0

18. Rabinovici GD, Jagust WJ, Furst AJ, Ogar JM, Racine CA, Mormino EC, et al. Abeta amyloid and glucose metabolism in three variants of primary progressive aphasia. *Ann Neurol.* (2008) 64:388–401. doi: 10.1002/ana.21451

19. Lehmann M, Ghosh PM, Madison C, Laforce R Jr, Corbetta-Rastelli C, Weiner MW, et al. Diverging patterns of amyloid deposition and hypometabolism in clinical variants of probable Alzheimer's disease. *Brain.* (2013) 136:844–58. doi: 10.1093/brain/aws327

20. Ossenkoppele R, Schonhaut DR, Schöll M, Lockhart SN, Ayakta N, Baker SL, et al. Tau PET patterns mirror clinical and neuroanatomical variability in Alzheimer's disease. *Brain.* (2016) 139:1551–67. doi: 10.1093/brain/aww027

21. de Souza LC, Lamari F, Belliard S, Jardel C, Houillier C, De Paz R, et al. Cerebrospinal fluid biomarkers in the differential diagnosis of Alzheimer's disease from other cortical dementias. *J Neurol Neurosurg Psychiatry.* (2011) 82:240–6. doi: 10.1136/jnnp.2010.207183

22. Ossenkoppele R, Mattsson N, Teunissen CE, Barkhof F, Pijnenburg Y, Scheltens P, et al. Cerebrospinal fluid biomarkers and cerebral atrophy in distinct clinical variants of probable Alzheimer's disease. *Neurobiol Aging.* (2015) 36:2340–47. doi: 10.1016/j.neurobiolaging.2015.04.011

23. Paterson RW, Toombs J, Slattery CF, Nicholas JM, Andreasson U, Magdalinou NK, et al. Dissecting IWG-2 typical and atypical Alzheimer's disease: insights from cerebrospinal fluid analysis. *J Neurol.* (2015) 262:2722–30. doi: 10.1007/s00415–015–7904–3

24. Whitwell JL, Kantarci K, Weigand SD, Lundt ES, Gunter JL, Duffy JR, et al. Microbleeds in atypical presentations of Alzheimer's disease: a comparison to dementia of the Alzheimer's type. *J Alzheimers Dis.* (2015) 45:1109–17. doi: 10.3233/JAD–142628

25. Preische O, Schultz SA, Apel A, Kuhle J, Kaeser SA, Barro C, et al; Dominantly Inherited Alzheimer Network. Serum neurofilament dynamics predicts neurodegeneration and clinical progression in presymptomatic Alzheimer's disease. *Nat Med.* (2019) 25:277–83. doi: 10.1038/s41591-018-0304-3.

26. Dhiman K, Gupta VB, Villemagne VL, Eratne D, Graham PL, Fowler C, et al. Cerebrospinal fluid neurofilament light concentration predicts brain atrophy and cognition in Alzheimer's disease. *Alzheimers Dement (Amst).* (2020) 12(1):e12005. doi: 10.1002/dad2.12005.

27. Antonell A, Mansilla A, Rami L, Lladó A, Iranzo A, Olives J, et al. Cerebrospinal fluid level of YKL-40 protein in preclinical and prodromal Alzheimer's disease. *J Alzheimers Dis.* (2014) 42:901–8. doi: 10.3233/JAD-140624.

28. Banerjee G, Ambler G, Keshavan A, Paterson RW, Foiani MS, Toombs J, et al. Cerebrospinal Fluid Biomarkers in Cerebral Amyloid Angiopathy. *J Alzheimers Dis.* (2020) 74:1189–1201. doi: 10.3233/JAD-191254.

29. Folstein MF, Folstein SE, McHugh PR. ‘‘Mini-mental state’’. A practical method for grading the cognitive state of patients for the clinician. *J Psychiatr Res.* (1975) 12:189–98.

doi: 10.1016/0022-3956(75)90026–6

30. Nasreddine ZS, Phillips NA, Bedirian V, Charbonneau S, Whitehead V, Collin I, et al. The Montreal Cognitive Assessment, MoCA: A brief screening tool for mild cognitive impairment. *J Am Geriatr Soc.* (2005) 53:695–9. doi: 10.1111/j.1532-5415.2005.53221.x

31. Dubois B, Slachevsky A, Litvan I, Pillon B. The FAB: A Frontal assessment battery at bedside. *Neurology.* (2000) 55:1621–26. doi: 10.1212/wnl.55.11.1621

32. Holsinger T, Deveau J, Boustani M, Williams JW Jr. Does this patient have dementia? *JAMA.* (2007) 297:2391–2404. doi: 10.1001/jama.297.21.2391

33. McKhann G, Drachman D, Folstein M, Katzman R, Price D, Stadlan EM. Clinical diagnosis of Alzheimer's disease: report of the NINCDS-ADRDA Work Group under the auspices of department of health and human services task force on Alzheimer's disease. *Neurology.* (1984) 34:939–44. doi: 10.1212/wnl.34.7.939

34. Mimura M, Kato M, Kato M, Sano Y, Kojima T, Naeser M, Kashima H. Prospective and retrospective studies of recovery in aphasia. Changes in cerebral blood flow and language functions. *Brain.* (1998) 121:2083–94. doi: 10.1093/brain/121.11.2083

35. Ikeda M, Yonemura K, Kakuda S, Tashiro Y, Fujita Y, Takai E, et al. Cerebrospinal fluid levels of phosphorylated tau and Aβ1-38/Aβ1-40/Aβ1-42 in Alzheimer's disease with PS1 mutations. *Amyloid.* (2013) 20:107–12. doi: 10.3109/13506129.2013.790810

36. Andreasen N, Minthon L, Davidsson P, Vanmechelen E, Vanderstichele H, Winblad B, et al. Evaluation of CSF-tau and CSF- Aβ42 as diagnostic markers for Alzheimer's disease in clinical practice. *Arch Neurol.* (2001) 58:373–9. doi: 10.1001/archneur.58.3.373

37. Norgren N, Rosengren L, Stigbrand T. Elevated neurofilament levels in neurological diseases. *Brain Res.* (2003) 987:25–31. doi: 10.1016/s0006–8993(03)03219–0

38. Ikeda M, Kuwabara T, Takai E, Kasahara H, Furuta M, Sekine A, et al. Increased neurofilament light chain and YKL-40 CSF levels in one Japanese IBMPFD patient with

VCP R155C mutation: a clinical case report with CSF biomarker analyses. *Front Neurol.* (2020) 11:757. doi: 10.3389/fneur.2020.00757.

39. Molinuevo JL, Ayton S, Batrla R, Bednar MM, Bittner T, Cummings J, et al. Current state of Alzheimer's fluid biomarkers. *Acta Neuropathol.* (2018) 136:821–53. doi: 10.1007/s00401-018-1932-x.

40. Baldacci F, Lista S, Palermo G, Giorgi FS, Vergallo A, Hampel H. The neuroinflammatory biomarker YKL-40 for neurodegenerative diseases: advances in development. *Expert Rev Proteomics.* (2019) 16:593–600. doi: 10.1080/14789450.2019.1628643.

41. Gregoire SM, Chaudhary UJ, Brown MM, Yousry TA, Kallis C, Jäger HR, et al. The microbleed anatomical rating scale (MARS): reliability of a tool to map brain microbleeds. *Neurology.* (2009) 73:1759–66. doi: 10.1212/WNL.0b013e3181c34a7d

42. Matsuda H, Mizumura S, Nagao T, Ota T, Iizuka T, Nemoto K, et al. Automated discrimination between very early Alzheimer disease and controls using an easy Z-score imaging system for multicenter brain perfusion single-photon emission tomography. *Am J Neuroradiol.* (2007) 28:731–6

43. Ito K, Shimano Y, Imabayashi E, Nakata Y, Omachi Y, Sato N, et al. Concordance between ^{99m}Tc-ECD SPECT and ^{18}F-FDG PET interpretations in patients with cognitive disorders diagnosed according to NIA-AA criteria. *Int J Geriatr Psychiatry.* (2014) 29:1079–86. doi: 10.1002/gps.4102

44. Klunk WE, Engler H, Nordberg A, Wang Y, Blomqvist G, Holt DP, et. Imaging brain amyloid in Alzheimer's disease with Pittsburgh Compound-B. *Ann Neurol.* (2004) 55:306–19. doi: 10.1002/ana.20009

45. Lopresti BJ, Klunk WE, Mathis CA, Hoge JA, Ziolko SK, Lu X, et al. Simplified quantification of Pittsburgh Compound B amyloid imaging PET studies: A comparative analysis. *J Nucl Med.* (2005) 46:1959–72

46. McNamee RL, Yee SH, Price JC, Klunk WE, Rosario B, Weissfeld L, et al. Consideration of optimal time window for Pittsburgh compound B PET summed uptake measurements. *J Nucl Med.* (2009) 50:348–55. doi: 10.2967/jnumed.108.057612

47. Yamane T, Ishii K, Sakata M, Ikari Y, Nishio T, Ishii K, et al. Inter-rater variability of

visual interpretation and comparison with quantitative evaluation of ^{11}C-PiB PET amyloid images of the Japanese Alzheimer's Disease Neuroimaging Initiative (J-ADNI) multicenter study. *Eur J Nucl Med Mol Imaging.* (2017) 44:850–7. doi: 10.1007/s00259–016–3591–2

48. Kasahara H, Ikeda M, Nagashima K, Fujita Y, Makioka K, Makioka K, et al. Deep white matter lesions are associated with early recognition of dementia in Alzheimer's disease. *J Alzheimers Dis.* (2019) 68:797–808. doi: 10.3233/JAD-180939

49. Shams S, Granberg T, Martola J, Li X, Shams M, Fereshtehnejad SM, et al. Cerebrospinal fluid profiles with increasing number of cerebral microbleeds in a continuum of cognitive impairment. *J Cereb Blood Flow Metab.* (2016) 36:621–8. doi: 10.1177/0271678X15606141

50. : Noguchi-Shinohara M, Komatsu J, Samuraki M, Matsunari I, Ikeda T, Sakai K, et al. Cerebral Amyloid Angiopathy-Related Microbleeds and Cerebrospinal Fluid Biomarkers in Alzheimer's Disease. *J Alzheimers Dis*. (2017) 55:905–13. doi: 10.3233/JAD–160651

51. Mendes A, Bertrand A, Lamari F, Colliot O, Routier A, Godefroy O, et al. Cerebral microbleeds and CSF Alzheimer biomarkers in primary progressive aphasias. *Neurology.* (2018) 90:e1057–e1065. doi: 10.1212/WNL.0000000000005165

52. Wellington H, Paterson RW, Suárez-González A, Poole T, Frost C, Sjöbom U, et al. CSF neurogranin or tau distinguish typical and atypical Alzheimer disease. *Ann Clin Transl Neurol.* (2018) 5:162–71. doi: 10.1002/acn3.518

53. Petersen C, Nolan AL, de Paula França Resende E, Miller Z, Ehrenberg AJ, Gorno-Tempini ML, et al. Alzheimer's disease clinical variants show distinct regional patterns of neurofibrillary tangle accumulation. *Acta Neuropathol.* (2019) 138:597–612. doi: 10.1007/s00401-019-02036-6.

54. Munoz DG, Woulfe J, Kertesz A. Argyrophilic thorny astrocyte clusters in association with Alzheimer's disease pathology in possible primary progressive aphasia. *Acta Neuropathol.* (2007) 114: 347–57. doi: 10.1007/s00401–007–0266–x

55. Resende EPF, Nolan AL, Petersen C, Ehrenberg AJ, Spina S, Allen IE, et al. Language and spatial dysfunction in Alzheimer disease with white matter thorn-shaped astrocytes. *Neurology.* (2020) 94:e1353-e1364. doi: 10.1212/WNL.0000000000008937.

56. Buciuc M, Duffy JR, Machulda MM, Spychalla AJ, Gunter JL, Jack CR Jr, et al. Association of amyloid angiopathy with microbleeds in logopenic progressive aphasia: an imaging-pathology study. *Eur J Neurol.* (2021) 28:670–5. doi: 10.1111/ene.14594.

57. van Veluw SJ, Biessels GJ, Klijn CJ, Rozemuller AJ. Heterogeneous histopathology of cortical microbleeds in cerebral amyloid angiopathy. *Neurology.* (2016) 86:867–71. doi: 10.1212/WNL.0000000000002419

58. Whitwell JL, Jones DT, Duffy JR, Strand EA, Machulda MM, Przybelski SA, et al. Working memory and language network dysfunctions in logopenic aphasia: a task-free fMRI comparison with Alzheimer's dementia. *Neurobiol Aging.* (2015) 36:1245-52. doi: 10.1016/j.neurobiolaging.2014.12.013.

Figure 1.TIF

TABLE 1.

	Typical AD	Atypical AD	ND	Typical AD vs. Atypical AD (p value)
No.	85	32	40	
Male %	42.05	53.13	50.00	0.307 (χ^2)
Age at onset (years)	65.99±11.08	65.09±8.35	NA	0.379
Duration of Illness (years)	3.24±2.07	3.50±2.34	NA	0.755
Age at lumber puncture	69.75±8.43	68.59±7.61	NA	0.429
Education (years)	12.02±1.72	12.09±1.11	NA	0.727
Hypertension (%)	18 (21.18)	5 (18.52)	NA	0.680 (χ^2)
Diabetes (%)	12 (14.12)	3 (9.38)	NA	0.709 (χ^2)
Hypercholesterolemia (%)	15 (17.65)	5 (18.5)	NA	0.987 (χ^2)
MMSE (/30)	19.34±4.82*	17.81±4.32*	29.15±1.05	0.075
MoCA (/30)	14.65±4.85	12.53±4.05	NA	0.017
FAB (/18)	8.74±3.23	7.38±3.49	NA	0.081
APOE ε4 (%)	57.65	46.88	NA	0.214 (χ^2)
CSF Aβ1-42 (pg/ml)	182.81±58.07*	176.7±29.66*	425.06±126.31	0.752
CSF Aβ1-40 (pg/ml)	4503±1745	4193±1085	7062.96±4163.42	0.616
CSF Aβ1-38 (pg/ml)	3255±1181	2183±629.5	2533.64±1253.03	0.002
CSF P-Tau (pg/ml)	83.07±31.63*	78.27±34.19*	36.37±14.17	0.409
CSF T-Tau (pg/ml)	593.95±175.75*	578.21±232.20*	151.50±72.27	0.717
CSF NFL (pg/ml)	1906±1140*	2468±1681*	579.89±322.96	0.306
CSF YKL-40 (ng/ml)	120.41±48.14*	124.16±49.93*	60.53±22.25	0.681

Figure 2.TIF

TABLE 2.

	lvPPA	PCA	EOAD	LOAD	Comparing AD subtypes ANOVA (p value)	Post hoc differences (p value)
No.	20	12	39	46		
Male %	55.00	50.00	38.46	45.65	0.05 < p (χ^2)	
Age at onset (years)	68.70±6.95	60.00±8.34	57.31±10.41	73.35±4.13	< 0.0001	PCA<lvPPA (0.046) EOAD<PCA (0.0002) PCA<LOAD (<0.0001) EOAD<LOAD (<0.0001)
Duration of Illness (years)	3.65±2.58	3.25±1.96	3.92±2.53	2.98±2.04	0.315	
Education (years)	11.58±1.04	12.75±2.34	12.18±1.32	12.02±0.91	0.085	
MMSE (/30)	17.10±4.12	19.00±4.57	18.67±4.89	19.91±4.73	0.101	
MoCA (/30)	11.35±3.88	13.83±4.15	14.21±5.10	15.02±4.65	0.025	lvPPA<LOAD (0.015)
FAB (/18)	6.35±3.15	9.08±3.50	8.79±3.69	8.70±2.82	0.039	lvPPA<EOAD (0.045)
Hypertension (%)	3 (15)	3 (25)	7 (17.95)	10 (21.74)	0.05 < p (χ^2)	
Diabetes mellitus (%)	2 (10)	1 (8.33)	6 (15.38)	11 (23.91)	0.05 < p (χ^2)	
Hypercholestrolemia (%)	4 (20)	2 (16.67)	6 (15.38)	12 (26.09)	0.05 < p (χ^2)	
Language:	**lvPPA**	**PCA**	**EOAD**	**LOAD**	Comparing AD subtypes ANOVA (p value)	**Post hoc differences (p value)**
Confrontation Naming (0-2) #	1.45±0.83	1.67±0.49	1.85±0.43	1.76±0.48	0.149	
Single word repetition (0-3) #	2.20±1.24	2.75±0.45	2.56±0.72	2.61±0.68	0.719	
Single word recall (0-3) #	0.60±0.75	0.75±0.86	0.82±0.88	0.89±1.08	0.849	
Sentence repetition (0-1) #	0.40±0.50	0.75±0.45	0.69±0.47	0.65±0.48	0.112	
Auditory sentence comprehension (0-3) #	1.40±1.05	2.58±0.67	2.15±1.09	2.48±0.89	0.0007	lvPPA<PCA (0.015) lvPPA<EOAD (0.042) lvPPA<LOAD (0.0005)
Calculation:	**lvPPA**	**PCA**	**EOAD**	**LOAD**	Comparing AD subtypes ANOVA (p value)	**Post hoc differences (p value)**
Serial seven (0-5) #	1.25±1.07	1.33±0.98	1.69±1.52	1.91±1.54	0.468	
Digit span backward (0-2) #	0.60±0.74	0.33±0.49	0.54±0.55	0.74±0.61	0.167	
Visuospatial functioning:	**lvPPA**	**PCA**	**EOAD**	**LOAD**	Comparing AD subtypes ANOVA (p value)	**Post hoc differences (p value)**
Intersecting pentagons (0-1)	0.50±0.51	0.08±0.29	0.56±0.50	0.69±0.46	0.0022	PCA<EOAD (0.021) PCA<LOAD (0.0009)
Clock drawing test (0-3)	0.95±0.99	0.42±0.51	1.18±0.91	1.26±0.97	0.0284	PCA<LOAD (0.028)

Figure 3.TIF

TABLE 3.

	lvPPA	PCA	EOAD	LOAD	Comparing AD subtypes ANOVA (p value)	Post hoc differences (p value)
No.	20	12	39	46		
Lobar CMBs (1≦) (%)	10 (50.00)	4 (25.00)	9 (23.08)	17 (36.96)	0.024	EOAD<lvPPA (0.082) PCA<lvPPA (0.036) LOAD<lvPPA (0.322)
Mean Lobar CMBs No. (Bilateral) (per a patient with lobar CMBs)	11.60±9.87	3.33±3.22	8.39±14.69	10.85±10.30	0.312	
Mean lobar CMBs No. (Right) (per a patient with lobar CMBs)	4.75±3.69	2.00±3.64	5.20±8.23	6.15±6.36	0.715	
Mean lobar CMBs No. (Left) (per a patient with lobar CMBs)	7.80±6.13	1.33±0.33	4.50±8.14	5.31±3.68	0.259	
Comparing mean lobar CMBs No. (Right vs Left) Kruskal-Wallis test	0.161	0.600	0.987	0.602		

Figure 4.TIF

TABLE 4.

Typical AD vs. ND	Cut-point	95% CI	p	Sensitivity (%)	Specificity (%)
Aβ1-42	< 308.7	0.8883 ~ 0.9961	< 0.0001	96.77	90.91
P-Tau	> 47.43	0.8411 ~ 0.9764	< 0.0001	92.86	81.58
T-tau	> 270.2	0.8992 ~ 0.9965	< 0.0001	97.10	94.74
NFL	> 858.8	0.8203 ~ 0.9674	< 0.0001	91.30	85.71
YKL-40	> 78.59	0.7381 ~ 0.9303	< 0.0001	85.25	75.00

Figure 5.TIF

TABLE 5.

CSF markers	lvPPA	PCA	EOAD	LOAD	ND	Comparing AD subtypes (p value)	Post hoc differences (p value)
No.	18	12	34	38	33		
Aβ1-42	174.67±29.72[a]	181.074±49.88[a]	181.18±58.39[a]	184.871±58.68[a]	441.1±90.13	0.983	
Aβ1-40	4415.82±1073.98	4489.73±1887.83	4202.36±1585.82	4735.38±1844.25	6196±1325	0.379	
Aβ1-38	2224.77±651.98	2036.91±645.98	3053.18±990.84	3390.02±1287	2640±1032	0.035	no significant difference
P-Tau	84.68±37.05[a]	58.71±28.71[d]	87.24±33.45[a]	79.55±30.01[a]	34.86±12.84	0.389	
T-Tau	547.74±234.98[a]	568.66±251.81[a]	596.29±196.32[a]	592.04±197.93[a]	157.89±68.25	0.756	
NFL	2731.43±1227.88[a]	1101.18±269.37[d]	1781.57±1260.64[a]	2041.86±994.38[a]	541.1±273.5	0.002	PCA<lvPPA (0.003) EOAD<lvPPA (0.014) LOAD<lvPPA(0.045)
YKL-40	135.54±54.56[a]	96.49±36.12[d]	107.96±42.83[b]	130.97±50.54[a]	60.53±22.25	0.148	
APOE ε4 carrier (%)	11 (55.00)	5 (41.67)	25 (64.10)	24 (52.17)	—	0.646 (χ^2)	
Global PiB retention	1.94±0.48	1.99±0.49	1.82±0.41	1.93±0.49	—	0.072	

Figure 6.TIF

TABLE 6.

C.I. (p value)	R/L	lvPPA	PCA	EOAD	LOAD
No.		17	12	32	36
Frontal	R	-0.285 (0.099)	-0.412 (0.250)	-0.001 (0.498)	0.061 (0.383)
	L	-0.316 (0.076)	-0.577 (0.250)	0.119 (0.299)	-0.066 (0.375)
Temporal	R	0.106 (0.319)	0.082 (0.500)	-0.052 (0.410)	-0.345 (0.042)
	L	-0.382 (0.046)	-0.252 (0.321)	0.052 (0.410)	-0.368 (0.027)
Parietal	R	0.099 (0.329)	0.082 (0.500)	-0.148 (0.251)	-0.397 (0.020)
	L	-0.303 (0.085)	-0.405 (0.179)	-0.129 (0.278)	-0.345 (0.042)
Occipital	R	0.012 (0.478)	-0.143 (0.725)	-0.052 (0.410)	-0.353 (0.042)
	L	0.079 (0.362)	-0.417 (0.268)	-0.051 (0.409)	-0.408 (0.043)

Figure 7.TIF

FIGURE 1.

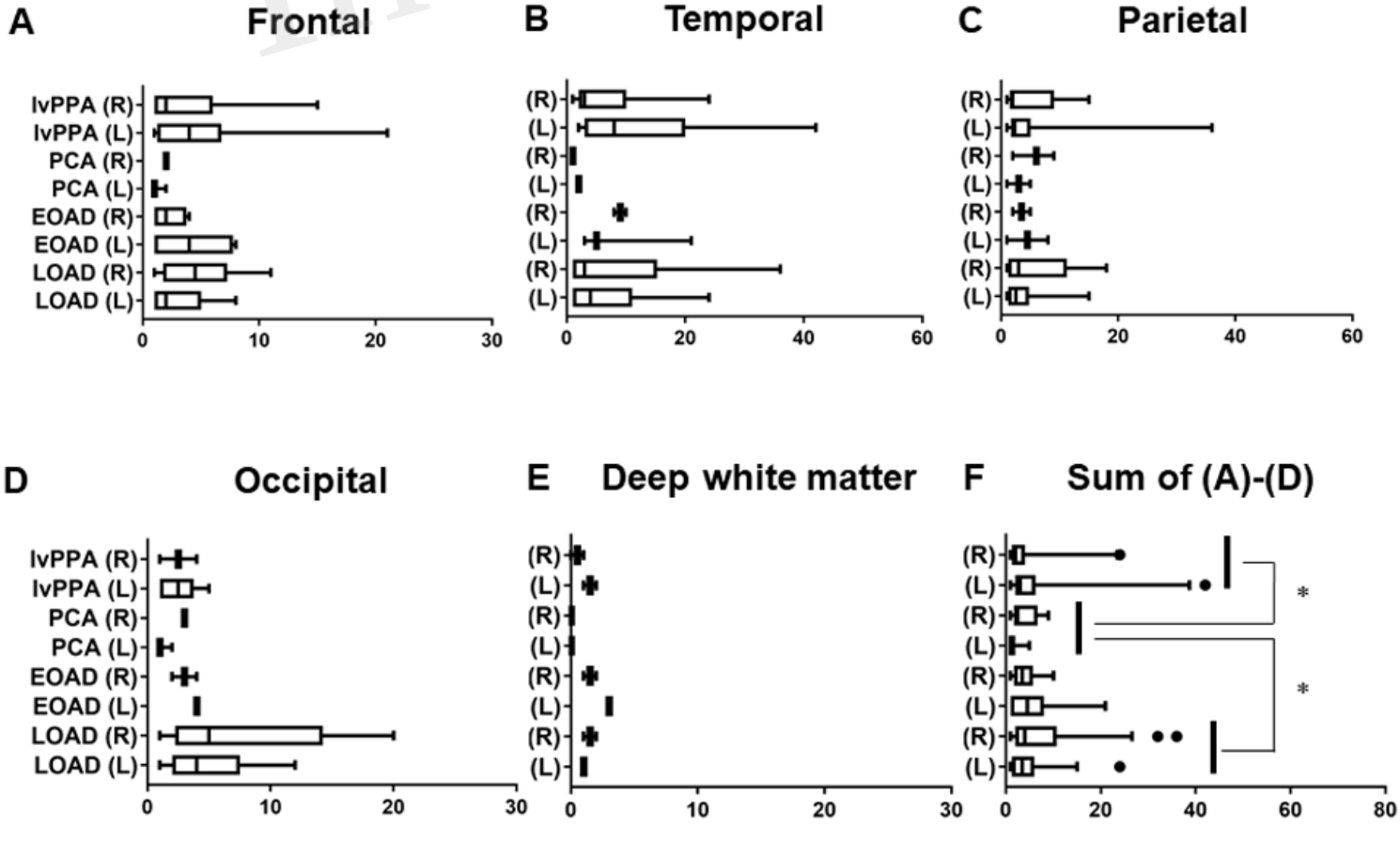

Figure 8.TIF

FIGURE 2.

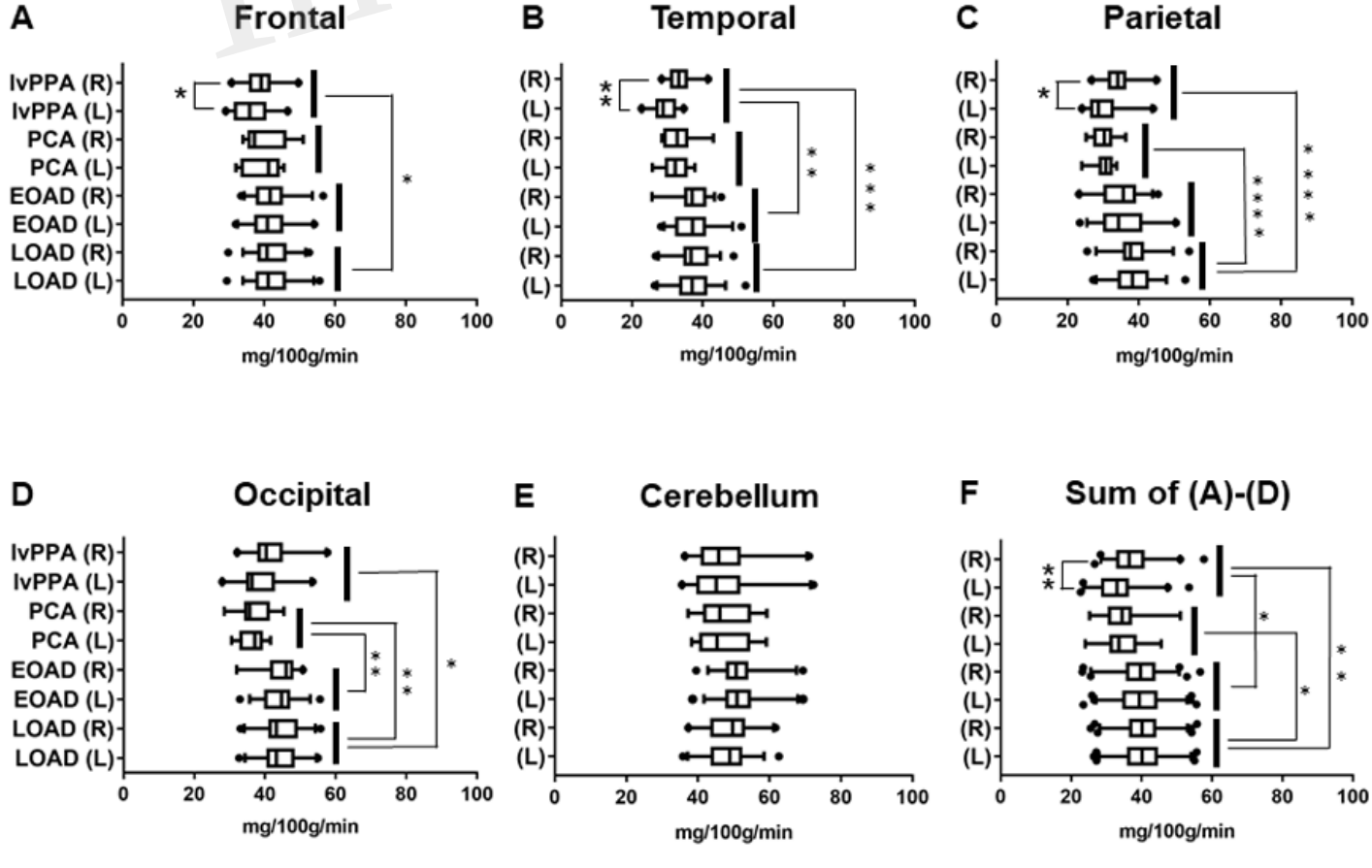

Figure 9.TIF

FIGURE 3.

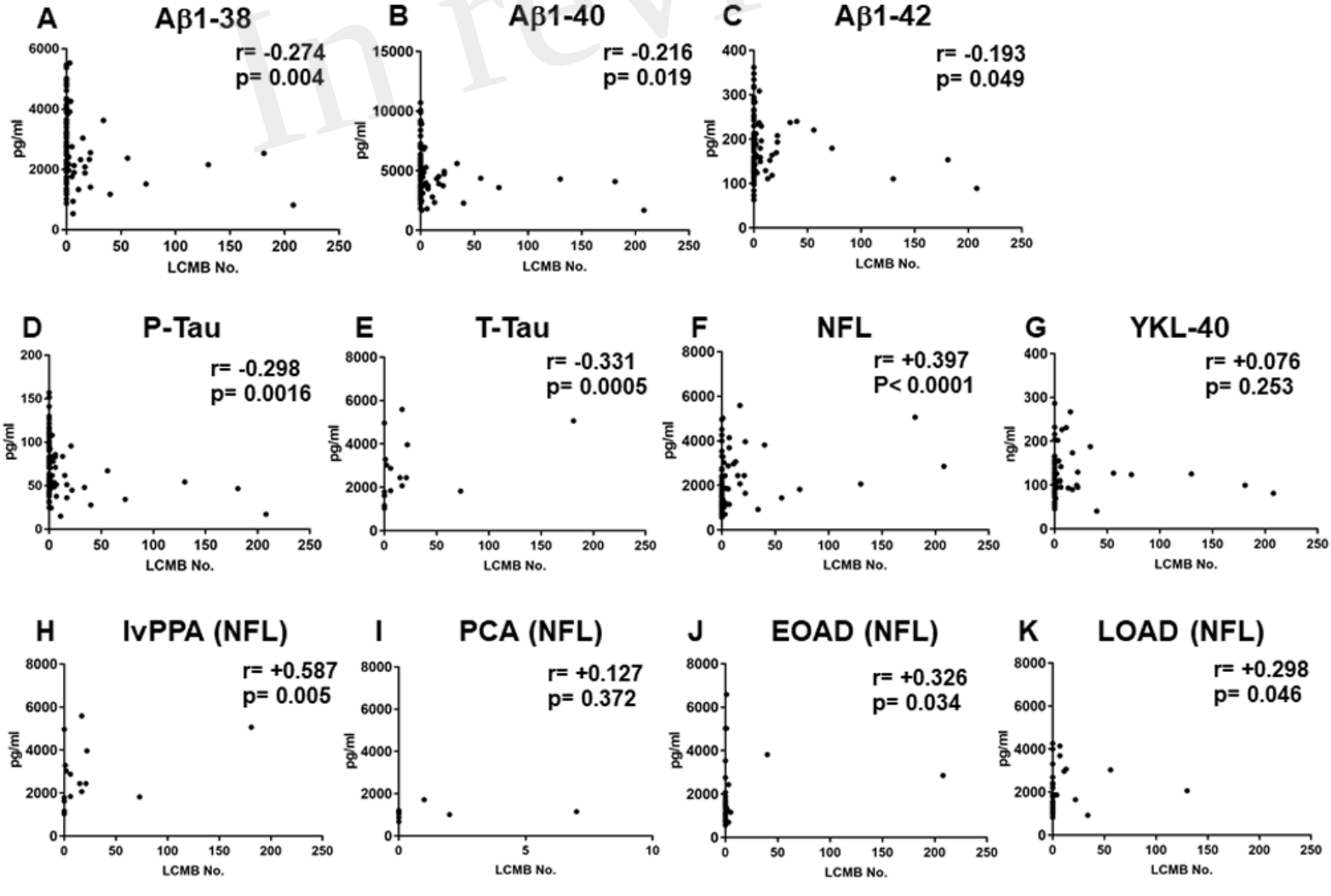

frontiers in Neurology

CASE REPORT
published: xx June 2021
doi: 10.3389/fneur.2021.645625

Recurrent Lobar Hemorrhages and Multiple Cortical Superficial Siderosis in a Patient of Alzheimer's Disease With Homozygous APOE ε2 Allele Presenting Hypobetalipoproteinemia and Pathological Findings of ^{18}F-THK5351 Positron Emission Tomography: A Case Report

Masaki Ikeda[1,2,3], Koichi Okamoto[2], Keiji Suzuki[4], Eriko Takai[3], Hiroo Kasahara[3], Natsumi Furuta[3], Minori Furuta[3], Yuichi Tashiro[5], Chisato Shimizu[2], Shin Takatama[6], Isao Naito[6], Mie Sato[7], Yasujiro Sakai[2], Manabu Takahashi[8], Masakuni Amari[2], Masamitsu Takatama[2], Tetsuya Higuchi[9], Yoshito Tsushima[9], Hideaki Yokoo[10], Masahiko Kurabayashi[11], Shun Ishibashi[10], Kenji Ishii[12] and Yoshio Ikeda[3]*

[1] Division of General Education (Neurology), Faculty of Health & Medical Care, Saitama Medical University, Saitama, Japan, [2] Department of Neurology, Geriatrics Research Institute and Hospital, Maebashi, Japan, [3] Department of Neurology, Gunma University Graduate School of Medicine, Maebashi, Japan, [4] Department of Pathology, Geriatrics Research Institute and Hospital, Maebashi, Japan, [5] Department of Neurology, Mito Medical Center, Mito, Japan, [6] Department of Neurosurgery, Geriatrics Research Institute and Hospital, Maebashi, Japan, [7] Department of Anesthesiology, Geriatrics Research Institute and Hospital, Maebashi, Japan, [8] Department of Cardiovascular Medicine, Gunma University Graduate School of Medicine, Maebashi, Japan, [9] Department of Diagnostic Radiology and Nuclear Medicine, Gunma University Graduate School of Medicine, Maebashi, Japan, [10] Division of Endocrinology and Metabolism, Department of Internal Medicine, Jichi Medical University, Tochigi, Japan, [11] Department of Pathology, Gunma University Graduate School of Medicine, Maebashi, Japan, [12] Team for Neuroimaging, Tokyo Metropolitan Institute of Gerontology, Tokyo, Japan

In Alzheimer's disease, the apolipoprotein E gene *(APOE)* ε2 allele is a protective genetic factor, whereas the *APOE* ε4 allele is a genetic risk factor. However, both the *APOE* ε2 and the *APOE* ε4 alleles are genetic risk factors for lobar intracerebral hemorrhage. The reasons for the high prevalence of lobar intracerebral hemorrhage and the low prevalence of Alzheimer's disease with the *APOE* ε2 allele remains unknown. Here, we describe the case of a 79-year-old Japanese female with Alzheimer's disease, homozygous for the *APOE* ε2 allele. This patient presented with recurrent lobar hemorrhages and multiple cortical superficial siderosis. The findings on the ^{11}C-labeled Pittsburgh Compound B-positron emission tomography (PET) were characteristic of Alzheimer's disease. ^{18}F-THK5351 PET revealed that the accumulation of ^{18}F-THK 5351 in the right pyramidal tract at the pontine level, the cerebral peduncle of the midbrain, and the internal capsule,

OPEN ACCESS

Edited by:
Achim Gass,
University of Heidelberg, Germany

Reviewed by:
Katsutoshi Furukawa,
Tohoku University, Japan
Lukas Sveikata,
Massachusetts General Hospital and Harvard Medical School, United States
Kenjiro Ono,
Showa University, Japan

***Correspondence:**
Masaki Ikeda
ikedam8@gmail.com

Specialty section:
This article was submitted to Applied Neuroimaging, a section of the journal Frontiers in Neurology

Received: *15 January 2021*
Accepted: *05 May 2021*
Published: *xx June 2021*

Citation:
Ikeda M, Okamoto K, Suzuki K, Takai E, Kasahara H, Furuta N, Furuta M, Tashiro Y, Shimizu C, Takatama S, Naito I, Sato M, Sakai Y, Takahashi M, Amari M, Takatama M, Higuchi T, Tsushima Y, Yokoo H, Kurabayashi M, Ishibashi S, Ishii K and Ikeda Y (2021) Recurrent Lobar Hemorrhages and Multiple Cortical Superficial Siderosis in a Patient of Alzheimer's Disease With Homozygous APOE ε2 Allele Presenting Hypobetalipoproteinemia and Pathological Findings of ^{18}F-THK5351 Positron Emission Tomography: A Case Report. Front. Neurol. 12:645625. doi: 10.3389/fneur.2021.645625

reflecting the lesions of the previous lobar intracerebral hemorrhage in the right frontal lobe. Moreover, ^{18}F-THK5351 accumulated in the bilateral globus pallidum, amygdala, caudate nuclei, and the substantia nigra of the midbrain, which were probably off-target reaction, by binding to monoamine oxidase B (MAO-B). ^{18}F-THK5351 were also detected in the periphery of prior lobar hemorrhages and a cortical subarachnoid hemorrhage, as well as in some, but not all, areas affected by cortical siderosis. Besides, ^{18}F-THK5351 retentions were observed in the bilateral medial temporal cortices and several cortical areas without cerebral amyloid angiopathy or prior hemorrhages, possibly where tau might accumulate. This is the first report of a patient with Alzheimer's disease, carrying homozygous *APOE* ε2 allele and presenting with recurrent lobar hemorrhages, multiple cortical superficial siderosis, and immunohistochemically vascular amyloid β. The ^{18}F-THK5351 PET findings suggested MAO-B concentrated regions, astroglial activation, Waller degeneration of the pyramidal tract, neuroinflammation due to CAA related hemorrhages, and possible tau accumulation.

Keywords: Alzheiemer's disease, apolipoprotein ϵ allele, cerebral amyloid angiopathy, cortical superficial siderosis, recurrent lobar brain hemorrhages, hypobetalipoproteinemia, ^{18}F-THK5351 PET, ^{11}C-PiB PET

INTRODUCTION

The apolipoprotein E gene *(APOE)* ε2 allele has an exceptionally low likelihood of causing Alzheimer's dementia in *APOE2* homozygotes (1) and, it protects against Alzheimer's disease (AD) (2). In contrast, the *APOE* ε4 allele is a genetic risk factor of AD (3). However, the *APOE* ε2 and the *APOE* ε4 alleles, responsible for causing severe alterations in the vascular wall structure causing cerebral amyloid angiopathy (CAA), are common genetic risk factors for lobar intracerebral hemorrhage (ICH) (4–7). The reason for the high prevalence of lobar ICH despite the very low prevalence of AD in individuals with the *APOE* ε2 allele remains unknown. ^{18}F-THK5351, which was developed as a tau binding tracer (8, 9), has been shown to strongly bind to monoamine oxidase B (MAO-B) (10). Recently, in a patient of cerebral infarction, the off-target retentions of ^{18}F-THK5351 revealed Wallerian degeneration of the pyramidal tract, basal ganglia, thalamus, and cerebral cortices (11). In this report, we describe a patient with AD who carried a homozygous *APOE* ε2 allele. This patient presented with recurrent lobar hemorrhages and multiple cortical superficial siderosis (cSS) with hypobetalipoproteinemia. Additionally, several ^{18}F-THK5351 PET findings reflected an increase in the MAO-B, reactive astrogliosis, and Wallerian degeneration of the pyramidal tract due to lobar ICH, as well as the possible accumulation of tau, related to AD pathology, in cerebral cortical areas.

Abbreviations: *APOE*, apolipoprotein E gene; AD, Alzheimer's disease; ICH, intracerebral hemorrhage; CAA, cerebral amyloid angiopathy; MAO-B, monoamine oxidase B; cSS, cortical superficial siderosis; ^{11}C PiB-PET, ^{11}C-labeled Pittsburgh Compound B-positron emission tomography; Aβ, amyloid β; P-Tau, phosphorylated tau 181; T-Tau, human total tau; CSF, cerebrospinal fluid; SAH, subarachnoid hemorrhage; MRI, magnetic resonance imaging; WMH, white matter hyperintensities; PVC, perivascular spaces; ADL, activities of daily living.

METHODS

^{11}C-PiB PET and ^{18}F-THK5351 PET Neuroimages

^{11}C-labeled Pittsburgh Compound B positron emission tomography (^{11}C-PiB PET) was performed at the Gunma University Hospital as described previously by the authors (12, 13). ^{18}F-THK5351 PET examinations were performed at the Tokyo Metropolitan Institute of Gerontology using the Discovery PET/CT 710 scanner (GE Healthcare, Milwaukee, WI, USA). Emission data were acquired for 20 min, starting 40 min after intravenous injection of ^{18}F-THK5351 at a dose of approximately 190 MBq (5.1 mCi). In total, 47 slice images, with a voxel size of 2 × 2 × 3.27 mm and a matrix size of 128 × 128, were obtained. The data, collected in three-dimensional mode, were reconstructed after correcting for decay, attenuation, and scatter. ^{18}F-THK5351 PET images were then normalized using the cerebellum as a reference region; cerebellar uptake was set to the value of one, as in the previously reported method (11, 14).

Analyses of the Cerebrospinal Fluid (CSF)

A Cerebrospinal fluid was obtained by a lumbar puncture of the L3/L4 or L4/L5 intervertebral space, and the CSF samples were centrifuged for 10 min at 1,800 × g at 4°C within 3 h of collection. Samples were divided into aliquots of 0.5 mL and stored at −80°C in polypropylene tubes until they were analyzed using enzyme-linked immunosorbent assay (ELISA) kits for human CSF amyloid β (Aβ) Aβ1-42 and Aβ1-40 (FUJIFILM Wako Pure Chemical Corporation, Osaka, Japan) (12). Phosphorylated tau 181 (P-Tau) and human total tau (T-Tau) levels in the CSF were measured using the sandwich using ELISA INNOTEST® PHOSPHO-TAU (181P) (15) and the sandwich ELISA INNOTEST® T-Tau-Ag (both FUJIREBIO, Ghent, Belgium) (16), respectively, as described previously (12, 17).

Pathological Examinations

Brain tissue samples were obtained when the patient underwent surgery for hematoma. Immunohistochemical studies were performed on using an anti-Aβ1-42 antibody and an anti-Aβ1-40 antibody (both IBL, Fujioka, Gunma, Japan).

APOE Genotyping and Apolipoprotein E Protein Analyses

After obtaining informed consent for the genetic test of the *APOE* gene, we purified genomic DNA from lymphocytes in the peripheral blood of the patient. For the analysis of *APOE* allele polymorphism, purified genomic DNA samples were examined as previously described (12). The Apolipoprotein E protein was confirmed by the LSI Medience Corporation (Tokyo, Japan).

CASE PRESENTATION AND RESULTS

This report describes the case of a 79-year-old Japanese woman diagnosed with AD, presenting with recurrent hemorrhages despite the absence of vascular risk factors such as hypertension, diabetes mellitus, hypercholesterolemia, coronary heart disease, and smoking. However, fatty liver and hypocholesterolemia were observed on medical examination. Although her mother had died of a subarachnoid hemorrhage (SAH). At age 70 years, the patient experienced a loss of recent memory, and since then, the amnesia has gradually progressed. At the age of 72 years, she was admitted to the Gunma University Hospital for a headache caused by a brain hemorrhage; she felt a little headache and dullness without nausea, vomiting or loss of consciousness, a state that were quite different from a typical acute SAH. At the time of her first admission, cerebral magnetic resonance imaging (MRI) revealed a hemorrhage in the left parietal subcortical area (**Figure 1A**) and multiple regions of cSS (**Figures 1A,B**). Although there were no white matter hyperintensities, perivascular spaces, chronic ischemic infarcts, or lacunae, there were multiple regions of cSS and a few lobar microbleeds. On neuropsychological examinations, the scores were 23/30 in the Mini-Mental State Examination (MMSE) (disorientation of time, delayed recall deficits, acalculia, and agraphia), 19/30 in the Montreal Cognitive Assessment (MoCA) (visual-spatial disorientation, clock drawing, delayed recall, and disorientation of time), and 9/18 in the Frontal Assessment Battery (FAB) (deficits of similarities, motor series, conflicting instructions, and prehension behavior). The Instrumental Activities of Daily Living scales (IADL) (18) was 4/8 (Abilities required for shopping, food preparation, responsibility for own medications, and handling finances were disturbed). She could do activities of daily living (ADL) to some extent but needed some assistance from her family. According to gradual amnestic progression and executive dysfunction of ADL, she was diagnosed with mild dementia with AD at the first admission; the findings were also suggestive of possible CAA according to the modified Boston criteria (19). At age 73 years, the second cerebral hemorrhage occurred. This time she was admitted to the Geriatric Research Institute and Hospital for a left hemiparalysis with a lobar ICH at the right frontal lobe (**Figure 1C**). The hematoma was removed by a neurosurgical operation. The score of MMSE at the time of the second admission had decreased to 18/30, implying a cognitive decline, when compared to the first admission. The score of the revised Hasegawa Dementia Scale (HDS-R) (20) was 17/30, suggesting moderate dementia. At age

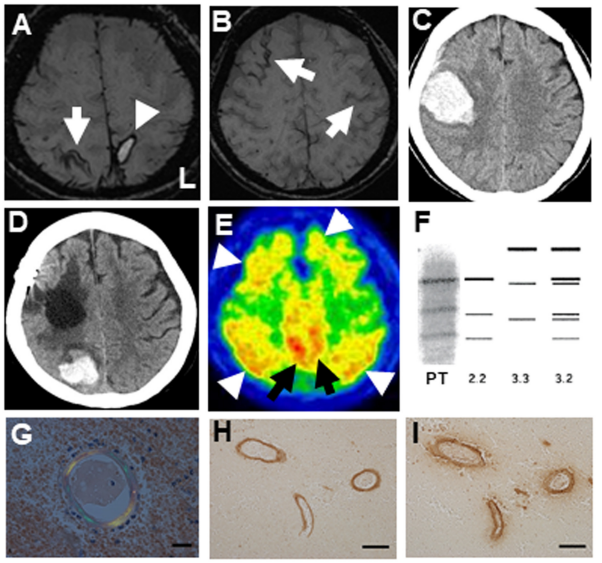

Serum (mg/dl)	Patient	standard value
Total C	108	128-219
HDL C	48	45SD-67SD
LDL C	25	59-139
TG	103	30-149
Apo A-1	129	126-165
Apo A-2	23.4	24.6-33.3
Apo B	26	66-101
Apo C-2	4.2	1.5-3.8
Apo C-3	8.5	5.4-9.0
Apo E	4.8	2.8-4.6
Lip (a)	<3.0	0.0-40.0
RLP	18	<7.5
Lipoprotein fraction (%)	**Patient**	**standard value**
1 HDL	40	26-53
2 LDL	13	42-65
3 IDL	25	0
4 VLDL	22	4∼7

FIGURE 1 | (A) Brain magnetic resonance imaging (MRI; 3T System, Skyra, Siemens, Germany) at the first admission. Susceptibility weighted images (SWI) showing a cortical hemorrhage (arrowhead) at the left parietal lobe cortex and cortical superficial siderosis (cSS) in the right parietal cortex (arrow). **(B)** In the same MRI, cSS was additionally observed in the left and right frontal cortices (arrows). **(C)** Brain computed tomography (CT) showing a second lobar hemorrhage at the right frontal subcortical area concurrent with left hemiparesis. **(D)** Brain CT showing a third lobar hemorrhage at the right parieto-occipital subcortical region. **(E)** ^{11}C-PiB PET revealing widespread ^{11}C-PiB retentions in the cerebral cortices (arrowheads) and precuneus (arrows). **(F)** Electrophoresis revealing a 2/2 pattern in the apolipoprotein E phenotype for this patient (PT). **(G)** Congophilic amyloid deposits shown in blood vessels of the resected brain tissue, as shown using polarizing microscopy (Scale bar: 20 μm). **(H,I)** Aβ-reactive structures in blood vessel walls identified by immunohistochemistry using anti-Aβ1-42 **(H)** and anti-Aβ1-40 **(I)** antibodies. Scale bars: 100 μm. **(J)** Laboratory serum results from the patient's first admission. **(K)** Serum lipoprotein electrophoresis reveals a broad-β pattern (bar), where intermediate-density lipoprotein (fraction 3) and very-low-density lipoprotein (fraction 4) are aberrantly elevated.

77 years, she was admitted for a headache for the third time; this time she had left hemispatial neglect, caused by a lobar ICH in the right parieto-occipital lobes (**Figure 1D**). Currently, she has no additional hemorrhages but is still affected by dementia and left hemiparalysis. The patient has not on any anti-platelet, anti-coagulation, or antihyperlipidemic drugs for the clinical course.

At the time of the first hospitalization, ^{11}C-PiB PET revealed widespread ^{11}C-PiB retentions in the cerebral cortices and precuneus, which were compatible with those of AD (**Figure 1E**).

The *APOE* genotyping revealed a homozygous ε2 allele (not shown). The apolipoprotein E (ApoE) was confirmed as a 2/2 protein by the western blot (**Figure 1F**). Congophilic amyloid deposits in blood vessels were confirmed on polarizing microscopy, undertaken using tissue resected during the second hospitalization (**Figure 1G**). Aβ-immunoreactive structures in blood vessels walls were revealed by an anti-Aβ1-42 antibody (**Figure 1H**) and an anti-Aβ1-40 antibody (**Figure 1I**) on immunohistochemical studies. Based on the pathological results, this case was suggestive of "probable CAA" with supporting pathological evidence according to the modified Boston criteria (19). Laboratory examination of the serum at the first admission demonstrated hypolipidemia, defined by low serum levels of total cholesterol (Total C), low-density lipoprotein cholesterol (LDL C), apolipoprotein A-2 (ApoA-2), and apolipoprotein B (Apo B). Chylomicrons were scarcely detectable (data not shown). The serum levels of apolipoprotein C-2 (ApoC-2), apolipoprotein E (ApoE), remnant-like lipoprotein (RLP), intermediate-density lipoprotein (IDL), and very-low-density lipoprotein (VLDL) were increased (**Figure 1J**). Furthermore, polyacrylamide gel (PAGE) electrophoresis of her serum revealed a broad-β band which seemed to be mimicking type III dysliplidemia (**Figure 1K**) (BML Co. Tokyo, Japan). There was no detection of aberrantly truncated apolipoprotein B on the western blot (data not shown). In the case, the CSF level of Aβ1-42 was 144.49 pg/mL, which was lower than that in non-dementia subjects (mean ± standard deviation, 431.55 ± 103.46 pg/mL, $n = 20$) and comparable to that in age-matched AD patients (183.32 ± 14.68 pg/mL, $n = 25$); the Aβ1-40 was 3037.22 pg/mL, which was lower than that in non-dementia subjects (mean ± standard deviation, 5118.79 ± 1882.47 pg/mL, $n = 20$) and age-matched AD patients (5358.47 ± 2376.80 pg/mL, $n = 25$); the P-Tau level was 42.94 pg/mL, which was higher than that in non-dementia subjects (29.33 ± 11.36 pg/mL, $n = 20$) and comparable to those of age-matched AD patients (75.40 ± 7.5 pg/mL, $n = 25$); and the T-Tau level was 424.50 pg/mL, which was higher than that in non-dementia subjects (143.55 ± 14.63 pg/mL, $n = 20$) and comparable to that in age-matched AD patients (503.30 ± 53.03 pg/mL, $n = 25$). These findings of CSF biomarkers and ^{11}C-PiB PET of the patient were compatible with those of AD. Post-discharge the second hemorrhage at the age of 73 years, the 76-year-old patient was examined using ^{18}F-THK5351 PET in a stable condition.

^{18}F-THK5351 retentions areas were observed at the right side of the pyramidal tract at the pontine level, the cerebral peduncle of the midbrain, and the internal capsule (red circles in **Figure 2 A-G-M-S, B-H-N-T, C-I-O-U**, and **D-J-P-V**). The off-target ^{18}F-THK5351 retentions, binding to MAO-B derived from astrocytes, located in the pyramidal tract, were considered a result of a previous right frontal lobar hemorrhage.

In addition, they were detected at the bilateral substantia nigra of the midbrain, medial areas of the thalamus, the amygdala, the globus pallidum (**black circles** in **Figure 2 T, C-I-O-U, D-J-P-V**), and the anterior caudate nuclei (**black circles** in **Figure 2 D-J-P**), in which originally contained a high concentration of MAO-B.

Besides, ^{18}F-THK5351 retentions were visible along with previous lobar hemorrhagic lesions in the left parietal cortex (at the first hemorrhage) and the right frontal lobe (at the second hemorrhage), and an asymptomatic old cortical SAH lesion in the right parietal cortex (yellow circles in **Figure 2 E-K-Q-W** and **F-L-R-X**).

Additional ^{18}F-THK5351 retentions were observed in the bilateral medial temporal areas (blue circles in **Figure 2 A-G-M-S** and **B-H-N-T**), the bilateral areas of entorhinal and parahippocampal gyruses, and hippocampus (blue circles in **Figure 2 B-H-N-T, C-I-O**), the bilateral areas of parahippocampal, fusiform, and lingual gyruses (blue circles in **Figure 2 C-I-O**), the left anterior frontal cortical areas (blue circles in **Figure 2 B-H-N** and **C-I-O**), the bilateral posterior areas in the temporal cortices (blue circles in **Figure 2 C-I-O** and **D-J-P**), bilateral basis areas in the temporal lobes (blue circles in **Figure 2 S, T, U, V,** and **W**), the left calcarine sulcus (blue circles in **Figure 2 D-J-P**), the left precuneus area and the left frontal cortex (blue circles in **Figure 2 E-K-Q-W**).

DISCUSSION

To our knowledge, this is the first report of an AD patient, homozygous for the *APOE* ε2 allele, presenting with recurrent lobar hemorrhage, vascular Aβ amyloid deposits, hypobetalipoproteinemia, and pathological ^{18}F-THK5351 findings. The vasculopathologic changes associated with the *APOE* ε2 allele might have a crucial role in the severity and clinical course of lobar ICH, and the screening of patients with ICH for the *APOE* ε2 may identify those at increased risk of mortality and poor functional outcomes (21). The *APOE* ε2, as well as the *APOE* ε4, allele was reported to be significantly associated with lobar ICH and cSS (21, 22), and their presence may predict the recurrence of anti-coagulation-associated ICH (23). Clinically, some patients with the *APOE* ε2 allele present with hypocholesterolemia (24). In animal study, *APOE* ε2 transgenic mice showed a decreased serum level of low-density lipoprotein cholesterol (25). These biochemical aberrations may lead to the fragility in the structure of cerebral blood vessel walls, resulting in recurrent ICH in AD patients with the *APOE* ε2 allele (26, 27). *APOE* ε2/ε3 carriers have larger total volumes of white matter hyperintensities compared to *APOE* ε4 carriers and a higher prevalence of microbleeds compared to *APOE* ε3 homozygotes (28). Because the homozygous *APOE* ε2 allele has an extremely low frequency (1), no prior publication has confirmed a proven vascular amyloid pathology, in a homozygous *APOE* ε2 allele carrying AD patient with recurrent lobar ICH, using ^{18}F-THK5351 PET and ^{11}C-PiB PET. *In vivo* study revealed that the levels of Aβ40 and Aβ42 in both soluble

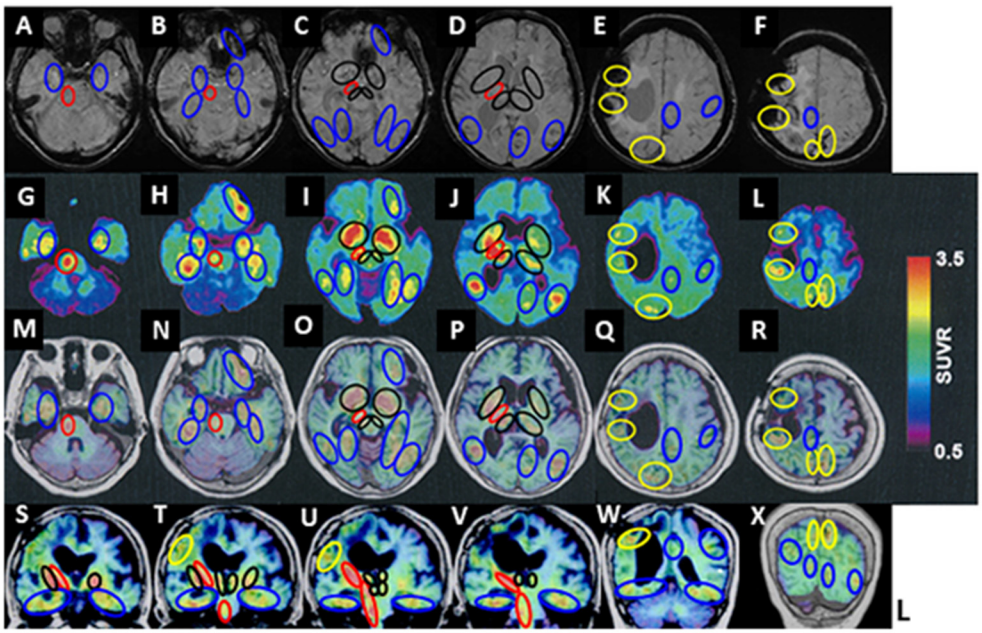

FIGURE 2 | ^{18}F-THK5351 imaging and MRI of the patient's brain. **(A–F)** Susceptibility-weighted MRI. **(G–L)** ^{18}F-THK5351. **(M–R)** ^{18}F-THK 5351 on transverse MRI (T1-weighted images). **(S–X)** ^{18}F-THK 5351 on coronal MRI (T1-weighted images). ^{18}F-THK5351 retentions areas were observed in the pyramidal tract at the pontine level, the cerebral peduncle of the midbrain, and the internal capsule, all at the right side (red circles: **A-G-M-S**, **B-H-N-T**, **C-I-O-U**, and **D-J-P-V**). The bilateral substantia nigra of the midbrain, the globus pallidum, the anterior caudate nuclei, amygdala, and the medial areas of thalamus (**black circles**: **C-I-O-U** and **D-J-P-V**) were considered the off-target retentions of ^{18}F-THK5351 binding to MAO-B. They were also visible along the previous lobar hemorrhagic lesions in the right frontal lobe and the left parietal cortex, as well as an asymptomatic old cortical SAH lesion in the right parietal cortex (yellow circles: **E-K-Q-W** and **F-L-R-X**). Additional ^{18}F-THK5351 retentions were observed in the bilateral medial temporal areas (blue circles: **A-G-M-S** and **B-H-N-T**), the left anterior frontal cortical areas (blue circles: **B-H-N-T** and **C-I-O-U**), the posterior areas in bilateral temporal cortices, and the bilateral fusiform, lingual, and parahippocampal gyruses (blue circles: **C-I-O** and **D-J-P**).

and insoluble fractions of the brain lysate were reduced in *APOE* ε2, but not in *APOE* ε3 or *APOE* ε4 gene integrated in human amyloid precursor protein/human presenilin 1 (APP/PS1) double transgenic mice (29). The CAA patients had a distinctive CSF biomarker profile, with significantly lower concentrations of Aβ40 and Aβ42 than those of non-demented controls and AD patients, which were found in *APOE* ε2, ε4, and ε3 genotypes (30–33). Lower CSF levels of Aβ1-40 and Aβ1-42 in an AD patient with CAA carrying *APOE* ε2 homozygote had not been reported before this case. So far, pathological reports of autopsy studies showed reduced neurofibrillary tangles (NFTs) in postmortem AD brains of *APOE* ε2 carriers (2, 34, 35). Although the mechanism underlying this reduction of NFTs is poorly understood; as *APOE* ε2 was significantly correlated with tau pathology only in Aβ positive AD patients but not with those in Aβ negative individuals, the protective effect of *APOE* ε2 against AD tau may be partially mediated through its effect on Aβ deposition (36). It remains still controversial why *APOE* ε2 may protect against tau pathology independently of Aβ in AD (37–39). ^{18}F-THK5351 was initially developed to target tau aggregates in NFTs (8, 9), however, ^{18}F-THK5351 has been shown to strongly bind off-target to MAO-B in the basal ganglia and thalamus (10), as well as the melanin-containing cells of the substantia nigra (40). ^{18}F-THK5351 is also highly concentrated in astrocytes, compared to other types of glial cells (41, 42). The MAO-B concentration is also increased in reactive astrogliosis (43), which describes a spectrum of astrocytic changes that occur in response to brain injury (44). On the other hand, Wallerian degeneration, the progressive anterograde demyelination and disintegration of distal axons, develops following a brain injury to neuronal soma or proximal axons (45). In the early stage of brain injury, axonal swelling, and breakdown of myelin sheath occur, followed by loss of myelinated fibers and infiltration of macrophages. In the later stage, the degenerated axons are replaced by gliosis, which is primarily the proliferation of astrocytes to form a scar. A previous case report demonstrated ipsilateral myelin loss and gliosis in the pyramidal tract lesion 5 years after a left middle cerebral artery infarction (45). As for the other tau PET tracers and CAA, two reports of Tau PET have been published (46, 47). In the former report, paired helical filament (PHF) tau burden overlapped cerebral microbleeds and/or cSS on ^{18}F-AV1451 PET, raising the possibility that the characteristic markers of vascular amyloid were associated with local production of PHF tau (46). In the latter report, the amyloid deposition, evaluated by ^{18}F-florbetaben PET, was not different in vicinity of cSS, but tau depositions were elevated in vicinity of cSS-affected regions compared to non-cSS-affected brain regions. Their case of probable CAA suggested that cSS may be associated

with an elevation in local tau accumulation but not with an increase in fibrillary amyloid deposition (47). ^{18}F-THK5351 PET has been reported to strongly bind to MAO-B derived from astrocytes and possibly tau, probably reflecting astrogliosis related CAA hematoma and cSS, also possibly tau accumulation in AD pathology (48). In our case, 3 year have passed since the ^{18}F-THK5351 PET examination for the previous ICH in the right frontal lobe presenting as contralateral hemiparalysis. In this patient, Wallerian degeneration may have developed in the ipsilateral pyramidal tract followed by astrogliosis, and the marker ^{18}F-THK5351 PET, targeting MAO-B containing tissues, may have identified this Wallerian degeneration. The ^{18}F-THK5351 is now recognized as a dual-purpose compound that binds to both MAO-B and tau aggregates, thus tau isoforms might have accumulated in the damaged fasciculus. MAO-B is highly concentrated in astrocytes and serotonergic and histaminergic neurons (43), astrocytes proliferate in response to inflammation caused by brain injury (44). Therefore, regional changes in MAO-B concentration can be an index of astrogliosis and be detected on ^{18}F-THK5351 PET imaging, although tau accumulation may co-exist in the AD brain (48). These findings suggest that ^{18}F-THK5351 accumulates in lesions where astrogliosis occurs and that ^{18}F-THK5351 PET can be an imaging modality to visualize and quantify astrogliosis, as recently demonstrated in patients with a cerebral infarction or neurological disorders (49–51). In our case, ^{18}F-THK5351 retentions were observed in some, but not all, regions with cSS, presumably because this effect might depend on severity of cSS and the degree of astrogliosis that is correlated with the extent of hemosiderin deposition (52). ^{18}F-THK5351 retentions were observed only in some areas rather than all peripheral regions at the lobar hemorrhage in this patient. Several cSS lesions reflected ^{18}F-THK5351 PET retentions, however, the other cSS lesions did not reflect, which might probably depend upon severity of cSS or neuroinflammation of CAA. It seems that old cSS showed less or no THK5351 retention [such as in bilateral prefrontal lobes cortices/subcortices (**Figure 2 D-J-P and E-K-Q**)], while the recent lesions of hematoma or siderosis showed THK5351 retentions [such as in left parietal cortical area (hematoma at the first admission) and right frontal cortico-subcortical areas (hematoma at the second admission)]. This case signifies that both AD and CAA pathologies could co-occur and contribute to cognitive decline (53), indicating that CAA, especially, cSS strongly increases the risk of hemorrhages, even when the clinical changes are gradual. We found that CSF Aβ1-40 of this patient was lower than those of AD patients and non-demented subjects, as, in the recent publication, the levels of CSF Aβ1-40 in AD with disseminated cSS were lower than that in AD patients with focal cSS and those without cSS (54, 55). This result is thought be in accordance with neuropathological reports demonstrating deposition of Aβ40 within the vessel walls of CAA patients (56). CSF P-Tau levels, in this case, were not significantly higher than those in AD patients, because CSF P-Tau levels in AD patients with CAA pathology have been reported to be either slightly elevated or within the normal levels (55, 57, 58). This could be because of the change in permeability of the cerebral blood vessels due to CAA; decreased ability of parenchymal P-Tau to flow out into the lumen of vessels or less amount of tau phosphorylation in CAA than in AD patients may have led to lower P-Tau levels in CSF. On the other hand, Aβ 40 is thought to deposit in the blood vessels affected by CAA, rather than flowing into the lumen of vessels (59). Although the fact that the pathophysiologic mechanisms are not completely understood, recent studies show that *APOE2* allele is strongly associated with cSS and increased frequency and severity of lobar ICH (22). Furthermore, while *APOE* ε2 promotes so-called CAA-related vasculopathic changes (vessel cracking, detachment, and delamination of the outermost layer of the tunica media, and fibrinoid necrosis), this can lead to vessel rupture (5, 22), another evidence of increased ICH risk in *APOE* ε2 carriers was recently reported, with or without AD (60). Hypobetalipoproteinemia may not be a direct cause for the ICH in this case, but might be an additional contributing factor, because hypocholesterolemia was reported to be a risk factor of ICH (61–63). This AD case carried the homozygous *APOE* ε2 allele and severe hypocholesterolemia, which may have exacerbated vascular changes in the CAA, thereby leading to more severe CAA, multiple cSS, and recurrent lobar ICH. The mechanism underlying the risk for ICH because of an *APOE* ε2 genotype is still unclear and perhaps complex (60), which should be elucidated hereafter. In future, a large-scale investigation of cholesterol levels in AD patients with a homozygous *APOE* ε2 allele will be required to define its clinical significance and etiologies. This AD case with multiple cSS regions and lobar hemorrhages is also worth reporting; it demonstrates that ^{18}F-THK5351 retentions reflected MAO-B, reactive astrogliosis, and Wallerian degeneration of the pyramidal tract due to CAA related lobar ICH, and possibly tau accumulation.

Finally, the therapies targeting *APOE* ε2 and APOE2 for AD have been extensively developed; a viral-mediated *APOE* ε2 overexpression, converting *APOE* ε4 to *APOE* ε2, and plasma APOE-based therapy were described detail in a recent review (64). Although these trials have some effect, unfortunately, they have not been effective, regardless of their successful experimental results. Besides severe CAA pathology, this case presented with hypobetalipoproteinemia, however, we could not elucidate the clear molecular and pathological relationships between them. To validate the mechanisms of effective therapies targeting APOE2/*APOE* ε2, more evidence from humans and animal models is required. Further, more AD patients carrying the *APOE* ε2 allele are required to analyze pathological and biochemical findings. Furthermore, improved understanding of the roles of APOE2/*APOE* ε2 in other diseases, CAA/Stroke and different proteinopathies, including tau, TDP-43, and α-synuclein pathologies, may allow a comprehensive assessment of the safety of APOE2 targeted therapeutics for AD.

A limitation of this study is that it includes only one AD patient carrying a homozygous *APOE* ε2 allele with recurrent hemorrhages and multiple cSS regions. This impedes statistical analyses for cholesterol levels in comparison to other *APOE* alleles or healthy control groups. The other limitation is that we could not confirm how histopathological association between ^{18}F-THK5351 retention and astrogliosis pathology since we

histologically observed only a part of the brain. To better understand the pathological mechanism, a detailed investigation using neuroradiological, biochemical, genetical, and pathological methods is required in CAA and AD patients.

DATA AVAILABILITY STATEMENT

The raw data supporting the conclusions of this manuscript will be made available by the authors, without undue reservation, to any qualified researcher.

ETHICS STATEMENT

The studies involving human participants were reviewed and approved by the ethics committee of the Gunma University Hospital. The patients/participants provided their written informed consent to participate in this study. Written informed consent was obtained from the individual(s) for the publication of any potentially identifiable images or data included in this article. Written consent to publish the clinical information was obtained from the patient's family.

AUTHOR CONTRIBUTIONS

MI collected the clinical data, interpreted the data, and wrote the manuscript. ET analyzed genomic DNA from the patient's blood samples and CSF biomarkers from the patient. KO, KS, and HY performed pathological examinations and evaluation of the results. TH and YTs performed the neuroimaging examination for ^{11}C PiB-PET, and KI performed and evaluated the neuroimaging examination for ^{18}F THK5351-PET. MF, NF, YTa, CS, MS, YS, MA, and MTakat collected the clinical information. SI, MK, and MTakah performed and evaluated the western blot of ApoB protein, also discussed the hypobetalipoproteinemia in this patient. ST and IN performed the neurosurgical operation to removal the hematoma at the second admission. MI performed the clinical data analysis and evaluated the specificities and neurological significances. All authors contributed to the article and approved the submitted version.

FUNDING

This study was supported by a Grant-in-Aid for Scientific Research (C) (MI: 18K07491, MTakah: 20K08870, TH: 19K08220, YTs: 18K07627, HY: 19K07411, KI: 17K09813, YI: 19K07813), (B) (SI: 19H03712, MK: 20H03671) from the Ministry of Education, Culture, Sports, Science and Technology of Japan, MI also received a Donation of love from the JOMO-SHINBUN newspaper company (Maebashi, Gunma, Japan).

ACKNOWLEDGMENTS

The authors thank the patient and his family for providing clinical data and allowing the publication of this case report. We especially thank Dr. Hirofumi Kawakami, an Advanced Application Specialist who belongs to Headquarter of Academy, GE Healthcare Japan, and Yoshikatsu Tsunemi (Inspection Specialist), Department of Clinical Laboratory Medicine, Geriatrics Research Institute and Hospital, for their excellent technical assistance. We thank Dr. Mikio Shoji for academic discussion about this manuscript. We would like to thank Editage (www.editage.com) for American English language editing.

REFERENCES

1. Reiman EM, Arboleda-Velasquez JF, Quiroz YT, Huentelman MJ, Beach TG, Caselli RJ, et al. Exceptionally low likelihood of Alzheimer's dementia in APOE2 homozygotes from a 5,000-person neuropathological study. *Nat Commun.* (2020) 11:667. doi: 10.1038/s41467-019-14279-8
2. Serrano-Pozo A, Qian J, Monsell S, Betensky R, Hyman B. APOEε2 is associated with milder clinical and pathological Alzheimer's disease. *Ann Neurol.* (2015) 77:917–29. doi: 10.1002/ana.24369
3. Corder EH, Saunders AM, Strittmatter WJ, Schmechel DE, Gaskell PC, Small G, et al. Gene dose of apolipoprotein E type 4 allele and the risk of Alzheimer's disease in late onset families. *Science.* (1993) 261:921–3. doi: 10.1126/science.8346443
4. Nicoll JA, Burnett C, Love S, Graham DI, Dewar D, Ironside JW, et al. High frequency of apolipoprotein E ε2 allele in hemorrhage due to cerebral amyloid angiopathy. *Ann Neurol.* (1997) 41:716–21. doi: 10.1002/ana.410410607
5. Greenberg SM, Vonsattel JP, Segal AZ, Chiu RI, Clatworthy AE, Liao A, et al. Association of apolipoprotein E ε2 and vasculopathy in cerebral amyloid angiopathy. *Neurology.* (1998) 50:961–5. doi: 10.1212/wnl.50.4.961
6. O'Donnell HC, Rosand J, Knudsen KA, Furie KL, Segal AZ, Chiu RI, et al. Apolipoprotein E genotype and the risk of recurrent lobar intracerebral hemorrhage. *N Eng J Med.* (2000) 342:240–5. doi: 10.1056/NEJM200001273420403
7. Rannikmäe K, Kalaria RN, Greenberg SM, Chui HC, Schmitt FA, Samarasekera N, et al. APOE associations with severe CAA-associated vasculopathic changes: collaborative meta-analysis. *J Neurol Neurosurg Psychiatry.* (2014) 85:300–5. doi: 10.1136/jnnp-2013-306485
8. Harada R, Okamura N, Furumoto S, Furukawa K, Ishiki A, Tomita N, et al. 18F-THK5351: a novel PET radiotracer for imaging neurofibrillary pathology in Alzheimer disease. *J Nucl Med.* (2016) 57:208–14. doi: 10.2967/jnumed.115.164848
9. Tago T, Furumoto S, Okamura N, Harada R, Adachi H, Ishikawa Y, et al. Structure-activity relationship of 2-arylquinolines as PET imaging tracers for tau pathology in Alzheimer disease. *J Nucl Med.* (2016) 57:608–14. doi: 10.2967/jnumed.115.166652
10. Ng KP, Pascoal TA, Mathotaarachchi S, Therriault J, Kang MS, Shin M, et al. Monoamine oxidase B inhibitor, selegiline, reduces ^{18}F-THK5351 uptake in the human brain. *Alzheimers Res Ther.* (2017) 9:25. doi: 10.1186/s13195-017-0253-y
11. Ishibashi K, Kameyama M, Tago T, Toyohara J, Ishii K. Potential use of 18F-THK5351 PET to identify wallerian degeneration of the pyramidal tract caused by cerebral infarction. *Clin Nucl Med.* (2017) 42:e523–4. doi: 10.1097/RLU.0000000000001868
12. Ikeda M, Tashiro Y, Takai E, Kurose S, Fugami N, Tsuda K, et al. CSF levels of Aβ1-38/Aβ1-40/Aβ1-42 and ^{11}C-PiB PET studies in three clinical variants of primary progressive aphasia and Alzheimer's disease. *Amyloid.* (2014) 21:238–45. doi: 10.3109/13506129.2014.949231
13. Kasahara H, Ikeda M, Nagashima K, Fujita Y, Makioka K, Tsukagoshi S, et al. Deep white matter lesions are associated with early recognition of dementia in Alzheimer's disease. *J Alzheimers Dis.* (2019) 68:797–808. doi: 10.3233/JAD-180939

14. Ishibashi K, Miura Y, Hirata K, Toyohara J, Ishii. Relationship between the temporal course of astrogliosis and symptom improvement in cerebral infarction: report of a case monitored using ^{18}F-THK5351 positron emission tomography. *BMC Med Imaging.* (2020) 20:81. doi: 10.1186/s12880-020-00481-4
15. Vanmechelen E, Vanderstichele H, Davidsson P, Van Kerschaver E, Van Der Perre B, Sjögren M, Andreasen N, et al. Quantification of tau phosphorylated at threonine 181 in human cerebrospinal fluid: a sandwich ELISA with a synthetic phosphopeptide for standardization. *Neurosci Lett.* (2000) 285:49–52. doi: 10.1016/s0304-3940(00)01036-3
16. Andreasen N, Minthon L, Davidsson P, Vanmechelen E, Vanderstichele H, Winblad B, et al. Evaluation of CSF-tau and CSF-Aβ42 as diagnostic markers for Alzheimer's disease in clinical practice. *Arch Neurol.* (2001) 58:373–9. doi: 10.1001/archneur.58.3.373
17. Ikeda M, Kuwabara T, Takai E, Kasahara H, Furuta M, Sekine A, et al. Increased neurofilament light chain and YKL-40 CSF Levels in one Japanese IBMPFD patient with VCP R155C mutation: a clinical case report with CSF biomarker analyses. *Front Neurol.* (2020) 11:757. doi: 10.3389/fneur.2020.00757
18. Lawton MP, Brody EM. Assessment of older people: self-maintaining and instrumental activities of daily living. *Gerontologist.* (1969) 9:179–86.
19. Linn J, Halpin A, Demaerel P, Ruhland J, Giese AD, Dichgans M, et al. Prevalence of superficial siderosis in patients with cerebral amyloid angiopathy. *Neurology.* (2010) 74:1346–50. doi: 10.1212/WNL.0b013e3181dad605
20. Katoh S, Shimogaki H, Onodera A, Ueda H, Oikawa K, Ikeda K, et al. Development of the revised version of Hasegawa's Dementia-Scale (HDS-R). *Jpn J Geriatr Psychiatry.* (1991) 2:1339–47. (Japanese)
21. Biffi A, Anderson CD, Jagiella JM, Schmidt H, Kissela B, Hansen BM, et al. APOE genotype and extent of bleeding and outcome in lobar intracerebral haemorrhage: a genetic association study. *Lancet Neurol.* (2011) 10:702–9. doi: 10.1016/S1474-4422(11)70148-X
22. Charidimou A, Zonneveld HI, Shams S, Kantarci K, Shoamanesh A, Hilal S, et al. APOE and cortical superficial siderosis in CAA: meta-analysis and potential mechanisms. *Neurology.* (2019) 93:e358–71. doi: 10.1212/WNL.0000000000007818
23. Biffi A, Urday S, Kubiszewski P, Gilkerson L, Sekar P, Rodriguez-Torres A, et al. Combining imaging and genetics to predict recurrence of anticoagulation-associated intracerebral hemorrhage. *Stroke.* (2020) 51:2153–60. doi: 10.1161/STROKEAHA.120.028310
24. Mahley RW, Huang Y, Rall SC. Pathogenesis of type III hyperlipoproteinemia (dysbetalipoproteinemia): questions, quandaries, and paradoxes. *J Lipid Res.* (1999) 40:1933–49.
25. Huang Y, Liu XQ, Rall SC, Mahley RW. Apolipoprotein E2 reduces the low-density lipoprotein level in transgenic mice by impairing lipoprotein lipase-mediated lipolysis of triglyceride-rich lipoproteins. *J Biol Chem.* (1998) 273:17483–90. doi: 10.1074/jbc.273.28.17483
26. McCarron MO, Nicoll JA, Stewart J, Ironside JW, Mann DM, Love S, et al. The apolipoprotein E epsilon2 allele and the pathological features in cerebral amyloid angiopathy-related hemorrhage. *J Neuropathol Exp Neurol.* (1999) 58:711–8. doi: 10.1097/00005072-199907000-00005
27. Nelson PT, Pious NM, Jicha GA, Wilcock DM, Fardo DW, Estus S, et al. APOE-ε2 and APOE-ε4 correlate with increased amyloid accumulation in cerebral vasculature. *J Neuropathol Exp Neurol.* (2013) 72:708–15. doi: 10.1097/NEN.0b013e31829a25b9
28. Groot C, Sudre CH, Barkhof F, Teunissen CE, van Berckel BN, Seo SW, et al. Clinical phenotype, atrophy, and small vessel disease in APOEε2 carriers with Alzheimer disease. *Neurology.* (2018) 91:e1851–9. doi: 10.1212/WNL.0000000000006503
29. Hudry E, Dashkoff J, Roe AD, Takeda S, Koffie RM, Hashimoto T, et al. Gene transfer of human ApoE isoforms results in differential modulation of amyloid deposition and neurotoxicity in mouse brain. *Sci Transl Med.* (2013) 5: 212ra161. doi: 10.1126/scitranslmed.3007000
30. Costa AS, Pinho J, Kučikiene D, Reich A, Schulz JB, Reetz K. Cerebral amyloid angiopathy in amyloid-positive patients from a memory clinic cohort. *J Alzheimers Dis.* (2021) 79:1661–72. doi: 10.3233/JAD-201218
31. Banerjee G, Ambler G, Keshavan A, Paterson RW, Foiani MS, Toombs J, et al. Cerebrospinal fluid biomarkers in cerebral amyloid angiopathy. *J Alzheimers Dis.* (2020) 74:1189–1201. doi: 10.3233/JAD-191254
32. Charidimou A, Imaizumi T, Moulin S, Biffi A, Samarasekera N, Yakushiji Y, et al. Brain hemorrhage recurrence, small vessel disease type, and cerebral microbleeds: a meta-analysis. *Neurology.* (2017) 89:820–29. doi: 10.1212/WNL.0000000000004259
33. Shams S, Martola J, Charidimou A, Cavallin L, Granberg T, Shams M, et al. Cortical superficial siderosis: prevalence and biomarker profile in a memory clinic population. *Neurology.* (2016) 87:1110–7. doi: 10.1212/WNL.0000000000003088
34. Bennett DA, De Jager PL, Leurgans SE, Schneider JA. Neuropathologic intermediate phenotypes enhance association to Alzheimer susceptibility alleles. *Neurology.* (2009) 72:1495–503. doi: 10.1212/WNL.0b013e3181a2e87d
35. Nagy Z, Esiri MM, Jobst KA, Johnston C, Litchfield S, Sim E, et al. Influence of the apolipoprotein E genotype on amyloid deposition and neurofibrillary tangle formation in Alzheimer's disease. *Neuroscience.* (1995) 69:757–61. doi: 10.1016/0306-4522(95)00331-c
36. Farfel JM, Yu L, De Jager PL, Schneider JA, Bennett DA. Association of APOE with tau-tangle pathology with and without β-amyloid. *Neurobiol Aging.* (2016) 37:19–25. doi: 10.1016/j.neurobiolaging.2015.09.011
37. Goldberg TE, Huey ED, Devanand DP. Association of APOE ε2 genotype with Alzheimer's and non-Alzheimer's neurodegenerative pathologies. *Nat Commun.* (2020) 11:4727. doi: 10.1038/s41467-020-18198-x
38. Zhao N, Liu CC, Van Ingelgom AJ, Linares C, Kurti A, Knight JA, et al. APOE ε2 is associated with increased tau pathology in primary tauopathy. *Nat Commun.* (2018) 9:4388. doi: 10.1038/s41467-018-06783-0
39. Ghebremedhin E, Schultz C, Botez G, Rüb U, Sassin I, Braak E, et al. Argyrophilic grain disease is associated with apolipoprotein E epsilon 2 allele. *Acta Neuropathol.* (1998) 96:222–4. doi: 10.1007/s004010050886
40. Tago T, Toyohara J, Harada R, Furumoto S, Okamura N, Kudo Y, et al. Characterization of the binding of tau imaging ligands to melanin-containing cells: putative off-target-binding site. *Ann Nucl Med.* (2019) 33:375–82. doi: 10.1007/s12149-019-01344-x
41. Gulyás B, Pavlova E, Kása P, Gulya K, Bakota L, Várszegi S, et al. Activated MAO-B in the brain of Alzheimer patients, demonstrated by [^{11}C]-L-deprenyl using whole hemisphere autoradiography. *Neurochem Int.* (2011) 58:60–8. doi: 10.1016/j.neuint.2010.10.013
42. Levitt P, Pintar JE, Breakefield XO. Immunocytochemical demonstration of monoamine oxidase B in brain astrocytes and serotonergic neurons. *Proc Natl Acad Sci USA.* (1982) 79:6385–9. doi: 10.1073/pnas.79.20.6385
43. Saura J, Luque JM, Cesura AM, Da Prada M, Chan-Palay V, Huber G, et al. Increased monoamine oxidase B activity in plaque-associated astrocytes of Alzheimer brains revealed by quantitative enzyme radioautography. *Neuroscience.* (1994) 62:15–30. doi: 10.1016/0306-4522(94)90311-5
44. Sofroniew MV. Molecular dissection of reactive astrogliosis and glial scar formation. *Trends Neurosci.* (2009) 32:638–47. doi: 10.1016/j.tins.2009.08.002
45. Jones KC, Hawkins C, Armstrong D, Deveber G, Macgregor D, Moharir M, et al. Association between radiographic Wallerian degeneration and neuropathological changes post childhood stroke. *Dev Med Child Neurol.* (2013) 55:173–7. doi: 10.1111/dmcn.12010
46. Kim HJ, Cho H, Werring DJ, Jang YK, Kim YJ, Lee JS, et al. 18F-AV-1451 PET imaging in three patients with probable cerebral amyloid angiopathy. *J Alzheimers Dis.* (2017) 57:711–6. doi: 10.3233/JAD-161139
47. Brendel M, Catak C, Beyer L, Linn J, Wahl H, Janowitz D, et al. Colocalization of tau but not β-amyloid with cortical superficial siderosis in a case with probable CAA. *Case Rep Neurol.* (2020) 12:232-7. doi: 10.1159/000506765
48. Harada R, Ishiki A, Kai H, Sato N, Furukawa K, Furumoto S, et al. Correlations of ^{18}F-THK5351 PET with postmortem burden of tau and astrogliosis in Alzheimer disease. *J Nucl Med.* (2018) 59:671–4. doi: 10.2967/jnumed.117.197426
49. Ishibashi K, Miura Y, Hirata K, Toyohara J, Ishii K. ^{18}F-THK5351 PET can identify astrogliosis in multiple sclerosis plaques. *Clin Nucl Med.* (2020) 45:e98–100. doi: 10.1097/RLU.0000000000002751
50. Schönecker S, Brendel M, Palleis C, Beyer L, Höglinger GU, Schuh E, et al. PET imaging of astrogliosis and tau facilitates diagnosis of Parkinsonian syndromes. *Front Aging Neurosci.* (2019) 11:249. doi: 10.3389/fnagi.2019.00249

51. Takami Y, Yamamoto Y, Norikane T, Mitamura K, Hatakeyama T, Nishiyama Y. ^{18}F-THK5351 PET can identify lesions of acute traumatic brain injury. *Clin Nucl Med.* (2020) 45:e491–2. doi: 10.1097/RLU.0000000000003165
52. Charidimou A, Perosa V, Frosch MP, Scherlek AA, Greenberg SM, van Veluw SJ. Neuropathological correlates of cortical superficial siderosis in cerebral amyloid angiopathy. *Brain.* (2020) 143:3343–51. doi: 10.1093/brain/awaa266
53. Boyle PA, Yu L, Wilson RS, Leurgans SE, Schneider JA, Bennett DA. Person-specific contribution of neuropathologies to cognitive loss in old age. *Ann Neurol.* (2018) 83:74–83. doi: 10.1002/ana.25123
54. Martínez-Lizana E, Carmona-Iragui M, Alcolea D, Gómez-Choco M, Vilaplana E, Sánchez-Saudinós MB, et al. Cerebral amyloid angiopathy-related atraumatic convexal subarachnoid hemorrhage: an ARIA before the tsunami. *J Cereb Blood Flow Metab.* (2015) 35:710–7. doi: 10.1038/jcbfm.2015.25
55. Catak C, Zedde M, Malik R, Janowitz D, Soric V, Seegerer A, et al. Decreased CSF levels of ß-amyloid in patients with cortical superficial siderosis. *Front Neurol.* (2019) 10:439. doi: 10.3389/fneur.2019.00439
56. Vinters HV. Emerging concepts in Alzheimer's disease. *Annu Rev Pathol.* (2015) 10:291–319. doi: 10.1146/annurev-pathol-020712-163927
57. van Etten ES, Verbeek MM, van der Grond J, Zielman R, van Rooden S, van Zwet EW, et al. β-Amyloid in CSF: biomarker for preclinical cerebral amyloid angiopathy. *Neurology.* (2017) 88:169–76. doi: 10.1212/WNL.0000000000003486
58. Shams S, Granberg T, Martola J, Li X, Shams M, Fereshtehnejad SM, et al. Cerebrospinal fluid profiles with increasing number of cerebral microbleeds in a continuum of cognitive impairment. *J Cereb Blood Flow Metab.* (2016) 36:621–8. doi: 10.1177/0271678X15606141
59. Viswanathan A, Greenberg SM. Cerebral amyloid angiopathy in the elderly. *Ann Neurol.* (2011) 70:871–80. doi: 10.1002/ana.22516
60. Goldberg TE, Huey ED, Devanand DP Associations of APOE e2 genotype with cerebrovascular pathology: a postmortem study of 1275 brains. *J Neurol Neurosurg Psychiatry.* (2021) 92:7–11. doi: 10.1136/jnnp-2020-323746
61. Yilmaz P, Ikram MA, Ikram MK, Niessen WJ, Viswanathan A, Charidimou A, et al. Application of an imaging-based sum score for cerebral amyloid angiopathy to the general population: risk of major neurological diseases and mortality. *Front Neurol.* (2019) 10:1276. doi: 10.3389/fneur.2019.01276
62. An SJ, Kim TJ, Yoon BW. Epidemiology, risk factors, and clinical features of intracerebral hemorrhage: an update. *J Stroke.* (2017) 19:3–10. doi: 10.5853/jos.2016.00864
63. Mustanoja S, Strbian D, Putaala J, Meretoja A, Curtze S, Haapaniemi E, et al. Association of prestroke statin use and lipid levels with outcome of intracerebral hemorrhage. *Stroke.* (2013) 44:2330–2. doi: 10.1161/STROKEAHA.113.001829
64. Li Z, Shue F, Zhao N, Shinohara M, Bu G. APOE2: protective mechanism and therapeutic implications for Alzheimer's disease. *Mol Neurodegener.* (2020) 15:63. doi: 10.1186/s13024-020-00413-4

Conflict of Interest: The authors declare that the research was conducted in the absence of any commercial or financial relationships that could be construed as a potential conflict of interest.